IAEA-TECDOC-678

Advanced calculational methods for power reactors and LWR core design parameters

Proceedings of a Specialists Meeting, held in Cadarache, France, 10–14 September 1990 and a Technical Committee Meeting and Workshop held in Řež, Czechoslovakia, 7–11 October 1991

INTERNATIONAL ATOMIC ENERGY AGENCY IAEA

December 1992

The IAEA does not normally maintain stocks of reports in this series. However, microfiche copies of these reports can be obtained from

INIS Clearinghouse
International Atomic Energy Agency
Wagramerstrasse 5
P.O. Box 100
A-1400 Vienna, Austria

Orders should be accompanied by prepayment of Austrian Schillings 100,— in the form of a cheque or in the form of IAEA microfiche service coupons which may be ordered separately from the INIS Clearinghouse.

ADVANCED CALCULATIONAL METHODS FOR POWER REACTORS
AND LWR CORE DESIGN PARAMETERS
IAEA, VIENNA, 1992
IAEA-TECDOC-678
ISSN 1011–4289

Printed by the IAEA in Austria
December 1992

FOREWORD

In the framework of its reactor physics activities, the Agency has long been providing Member States with a forum for the exchange of technical information on in-core fuel management.

The Agency published the technical documents entitled "Computer Programs for the In-core Fuel Management of Power Reactors", IAEA-TECDOC-250, in 1981, and "In-core Fuel Management Programs for Nuclear Power Reactors, IAEA-TECDOC-314, in 1984, which describes available computer code packages. The Agency has also initiated a number of Co-ordinated Research Programmes (CRPs) on selected reactor core physics aspects of water reactors. The CRP on In-core Fuel Management Code Package Validation was set up to obtain well defined cases for the verification of code packages for PWRs, BWRs and WWERs, with the participation of 16 contract/agreement holders and observers.

The purpose of the Specialists Meeting on Advanced Calculational Methods for Power Reactors, held in Cadarache, France, 10-14 September 1990, was to provide a forum for reviewing and discussing selected core physics of water cooled reactors (including high convertors). New methods of advanced calculation for advanced fuels and complex geometries of next generation reactors with a high level of accuracy were discussed and the importance of supercomputing and on-line monitoring was also acknowledged. The meeting was attended by about 60 participants from 20 countries who presented 30 papers.

The Technical Committee Meeting on LWR Core Design Parameters, held in Rez, Czechoslovakia, 7-11 October 1991, provided an opportunity for participants to exchange their experience on reactor physics aspects of benchmark calculations of various lattices, methods for core parameter calculations, core monitoring and in-core fuel management. At the Workshop there were further discussions related to the benchmark problems, homogenization techniques and cross-section representations. Thirty-five papers were presented by about 43 participants from 19 countries.

EDITORIAL NOTE

In preparing this material for the press, staff of the International Atomic Energy Agency have mounted and paginated the original manuscripts as submitted by the authors and given some attention to the presentation.

The views expressed in the papers, the statements made and the general style adopted are the responsibility of the named authors. The views do not necessarily reflect those of the governments of the Member States or organizations under whose auspices the manuscripts were produced.

The use in this book of particular designations of countries or territories does not imply any judgement by the publisher, the IAEA, as to the legal status of such countries or territories, of their authorities and institutions or of the delimitation of their boundaries.

The mention of specific companies or of their products or brand names does not imply any endorsement or recommendation on the part of the IAEA.

Authors are themselves responsible for obtaining the necessary permission to reproduce copyright material from other sources.

Throughout the text names of Member States are retained as they were when the text was compiled.

CONTENTS

SPECIALISTS MEETING ON ADVANCED CALCULATIONAL METHODS FOR POWER REACTORS, CADARACHE, FRANCE, 10–14 SEPTEMBER 1990

TECHNICAL COMMITTEE MEETING AND WORKSHOP ON LWR CORE DESIGN PARAMETERS, ŘEŽ, CZECHOSLOVAKIA, 7–11 OCTOBER 1991

SPECIALISTS MEETING ON
ADVANCED CALCULATIONAL METHODS FOR POWER REACTORS

CADARACHE, FRANCE, 10-14 SEPTEMBER 1990

SUMMARY OF THE SPECIALISTS MEETING

Session 1: LWR Cell & Assembly calculations
(Chairmen: M.J. Halsall & G.B. Bruna)

The session provided an interesting contrast between computer-intensive solutions of exact geometries, and computer-economical solutions based on theoretical extensions of methods to achieve acceptable accuracies.

An extension to the fast, but rather approximate interface current collision probability method was recommended, in which the use of DP_1 instead of DP_0 was suggested in order to achieve a flux profile comparable to a CP (P_{13}) treatment, but at approximately 20% the cost of the latter. The speed of the conventional method is due to the fact that the probability increases only linearly with the number of regions, but it is approximate because isotropy is assumed at every boundary. The extended method is based instead on a spherical harmonic expansion at each boundary, improving the accuracy by including directional terms. A factor of about 5 was observed in the accuracy of fluxes, at little expense in computation time.

A new and interesting approach for differentiating the axial and radial leakages in a heterogeneous assembly was proposed. This method, which is based on the definition of direction-dependant migration areas, represents an improvement over the standard one, which operates only on an homogeneous system, defining thereby an averaged diffusion coefficient. The results show quite a low sensitivity of the local diffusion coefficient to the computational options, in PWR nominal conditions, but this sensitivity increases significantly in advanced reactor lattices. Its drawback lies in the fact that it computes the neutron leakage rate DB^2 for a medium representing the assembly, not the leakage of the assembly itself.

A new module called CACTUS was described, which solves the differential form of the neutron transport equation by a method of characteristics in a complex mixed geometry of cylindrical rods in a square or hexagonal array. Applications for this system can be found that extend to very complex 2D geometries. Despite rather prohibitive computational costs, it could still be used for benchmarking purposes.

The fortuitous success of a center-mesh one mesh per pin diffusion treatment was brought out, vis-s-vis a rigorous transport treatment for worth evaluation of RCCA in a PWR fuel assembly. The interest in performing an equivalence was also analyzed, and compensation phenomena between transport and diffusion calculations were pointed out.

Simple, heuristic 1-D supercell calculational procedures were applied to some difficult problems of two adjacent Gd pins in a 4x4 square array, and for Gd as BAF or absorber rods in hexagonal lattice assembly/core. Despite the simplifying assumptions made in the methods, agreement with accepted benchmark solutions and experimental measurements was generally good.

Session 2: Computational Techniques/Posters/Demonstrations
(Chairmen: V. Jagannathan & J.B. Thomas)

The advent of supercomputing can be likened to the invention of the microscope and the telescope, since it could add a whole new dimension to the art of 3D visualization, and to the real-time follow-up of 3D phenomena in a nuclear reactor. The consensus is that supercomputing is necessary, and that it will arrive on the scene anyway, since yesterday's supercomputing is simply, after all, today's computing. The gigantic computational power that will be provided by these machines (gigaflops, teraflops, and perhaps beyond), will require increasing control of a huge amount of data, and of a great number of choices to be made for optimizing modeling and computation. The solution to this will probably come from Computer Aided Software Engineering (CASE), with knowledge-based systems that will act on generic, multipurpose and modular integrated software systems. This will simultaneously provide, from a single toolkit:

- simple, specialized methods for industrial applications that are highly concerned with computational time, and
- advanced methods for reference calculations and cross-validation, and for the calibration of standard models and procedures.

The high-standard presentations made during the poster and demonstration session provided a representative sampling of the tools developed for various industrial purposes. These ranged from off-line design and safety calculations to on-line computer aided monitoring and operation, and from them the two main classes of tools can be identified; namely, that of generic, multipurpose software tools, and that of specialized, automated, fast-running tools.

The software packages presented were APOLLO, CRONOS, CESAR, CAROLINE AND RITME. In its new version, the first of these incorporates collision probabilities with 2D discrete ordinate capabilities. Transport/transport and transport/diffusion equivalence procedures, providing identical calculation of reaction rates on reference lattices, are built-in. CRONOS2 is a 3D kinetics code oriented towards core calculations in normal and off-normal situations. It combines finite difference and various levels of finite elements diffusion approximations with discrete ordinate transport capabilities. The kinetics and thermal hydraulics are tightly coupled in CRONOS2, by the use of a simplified model or of the FLICA4 3D two-phase flow code. The modular structure of SAPHYR (the computer code system into which both APOLLO and CRONOS are embedded), and the availability of a control language (GIBIANE), allow the user to build up computational procedures oriented towards the optimized calculation of specific problems.

CESAR, a PWR rod ejection computational system, combines 3D kinetics and thermal hydraulics in a very optimized fashion. The comparison with conventional, standard synthesis previously used in parametric design and fuel management studies (which lead to numerous accident simulations) demonstrated to be very favorable, and allowed the adoption of CESAR as a routine computational tool. As a consequence, a great part of the conservatism deriving from synthesis approximation has been relaxed, providing a more realistic computation, and correlative gains.

CAROLINE is a surveillance-protection system that uses on-line 3D calculations. It is derived from the 3D nodal code COCCINELLE, which was developed for core design and fuel management. As such, CAROLINE can be compared consistently

with more detailed models of the core. On-line correction with measured axial off-set data is feasible with it, and a 3D burnup profile can be updated by a special module. A slightly more detailed model, SUPER-CAROLINE, provides a precision very close to that of COCCINELLE.

Another fast 3D integral transport code is RITME, which uses the nodal Greene function method. A time step requires about 1 second on a conventional workstation. On-line, RITME uses calibration on the ex-core measurements providing the axial-offset of the core. This methodology proved to lead to a satisfactory precision on the whole core 3D power distribution. More detailed models are under development in the framework of the LOGARITME system.

The software presented in the poster and demonstration session illustrates the evolution towards modular, multi-function and multilevel codes. Attempts are being made to build computational schemes for handling many different problems with the same toolkit, and encompassing various models from different fields (neutronics, thermal-hydraulics, etc.). Furthermore, the codes are being developed in such a fashion as to allow the building of an optimized computation by picking up in the toolkit the right level of modeling for every sub-problem, thereby broadening the field of operations. Also desirable is the ability to build, calibrate, validate and optimize simplified models intended to perform specific industrial on- or off-line computations, and to perform cross-validations between different methods (Monte-Carlo, SN, collision probabilities, etc.). These codes are intended to capitalize, in a unique, long-lived and more easily maintainable fashion, every improvement in modeling, numerical analysis, computational scheme, nuclear data and qualification. Simultaneously, new, specialized products are emerging as tools dedicated to industrial applications concerning off-line parametric studies, or on-line computer-aided operation. In both cases, the specialization is intended to provide a high computational efficiency and to reduce or even cancel (on-line) the human work necessary to run the code. The codes oriented towards on-line computation have proved capable of running in one to ten seconds by time-step on hardware typically capable of one to ten MFlops. The precision is still improving, and comes close to that of typical off-line calculations.

The main goals and future needs for the development of computer codes for reactor physics dictate a reduction of the manpower required by the whole computational process. This includes the development, maintenance, and daily "operation" of the code by the users (the field of "computer-aided computation"). Simultaneously, the quality and reliability need to be increased, as does the automation of the QUALIFICATION process. Precision of the computations can be optimized through the combination of models from various fields, with special attention given to the core and primary system thermal-hydraulics, and by careful selection of the right models ("the right model in the right place"). For on-line computations, the methodology for calibration by comparison with measurements needs to be improved as well.

The limits on future developments have their roots in the precision of basic nuclear data, and data on critical experiments and on the physical state of the core, which will be available for qualification and calibration. A factor is also the time that is needed to develop and assess a new, improved computational scheme, without any "weak link" (for instance, when introducing 3D transport with thermal hydraulic feedback in the core computation). Last, but not least, is the problem of raw computing power, which leads us back to the subject of "supercomputing".

The means to achieve future goals is to follow the current lines of progress, while adding boosters to tackle the complexity problem. Important aids to this would be knowledge-based systems providing the power of the expert's heuristics, with the assistance of data banks oriented towards qualification in relation to various experiments, cross-comparison, and operational feedback. Given some improvements and increasing resources in power and memory available on workstations, two fields seem to be open to a massive use of computation. One is on-line monitoring, surveillance and control, which involves improved thermal-hydraulics and calibration methodology. The other is optimization, with a new methodology involving automated computation and interpretation of the results and decision, in a closed-loop feedback.

Session 3: Methods for Advanced and MOX Fuelled Reactors

(Chairmen: A. Casadei, A. Vallee)

It is necessary to provide a fresh validation of codes for application to HCLWRs. Through a Monte Carlo comparison, it has been shown that 1D modeling and 2D diffusion, vis-a-vis 2D Sn calculations, are inadequate. This is especially the case for strong perturbation with RCCPs.

An approach is being developed to improve reactor calculation efficiency by generating a multi-parameter cross-section library for PWR design calculations used in the APOLLO code. This would help avoid large numbers of costly assembly spectrum calculations. Reactivity differences noted between the reconstructed cross-sections and explicit calculations, covering the first phase of the project (i.e. data generation), were small. These acceptable differences indicate that the approach is feasible. Exactly how feasible it is will be determined by the results of further work that is planned to test the performance for core calculations.

Pu recycling with a maximum of 30% of MOX assemblies in each reload has been successfully implemented. With the updating of Pu data, the inclusion of some minor and otherwise neglected actinides, and the revision of equivalent fusion product cross-sections, accuracies comparable to those for uranium cores were obtained for MOX fuelled cores.

The preparation of multi-group cross-sections by using a rigorous resonance treatment for U and Pu was described. It is probable that MOX fuel may need a 2D modelling of fuel assemblies due to greater complexity. The contribution of some normally neglected chains, such as U-234, Pu-238, Np-231, etc. were evaluated as a function of burnup. The results presented are useful in assessing changes made to the specific nuclide chain, but care must be exercised in generalizing some of the conclusions to other systems.

Session 4: Calculational Methods for VVER-Type Reactors

(Chairmen: M.R. Becker, M. Salvatores)

Spectral rods, based on the numerical solution of the multi-group transport equation, were validated against a set of experimental and numerical benchmarks. Generally, their performance was satisfactory for regular lattices. Increasing attention is being paid to lattices with Gd as a burnable absorber, some results for which were presented both for numerical benchmarks and for critical experiments. The accuracy of these codes allows their use for preliminary design studies.

Assembly homogenization is performed either in transport or in diffusion approximation. At this stage, the actual hexagonal geometry must be correctly described.

Two methods are used to account for the spectrum perturbations. For the first one, a method of spectral indices, extensive validation of the code system with uniform and heterogeneous lattice has been done. The performance has been very good for uniform lattice cores, although in the ZR-6 experiment with Gd, the k_{eff} was somewhat over-predicted. The results of power distribution comparison from Czechoslovakia proved to be similar to those of India. For LR_o experiments, there is a strong under-prediction of Gd pin power, which may be due to the neglect of net leakage across the assembly.

The second is a hexagonal nodal method, based on a representation of neutron distribution in a cell as a sum of some trial functions. It is capable of taking into account the effects of thermal neutron spectrum deformations and cell heterogeneities, and therefore significantly increasing calculational accuracy. Substantial improvement in power distribution was obtained for the strongly perturbed (D7) lattice experiments of ZR-6.

Generally good agreement was found for all uniform and regularly perturbed lattices, in the validation of the NESSEL 4 code with numerical and experimental benchmarks. The effects of fine divisions on the micro-depletion behaviour of burnable absorber rods were described.

A code system which uses neutrons and thermal hydraulics modules to treat steady state, and slow transient situations was presented, together with typical subchannel analyses of the latter. The neutronics part has been validated with TRX and ZR-6 experiments.

Many of the ZR-6 experiments, and other VVER-type benchmarks, can be useful in assessing the performance of hexagonal codes. It may be increasingly important due to increasing interest in LWHCRs. The code systems that were presented at this session should additionally be validated in the solution of applied problems such as reactor operation and control, load following, incidental and accidental transients, safety-related difficulties, and the assessment of safety margins. The comparison of safety-related critical and postulated accidents analyzed in PSAR for VVERs and PWRs could help to resolve some of the problems for VVER users. Further studies should be devoted to a consistent inter-comparison of the different schemes used for VVER calculations.

Session 5a: Core/Reflector Interface; Fuel Management
(Chairmen: J. Mondot, G. Naudan)

Two methods of PWR reflector treatment in modern nodal diffusion codes were presented. Both of them aim at the substitution of the theoretically and potentially complicated reflector by simpler models.

In the first, the complicated water-steel reflector region was approximately modeled in 1D, which proved to be sufficient for design purposes (1% error compared to the 2D treatment). A generalized equivalence theory based on nodal techniques was used to obtain the environment-independent response matrices for the reflector region. For theoretical benchmark studies, accurate results of core power distribution were obtained.

An alternate method is based on the coupling of different methods for the treatment of neighbouring regions. This system allows for simultaneous diffusion/transport calculations connected by means of multi-group boundary conditions. In particular the reflector, including any heterogeneities, can be implicitly represented by a simple albedo matrix. Simple modifications in the Monte Carlo technique, which was used, could facilitate a parametric variation of reflector constraints, even by a single Monte Carlo run. The comparison of the average assembly power distribution in a reactor core shows a good agreement between standard explicit calculation of the reflector, and the albedo boundary condition.

Both models are very interesting and complementary in the sense that they allow accurate simulations of the reflector effects for different core calculational methods. However, the homogenization and collapsing processes are based on equivalences which preserve boundary conditions. Hence, the precision of the final results depends on the validity of a "reference" calculation, which has to be capable of explicitly treating the hard spectrum and flux transients close to the core/reflector interface.

The subject of fuel management led to the discussion of problems of Quality Assurance (QA) and portability of software. A strict QA procedure, including benchmarks on a large database, is indispensable for ensuring the portability of the code package to every kind of hardware and operating system. It is also preferable to have a single, validated version than several versions that are optimized for individual systems. Both these points are valid, in fact, for any kind of code system. The general features of a code package that had been completely rewritten in the framework of this QA procedure, and its validation were described subsequently. Further enhancements have been incorporated into the new generation of codes, which are directed towards the complete integration of reactor physics methods for a broad range of applications from core design, safety analysis, core monitoring, operations support, and operators training.

Session 5b: Reactor Calculational Methods and Codes
(Chairmen: H. Finneman, J.P. West)

Three complex code systems were presented, all of which have reached a certain level of maturity with respect to the methods used. The authors were aware of the necessity for producing high-quality, user-friendly and portable software, as highlighted in the previous session, and consequently yet further effort is being devoted to these aspects.

The SAPHYR code system, which relies on the well-known APOLLO code for assembly transport calculations, and on the diffusion code CRONOS for global reactor calculations, was described. APOLLO has a built-in 99 group library, and is capable of handling other libraries as well. The heterogeneous fuel assembly is normally treated by a 2-D transport method with either Roth approximation (multicell) or by J^*/DPDO treatment. An exact 2-D P_{ij} calculation may also be opted for benchmarking purposes. The CRONOS module solves core problems by FD, FE and synthesis methods. An outstanding feature of the code system is the FLICA IV module, which provides the thermal hydraulic feedback.

The space-time kinetics code system PANBOX is completely based on advanced nodal methods that have been improved over the past years, as demonstrated by their recent extension to include hexagonal geometry. A new approach, applicable to cartesian and hexagonal geometry for the calculation of the homogeneous flux distribution inside the node, was presented which uses elementary Helmholtz solutions for the representation of the group fluxes. The PANBOX code system then uses the reconstructed pin power distributions to evaluate safety-related parameters by

explicitly recalculating the hot channel thermal-hydraulics. Different local refinements are still under investigation.

The capabilities of the emerging code system COCCINELLE include static and transient calculations applied to core design, fuel management, safety, monitoring and on-line surveillance. For space-time kinetics calculations, a detailed 3D thermal-hydraulic module has been implemented (THYC), and an external coupling with the CATHARE code (for overall NSSS operation calculations) has been tested. First results for such accidents as control rod ejection and steam line break can already be obtained, which show that a detailed modelling is feasible and necessary. An interesting new approach was presented for the calibration of neutron parameters, based upon an application of the GPT, and on the calculations of 3D importance functions.

The physical characteristics of the core of a Nuclear District Heating Plant (NDHP), and the associated core studies were presented. The NDHP concept had been designed for implementation in the vicinity of large cities, which requires them to have enhanced safety features. Results from core analyses performed on the basis of experimental assembly geometries and full scale cores showed good agreement with the calculations.

The use of discontinuity factors in a 1D modelling was attempted, to obtain an approximate coarse mesh solution method for solution of the diffusion equation in RZ geometry. 2D RZ calculations can already be performed on PC-XTs with reasonable accuracy, and within reasonable time. This is true even if the quadratic variant of the nodal expansion method is coupled with a 1D algorithm for the calculation of discontinuity factors, which are used as correction factors to increase the accuracy of the 2D calculation. Such methods are of interest in and of themselves, and are related to more general multilevel techniques.

Session 6: Core Monitoring Codes and Methods

(Chairman: V.V. Pshenin, P. Bernard)

The LOGARITME concept of core monitoring, mentioned in a previous session, was presented. The method is based on the evaluation of nodal Green functions, which can be parametrically precalculated and tabulated for subsequent construction of the core flux profile. It is found to be adaptable to on-site work stations for very low computational cost.

The Toshiba Advanced Reactor Management System (TARMS) for BWR core monitoring uses adaptive methods to estimate biasing factors for nodal powers and eigenvalue, and is able to accurately predict the core behaviour even during Xenon transient conditions. Use of exponential interpolation provides the possibility of a more precise local power peak estimation.

Also presented was the full scale computer simulation code complex for a RBMK type reactor. A one group time dependant diffusion equation is solved by explicit scheme, and it is possible to display the 3D transient behaviour for any vertical/horizontal section of the core using coloured graphics.

In conclusion of the session, it is evident that great progress has been made in this field, and some very good physical models are presently being used. It was suggested, however, that the pin by pin calculations and/or reconstruction be improved, especially for MOX, complex enrichment, and refuelling. It is clear that in on-line calculations, there exists inherent amplification of even slight uncertainties, and that adequate calculation-measurement combinations are necessary.

General Conclusions and Recommendations

A high level of maturity has been reached in the development of code systems for PWRs. Though these codes may not be directly available to developing countries, it is in principle possible for even non-OECD members to gain access to specific benchmark problems and their solutions from NEA. IAEA may act as the coordinator for making a particular choice of codes/problems benchmark, etc. for countries which are without any on-going nuclear programme, but are aspiring to have one in the near future. It was suggested that the choice of a particular reactor type must be made by every country, and developed countries can provide assistance on a need-basis for developing expertise in specific areas.

Even if a reactor type is not chosen by a developing country, it might be possible for them to participate in simple, reactor independent problems.

USSR and other socialistic bloc countries expressed the possibility of identifying certain cold-clean experiments of the ZR-6 facility, performed over the last two decades under TIC. Interest in these experiments exists in all countries opting for a VVER type reactor. From the advanced countries' point of view, the ZR-6 experiments may be useful in testing out some HCLWR concepts, and eventually formulating a serious benchmark for a prospective HCLWR design.

USSR also mentioned that the operational data on VVER-440 and VVER-1000 type reactors be presented at the TIC meetings. They can be made available to other interested member states by the Agency, for verification of the hexagonal code system, developed by various states.

The Federal Republic of Germany expressed the need for reviving interest in 3D transient benchmark analysis with thermal hydraulic feedback, since far more 3D space-time codes are available compared to two decades earlier, and computing costs are also less prohibitive.

SOLVING THE INTEGRAL TRANSPORT EQUATION USING THE DP1/$J_\pm$ TECHNIQUE

G. MARLEAU, A. HÉBERT
Groupe d'analyse nucléaire,
Institut de génie énergétique,
Ecole polytechnique de Montréal,
Montréal, Québec,
Canada

Abstract

The collision probability method has been used extensively to solve the neutron integral transport equation for lattice cells. The main problem with this technique is that in order to converge on the exact neutron flux distribution inside the cell, a fine calculation mesh is required. However this substantially increases the amount of computation time required for a transport calculation since the number of collision probabilities that must be computed is quadratic in N, the number of regions. An alternative to this technique, which is expensive in terms of computer resources is the $J_\pm$ technique which is also based on the collision probability method. This technique involves performing a n-terms series expansion for the angular fluxes at each interface (the DPn approximation) and then computing the collision, leakage and transmission probabilities associated with each individual homogeneous region inside the cell independently of its surroundings. These probabilities are then coupled using the angular fluxes at each interface surrounding a cell. In the DP0 approximation, only the first order term in this series expansion is considered. This results in fast (since the number of probabilities to compute is linear in N) but often inaccurate solutions to the transport equation. Here we present the DP1 approximation where, in addition to the uniform angular flux contributions, linearly anisotropic contributions are also considered. This approximation retains most of the speed of the DP0 approximation (since the number of CP to compute is still linear in N) while providing an improved solution to the transport problem. We will illustrate this affirmation by looking at 1D cylindrical and 2D square and hexagonal geometry problems. As will be shown, even if the DP1 results are more approximative than the standard CP method, they gives a very good description of the behaviour of the neutron flux inside a cell.

I. INTRODUCTION

One method which is widely used throughout the world to solve the neutron transport equation is the collision probability (CP) technique [1, 2]. The results obtained using this method can be made as accurate as desired provided the mesh discretization is sufficiently fine. However, a very fine discretization of the mesh has important effects on the computation time since the number of collision probabilities that need to be computed is quadratic in N, the number of regions in the cell. Moreover, upon changing the physical properties of a single region in the cell, either for self-shielding problems of during depletion calculations, the complete collision probability matrix must be recomputed. Therefore, there is a need for a faster technique for solving the transport equation when the number of regions to consider is large.

One alternative to this method lies in the use of the $J_\pm$ technique[3]. Here, one first uses a series expansion for the interface currents in terms of spherical harmonics. This series expansion is then truncated after n terms (the DPn approximation). Then, the collision, leakage, and transmission probabilities are computed for each region and for each component of the angular flux expansion. All the regions inside the cell are finally coupled via the currents at each interface using a transmission/reflection matrix. The main advantage here is that the number of probabilities that need to be evaluated for the complete mesh is linear in N as opposed to the quadratic dependence of the CP technique, and these probabilities depend only on the cross section of each individual region. However, in the case where the order of the series expansion is too large, this linearity in N is soon overcome by the need to compute the additional leakage and transmission probabilities associated with each component in the current.

The $J_\pm$ technique was initially used assuming uniform angular fluxes at each interface (the DP0 approximation). This lead to a fast solution to the transport equation which was found to be innacurate in many situations. In order to improve on this problem of precision, Sanchez[5] proposed to use linear current expansion at each interface (the DP1 approximation). This should improve considerably on the DP0 flux results since one takes into account, in addition to the cosine current contribution at each interface, the contribution from the anisotropic currents. However, this implies the computation of additional transmission and leakage probabilities associated with the various components of the current considered. This increased complexity has for effect to effectively slow down the collision probability calculation process with respect to the DP0 technique, however the number of probabilities to compute is still linear in N, and each region remains independent. In fact, the improvements in the flux solutions obtained using the DP1 as compared to the DP0 technique are very substantial.

The main advantage of the $J_\pm$ method is that it allows one to perform a complete self-shielding calculations in its exact geometry, using few computer resources. This is because only the CP associated with the fuel rods must be recomputed at each stage of the self-shielding process. This made possible the replacement of the very crude 1D/4 regions (annular) self-shielding approximation previously used in WIMS-AECL[2] by an exact geometry analysis without noticeable increase in the calculation time. It also speeds up the burnup calculation since only the CP associated with regions where depletion takes place must be reevaluated at each time step.

This paper will describe the DP1 approximation to the $J_\pm$ method and its implementation in the lattice code DRAGON[4]. In section II. of this paper we will describe the basics of the $J_\pm$ method while in section III. we discuss the evaluation of the DP1 transmission probabilities for various type of 1 and 2 dimensional geometries. In section IV. we show how these probabilities can be used directly in a lattice code. In section V. we analyze the performance of the DP1 approximation as compared with either the CP method and the DP0 approximation. Finally in section VI. we present possible extensions of this method to multicell calculations and conclude.

II. THE DP1 TRANSMISSION PROBABILITIES CALCULATION

The monoenergetic integral transport equations for the scalar and angular fluxes inside a region V of total cross section $\Sigma(\vec{r})$ with isotropic source $Q(\vec{r})$ and bounded by a surface S take the form[6]:

$$\phi(\vec{r}) = \int_S \psi_-(\vec{r}_s,\vec{\Omega})\,\frac{\exp(-\tau(R))}{R^2}(\vec{\Omega}\cdot\vec{N}_-)d^2r_s + \int_V Q(\vec{r}-s\vec{\Omega})\frac{\exp(-\tau(s))}{4\pi s^2}d^3r \quad (1)$$

$$\psi_+(\vec{r}'_s,\vec{\Omega}) = \psi_-(\vec{r}_s,\vec{\Omega})\exp(-\tau(R)) + \frac{1}{4\pi}\int_0^R Q(\vec{r}_s - s\vec{\Omega})\,\exp(-\tau(s))\,ds \quad (2)$$

$$\psi_-(\vec{r}_s,\vec{\Omega}) = \int \psi_+(\vec{r}_s,\vec{\Omega}')T(\vec{r}_s,\vec{\Omega}'\to\vec{\Omega})\,d^2\Omega' \quad (3)$$

where the first equation is for the scalar flux, the second equation represents the behaviour of the angular flux on each surface and the last equation incorporates the boundary conditions. In the above, $\vec{r}_s = \vec{r} - R\vec{\Omega}$ is a point on S and $\tau(s)$ is the optical neutron path.

These equations will be discretized in the following way. We assume a constant scalar flux ϕ^i inside each homogeneous region of the cell (volume V^i, boundary surface $\sum_\lambda S^i_\lambda$ and cross section Σ^i) and use a series expansion in terms of spherical harmonics for the angular flux of the form:

$$\psi^i_\pm(\vec{r}_s,\vec{\Omega}) = \frac{1}{4\pi}\{J^{0,i}_{\pm,\lambda}\Psi^{00}_\pm(\vec{r}_s,\vec{\Omega}) + \sum_{\rho=1}^{3} J^{\rho,i}_{\pm,\lambda}\Psi^{1\rho}_\pm(\vec{r}_s,\vec{\Omega})\} \qquad \vec{r}_s\in S^i_\lambda;\ (\vec{\Omega}\cdot\vec{N}_\pm)\geq 0 \quad (4)$$

where the $\Psi^{m\rho}_\pm(\vec{r}_s,\vec{\Omega})$ form sets of orthonormalized functions:

$$\int \Psi^{m\mu}_\pm(\vec{r}_s,\vec{\Omega})\Psi^{n\nu}_\pm(\vec{r}_s,\vec{\Omega})(\vec{\Omega}\cdot\vec{N}_\pm)d^2\Omega = \pi\delta^{mn}\delta^{\mu\nu} \quad (5)$$

Note that the above series expansion is divided into parts: the DP0 term ($m=0$), which is proportional to $\Psi^{00}_\pm(\vec{r}_s,\vec{\Omega})$ and the DP1 contributions ($m=1$), which contains 3 independent terms $\rho = 1,3$:

$$\begin{aligned}
\Psi^{00}_\pm(\vec{r}_s,\vec{\Omega}) &= 1,\\
\Psi^{11}_\pm(\vec{r}_s,\vec{\Omega}) &= \sqrt{2}(3\vec{\Omega}\cdot\vec{n}^1_\pm - 2),\\
\Psi^{12}_\pm(\vec{r}_s,\vec{\Omega}) &= 2(\vec{\Omega}\cdot\vec{n}^2_\pm),\\
\Psi^{13}_\pm(\vec{r}_s,\vec{\Omega}) &= 2(\vec{\Omega}\cdot\vec{n}^3_\pm).
\end{aligned}$$

with $\vec{N}_\pm = \vec{n}^1_\pm$ and the unit vectors $\vec{n}^1_\pm,\vec{n}^2_\pm,\vec{n}^3_\pm$ form a three-dimensional bases on S^i_λ. This discretization procedure results in the following set of linear equations:

$$\phi^i = \sum_{\lambda=1}^{\Lambda_i}\sum_{\rho=0}^{N}\frac{S^i_\lambda}{4V^i}p^\rho_{\lambda,i}\,J^{\rho,i}_{-,\lambda} + p_{ii}Q^i \quad (6)$$

$$J^{\nu,i}_{+,\alpha} = \sum_{\lambda=1}^{\Lambda_i}\sum_{\rho=0}^{N}\frac{S^i_\lambda}{S^i_\alpha}P^{\rho\nu,i}_{\lambda\alpha}\,J^{\rho,i}_{-,\lambda} + \frac{4V^i}{S^i_\alpha}P^\nu_{i\alpha}Q^i \quad (7)$$

$$J^{\nu,i}_{-,\alpha} = \sum_{j=1}^{M}\sum_{\lambda=1}^{\Lambda_j}\sum_{\rho=0}^{3}T^{\rho\nu,ij}_{\alpha\lambda}\,J^{\rho,j}_{+,\lambda} \quad (8)$$

where $T^{\rho\nu,ij}$ is the discretized coupling matrix.

We defined in Eq. (6) and Eq. (7) four different types of CP matrices. These are not all independent since they satisfy symmetry and conservation relations:

Symmetry relations	Conservation relations
$S_\lambda P^{\rho\nu}_{\lambda\alpha} = S_\alpha P^{\nu\rho}_{\alpha\lambda}$	$\sum_\alpha P^{\rho 0}_{\lambda\alpha} = \delta^{\rho 0} - \Sigma^i\,p^\rho_{\lambda,i}$
$4V_i P^\rho_{i\lambda} = S_\lambda p^\rho_{\lambda,i}$	$\sum_\alpha P^0_{i\alpha} = 1 - \Sigma^i\,p_{ii}$

In fact it is sufficient to compute a subset of the transmission probabilities $P^{\rho\nu,i}_{\lambda\alpha}$ which is given by:

$$P^{\rho\nu,i}_{\lambda\alpha} = \frac{1}{\pi S^i_\lambda}\int_{S^i_\lambda}d^2r_s\int_{S^i_\alpha}d^2r'_s\,(\vec{\Omega}\cdot\vec{N}_-)\Psi^{m\rho}_-(\vec{r}_s,\vec{\Omega})(\vec{\Omega}\cdot\vec{N}_+)\Psi^{n\nu}_+(\vec{r}'_s,\vec{\Omega})\frac{\exp(-\tau(s))}{s^2} \quad (9)$$

From further symmetry considerations, it can be shown that for 1 dimensional geometries the contributions of two current components ($\rho = 2,3$ components) are completely uncoupled from the scalar flux equations. Similarly, for 2 dimensional geometries the $\rho = 3$ current component will not contribute to the neutron flux. Accordingly, the transmission probabilities associated with these terms in the angular flux expansion will not be evaluated.

A final advantage of this technique is that the collision, leakage, and transmission probabilities associated with void regions can be easily evaluated[7].

III. APPLICATION TO 1 AND 2 DIMENSIONAL GEOMETRIES

We will first present the computation of the DP1 transmission probabilities for the 1D cylindrical geometry described in Fig. 1.

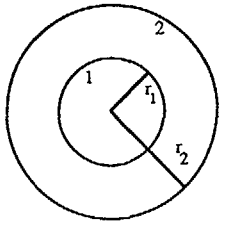

Figure 1: Example of a 1 dimensional cylindrical geometry

In this case we only need to evaluate $P_{11}^{\mu\nu,1}$ for the filled cylindrical region and $P_{12}^{\mu\nu,2}$ and $P_{22}^{\mu\nu,2}$ for the hollow cylinder with $\mu,\nu = 0,1$[7]. Here we use the notation

$$\begin{array}{ll} P_{\alpha\alpha'}^{00,i} = \mathcal{I}_1^i & P_{12}^{00,2} = \mathcal{I}_{00}^0 \\ P_{\alpha\alpha'}^{01,i} = \sqrt{2}(3\mathcal{I}_2^i - 2\mathcal{I}_1^i) & P_{12}^{01,1} = \sqrt{2}(3\mathcal{I}_{01}^1 - 2\mathcal{I}_{00}^0) \\ P_{\alpha\alpha'}^{10,i} = P_{\alpha\alpha}^{01,i} & P_{12}^{10,1} = \sqrt{2}(3\mathcal{I}_{10}^1 - 2\mathcal{I}_{00}^0) \\ P_{\alpha\alpha'}^{11,i} = 18\mathcal{I}_3^i - 24\mathcal{I}_2^i + 8\mathcal{I}_1^i & P_{12}^{11,1} = 18\mathcal{I}_{11}^2 - 12\mathcal{I}_{01}^1 - 12\mathcal{I}_{10}^1 + 8\mathcal{I}_{00}^0) \end{array}$$

where $\mathcal{I}_k^i$ and $\mathcal{I}_{mn}^k$ involve 4 dimensional integrals as described in Eq. (9). From the symmetries of the problem, these expressions can be reduced to a final one dimensional quadrature of the form:

$$\mathcal{I}_n^i = \frac{8}{\pi}[\int_0^{\sqrt{1-x_i}} x^n\, dx\, (2-x^2)^{(n-1)/2}\mathrm{Ki}_{n+2}[2\Sigma r_i x\sqrt{(2-x^2)}] \tag{10}$$

$$\mathcal{I}_{nm}^k = \frac{8}{\pi}\int_0^1 dx x^{n+1}(\sqrt{2-x^2})^n(\sqrt{1-(z_2-z_2x^2)^2})^m \mathrm{Ki}_{k+3}[\Sigma A(\sqrt{1-(z_2-z_2x^2)^2} - z_2x\sqrt{2-x^2})] \tag{11}$$

where $z_1 = 0$, $z_2 = r_1/r_2$ and $Ki_n[u]$ is the Bickley-Naylor function of order n. This final expression will be evaluated numerically using a Gauss-Jacobi quadrature. Spherical and slab geometries can be treated in exactly the same way and the results we obtained either involve a single integral or are analytic.

We also analyzed various types of two dimensional geometries including rectangular, hexagonal and cluster geometries[8] which are illustrated in Fig. 2.

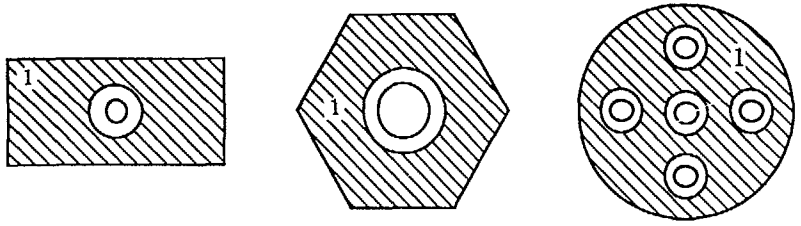

Figure 2: Examples of 2 dimensional geometries analysed using the $J_\pm$ technique

In these cases, the collision probabilities associated with each of the cylindrical regions will be computed using the technique previously described, which involves a single Gauss numerical quadrature, while the strictly two dimensional contributions corresponding to region 1 will be evaluated independently. In fact the transmission probabilities for these regions all involve a double numerical integration. This is in contrast with the standard CP technique where the geometry is always treated as a whole which implies that the collision probabilities associated with the cylindrical region are also computed using a 2D numerical quadrature.

IV. USE OF THE DP1 TRANSMISSION PROBABILITIES

Once all the probabilities associated with a given homogeneous regions have been evaluated numerically, the problem of using them directly in various parts of a transport calculation remains. In fact, collision probability matrices are used in two different parts of a complete lattice cell calculation: for the solution of the transport equation itself and in the self-shielding calculation. In both cases, the straight forward option is to reconstruct the complete collision probability matrix for the heterogeneous cell ($\tilde{\mathbf{p}}_{\mathbf{vv}}$), starting with the known probabilities for the N individual regions:

$$\tilde{\mathbf{p}}_{\mathbf{vv}} = \mathbf{p}_{\mathbf{vv}} + \mathbf{P}_{\mathbf{vs}}\tilde{\mathbf{P}}_{\mathbf{ss}}\mathbf{p}_{\mathbf{sv}} \tag{12}$$

$$\tilde{\mathbf{P}}_{\mathbf{ss}} = \mathbf{T}\{\mathbf{I} - \mathbf{P}_{\mathbf{ss}}\mathbf{T}\}^{-1} \tag{13}$$

where $\mathbf{I}$ is the identity matrix. This approach is expensive in terms of computer resources since it requires one matrix inversion and four matrix products to be performed.

For the solution the transport equation, a totally different approach, which involves the direct solution of the current-flux equations using sparse matrix algebra techniques, can be considered[7]. An additional benefit of this method is that the various components of interface currents are also computed during the resolution process. The first step here consists in extracting from the isotropic neutron source Q^i, which appears in Eq. (1) and Eq. (2), contributions arising from within-group scattering:

$$Q^i = \Sigma_{s0}^i\phi^i + Q^{*i}$$

where Σ_{s0}^i is the within-group macroscopic scattering cross section and Q^{*i} is the reduced neutron source which includes neutrons generated from all other origins. Using this notation, the transport equation can be cast in the form:

$$\phi^i = \sum_{\lambda=1}^{\Lambda_i}\sum_{\rho=0}^{3} \mathrm{W}_{i\lambda}^{\rho}\, J_{-,\lambda}^{\rho,i} + \mathrm{w}_{ii}Q^{*i} \tag{14}$$

$$J_{+,\alpha}^{\nu,i} = \sum_{\lambda=1}^{\Lambda_i}\sum_{\rho=0}^{3} \mathrm{W}_{\alpha\lambda}^{\rho\nu,i}\, J_{-,\lambda}^{\rho,i} + \mathrm{w}_{\alpha i}^{\nu}Q^{*i} \tag{15}$$

where the scattering modified CP matrices are defined as

$$\mathrm{w}_{ii} = \frac{1}{1-\Sigma_{s0}^i p_{ii}}p_{ii}$$

$$\mathrm{w}_{\alpha i}^{\nu} = \frac{1}{1-\Sigma_{s0}^i p_{ii}}\left(\frac{4V^i}{S_\alpha^i}P_{i\alpha}^{\nu}\right)$$

$$\mathrm{W}_{i\lambda}^{\rho} = \frac{1}{1-\Sigma_{s0}^i p_{ii}}\left(\frac{S_\lambda^i}{4V^i}p_{\lambda i}^{\rho}\right)$$

$$\mathrm{W}_{\alpha\lambda}^{\nu\rho,i} = \frac{S_\lambda^i}{S_\alpha^i}P_{\lambda\alpha}^{\rho\nu,i} + \frac{\Sigma_{s0}^i}{1-\Sigma_{s0}^i p_{ii}}\left(\frac{S_\lambda^i}{S_\alpha^i}p_{\lambda i}^{\rho}P_{i\alpha}^{\nu}\right)$$

Note that the w-matrices satisfy the same symmetry and conservation relations as the standard CP matrices provided that the total cross section Σ^i is replaced by $\Sigma^i - \Sigma^i_{s0}$.

The resulting linear system of equations to solved can be reduced to the following form:

$$\vec{J}_+ = [\mathbf{I} - \mathbf{W}_{ss}\mathbf{T}]^{-1}\mathbf{w}_{sv}\vec{Q}^* \quad (16)$$

$$\vec{\phi} = \mathbf{W}_{vs}\mathbf{T}\vec{J}_+ + \mathbf{w}_{vv}\vec{Q}^* \quad (17)$$

where $\vec{\phi}$, $\vec{J}_+$ and $\vec{Q}^*$ are vectors made up of the fluxes, the currents and the reduced sources Q^{*i}, and we have solved Eq. (8) explicitly for $\vec{J}_-$.

These two equations are those actually used to evaluate the neutron flux inside each region. As may be seen, solving Eq. (16) involves the inversion of a rather large matrix. However, this matrix has a diagonal banded structure with a constant bandwidth. A **LU** factorization of the matrix may therefore be performed using a compressed diagonal storage mode where the **LU** factors occupy the same locations as the elements of the original matrix. The complete algorithm of the solution then proceeds as follows: 1) find the elements of the lower (**L**) and upper (**U**) triangular matrix such that $\mathbf{LU} = [\mathbf{I} - \mathbf{W}_{ss}\mathbf{T}]$; 2) solve successively the two linear systems $\mathbf{L}\vec{x} = \mathbf{w}_{sv}\vec{Q}^*$ and $\mathbf{U}\vec{J}_+ = \vec{x}$ by forward and backward substitution, respectively; 3) solve the flux equations using Eq. (17). This algorithm will generally be efficient and economical.

For self-shielding calculations, the evaluation of an escape matrix is required:

$$\mathbf{E} = \tilde{\mathbf{p}}_\mathbf{o}^{-1}[\mathbf{I} - \tilde{\mathbf{p}}_\mathbf{o}\Sigma^*_\mathbf{o}]$$

where $\mathbf{\Sigma}^*_\mathbf{o}$ is a diagonal matrix containing the macroscopic cross section of the resonant isotopes in each fuel region and $\tilde{\mathbf{p}}_\mathbf{o}$ is a matrix formed by the components of $\tilde{\mathbf{p}}_{\mathbf{vv}}$ related to fuel regions. The computation of the $\tilde{\mathbf{p}}_\mathbf{o}$ matrix can be speed-up using again sparse matrix algebra: 1) use an **LU** decomposition for $[\mathbf{I} - \mathbf{P}_{ss}\mathbf{T}]$ with **L** a lower and **U** an upper triangular matrix; 2) for each fuel region i, successively solve the two linear systems $\mathbf{L}\vec{x}_i = \vec{S}_i$ and $\mathbf{U}\vec{y}_i = \vec{x}_i$ where $\vec{S}_i$ is a column of the $\mathbf{p}_{\mathbf{sv}}$ matrix corresponding to the fuel region i; 3) compute $\tilde{\mathbf{p}}_\mathbf{o}$ by applying Eq. (12) and Eq. (13) only to the fuel components:

$$\tilde{\mathbf{p}}_\mathbf{o} = \mathbf{p}_\mathbf{o} + \mathbf{P}^\mathbf{o}_{\mathbf{vs}}\mathbf{TY}$$

with $\mathbf{P}^\mathbf{o}_{\mathbf{vs}}$ a subset of the $\mathbf{P}_{\mathbf{vs}}$ matrix and where **Y** is a matrix formed with the $\vec{y}_i$. Note that a special treatment is required in cases where one or more components of $\mathbf{\Sigma}^*_\mathbf{o}$ become infinite. In these cases, the Hospital rule can be consistently applied and leads to finite components for the **E** matrix.

V. NUMERICAL RESULTS

We will now compare the results obtained using the DP0 and DP1 approximation to the $J_\pm$ method with standard CP calculation results. Three types of geometry will be considered: a one dimensional cylindrical geometry, a two dimensional square geometry and a two dimensional hexagonal geometry.

We will first compare the reconstructed collision probabilities obtained using the DP1 and DP0 approximation with the exact CP probabilities for a two region hexagonal geometry (side 1.0 cm). We will consider various cross section values for the inner cylindrical region of radius 0.5 cm (Σ_1) and for the outer region (Σ_2). The results we obtained for p_{22} and p_{12} are presented in Table 1. As can be seen the DP1 results are all within 2% of the CP results while the DP0 results may differ by as much 3%.

Table 1: Comparison of the DP0 and DP1 results with the exact p_{22} and p_{12} probabilities

Cross Section		p_{22}			p_{12}		
$\Sigma_1(\text{cm}^{-1})$	$\Sigma_2(\text{cm}^{-1})$	DP0	DP1	CP	DP0	DP1	CP
1.0	1.0	0.4085	0.4116	0.4169	0.2581	0.2538	0.2510
1.0	2.0	0.2948	0.2959	0.2972	0.1991	0.1969	0.1945
2.0	1.0	0.3908	0.3938	0.4022	0.1763	0.1734	0.1698
2.0	2.0	0.2843	0.2854	0.2877	0.1360	0.1345	0.1322

For the second set of tests we solve the neutron transport equation in a multiplicative media with reflective boundary conditions (k_∞ calculation). We first considered the cylindrical geometry problem described in Fig. 3.

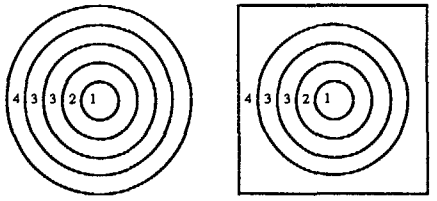

material	Σ_t	Σ_s	$\nu\Sigma_f$
1	14.0	0.0	0.0
2	2.0	1.242	0.0
3	0.625	0.355	0.3
4	1.250	1.242	0.0

Figure 3: Geometrical and physical properties for Test2 (cylindrical) and Test3 (square). the outer radii of each cylindrical region are respectively 1.0, 2.0, 3.0, 4.0 and 5.0 cm while the square has sides 10.0 cm

The calculations were first performed over the 5 mesh regions using an 8-points Gauss-Jacobi quadrature for collision probability integration for both the $J_\pm$ and the complete CP calculations. We then successively subdivided each of the annulii into 2, 4 and 8 subregions. The results we obtained for k_∞ and the averaged relative error on the neutron fluxes relative to the complete CP calculation are presented in Table 2. All the DP1 results lie within 50 pcm (0.5 mk) of the CP results which is a noticable improvement over the DP0 results which may be in error by as much as 360 pcm (3.6 mk). Note that the relative error in the flux increases as the number of regions increases from 5 to 40. Large flux errors arise in the highly absorptive region when it is finely discretized. This is illustrated by the 33 region calculations (only regions 2 to 5 subdivided into 8 subregions) which result in a value for k_∞ identical to the 40 region calculations while the averaged error in fluxes is reduced to less than 1%.

Table 2: Results for k_∞ and average relative flux error for Test2 and Test3

nb. regions	k_∞			flux error(%)	
	DP0	DP1	CP	DP0	DP1
Test2					
5	0.8616	0.8633	0.8631	0.57	0.06
10	0.8739	0.8756	0.8753	1.98	0.28
20	0.8813	0.8811	0.8807	3.53	0.70
33	0.8861	0.8830	0.8825	3.81	0.68
40	0.8861	0.8830	0.8825	5.05	1.26
Test3					
5	0.8499	0.8518	0.8516	0.74	0.10
9	0.8615	0.8638	0.8633	2.16	0.33
17	0.8685	0.8691	0.8685	3.50	0.56
26	0.8617	0.8643	0.8638	2.33	0.37
33	0.8730	0.8710	0.8703	4.86	1.07

The relative error in the flux distribution in each region is also presented in Fig. 4 for the 33 subregions case. As one can see, the DP1 results are very close to the reference CP results. For the 5 region calculations the CPU required by the CP calculations amounted to 0.17 sec while the DP0 and DP1 calculations required only 0.17 and 0.16 sec respectively. For the 33 region calculations, the respective CPU amounted to 0.60 sec and 0.19 sec for the CP and DP1 calculations which is an improvement of 3 times by the DP1 method.

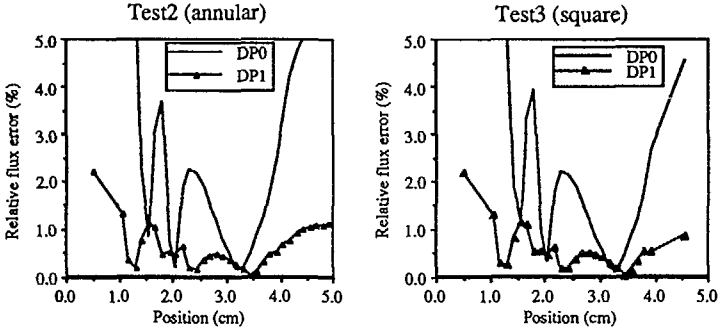

Figure 4: Relative error in flux for DP0 and DP1 calculation with respect to a CP calculation for Test2 and Test3

For the second test case (Test3), we also considered various mesh sizes. Here, the four internal cylinders were divided successively into 2, 4 and 8 subregions for a total of 9, 17 and 33 regions. The results we obtained for k_∞ are also presented in Table 2.

As one can see, there is again very good agreement between the DP1 calculations and CP calculations. Here the relative errors on the fluxes increases quite substantially as the discretization is increased, however, this error arises mostly in the very absorptive material and is reduce dramatically when the first region is not subdivided as illustrated in the 26 region results. Finally, one will find in Fig. 4 a plot representing the relative error on the DP0 and DP1 flux (with respect to the CP flux) with respect to the position in the mesh. Again the DP1 results are relatively good while the DP0 results are are very poor. Finally for the 33 region test case, the respective CPU requirement are: 1.18 sec for the CP method, 0.25 sec for the DP1 results and 0.22 sec for the DP0 calculations. Here the gain in computation time for the DP1 method over the CP is even larger that for Test2.

VI. CONCLUDING REMARKS

The DP1 approximation gives solution to the transport equation that are more reliable than the DP0 approximation while the benefits of the $J_\pm$ technique, which are its speed and the fact that the CP to compute are associated with a single region, remains. Moreover, the method can be used directly for assembly calculations where a large number of cells are coupled.

Acknowledgments — This work was supported, in part, by a grant from the Natural Science and Engineering Research Council of Canada and by Hydro-Québec.

REFERENCES

[1] A. Hoffmann et al., "APOLLO: Code multigroupe de résolution de l'équation du transport pour les neutrons thermiques et rapides" CEA-N-1610, Commissariat à l'Énergie Atomique, France (1973);

[2] J.V. Donnelly, "WIMS-CRNL: A User's Manual for the Chalk River Version of WIMS." AECL-8955, Atomic Energy of Canada Limited (1986);

[3] F.E. Driggers, "A Method for Calculating Neutron Absorptions and Flux Spectra at Epithermal Energies," AECL-1996, Atomic Energy of Canada Limited (1964);

[4] G. Marleau and A. Hébert, "A New Driver for Collision Probability Transport Code.", Proc. Int. Top. Mtg. Reactor Physics, Mathematics and Computation,American Nuclear Society, Santa Fe, New Mexico, April 9-13 1989;

[5] R. Sanchez, *Nucl. Sci. Eng.*, **64**, 384 (1977);

[6] R. Sanchez and N.J. McCormick, *Nucl. Sci. Eng.*, **80**, 481 (1982);

[7] G. Marleau, M.L. Vergain, A. Hébert and R. Roy, *Ann. nucl. Energy*, **17**, 119 (1990);

[8] G. Marleau and A. Hébert, "DP1 Transmission Probability Calculations for Cluster Geometries" to be published; M. Ouisloumen, G. Marleau, A. Hébert and R. Roy, "Computation of Hexagonal Cells Collision Probabilities Using the DP1 Technique" to be published;

IMPROVEMENTS IN THE CALCULATIONAL METHODS OF NUCLEAR REACTOR ASSEMBLIES

P BENOIST, I PETROVIC*, Z STANKOVSKI
Direction des réacteurs nucléaires,
Département de mécanique et de technologie,
Commissariat à l'énergie atomique,
Centre d'études nucléaires de Saclay,
Gif-sur-Yvette, France

Abstract

The standard procedure for the calculation of neutron leakage rate of an assembly is based on calculating this rate for a homogeneous medium representing approximately the assembly, but not the lekage rate of the assembly itself The method presented here allowes to take into account, with some approximations the influence of heterogeneous structure of the assembly on the leakage The anisotropic buckling-dependent migration area of the assembly in the direction k, which relates buckling in the same direction to the effective and the infinite multiplication factor, can be calculated using the anisotropic buckling-independent migration area corrected in an approximately way by the buckling-dependent and the buckling-independent migration areas of the homogenized madium The mentioned migration areas are calculated by means of the first flight collision probability and the first flight directional collision probability The numerical results show that for ordinary PWR fuel assembly the influence of heterogenity on the leakage is relatively small and that the effect increases when the concentration of water decreases This effect could be much more important in more heterogeneous types of reactors

I - INTRODUCTION

The calculation of a nuclear reactor as a whole remaining, at least at the time being, beyond the possibilities of computers, certain codes used at present for the calculation of reactors, for instance APOLLO (Ref 1), begin by calculating the transport multigroup flux chart in a perfectly reflected assembly by means of the collision probability method This calculation can be made with some approximations at the boundary of each elementary cell,such as in the multicell codes CALLIOPE and NAUSICAA (Ref 2) and EURYDICE (Ref 3) it can also be made without any approximation other than numerical ones, such as in MARSYAS (Ref 4) Once obtained the multigroup flux chart in a perfectly reflected assembly, one can define for the whole assembly a homogenized medium by weighting all the cross-sections on the volume and the flux in each energy group This medium without leakage is not critical In order to make it critical, it is necessary to introduce a spatial dependence in $\exp(i\vec{B}\,\vec{r})$ A subroutine of APOLLO, DIFFON, calculates, in a multigroup scheme, the critical buckling B_o^2 and the diffusion coefficient D^g in each group g of this homogenized medium The next step consists in introducing this leakage rate as an uniform absorption cross-section in a new heterogeneous reflected assembly transport calculation This is made by replacing the scattering cross-section $\Sigma_s^{g\to g}$ by $\Sigma_s^{g\to g} - D^g B^2$ The new assembly flux chart allows to define a new homogenized medium, a new critical buckling B_o^2 and a new diffusion coefficient D^g are obtained for this medium The same procedure is continued until convergence (K=1) Finally, one obtain by MARSYAS a flux chart taking into account the leakage of the assembly, and the critical buckling B_o^2 is given by DIFFON Analogous calculations are now made by the APOLLO-2 code (Ref 10)

II - A NEW PROCEDURE FOR LEAKAGE CALCULATION

The drawback of this procedure lies on the fact that it calculates the neutron leakage rate $D^g B^2$ of a homogeneous medium representing approximately the assembly, not the leakage rate of the assembly itself We propose here an improvement of the method allowing to take into account (with some approximations) the influence of the heterogeneous structure of the assembly on the leakage

Let us start with the initial case, concerning a perfectly reflecting heterogeneous assembly without buckling Considering a reflection condition is equivalent to consider an infinite and regular lattice of similar assemblies This lattice can be critical only if a macroscopic dependence $\exp(i\vec{B}\,\vec{r})$ is superimposed to the microscopic flux The buckling vector $\vec{B}$ is related to the effective multiplication factor K by the relationship

$$\frac{1}{K} = \frac{1}{K_\infty}\left[1 + \sum_k M_k^2(\vec{B})\, B_k^2\right] \qquad (1)$$

* On leave from the Boris Kidrič Institute — Vinca, Belgrade, Yugoslavia

where K_∞ is the infinite multiplication factor (i.e. with a zero-buckling), where B_k is the k-component of $\vec{B}$ (with k=x,y,z), and where $M_k^2(\vec{B})$ is the anisotropic buckling - dependent migration area in the direction k. The quantity $M_k^2(\vec{B})$ being difficult to calculate, we shall calculate the quantity $M_k^2(0)$ (buckling-independent migration area), and correct it approximately as follows in order to obtain $M_k^2(\vec{B})$ (Ref. 9).

$$M_k^2(\vec{B}) = M_k^2(0) \frac{M_{hom}^2(B_o)}{M_{hom}^2(0)} \tag{2}$$

where $M_{hom}^2(B_o)$ is the migration area of the homogenized medium obtained by flux weighting, and corresponding to the critical buckling B_o of this medium. This quantity can be obtained by means of the DIFFON module of APOLLO. The calculation of $M_{hom}^2(0)$ is a simple particular case of the calculation of $M_k^2(0)$ in a lattice, that we shall see later.

Assuming that the lattice is such that

$$M_x^2(\vec{B}) = M_y^2(\vec{B}) \tag{3}$$

Eq. 1 gives a relation between K, B_r^2 and B_z^2, where B_r^2 is the radial buckling. Let us assume that B_z^2 is known; Eq. 1 defines then the critical radial buckling B_r^2 corresponding to K=1.

III - CALCULATION OF $M_k^2(0)$

The expression $M_k(0)$ of the migration area in a lattice at the limit $\vec{B}\to 0$ has been obtaind by Deniz (Ref. 5,6)

$$M_k^2 = K_\infty \frac{\langle \psi_o^+, \Omega_k \psi_{1k} \rangle}{\langle \psi_o^+, F\psi_o \rangle} \tag{4}$$

where the brackets mean a summation over the volume of the reflected assembly, over the solid angle 4π and over all the groups g.

The "classical" angular flux $\psi_o^g(\vec{r},\vec{\Omega})$ is the solution of the equation

$$T\psi_o - \frac{1}{K_\infty} F\psi_o = 0 \tag{5}$$

where T is the integro-differential transport operator (taking into account the energy group transfer) and where F is the fission operator. The adjoint flux $\psi_o^{+g}(\vec{r},\vec{\Omega})$ is the solution of the adjoint equation.

The "directional" angular flux $\psi_{1k}^g(\vec{r},\vec{\Omega})$ is the solution (the existence of which is guaranteed by Fredholm's theorem) of the equation with source (Ref. 7,8)

$$T\psi_{1k} - \frac{1}{K_\infty} F\psi_{1k} = \Omega_k \psi_o \tag{6}$$

In order to avoid handling of angular fluxes, let us assume that $\psi_o^g(\vec{r},\vec{\Omega})$ and $\psi_o^{+g}(\vec{r},\vec{\Omega})$ can be replaced by their average value $\varphi_o^g(\vec{r})$ and $\varphi_o^{+g}(\vec{r})$ over de solide angle 4π. Moreover let us assume that we can keep only the uncollided part of the directional flux $\psi_{1k}^g(\vec{r},\vec{\Omega})$, which is equivalent to neglecting the "angular correction term"; this approximation is reasonable in a lattice such a PWR one, which is not extremly far from homogeneity. Then $M_k^2(0)$ becomes

$$M_k^2(0) = \frac{K_\infty}{3} \frac{\sum_g \sum_i \sum_j \varphi_j^{+g} V_i \varphi_i^g \frac{1}{\Sigma_{tj}^g} P_{ij,k}^g}{\sum_g \sum_{g'} \sum_i \varphi_i^{+g} V_i \chi_i^g \nu\Sigma_{fi}^{g'} \varphi_i^{g'}} \tag{7}$$

where the sumations are extended to all the calculatonal regions i and j of the reflected assembly, and to all the groups, V_i being the volume of region i and φ_i^g and φ_i^{+g} being the average value of $\varphi_o^g(\vec{r})$ and $\varphi_o^{+g}(\vec{r})$ over region j.

The first flight directional collision probability $P_{ij,k}^g$ is defined by (Ref. 7,8)

$$P^{g}_{ij,k} = \frac{\Sigma^{g}_{tj}}{V_i} \int_{V_j} d^3r \int_{V_i} d^3r' \, \frac{\exp(-\Sigma R)^g}{4\pi R^2} \, 3\Omega^2_k \qquad (8)$$

with $\vec{R}=\vec{r}-\vec{r}'$, $\vec{\Omega}=\vec{R}/R$ and where ΣR^g is the optical path between $\vec{r}$ and $\vec{r}'$ (with the total cross-section Σ^g_t).

The $P^g_{ij,k}$ are very close to the classical first flight collision probabilities P^g_{ij}, and since the P^g_{ij} are anyway necessary to calculate the flux chart in the assembly, the determination of the $P_{ij,k}$ requires only a small additional work.

REMARK

A small difficulty arises here due to the fact that $\varphi^{+g}_o(\vec{r})$ is not the solution of the adjoint integral transport equation. It can be shown (Ref. 9) that it is the solution of the direct integral transport equation in which the transfer cross-section $\Sigma^{g'\to g}_s(\vec{r})$ is replaced by $\Sigma^{g\to g'}_s(\vec{r})$. This is important to point out since the collision probability method is based on the integral form of the transport equation.

IV - NUMERICAL RESULTS

The method presented above was performed by the APOLLO-2 code (Ref. 10) and applied to several situations of a PWR assembly. The normal fuel assembly is a 17x17 square pattern of fuel pins, this fuel being a typical MOX mixture of uranium oxide and plutonium oxide. The pin radius is 0.413cm, the clad radius 0.474cm; the pitch is 1.265cm; the central cell is a water hole; for the calculation the structure materials are homogenized with water.

The table presents the values of the migration area $M^2_o=M^2_{hom}(B_o)$ obtained by the standard APOLLO procedure, and the values M^2_k of the radial and axial migration areas given by the proposed method. This table gives also the relative changes

$$\frac{\delta M^2_k}{M^2_o} = \frac{M^2_k - M^2_o}{M^2_o} \qquad (9)$$

	Normal water density d	d/5	d/10	Control assembly
M^2_o	36.69	183.93	281.45	34.37
M^2_r cm^2	36.94	185.32	284.56	34.54
M^2_z	37.11	187.94	291.27	34.77
$\delta M^2_r/M^2_o$ %	0.68	0.76	1.10	0.49
$\delta M^2_z/M^2_o$ %	1.14	2.18	3.49	1.16

The first case concerns a normal fuel assembly in which the water temperature is 306°C (the boron concentration is 1.2 10^{-5}). In the two following cases, the density of water (and boron) has been reduced by a factor 5 and 10. In the last case, we considered a critical assembly with 24 boron carbide pins.

V - CONCLUSIONS

It can be seen that for a normal fuel assembly the influence of the heterogeneity on the leakages is relatively small;the effect increases when the concentration of water decreases. Anyway, the effect of heterogeneity on leakages does not seem to be fundamental in a PWR assembly. But this effect could be much more important in more heterogeneous types of reactors as for example HTR.

ACKNOWLEDGEMENTS

We would like to thank Miss. M. Coste, R. Sanchez and I. Zmijarevic for helpful discussions and useful advices in the use of the APOLLO-2 code.

REFERENCES

1 A. Hoffmann, A. Kavenoky, at all Note CEA-N-1610, Saclay (1973).

2. R. Sanchez, Nucl. Sci. Eng. 64 384 (1977).

3. A. Hébert et A. Kavenoky, Proc. International Mtg. in Math. Methods for the Solution of Nucl. Eng. Problems, ENS, Munich, Vol 1, 195 (1981).

4. Z.Stankovski, Traitement par la méthode de Galerkin du transport des neutrons dans un milieu hétérogène à géométrie X-Y. Thèse de 3è Cycle, Belgrade, Yougoslavie, (1978). see also:

A. Kavenoky, M. Lam-Hime et Z. Stankovski, Proc. Topical Mtg. on Computational Methods in Nucl. Eng, ANS, Williamsbourg, Vol II, 7-55 (1979).

5. V.C. Deniz, Nucl. Sci. Eng., 28, 397
see also: Raport CEA-R-3080 (1967).

6. V.C. Deniz, CRC Handbook of Nuclear Reactor Calculations, Vol II, p.p. 409-508 (1986).

7. P. Benoist, Raport CEA-R-2278, Saclay (1964).

8. P. Benoist, Nucl. Sci. Eng. 34, 285 (1968).

9. P. Benoist, Note CEA-N-2619, Saclay (1989).

10. R. Sanchez, J. Mondot, Z. Stankovski, A. Cossic, I. Zmijarevic, Proc. 12th Int. Top. Mtg. Advances in Reactor Physics, Mathematics and Computations, Paris, France, April 27-30, Vol 3, p. 1563, (1987).

THE CACTUS TRANSPORT METHOD IN WIMS

M.J. HALSALL
Physics and Thermal Hydraulics Division,
AEA Thermal Reactor Services,
Winfrith Technology Centre,
Dorchester, Dorset,
United Kingdom

Abstract

The WIMS lattice codes, written at Winfrith in the UK, have a long pedigree, dating back to about 1964 (and earlier for several of the physics methods). It was in 1969 that serious efforts were made to develop the first 'modules' of a new version to be known as WIMSE. This modular scheme is now the major lattice code at Winfrith for the exploitation of new methods; because it is modular with a standard interface between the individual components, it is relatively easy to add new ones. The method we call CACTUS is such a module.

CACTUS solves the differential transport equation in two dimensions by the so-called Characteristics Method. By means of a combination of carefully selected numerical 'tracks' and a general, if somewhat tedious method of geometry description, the method has been used to solve a wide range of very complicated geometries from simple pincells to supercells (colorsets) of Advanced Gas-cooled Reactor (AGR) channels. In all of these cases the 2D geometry is solved exactly without the need to smear fuel pins.

This Paper describes the rather simple equations solved by CACTUS and explains the tracking methods that automatically impose the required boundary conditions. The accuracy of the solution is dependent on the number of angles at which tracks are evaluated, and also on the spacing between them. In this respect, the method has similarities with numerical methods of integrating collision probabilities; it is significantly different in that the transport equation is solved along each track segment in turn. One disadvantage of the method is that both azimuthal and polar angles must be integrated numerically; in collision probability methods the polar integration is analytic.

The methods have only been worked out in detail for rectangular outer boundaries, ie. for square or rectangular pitch lattices, but could be applied equally well to hexagonal systems. It is these tracking methods and efficient ways of processing the data produced by them that are at the heart of CACTUS and its successful exploitation.

The generality of the CACTUS geometry has made it possible to analyse some problems for which no other method in WIMS

would be appropriate. The Paper gives two examples of these applications.

Essentially the same CACTUS module has been implemented in the 'semi- modular' Light Water Reactor version of WIMS known as LWRWIMS. In LWRWIMS the geometry interface is automatic, but is restricted to standard LWR assembly (or supercell) geometries. Comparisons are quoted of the relative efficiencies for practical design calculations of CACTUS and the standard LWRWIMS design route.

The specification of a theoretical benchmark based on a mixed oxide PWR is given as an Appendix, together with sample solutions derived by various methods, including CACTUS, that are available within the WIMS family of codes.

1. INTRODUCTION

The WIMS lattice codes, written at Winfrith in the UK, have a long pedigree, dating back to about 1964 (and earlier for several of the physics methods). It was in 1969 that serious efforts were made to develop the first 'modules' of a new version to be known as WIMSE. This modular scheme is now the major lattice code at Winfrith for the exploitation of new methods; because it is modular with a standard interface between the individual components, it is relatively easy to add new ones. The method we call CACTUS is such a module.

An early stand-alone version of CACTUS is described in Ref 1, and testing on a 'simple' benchmark case in Ref 2. Ref 3 contains a slightly more recent description of the options of the code as first implemented in WIMSE.

CACTUS solves the differential transport equation in two dimensions by the so-called Characteristics Method. By means of a combination of carefully selected numerical 'tracks' and a general geometry description, the method has been used to solve a wide range of very complicated geometries from simple pincells to supercells (colorsets). In all of these cases the 2D geometry is solved exactly without the need to smear fuel pins. Section 2 of this Paper describes the rather simple equations solved by CACTUS. Sections 3 to 5 describe the numerical tracking methods used to integrate them.

Essentially the same CACTUS module has been implemented in the 'semi-modular' Light Water Reactor version of WIMS known as LWRWIMS. In LWRWIMS the geometry interface is automatic, but is restricted to near-standard LWR assembly (or supercell) geometries.

The generality of the CACTUS geometry has made it possible to analyse some problems for which no other method in WIMS would be appropriate. Section 6 gives examples from WIMSE and LWRWIMS, and also gives an indication of the relative efficiencies for practical design calculations of CACTUS and the standard LWRWIMS diffusion theory based design route.

2. THE TRANSPORT EQUATION

One of the principle attractions of the methods used in CACTUS is the simplicity of the formulation. The Boltzmann form of the neutron transport equation for an isotropic source can be written:

$$\frac{dN}{dS} + \Sigma N = \frac{Q}{4\pi} \qquad (1)$$

where N is the angular flux along a 'line' or 'track' in the problem (otherwise known as a 'characteristic')
S is the distance measured along the line
Σ is the total macroscopic cross section
Q is the neutron source (fission-yield and scattering) assumed to be isotropic.

For any line segment of length t and constant properties Σ and Q we can integrate Equation 1 to obtain:

$$N_{out} = N_o e^{-\Sigma t} + \frac{Q}{4\pi\Sigma} (1-e^{-\Sigma t}) \qquad (2)$$

or $$\Sigma t\bar{N} = \Sigma\int_o^t N dS = (N_o - \frac{Q}{4\pi\Sigma})(1-e^{-\Sigma t}) + \frac{Qt}{4\pi}$$

Hence $$\bar{N} = \frac{Q}{4\pi\Sigma} + \frac{\Delta}{\Sigma t} \qquad (3)$$

where $\bar{N}$ is the average angular flux along the line
N_o is the inward value of the angular flux at S=0
N_{out} is the outward value at S=t
Δ is $N_o - N_{out}$

Thus for any line intersecting a system, we may, by repeated application of Equations 2 and 3, form the average flux along each line segment, given an initial boundary condition.

3. NUMERICAL INTEGRATION

The entire procedure of calculating the neutron flux in CACTUS revolves around numerical integration of the line segments as described above. By choosing a family of parallel

lines it is possible to carry out the required spatial integration. If these lines are also rotated through a number of discrete angles in the azimuthal direction (x-y plane) and in the polar direction (the z direction) the angular integration can also be carried out.

This approach has significant similarities with the numerical type of tracking that is frequently adopted in collision probability methods for geometries where the probabilities cannot be expressed analytically. Some sort of geometrical algorithm has to be programmed to evaluate the track lengths through whatever geometry is of interest. In the WIMS PIJ code this geometry is generally of a cylindrical cluster type, with options to subdivide annuli and pins azimuthally. In CACTUS a more general approach was adopted to permit almost any type of geometry within a rectangular boundary to be investigated.

The differences between CACTUS and PIJ tracking are:

- the polar angle integration must be done numerically rather than analytically through the use of Bickley functions. In this respect, CACTUS has a similarity with Sn methods. In CACTUS, it is convenient, though not essential, to adopt the same azimuthal angles at each polar angle, whereas in Sn methods the number of azimuthal angles is normally reduced at high polar angles.

- because the flux is being solved directly, the boundary conditions must be built into the tracking routine, and provision must be made for iteration of the solution. In this respect, also, the method has a similarity with Sn methods.

The method by which the boundary conditions are introduced into the solution at present restricts the use of CACTUS to rectangular boundary problems with reflection or translation. Consider the simple track in Figure 1 which illustrates reflecting boundary conditions.

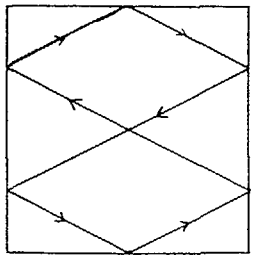

Figure 1. Simple Reflecting Track

With the right choice of angle this track has been arranged so that it ends at its own starting point. If a guess is made of the angular neutron flux at a starting point on this track (N_o in equation 2), then the final value of N_{out} should equal this if the solution has been properly converged.

Several parameters are important in achieving an accurate solution from CACTUS. These are:

the size of region within the problem over which the source Q is assumed to be spatially constant,
the spacing between tracks,
the number of azimuthal angles,
the number of polar angles.

The user has control over all of these parameters, but the precise choice of track spacing and azimuthal angle is constrained by the requirement that the track shall return to its starting point. The way this constraint works is easier to visualise in a case with translational (or cyclic) boundary conditions.

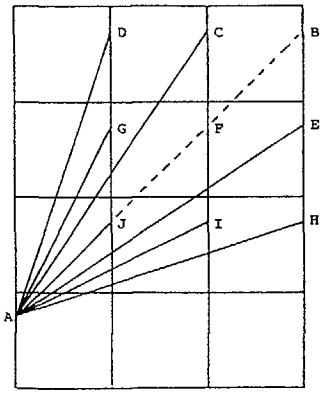

Figure 2. Translating Tracks

In Figure 2, assume that each 'box' is an identical assembly with cyclic boundary conditions, and each lettered point is at an equivalent position on the assembly boundary. Then a track from A to any other lettered point will simply repeat itself if further extended, and the angular flux at A in the direction of the track will be equal to that at all other points in the same direction. This will be our basic boundary condition assumption; on a track from A to C, for example, we insist that the computed outward angular flux at C be equal to the inward angular flux at A in a converged solution.

Along any track where Nx assemblies are traversed in the x-direction, and Ny in the y-direction, then Nx and Ny should

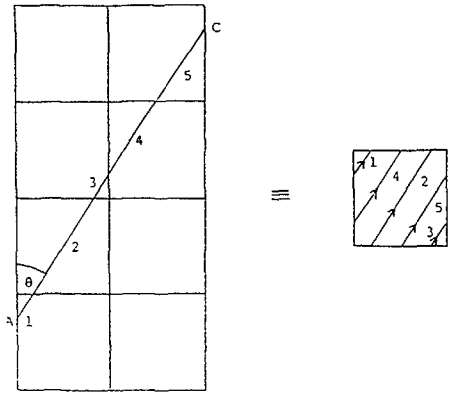

Figure 3.
Translating
Boundary Condition

be co-prime (they must not have a common factor greater than unity) otherwise tracks will be duplicated. (See for example, tracks AJ and AF in Figure 2.)

Along AC, Nx=2 and Ny=3, and the within assembly track is as shown in Figure 3, where θ is the azimuthal angle.

A further constraint on the choice of tracks is the required track separation; the closer the tracks and the better the calculation, but the computing cost will also be increased. The track separation will obviously vary inversely as the total length of track within the assembly, and hence for a given required separation we have further constraints placed upon the values of Nx and Ny.

The choice of azimuthal angles, θ, is therefore rather complicated. We have first to choose a range of 'ideal' angles and then for each one, evaluate the co-prime pair of numbers Nx and Ny so that the required angle and the required track separation are most nearly achieved.

The easiest way to consider the reflecting boundary case is to take units of four assemblies which then have cyclic boundary conditions. The track illustrated in Figure 4(a) across 4 assemblies is equivalent to the reflecting track illustrated in Figure 4(b) around a single assembly. It should be noted that for the translational case it is necessary to spread the azimuthal angles between 0 and 2π, but for the reflectional case tracks starting at angles between 0 and $\pi/2$ achieve a similar coverage.

CACTUS does not presently have a capability for hexagonal geometries, but there is no reason in principle why these should not be implemented. For example, tracks across a single assembly with cyclic boundary conditions would work as illustrated in Figure 5.

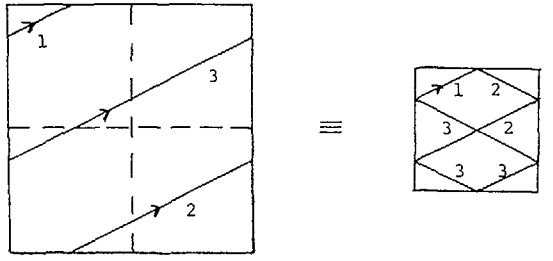

Figure 4. Reflecting Boundary Condition

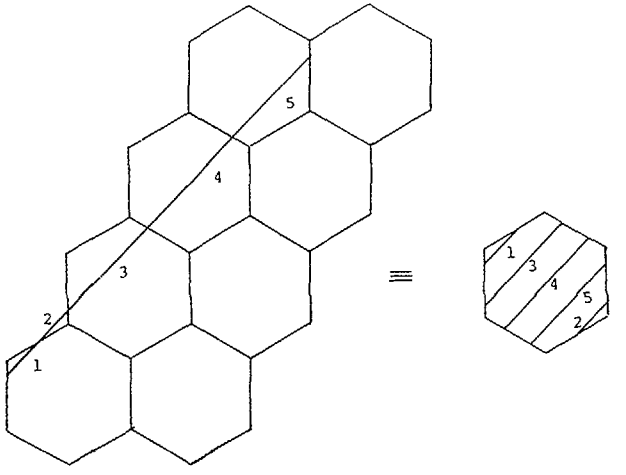

Figure 5. Translating Boundary Condition in Hexagonal Geometry

As noted earlier, the integration over polar angles in CACTUS, as in Sn methods, is numerical. The choice of polar angles is not constrained in any way, but some choices are better than others. For convenience, the same azimuthal angles are tracked at each polar angle; this simplifies the logic of the tracking routine itself. In the x-y plane it is not possible to choose tracks that preserve a mean chord length (although the actual track lengths can be used to integrate region areas numerically, and the true track lengths in each region can be scaled to give the analytic areas). In the polar direction, it is straightforward and desirable to choose angles that reproduce mean chords. As a simple example, an infinite cylinder (of volume V, surface area S, and radius r) has a mean

chord of $4V/S = 2r$. Tracks in the horizontal plane (of area A and diameter d) have a mean length of $A/d = \pi r/2$. To achieve the required mean chord for the cylinder the horizontal tracks must be multiplied by $4/\pi$, which is the secant of the required polar angle. For several polar angles it has been shown semi-empirically that the best choice is to divide the range 0 to $\pi/2$ into equal angles and to select the mean secant within each range.

In practical cases good accuracy is obtained by choosing a track separation of the order of 2mm, 5 azimuthal angles, and 2 or 3 polar angles. Even with a single polar angle the solution is not unrealistic (typically within 1% in k).

4. REPRESENTATION OF GEOMETRY

There are many ways of describing geometry, even in two dimensions. With hindsight, the method used in CACTUS is not ideal. It is extremely flexible but is very onerous for the user who wishes to set up a large complicated problem. Within LWRWIMS, which is used for standard geometries, an interface is generated automatically, and the user is spared this chore. In the modular WIMS code, WIMSE, the user is required to specify the geometry as follows:

- define the rectangular boundary of the problem,
- locate by means of x-y coordinates any number of 'nodes' or points within the boundary,
- join pairs of nodes by straight lines or circular arcs (with a specified centre of curvature) to define any number of 'edges',
- define 'elements' by specifying a sequence of edges,
- define 'inserts' of concentric regions that make up fuel pins for example,
- specify the material contents of each region (elements + inserts).

The above sequence provides an extremely general capability for defining any geometry that can be represented by straight lines and circular arcs. Graphical procedures have been written to output the geometry as defined but these are useful only for checking, and not for data generation. Ad hoc procedures have been written by some users with special requirements for very large problems, but this is an area of the code development that will be given attention, now that we have convinced ourselves of the power of the method.

5. ACCELERATION OF THE SOLUTION

Several methods have been employed. The original code used an Aitken extrapolation of the fluxes every few iterations. This had limited success and has now been replaced by a Chebyshev technique. In addition, the energy rebalance, which is particularly important in multigroup light water cases, has been speeded up by a simple homogenisation procedure. After each iteration, the problem is smeared using conventional flux and volume weighting, and the homogeneous eigenvalue problem is solved. (At present this is a simple unaccelerated iterative solution which is adequate for few group cases, but as bigger problems are now being run, this will be replaced by a better inversion method). The homogeneous flux solution is used to rescale the group spatial fluxes derived by CACTUS, and it is these rescaled fluxes that are accelerated using the Chebyshev method.

A standard calculation is started by assuming a scalar flux of unity in all groups and regions, and a boundary angular flux of $1/4\pi$. A less obvious way of obtaining a faster solution is to run a calculation with only one polar angle to obtain a starting flux guess. This strategy is attractive because a better solution with more polar angles does not involve any further analysis of the geometry. Even better, in a depletion calculation, is to save all the track lengths from one time step to the next for multiplication by an updated set of cross sections, and to use the previous time step fluxes (scalar and boundary) as a starting guess. This typically speeds up subsequent CACTUS calculations by a factor of about three.

6. EXAMPLES OF THE USE OF CACTUS

An early version of the CACTUS code was in use at Winfrith about 10 years ago. At that time it was prone to tracking errors and expensive to run on our main-frame computers. Double precision arithmetic in the tracking routines has cured the tracking error problems and modern workstations have made very large problems a practical proposition.

An early application of CACTUS was a problem that was not easily solved by other methods available at the time. An important consideration in the study of PWR clad ballooning is the local distribution of pin powers, and the question asked was 'How important to local pin power distribution is the possible displacement of a pin from its nominal position in the assembly?'. The answer can be obtained simply by use of CACTUS in LWRWIMS. A 5 by 5 array of identical pincells at normal conditions gives a flat power distribution; with the centre pin displaced 2mm along the diagonal the following power map was obtained, ie with about a 1% perturbation in the pin powers adjacent to the displaced pin.

o	o	o	o	o	1.000	0.999	0.997	0.997	0.998
o	o	o	o	o	1.001	1.000	0.990	0.992	0.997
o	o		o	o	1.003	1.011	0.996	0.990	0.997
o	o	o	o	o	1.003	1.007	1.010	1.000	0.999
o	o	o	o	o	1.003	1.003	1.003	1.002	1.001

Figure 6. Displaced Pin Geometry and Power Map

A more complicated case that was analysed in early CACTUS days concerned fast neutron damage to the structure of the bulk graphite moderator in an AGR core. The case was a difficult one because it involved calculating the fast flux gradient along a straight line junction between blocks of graphite some distance from the cylindrical cluster of fuel pins.

The biggest case in terms of regions and track data that has been analysed was a 9 by 9 supercell of AGR fuel channels, each comprising 36 fuel pins in a cluster, surrounded by graphite sleeves and bulk graphite moderator. Control absorbers were placed at interstitial positions (Ref 4).

A sample case that has been used as a benchmark in the UK is described below. The problem is a two-dimensional representation of a PWR supercell (colorset) designed to highlight the interaction between U and Pu assemblies.

Geometry

```
c c c c c c b w 1 1 1 1 1 1 1
c c c c g c b w 1 1 g 1 1 1 1
c c g c c c b w 1 1 1 1 g 1 1
c c c c c c b w 1 1 1 1 1 1 1
c g c c g b b w 1 1 g 1 1 g 1
c c c c b b a w 1 1 1 1 1 1 1
b b b b b a a w 1 1 1 1 1 1 1
w w w w w w w w w w w w w w w
2 2 2 2 2 2 2 w 3 3 3 3 3 3 3
2 2 2 2 2 2 2 w 3 3 3 3 3 3 3
2 g 2 2 g 2 2 w 3 3 g 3 3 g 3
2 2 2 2 2 2 2 w 3 3 3 3 3 3 3
2 2 g 2 2 2 2 w 3 3 3 3 g 3 3
2 2 2 2 g 2 2 w 3 3 g 3 3 3 3
2 2 2 2 2 2 2 w 3 3 3 3 3 3 3
```

Key

```
a = 2.359 w/o Pu fissile pin
b = 2.993 w/o Pu fissile pin
c = 4.252 w/o Pu fissile pin
1 = 1.053 w/o U235 pin
2 = 1.349 w/o U235 pin
3 = 3.400 w/o U235 pin
g = guide tube
w = water gap
```

Other data: fuel radius 0.4645 cm, temperature 900K
clad i.r. 0.4742 cm, o.r 0.5360 cm, temperature 600K
guide tube i.r. and o.r. as clad, temperature 550K
coolant temp 550K
water gap 0.1 cm, pin pitch 1.4122 cm, assembly pitch 19.8708 cm

Fuel compositions as weight percentages:

	a	b	c	1	2	3
U235	0.2097	0.2097	0.2174	0.9282	1.1891	2.9971
U238	85.0612	84.3323	82.7772	87.2218	86.9609	85.1529
Pu238	0.0305	0.0396	0.0580			
Pu239	1.7691	2.2219	3.1574			
Pu240	0.6772	0.8466	1.2208			
Pu241	0.2540	0.3153	0.4495			
Pu242	0.1179	0.1473	0.2165			
Am241	0.0323	0.0397	0.0567			
Oxygen	11.8481	11.8476	11.8465	11.8500	11.8500	11.8500
Density	10.198	10.199	10.202	10.422	10.422	10.422

Clad and guide tube zirconium density 6.5g/cc

Water composition to be used throughout (density 0.85943 g/cc includes smeared grid material and 900 ppm boron):

Hydrogen	9.8574	Natural boron	0.0794
Oxygen	78.2332	Zirconium	11.8300

Boundary conditions are reflecting on all four sides, and correspond to a problem of infinite extent axially. The low, medium and high enrichments of uranium correspond in reactivity to two representative fuel burnups and to fresh fuel. Requested output is a normalised (to an average of unity) pin power map, a similarly normalised assembly power map, and k-infinity.

For an accurate calculation of the above problem, the CACTUS solution takes over 100 times longer than a straightforward diffusion solution. This may seem prohibitive for design work, but in a typical case with depletion, the breakdown of running times is as follows:

	Diffusion	CACTUS
Microscopic cross section processing	5	5
Multicell collision probabilities	5	5
Few group constants	1	1
Smear & modified diffusion coefficients	1	0
Transport solution (GOG/CACTUS)	1	150
Edits and depletion	3	3
Total	16	164

Note that the derivation of modified diffusion coefficients also relies on CACTUS calculations for small sections of the problem (Ref 5). Bearing in mind that CACTUS calculations after the first in a depletion run (using previous flux solutions as starting guesses) are three times quicker, we see that the overall factor in running time ranges from 10 down to about 4. A factor of 4 in computing time in the context of a workstation environment, where computing is cheap and machine

speeds are increasing every year, is not serious. The benefit of using a more reliable transport solution in design applications is considerable and it is reasonable to anticipate that the CACTUS approach will become the standard LWRWIMS method in the not-too-distant future.

REFERENCES

1. Halsall M J
CACTUS, a Characteristics Solution to the Neutron Transport Equation in Complicated Geometries.
AEEW R 1291 (1980)

2. Halsall M J
The Analysis by Several Neutron Transport Methods of a Small PWR Model Problem.
AEEW R 1378 (1980)

3. Halsall M J
A User's Guide to the WIMS-E Module W-CACTUS.
AEEW R 1710 (1983)

4. Hutton J L, Phenix J & Course A F
Advanced Modelling Methods in WIMSE.
International Conference on the Physics of Reactors (PHYSOR 90) Page IX-14 (Marseille, April 1990)

5. Halsall M J, Powney D & Moxom Mrs M R
LWRWIMS, the WIMS Code for Light Water Reactors.
International Conference on Physics of Reactors (PHYSOR 90) Page IV-45 (Marseille, April 1990)

ANALYSIS OF THE MAIN PHYSICAL AND NUMERICAL ASPECTS IN THE MODELLING OF CONTROL CLUSTERS FOR PROJECT CALCULATIONS

G.B. BRUNA, P.L. CORNILUS,
C. POINOT, C. VAN FRANK
Framatome,
Paris-La Défense,
France

Abstract

Calculation of the reactivity worth of control and safety clusters is generally a major issue in the project studies of the PWR type nuclear reactors

Adapted procedures are to be searched for obtaining suitable data, because, in practice, computing the absorber cross-sections always implies a compromise between the often contrasting requirements of the physics and those imposed by the environment in the computational chain

In this paper, we summarize some elements of a wide research and development work carried out in FRAMATOME in the aim of getting a deeper understanding on the whole matter, taking into account both its physical and computational aspects.

All these elements contributed, in various ways, to the definition of a project oriented preliminary cross-section generation scheme, well adapted to fulfill the requirements of a calculation chain based on two group, finite difference, discrete, diffusion codes.

The analysis was performed either with the multigroup, collision probability, two dimensional, transport APOLLO code, or with the finite difference, centered mesh, diffusion module of the project chain

All calculations were made in an infinite medium assembly approximation

In the whole work, four main items were analyzed, in some detail

- the origin and splitting of the reactivity worth of control clusters,
- the influence of the transport scheme,
- the effect of the diffusion approximations,
- the overall impact of these items on the structure of a project computational chain

1 FUNDAMENTAL ANALYSIS ON REACTIVITY EFFECT

The sample we considered in our investigation was a standard 17x17 Uranium fueled PWR assembly, the main features of which are summarized in tab 1 , Fig 1 shows its typical layout As said, the assembly was either in nominal wet full power conditions, (24 water holes), or in a clustered full power configuration, (24 AIC - Silver, Indium, Cadmium-pins in)

When a control cluster is inserted into a reactor, the reactivity of the system is changed by the action of several contrasting effects of different magnitude and opposite sign

- a direct effect, a big, strongly negative one, which is due to the net increase of the absorption reaction rates in the poison region,
- a main spectral effect, which is due to the change in the reactivity worth of all the fuel, coolant and structural materials of the medium, produced by the selective action of the cluster on the thermal and epithermal energy regions,
- a minor spectral effect, which is due to the average change in the medium coolant to fuel ratio

In a standard PWR infinite medium assembly calculation, the direct component of the worth is up to about 90 % of the total, the spectral components accounting for about 9 % and 1 % respectively

An accurate splitting of the reactivity worth into individual components per isotope can be obtained via a two group zero-dimensional exact perturbation formula as shown, for instance, in [Ref /2/]

If the small moderation effect is neglected, the results summarized in tab 2 show that, owing to the mutual compensations in the fuel and structural material contributions to the reactivity change, the overall reactivity effect can be reduced to two main contributions

- the direct effect of the absorber,

TAB. 1

17x17 PWR ASSEMBLY FEATURES

The Uranium fueled PWR assembly is composed as follows, according to an orthogonal 17x17 array

264	fuel pins
24	guide-tubes
1	central thimble tube

DIMENSIONS inter-assembly gap = 21 5 cm
inter-pin gap = 1 26 cm

URANIUM FUEL PIN CARACTERISTICS

		Unit, material	Value
PELLET			
* density	Theoretical (T D)	UO2	10 96
	Nominal	% T D	95
* diameter		mm	8 19
CLAD		Zircaloy4	
* outlet diameter		mm	9 50
* thickness		mm	0 57

- the spectral effect associated to the change in the slowing-down properties of the water

This fact, if confirmed and broadly proved, could be usefully exploited in the definition of the project computational scheme, in order to account for the spectral effect of the cluster in a simplified way

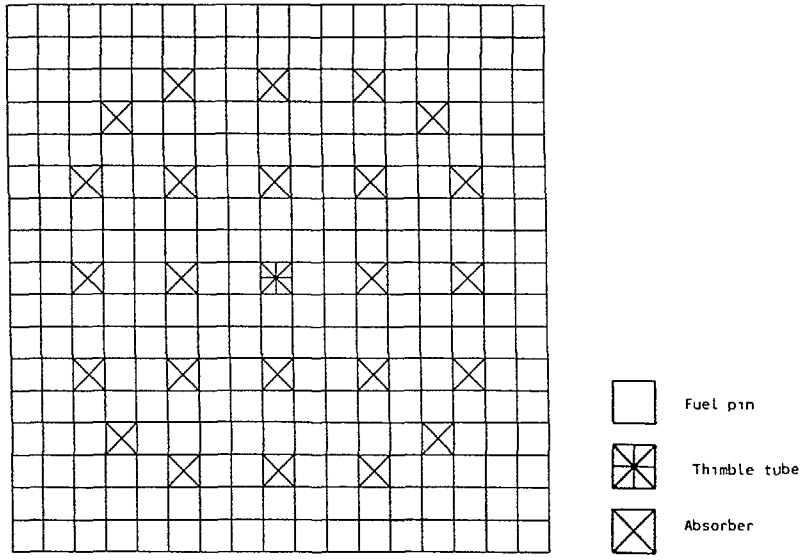

FIG.1
ASSEMBLY LAYOUT

Anyway, it must be noticed that the infinite medium assembly approximation, very practical in the analysis phase, exacerbates the spectral effect in the fuel region surrounding the absorber, because, in the core, the sharp spectral shift produced by the cluster is significantly mitigated by the leakage of the unclustered assemblies.

In the following, for practical reasons, only the direct effect component will be explicitly taken into account.

2 INFLUENCE OF THE TRANSPORT SCHEME

In a transport PIJ computational scheme, like the one built in the APOLLO code/1/, the results may significantly depend on the approximations made in the treatment of the probability collision exchange matrix These approximations may generate important discrepancies on the calculated power values, when black absorbers are studied in a simplified "multicell" scheme,[Ref /3/]

TAB. 2

SPLITTING OF THE CLUSTER REACTIVITY
INTO COMPONENTS (TYPICAL UO2 CASE)

ISOTOPE	DIRECT CONTRIBUTION	SPECTRAL CONTRIBUTION	HIGHER ORDER CONTRIBUTION	TOTAL
URANIUM 235	0	- 134	0	- 134
URANIUM 238	0	187	0	187
WATER	621	861	- 56	1426
OXYGEN	0	15	0	15
BORON	- 126	- 37	2	- 161
ZIRCONIUM	0	4	0	4
HAFNIUM	0	- 1	0	- 1
CHROMIUM	39	- 8	- 12	19
IRON	110	- 12	- 44	54
NICKEL	29	- 11	- 4	14
OTHER STAINLESS STEEL	13	0	0	13
CADMIUM	3472	0	0	3472
SILVER	3196	0	0	3196
INDIUM	1896	0	0	1896
TOTAL	9250	864	- 114	10000

Features : U^{235} enrichment = 1.8 %
nominal conditions
boron concentration = 1050 10^{-6}
24 AIC control cluster

All these approximations were widely investigated and their impact quantified in a previous paper, [Ref /3/], so that we focus here only on the other approximations, usually made in the transport assembly calculations, i e

- "cell" homogenisation in space, eventually via a transport/transport equivalence procedure,

- finite meshing in space and energy, (coarse mesh and collapsing),

- assembly spatial amalgamation of several physically "equivalent" cells, in order to reduce the memory size in computations and simplify the data storage

Fig 2 presents a structured synthetic flow-chart of the whole transformation process , the relative weight of the different steps are quantified in fig 3

These approximations generate effects, which can be individually higher than the ones strictly related to the use of a two group diffusion approximation in a theoretical continuous meshing

An equivalence procedure is generally set up in the cell code in order to account for these approximations in a simplified way this procedure, often quoted as a "transport/diffusion equivalence", actually acts as an overall equivalence operator, which transforms fine transport calculated, multimedia, multigroup data into "equivalent" homogeneous, two media, two group diffusion ones

3 EFFECT OF DIFFUSION APPROXIMATIONS

The main issue in the search of a finite difference numerical solution of the diffusion equation, containing homogeneous pin data coming from a transport computational scheme, as seen before, is to discretize the gradient operator on a given meshing in order to set up a system of linear equations, [Ref /4/]

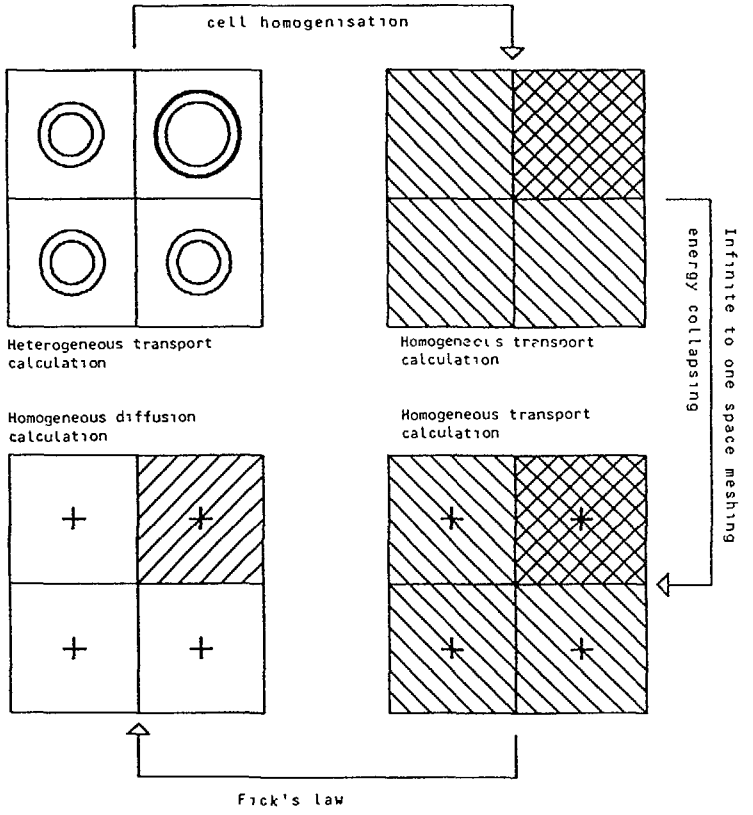

FIG.2

STRUCTURED FLOW CHART
OF THE TRANSPORT-DIFFUSION PROCESS

A very usual system is based on a linear expansion of the Laplacian operator over the mesh This procedure generates an error which is proportional to the square of the mesh size, [Ref /5/]

Different expressions of the error show up, depending on whether the problem is either a centered mesh or a non centered mesh, but, in both cases, the asymptotic continuous meshing expressions of the gradient and k effective will be the same [Ref /6/]

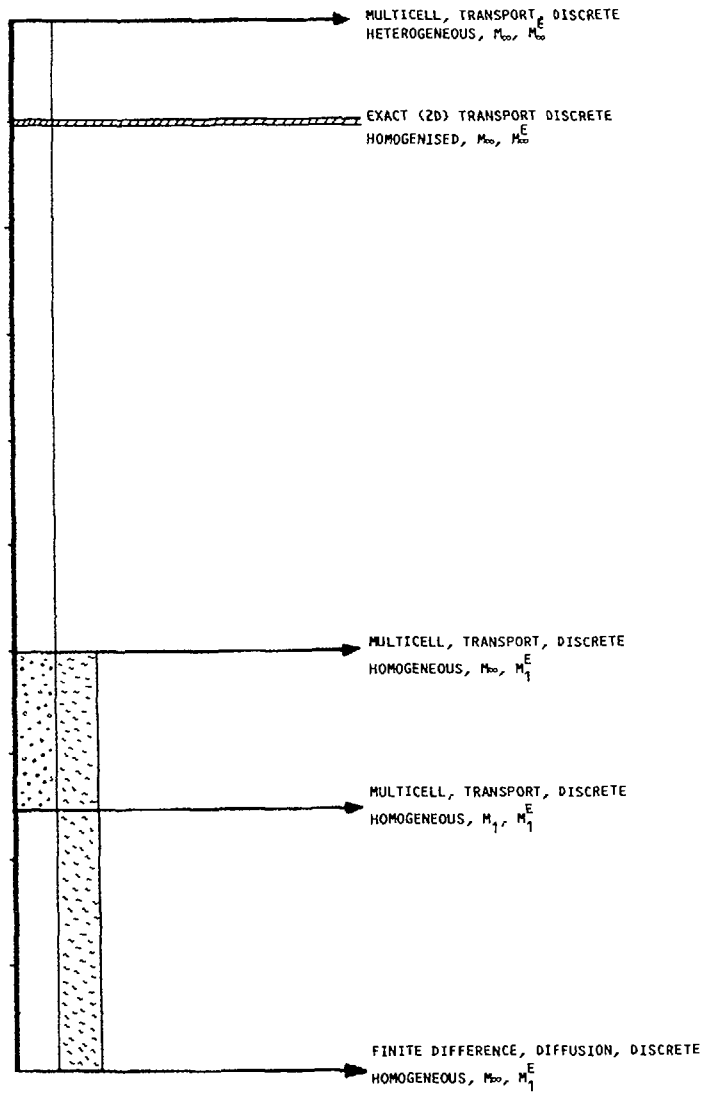

FIG. 3

RELATIVE WEIGHT OF
THE TRANSPORT APPROXIMATIONS :
INFINITE MEDIUM CLUSTERED ASSEMBLY CALCULATION

Fig.4 shows the relative weights of the first, second and higher order corrections to the eigenvalue in a finite difference scheme. Informations on the equivalent results obtained with different polynomial expansions at finite elements are also given, for comparison.

This problem being a general matter in neutronics, the analysis we performed on the topic is straightforward and will not be presented here in detail.

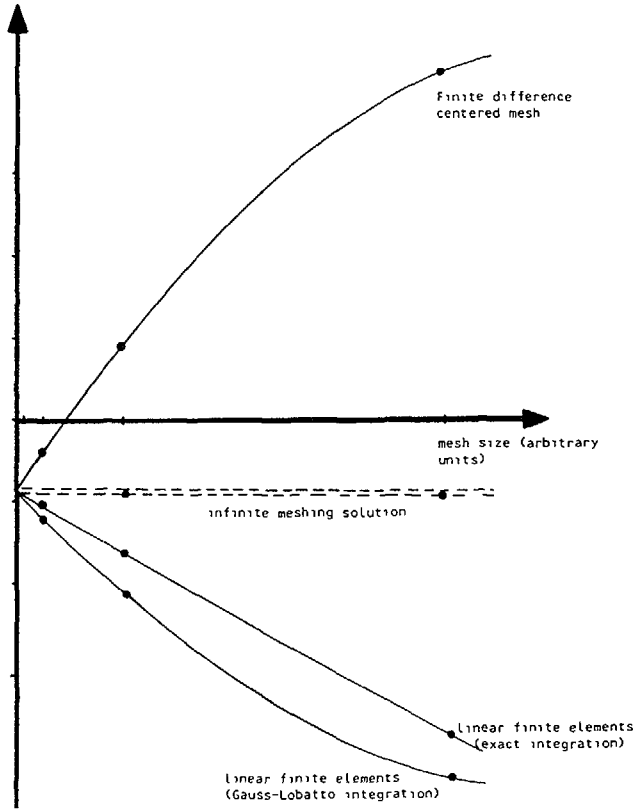

FIG. 4

MESHING EFFECT ON k_∞ :
INFINITE MEDIUM CLUSTERED ASSEMBLY DIFFUSION CALCULATION

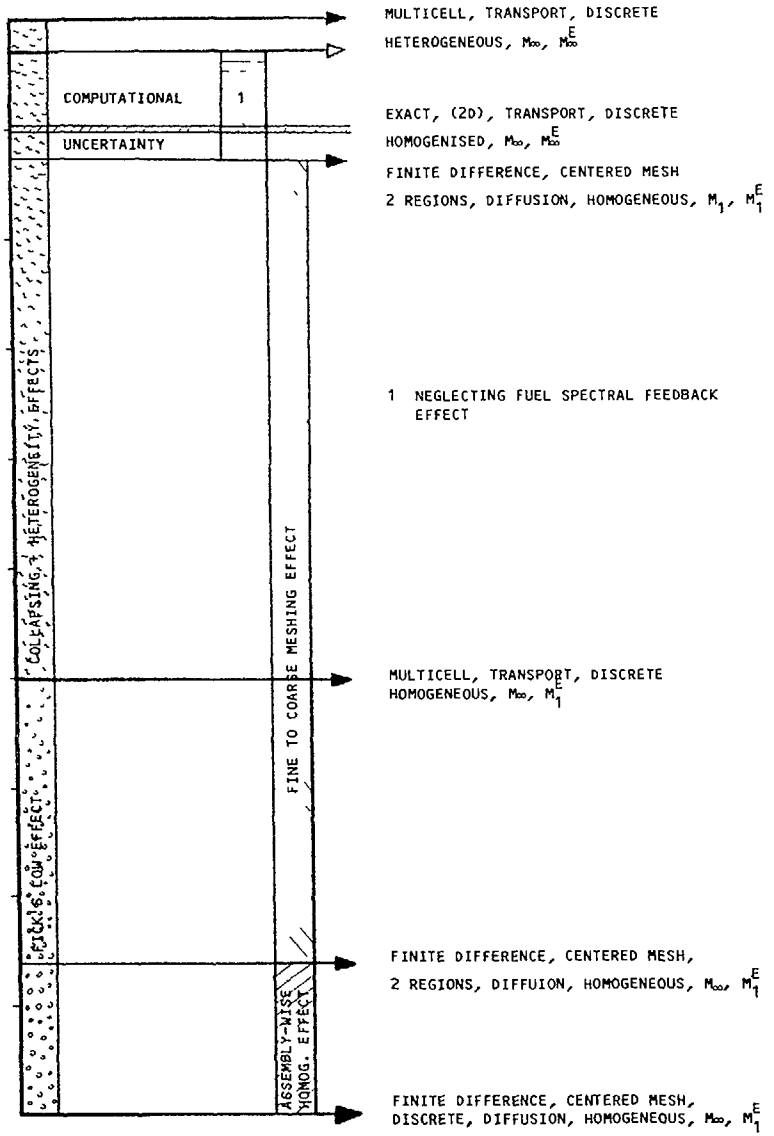

FIG. 5

RELATIVE WEIGHT OF THE DIFFERENT TRANSPORT AND DIFFUSION APPROXIMATIONS : INFINITE MEDIUM CLUSTERED ASSEMBLY CALCULATION NOTE COMPENSATION AMONG CONTRIBUTIONS

The practical information to be retained from this analysis is the huge sensitivity of the calculated parameters to the mesh size, and its dependence on the discretisation scheme used in the diffusion calculations.

4 OVERALL IMPACT ON THE COMPUTATIONAL CHAIN

All the informations obtained in the studies presented above allowed the definition of a simplified preliminary procedure for the generation of the absorber constants for the project calculations

Being aware that our project chain is based on an homogeneous pin by pin description of the core and that a finite difference discretisation of the diffusion equation with one mesh per pin is chosen at two energy groups, the overall results summarized in Fig 5 show that, owing to compensations among transport and diffusion effects, [Refs /7/, /8/] a systematic transport/diffusion equivalence can be avoided in the general case, without affecting the project chain computed results, significantly.

This conclusion remains strictly dependent an the overall structure of the chain and on the design features, (assembly layout, fueling, enrichment, etc...), so that any too hasty generalisation should be avoided.

5 CONCLUSIONS

We present in this paper some elements of an analysis aimed at getting a deeper understanding on the process which allows the generation of suitable data for the project calculations of the absorbing clusters

Preliminary results allow the definition of a simplified procedure which avoids a systematic use of a transport/diffusion equivalence, in a fixed scheme project chain

REFERENCES

/1/ A KAVENOKY, "APOLLO a General Code for Transport, Slowing-Down and Thermalisation Calculations in Heterogeneous Media", Proceedings of the National Topical Meeting on Mathematical Models and Computational Techniques for Analysis of Nuclear Systems, Ann-Arbor, Michigan, April 9-11, 1973 ;

/2/ J. PORTA, J.Y. DORIATH, A. MOURGUES, M NOBILE, A VALLEE and G.B. BRUNA, Nucl Sci Eng , 95, 266-281, (1987) ,

/3/ G.B BRUNA, J P CHAUVIN, M. NOBILE, G PALMIOTTI, C VAN FRANK, M.L. VERGAIN, "Search for a Transport Method for the Calculation of the PWR Control and Safety Clusters", Proceedings of the Physor '90, Marseille, April 23-27, 1990 ;

/4/ R.S. VARGA, "Matrix Iterative Analysis", Prentice-Hall Series in Automatic Computation, Englewood Cliffs, N.J, 1962 ;

/5/ Y. KATO, T. TAHEDA, S. TAKEDA, Nucl. Sci. Eng , 61, 127-141, (1976) ,

/6/ J.C. ESTIOT, D. HONDE, G. PALMIOTTI, M SALVATORES, Annals of Nuclear Energy, Vol. 8, 609-620, (1981);

/7/ A. HEBERT, P BENOIST, "Application of the SPH Method to the Homogeneous Diffusion Procedure", Proceedings of the Physor '90 Meeting, Marseille, April 1990 ;

/8/ A. HEBERT, private communication

BENCHMARKING THE CALCULATIONAL MODEL FOR GADOLINIUM PINS IN SQUARE AND HEXAGONAL LATTICE ASSEMBLIES

V. JAGANNATHAN, R.P. JAIN, V. KUMAR
Theoretical Physics Division,
Bhabha Atomic Research Centre,
Trombay, Bombay,
India

Abstract

This paper presents the benchmarking of lattice codes against two theoretical benchmarks, one for square and another for hexagonal geometry. Both these benchmarks lay emphasis on the modelling of burnable absorber rods. The validation of the hexagonal lattice and core simulation codes against the experiments done in the ZR-6 facility of Hungary and in the LR-0 research reactor of Czechoslovakia with Gd as absorber or poisoned pin respectively is also presented in this paper.

1 INTRODUCTION

A lattice burnup model based on one dimensional (1-D) supercell approach offers one of the most computationally efficient tool to analyse the complex square or hexagonal Light Water Reactor (LWR) fuel assemblies. The code SUPERB [1] was developed for the depletion calculation of a BWR fuel assembly lattice cell. The lattice constants of SUPERB code are used in the coupled neutronics and thermal hydraulics core simulator code COMETG [2]. These codes have been tested against the operational data of Tarapur BWRs [3]. We have recently developed another lattice code EXCEL based on the same 1-D supercell method for burnup analyses of hexagonal lattice assemblies.

2 CALCULATIONAL MODEL

The basic cross section library is the 69 group WIMS library of U.K. The cross sections for Gd isotopes Gd-155, Gd-156 and Gd-157 were generated from the respective resonance parameters and appended to the WIMS library in WIMS format. For routine design calculations the 69 group library is condensed with a typical LWR spectrum to 28 groups with the group structure recommended in LWR-WIMS [8].

We perform the multigroup transport calculations invariably in one dimensional (one-d) cylindrical geometry in order to keep the computer memory and time requirements to a minimum value. The 2-D calculations are done in few groups by diffusion theory.

We classify the fuel pins in the assembly cell into many pincell types depending on enrichment and Dancoff factors. The resonance group cross sections are obtained by the standard WIMS procedure. For the one-d transport calculations we use the interface current approach ($J\pm$) of the MURLI code which is found to give as accurate a result as P_{ij} method [9].

In a fuel assembly heterogeneities in the form of a water rod, poisoned pin or an absorber rod influence the normal uniform lattice spectrum to different extent depending on the proximity or otherwise of a given type of heterogeneity. We perform a series of one-d supercell calculations in multigroups for each of the above heterogeneities. We consider a given heterogeneity at the centre of the supercell, surrounded by rings of fuel pincell paste regions. Multiple rings are considered for the poisoned fuel pin. The presence of other heterogeneities in the surrounding rings is ignored in this calculation. This calculation is also done by $J\pm$ method in 28 groups. The cross sections are collapsed to few (five) groups by using the appropriate supercell ring spectra.

The 2-D fuel assembly cell is analysed by few group diffusion theory in square or hexagonal geometry with one mesh per fuel pincell.

The burnup equations are solved for several burnup zones. We follow the nephew scheme of five pseudo-fission products recommended in LWR-WIMS [8]. At present the burnup chain of even isotopes of Gd is completely ignored in our codes i.e., Gd-155 and Gd-157 become non-absorbers after absorption of a neutron.

3. THEORETICAL BENCHMARKS

3.1 Square Lattice

The square lattice benchmark [4] considers a simple 4X4 regular fuel pin array with two central diagonally adjacent pins containing 3% of Gd_2O_3. We give in Tables 1 and 2 the results of regular and poisoned pin lattices obtained by SUPERB. Our results are updated due to changes in transport cross section of hydrogen [10], use of resonance table 3238.4 for cold and hot conditions and a DB^2 leakage model of criticality adjustment during burnup. At zero burnup results of a Monte Carlo (MC) analysis are also given [11]. It is found that SUPERB results agree with MC results. It is observed that for regular lattice the deviations in various international results are essentially due to cross section library and our results are within the overall spread. For poisoned lattice, SUPERB underpredicts the

Table-1 Results of Square Lattice Benchmark - Regular Lattice

Burnup (GWD/T)	K-inf	Number densities in units of 10^{24} U-235	Pu-239	Pu-240
0.0 (No Xe)	1.3396	6.776-4	0.0	0.0
1.0	1.2830	6.510-4	1.176-5	2.609-7
2.0	1.2686	6.258-4	2.214-5	9.395-7
3.0	1.2543	6.010-4	3.161-5	1.953-6
4.0	1.2405	5.769-4	4.024-5	3.213-6
5.0	1.2267	5.545-4	4.772-5	4.608-6
6.0	1.2136	5.328-4	5.449-5	6.116-6
7.0	1.1995	5.104-4	6.100-5	7.844-6
8.0	1.1870	4.901-4	6.650-5	9.518-6
9.0	1.1747	4.706-4	7.145-5	1.125-5
10.0	1.1627	4.516-4	7.592-5	1.302-5

Code	K-inf	Burnup = 0.0 Percentage Absorption in Fuel	Clad	Coolant
SUPERB	1.3396	93.60	1.388	5.02
MONALI (MC)	1.3404	93.53	1.389	5.09

Table-2 Results of Square Lattice Benchmark - Poisoned Lattice

Burnup (GWD/T)	K-inf	Number densities in units of 10^{24} U-235	Pu-239	Pu-240	Gd-155	Gd-157	Power in Pin 4	Gd Pin
0.0	1.0164	6.573-4	0.0	0.0	1.47-4	1.56-4	1.166	0.368
1.0	1.0180	6.471-4	1.164-5	1.477-7	1.22-4	9.22-5	1.140	0.461
2.0	1.0491	6.349-4	2.244-5	5.986-7	9.00-5	5.22-5	1.112	0.562
3.0	1.0764	6.210-4	3.239-5	1.339-6	6.42-5	2.89-5	1.088	0.654
4.0	1.1042	6.057-4	4.119-5	2.330-6	4.21-5	1.29-5	1.064	0.745
5.0	1.1327	5.888-4	4.905-5	3.564-6	2.50-5	3.45-6	1.041	0.833
6.0	1.1648	5.704-4	5.594-5	5.022-6	1.16-5	2.27-6	1.017	0.928
7.0	1.1794	5.509-4	6.195-5	6.642-6	4.44-6	3.66-9	1.002	0.983
8.0	1.1832	5.307-4	6.727-5	8.386-6	1.14-6	--	0.994	1.017
9.0	1.1760	5.104-4	7.199-5	1.020-5	2.55-7	--	0.992	1.027
10.0	1.1655	4.904-4	7.622-5	1.203-5	5.44-8	--	0.991	1.027

Burnup = 0.0

Code	K-inf	Relative Power in Pins 1	2	3	4	5	Gd	Worth of Gd
SUPERB	1.0164	1.119	1.062	1.113	1.166	0.999	0.368	0.237
MONALI (MC)	1.0122	1.118	1.060	1.120	1.166	0.988	0.366	0.243

absorption in Gd and hence initially there is a significant overprediction of K_∞. The lower depletion rate of Gd results in somewhat closer prediction of K_∞ at higher burnups.

3.2 Hexagonal Lattice

The hexagonal lattice benchmark [5] was analysed by EXCEL code. The benchmark considers two half pins with about 4 % Gd_2O_3 in a 60° symmetric sector of the fuel assembly type used in VVER-1000 MWe reactor. For calculations the regular lattice (pincell case), the macrocell with one Gd pin (Supercell case) and the assembly cell case were considered separately. The results are presented in Tables 3 to 5. The results are found to be generally agreeing with the Finnish and Russian results presented at the IAEA meeting. Our results are updated due to reasons given above. There are significant differences noted mainly in Gd pin (BA rod). We give in Tables 4 and 5 the results for BA rod of supercell and assembly cell. It is presumed that the difference in basic cross sections of Gd is more responsible for the deviations.

4. VALIDATION WITH EXPERIMENTS

4.1 ZR-6 Experiments

In the ZR-6 facility of Budapest, Hungary, the uniform hexagonal fuel lattice of 3.6% enriched uranium fuel with pitch of 12.7 mm was perturbed regularly by replacing the central and every seventh fuel pin from central pin with either water (E7) or absorber rods (I7,..,N7). The absorber rod contained 0 to 7.5% of Gd_2O_3 in Al_2O_3. Experimental data were presented at a TCM at IAEA [6].

The supercell model of EXCEL code was used to simulate the macrocells. We used the modifications in model mentioned above. The K_{eff} values of zero dimensional diffusion calculations with the recommended measured bucklings are given in Table 6. The percentage deviations in the normalised pin powers of the central macrocell are also given in Table 6. We see that the K_{eff} is over-predicted by about 1.1%. The pin powers agree within 2%. The spectral ratios (Np/Ce) representing the ratio of U-238 captures to total fissions, were compared for J7 and N7 lattices. They were overpredicted by 8-10% (not included in the table).

4.2 LR-0 Experiments [7]

In the LR-0 facility of Czechoslovakia, 19 fuel assemblies of the hexagonal VVER-440 type reactor constitute the core. In two symmetric assemblies near the central assembly one of the pins is replaced by Gd bearing fuel rods. The Gd_2O_3 content varied from 0.5% to 2.0%. The 2-D energy release profile at the mid-plane in about 37 pins of the two symmetric assemblies were measured twice for five core configurations

Table-3 Results of Hexagonal Lattice Benchmark - Pincell Case

Burnup MWD/MTU	K-inf	Number densities in units of 10^{24} U-235	Pu-239	Pu-240	Pu-241
0	1.4569	(Cold no Xe)			
0	1.3686	(Hot no Xe)			
0	1.32288	9.0 -4	0.0	0.0	0.0
1000	1.30539	8.744-4	1.104-5	1.883-7	8.421-9
2000	1.29092	8.491-4	2.139-5	7.045-7	6.403-8
3000	1.27785	8.252-4	3.070-5	1.449-6	1.952-7
4000	1.26542	8.020-4	3.930-5	2.378-6	4.202-7
5000	1.25287	7.794-4	4.726-5	3.452-6	7.486-7
6000	1.24099	7.574-4	5.465-5	4.630-6	1.180-6
7500	1.22336	7.255-4	6.474-5	6.557-6	2.019-6
10000	1.19594	6.748-4	7.937-5	1.004-5	3.857-6
15000	1.14709	5.822-4	1.020-4	1.749-5	8.747-6
20000	1.10507	4.999-4	1.180-4	2.498-5	1.447-5

Table-4 Results of Hexagonal Lattice Benchmark - Supercell Case

K∞ For Supercell ; Isotopic densities for BA rod

Burnup MWD/MTU	K-inf	Number densities in units of 10^{24} U-235	Pu-239	Pu-240	Pu-241	Gd-155	Gd-157
0	1.3454	(Cold no Xe)					
0	1.2463	(Hot no Xe)					
0	1.20858	4.000-4	0.0	0.0	0.0	1.920-4	2.030-4
1000	1.20561	3.951-4	1.009-5	9.884-8	4.189-9	1.646-4	1.352-4
2000	1.20343	3.893-4	1.999-5	4.073-7	3.476-8	1.346-4	9.400-5
3000	1.20168	3.831-4	2.938-5	9.177-7	1.155-7	1.080-4	6.475-5
4000	1.19993	3.763-4	3.814-5	1.623-6	2.568-7	8.571-5	4.408-5
5000	1.19768	3.690-4	4.639-5	2.516-6	4.794-7	6.508-5	2.723-5
6000	1.19598	3.612-4	5.412-5	3.590-6	7.875-7	4.722-5	1.490-5
7500	1.19300	3.483-4	6.488-5	5.621-6	1.397-6	2.630-5	4.279-6
10000	1.18480	3.253-4	7.964-5	9.712-6	2.812-6	5.772-6	3.177-8
15000	1.14241	2.790-4	1.009-4	1.876-5	7.041-6	3.715-8	--
20000	1.10051	2.371-4	1.157-4	2.734-5	1.274-5	--	--

(unperturbed and perturbed with the above Gd pins). The mean of the four measured data for a given pin was obtained. Experimental data were presented at a RCM at IAEA.

For calculations we used EXCEL code to obtain five group cross sections of different pincell types, water rods, poisoned pins, channel and water gap regions and reflector by appropriate supercell calculations. These five group cross sections were then used in a

Table-5 Results of Hexagonal Lattice Benchmark - Assembly Cell Case

K_∞ For Assembly cell ; Isotopic densities for BA rod

Burnup MWD/MTU	K-inf	Number densities in units of 10^{24} U-235	Pu-239	Pu-240	Pu-241	Gd-155	Gd-157
0	1.4114	(Cold no Xe)					
0	1.3182	(Hot no Xe)					
0	1.27566	4.000-4	0.0	0.0	0.0	1.920-4	2.030-4
1000	1.26367	3.952-4	9.884-6	9.323-8	3.910-9	1.660-4	1.376-4
2000	1.25418	3.896-4	1.977-5	3.921-7	3.349-8	1.365-4	9.629-5
3000	1.24570	3.834-4	2.910-5	8.871-7	1.125-7	1.102-4	6.700-5
4000	1.23676	3.767-4	3.807-5	1.582-6	2.608-7	8.769-5	4.574-5
5000	1.22842	3.694-4	4.652-5	2.467-6	4.986-7	6.669-5	2.841-5
6000	1.22063	3.618-4	5.420-5	3.497-6	8.193-7	4.902-5	1.600-5
7500	1.20867	3.496-4	6.466-5	5.328-6	1.474-6	2.862-5	5.173-6
10000	1.18915	3.277-4	7.942-5	9.008-6	3.009-6	7.281-6	6.939-8
15000	1.14378	2.818-4	1.011-4	1.746-5	7.535-6	5.684-8	--
20000	1.10196	2.397-4	1.159-4	2.579-5	1.320-5	--	--

Table-6 Results of ZR-6 Experiments with Gd2O3 Absorber Rods

Lattice type	% Gd_2O_3	K-inf	M^2 cm^2	K-eff	Pin Location	% Deviation in Relative Pin Powers I7	J7	K7	L7	M7	N7
E7	--	1.42546	41.13	1.0024	1*	--	--	--	--	--	--
G7	0.0	1.42252	41.56	1.0063	2	-0.10	1.06	0.81	0.80	-0.21	2.01
J7	0.2	1.39864	41.36	1.0090	3	-0.42	0.66	0.27	0.00	-0.24	0.85
K7	1.0	1.37995	41.24	1.0052	4	-0.41	-0.70	-0.85	-0.75	-0.97	-0.90
L7	2.0	1.37468	41.21	1.0047	5	0.19	0.15	0.97	0.17	-0.39	0.03
M7	5.0	1.36885	41.12	1.0091	6	-0.14	-0.59	-0.78	-0.24	1.11	-0.54
N7	7.5	1.36610	41.09	1.0108	7	-0.03	-0.18	0.14	-0.17	-0.29	-0.73
					8	0.51	-0.20	0.17	0.00	-0.44	-0.45

* Location of water rod or absorber rod

hexagonal finite difference diffusion code TRIHEX-3D [12]. In the core calculation we represented each individual fuel pincell region and other heterogeneities explicitly. Reflector thickness equivalent to one additional fuel assembly layer was considered. Axial buckling was adjusted such that the reactor was nearly critical. Fig.1 gives the relative pin locations within a fuel assembly which are referred to in the following table. Percentage deviations in relative pin powers for the measured locations after normalising at the measured peak (location 1012) are given in Table 7. For the poisoned pin cases the pin powers relative to no Gd case were obtained and deviations in these are also given in Table 7. We see that Gd pin powers are predicted within 2%. The maximum pin power deviation is about 6%. The r.m.s. error is about 3%.

Table-7 LRO Experiments Power distribution comparison

S.No.	Location of measured Pin	No Gd	Percentage Deviation in Relative Pin Powers Two Gd Pins with Gd2O3 Content of 0.5%		1.0%		1.5%		2.0 %	
		A	A	B	A	B	A	B	A	B
1	1011	1.3	0.0	-1.2	0.7	-0.6	2.0	0.7	0.3	-1.0
2	1012	0.0	0.0	0.0	0.0	0.0	0.0	0.0	0.0	0.0
3	1019	-2.1	-2.5	-0.4	-2.5	-0.3	-2.6	-0.5	-2.2	-0.1
4	1022	0.4	-0.5	-0.9	-1.7	-2.1	-0.4	-0.8	-0.6	-1.1
5	1026	--	1.6	--	-0.5	--	1.8	--	1.8	--
6	1027	-1.9	-0.2	1.7	-1.4	0.5	-2.2	-0.3	-0.8	1.1
7	1028	-4.1	-3.7	0.4	-3.8	0.3	-3.5	0.6	-3.8	0.3
8	1033	0.9	0.2	-0.6	0.5	-0.3	-2.6	-3.4	0.6	-0.2
9	1036	1.5	2.2	0.7	2.4	0.9	2.2	0.7	2.9	1.4
10	1037	-2.1	-2.1	0.0	-1.0	1.1	-0.9	1.3	-0.3	1.9
11	1038	-4.2	-3.7	0.6	-4.7	-0.5	-4.1	0.2	-3.7	0.6
12	1039	-5.9	-6.3	-0.5	-5.3	0.6	-6.8	-1.0	-6.3	-0.5
13	1044	0.9	1.3	0.4	-1.1	-2.0	0.8	-0.1	1.0	0.1
14	1047	3.5	3.0	-0.5	3.3	-0.2	2.2	-1.3	4.0	0.5
15	1048	-1.2	0.9	2.1	1.3	2.5	1.1	2.4	3.4	4.7
16	1049	-3.4	-3.5	-0.1	-2.8	0.6	-2.4	1.0	-2.9	0.5
17	1050	-6.1	-6.4	-0.3	-5.9	0.3	-6.5	-0.4	-5.6	0.5
18	1060*	1.3	3.0	1.7	3.2	1.8	5.8	4.5	4.1	2.7
19	1061*	-2.8	-0.2	2.7	-0.6	2.3	-2.0	0.9	1.3	4.2
20	1062	-5.5	-3.2	2.5	-4.4	1.1	-5.2	0.4	-3.1	2.6
21	1067	-0.1	-1.2	-1.1	-1.3	-1.2	-2.9	-2.8	-1.0	-0.9
22	1071	3.2	4.9	1.7	4.6	1.4	4.6	1.4	5.4	2.1
23	1072	-2.2	0.3	2.5	0.4	2.6	1.6	3.9	1.8	4.0
24	1073	-3.5	-2.7	0.8	-2.2	1.3	-2.6	0.9	-1.5	2.0
25	1074	-5.6	-6.6	-1.0	-6.1	-0.4	-6.0	-0.4	-4.5	1.2
26	1083	2.7	3.8	1.1	3.4	0.7	4.1	1.4	3.2	0.5
27	1084	-1.1	-1.6	-0.4	-0.5	0.6	-2.0	-0.9	-1.3	-0.2
28	1085	-3.6	-3.6	0.0	-3.9	-0.4	-4.8	-1.3	-2.7	0.9
29	1086	-5.7	-5.3	0.4	-5.5	0.3	-5.3	0.5	-5.6	0.2
30	1091	-1.7	-2.8	-1.1	-2.1	-0.5	-3.3	-1.7	-2.0	-0.4
31	1094	2.9	2.6	-0.4	2.4	-0.6	1.0	-1.9	3.1	0.1
32	1095	-0.9	-1.8	-1.0	-1.1	-0.3	-1.6	-0.8	-0.4	0.5
33	1096	-1.6	-3.3	-1.7	-2.7	-1.2	-2.6	-1.0	-0.6	1.0
34	1101	0.1	-1.7	-1.8	-1.7	-1.8	-0.9	-1.0	-1.0	-1.1
35	1106	-1.4	-2.2	-0.8	-1.7	-0.3	-2.5	-1.1	-0.8	0.6
36	1109	-1.9	-1.1	0.8	-1.2	0.7	-2.4	-0.5	-1.2	0.7
37	1115	1.1	-0.2	-1.3	1.0	-0.1	0.0	-1.1	1.4	0.2
38	1116	0.8	-0.8	-1.6	0.2	-0.6	-0.9	-1.7	1.1	0.3
r.m.s.	--	2.96	3.00	1.22	2.88	1.15	3.30	1.55	2.84	1.64

A - Maximum pin power normalised with measured value
B - Deviations of Pin powers relative to no Gd case
* - Gd pin location

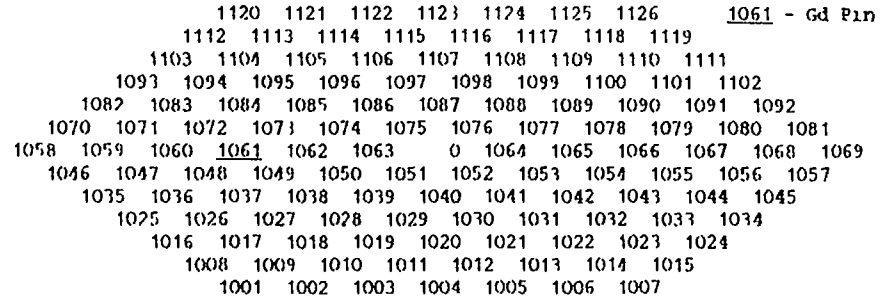

FIG 1 Location of pins in a LR-0 reactor fuel assembly.

5 CONCLUSIONS

The lattice codes SUPERB and EXCEL and the hexagonal core analysis code TRIHEX-3D have been used to analyse two theoretical benchmarks and ZR-6 and LR-0 experimental data on Gd as absorber or burnable absorber rod. It is found that our modelling in our lattice codes are resonably good to predict the zero burnup K_∞ and power distributions. With burnup there is still some discrepancy which may be attributed to the Gd cross section data used.

ACKNOWLEDGEMENTS

The authors are grateful to Dr.I.Vidovszky, and Dr.J.Gado of CRIP, Hungary and Dr.J.Bardos, NRI, Czechoslovakia for furnishing the experimental data. We are grateful to Dr.H.C.Gupta for providing the Monte Carlo results of square lattice benchmark.

REFERENCES

1. V.Jagannathan et al., Annals of Nuclear Energy, 7, 641 (1980)
2. S.R.Dwivedi et al. Report B.A.R.C.-864. (1975)
3. V.Jagannathan et al., Annals of Nuclear Energy, 10, 339. (1983)
4. C.Maeder and P.Wydler, Report NEACRP-A-567. (1983)
5. V.D.Siderenko, 'Test Problem for Calculating Reactor Lattices With Gadolinium Bearing Fuel Pins', TIC internal material. (1988)
6 I.Vidovzsky and J.Gazso, 'Experimental Investigations of VVER-Type Lattices Containing Gd Absorber Rods', Presented at the IAEA Tech. Comm. Mtg. on Incore Fuel Management, Vienna, Dec 4-7, 1989
7. J.Bardos et al., 'Burnable Absorbers in VVER-Type Fuel Lattices', presented at the IAEA Research Coor. Mtg. on 'Safe Core Management with Burnable Absorbers in VVERs', Vienna, Dec. 11-14, 1989.
8. F.J.Fayers et al., Report AEEW-R-785. (1972)
9. P.Mohanakrishnan and H.C.Huria, Nucl. Sci. Engg., 68, p.220.(1978)
10. Vinod Kumar and R.D.S.Yadav, private communication. (1990)
11. H.C Gupta, B.A.R.C. Report, under preparation. (1990)
12. V.Jagannathan and R.P.Jain, Report B.A.R.C.-1515. (1990)

THE APOLLO-I ASSEMBLY SPECTRUM CODE

G. MATHONNIÈRE, Z. STANKOVSKI
Direction des réacteurs nucléaires,
Département de mécanique et de technologie,
Commissariat à l'énergie atomique,
Centre d'études nucléaires de Saclay,
Gif-sur-Yvette, France

Abstract

APOLLO-I is a general purpose assembly spectrum code, the only used by the Commissariat à l' Energie Atomique (CEA) and by the french utility Electricité de France (EDF) for PWR's calculations. It is also used by the french manufacturer FRAMATOME for reference calculations and, of course, in CEA for development of new reactors and to analize experimental results.

As its development begun as soon as in 1970, the code and its associated external cross section library, called APOLIB, has been widely tested and qualified, by comparison with experimental results coming from test facilities or EDF's PWRs.

Many studies have been carried out with APOLLO-I as different as reference calculations for PWR using MOX assemblies, or benchmark calculations on fuel dissolver.

The APOLLO-I assembly spectrum code is currently run at the IBM and CRAY computers, and can be easily installed on workstations.

The APOLLO-I code has been widely described in international publications and specially in [1] a very detailed presentation of the code formalism has been presented.

So, in the present paper we will be satisfied with giving in brief the main capabilities and features of the code.

Library. The standard 99 groups APOLIB library contains multigroup cross section data for over 400 isotopes and also pretabulated effective reaction rates used in the frame of selfshielding calculations. This library is continously improved through modifications in the basic data files and through experimental results taken into account owing to the "search of tendancies" [2].

Selfshielding. For isotopes with epithermal resonances, the selfshielding is performed, according Livolant-Jeanpierre theory [3], and using pretabulated reaction rates of the library.

Flux calculations. APOLLO is based on the resolution of the multigroup integral transport equation by the collision probability method. The choice among the various possibilities offered by the code is rather large: it is possible to deal with one and two-dimension geometries, to take into account an isotropic or a linearly anisotropic scattering, to treat a double heterogenity (media containing a dispersion of grains).

Furthermore it is possible to select either modules based on a rigorous discretisation of the integral transport equation, or modules using physical approximation to simplify calculations. The first ones are used for reference calculation, the seconds for route calculation.

Leakage. The diffusion coefficient and the material buckling are calculated in an equivalent flux-homogenized infinite medium. It is also possible to perform a streaming correction based on Benoist's theory [4].

Depletion calculations. The variation of the isotopic compositions in the various media is taken into account as a function of the burn-up, steps being chosen by the user.

Post processing capabilities. APOLLO-I computes reaction rates and average cross sections for any isotope and any spatial region or energy mesh; but it is also able to generate a set of cross sections either in the APOLIB or NEPLIB formats. The APOLIB library is created in order to homogenize isotopes in space and/or energy, which can be used for other APOLLO transport calculations. The cross sections are created by using the SPH process [5], which allows to generate the same reactions rates as the original calculation.

For the NEPLIB libraries it is exactly the same, but these cross sections are destinated to be used in a diffusion calculation code like CRONOS. The NEPLIB structure, whose one parameter is the burnup, is suitable for dealing with water density and temperatures feedback, which are very important for PWRs [6].

For creating a multiparameter (for exemple burn-up, fuel temperature, water density, xenon concentration, boron concentration) tabulated NEPLIB, a specific feature, the GENALIB module may be used [7] It allows to generate the full NEPLIB by executing only one job The process is the following firstly basic calculations are performed, at the first and last step a full grid comprising all the parameters combinations is calculated, but for the other steps only the nominal combination is calculated Secondly the full NEPLIB is got by using a factorisation hypothesis allowing to calculate the full grid for each step from the basic calculations

Examples Apart from its utilisation as a main step of a routine code route for PWR's calculations, its versatility and its accuracy allows to deal with many various physical problems

For instance it was widely used for neutronic investigations of an advanced pressurised water reactor with spectral shift made in CEA [8]

It was also used to determine the influence on the power peaking factor by using different isotopic compositions for various pins of the same MOX assembly [9]

As a last example, it is possible to quote a recent study devoted to the fuel cycle and to the difficult dissolver calculation problem [10]

CONCLUSIONS

The great versatility of the APOLLO-I assembly spectrum code, the importance and the accuracy of its associated library, the qualification of its formalism allow to deal successfully with many various difficult physical problems, but also to be a very precious step in a routine code route

REFERENCES

1 **A. Kavenoky, R Sanchez**
The Apollo assembly spectrum code
ANS International Topical Meeting on Advances in Reactor Physics, Mathematics and Computations, Paris, April 27-30, 1987

2 **H. Tellier and al.**
Joint Evaluated File Qualification for Thermal Neutron Reactors
ANS Saratoga Springs September 11-14, 1986

3 **M. Livolant, F Jeanpierre**
Autoprotection des resonances dans les reacteurs nucleaires Application aux isotopes lourds
Rapport CEA-R 4533

4 **P Benoist**
Theorie du coefficient de diffusion des neutrons dans un reseau comportant des cavites
Rapport CEA-R 2278

5 **A. Kavenoky**
The SPH Homogenization Method
IAEA Technical Meeting on Homogenization Methods in Reactor Physics,

6 **J. Krebs and al**
Calculational Methods for PWR
this Meeting

7 **V Brun and al.**
Reactor Calculation Multigroup Parametred Libraries
This Meeting

8 **J Bergeron, R Lenain**
Investigation of an Advanced Reactor with Plutonium Fuel Controlled without Soluble Boron
ANS International Reactor Physics Conference, Jackson Hole, Septembre 18-22, 1988

9 **G. Mathonniere, M. Rohart**
Influence on the Power Peak of Different Plutonium Isotopic Compositions in PWR MOX Fuel Assemblies
AIEA Technical Commitee on Recycling of Plutonium and Uranium in water reactor fuels, Cadarache, Novembre 13-16, 1989

10 **A. Santamarina and al**
NEACRP standard problem exercise on criticality codes for dissolving fissile oxides in acides, A reference method for treating the fuel double heterogeneity
PHYSOR International Conference on the Physics of Reactors, Marseille, April 23-27, 1990

CRONOS: A MODULAR COMPUTATIONAL SYSTEM FOR NEUTRONIC CORE CALCULATIONS

J.J. LAUTARD, S. LOUBIÈRE, C. FEDON-MAGNAUD
Direction des réacteurs nucléaires,
Département de mécanique et de technologie,
Commissariat à l'énergie atomique,
Centre d'études nucléaires de Saclay,
Gif-sur-Yvette, France

Abstract

The CRONOS code has been designed to provide all the computational means needed for Pressurized Water Reactor calculations, including design, fuel management, follow up and accidents. CRONOS allows steady state, kinetic and transient multigroup calculations of power distribution taking into account the thermal-hydraulic feedback effects. All this can be done without any limitation on any parameter (energy groups, meshes...).

The code solves either the diffusion equation or the even parity transport equation with isotropic scattering and sources. Different geometries are available such as 1, 2 or 3 dimensions cartesian geometries, 2 or 3D hexagonal geometries and cylindrical geometries. The numerical method is based on the finite difference or finite element methods.

CRONOS 2 has been written with the constant will of optimizing its portability. Presently it is running on very different computers such as IBM 3090, CRAY 1, CRAY 2, SUN 4, MIPS RS2030 or IBM RS6000. A special data structure is used in order to improve vectorization.

CRONOS is based on a modular structure thas allows a great flexibility of use. It is implemented in the SAPHYR system which includes assembly calculation code (APOLLO [1]), and thermal-hydraulic core calculation code (FLICA IV [2]). A special object oriented language, named GIBIANE, and a common tool library have been developed to chain the various computation modules of those codes.

1) Cross section representation

The cross sections used come from a group collapse of a two dimensional transport calculation of an assembly in an infinite medium using the APOLLO code in a 99 energy group representation. We have to apply a transport/diffusion equivalence to those cross sections. To do so we modify the library so that the reaction rates in each cell in diffusion theory is equal to the same reaction rate in the transport theory.

The library is tabulated by depletion parameters such as burnup or fluence, by thermal-hydraulic ones - water density, fuel temperature - or even by some characteristic isotope concentrations such as Xenon, Boron or any parameters wished by user. In CRONOS the parameters are stored plane by plane and isotope by isotope, because of the great number of their values. A memory management system is used, so that at any time of the process no more than one plane of the parameters is loaded in the central memory. The calculation either of the macroscopic cross sections or the isotopic concentration evolution are vectorized by working on all the cells containing the same medium, at a time.

Regarding homogeneous calculation the cross sections used are coming from the homogeneization of heterogeneous ones with the transport flux resulting from the transport assembly code (APOLLO). The homogeneous calculation can be dramatically improved if we use not only constant parameters and isotopic concentrations in each homogeneized medium but also polynomial space dependent ones. This case induces polynomial space dependent cross sections [3]. The CRONOS code allows to use polynomials up to order 2 in each direction.

2) Weak formulations

2.1 Diffusion calculation (primal form) [4]

Let us consider the simplified one group source problem :

$$-\nabla D \nabla \Phi + \Sigma \Phi = f \qquad (r \in \Omega) \qquad (1)$$

with the boundary condition :

$$\Phi = 0 \text{ on } \Gamma_1 \qquad (2)$$

$$D \frac{\partial \Phi}{\partial n} + \gamma \Phi = 0 \text{ on } \Gamma_2 \qquad (3)$$

The weak formulation can be obtained by multiplying the two members of equation (1) by any fonction Ψ belonging to the well-known Sobolev space H_0^1 and by integrating the result over Ω.

$$a(\Phi,\Psi) = f(\Psi) \qquad \forall \Psi \in H_0^1$$

with

$$\begin{cases} a(\Phi,\Psi) = \int_\Omega (D \vec{\nabla}\Phi.\vec{\nabla}\Psi + \Sigma \Phi \Psi) + \int_{\Gamma_2} \gamma \Phi \Psi \\ f(\Psi) = \int_\Omega f \Psi \end{cases} \qquad (4)$$

2.2 Transport calculation (primal form) [5]

On each energy group assuming isotropic scattering processes we have :

$$\vec{\Omega}.\vec{\nabla}\varphi + \Sigma_t \varphi = \Sigma_s \Phi + Q \qquad (5)$$

where $\Phi(\vec{r}) = \frac{1}{4\pi}\int_S \varphi \, d\vec{\Omega}$ is the scalar flux

and $Q(\vec{r})$ for $\vec{r} \in E$ is an isotropic source

with boundary conditions :

- symmetry $\varphi(\vec{\Omega}) = \varphi(\vec{\Omega}')$ $\vec{\Omega}.\vec{n} = -\vec{\Omega}'.\vec{n}$

$(\vec{\Omega} \times \vec{\Omega}').\vec{n} = 0$ on $\partial E_1 \times S$

- vacuum $\varphi(\vec{\Omega}.\vec{n}<0) = 0$ on $\partial E_2 \times S$

Following the standard development we derive an equation for the even parity flux :

$$-\vec{\Omega}.\vec{\nabla}\left[\frac{1}{\Sigma_t}\vec{\Omega}.\vec{\nabla}\varphi^+\right] + \Sigma_t\varphi^+ = \Sigma_s \Phi + Q \qquad (6)$$

with : $$\varphi^+ = \frac{1}{2}\left[\varphi(\vec{\Omega}) + \varphi(-\vec{\Omega})\right] \qquad (7)$$

with boundary conditions :

- symmetry $\varphi^+(\vec{\Omega}) = \varphi^+(\vec{\Omega}')$ $\vec{\Omega}.\vec{n} = -\vec{\Omega}'.\vec{n}$

$(\vec{\Omega} \times \vec{\Omega}').\vec{n} = 0$ on $\partial E_1 \times S$

- vacuum $\pm\left[\frac{1}{\Sigma}\vec{\Omega}.\vec{\nabla}\varphi^+\right] + \Sigma_t\varphi^+ = 0$ on $\partial E_2 \times S$

Using the same method as in the diffusion case we get the following weak formulation : (φ and ψ being the even parity fluxes)

$$a(\varphi,\psi) = f(\Phi,\Psi) \qquad \forall\, \psi \in V \qquad (8)$$

where $$a(\varphi,\psi) = \int_{E\times S} \frac{1}{\Sigma_t}(\vec{\Omega}.\vec{\nabla}\varphi)(\vec{\Omega}.\vec{\nabla}\psi)\, d\vec{r}\, d\vec{\Omega} + \int_{E\times S} \Sigma_t \varphi\, \psi\, d\vec{r}\, d\vec{\Omega} + \int_{\partial E_2 \times S} |\vec{\Omega}.\vec{n}|\, \varphi\, \psi\, d\Gamma\, d\vec{\Omega}$$

and $$f(\Phi,\Psi) = \int_E \Sigma_s \Phi\, \Psi\, d\vec{r} + \int_E Q\, \Psi\, d\vec{r}$$

This equation has already been well investigated, and has a unique solution.

The "a" bilinear form needs an integration over the angular variable $\vec{\Omega}$. The usual method to estimate this integral is to use finite differences (Discrete Ordinates Method). Using this method we get a serie of coupled variationnal problems :

$$a_i(\varphi_i,\psi) = f(\Phi,\psi) \qquad \forall\, \psi \in H^1 \qquad (9)$$

with $\Phi = \sum \omega_i \varphi_i$ ω_i beeing the quadrature weights

This problem is very close to the diffusion one, except that :

- the unknown space function is replaced by a vector of functions depending on the number of angular points
- cross derivatives appear in the variationnal forms which do not exist in diffusion

3) Spatial approximation

The 3D reactor core is divided into elements (rectangular parallelepiped ones in the case of the cartesian geometries and equilateral triangles for the hexagonal ones). On each element the flux is expanded over a truncated polynomial basis. A large number of polynomial approximations are provided from which the more used are the Lagrange basis.

We will develop here-after the case of the cartesian geometries. For each variable x_j, the user may choose the degree of the polynomial P_i^j between 1 and 3 ; the standard elements available in CRONOS are presented in § 3.3.

The weak form of the diffusion equation involves integrals of basis fonction products :

$$M_{ij}^k = \int P_i^k(x).P_j^k(x).dx \qquad (10)$$

$$S_{ij}^k = \int \nabla P_i^k(x).\nabla P_j^k(x).dx \qquad (11)$$

Two improvements have been added to the standard calculations : choice of a basis reducing the number of terms to be accounted for, and numerical integration [6].

3.1 Refined basis

In order to speed up the numerical solution, the P_i^k polynomial are chosen so that the number of M_{ij}^k non equal to zero is minimized : our basis beeing factorized, the treatment is presented in 1D. If the standard Lagrange polynomials are used (corresponding to the nodes), no element of M_{ij}^k is equal to zero. In our treatment the polynomials corresponding to the edges of the element core are kept. The others are replaced by orthogonal linear combinations of them. These combinations are chosen to be orthogonal to the first two polynomials.

Figure 1 presents the third order M^k_{ij} matrix corresponding to the standard and modified basis : the number of terms is reduced from 16 to 6.

Standard Lagrange M^k_{ij} matrix Modified M^k_{ij} matrix

Figure 1

3.2 Numerical integration providing super-convergence

The standard finite element method is based on analytical calculation of equations (10) and (11) ; some theoretical attempts have shown that better results may be obtained if these integrals are computed using Gauss formula ; all the polynomials of our basis beeing of the same order q, the Gauss formula using q integration points had to be used. This formula integrates rigorously polynomials of order 2q-1 ; the S^k_{ij} matrix is exact but an integration error remains for M^k_{ij} (the order of the integral beeing 2q).

Another interesting property of the numerical integration is to use the Gauss Lobatto integration formula. It can be shown that in this case and for the linear approximation we obtain the vertex centered finite difference approximation (the M^k_{ij} matrix is then diagonal). This one leads to more regular matrices and this can be used to improve the vectorization. A special treatment for this kind of matrices is done in CRONOS (it will be described later in this paper).

3.3 Set of implemented elements

The 3D basis are tensorial products of 2D basis with 1D axial basis.
(• represents a flux node, × an integration point, ~ a mean value, and → a current node)

- Two dimensional cartesian elements

* Standard linear Lagrange  (LL4)
* Linear Lagrange using Gauss formula  (LL4#)
* Linear Lagrange using Gauss Lobatto formula (vertex centered finite differences VCDF)  (LL4$)
* Standard parabolic Lagrange 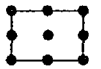 (PL9)
* Orthogonalized parab.Lag. using Gauss formula  (PL9#)
* Standard cubic Lagrange  (CL16)
* Orthogonalized cubic Lag. with Gauss formula  (CL16#)

- Two dimensional hexagonal elements

* Standard Linear Lagrange 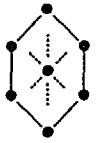 (HXL7)
* Linear Lagrange using Gauss Lobatto formula (vertex centered finite differences) 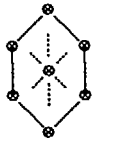 (HXL7$)
* Standard Parabolic Lagrange 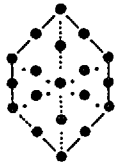 (HXP19)

- Axial elements

* Linear Lagrange  (L2)
* Linear Lagrange using Gauss formula  (L2#)
* Parabolic Lagrange  (P3)

4) Mixed-dual approximation of diffusion calculation

Mixed diffusion approximations have been recently applied to the diffusion equations [7]. This method is based on a numerical approximation of the equation that links fluxes and currents. Two kinds of approximations can be considered .

The first one is a mixed primal approximation which needs a flux continuity at the element boundary (currents can be discontinuous). It can be shown that this approximation is equivalent to the classical primal one. So it is of no interest.

The second method is the mixed dual approximation. In this case the flux can be discontinuous and the current has to be partly continuous at the element boundaries. This method is quite interesting, it presents some relations with the nodal methods [8]. Moreover the numerical integration of the linear current approximation leads to the classical mesh centered finite difference method (MCDF).

4.1 Method

The mixed dual variational formulation can be written as follows :

$$(12)\quad \begin{cases} \text{Find } (\vec{p},u) \in H_{0,\Gamma_1}(\text{div},\Omega) \times L^2(\Omega) & \text{so that} \\ \displaystyle\int_\Omega \frac{1}{D}\,\vec{p}.\vec{q} + \vec{\nabla}.\vec{q}\;u = 0 & \forall\, \vec{q} \in H_{0,\Gamma_1}(\text{div},\Omega) \\ \displaystyle\int_\Omega -\vec{\nabla}.\vec{p}\;v + \Sigma\, u\, v = \int_\Omega f\, v & \forall\, v \in L^2(\Omega) \end{cases}$$

$$\text{with } H_{0,\Gamma_1}(\text{div},\Omega) = \left\{ \vec{q} \in H(\text{div},\Omega) \mid \vec{q}.\vec{n} = 0 \text{ on } \Gamma_1 \right\}$$

This problem has a unique solution which is $(D\vec{\nabla}u,u)$, where u is a solution of the initial source diffusion problem.

4.2 Finite element approximation

The spaces $H_{0,\Gamma_1}(\text{div},\Omega)$ and $L^2(\Omega)$ are approximated by finite dimensional spaces:

$$Q_h = \left\{ \vec{q}_h \in H_{0,\Gamma_1}(\text{div},\Omega) \mid q_h|_K \in Q_K \quad \forall\, K \in T_h \right\}$$

$$V_h = \left\{ v_h \in L^2(\Omega) \mid v_h|_K \in P_K \quad \forall\, K \in T_h \right\}$$

built on a triangulation, T_h, P_K and Q_K being polynomial spaces. Usually Q_K and P_K are Raviart and Thomas spaces :

$$Q_K = P_{m+1,m} \times P_{m,m+1} \qquad P_K = P_{m,m} \qquad m \text{ beeing a given integer.}$$

4.3 Set of implemented elements

Flux Current

- First order elements

$P_K = P_{0,0}$
$Q_K = P_{1,0} \times P_{0,1}$

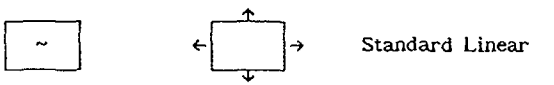

Standard Linear

$P_K = P_{0,0}$
$Q_K = P_{1,0} \times P_{0,1}$

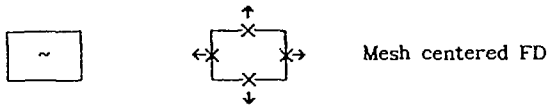

Mesh centered FD

With Gauss Lobatto formula

- Second order element

$P_K = P_{1,1}$
$Q_K = P_{2,1} \times P_{1,2}$

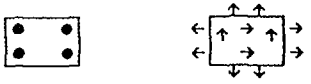

Standard Parabolic

5) Numerical resolution

The element discretization leads to large 3D matrices. Due to the special choice of the finite element basis (tensorial product of 2D and 1D basis) the 3D matrix has a block symetric structure in each energy group. Each block represents coupling terms between plans.

The iterative scheme used to solve eigenvalue problems (power iteration accelerated by Tchebychev or L^2 minimization) or to solve steps equations in the kinetic problems, needs the resolution of 3D systems within each energy group. These systems are solved iteratively by the usual axial block SOR method. The 2D plane block systems are solved by a direct Choleski method or by iterative methods.

A specific numerical treatment and data storage of the linear system is used when CRONOS runs on vector computers as CRAY1 or CRAY2. For a rectangular mesh grid, the non zero terms appear only on a small number of subdiagonals (5 subdiagonals for the linear Lagrange approximation and 13 for the parabolic Lagrange). When CRONOS runs on a vector computer the matrices are stored subdiagonal by subdiagonal, some zero terms being added so that all the stored terms on a subdiagonal have a constant increment. Thus all the matrix vector products are fully vectorized. The matrix system are solved iteratively using special vectorized preconditionners based on finite difference system structure.

6) Special treatment of finite difference systems

In the finite difference approximation the matrices do not represent the main storage requirements. The iteration process to get the eigenvalue takes an important part of the computing time, so we have used special vectorization methods. Here-below we will consider the case of axial finite difference.

6.1 Matrix normalization

At each iteration of the power method, we have to solve a linear system, which is solved using a line Jacobi preconditioning method :

$$(D + A_x).\varphi^{j+1}_{n+1} = b - (A_y + A_z).\varphi^{j}_{n+1} \qquad \varphi^{0}_{n+1} = \varphi_n \tag{13}$$

Where A_x (resp. A_y, A_z) represents the coupling terms along the X (resp. Y, Z) axis.

Decomposing ($D + A_x$) in the Choleski form as in equation (14),

$$D + A_x = L.L^t = \tilde{D}.\tilde{L}.\tilde{L}^t.\tilde{D} \tag{14}$$

(where $\tilde{L}$ is an unitary lower triangular matrix and $\tilde{D}$ a diagonal matrix)

multiplying all the matrices by $\tilde{D}^{-1}$ and taking as new unknown $\psi = \tilde{D}.\varphi$

we get a new eigenvalue problem with ψ as unknown. The associated inner iteration can be written :

$$L.L^t.\psi^{j+1}_{n+1} = \tilde{D}^{-1}.b - (\tilde{D}^{-1}.A_y.\tilde{D}^{-1} + \tilde{D}^{-1}.A_z.\tilde{D}^{-1}).\psi^{j}_{n+1} \tag{15}$$

We thus avoid operations on diagonal terms. Equation (15) can be solved in vector mode by solving all the tridiagonal systems along X simultaneously.

6.2 Acceleration methods

The inner iterations are accelerated by a conjugate gradient method.

Regarding the power iterations the acceleration is done by using a finite element coarse mesh rebalancing method. If we consider a finite element representation of the flux Φ developed on a basis P_k :

$$\text{on each element} \qquad \Phi = \sum \phi_k.P_k \tag{16}$$

Instead of looking for Φ in the P_k basis, we represent it on the $P_k.\varphi_n$ basis, where φ_n is the fine flux obtained at iteration n of the power method.

This leads to the finite element matrix system :

$$A_{ij} = a(i,j) = \int_\Omega D.\nabla.(P_i.\varphi_n).\nabla.(P_j.\varphi_n) + \Sigma.P_i.P_j.\varphi^2_n \tag{17}$$

This system is very similar to a classical finite element system except that some source matrices are no more symetrical. All the usual finite element bases available in CRONOS can be used (linear, parabolic, cubic).

This acceleration method allows a good vectorization rate, so it is very efficient on vector processors such as CRAY-1 and CRAY-2.

7) Kinetic approximation [9]

We consider the standard kinetic equations, each of the precursor equations being integrated over the time variable.

$$\frac{1}{v_g}\frac{\partial \Phi_g}{\partial t} = \nabla D_g \nabla \Phi_g - \Sigma_{tg}\Phi_g + \sum_{g'}^{G} \Sigma_{r,g'\to g}\Phi_{g'} + \chi_g \sum_{g'}^{G} (1-\beta_{g'})\nu\Sigma_{fg'}\Phi_{g'} + \sum_{l}^{L} \chi_{lg}\lambda_l C_l \tag{18}$$

$$C_l(r,t) = C_{l0}(r)\, e^{-\lambda l t} + \int_0^t e^{-\lambda l (t-s)} \left(\sum_{g'}^{G} \beta_{lg'} \nu \Sigma_{fg'}\Phi_{g'} \right) ds \tag{19}$$

where C_l is the density of the l^{th} group of precursors.

The kinetic equations are discretized using a finite element representation for the spatial variable. The flux is developed on a finite element basis P_i:

$$\Phi_g(r,t) = \sum_{i=1}^{N} \varphi_{ig}(t)\, P_i(r) \tag{20}$$

The time interval [0,T] is divided into time steps $[t_p, t_{p+1}]$. On each one we suppose :

- A linear variation of the cross sections

$$\Sigma(t) = \Sigma_p \, l_p(t) + \Sigma_{p+1} \, l_{p+1}(t) \qquad (21)$$

$$l_p(t) = \frac{t_{p+1} - t}{t_{p+1} - t_p} \qquad l_{p+1}(t) = \frac{t - t_p}{t_{p+1} - t_p}$$

- An approximation of the flux coefficients φ_{lg} which depends only on their values at the limits of the time step.

$$\varphi_{lg}(t) = \varphi_{lg}^{p} \, \omega_p(t) + \varphi_{lg}^{p+1} \omega_{p+1}(t) \qquad (22)$$

Then discretized kinetic equations are obtained by projection on the finite element basis and integration over the time step. On each step we have then to solve the following linear system :

$$A_{p+1} \varphi_{p+1} = - A_p \varphi_p + R_p \qquad (23)$$

where R_p is a source vector representing the neutrons yielded by the precursors.

Different choices for the ω_p functions lead to different schemes :

- the Crank Nikolson scheme : $\omega_p = l_p$, $\omega_{p+1} = l_{p+1}$
- the implicit backward scheme : $\omega_p = (1-u)(1-3u)$, $\omega_{p+1} = u(4-3u)$

with $u = \dfrac{t - t_p}{t_{p+1} - t_p}$

8) Fine flux reconstruction

One of the recent developments in the core calculation codes is the local flux reconstruction. In the case of the finite element method the solution we have developed and implemented in CRONOS is based on a superposition of a fine shape spectrum to the result of an homogeneous calculation :

$$\varphi_{ij}^{g} = \mathcal{F}_{ij}^{g} \cdot \Phi_{ij}^{g} \qquad (24)$$

where φ_{ij}^{g} is the reconstructed flux in location (i,j) for the g^{th} energy group, Φ_{ij}^{g} is the homogeneous flux and $\mathcal{F}_{ij}^{g}$ is the fine shape factor.

The fine shape factors are calculated in the case of infinite medium calculations or lattice calculation representative enough of the situation encountered in a core.

$$\mathcal{F}_{ij}^{g} = K \frac{\psi_{ij}^{g}}{\Psi_{ij}^{g}} \qquad (25)$$

where ψ_{ij}^{g} is the local flux resulting from an heterogeneous lattice or infinite medium calculation and Ψ_{ij}^{g} is the one coming from the homogeneous calculation of the same problem.

This local flux reconstruction method can be integrated into an iterative homogeneisation/flux reconstruction process to solve an heterogeneous problem by successive homogeneous calculations.

9) Other physical posssibilities

9.1 Depletion calculation

As we said before cross sections come from the Apollo assembly code. They are tabulated by depletion parameters (burn-up for the fissile zones or fluence for the other media). The macroscopic cross section is given by the following formula :

$$\Sigma(bu,r) = \Sigma_0(bu,r) + \sum_i c_i(r) . \sigma_i(bu,r) \qquad (26)$$

Where c_i is the isotopic concentration and $\sigma_i(bu,r)$ is the microscopic cross section.

The depletion calculations are done in two steps. The first one updates the depleted variables for the different zones. In case of polynomial space dependant parameters each polynomial is expanded over a nodal basis and a burn-up or fluence calculation is performed for each node.

The second steps consists in the resolution of evolution equation to update the isotopic concentrations. These equations take into account any kind of radioactive decay. For each zone and node within the medium the diffential equation is solved by a Runge-Kutta method. The calculations are vectorized when they are run on the CRAY computers.

9.2 Thermal-hydraulic feedback effects

Cross sections can also be tabulated by thermal-hydraulic parameters (such as fuel temperature and moderator density). Presently two modules have been implemented in CRONOS 2. They are based on a simplified model treating fuel conduction and heat transfer through the gap beetwen the fuel pellet and the clad. The exchange heat transfer coefficient can be given by the user. In each thermal mesh the enthalpy rise is proportional to the power.

The thermal-hydraulic mesh can be coarser than the neutronic one.In the next future the coupling with the FLICA IV system will provide more accurate methods.

The thermal-hydraulic feedback is obtained by a simple iteratlve process that alternates neutronic modules, which calculate power distributions, and thermal-hydraulic modules, that deduce from them the new values of the parameters, inducing a new set of macroscoplc cross sections.

10) The data processing system

The CRONOS 2 system has been organized into a modular structure and uses three auxilliary software package the ESOPE precompiler for data structuralization and dynamic management, the ARCHIVE modules for permanent data storage and the GIBIANE macro-language program.

10.1 The ESOPE system

The ESOPE language is a super-set of FORTRAN 77 allowing storage management controlled by the system itself. The precompiler generates FORTRAN 77 source code. Each of the data used in the programs are arranged into entities called "segment". Each of the segments are activated and desactivated before and after their use. The ESOPE system manages itself the central memory allocated by the user and a disk overlapping zone. At each activation of a segment the ESOPE system can write on the disk memory an already desactivated segment. This is done with a total transparency for the user.

The special structuration of the datas in CRONOS is done so that the maximum memory size of each segment cannot exceed the storage of a 2D plane, so each of the 3D calculations can run with the same central memory as the one needed for a 2D calculation.

It is also interesting to mention that ESOPE allows object oriented programing.

10.2 The GIBIANE macro-language

The logical chaining of the computing modules is controlled by the GIBIANE system. Each of them have input and output datas which are gathered into collections of ESOPE segments named "stucture". They are defined by a name, a type and a pointer. A special object oriented language has been defined. The GIBIANE language allows to execute a module giving its name and the name of the input and output data structures. Thus the users can define their own algorithms.

10.3 The ARCHIVE modules

The ARCHIVE system is a set of modules that allows the users to read or write structures on a storage device. This can be done either in a binary or a formated record that allows the transfer of those datas from computer to computer.

10.4 The post-treatment modules

The CRONOS code manage a huge amount of numerical values (parameters, cross sections, matrices, flux, power etc.). A lot of modules have been implemented in the code in order to help the user to analyse the calculation results. Those modules can display synthetic listing editions and graphical visualisation of various physical quantities such as reaction rates, power distribution, integrated fluxes, albedos, cross sections... The graphical modules can display geometries, power distribution maps, isopower or isoflux curves and power or flux shapes.

11) Examples of calculations

11.1 Diffusion core calculation

- Cartesian geometry

Table 1 gathers the results of various methods and approximations available in CRONOS to solve a typical 2D calculation for a french 900 MWe PWR. Those results take into account the feedback effects. Those results are developed and commented in a companion paper by J. Krebs, M.C. Laigle, R. Lenain, G. Mathonnière and A. Nicolas [10].

Table 1
Various diffusion results with feedback effects
for the same 2D core problem

	Ref	1	2	3	4	5	6	7
Type	Homog	Homog	Homog	Homog	Homog	Homog	Heter	Heter
Approx.	CL16	CL16	PL9#	PL9#	V.C.FD.	M.C.FD.	V.C.FD.	M.C.FD.
Neut.mesh	2x2	1x1	1x1	2x2	8x8	8x8	17x17	17x17
Ther.mesh	2x2	1x1	1x1	2x2	2x2	1x1	1x1	1x1
Keff	0.99961	0.99959	0.99992	0.99965	0.99902	1.00052	0.99993	0.99771
K∞	1.03433	1.03421	1.03479	1.03440	1.03338	1.03575	1.03459	1.03249
Leakage	- 3414.	- 3405.	- 3428.	- 3417.	- 3382.	- 3461.	- 3408.	- 3427.
Max ΔP	-	- 0.66	0.90	0.20	- 2.58	3.80	0.80	2.06
σ(P)	-	0.30	0.47	0.10	1.42	2.01	0.38	1.08
Δ Keff	-	- 2.	31.	4.	- 59.	91.	32.	- 190.
Δ K∞	-	- 12.	44.	7.	- 92.	137.	25.	- 178.
Δ Leakage	-	10.	- 13.	- 3.	33.	- 46.	7.	- 12.
Δ Pmax	-	0.31	- 0.54	- 0.08	1.25	- 1.79	- 0.31	- 0.93

Table 2 shows the power distibution in the core, for the reference case. This distribution is renormalized so that the average power over the core is equal to 1.

Table 2
2D assembly per assembly power distribution

0.961	0.764						
1.039	1.178	1.026	0.711				
1.168	1.023	0.860	1.118	0.418			
0.863	0.911	1.231	0.881	1.027	0.418		
1.285	1.249	1.147	1.220	0.882	1.118	0.711	
1.049	1.078	1.075	1.148	1.231	0.860	1.026	
0.989	1.180	1.078	1.249	0.911	1.023	1.178	0.764
0.805	0.989	1.049	1.285	0.863	1.168	1.039	0.961

CRONOS 2 allows to do 3D heterogeneous core calculation which represent around 10 million unknowns and a 306 X 306 X 50 calculation mesh for an entire core. We present in Table 3 the result of such a calculation in the case of a uniform zero burnup 900 MWe PWR core (quarter core), using for both calculations the same set of cross sections.

Table 3
3D heterogeneous quarter core calculation

approximation	K_{eff}	power peak	cpu time (s)
Mesh Centered FD	1.24806	3.560	806 / 1015
Vertex Centered FD	1.24993	3.556	721 / 1058

- Hexagonal geometry

Hexagonal core calculations have been done with CRONOS on tight lattices core studies. Table 4 shows the comparison of the different approximations available in the code for a sixth core calculation, the core being composed of 11 concentric rings of assemblies.

Table 4
Hexagonal core results comparison

Approximation	ΔK_{eff} (pcm)	ΔP_{max} (%)	ΔCPu time
HXL7	- 42	- 0.8	0.11
HXL7#	- 86	- 0.7	0.12
HXL7$	11	- 0.6	0.11
HXL19	- 1	- 0.2	0.33
HXL19$	21	0.0	0.30
HXP19	10	0.1	0.30
XXL37$	15	0.1	0.90
Reference:HXC37	1.08851	1.801	401 s

Table 5
Eigenvalues of the 2D transport test

Mesh	Approx	Diffusion	S2	S4	S8
20X20	LL4	1.18324	1.18314	1.18354	1.18348
20X20	PL9	1.18401	1.18323	1.18439	1.18432
40X40	LL4	1.18382	1.18373	1.18419	1.18412
60X60	LL4	1.18401	1.18393	1.18440	1.18433
80X80	TWODANT [11]	-	1.18393	1.18442	1.18436

11.2 Transport calculations

Table 5 shows the Keff results using various fine mesh, angles order and Finite Element. This is done for a 2D transport test problem representing a non fissile absorbing zone (40 X 40 cm, $\sigma_t = 2.$, $\sigma_s = \sigma_f = 0.$), surrounded by a fissile medium (20 cm thick, $\sigma_t = 1.$, $\sigma_s = 0.5$, $\sigma_f = 1.$). The boundary conditions are supposed to be vacuum ones. A paper to be submited to the Pittsburgh ANS meeting next spring will develop this implementation.

REFERENCES

[1] : "APOLLO2 an user oriented portable modular code for multigroup transport assembly calculations".
by R. Sanchez and J. Mondot
Proc. Topical meeting on Advances in Reactor Physics, Mathematics and Computation, Paris, FRANCE, (27-30 April 1987)

[2] : "FLICA IV A finite volume implicit computer code for 3D two phase flows computation of P.W.R. cores".
by D. Caruge and P. Raymond
European Two-Phase Flow Group Meeting, Paris, FRANCE (May 1989)

[3] : "A Finite Element Depletion Diffusion Calculation Method with Space Dependent Cross Sections".
by A. Kavenoky and J.J. Lautard
Nuclear Science and Engineering, 64, 563-575 (1977)

[4] : "State of the Art in using Finite Element Method for Neutron Diffusion Calculations"
by A. Kavenoky and J.J. Lautard
Proc. Topical meeting on Advances in Reactor computations, Salt Lake City (Utah), U.S.A., (March 1983)

[5] : "Computational Methods of Neutron Transport"
by E.E. Lewis and W.F. Miller
Wiley-Interscience Publication (1985)

[6] : "New Finite Element Representation for 3D reactor calculations".
by J.J. Lautard
ANS/ENS Meeting, Munich, GERMANY (27-29 April 1981)

[7] : "Mixed and Mixed-hybrid elements for the Diffusion Equation"
by F. Coulomb, C. Fedon-Magnaud
Proc. Topical meeting on Advances in Reactor Physics, Mathematics and Computation, Paris, FRANCE, (27-30 April 1987)

[8] : "On the Relationship Between some Nodal Schemes and the Finite Element Method in Static Diffusion calculations".
by C. Fedon-Magnaud, J.P. Hennart and J.J. Lautard
Proc. Topical meeting on Advances in Reactor computations, Salt Lake City (Utah), U.S.A., (March 1983)

[9] : "The Neutron Kinetics and Thermal-hydraulic transient computation module of Neptune System CRONOS".
by A. Kavenoky and J.J. Lautard
Proc. Topical Meeting on Advances in Reactor Physics and Core Thermal-hydraulics, Klamesha Lake (N.Y.), U.S.A., (September 1982)

[10]: "Calculational Methods for PWR"
by J. Krebs, M.C. Laigle, R. Lenain, G. Mathonnière and A. Nicolas
Proc. this meeting.

[11]: "User's Guide for TWODANT : a code Package for Two Dimensional, Diffusion accelerated, Neutral-Particle Transport"
by R.E. Alcouffe, F.W. Brinkley, D.R. Marr and R.D. O'Del
LA-10049-M, Los Alamos National Laboratory (march 1984)

ROD EJECTION ANALYSIS IN PWRs WITH A 3D KINETIC NEW CODE

M. GONNET, C. NEAUME, T. BISIAUX
Framatome,
Paris-La Défense,
France

Abstract

Standard synthesis method in control rod ejection analysis is usually over-conservative and may affect significantly the PWR project parameters. A 3D kinetic applied to standard safety analysis and to a series of penalizing transients (simultaneous ejection of 2 rods) is presented here. For this purpose a 3D kinetic code involving 2-group time dependent diffusion and fine thermal-hydraulic models was developed at FRAMATOME. The large number of meshes used (30000 to 45000) allows a sufficient accuracy to clearly show the margins imposed by the standard approach.

INTRODUCTION

A typical application of such a 3D kinetic code to the study of a rod ejection in a PWR is presented here. In such reactors,the introduction of clusters is made by gravity starting from the uppermost part of the core. Rod ejection is an accident which could occur in case of rupture of the control rod drive mecanism casing located on the top of the pressure vessel. This rupture would affect the primary system pressure (155 bars) and this could propel the rod out of the core at a very high speed. When the reactivity worth is high, the ejection could bring up the core to be prompt-critical. The consequences of the increase in nuclear power on the fuel integrity have to be examined. This accident, rated ANS condition IV, should lead neither to a stored energy of more than 840 J/g at the hot point, nor to an excessive clad temperature. Respect of these criteria commonly leads to set up rod bank insertion limits.

In this presentation, the results of the 3D and standard methods in term of global core behaviour (nuclear power),local energy and temperature variations for various initial conditions and rod worth are compared. Two types of transients are considered. First type transients are classical cases of project studies, selected on 1450 MWe or 1300 MWe plants (refered as N4 and P4 in the text), leading to violation of criteria under the standard approach. Second type are more pessimistic ones (simultaneous ejection of two rods).

The standard FRAMATOME method for rod ejection analysis is based on a synthesis of 2D static discrete (with frozen feedbacks) and 1D kinetic calculation , followed by thermal calculation for the hot spots. This simplified method allows to analyse a great number of situations, particulary in case of load follow, regarding to computing time required

by 1D code. However this method is usually much more conservative than direct 3D kinetic calculation. So this analysis aims at pointing out the margins that could be gained with 3D kinetic calculations.

METHODOLOGY

Code description:

CESAR is a 3-dimensional, diffusion, kinetic code. It solves the two-group diffusion equation in rectangular lattice. Macroscopic cross sections are tabulated as a function of burnup and ajusted in every meshes to take into account all pointwise feedback effects (xenon, boron concentration, water density, spectral effect).

CESAR neutron model solves a system of eight time dependent differential equations: the two group neutron balance and the six delayed neutron precursor equations. Time integration is performed by the Krank-Nicholson method and space integration by finite differences with centered meshes. Delayed neutron parameters are evaluated as a function of the fuel local characteristics in each mesh by polynomial expansion.

CESAR thermal model solves heat transfer equation in R-Z geometry in each axial element of a channel. Various correlations are used to describe the fuel thermal properties and heat transfer in the gap and clad surface. Effective temperature required for Doppler feedback calculation is estimated by the Rowland's formula. In addition, the code includes a decay heat model.

The number of meshes in the core description only depends on computer memory size. Our CRAY-XMP allows about 50 000 meshes i.e. 30 to 40 axial meshes and 4 meshes per assembly for full core computations, to 9 for reduced samples.

Figure 1 shows an exemple of graphical display provided by the post-processor of the code, for a transient calculation.

Synthesis method:

In conventional 2D-1D approach, the two and one dimensional calculations are statics with frozen feedback conditions. They provide the radial and axial peaking factors, respectively called Fxy and Fz. The hot spot factor (FQ) is approximated by (1) and (2) :

$$FQi = Fxyi * Fzi \quad \text{calculated before the rod ejection} \qquad (1)$$

$$FQf = Fxyf * Fzf \quad \text{after ejection with frozen feedbacks} \qquad (2)$$

During the ejection, change in FQ is supposed to be linear. Change of mean core power as a function of time is calculated with the 1D kinetic code. The hot spot power evolution is then estimated by (3):

$$Pmax(t) = FQ * P(t) \qquad (3)$$

Design assumptions:

In order to compare thermal results such as fuel and clad temperature and stored energy to criteria, project penalties are added on FQ and the

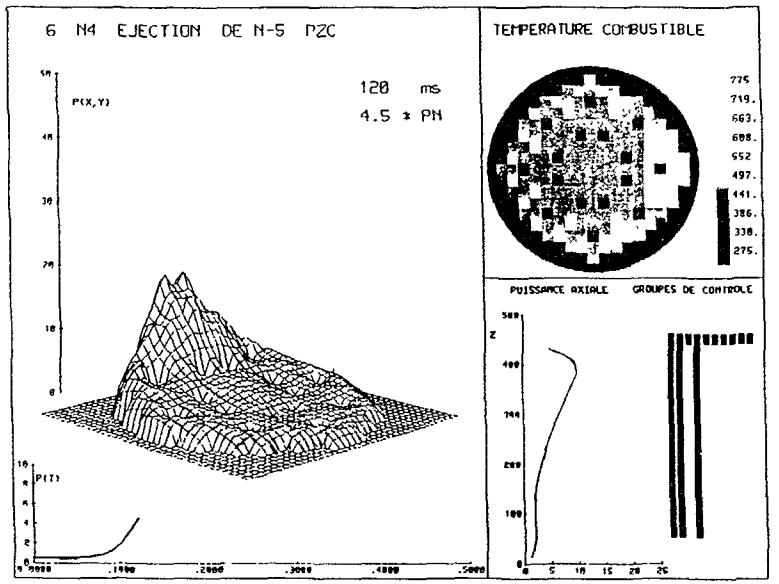

Figure 1 : Sample of screen display issued by CESAR post-processor.

1D kinetic parameters (Doppler coefficient, delayed neutron fraction, rod worth and rod ejection time).
Penalizing axial xenon distributions are used in 3D and 1D calculations in order to maximize axial peaking factor (Fz) and rod worth.
All 3D and 1D calculations are made with the same assumptions.

CALCULATIONS AND RESULTS

Table I summarizes the sample of 9 cases presented here.Cases 1 to 5 present the higher level of realism. They are selected on N4 and P4 plants at different power level for peripheral rods (fig 2). Cases 1,2 and 5 are transients used as design basis of standard safety analysis.

The next three cases, in table I, allow to appreciate the consequences on transient of the position of ejected rod; in these cases, rods have the same worth, but they are inserted at different locations. The last case, the most hypothetic one, shows the behaviour of the reactor in presence of a reactivity insertion of very high magnitude.

Table II summarises the main thermal results selected on P4 cases, obtained with both 3D and synthesis methods. Thermal parameters of interest are the temperature in the center of the pellet (Tf max), the clad temperature (Tc max) and energy stored for the fuel pellet at the hot spot.

TABLE I

Presentation and summarize of studied cases

CASE NUMBER	PLANT	INITIAL POWER LEVEL % N P	INITIAL ROD INSERTION %	ROD POSITION	ROD WORTH pcm
1	N4	100	D 55 % IN	J3	455
2	N4	0	D,C,B resp. at 83,65,15 % IN	N5	770
3	P4	100	R 30 % IN	H14	200
4	P4	40	R,N1,G1,G2 30,60,100,100	H14	520
5	P4	0	R,N1,N2,G1,G2 30,75,15,100,100	D12	670
6	P4	100	R 100 % IN	H14	750
7	P4	100	R 100 % IN	E11	750
8	P4	100	R 100 % IN	H8	750
9	N4	0	ALL RODS IN	J3+H2	4300

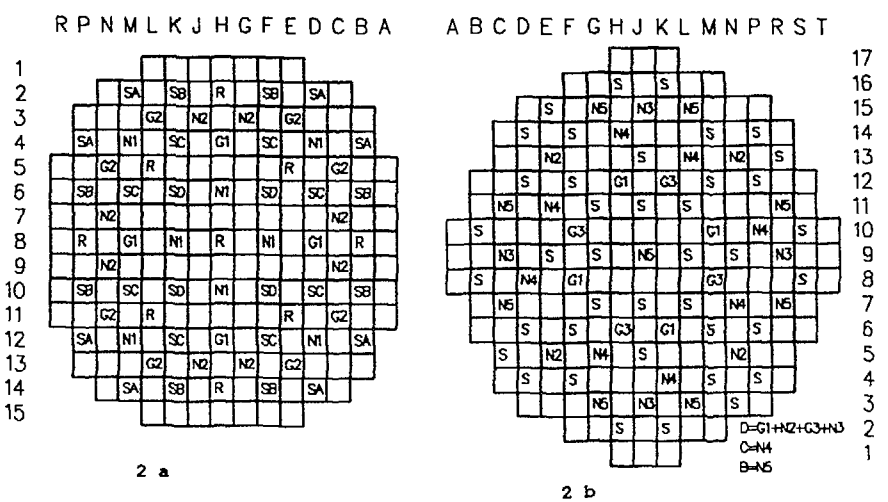

Figure 2 Control rod pattern on P4 (2 a) and N4 (2 b) plants

TABLE II

Comparative thermal results on P4 plant

Case 3	3D	Synthesis	Case 4	3D	Synthesis
Tf max (C)	2100	2400	Tf max (C)	2110	2480
Tc max (C)	820	855	Tc max (C)	990	1190
Stored En J/g	440	520	Stored En J/g	490	610

Case 5	3D	Synthesis	Case 6	3D	Synthesis
Tf max (C)	750	1070	Tf max (C)	2660	3630
Tc max (C)	410	460	Tc max (C)	1080	1430
Stored En J/g	170	230	Stored En J/g	630	1120

These parameters are to be compared with safety criteria related to rupture threshold of fuel rods They are based mainly on results of SPERT experiment [ref 1] Criteria used in FRAMATOME are
- Fuel enthalpy at hot spot should be lower than 940 J/g for fresh fuel and 840 J/g for spent fuel
- Fuel centerline melting is limited to 10% of pellet volume at hot spot
- Clad temperature should not exceed 1480 C

Table III shows up, that in cases 3 and 4, the pellet center temperature approach the limit (2600 C) with synthesis method The use of a 3D model leads to release of about 15% on margins In case 6, 3D fuel temperature is close to the limit when synthesis method exceeds it of 36%

Moreover, these results indicate that the extra-margin due to the synthesis method are strongly related to the ejected rod worth 14% for 200 pcm to 36% for 750 pcm

ANALYSIS AND DISCUSSION OF RESULTS

In this paragraph we analyse the origin of the conservatism in the synthesis method for rod ejection analysis Two issues are to be studied margins on hot peaking factor and on mean core power calculation

Nuclear power behaviour

Core power behaviour is approximately the same in all cases However, the maximum core power can be reached between 110 to 140 ms depending on the starting fuel temperature (300 to 800 C) and its value depends on the ejected rod worth Figure 3 shows, for case 2, a large difference in 3D and 1D calculated nuclear power peak Conservatism is here very large (about 100%)

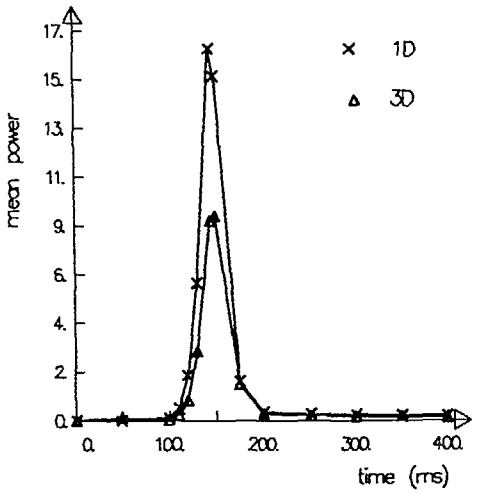

Figure 3: Comparison between 3D and 1D calculated mean power for an ejected rod worth of 770 pcm (case 2 of table I).

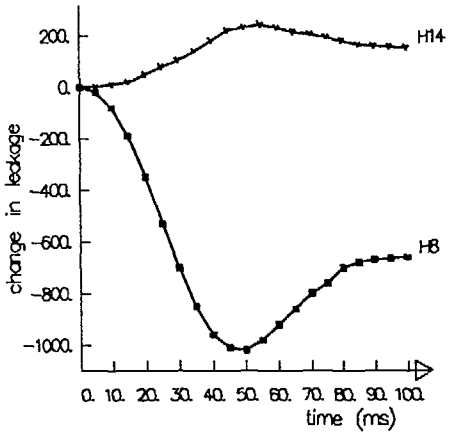

Figure 4: Change in radial buckling in pcm induced by ejection of H14 and H8 with ajusted worths of 750 pcm.

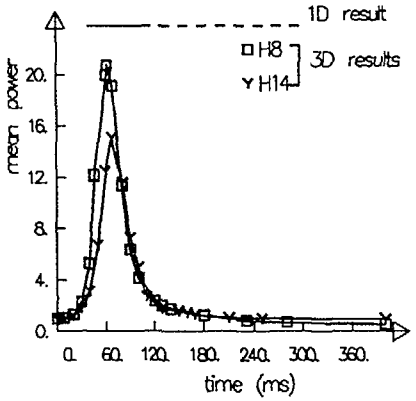

Figure 5: Mean core power change in pcm induced by ejection of H14 and H8 with ajusted worths of 750 pcm.

This conservatism increases as a function of control rod worth. Figure 4 shows the change in radial buckling, expressed in pcm (1 pcm= 1.E-5), produced by the rod ejection. One can see that the ejection of peripheral rod, like H14 (see figure 2), leads to a small amount of neutron leakage when central rod ejection induces a fall in leakage corresponding to a reactivity excursion of about 1000 pcm. This explains the most important part of the deviation between 3D and 1D calculations as shown on figure 5.

Hot peaking factor:

In synthesis method the hot spot factor is calculated with frozen feedback in both 1D and 2D codes,so that flux flattening due to Doppler effect is not taken into account. Consequently conservatism on FQ can reach 50% as it is shown on figure 6.Moreover in this approach the decrease of FQ according to fuel heatening is not considered since the maximum value is imposed from the peak time to the scram.

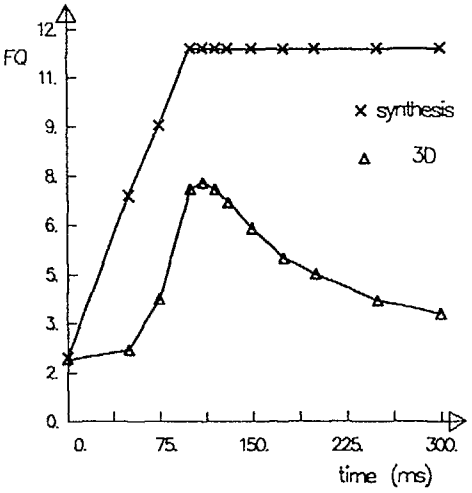

Figure 6: Comparison between hot peaking factor 3D calculated and those used in synthesis method.

Effects of partial initial insertion:

1D rod worth are ajusted on 2D caculations which supposes a fully inserted rod. With partially inserted rod, 1D and 3D worth results are different: in cases 1 and 2, 3D rod worth static results are respectively 455 and 550 pcm , whereas 1D results give 540 and 600 pcm. This difference is explained by the fact that the 3D axial assembly flux is more shifted toward the bottom than the 1D average axial core flux. Associated conservatism can reach 100% (Figure 7).

Simultaneous ejection of two rods:

Now let's see what happens when the reactor is driven to extreme eventuality: the simultaneous ejection of two adjacent rods, both of which belong to control banks of high efficency. It's not a very realistic situation because the core is considered at zero power with all control and safety banks inserted, as if a scram had just occured. However the core is supposed to be critical.

This accident is much more rapid and violent than in previous cases. Prompt criticality is attained after only 30 ms, when the rods are 30% withdrawn.

The power peak is attained at 40 ms.Locally,the power hits 3000 times its nominal value. Power immediatly falls, thanks to the Doppler effect, but built-in reactivity of the two rods is sufficient to bring up the core prompt critical again. This explains, what it is shown on figure 8. Note that maximum fuel temperature reachs 2670 C in H2 assembly. The fuel melting criteria is slightly exceeded but clad temperature limit, in this case is violated. Stored energy reachs 840 J/g at 120 ms.

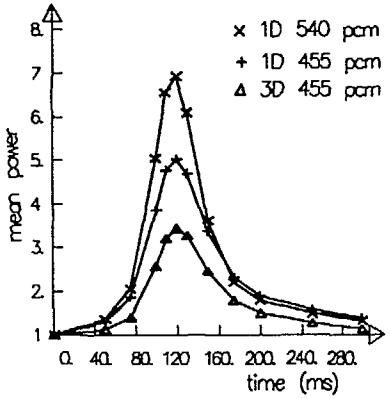

Figure 7: Dependance of power evolution with 1D and 3D worth result.

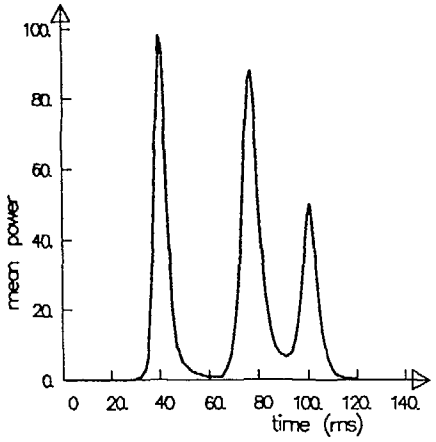

Figure 8. Mean core power evolution for two ejected rods of 4300 pcm.

CONCLUSION

The rod ejection analyses presented here shows that:

- the transients in the safety report were up to now very conservatively analysed.
- out of design basis transients , such as two simultaneous rods ejection do not lead to very extreme conditions on the fuel rods , as could be supposed .

REFERENCE

1. T.G. TAXELIUS and IDAHO NUCLEAR CORPORATION, "SPERT project - annual report 1968-1969 ", Reactors Technology, TID 4500 (1970).

VALIDATION OF A METHOD FOR HCLWR FUEL ASSEMBLY CALCULATION

V. ISHIDA, N.E. PATIÑO,
M.J. ABBATE, M.M. SBAFFONI
Centro Atómico Bariloche,
Comisión Nacional de Energía Atómica,
San Carlos de Bariloche, Argentina

Abstract

The present work involves a validation of the nuclear data processing and calculational system, presently used at Centro Atómico Bariloche (CAB), for its application to High Conversion Reactors (HCR) fuel assembly calculations.

The chosen reference problem was a Montecarlo High Conversion Boiling Water Reactor (HCBWR) numerical benchmark.

Several cases were calculated considering controlled and uncontrolled situations, in cold and hot conditions and as a function of void fractions.

Comparisons were performed on multiplication factors and reaction rates, and on power maps and peaking factors.

An analysis on the number of typical cells, approximations (Sn or diffusion), 1D or 2D representations, and spatial mesh employed, was also done in order to show their influence on the parameters values and to select the best combinations to be used for this type of problems.

1. INTRODUCTION

The treatment of High Conversion Light Water Reactor (HCLWR) assemblies is not a standard case from the point of view of the methods and calculational tools to be used. It is not valid that the procedures utilized in thermal and fast reactors can be directly applied; instead, careful validations using suitable benchmarks must be carried out.

But in face of the lack of experimental results, theoretical or numerical ones must be considered, like those obtained with the most refined methods, i.e. Montecarlo calculations.

The present work involves the validation of a nuclear data processing and calculational system implemented at CAB /1/, and based on the ENDF/B-IV library, the AMPX-II code system and XSDRNPM and DOT3.5-CAB /2/ codes, in order to be used in HCLWR cell and fuel assembly calculations.

2. BENCHMARK DESCRIPTION

The problem selected as numerical benchmark was a Montecarlo calculation, performed with the MERIT MC code (MC), of a high conversion BWR (HCBWR) assembly reported in /3/. In this reference, results of calculations with the HELIOS.HX (H.HX) code, specially developed for this type of reactors, are also available.

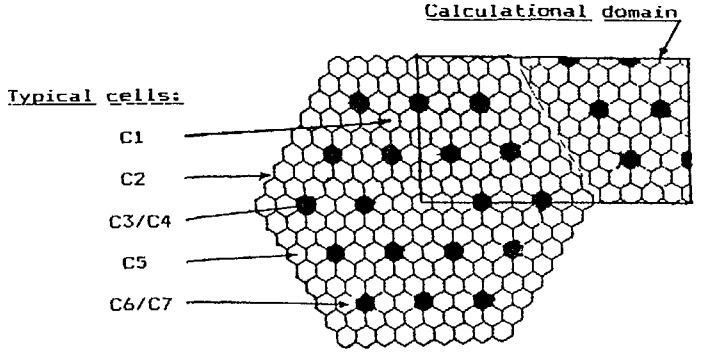

FIGURE 1: Geometrical configuration of the fuel assembly

TABLE I
Fuel assembly specifications

Assembly pitch:	22.40 cm.
Fuel rod diameter:	1.21 cm.
Cladding thickness:	0.06 cm.
Fuel rod pitch:	1.47 cm.
Rod clearance:	0.26 cm.
Cladding-to-channel distance:	0.24 cm.
Channel box wall thickness:	0.13 cm.
Moderator to fuel volume ratio (Vm/Vf):	1.03
Fuel composition:	mixed oxide

The fuel assembly comprises 199 fuel cells and 18 control rods; its geometrical shape and other data are included in figure 1 and table I, /3/.

The fuel density was assumed to be 10.34 g/cm**3, typical of MOX fuels, and the B4C density was taken to be 1.844 g/cm**3.

It must be pointed out that this work also includes a validation of the working libraries used because, in the present case, the group constants were completely derived from the ENDF/B-IV library, while in the benchmark, they were obtained from the ENDF/B-V library for the heavy nuclides and from the ENDF/B-IV for the remainder.

3. CALCULATIONAL METHODOLOGY

The methodology includes the preparation of the suitable group constants, that requires two steps, and the calculations of the assembly:

3.1. Generation of the working libraries:

Two working libraries were prepared with AMPX-II system: cold library, at 300 K, and hot library, at 900 K for fuel and 560 K for the remainder; they were obtained in a 108 groups structure, derived from the WIMS 69 group energy mesh.

The resonance and heterogeneities treatments used, were different from the reference case. Here, Nordheim's method was employed (NITAWL module) together with a specially defined Dancoff factor /4/. In the reference case, an improved intermediate resonance and hyperfine treatments were applied; the Dancoff factor was calculated taking into account all the rods seen by the considered cell /5/.

It must be noted that the corresponding libraries were obtained at 0, 40 and 85% of void. It was verified that to use only zero void data together with a density factor is not acceptable, specially, in high void fraction cases.

3.2. Calculation of cell-homogenized libraries:

In this step, the "typical cell" approach was followed, and seven cells were defined and considered:

-C1: fuel cell in an infinite array of equal cells.
-C2: outer water gap, including the channel box wall.
-C3: water cell (empty guide tube) surrounded by 6 fuel cells, C1.
-C4: control rod cell, surrounded by 6 C1 cells.
-C5: fuel cell surrounded by 4 C1 cells and external water gap, C2.
-C6: fuel cell surrounded by 5 C1 cells and 1 of water, C3.
-C7: fuel cell surrounded by 5 C1 cells and 1 of control, C4.

These macrocell arrangements permit to take into account the coupling effect among the cell to be homogenized and its neighbours. Each inner cell is explicitly modelled in 3 zones, and the outer region is assumed as homogeneous, employing the group constants already homogenized in previous steps.

The flux was obtained by an Sn transport 1D calculation (XSDRNPM code in S4-P0 approximations) and was used for collapsing to 20 groups and homogenizing the cross-sections of the inner cell.

3.3. Fuel assembly calculation:

At the fuel assembly level, the following cases were calculated for considering normal dependence on temperature, control rods and void:

-uncontrolled and controlled cold fuel element.
-uncontrolled hot fuel element at 0, 40 and 85% void fractions.
-controlled hot fuel element at 40% void fraction.

As main results, integral parameters like multiplication factors and reaction rates, and local ones, like power maps and peaking factors were calculated. The methods employed in the calculations were transport with discrete ordinates (Sn) and diffusion theory.

For 2D calculations, the DOT3.5-CAB code was used, considering an X-Y representation of the fuel assembly. The geometry is also shown in figure 1; two quarters of the fuel element were included in the calculational domain with reflective boundary conditions.

In 1D geometry, the fuel assembly was cylindricalized and the XSDRNPM code was used for the calculations.

With an auxiliary module (POSTDOT) power maps and peaking factors were derived.

4. RESULTS

4.1. Comparisons with reference results:

The results presented here were obtained with 2D transport calculations in S4-P0 approximation.

Table II shows the k-infinite calculated with MC, together with their differences (Δk *100) with the results of this work and

TABLE II
Calculated k-infinite and H.HX values, compared with benchmark

Cases	Benchmark results(MC)	Differences (%) (H.HX-MC)	(This work-MC)
a.Uncontrolled			
Cold	1.2074	- 0.58	- 1.03
Hot, 0% void.	1.1442	- 0.62	- 1.13
Hot, 40% void.	1.1126	- 0.52	- 0.74
Hot, 85% void.	1.0918	+ 0.19	+ 0.53
b.Controlled			
Cold	0.9602	+ 0.21	- 1.18
Hot, 40% void.	0.8589	+ 0.54	- 0.08

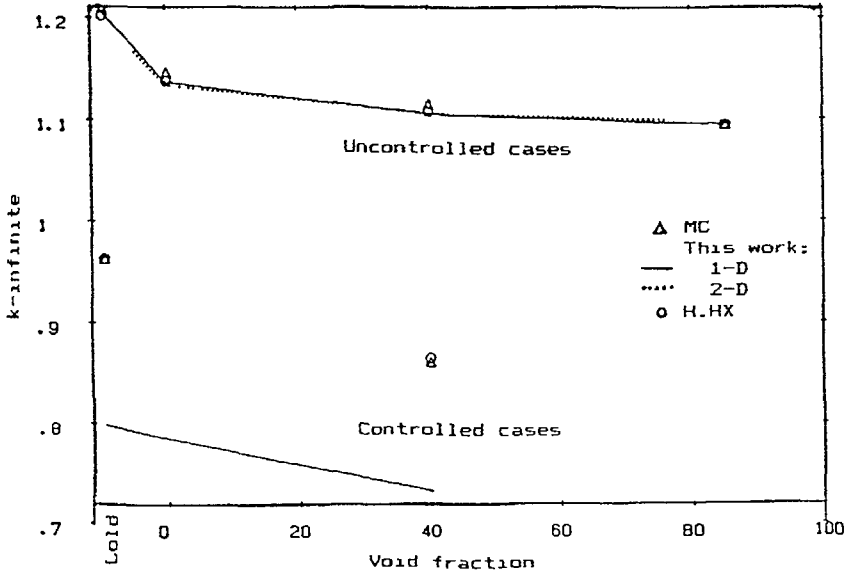

FIGURE 2: Calculated and reported k-infinite values as a function of void fraction

H.HX. As it can be seen there, a good agreement is obtained for all the cases between these calculations and MC and H.HX ones (of the order of 1000 pcm in Δk or better). See also figure 2.

Table III shows control rod and void reactivity worths, the general agreement is also very good, better than 0.5% , although there is a difference of approximately 1% in the transition between 40 and 85% void, which shows a smaller slope than the reported values. This behaviour can be observed also with H.HX

TABLE III
Comparison of reactivity worths

Cases	Benchmark results(MC)	Differences (%Δk) (H.HX-MC)	(This work-MC)
a. Of control rods			
Cold	24.27	- 0.78	+ 0.15
Hot, 40% void.	25.37	- 1.08	- 0.66
b. Of moderator void, uncontrolled cases			
Transition:			
-from cold to 0%	- 6.32	- 0.05	- 0 10
-from 0 to 40%	- 3 16	+ 0.09	+ 0.39
-from 40 to 85%	- 2.08	+ 0.73	+ 1.27

Figure 3 shows the power peaking factors (fission rates) as a function of void fraction. The values are contained within the standard deviation of MC results for the uncontrolled cases; in the controlled state, the discrepancies are somewhat larger.

Figures 4 and 5 present the percentual differences in power distributions at different stages for 1/12 of the fuel element, showing a very good agreement with the reference results.

The contribution of main individual isotopes to the variation of k-infinite between two voidage states was calculated (S4P0-1D) and compared in accordance with the definition of the reference (k=Production/Absorption). The results are shown in table IV.

This test is related directly with the reaction rates and can give information about cross-sections. The discrepancies in the transition from cold to 0% void are reasonable; it can be noted that big deviations are reported with H.HX for Pu240 and U238. In the transition from 0 to 40% void, a 9% deviation was found in U238 and a bigger difference in Pu241 (the same that with H.HX). In the last part (40 to 85% void), where a smaller slope was found, the reactivity contributions of U238 and Pu240 show a large discrepancy with MC results, although they cancel each other. In this case, most of the contributions show positive differences, causing the mentioned less negative slope. And, the results for Pu239, Pu241 and net are also deviated more than 10%, similar to H.HX.

4.2 Sensitivity to the scattering order and quadratures

In order to verify the adequacy of the P0 approximation, some cases were recalculated with the scattering matrices expanded up to order P1. In the controlled cold assembly a difference of approximately 1% exists between P0 and P1 results, and in the uncontrolled hot 0% void case the difference is negligible.

Changes in the order of quadrature from S4 to S10 do not produce signicant differences in the multiplication factors

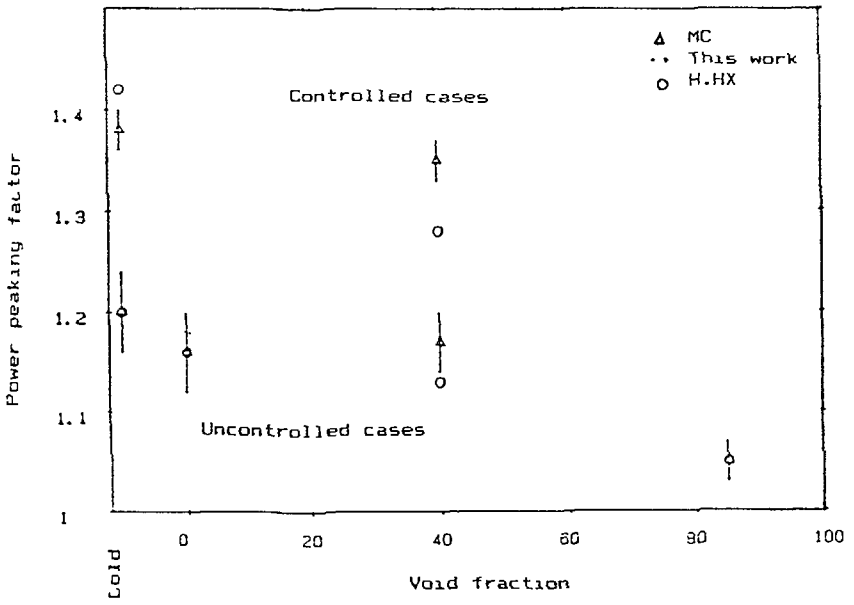

FIGURE 3: Power peaking factors

TABLE IV

Contribution of individual isotopes to the variation of k-infinite (differences related to MC results)

Isotope	Transition: Cold to 0% void (1)	Cold to 0% void (2)	0 to 40% (1)	0 to 40% (2)	40 to 85% (1)	40 to 85% (2)
U238	- 33	- 15	+ 0	- 31	+ 35	- 285
Pu239	+ 2	- 11	+ 1	- 2	+ 23	+ 32
Pu240	+ 30	- 11	- 7	+ 13	- 3	+ 330
Pu241	- 1	- 1	+ 7	+ 16	+ 5	- 13
Others	- 3	- 11	+ 8	+ 3	+ 13	+ 33
Net	- 5	- 49	+ 9	- 1	+ 73	+ 97

Notes: (1). (Δk(H.HX) - Δk(MC))
(2) (Δk(This work) - Δk(MC))

where $\Delta k = (\Delta \text{Production} - k\text{-infinite} * \Delta \text{Absorption}) * 10^{-4}$

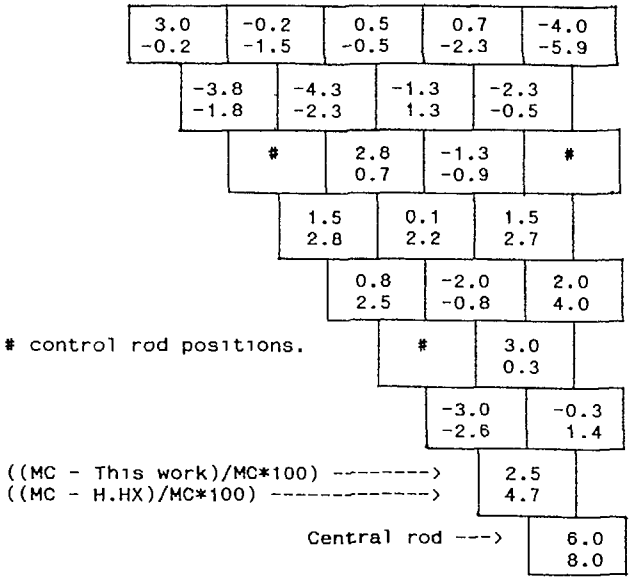

FIGURE 4: Power map. Case: uncontrolled, 0 % void

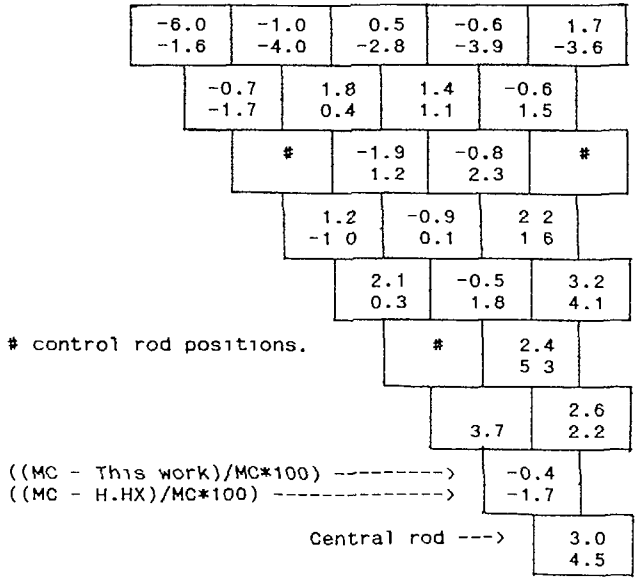

FIGURE 5: Power map. Case controlled 40 % void

TABLE V
Sensitivity with geometrical representation and theory used

Parameter and cases	Calculational Method: One-dimensional S4-P0	One-dimensional Diffusion(1)	Two-dimensional Diffusion	Two-dimensional Diffusion(2)
1.k-infinite				
a.Uncontrolled				
Cold	+ 0.68	+ 0.75	- 0.16	- 0.23
Hot, 0% void	+ 0.53	+ 0.44	- 0.01	N/C
Hot, 40% void	+ 0.10	+ 0.03	- 0.02	- 0.10
Hot, 85% void	- 0.30	- 0.32	+ 0.20	+ 0.12
b.Controlled				
Cold	N/C	-14.04	+ 0.30	N/C
Hot, 40% void	-12.63	-13.14	- 0.42	- 0.56
2.Reactivity worth of control rods (%)				
Cold	N/C	+14.79	- 0.46	N/C
Hot, 40% void	+12.65	+13.17	+ 0.40	+ 0.46
3.Reactivity worth of moderator void (%)				
Transition from:				
Cold to 0%	- 0.15	- 0.31	+ 0.15	N/C
0 to 40%	- 0.43	- 0.41	- 0.01	N/C
40 to 85%	- 0.40	- 0.35	+ 0.22	+ 0.22

Notes: (1). no changes between considering C5 type cell or not.
(2): diffusion calculation considering C1 type cell instead C5 type.
N/C: not calculated.

4.3.Evaluation of other approximations:
To determine the crudest approximations that can be used for design purposes, which could imply important reductions in running times without loosing the accuracy of the results, the following aproximations were also tried:

a. 2D diffusion and 1D Sn and diffusion calculations:
Table V shows the differences of the various approximations employed for the calculation of fuel assembly, referred to the S4-P0 bidimensional results.
If only the k-infinite values are taken into account, 1D results did not show differences between Sn or diffusion cases. Both, in uncontrolled cases, agree reasonably well (differences lower than 1%), but are highly inadequate for the controlled ones. This is due to the smearing of the control rods in concentric rings that overestimates their reactivity worth by more than 10% . The k-infinite results, together with the 2D ones, are shown in figure 2.
On the other hand, a 2D diffusion calculation showed to be enough for all the uncontrolled cases, but for the controlled configurations, even if that suffices to get a first-order result, better values are obtained using discrete ordinates. Of course the use of diffusion theory reduces the running times, in this case by a factor of twenty.

From the fluxes point of view very important differences were found between diffusion and Sn.
In the one-dimensional calculations the power maps and power peaking factors are not good enough.

b. Reduction in the number of typical cells considered:
Table V also shows in the last column the effect of eliminating the C5 type cell (fuel surrounded by 4 fuel cells and water gap), and replacing its group constants by those of C1 type cell. The changes in k-infinite are negligible, (not larger than 150 pcm) for controlled and uncontrolled cases, for 2D calculations and, negligible for 1D ones.

c. Relaxation of the spatial mesh employed in the calculations.
A very fine and detailed spatial discretization was used, (approximately 700 intervals) with a precise description of the water gap. However, if the actual geometry is slightly modified in order to align both quarters of fuel element from the point of view of the spatial grid (figure 1), this could imply a significant reduction in the number of intervals (approximately 250).
These changes reduced the running times by a factor of two, with the following effects on the results. k-infinite was modified by less than 100 pcm and the discrepancies in the power maps were not important, but the fluxes were not satisfactory because they do not represent the depletion in the water rod position and the condensed group constants for reactor calculations showed big differences; moreover, there were also discrepancies with peaking factors.

4.4.Group constants for reactor calculation:
As a last test of the methodology, group constants for reactor calculation were prepared condensing, the previous 20 groups cross sections, to 8 energy groups. Those obtained with weighting spectra calculated by diffusion showed big differences, specially, at thermal energies; the same was found in the case of Sn 1D spectra.

5.CONCLUSIONS

As summary, it can be said that all the parameters here calculated are in satisfactory agreement with benchmark results (MC) and also with H.HX results.
In more detail:
- k-infinite:
For the uncontrolled element the discrepancies are at most +/- 1 % in Δk with the MC code and much lower with the H.HX, in both one- and bidimensional cases, which is a very good agreement with the reference.
For the controlled cases, there is a very good agreement with the bidimensional calculation, while one-dimensional one is not adequate at all.
- Void coefficient:
It has shown to be less negative than MC results in the transition from 40 to 85% of voidage, due to a cancellation of a very negative contribution of U238 and a positive one of Pu240. The differences are lower if compared with H.HX results, which have the same tendencies.
- Power maps:
They have an excellent agreement with the reference calculations, with discrepancies very similar to those of H.HX.

- Power peaking factors:
They are within the statistical deviations of MC and quite close to H.HX in bidimensional calculations for both controlled and uncontrolled cases.

As conclusions, and to be applied to future work, it can be said that:
- Sn (transport), 2D calculations is the most recommendable method.
- even though, a 2D diffusion calculation could be accurate enough and cost effective, from the computational point of view, for all the uncontrolled cases; and, for the controlled cases, they can give first order results.
- S4 approximation showed to be good enough; and, it can be inferred that a small improvement in the results could be obtained if anisotropy (P1) is considered.
- high sensitivity with the weighting spectra was found for the few groups cross sections, supporting even more the first conclusion.
- it is not necessary to explicitly consider the coupling effect in calculating the group constants of the cells of the border, at least if the channel between elements is of the size of the present one or lower; this result can be extrapolated to HCPWR fuel element calculation, where these channels do not exist.
- the water gap must be accurately represented by the spatial grid to obtain adecquate weighting spectra.
- as soon as new libraries become worldwide available, it is convenient to check (or change) the data of the main heavy isotopes.
- as the presented and H.HX systems results, on reaction rates, showed similar discrepancies with MC, in spite of using different libraries, specially in the 40% void case, maybe this MC results should be checked.

Finally, the whole system, which was previously tested with the PROTEUS cell /1/, has also proved to be completely acceptable from the point of view of fuel elements calculations. Further tests will be done as soon as new fuel element benchmarks become available.

ACKNOWLEDGEMENTS

The authors deeply appreciate the contributions of P.C.Florido and S.E.Gómez, members of the research group.
This work was partially supported by the UNDP and the IAEA through projects ARG/78/020 and ARG/89/012 'Nuclear Engineering .

REFERENCES

/1/ M.J.Abbate et al., "Progress report on the research activities on high conversion reactors at Centro Atomico Bariloche - Argentina", Technical Committee Meeting on Technical and Economical Aspects of High Converters, Nuremberg, FRG (March 1990).

/2/ M.M.Sbaffoni and M.J.Abbate, 'DOT3.5-CAB. A new version of DOT3.5 code", CNEA/NT 18/85 (1985), sent to RSIC and NEA data bank (1985).

/3/ M.Yamamoto et al, "Validation of HELIOS.HX code for high conversion light water reactor lattice analysis", Nucl. Technol., 80, 240 (1988).

/4/ N.E.Patiño, M.J.Abbate and M.M.Sbaffoni, 'Evaluation of some resonance self-shielding procedures employed in high conversion light water reactor design", PHYSOR conference, Marseille, France, (April 1990).

/5/ Y.Ishiguro and K.Okumura, 'Pancake core high conversion LWR concept", Nucl. Technol., 84, 331 (1989).

REACTOR CALCULATIONS WITH A MULTIPARAMETERS LIBRARY

V. BRUN, B. CHANARON, J.M. DUBOIS
Commissariat à l'énergie atomique,
Centre d'études nucléaires de Cadarache,
Saint-Paul-lez-Durance, France

Abstract

In this paper we propose an approach to compute multi-parameter cross sections files. This is the first step of our programme. Our goal consists in improving the calculation of a complete reactor cycle taking into account feedback effects. This reactor is the french St-Laurent-B1 reactor which is composed of a UO2 zone and a MOX zone. Assembly calculations will be performed with the APOLLO-1 transport code. Core calculation will be performed with the CRONOS-2 diffusion code which determines the evolution of local isotopic concentrations. We are therefore looking for a library which contains microscopic two groups cross sections for all heavy isotopes and some fission products.

We evaluate in this paper the effects of the approximations only by cell calculations. The good agreement between all the results proves the validity of the approach. These results , nevertheless, need to be confirmed by a more global analysis of the experimental power distribution and reactivity coefficients of the complete core.

I METHOD

Let us consider a small zone of a fuel assembly. It is characterized, at the current moment, by four main parameters : TM=moderator temperature, TC=fuel temperature, CB=boron concentration, CX=xenon concentration. This zone evolves during the cycle along a certain path in the four dimensional space (TM,TC,CB,CX). The local microscopic cross sections at burnup B0 are a functional of this path. It is obviously not possible to store them for several pathes because of the very large quantity of datas.

Thus we will perform depletion calculation along a reference path, which is a straight line at a reference set of parameters (R), and then we calculate at burnup B0 cross sections at the current set of parameters. (In the core calculation, the correct path will be of course followed.) This is the basic approximation. We do not know any alternative way for this.

Let us now describe the complete method :

1) Choice of the parameters:
There are -a priori- 4 not negligeable parameters TM,TC,CB and CX.

TM and TC are necessary to calculate thermal-hydraulic feedback effects.

The effect of boron concentration on neutron spectrum and on two groups cross section of some isotopes is not negligeable. The difference between calculations performed with a boron free library and a 500 ppm library is more than 100 pcm.

We have shown that neglecting the influence of xenon concentration on microscopic cross sections is a good assumption. The reactivity errors are < 5 pcm.

In conclusion we will say that microscopic cross sections are a function of (TM,TC,CB).

2) Discretization of the parameters

It is obviously not possible to represent a continuous set. Cross sections are calculated at discrete values. For fuel temperature they are approximately proportional to the square root of TC. For moderator temperature they are approximately proportional to TM. Between these values cross sections are linearly interpolated. For moderator it is an interpolation with moderator density.

3) Reconstructing fluxes

At this point the computation time of multiparameter library is still to large: For the 1/8 of a 17*17 PWR assembly, the computation time with the EURYDICE module of APOLLO code needs 200 s. Let us compute the assembly depletion between 0 and 55 GWD/T using a burnup interval equal to 4GWD/T. We have 14 burnup values. If we consider for each burnup 4 moderator temperatures, 3 boron concentrations and 4 fuel temperatures we will perform 4.4.3.14=672 calculations. The global computation time is 37 hours. This time should be multiplied by the number of different types of fuel assemblies - 6 in our reactor - .The computation time becomes : 222 hours.

In order to simplify further calculations, fluxes are actually calculated at certain nodes as shown in figure 1 and reconstructed at the others nodes.(The CB axis is not represented in this figure). (i,j,k) denotes the set of the 3 discretized parameters (TM,TC,CB) and (ir,jr,kr) or (R) the same object in the particular case of the reference state. For the new assembly and the 55 GWD/T burned assembly, fluxes at the general parameter set are derived from the actually calculated fluxes by using the formula :

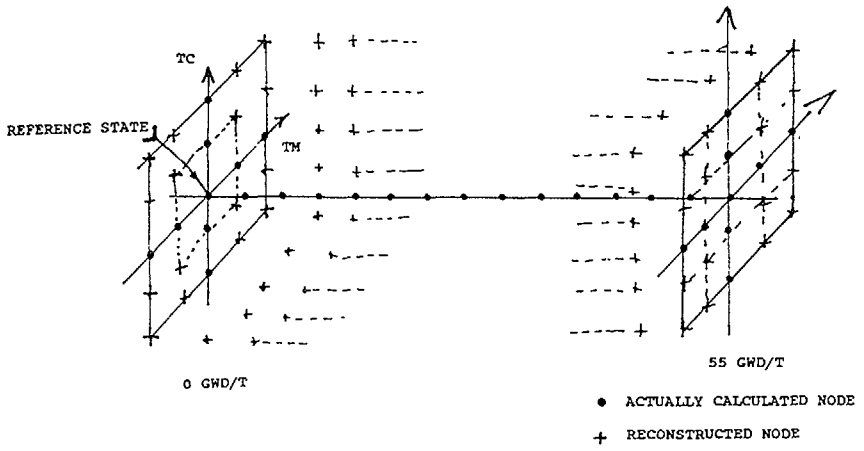

FIG. 1. Reconstructing fluxes.

$$f(i,j,k)=f(R)*\left(f(ir,jr,k)/f(R)\right)*\left(f(ir,j,kr)/f(R)\right)*\left(f(i,jr,kr)/f(R)\right)$$

In other words we assume that the ratios p(TM-1)/p(TM-2) do not depend on TC and CB, and in the same way for the other ratios. This is the "cross wise" approximation.

We have now to reconstruct fluxes at the general point (i,j,k) for all burnups. This is done by assuming that flux ratios depend linearly on the burnup. That is:

ri=f(i,j,k)/f(R) at 0 GWD/T
rf=f(i,j,k)/f(R) at 55 GWD/T
rl=f(i,j,k)/f(R) at burnup B

We assume that :

rl= ri . (55-B)/(55-0) + rf . (B-0)/(55-0)

Using this procedure the number of actually calculated nodes is 28. Thus the computation time is divided by the factor 28 /672. It becomes now realistic.

II NUMERICAL RESULTS

2-1

Let us summarize the approximations:

- 1) Isotopic concentrations are calculated at the reference state. (basic approximation)
The reference state is defined by:
TM=306°C,TC=650°C,CB=500 ppm

2) Discretization of parameters:

The values that we have chosen are:
TM=220°C,286,306,324,343
TC=220°C,286,650,1100,1700,2500
CB=0 ppm,500,1500

3) "Cross wise" approximation

4) Reconstuction of fluxes at intermediate burnups

We have to check the validity of these approximations. Our method to do this consists in elaborating a multi-parameter library of a simple cell as shown in part I, and in comparing calculations using this library with reference calculations of the same cell performed with APOLLO-1. This cell is a typical PWR cell with U5 enrichment = 2.5% , or a MOX cell with PU enrichment = 5%. These cell calculations are of course very fast. Since the errors related to boron are smaller than those related to temperature we will examine principaly the case of temperatures.

2-2

- Basic approximation : At a given set of parameters (TM,TC,CB) we compare two different cell calculations.

a) The first one, which is the reference is a direct depletion calculation at (TM,TC,CB).

b) The second one is also a depletion calculation at (TM,TC,CB), but uses the multiparameter library described in part 2-1. This work has been achieved for the 4 following sets of parameters.

TC=743°C TM=306°C
TC=561°C TM=306°C
TC=650°C TM=286°C
TC=650°C TM=343°C

The cross sections of the a) and b) models are compared in table I at 48 GWD/T. The isotopic concentrations of the models at the same burnup are compared in table II for UO2 cell and table III for MOX cell. One can see that the greatest relative difference between these models is less than 3% for concentrations and 4% for cross sections.

-Discretization of parameters: We consider three modera temperatures (TM=286°C,306,343) and three fuel temperatures (286°C,650,1000). Cross sections at intermediate temperatures are linearly interpolated. The differences between correct and interpolated cross sections at the middles of both TM intervals and both TC intervals are summarized in table IV for UO2 cell. The related reactivity differences are presented in table V.

TABLE I
BASIC APPROXIMATION
THERMAL CROSS SECTION ERRORS AT 48 GWD/T (%)

Isotope	a2 (UO2)	f2 (UO2)	a2 (MOX)	f2 (MOX)
U235	2,80	2,80	4,03	4,00
U238	2,49	-	3,48	-
PU38	3,37	3,26	4,61	4,47
PU39	1,34	1,46	3,53	3,55
PU40	1,16	0,58	1,82	1,17
PU41	2,44	2,56	4,23	4,31
PU42	2,22	2,55	3,20	3,63
XE35	3,49	-	4,80	-
SM49	3,22	-	4,54	-

TABLE II
BASIC APPROXIMATION
UO2 CELL : CONCENTRATION ERRORS AT 48 GWD/T (%)

Isotope	TC = 743, TM = 306	TC = 650, TM = 343
U235	- 0,41	- 1,99
U236	0,01	0,18
U238	3.10^{-3}	2.10^{-2}
NP37	0,03	0,16
PU38	- 0,10	- 2,21
PU39	- 0,27	- 1,48
PU40	- 0,20	- 2,15
PU41	- 0,24	- 1,23
PU42	0,05	1,00
AM41	- 0,29	- 0,45
AM42	- 0,49	- 3,15
CM42	- 0,12	- 0,49
XE35	- 0,36	- 2,88
SM49	1,02	- 2,33

TABLE III
BASIC APPROXIMATION
MOX CELL : CONCENTRATIONS ERRORS AT 48 GWD/T (%)

Isotope	TC = 743, TM = 306	TC = 650 TM = 343
U235	- 0,08	- 0,36
U236	0,03	0,11
U238	4.10^{-3}	2.10^{-2}
NP37	- 0,03	- 0,36
PU38	- 0,07	- 0,65
PU39	- 0,24	- 1,14
PU40	- 0,05	0,27
PU41	- 0,10	- 0,68
PU42	0,11	0,83
AM41	- 0,08	- 0,21
AM42	- 0,25	- 2,18
CM42	- 0,02	- 0,59
XE35	- 0,20	- 1,49
SM49	0,48	- 1,79

TABLE IV
TEMPERATURE INTERPOLATION (O GWD/T)
UO2 CELL : CROSS SECTION ERRORS (%)

	a1	a2	f1	f2
U235	0.027	0,18	0.030	0,19
U238	0.038	0,18	0.044	
PU239	0.028	0,13	0.028	0,10
PU240	0.075	0,10	0.025	
PU241	0.030	0.044	0.029	0.023
Bore		0,20		
XE		0,21		
H2O		0,19		

TABLE V
TEMPERATURE INTERPOLATION
UO2 CELL : REACTIVITY ERRORS

TC TM	O GWD/T	55 GWD/T
468 REF	+ 24 (4.8)	41 (6)
825 REF	- 13 (- 3)	5 (- 1,8)
REF 296	- 6 (- 5,3)	+ 3 (-4,5)
REF 324	1 (- 1,5)	- 15 (-4,4)

- First number : reactivity error (pcm) = eps
- number in parenthesis : relative error on feedback effect = eps / ((d /dT).(T-TREF))

TABLE VI
CROSS WISE APPROXIMATION
REACTIVITY ERRORS AT 0 GWD/T (pcm)

TC TM CB	UO2 Cell	MOX Cell
1700 324 REF	- 3	+ 3
1100 286 REF	- 8	- 9
1700 REF 1500	- 1	+ 5
REF 343 1500	- 9	- 4
REF 286 0	- 11	- 7

Comparing these results, the conclusion is that the maximum errors in the reactivities are 40 pcm for TC and 15 pcm for TM. They represent respectively 6% and 4.5% of the related feedback effects.

-"Cross wise" approximation : The reference library contain cross sections actually calculated at each node (TM,TC,CB) The differences between calculations using this reference library and the multiparameter one are presented in TABLE VI. The reactivity errors are very small. Thus the hypothesis which we used for the reconstuction of fluxes is quite well verified.

-Reconstruction of fluxes at intermediate burnups : For intermediate burnup we perform cell calculations with the multi parameter library and with a reference library actually calculated as this burnup. The relative differences are

TABLE VII
MOX CELL : RECONSTRUCTION OF FLUXES BETWEEN 0 AND 55 GWD/T
REACTIVITY ERRORS (PCM)

TC TM CB	12 GWD/T	28 GWD/T	44 GWD/T
REF 343 REF	+ 9	+ 3	- 3
REF REF 1500	- 2	- 1	+ 1
1100 REF REF	- 14	- 18	- 11

TABLE VIII
UO2 CELL : RECONSTRUCTION OF FLUXES BETWEEN 0 AND 55 GWD/T
REACTIVITY ERRORS (PCM)

TC TM CB	10 GWD/T	30 GWD/T	45 GWD/T
REF 343 REF	+ 75	+ 46	+ 20
1000 REF REF	+ 41	+ 40	+ 12
100 343 REF	+ 112	+ 67	+ 19

TABLE IX
UO2 CELL : RECONSTRUCTION OF FLUXES
INTERPOLATION IN (0-12) AND (12-55) GWD/T
REACTIVITY ERRORS (PCM)

TC TM CB	5 GWD/T	32 GWD/T
REF 343 REF	+ 9	- 2
1000 REF REF	- 6	- 11
REF REF 1500	- 3	- 4

presented in table VII for UO2 cell and in table VIII for MOX cell. In the case of MOX fuel the approximation is satisfying. Unfortunately it is not true in the case of UO2 assembly. The solution consists in adding a third burnup B2

$$0 < B2 < 55 \text{ GWD/T}$$

and in interpolating in the intervals 0-B2 and B2-55. One can see that greatest errors occur toward 10 GWD/T. We choose therefore B2=12 GWD/T. The errors become now acceptable. (See table IX).

ACKNOWLEDGMENTS

We would like to thank R LENAIN and A NICOLAS for helpful assistance with this work.

PROJECT CELL CODE UPDATING FOR MOX CALCULATION

A. VALLÉE, G.B. BRUNA,
M. DOUCET, D. DOUTRIAUX
Framatome,
Paris-La Défense,
France

Abstract

Recycling Plutonium in PWRs was obviously followed in FRAMATOME by a large scale research and development program, including theoretical inspections, parametrical studies, experimental analysis and contributions to international benchmarks.

The aim of this wide program is to acquire a full knowledge on the physics of the water cooled and moderated Plutonium lattices, in order to allow the project computational methods up-dating.

The results have allowed an overall significant up-dating of the FRAMATOME project computational methods, mainly at the "cell" code level.

The main achievements in this field are:

- an up-dating of the four most important Pu isotopes [239, 240, 241, 242] to the JEF-1 level,
- a correction of the Pu_{239} thermal ν, [Ref. 5],
- a simplified up-dating of the minor actinides,
- a reevaluation of the equivalent F.P. cross-sections.

An outline of the whole programme is presented and the main results are summarized. Several elements of the qualification are given which are essentially based on critical experiments and power plant measurements.

1. HISTORICAL BACKGROUND

Plutonium recycling in French PWRs was decided in June 1985. A generic safety report, established jointly by FRAGEMA and EdF in 1986, demonstrated the faisability of MOX (Mixed OXyde) recycling in such reactors, with a maximum 30 % of MOX assemblies in each reload [Ref./1/]

Since then, several reloadings were successfully made both in Saint-Laurent and Gravelines plants

The decision to go further with plutonium recycling in PWRs initiated at FRAMATOME a wide research and development program, dealing with a full knowledge of the physics of water moderated plutonium systems

A large scale faisability analysis, performed in FRAMATOME in the late eighties on HCLWRs (High Converter Light Water Reactors) [Ref./2/], was widely supported by a large experimental program carried on in a joint venture with EdF and CEA, [Ref./3/].

In the meantime, a global program of up-dating the project computational chain was started to verify the basic plutonium data and to adapt the methods to the new requirements of the system physics

A large-scale analysis, including calculation of the HCLWR benchmark proposed by NEA Data-Bank, [Ref /4/], gave the following main conclusions

- the old basic plutonium data included in the project libraries had to be significantly up-dated, in order to minimize the impact of cross-section errors,
- the treatment of the minor actinides had to be revised to account for their larger contribution to the reactivity of the system, (Table 1),
- the equivalent F P cross-section values had to be adapted to the new material and spectral environment

TABLE 1

Contribution to the overall reactivity
of a 5 % enriched MOX cell
(in the beginning of life conditions)
of Pu^{238} and Am^{241}, versus
the main Pu isotopes (arbitrary units)

ISOTOPES	δ ρ ı
Pu^{238}	- 100
Am^{241}	- 646
Pu^{239}	+ 31 307
Pu^{240}	- 11 110
Pu^{241}	+ 6 501
Pu^{242}	- 1 092

2 LIBRARY UP-DATING

The following main improvements were made to account for the learning of the physical analysis ·

- processing of the four main Pu isotope data from the JEF-1 Data File,
- simplified up-dating of the minor actinides to the JEF-1 level,
- correction of the thermal ν cross-section of Pu^{239},
- re-evaluation of the cross-sections of the pseudo F P. for burnup calculations

The cross-sections of the four main Pu isotopes (Pu^{239}, Pu^{240}, Pu^{241}, Pu^{242}) were processed from the JEF-1 Data File, [Ref /5/] and collapsed to the fine "cell" energy structure, including 54 groups in the 10 MeV - 0,625 eV region and 172 thermal, via the ETOG and ETOT codes, (Fig 1)

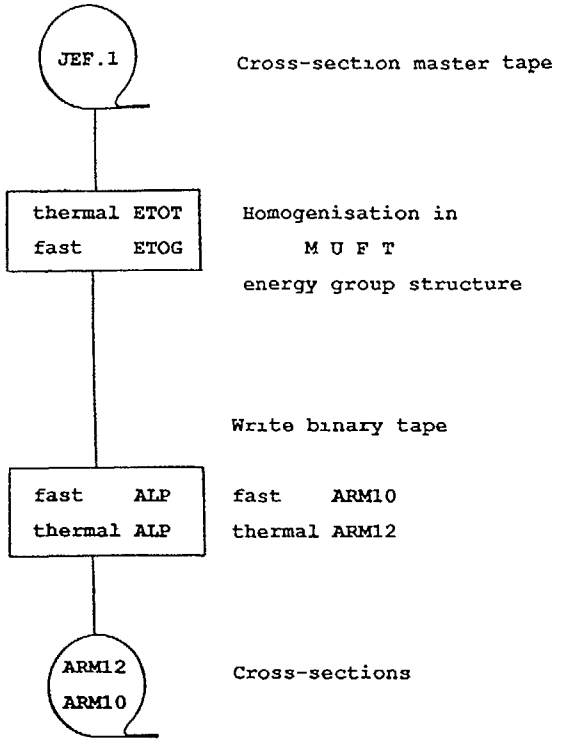

FIG. 1. Cross-section generation from JEF-1

Computations in the resolved resonance region were made with given "potential" cross-section values, i e

- 400 barn for Pu^{239}
- 1000 barn for Pu^{240}
- 2500 barn for Pu^{241}
- 5500 barn for Pu^{242}

Owing to the absence of resonances in the unresolved range of the Pu^{242} JEF-1 Data, the choice of the "sigma potential" had no effect on its cross-sections , besides, the other isotopes showed a slight sensitivity to this parameter, but its impact was small in the whole range of MOX enrichments

All minor actinide cross-sections were also checked by comparing them, in a simplified way, with JEF-1 data

The thermal ν cross-section of Pu^{239} was also revised by addition of the SANTAMARINA-TELLIER [Ref /6/] correction which accounts for the (n, γf) and spin effects in the range of the 0 3 eV large resonance According to this correction, the thermal production reaction rates of Pu^{239} were significantly reduced

3 VALIDATION

A full validation of the up-dated version of the project "cell" code was obtained from both benchmarkings and commercial reactor data

We summarize in the following chapters the main items of our validation program

3 1 Calculation of the HCLWR benchmark

As said before, calculation of the HCLWR benchmark entered into the preliminary analysis, which led to the definition of the project "cell" code improvements

An "average" reference was defined, as the one showing an average behaviour among all codes in the benchmark [Ref /7/]

Reactivity predictions of the project code, before and after up-dating, were compared systematically to those of the "average" code and the others, in the sample, via an exact zero-dimensional perturbation formula, [Ref /8/], getting results as the ones shown, for a fresh fuel, in Fig 2

Fig 3 presents the multiplication factor as a function of burnup, calculated by the up-dated project code, compared to APOLLO and WIMS-E results

3 2 Experimental validation critical experiments

The validation of a project computational scheme can be achieved on the basis of a reduced scale experiment if its "representativeness", defined as

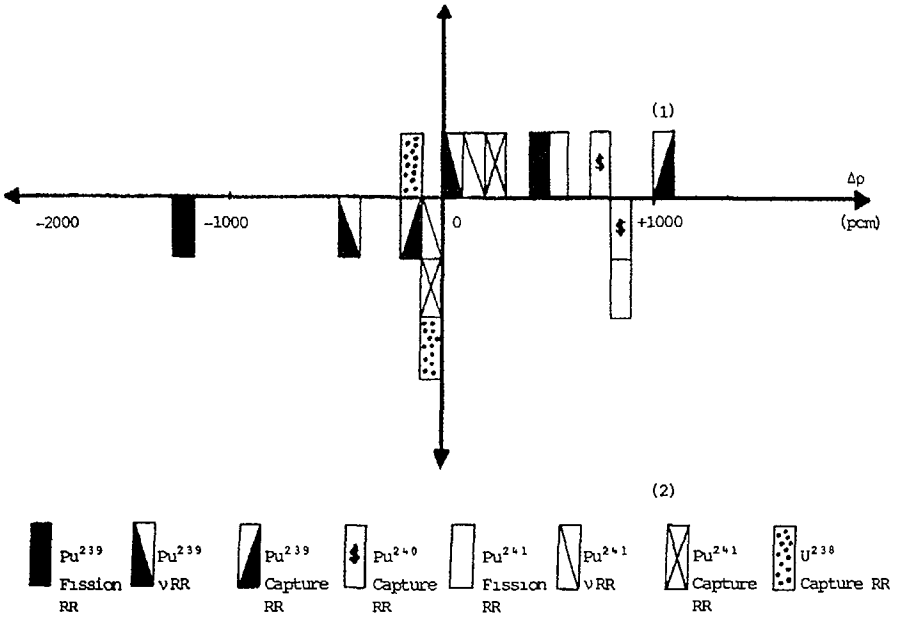

FIG 2 HCLWR NACRP benchmark contribution of different reaction rates (RR) to the differences in reactivity among the 'average' code and the non-updated (1), updated, JEF-1 level (2) cell code results (beginning of life)

the quantity able to carry-on the most of the physical background of a real system, is not too far from 1 0, [Ref /9/] The "representativeness" is then a function of a set of key parameters or "signatures", which can be different, depending on the real system features

On this basis, the only experiments, which could really be representative of the plutonium recycling in PWRs belong to the EPICURE program, now in progress at Cadarache, [Ref /10/] Unfortunately, owing to its time schedule, this program was not able to give useful informations for our qualification

Missing of these foundamental results, we based our validation on a series of experiments, none of them was fully representative of the actual MOX recycling, i e

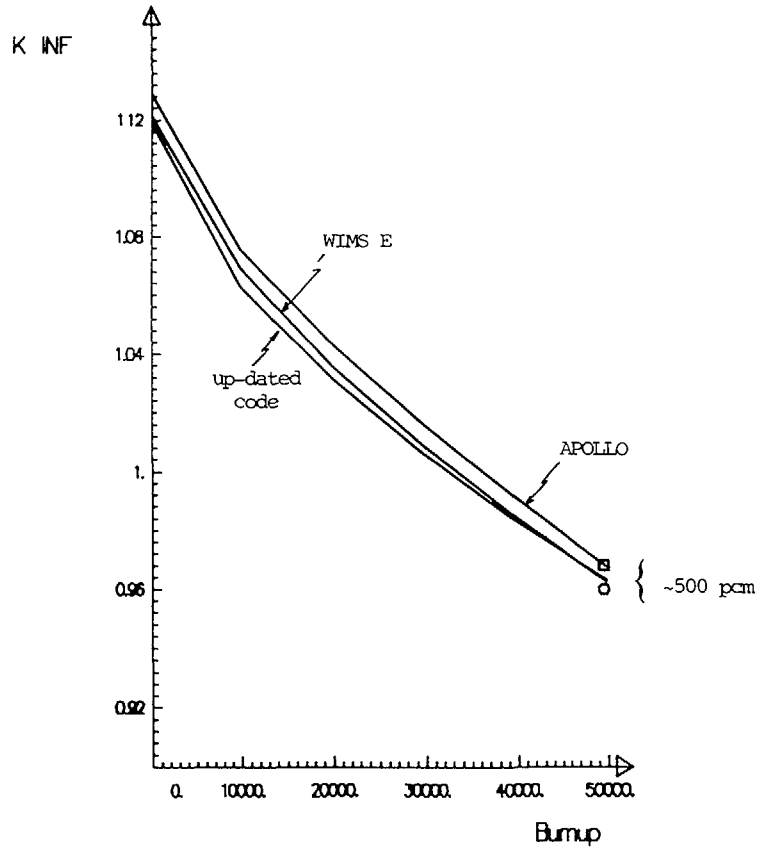

FIG. 3. Multiplication factor versus burnup: comparison between APOLLO, WIMS-E and updated code results.

- SAXTON [Ref./11/],
- JAERI [Ref./12/],
- ERASME [Ref./13/].

In order to allow appreciation of the "representativeness" of the experiment in the sample, the plutonium recycling physical conditions were compared to these of the experiments, (Fig 4) and the reactivity was plotted versus two different key parameters a coolant to fuel ratio and a spectrum index In

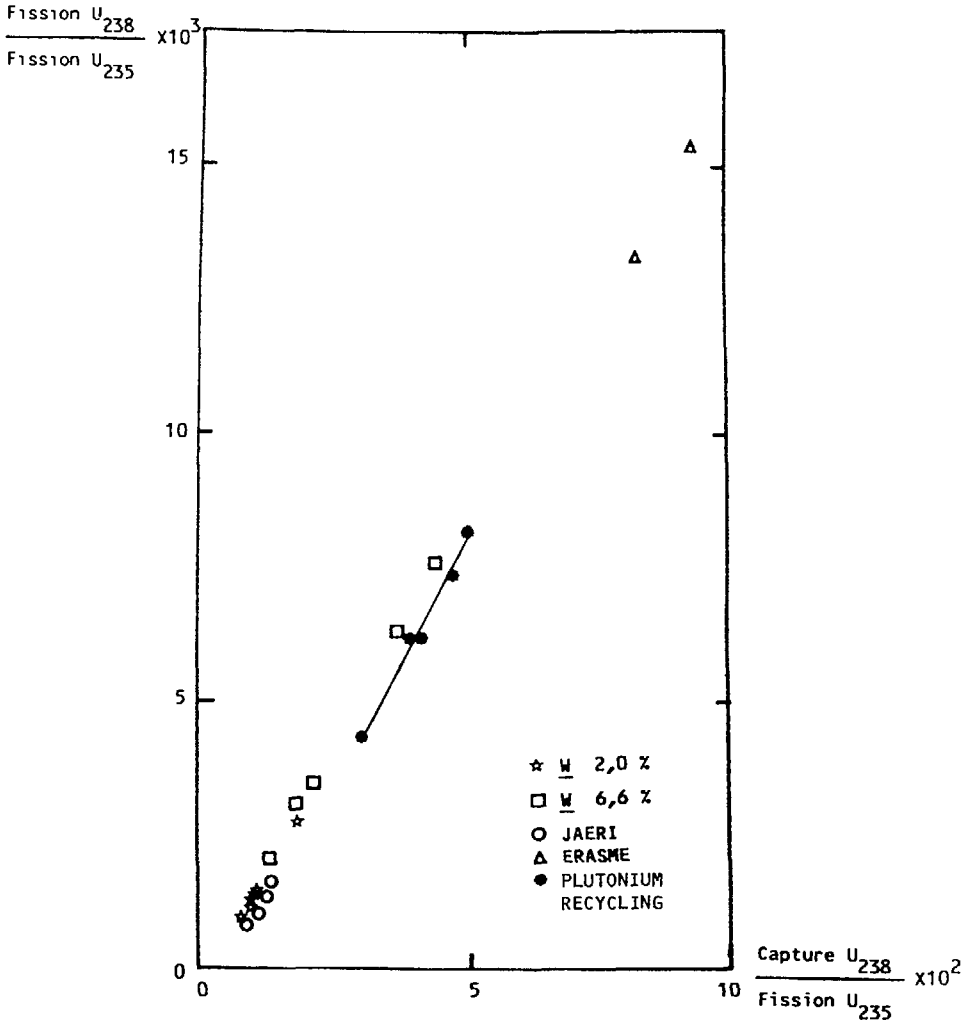

FIG. 4. Comparison of the plutonium recycling physical conditions to those of the experiments in the sample.

the Figs 5 and 6, arrows indicate the typical plutonium recycling range for these parameters. Moreover, an experimental uncertainty was evaluated and associated to each computed value

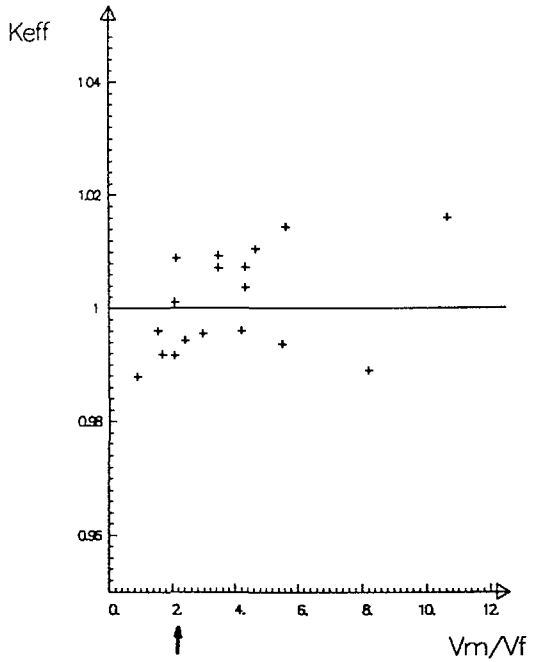

FIG. 5. K_{eff} versus moderation ratio.

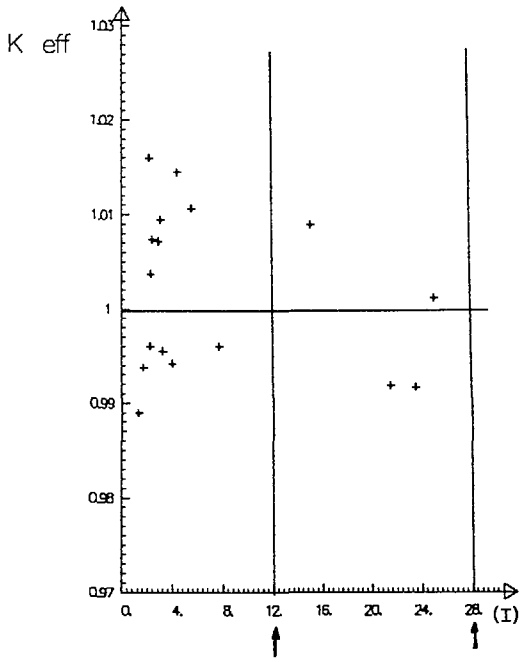

FIG. 6. K_{eff} versus fast and epithermal to thermal flux (I) (cut-off at 0.625 eV).

As can be seen from the figures, almost all the calculated points lay in the range ± 1000 10^{-5}, experimental uncertainly included, which corresponds to the qualification level of the project "cell" code for UO2 media.

Supplementary elements of validation were also drew from MINERVE "P/A" and "POWER" experiments and from the isotopical analysis of the CNA MOX fuel, (Fig 7), all giving satisfactory results

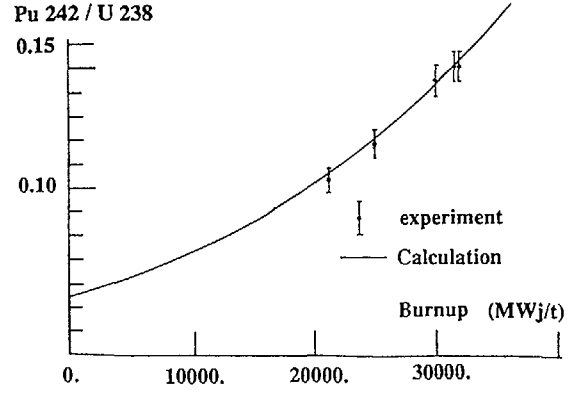

FIG. 7. Isotopic analysis of KO6 CNA MOX rod

3 3 Experimental validation . exploitation of measurements in situ

The new "cell" code was used in the standard project chain to generate data for core calculations with a sample of 7 reloadings (1), i.e :

Saint-Laurent B 105*
Saint-Laurent B 206*
Gravelines 308*
Gravelines 408*

Saint-Laurent B 106**
Saint-Laurent B 207**

Saint-Laurent B 107***

All the exploitable results were compared to experimental informations, mainly

- critical boron concentration at start-up,
- reactivity worth of different absorber clusters,
- power distribution per assembly,
- reactivity coefficients.

The main results, presented in a synoptic way in Tables 2 and 3 (2) and Figs.9 and 10 show the generally good agreement existing between computed and experimental values.

As far as it can be seen from these results, a satisfactory prediction is obtained not only in terms of reactivity, which is an integral parameter,

(1) The identification number of a reload indicates
— the plant which it is related to,
— its serial number, starting for the first loading (number 1),
— the number of MOX reloads (a MOX reload, one*)

(2) See Fig 8 for cluster positioning

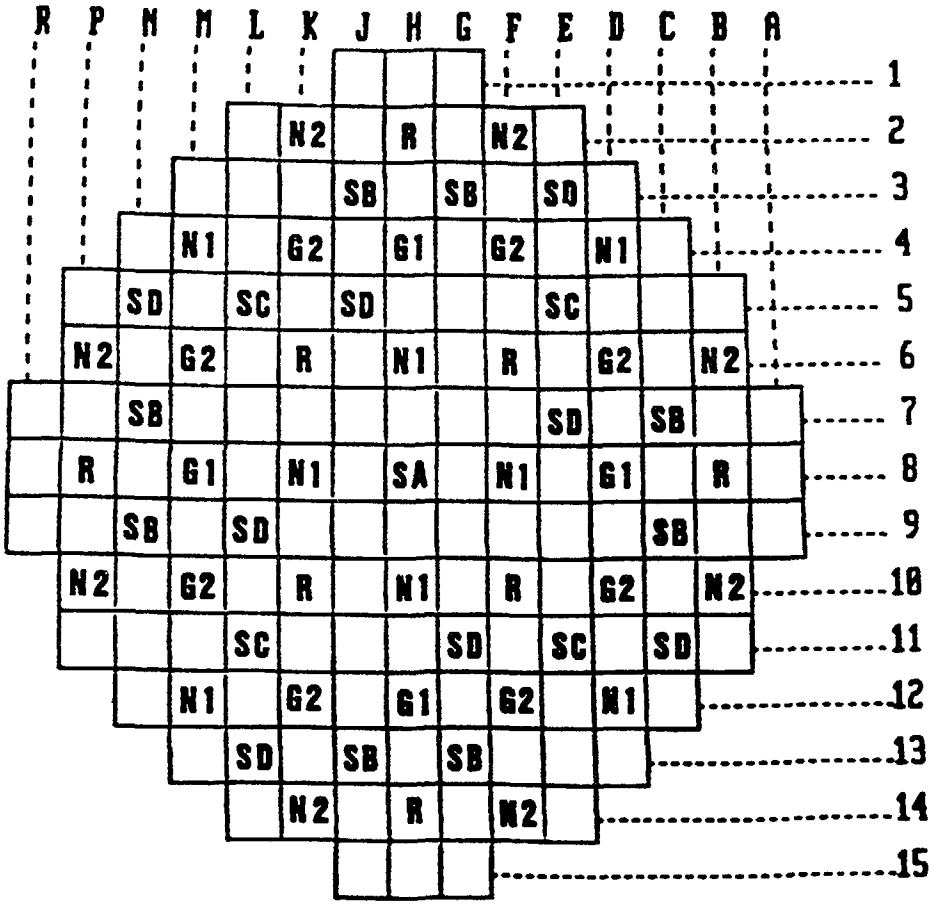

FIG 8 Cluster layout in a MOX refuelled plant

but also in terms of assembly-wise average power distribution, a local parameter, as claimed by :

- the power maps,
- the worth of the control clusters, which are not uniformly distributed over the core

TABLE 2

Critical boron concentrations at beginning of cycle, zero power ; core calculations. Comparaisons among predicted and experimental values.

RELOADING	DEVIATION (ppm) $
SB105*	- 30
SB206*	- 15
GR308*	+ 9
GR408*	+ 5
SB106**	+ 38
SB207**	+ 13

* 1 MOX reload

** 2 MOX reloads

$ 1 ppm = $1.0\ 10^{-6}$

Average deviation first reloads = 8 ± 18 ppm

Average deviation second reloads = 26 ± 16 ppm

4. CONCLUSION

Jointly with the start-up of the plutonium recycling in PWR, a wide analysis was made at FRAMATOME ; the aim was to up-date the project "cell" code in order to get its full validation for every computational circumstance for MOX reload projects.

The modified code was validated on both benchmarks and experiences.

The present paper summarizes most of the results obtained in the qualification program of the code.

TABLE 3

Comparison between predicted and experimental cluster worth, core calculations

Average deviation = + 1.1 ± 4.0 %

	SB105	SB206	GR408	SB106	SB207
	% DEVIATION	%DEVIATION	% DEVIATION	% DEVIATION	% DEVIATION
R	+ 3.9	+ 0.5	+ 2.5	+ 7.9	+ 5.9
G1	- 4.8	+ 5.0	+ 2.9	- 1.0	+ 8.0
G2	- 0.6	+ 1.5	- 5.5	- 1.8	+ 2.1
N1	+ 0.1	- 1.0	- 1.6	+ 4.1	+ 5.0
N2	+ 4.8	+ 1.4	- 0.4	- 3.0	- 5.9
SB	+ 6.1	+ 5.9	+ 5.1	- 3.2	- 4.5
SC	- 4.9	- 2.8	+ 1.7	+ 1.7	+ 8.7*
SA + SD2	+ 0.4	+ 1.9	-	+ 8.4	-
SD1	0	+ 0.5	-	- 0.9	-
SA + SD	-	-	- 3.5	-	+ 0.1

* In this case, SC cluster is inserted in MOX assemblies only

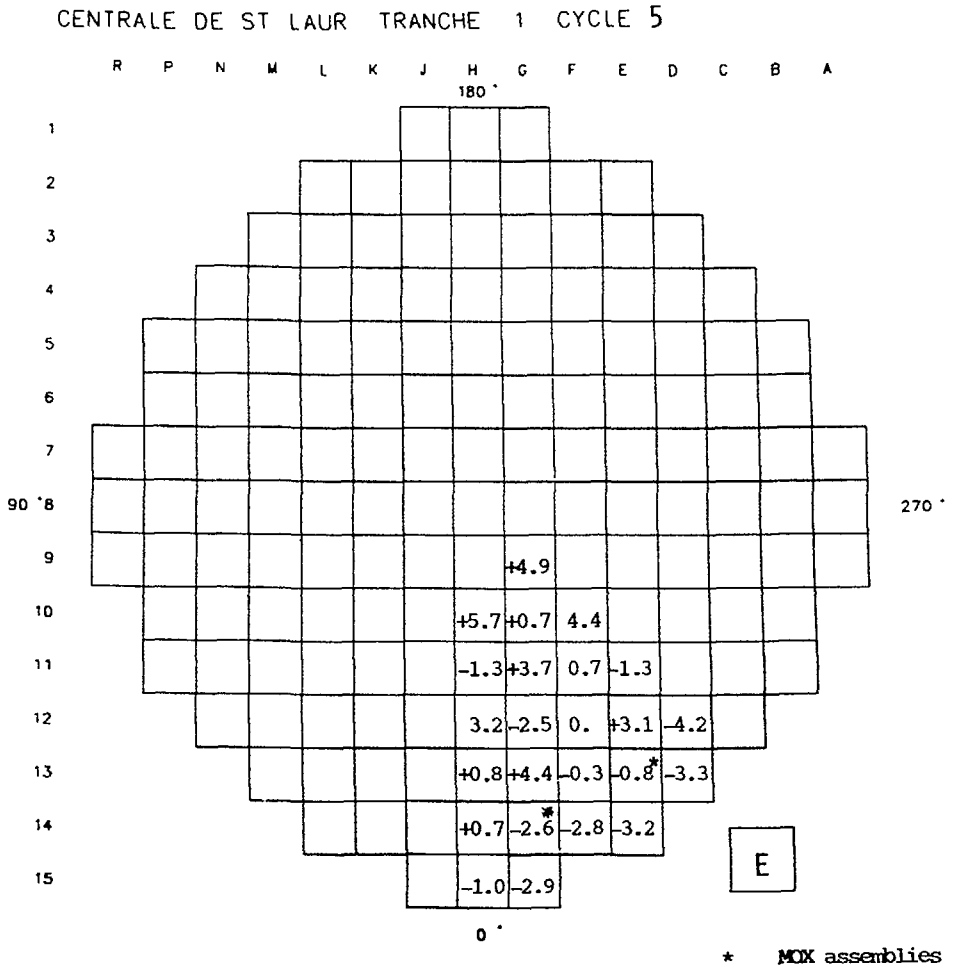

E = C-M (%) BEGINNING OF LIFE

FIG. 9.

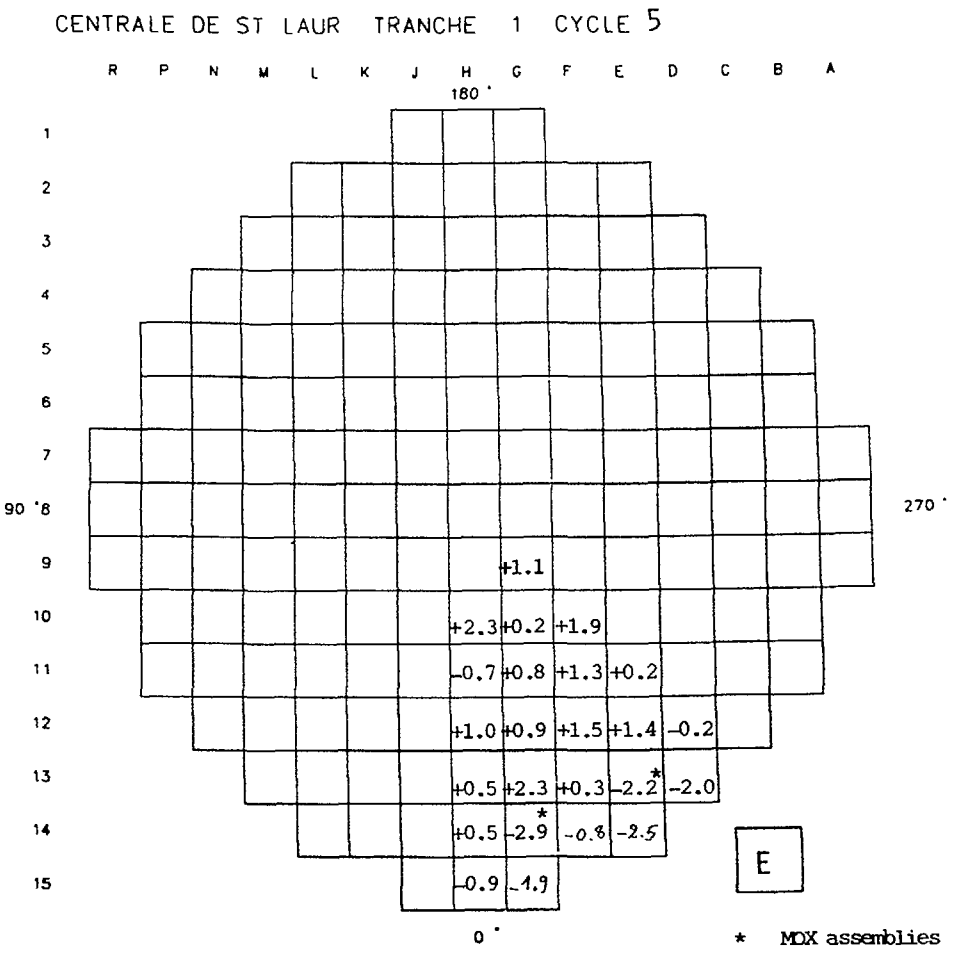

E = C-M (%) END OF CYCLE

FIG. 10.

REFERENCES

/1/ M. ROME, G. FRANCILLON, J LEBARS, "Plutonium Recylcing Experince in French PWR Plants : Neutronic Results", in AIEA Technical Meeting on Recycling of Plutonium and Uranium in Water Reactor Fuels, Cadarache, November 13-16, 1989 ;

/2/ A. VALLEE, J.P. MILLOT, G.B. BRUNA, "The FRAMATOME RCVS Concept and Physics", Proceedings of the ENC '86, Geneva, June 1-6, 1986 ;

/3/ B. BARRE, J.M. COURTAUD, M. DARROUZET, C. GOLINELLI, J.P. SCHWARTZ, G. GAMBIER, "Advenced PWRs : Prospects and Experimental Basis", Proceedings of the ENC '86 Meeting, Geneva, June 1-6, 1986 ;

/4/ W. BERNNAT, Y. ISHIGURO, E. SARTORI, J. STEPANEK, M. TAKANO, "Advances in the Analysis of the NEACRP High Conversion LWR Benchmark Problems", Proceedings of the Physor '90 Meeting, Marseille, April 23-27, 1990 ;

/5/ JEF Report 1, July 1985 OCDE - NEA Data-bank : "Index to the JEF 1 Nuclear Data Library" ;

/6/ A. SANTAMARINA, H. TELLIER, "The French CEA Multigroup Cross-Section Library and its Integral Qualification", Proceedings of the International Conference on Science and Technology Nuclear Data, Mito, Japan 1988 ;

/7/ Proceedings of the NEACRP Specialists' Meeting on HCLWR Burnup Benchmark, Saclay, June 1989 ;

/8/ J. PORTA, J Y. DORIATH, A. MOURGUES, M. NOBILE, A VALLEE and G.B. BRUNA, Nucl. Sci Eng, 95, 266-281 (1987) ;

/9/ G PALMIOTTI, P CHAUCHEPRAT, J. MONDOT, M SALVATORES, M NOBILE, A. VALLEE, "Uncertainty and Sensitivity Analysis for Power Distributions and Reactivity Coefficients", Proceedings of the ANS Topical Meeting on Advances in Nuclear Engineering, Computation and Radiation Schielding, Santa Fe, New Mexico, April 9-13 89 ;

/10/ J. MONDOT and al., "An Experimental Program Devoted to the Validation of the Schemes for Plutonium Recycling in PWRs, "Proceedings of Physor '90 Meeting. Marseille, April 1990.

/11/ E.G TAYLOR, "Critical Experiments for the SAXTON Partial Plutonium Core", Report WCAP-3385-54, EURAEC-1493 (1965) ;

/12/ I. KOBAYASHI al. "Critical Experiments and Analysis on Light Water Moderated Pu O2 - UO2 Lattices", JAERI, Memo 5745, (1974) ;

/13/ L MARTIN-DEIDIER, A. SANTAMARINA, S. CATHALAU, J.P. CHAUVIN, J.M. GOMIT, "Undermoderated PWR Neutronic Qualification Through the ERASME Experiments", Proceedings of the International Topical Meeting on Advances in Reactor Physics, Mathematics and Computation, Paris, April 27-30, 1987.

PREPARATION OF CROSS SECTION LIBRARIES FOR PWR URANIUM AND MOX ASSEMBLIES

D.C. LUTZ
Institut für Kernenergetik und Energiesysteme,
Universitat Stuttgart,
Stuttgart, Federal Republic of Germany

Abstract

This report regards the way from cross section data base to few group libraries for reactor calculations It starts with the calculation of a very detailed weighting spectrum for the generation of multigroup cross sections Special emphasis is lain on a good resonance treatment In a second step burnup calculations for assembly cells have been performed, which in most cases may be 1-dimensional, but are 2-dimensional for MOX assemblies Equivalence theory methods have been used to prepare homogeneous 2-group cross sections They are gathered in a multi-parameter representing the dependancies of macroscopic cross sections for operational conditions The applicability of the library is demonstrated by 2-dimensional cycle calculations for PWRs

1 Generation of Multigroup Cross Section Libraries

The cross section basis is the JEF-1 data file [1], which is processed [2] with the NJOY programm system [3] into multigroup data 3 libraries are available in following energy ranges

- fast and epithermal range, 100 groups,
- the resolved resonance region, 8500 groups,
- the thermal range, 151 groups

These libraries are used in the code CGM [4] for one dimensional spectral calculations for group collapsing to 45 (10 fast, 35 thermal) groups The generated data sets are dependent of the cell definition in CGM, mainly in the groups containing resonances They include the effects of self and mutual shielding and resonance overlapping Even for HCLWR problems this method can by applied successfully [5] Figure 1 shows the weighting spectrum for the fuel isotopes calculated with CGM for a MOX pin cell of a PWR assembly

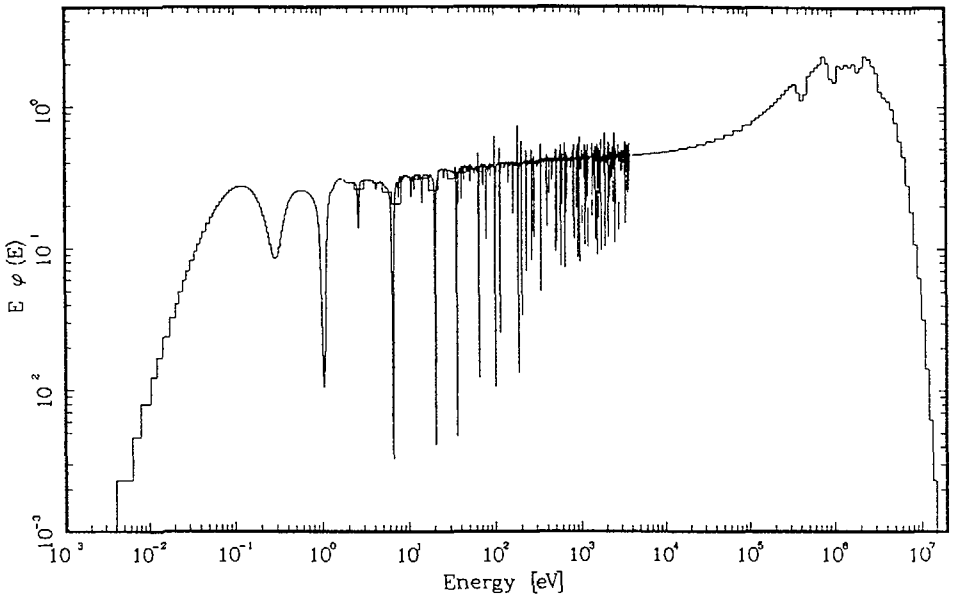

Figure 1 The weighting spectrum for MOX fuel calculated with CGM [4]

2 Cell Burnup Calculations for the Assemblies

2.1 One-dimensional Cell Models

The local dependancy of spectra in PWR Uranium assemblies isn't very strong Therefore one dimensional cylindrical models are a good approach for the assembly For Uranium assemblies a two stage cylindrical model is used as assembly cell Even if boron glas pins or control rods are inserted in the assembly the one dimensional Models give good results because of rather good symmetric distribution of the guide tubes The cell burnup calculations are done in RSYST1 [6] using a collision probability code For 16 Actinides and 64 fission product isotopes the burnup equations are solved For every burnup step a series of different assembly calculations is performed to take into account the influence of moderator and fuel temperature and boron concentration on the cell spektra

The first series of MOX assemblies inserted in a PWR in our country contained only 2 different pin types, low enriched at the boundary row and higher enriched ones at the other positions Such an assembly as a whole can also be presented by a cylindrical model, but the surrounding Uranium assemblies have

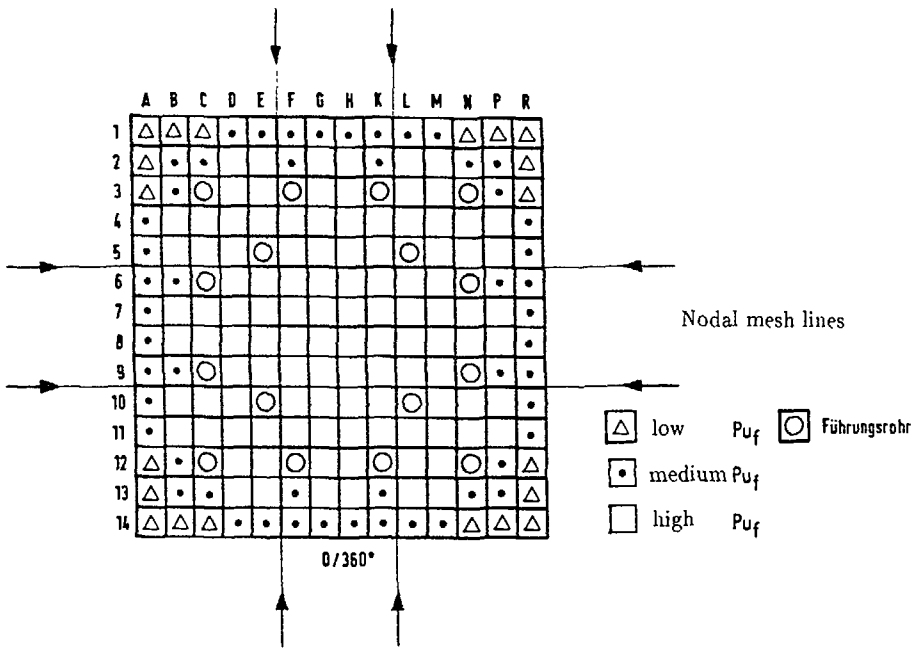

Figure 2: Enrichment distribution in a PWR MOX assembly

to be taken into account during the burnup calculations. The new MOX assembly developped for the KWO reactor [7] is shown in figure 2. It has 3 different enriched pins and it is hard to find a 1-dimensional model for it. The same statement goes for all BWR asssemblies mainly if they contain MOX.

2.2 Two-dimensional Cell Models

The RSYST code for 2-dimensional assembly calculations is ICM2D [8]. It works with the J -methode for homogeneous meshes, treats anisotropic scattering and includes a linear space and angular dependancy of the flux. The homogenized pin cell cross sections for this code are prepared using the SPH method [9]. Figure 3 shows the power density distribution in one eighth of the MOX assembly in figure 2 surrounded by Uranium assemblies. In the inner part of the MOX assembly the power density is low because of the shielding effect. The highest values are in the neighborhood of the outer waterholes. The power and burnup distribution in a colour set of BWR MOX and Uranium assemblies containing Gd poisoned pins represents figure 5. The fuel assemblies are arranged in a chessboard way. The

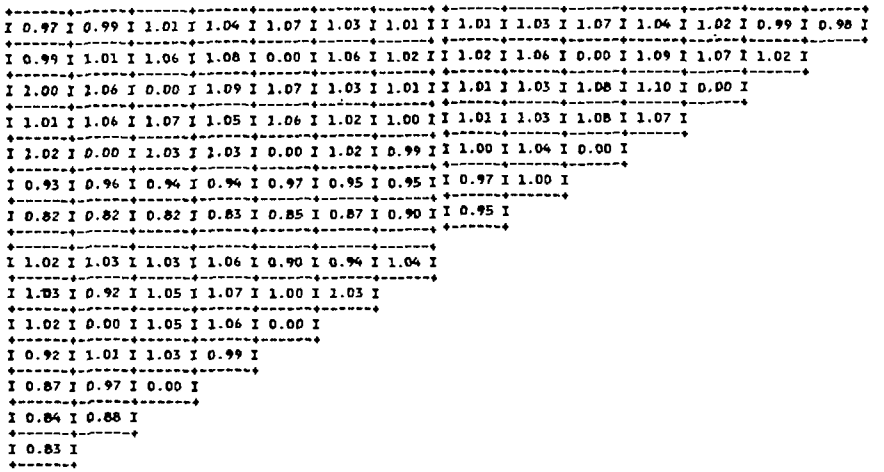

Figure 3: Power density in a cluster of PWR MOX and Uranium assemblies

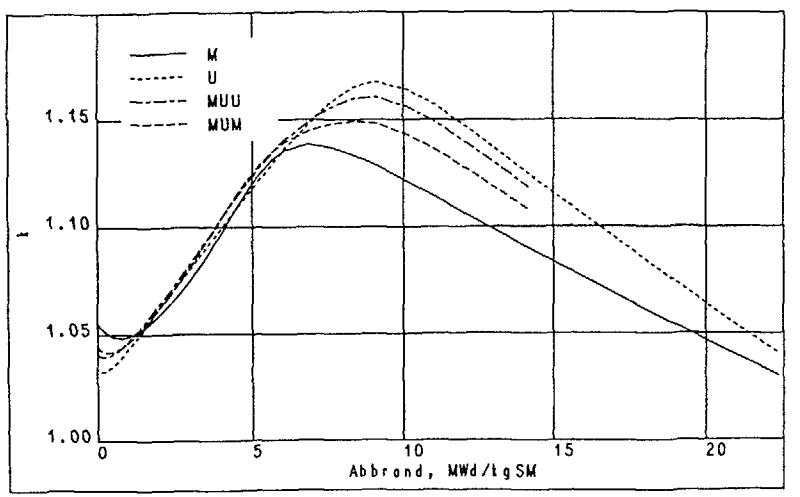

Figure 4: k_∞ of BWR MOX and Uranium assemblies in function of the burnup

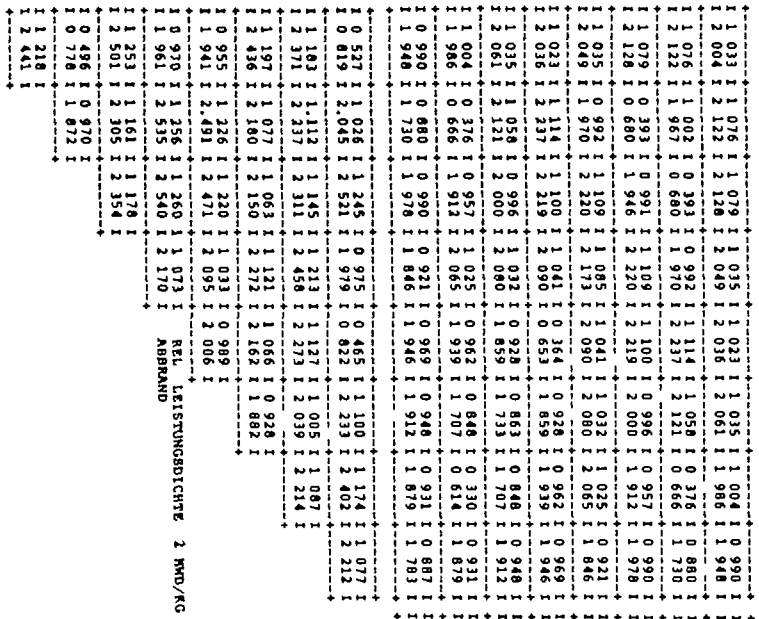

Figure 5 Power density in a cluster of BWR MOX and Uranium assemblies

average burnup is 2 MWd/kg, the k_∞ curves of the participating single assemblies (MOX A M, Uranium A U) and the of two different color sets (chessboard MUM, MOX A sorrounded by Uranium A MUU) are shown in figure 4

3 Generation of 2-Group Cross Sections for Diffusion Calculations

For the one dimensional assembly models with a reflectiv boundary at the surface of the homogenization region standard homogenization and condensation methods are applied, the only exception being the fast transport cross sections, which are averaged along Benoist's formula [10]

$$D_g = \frac{\sum_i V^i \Phi_g^i \lambda_{tr\,g}^i}{3 \sum_i V^i \Phi_g^i} \qquad \lambda_{tr\,g}^i = \sum_k P_g^{ik*} \lambda_{tr\,g}^k$$

In the 1 dimensional cases with U and MOX zones and for the 2 dimensional assembly models a tranport diffusion equivalence method has been used to get 2 group cross sections for the homogeneous nodes of the diffusion program This method is simular to that of Mondot [11] It conserves the multigroup transport reaction rates in the corresponding homogenized regions by an iterative way The local dependancy of enrichment and spectra in the MOX assemblies suggest a representation of MOX assembly by 9 meshes with 3 different homogeneous cross section sets It would be an advantage for a following pin power reconstruction to choose alternating nodal mesh sizes, which meet the pin cell boundaries (see fig 2)

4 The 2-Group Library for PWR

The aim of the library is to provide cross sections for operational conditions It contains

- macroscopic 2 group cross sections without Boron and Xe 135,
- macroscopic absorption cross section of 1 ppm Boron in the moderator,
- microscopic absorption cross section of Xe 135,
- fission yield of Xe 135 and energy release per fission

for mean parameter values of moderator density, fuel temperature and Boron density in the core tabulated in function of the burnup The dependancy of these parameters is represented in a linear approximation As additional parameter the historical moderator density is introduced Void content in the moderator isn't taken into account

This approach of cross section representation has been checked by calculations performed with fixed realistic exposition histories for pin cells [12] The deviations for the cross sections and k_∞ lay in the permille range

		1					
		1.0911					
		1.09					
		9	10				
		1.0261	1.1201				
		1.02	1.12				
		17	18	19			
		1.1591	1.0791	1.1991			
		1.15	1.07	1.18			
		25	26	27	28		
		1.1841	1.2251	1.1811	1.2031		
		1.16	1.21	1.16	1.18		
		33	34	35	36	37	
		1.2361	1.1831	1.1991	1.0721	1.2541	
		1.22	1.17	1.19	1.06	1.24	
		40	41	42	43	44	45
		1.1201	1.1541	1.0881	1.0831	0.9171	0.9881
		1.12	1.16	1.09	1.08	0.91	0.96
		47	48	49	50	51	52
		0.9851	0.9971	0.9561	0.9711	0.8471	0.5031
		1.02	1.02	0.99	0.97	0.82	0.46
		53	54	55	56		
		0.6831	0.7521	0.6331	0.5701		
		0.71	0.77	0.66	0.56		

Figure 6: Power distribution in a PWR containing Boron pins at BOC1

		1					
		1.0421					
		1.05					
		9	10				
		1.1021	1.0401				
		1.11	1.05				
		17	18	19			
		1.0391	1.1001	1.0431			
		1.05	1.11	1.05			
		25	26	27	28		
		1.1071	1.0441	1.1191	1.0701		
		1.12	1.05	1.13	1.07		
		33	34	35	36	37	
		1.0531	1.1221	1.0651	1.1441	1.1621	
		1.06	1.13	1.07	1.14	1.18	
		40	41	42	43	44	45
		1.1291	1.0631	1.1261	1.0521	1.0661	1.0061
		1.13	1.06	1.13	1.05	1.07	1.01
		47	48	49	50	51	52
		1.0031	1.1131	0.9751	1.0201	0.8821	0.6111
		1.01	1.12	0.98	1.03	0.86	0.57
		53	54	55	56		
		0.8021	0.8201	0.7511	0.6431		
		0.80	0.81	0.75	0.61		

Figure 7: Power distribution in a PWR containing Boron pins at EOC1

5 2-Dimensional Cycle Calculations

The initial cycle of a PWR with inserted Boron has been calculated using a 2-dimensional nodal diffusion code with axial bucklings and thermohydraulic feedback. Figures 6 and 7 show the resulting power distribution at BOC1 and EOC1,respectivly, together with the results of the manufacturer. The agreement is satisfactory.

Other applications are calculations of the cycles 18 and 19 of the KWO reactor. In its relativly small core (300 MWel) with 109 fuel assemblies 12 and 16, respectivly, MOX assemblies have been inserted. Local dependant axial bucklings taken of the results of a 3-dimensional calculation of a previous cycle simulated the third dimension. Figures 8 and 9 show a comparison of the calculated Boron curves with the measured ones. The figures contain the results based on ENDF/B-IV/V and JEF-1 base. The JEF-curves are shifted to higher Boron concentrations up to 50 ppm.

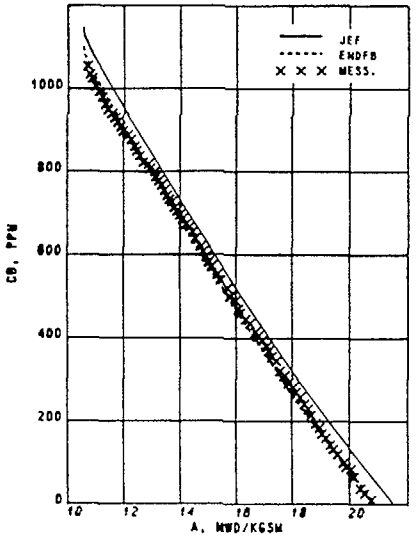

Figure 8: Measured and calculated Boron curves of 18. cycle of the KWO reactor

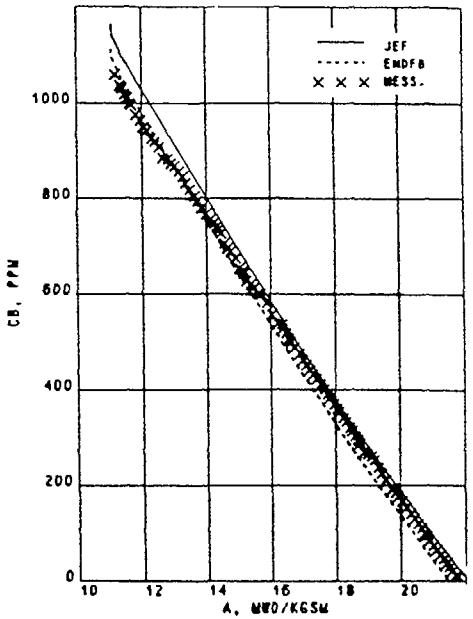

Figure 9: Measured and calculated Boron curves of 19. cycle of the KWO reactor

REFERENCES

[1] Rowlands, J.L.; Tubbs, N.: The Joint Evaluated File: A New Data Library for Reactor Calculations. Int. Conf. on Nuclear Data for Basic Applied Science, Santa Fe, 1985

[2] Mattes, M.: IKE, Internal Report, 1989

[3] Mac Farlane, R.E.; et al.: The NJOY Nuclear Data Processing System. LA-9309-M, 1985

[4] Arshad. M.: Development and Validation of a Program System for Calculation of Spectra and Weighted Group Constants for Thermal and Epithermal Systems. Theses University of Stuttgart (IKE 6-156), 1986

[5] Akie, H.;et al.: Summary Report on the International Comparison of NEACRP Burnup Benchmark Calculations for HCLWR Lattices. NEACRP-L-309, 1988

[6] Rühle, R.: RSYST. an Integrated Modular System for Reactor and Shielding Calculations. USAEC Conf-730 414-12, 1973

[7] Etzel, W.; et al.: Physikalische Auslegung des Reaktorkerns des Kernkraftwerks Obrigheim. Atom und Strom, 1968, p. 9

[8] Rückle, Th.: Lösung der Multigruppentransportgleichung für Brennelementanordnungen nach dem Erststossverfahren. Stuttgart: Universität,1985, Dissertation

[9] Kavenoky, A.: The SPH Homogenization Method. IAEA Meeting Würenlingen,1978

[10] Benoist, P.: Theorie du Coefficient de Duffusion des Neutron dans un Reseau comportant des Cavites.CEA-R 2278, 1964

[11] Mondot, J.: Determination de Constantes Equivalentes pour les Calculs de Diffusion. IAEA Meeting Lugano, 1978

[12] Memari, E.: Untersuchungen zur Genauigkeit von Abbrandrechnungen fü r Druckwasserreaktoren.IKE, 1984 (6-148)

MODIFICATIONS OF THE BURNUP CHAINS FOR ADVANCED FUEL CALCULATIONS

D.C. LUTZ
Institut für Kernenergetik und Energiesysteme,
Universität Stuttgart,
Stuttgart, Federal Republic of Germany

Abstract

The influences of some minor Actinides on k_∞ have been proven for standard Uranium fuel and some kinds of advanced fuel. Pin cell burnup calculations with modified Actinide chains showed, that in normal Uranium fuel the effects of (n,2n)-reactions and of the isotopes U-234 and Pu-238 are in the permille range and cancel each other rather well up to burnup values of 45 *Mwd/kg*. For higher burnups the connection between Np-237 and the Pu chain gets significant. The Am isotopes shouldn't be neglected in the burnup range higher 30 MWd/kg. Reprocessed Uranium has a higher U-234 concentration than fresh Uranium with an effect of 0.5 % on k_∞. Because of the initial U-236 content the connection from Np-237 to the Pu isotopes becomes earlier effective. It should be established if discharge burnups higher 30 MWd/kg are projected. In MOX fuel the Am isotopes play the leading role, of course, and have to be taken into account. Some of the Cm isotopes should be included also in the Actinide chain for MOX calculations.
The rest absorption of Gd poisoned fuel has been calculated for extended burnups for Gd oxide contents in fuel of 4 % and 10 %. The values at the minimum are 6 % and 14 %, respectivly. They increase with the burnup because of built up of Tb and Dy.

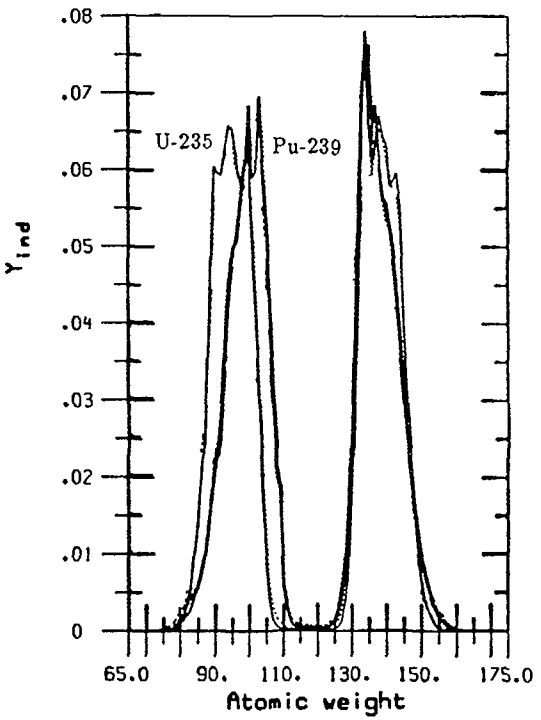

Figure 1: Fission yields of U-235 and Pu-239 [1]

1 Introduction

The tendency in fuel management to high burnup fuel and to insertion of spent and reprocessed fuel in LWR cores are arguments to review the calculational reactorphysical models. This has been done in this contribution with regard to the isotopic chains, for which the burnup equations have to be solved performing burnup calculations. The main effects are caused by the Actinide chain, of course. Therefore the main emphasis of this report is to look for an answer to the question of which Actinide isotopes have to be taken into account in calculations for different kinds of fuel. This point has been investigated for Uranium fuel with an enrichment of 4 % - the highest enrichment used in German LWRs -, for reprocessed Uranium fuel with an enrichment of 3.5 % and for MOX fuel with a content of 3.2 % of fissile Plutonium. Complementary, 2 effects, sometimes neglected, are taken into account and rated: (n,2n)-reaction and absorption of U-234. The most (n,2n)-neutrons are delivered in U-238. Their influence on the reactivity therefore is nearly the same in all kinds of LWR fuel. The initial concentration of U-234 in the fuel depends on the Uranium enrichment. It is higher in reprocessed Uranium because of its double enrichment.

The fission product chains don't make any trouble normally for high Plutonium content, provided the shift of fission yield curves of Plutonium isotopes against Uranium in the range of atomic weight 97 to 110 (see Fig.1) is paid attention to . In this range the U-235 yields are very low whereas those of Pu-239 are significant. In the other ranges the differences are not so high.

In addition a correlated problem - estimation of rest absorption in Gadolinium poisoned fuel - has been investigated taking into account the complete chain of Gadolinium isotopes and their successors.

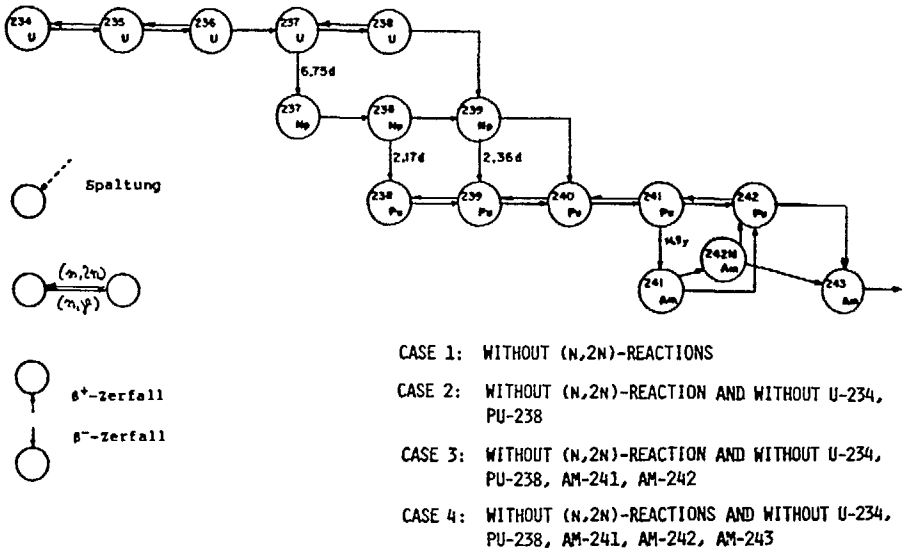

Figure 2: Actinide chain

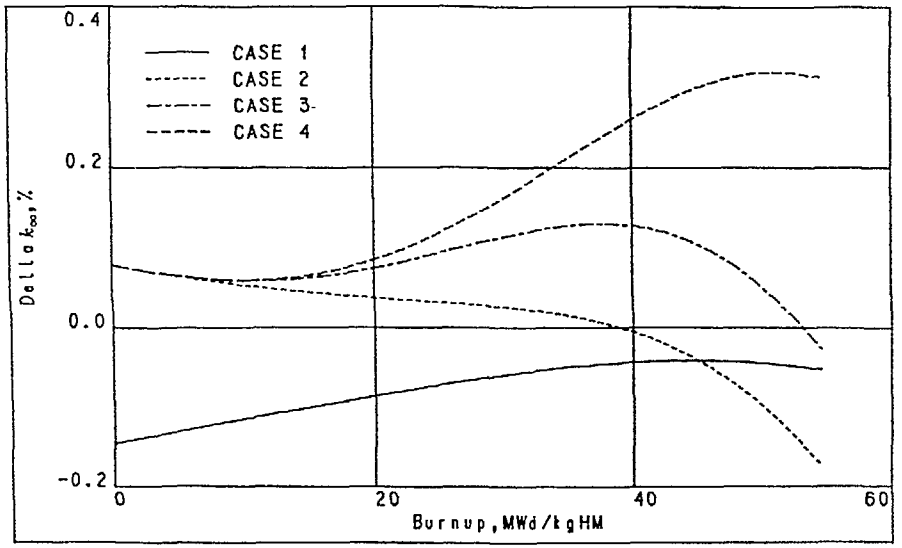

Figure 3: Effect of modified Actinide chains on k_∞ for Uran fuel (enrichment 4%)

2 Calculational Model

Standard pin cell calculations are performed using multigroup cross sections and number densities for operational conditions of a PWR. The composition of reprocessed Uranium is published in [2]. The missing number densities of U-234 have been calculated following a formula given by de la Garza [3]. The ratio of enrichment of U-234 to natural abundance is a little higher than the U-235 one. The burnup equations have been solved for 16 Actinides and 79 fission product isotopes including the Gadolinium chain.

The Actinide chain is shown in Fig. 2. For all these isotopes cross sections are available except for Np-238. For this isotope a 1/v cross section has been taken. The arrows showing to the left mark the (n,2n)-reactions. This chain has been taken as best estimate case. By some interruptions it has been modified in order to demonstrate the influence of special reactions or transitions, respectively.

- In a first change the (n,2n)-reactions are ommitted.
- In case 2 the isotopes U-234 and Pu-238 are additionally neglected.
- The connection between Pu-241 and Am-241 is interrupted, so the isotopes Am-241 and Am242m have no source (case 3).
- In case 4 Am-243 is neglected additionally.
- Case 5 combines the omissions of (n,2n)-reactions and of isotope Pu-238.

With these Actinide chains burnup calculations have been performed for the different fuel types. The resulting k_∞-values are compared with the results of the best estimate calculations. The differences are plotted in the Figures 3 to 5 and discussed in the following sections.

3 Results for Uranium Fuel

In Fig. 3 curve 1 shows the effect of the (n,2n)-reactions. For fresh fuel the k_∞-value is 0.16 % too low. The difference is lowered during burnup, mainly by the generation of Np-237. The U-234 absorption (curve 2) has an influence of more than 0.2 % on k_∞ at the start of exposition. The curve goes down because of transmutation of U-234 in U-235 and the missing connection of the Np-237 to the Plutonium isotopes. For burnup values until 45 MWd/kg these 3 effects cancel quite well. This is a rectification for a simple Actinide chain in this range.

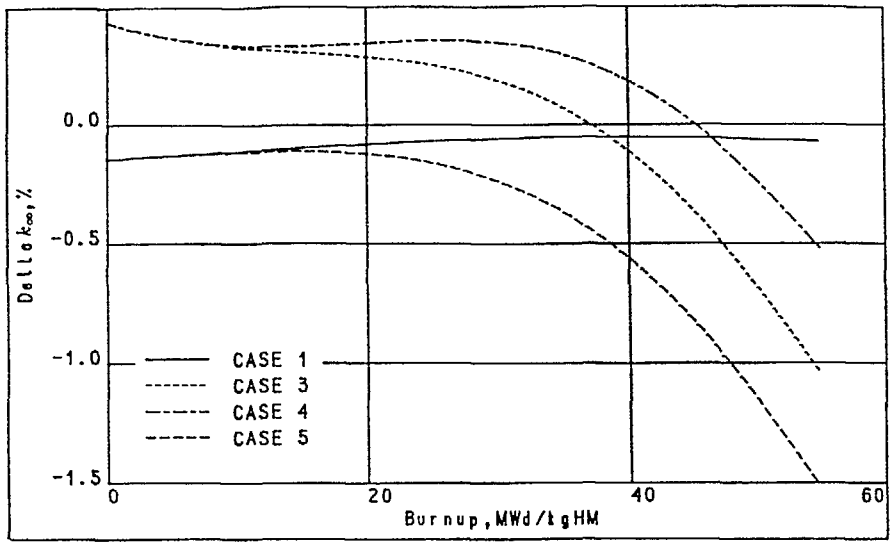

Figure 4: Effect of modified Actinide chains on k_∞ for reprocessed Uran fuel (enrichment 3.5%)

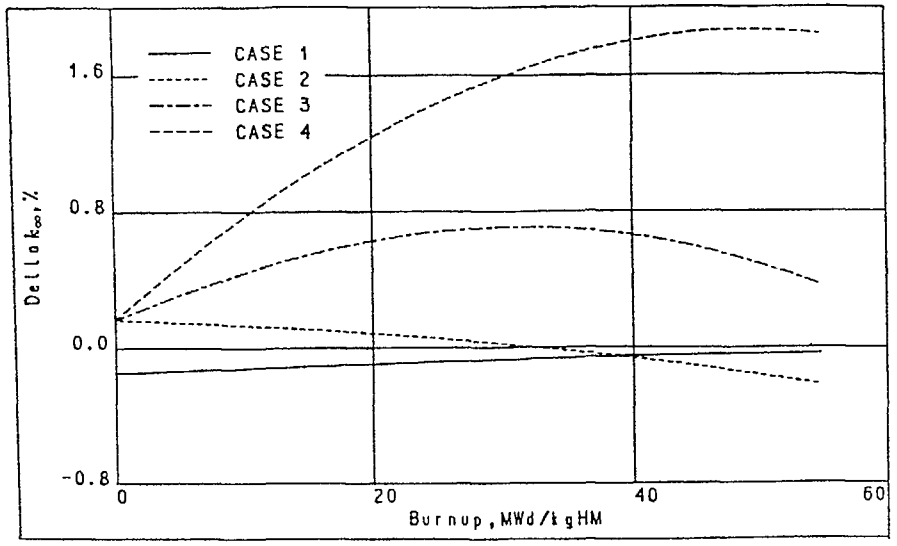

Figure 5: Effect of modified Actinide chains on k_∞ for MOX fuel (3.2% content of fissile Pu)

For higher burnup the connection between the U-235 and the Pu chain becomes more important. The neglection of the isotopes Am-241 and Am-242m causes an additional underestimation of k_∞ in the range of 0.1 % (case 3). The influence of the ommitted Am-243 gives the highest effect in Uranium fuel. It rises with burnup and becomes significant for values over 30 MWd/kg. In reality it is still higher because of the effect of Curium isotopes, which are not taken into account in the calculations.

4 Results for reprocessed Uranium Fuel

Reprocessed Uranium has a behaviour similar to fresh Uranium with respect to (n,2n)-effect (see Fig. 4). But the cut between Np-237 and the Plutonium chain has a higher influence on k_∞ in this case (see curve 5). The underestimation of k_∞ is nearly 0.5 % at 40 MWd/kg and grews very fast in the high burnup range. The effect of the U-234 absorption is higher than 0.5 % at the beginning of the exposition because of the higher initial U-234 number density in reprocessed and twice enriched Uranium (case 3). The contribution of the low Americium isotopes is not separated in this case. Am-243 has also a rising influence with burnup, 0.25 % at 40 MWd/kg, but the behaviour of the corresponding curve is determined by the missing connection of Np-237 to the Plutonium chain.

5 Results for MOX Fuel

The neglection of (n,2n)-reactions and of the isotopes U-234 and Pu-238 have in MOX fuel similar effects on k_∞ as in fresh Uranium fuel (case 1 and 2 in Fig. 5). Important influences are caused by the neglection of the Am isotopes, of course. The omission of Am-241 and Am-242m has an overestimation effect on k_∞ of up to 0.7 % (case 3). The Am-243 influence is twice as high. It reaches 1.1 % at 40 MWd/kg (case 4). Both effects are enlarged by the influences of the Cm isotopes, which should be taken into account in calculations for MOX fuel.

6 The Rest Absorption in Gadolinium Poisoned Fuel

An important question for the core designer applying burnable poisons is the height of the rest absorption. To get an impression of this term 2 burnup calculations for a supercell with poisoned fuel in the center surrounded by homogenized Uranium pin cells have been performed. The content of Gd-oxide was 4 % and 10 %, respectivly. A complete Gadolinium chain including Terbium and Dysprosium has been taken into account. In Fig. 6 the results for the lower Gadolinium

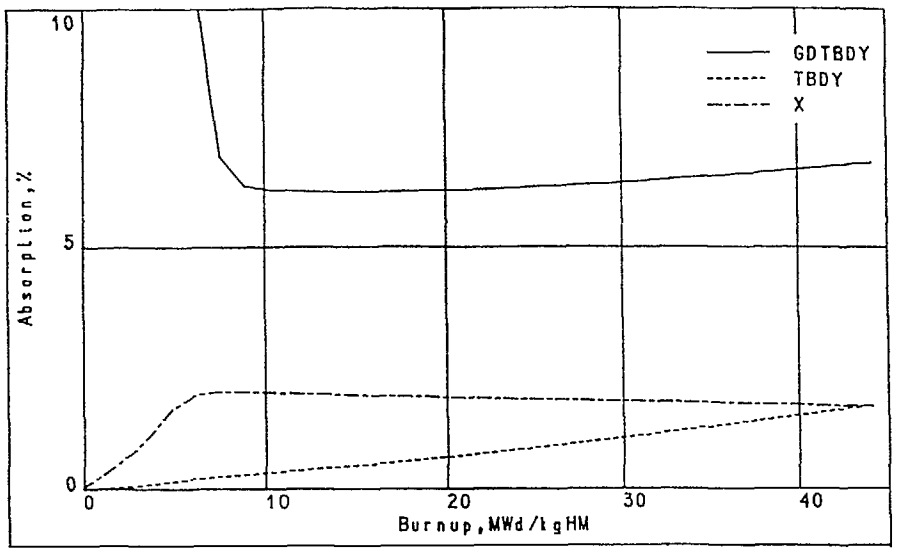

Figure 6: Rest absorption in a poisoned pin with 4% Gd oxide

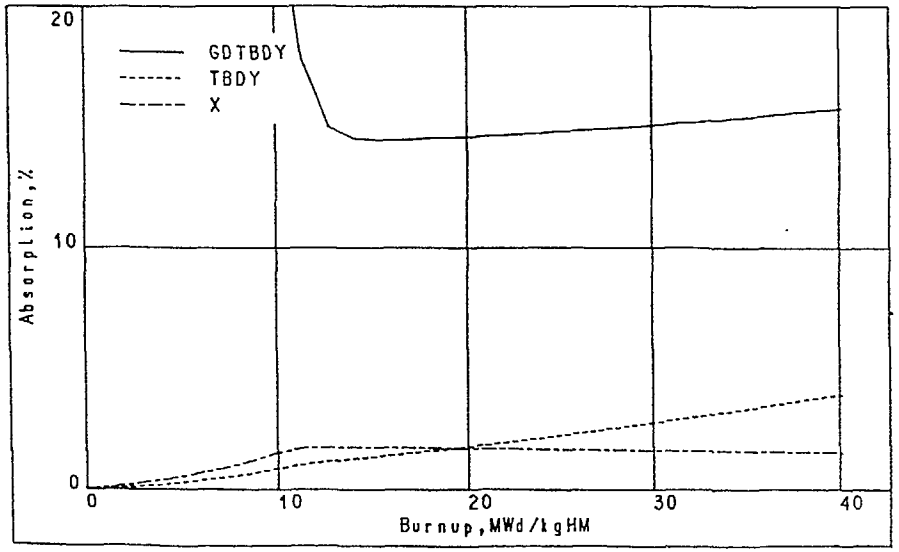

Figure 7: Rest absorption in a poisoned pin with 10% Gd oxide

concentration are shown. The upper curve presents the relative contribution of all Gadolinium, Terbium and Dysprosium isotopes to the absorption in the fuel pin as a funktion of the burnup. After the burnout of the high absorbing Gadolinium isotopes rests an effect of 6 %, which is slowly grewing with burnup. This increase is caused by the absorption in the Terbium and Dysprosium isotopes, which reaches 1 % at 30 MWd/kg. The relative absorption of Xe-135 in the fuel is the third curve in the figure. The corresponding results for the higher Gadolinium content are presented in Fig. 7. The rest absorption in this case is 14 % at the minimum. The absorption of the successor isotopes is also higher. At 30 MWd/kg it is 2.8 % and higher as the absorption of Xe-135.

REFERENCES

[1] Guidebook for the ENDF/B-V Nuclear Data Files, BNL-NCS-31451, BNL 1982

[2] Schlosser,G.; et al.: Uranrückführung. Jahrestagung Kerntechnik, Frankfurt, 1984. Bonn: Deutsches Atomforum, 1984, p.297

[3] de la Garza, A.:Uranium-236 in Light Water Reactor Spent Fuel Recycled to an Enriching Plant. Nucl.Technol.32,176(1977)

IMPROVED CODE SYSTEM FOR REACTOR CALCULATION AND VALIDATION FOR ADVANCED VVER CORE ANALYSIS

T.G. APOSTOLOV, K.N. IVANOV, R.I. PRODANOVA
Institute for Nuclear Research and Nuclear Energy,
Bulgarian Academy of Sciences,
Sofia, Bulgaria

Abstract

In the Institute for Nuclear Research and Nuclear Energy has been developed VVER core analysis code system on the base of our previous codes by incorporating improvements in accuracy and efficiency, as well as new advanced codes and methodologies. The code system consists of the NESSEL-IV-EC code - for lattice burnup calculations, HEXAB-3D code - three - dimensional core simulator with coupled thermohydraulic module and HEXAB-2D code - for two-dimensional rod by rod power distribution calculations.

Calculational models, recent improvements and test results on various VVER benchmark problems are presented. Future activities for development and validation of the code system are duscussed.

I. INTRODUCTION

VVER core analysis code system has been developed on the base of our previous codes by incorporating improvements in accuracy and efficiency, as well as new advanced codes and methodologies. The code system includes following interconnected computer codes and procedures:

- the NESSEL-IV-EC code - for cell calculations and cross section generation;
- the HEXAB-3D code - for global three - dimensional improved coarse-mesh core simulation;
- the HEXAB-2D code - for two - dimensional detailed (pin by pin) core calculations;
- thermohydraulic programme module THCALC - for calculating temperature field.

Two - dimensional few-group code HEXAB-2D [1] performs rod by rod power distribution calculations in hexagonal geometry for VVER cores. The 30°-sector of reactor core according to the reflective symmetry is represented. The detailed core-shroud and borated water are included in the fine-mesh grid Mesh points coinside with fuel pin centures.

The correct thermal-hydraulic model is used in THCALC module to determine the fuel and moderator temperatures and coolant mass flow rate. The general assumptions, which have been used for thermal-hydraulic analysis are treated in Ref.[2].

II.HEXAB-3D - THREE-DIMENSIONAL CORE SIMULATOR CODE IN HEXAGONAL GEOMETRY

II.1. Brief Description of Programme HEXAB-3D

The few-group diffusion code HEXAB-3D [3] is designed to calculate the three - dimensional flux distributions for power reactors which have a hexagonal core configuration with a heterogeneous region structure in the axial direction.

There are two versions of the code:

-HEXAB-III-30-the calculational model on horizontal plane is 30o - sector (the reflective conditions are used on the internal reactor boundaries);

-HEXAB-III-360~ the calculational model on horizontal plane is full core.

In the HEXAB-3D code is applied the mesh centered finite-difference formulation for neutron balance equation. The high effective two-sweep iterative method AGA DSOR has been used for the inner iterations in each energy group. This method belongs to the family of partial factorization techniques commonly used in the numerical solution of group - independent neutron diffusion equations in discrete form [4] The power method combined with Chebishev polynomial acceleration for outer iterations is applied in the code. There are two possibilities for the acceleration of outer iterations:

- by using two-term Chebishev polynomial method according to Ref [5];
- by using three-term Chebishev polynomial method according to Ref [6];

Optimized outer-inner iteration strategy has been applied in the code to minimize total CPU time.

II.2. Numerical Investigations for Determination of the Optimal Combination between Chebyshev Acceleration and Factorization Methods

Chebyshev method theory implicitly assumes that the matrix equation for each energy group is solved exactly during each outer iteration. For multidimensional problems, this is not the case, because the effect of solving this equation iteratively for each group is that the system of equations, being solved, bicomes modified. The dominance ratio of modified system is larger than that of the original system. One possible solution to this problem is to perform sufficient number of inner iterations for each group during each outer iteration, so that the effect on the dominance ratio to be not so significant. The more practical approach for optimal combination of the Chebyshev acceleration (for outer iterations) and AGA DSOR method (for inner iterations) is to use the method of preliminary inverse of inner iteration matrix [16], which allow to decrease the inner iteration number per outer iteration The efficiency of this method is connected with physical characteristic of VVER core.

The goal of the optimized iteration strategy is to reduce the number of outer iterations at the expense of investing relatively not so great efforts in the inner iterations performed during each outer iteration and in this way to minimize the total CPU time In order to determine the optimal parameters for AGA DSOR method and for to two- and three-term Chebyshev methods, the convergence characteristics have been investigated on VVER-440 and VVER-1000 three-dimensional test problems [13, 14]. The effectiveness of various combinations of the methods for outer and inner iterations have been compared and the convergence representation (outer iterations and CPU times) is given in table 1.

Table 1

Test problem	Outer iteration method	Number of mest points	hr/hz	Ω	Outer iterations	CPU* time T(s)
VVER-440	Power 2-term	528	0.588	1 195	91	157
	Chebyshev 3-term	-/-	-/-	1.188	48	90
	Chebyshev	-/-	-/-	-/-	45	84
	Power 2-term	5628	0 588	1.195	185	1608
	Chebyshev 3-term	-/-	-/-	1.188	93	1066
	Chebyshev	-/-	-/-	-/-	89	1048
	Power 2-term	1056	1.176	1 195	85	222
	Chebyshev 3-term	-/-	-/-	1 188	47	124
	Chebyshev	-/-	-/-	-/-	50	140
VVER-1000	Power 2-term	528	1.326	1 20	122	208
	Chebyshev 3-term	-/-	-/-	-/-	64	115
	Chebyshev	-/-	-/-	-/-	69	125

* All calculations were perfirming on IBM 3031 -1x10^6 oper per s

II.3. Approach for Improving Accuracy of Coarse-Mesh Finite-Difference Method

To improve the accuracy of the calculated integral and local reactor parameters without significant increase of computer time and storage it has been developed an effective coarse-mesh method. This method is based on the ICM method, proposed by Askew and Takeda [7]. It decreases errors due to the use of coarse-mesh by means of correcting the coefficients of finite-difference scheme. A consistent two dimensional procedure [8] is used in HEXAB-3D code to avoid some ICM method disadvantages, which are noted in [9]. As a result two problems have been solved - first it is improving of the radial neutron leakage expression and second - the introduction of average value for calculation of reaction rates in diffusion balance equation

The following expressions for the correction coefficients have been suggested [10]·

$$y_1^g = (1-2.4*h^2 * \beta_{1,g}^2 /27)*(1-4*h^2 * \beta_{1,g}^2 /81)$$

$$a_1^g = (1-2.4*h^2 * \beta_{1,g}^2 /27)/1-2.4 * \beta_{1,g}^2 /81)$$

for the absorber part of boron carbide control rods, and for the rest zones we have:

$$y_1^g = (1-1.8*h^2 * \beta_{1,g}^2 /27)*(1-4*h^2 * \beta_{1,g}^2 /81)$$

$$a_1^g = (1-1.8*h^2 * \beta_{1,g}^2 /27)/(1-1.8*h^2 * \beta_{1,g}^2 /81)$$

The computation time for correction procedure applied in HEXAB-3D code is only 30% of the total CPU time To attain correction parameters accuracy, required in practice, 3-5 recalculations are enough.

II.4. Validation of HEXAB-3D Code by VVER-440 and VVER-1000 Benchmarcs

A lot of numerical calculations with the code have been carried out on various test models of VVER-440 and VVER-1000 reactors and results are presented in [11] The code gives solutions (Keff and power distribution) comparable in accuracy to similar diffusion theory calculations with six mesh points per assembly The typical discrepancies between the reference and HEXAB results are

- Keff - within ± 0 15%;
- power distribution within ± 2%

The deviations are in any case within the designe and operational criteria, however the results should be analyse in order to get some improvement if possible

III. NESSEL-IV-EC CODE FOR CALCULATION OF THE LOCAL NEUTRON - PHYSICS PARAMETERS

III.1. Status and Recent Improvements

The NESSEL-IV-EC code [12] is intended to calculate the local neutron physics characteristics of light water moderated reactor cores. It calculates effective few-group diffusion parameters and depletion not only for a given subzone, but also the entire assembly, taking into consideration the strong inhomogeneities inherent to this type of reactor cores. It uses 34-group data library LIB4P containing microscopic data for about 200 isotopes. The energy distribution of neutron flux is calculated by using the multigroup approximation of transport equation. The spatial dependence is considered by applying the so called method of "step by step" homogenization. In this method the real assembly structure is represented by a set of cylindrical cells of Wigner-Zeitz, unified with respect to their properties in "homogeneous areas" (HA). Each HA contains either "elementary zones" (e.g. zones containing materials for which there are microscopic data in the data library and by the input data we give the number densities, temperatures etc.), or preliminary homogenized HA of lower rank. The present version of NESSEL-IV-EC can calculate maximum 5 steps of homogenization (5 HA) maintaining in this way up to 20 elementary zones. In order to improve the accuracy especially in the thermal region calculation we divide the zones by a reasonable number of thin fine (mathematical) zones (up to 40 in each HA) and apply the collision probability method for solving the integral transport equation.

In order to carry out ivestigations connected with the influence of burnable absorbers in VVERs the microscopic data library LIB4P have been extended recently to contain all necessary multigroup data for at least the most important gadolinium isotopes Gd-155 and Gd-157.

III.2. Burnup Calculations for Hexagonal Gadolinium Lattice Benchmark

For hexagonal geometry burnup calculations with this code system two different sets of infinite lattice were studied (the input data was specified according to Ref.15): supercell (Fig.1) and assembly (Fig.2). All calculations have been carried out with assumption of no leakage throughout the surfaces of the systems under consideration. Only the two most important Gd-isotopes (Gd-155 and Gd-157) have been taken into consideration. The multigroup library used is LIB4P containing 34 groups (12 fast, 12 resonance and 10 thermal groups), the cut off energy is 0.465 ev. In the thermal region calculation the Gd-bearing rod has been divided into 8 fine mathematical zones and the first collision probability method has been used. For the calculations of relative pin power distribution the HEXAB-II-30E code [1] has been used (applying

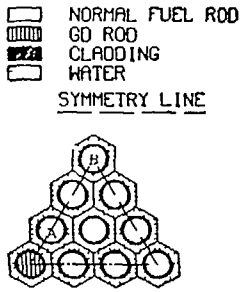

FIG. 1. Supercell case.

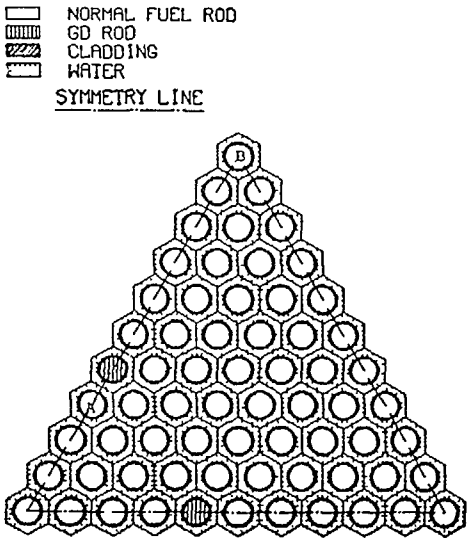

FIG. 2. Assembly case.

power normalization such as the average power of each fuel hexagonal is equal to 1.0) and results for the "supercell case" and for the "assembly case" at six burnup points are shown in Fig.3 and Fig.4a - 4f respectively.

IV. FUTURE ACTIVITIES

The code system will be further improved, new options will be added and benchmark calculations will be performed. In the nearest future the NESSEL-IV-EC will be improved not only

0 MWd/kgU

		3	5
		1.036	1.049
1	2	4	6
0.195	0.990	1.042	1.052

2 MWd/kgU

		3	5
		1.032	1.044
1	2	4	6
0.265	0.993	1.038	1.046

4 MWd/kgU

		3	5
		1.028	1.038
1	2	4	6
0.345	0.996	1.033	1.040

6 MWd/kgU

		3	5
		1.023	1.030
1	2	4	6
0.451	1.003	1.026	1.031

10 MWd/kgU

		3	5
		1.012	1.011
1	2	4	6
0.676	1.016	1.012	1.011

12 MWd/kgU

		3	5
		1.015	1.010
1	2	4	6
0.614	1.022	1.014	1.010

Figure 3. Pin power distributions in the supercell at six burnup points

from models point of view, but also with the aim to generate cross sections, necessary in the investigations of tight reactor latties. At the next stage we intend to incorporate burnup and thermal hydraulic feedback modelling and to validate the improved code system on NPP design and operational data.

										31
										1.049
							21	26	32	
							1.040	1.047	1.049	
					13	17	22	27	33	
					1.009	1.028	1.040	1.047	1.050	
				7	10	14	18	23	28	34
				0.975	0.983	1.004	1.027	1.041	1.049	1.051
			3	5	8	11	15	19	24	29	35
			0.995	0.976	0.939	0.949	1.001	1.030	1.044	1.051	1.053
1	2	4	6	9	12	16	20	25	30	36	
1.008	1.004	0.987	0.939	0.186	0.954	1.013	1.037	1.048	1.052	1.054	

Figure 4a. Pin power distibution in the assembly at 0 MWd/kgU burnup point

										31
										1.043
							21	26	32	
							1.036	1.041	1.043	
					13	17	22	27	33	
					1.010	1.025	1.036	1.042	1.044	
				7	10	14	18	23	28	34
				0.978	0.988	1.006	1.025	1.037	1.043	1.045
			3	5	8	11	15	19	24	29	35
			0.995	0.979	0.948	0.956	1.003	1.027	1.039	1.044	1.046
1	2	4	6	9	12	16	20	25	30	36	
1.006	1.002	0.988	0.947	0.263	0.960	1.013	1.033	1.042	1 046	1.047	

Figure 4b. Pin power distibution in the assembly at 2 MWd/kgU burnup point

										31
										1.034
							21	26	32	
							1.029	1.033	1.034	
					13	17	22	27	33	
					1.009	1.021	1.029	1.033	1.035	
				7	10	14	18	23	28	34
				0.987	0.990	1.005	1.020	1.029	1.034	1.036
			3	5	8	11	15	19	24	29	35
			1.000	0.988	0.962	0.969	1.003	1.022	1.031	1.035	1.037
1	2	4	6	9	12	16	20	25	30	36	
1.009	1.006	0.995	0.962	0.354	0.972	1.011	1.027	1.034	1.036	1.037	

Figure 4c. Pin power distibution in the assembly at 4 MWd/kgU burnup point

```
                                                31
                                              1 003

                                          21      26      32
                                        1 003   1 003   1 003

                                    13      17      22      27      33
                                  1 003   1 003   1 003   1 003   1 003

                              7      10      14      18      23      28      34
                            1 014   1 002   1 003   1 003   1 003   1 003   1 003

                        3       5       8      11      15      19      24      29      35
                      1 011   1 012   1 016   1 017   1 003   1 003   1 003   1 003   1 003

                1       2       4       6       9      12      16      20      25      30      36
              1 010   1 011   1 012   1 015   0 714   0 017   1 003   1 003   1 003   1 003   1 003
```

Figure 4d Pin power distibution in the assembly at 10 MWd/kgU burnup point

```
                                                31
                                              1 001

                                          21      26      32
                                        1 001   1 001   1 001

                                    13      17      22      27      33
                                  1 002   1 001   1 001   1 001   1 001

                              7      10      14      18      23      28      34
                            1 014   1 002   1 002   1 001   1 001   1 001   1 000

                        3       5       8      11      15      19      24      29      35
                      1 011   1 013   1 016   1 017   1 002   1 001   1 001   1 001   1 000

                1       2       4       6       9      12      16      20      25      30      36
              1 009   1 010   1 012   1 016   0 792   1 017   1 002   1 001   1 001   1 000   1 000
```

Figure 4e Pin power distibution in the assembly at 16 MWd/kgU burnup point

```
                                                31
                                              1 000

                                          21      26      32
                                        1 001   1 000   1 000

                                    13      17      22      27      33
                                  1 001   1 001   1 001   1 000   1 000

                              7      10      14      18      23      28      34
                            1 013   1 001   1 001   1 001   1 001   1 000   1 000

                        3       5       8      11      15      19      24      29      35
                      1 010   1 012   1 013   1 014   1 002   1 001   1 001   1 000   1 000

                1       2       4       6       9      12      16      20      25      30      36
              1 009   1 009   1 011   1 012   0 824   1 014   1 001   1 001   1 000   1 000   1 000
```

Figure 4f Pin power distibution in the assembly at 20 MWd/kgU burnup point

REFERENCES

1 Apostolov T , M Manolova, K Ivanov
HEXAB - A Family of Few Group Diffusion Codes for Hexagonal Geometry, KFKI-ZR6-562/89

2 Vasileva G , T Apostolov et al
Neutron- physics and thermal physics calculations for VVER-1000, XVIII Symposium of the Temporary International Collective (TIC) for joint research into the physics of VVER, 1989

3 Ivanov K ,M Manolova,T Apostoloov
An Application of Two-Sweep Method AGA DSOR in the HEXAB-3D code, Nuclear Energy, 28, 1990, Sofia

4 Woznicki Z
AGA Two-Sweep Method and Their Application in Critical Reactor Calculations, Nucleonica 9/23, 1978, pp 941-968

5 Nacamura Sh
Computational Methods in Engineering and Science, New-York, 1977

6 Ferguson D ,K Derstine
Optimized Iteration Strategies and Data Management Consideration for Fast Reactor Finite Diffusion Theory, Nucl Sci Eng Vol 64, 1978, pp 593-604

7 Komano Y , T Takeda, T Sekiya
Improved Few-Group Coarse-Mesh Method for Calculating Three-Dimensional Power Distribution in Fast Breeder Reactor NEACRP-L-204, 1978.

8 Seregin A
Increasing of the Solution Accuracy of Few - group Diffusion Coarse-mesh Problem in Three - dimensional Hexagonal Geometry, VANT, Ser Physics and technics of the nuclear reactors, 1985, N 5, pp 46-53

9 Azekura K ,H Aizava
Application of Coarse-Mesh Method to Neutron Diffusion Calculation for Fast Breeder Reactor, Nucl Sci Tech 22[5] 1985, pp 406-411

10 Ivanov K , T Apostolov, M Manolova
Methodical Investigations on Improving the Accuracy of Solution and Efficiency of HEXAB-3D Code, Nuclear Energy [to be published], Sofia

11 Apostolov T et al
Numerical Investigation for Verification of a Computer System for VVER Neutron - physics Calculation, XVIII Symposia of the Temporary International Collective (TIC) for joint research into physics of VVER, 1989

12 R Prodanova, T Apostolov
NESSEL-IV-EC Code for Calculation of the Local Neutron - Physics Parameters of Light Water Moderated Reactor Cores, Nuclear energy, 27, 1988

13 Zaidel F et al
20 and 30 - Diffusion Calculations for VVER-440 Benchmark, Symposium of the ITC, 1984

14 Shulch G
Model Problem for Calculation of Neutron Flux in VVER-1000, XV Symposium TIC, 1986

15 Consultants report on Proposed Programme for CRP on Safe Core Management with Burnable Absorber in VVERs IAEA, 1988

16 Krial V , Legman M
BORORO - A New 2D-Diffusion Code for Rod by Rod Calculations of Active Core, VII Symposium TIC, 1978

ŠKODA COMPUTATIONAL SYSTEM FOR VVER REACTORS

J. VACEK, P. MIKOLÁŠ,
J. ŠVARNÝ, V. KRÝSL
Škoda Plzeň,
Czechoslovakia

Abstract

The code system that is used in Škoda Plzeň for reactor safety analysis, in-core fuel management studies, criticality assesment of storage pools etc. for VVER-type reactor lattices, and some results of its validation, are described in this paper.

1. INTRODUCTION.

The code system that is used in Škoda Plzeň for reactor safety analysis, in-core fuel management studies, criticality assesment of storage pools etc. for VVER-type reactor lattices, consists of three main subsystems: lattice analysis subsystem, correlation subsystem and global reactor analysis subsystem.

The lattice analysis subsystem consists of following parts:

- WIMS-TRACA, a code used for the lattice calculations at a set of discrete lattice states that span the expected range of state variables (burnup, fuel temperature, moderator temperature and density, boron acid concentration etc.). Both cell-averaged and assembly-averaged few-group diffusion constants can be produced. The results of code validation against a set of a series of experimental and numerical benchmarks for different lattices, including non-uniform lattices containing control or burnable absorbers, justify the inclusion of WIMS into the production system of codes for VVER analyses.

- DIAMANT-2, a code used for studies of effects of different approximations (diffusion vs. transport, WIMS cylindrical representation vs. actual hexagonal 2-D geometry etc.).

- HOMOGS, a code for the assembly calculation in the diffusion approximation. It serves for the assembly homogenization at the stage of the preparation of the few-group diffusion data library.

- HECON, a code computing gamma-matrices, i.e. matrices relating flux to current at the core boundary (external or internal).

To describe the influence of history and environment, the method of spectral indices (i.e. the ratio of epithermal to thermal flux), is used. Not only assymptotic lattices but also lattices with disturbed spectrum are analyzed. Two types of spectral indices are used - the instantaneous one describing the influence of environment and local changes in values of technological parameters and the historical one, describing the influence of changing spectrum on the fuel isotopic composition.

Results of the lattice analysis subsystem for a set of lattice states enter the correlation subsystem. Here they are processed by the code APPRO that, on the basis of selected criteria of accuracy, correlates the lattice parameters and determines the coefficients of parametric expressions. These coefficients are then stored together with original tables in the library of few-group diffusion data. Both parametric expressions and interpolation in tables can then be used to retrieve diffusion constants for the given set of parameter values. So called implicit method is used, i.e. macroscopic cross sections dependent on the burn-up are processed and stored and burn-up equations are not solved in the core simulator. The only exceptions are the poisoning isotopes Xe^{135} and Sm^{149} and chemical shim control isotope B^{10}, that are treated explicitly and therefore their microscopic cross sections must be processed and stored.

The global reactor analysis subsystem consists of three-dimensional core simulators MOBY-DICK and BIPR. MOBY-DICK is the finite difference diffusion code using Boressen's approximation of diffusion coeffficient as the geometric mean instead of the usual harmonic one. This approximation results in substantial savings of both the computer memory and computing time and is acceptable when there are no great differences between the properties of neighbouring nodes. The code allows to perform fine-mesh and coarse-mesh calculations and also the combined calculations, i.e. it can solve fine-mesh 2-D diffusion equation for a selected horizontal plane with axial leakage calculated on the basis of the previous 3-D coarse mesh calculation. It also allows to account for the thermohydraulic feedbacks using simple correlations. MOBY-DICK can use few-group libraries in different formats. The code contains the built-in verification subsystem containing at present evaluated operational data for the LOVIISA reactor. It facilitates the fitting of the library to the operational data. Iteration accelaration strategies, treatment of feedback effects and some other details, together with results of the code verification, are presented in the paper.

BIPR is a member of the Soviet family of coarse mesh one-and-a-half group core simulators. Here it is mentioned for completness without any details. Through standardized interface files it can be coupled to MOBY-DICK and HEXALOK. HEXALOK is a code for the assembly dehomogenization at the stage of the analysis of detailed power distributions after the core coarse-mesh calculation.

2. LATTICE ANALYSIS SUBSYSTEM.

2.1. Calculational scheme.

The main task of the latice analysis subsystem is the preparation of multidimensional tables of the few-group diffusion constants dependent on

- technological parameters (fuel temperature, moderator temperature and density, boron acid concentration, position of control absorbers, specific power etc.),
- burn-up,
- spectral indices.

Spectral indices, defined as the double ratio of epithermal to thermal flux, describe the influence of the spectrum perturbations on the few-group diffusion data. The instantaneous spectral index reflects the influence of the departure of the actual values of technological parameters from the nominal ones, the historical spectral index is used to describe the influence of the spectral changes during burn-up on the fuel isotopic composition. The perturbation of the spectrum is achieved by adding an extra annulus to the structure studied (cell, supercell or assembly). Due to this, the spectrum of the interior structure is different from the assymptotic one.

Isotopic composition of the fuel and, through it, the few-group diffusion data, depends not only on the burn-up, but also on the spectrum, in which the fuel burns. We suppose that this dependence can be described by a single variable - historical spectral index S_I - defined by the formula

$$(\Phi_e / \Phi_t)_{micro} = S_I \, (\Phi_e / \Phi_t)_{ass} ,$$

where Φ_e is the epithermal flux, Φ_t thermal flux and $(..)_{ass}$ denotes the ratio of assymptotic fluxes, i.e. the fluxes in the uniform infinite lattice. In the macrocode, we determine the current value of S_I at a given burn-up A in mesh i so that

$$(\Phi_e / \Phi_t)_{macro} = (\Phi_e / \Phi_t)_{micro} \, (A_i, S_I).$$

Naturally, the isotopis composition is not determined by this current value $S_I(A)$, but by the value averaged over the lifetime of the fuel element. The following weigthed average that reflects the decreasing influence of the past, is used:

$$\bar{S}_I = \frac{\int_0^A S_I(A') \exp(\mu A') \, dA'}{\int_0^A \exp(\mu A') \, dA'}$$

The relaxation factor μ lies in the range of 10^{-4} tU/MWd.

Instantaneous spectral index s_I is determined in the macrocode as

$$(\Phi_e / \Phi_t)_{macro} = s_I \, (\Phi_e / \Phi_t)_{\infty} ,$$

where $(...)_{\infty}$ is the assymptotic ratio of epithermal to thermal flux that can be expressed as

$$\left(\frac{\Phi_e}{\Phi_t}\right)_{\infty} = \frac{\Sigma_a^t}{\Sigma_s^{e\to t}} ,$$

where Σ_a^t is the thermal absorption cross section, $\Sigma_s^{e->t}$ is the epithermal to thermal group scattering cross section.

The calculational scheme is illustrated in Fig.1. The burn-up calculations are performed for any materially and geometrically different lattice element in so called main branches. Each of them is characterized by nominal values of technological parameters and selected value of the historical spectral index. It means, that for any lattice element several main branch calculations are run for different values of historical spectral index. As a result, we obtain burn-up dependent isotopic inventories. Then, for selected points at the burn-up scale, calculations in auxiliary branches are performed. Any auxiliary branch is characterized by the departure of values of selected technological parameters from the nominal ones and/or the departure of the instantaneous spectral index from its main branch value. As a result, we obtain the tables of parameter dependent diffusion constants. The values of parameters are selected so that they span the supposed range of operational values for both cold and hot states.

Our code system is used for two types of VVER reactors. The older one, VVER-440, is composed of basically uniform fuel assemblies and controlled by control asemblies. At the lattice level, we can neglect two-dimensional effects and the assembly homogenization can be performed at the transport level. The situation is more complicated for VVER-1000 reactor, controled by clusters of control rods. Moreover, burnable control absorbers are used in this core. Therefore two-dimensional nonuniformity must be accounted for at the lattice analysis level. As two-dimensional transport calculations are rather expensive, they are used only for benchmarking purposes and two-stage process is used for the production of assembly homogenized data. The first stage is performed using the transport theory. Few-group diffusion constants are generated for the basic one-dimensional lattice elements (cells and supercells with central nonuniformity). The second stage homogenization is performad by the diffusion calculation of the hexagonal assembly.

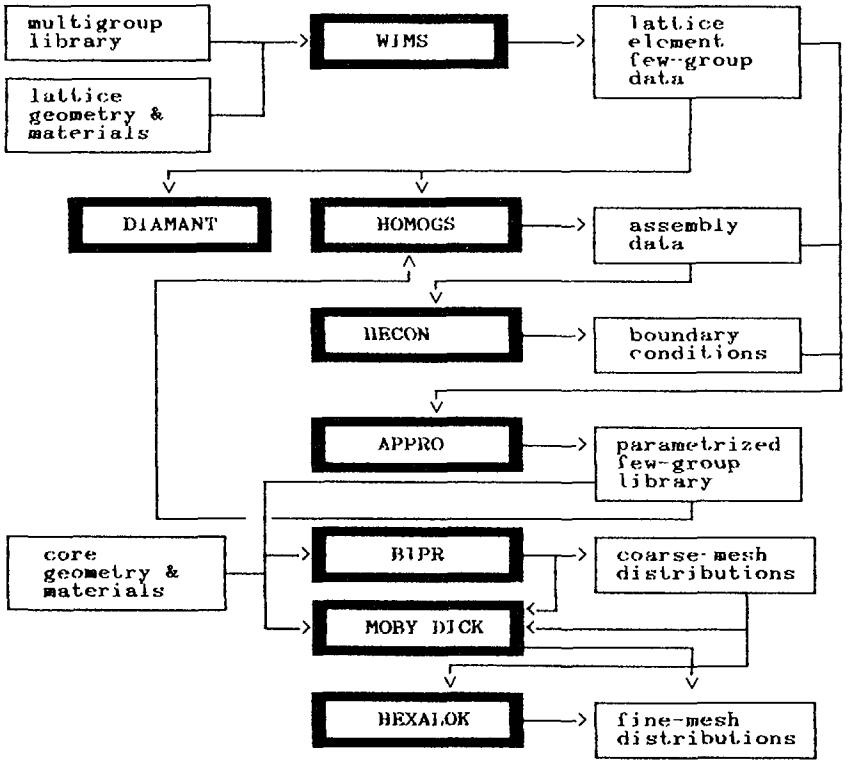

FIG. 1. Calculational system scheme.

The core boudaries are described by boundary conditions. For both core types, boundary conditions are applied at the external core boundary. For VVER-440, they may be applied also at the inner boundaries, i.e. at the control assemblies interfaces. At the lattice level, the set of parameter dependent γ-matrices is generated for different boundary types.

2.2. Components of the lattice subsytem.

2.2.1. WIMS.

The basic component of the lattice subsystem, the WIMS-TRACA [4] member of the WIMS-D family of codes, was aquired from the NEA Data Bank and slightly adapted to our needs. Later on, it was adapted to the IBM-PC/AT compatible computer. This code was selected among the available codes for its broad range of applicability and good international reputation. TRACA version was selected, as it allows regionwise homogenization and therefore several sets of data can be prepared simultaneously for different subregions of the modelled structure. For our calculational scheme it is also important, that we can model non-asymtotic cells by adding the extra region and calculate difusion constants of the inner regions averaged in the disturbed spectrum.

Before its routine use, the code was validated against a broad set of critical experiments and numerical benchmarks. Later on, lattices containing gadolinium were included into the validation process. The results of the validation were described in [1] and therefore only the brief review of the results is given here.

The results for a series of assymptotic criticals are summarized in Table 1. Series means $k_{ef,i}$ and standard deviations s_i^2 together with weighted means $\bar{k}_{ef}$ and standard deviations Δk_{ef} that are defined by the formulas [6]

$$\bar{k}_{ef} = \frac{\sum w_i \, k_{ef,i}}{\sum w_i} \quad , \quad w_i \sim \frac{1}{s_i^2}$$

$$\Delta k_{ef} = \sqrt{\frac{\sum w_i \, (k_{ef,i} - \bar{k}_{ef})^2 / (n-1)}{\sum w_i / n}} \quad ,$$

Table 1. Assymptotic lattices, series means

	mean k_{eff}	std.deviation	weight
ZR-6	1.006156	.009108	1.0472
BETTIS	1.002194	.001586	34.5358
WINFRITH	1.004557	.003641	6.5543
WAPD	.999919	.005538	2.8331
BNL	.999129	.003394	7.5412
TRX	.998811	.003210	8.4301
BAPL	1.001882	.002003	21.6452
SAXTON	.989248	.008326	1.2532
CAF	.991952	.015786	.3486
PNL	.997769	.002654	12.3312
Pu lattices	.996857	.003134	
U western	1.001589	.001676	

Table 2. Yankee - initial states

	WIMS	LASER[17]	experiment[17]
cold	1.1823	1.1840	-
hot,without power	1.1227	1.1210	1.1196+0.0033
hot,with power,unpoisoned	1.1029	1.1042	1.1035+0.0081
hot,with power,poisoned	1.0789		

where i denotes the values related to the series no. i, are presented here. we can see, that k_{eff} is slightly overestimated for uranium lattices and underestimated for Pu lattices. Among all U-lattices ZR-6 has greatest dispersion. Experience of several TIC laboratories shows that acceptable results are obtained, if two-dimensional calculations are performed with diffusion constants obtained by assymptotic cell calculations. It means, that ZR-6 results are not fully applicable as the benchmark for asymptotic cell calculations. Having this in mind, we can regard the agreement quite satisfactory. The applicability of WIMS to clean assymptotic lattices is confirmed by the analysis of numerical benchmarks.

In Table 2, results for the Yankee core are summarized. These results, together with the results of burn-up calculations of Maeder-Wydler [5] and Sidorenko [3] benchmarks for regular lattices without burnable absorber, illustrated in Figures 2 and 3, justify the inclusion of WIMS into the code system for the analyses of hot burnable lattices. In Fig.2, WIMS results are compared with the mean values of a series of codes presented in [5], in Fig.3 they are compared with results of Lutz [13].

The applicability of WIMS to the preparation of few-group diffusion data for nonuniformities such as control absorbers and water gaps was verified by the analyses of selected ZR-6 configurations. As an example, the results of the calculation of configurations 101/100 (B_4C rods) and 57/57 (water gaps) are presented in Figures 4 and 5.

Up to now, heterogeneous boron based burnable absorbers have been used in VVER-1000 cores, but they are supposed to be replaced by homogeneous burnable absorbers containing gadolinium. The research was started in this direction. Several internationally defined benchmarks were analyzed and results are in detail presented in [1]. In Figure 2, our results for Maeder-Wydler benchmark are compared with average values of [5], in Figure 3 our results for Sidorenko benchmark are compared with those of Lutz [13]. In both cases, WIMS overestimates k_{inf} in comparison with other codes for cells containing Gd. Due to this, k_{inf} is overestimated also for supercells and assemblies containing burnable absorbers.

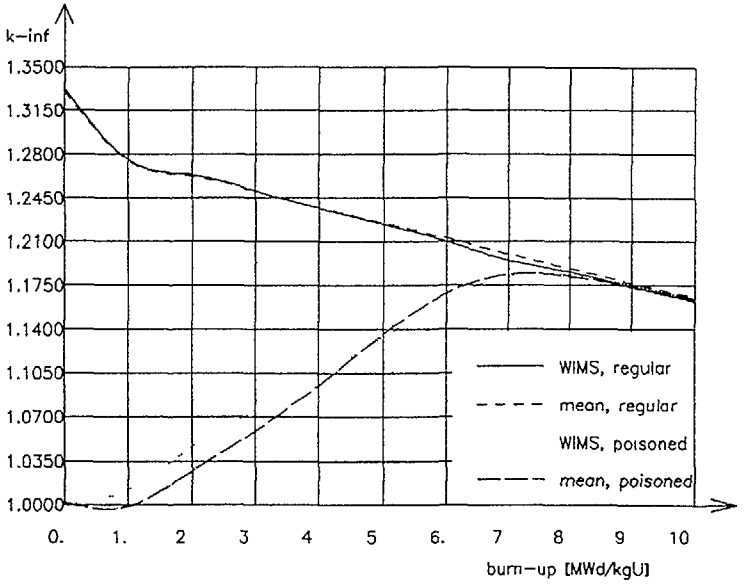

FIG. 2. Maedler-Wydler benchmark.

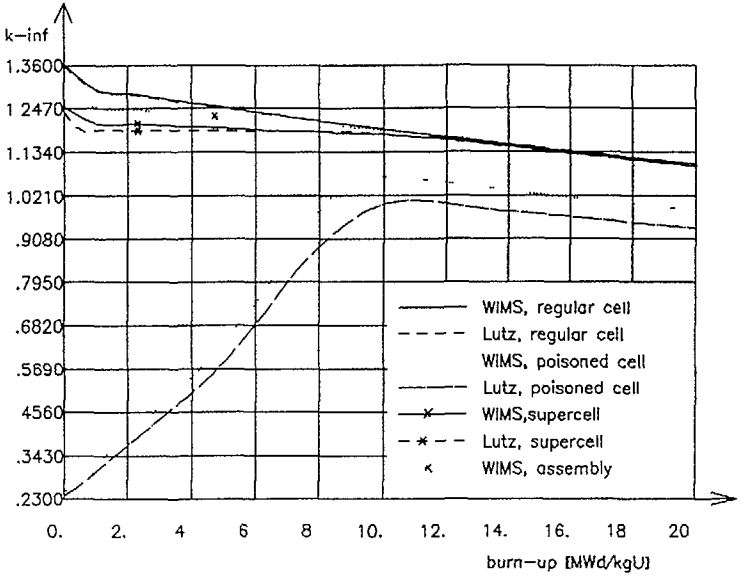

FIG. 3. Sidorenko benchmark.

Table 3. ZR-6 lattices of X7 type [10]

Lattice	k_{eff}	difference in power distribution [%] in annulus 1	2	3	4
I7	1.0136	0.33	-0.06	-0.29	0.33
J7	1.0160	1.34	0.46	-0.62	-0.18
K7	1.0125	1.08	0.64	-0.78	0.04
L7	1.0121	0.97	0.20	-0.38	-0.07
M7	1.0166	0.08	0.14	0.24	-0.25
N7	1.0184	2.17	0.53	-0.62	0.56

Table 4. Power distributions in LR-0 with UO_2-Gd_2O_3 [11]

Gd contents [%]	difference in power distribution [%] BA rod	annulus 1	annulus 2
0.5	-5.20	2.16	0.67
1.0	-7.30	2.25	0.70
1.5	-9.25	3.20	0.99
2.0	-14.24	2.96	0.92

Results of the comparison of calculations and experiments [2] for lattices containing Gd are presented in Table 3 for X7 type ZR-6 lattice. The order of the difference in k_{eff} is the same as for clean ZR-6 lattices. The differences between calculated and experimental values of power distributons show no systematic trends with changing Gd concentration.

In Table 4 we present the results for LR-0 lattice with UO_2 - Gd_2O_3 rods [11]. In this case, difference in the power in the absorber increases with increasing concentration of Gd. In contrast to results presented in [11], WIMS underestimates the power in the absorber. This indicates that the depression of the flux in the central cell is exaggerated, what can be caused by overestimating the Gd effectivity. It may imply that we should somewhat increase the gadolinium cross sections. We plan some investigations in this direction in the near future.

We can conclude that there exist some problems in the applicability of our computational models to lattices containing Gd absorbers but the discrepancies are of the same order as for other codes. We therefore regard our models acceptable for preliminary analyses and have in mind, that the research in this field should continue.

2.2.2. DIAMANT 2.

Using WIMS, only cylindricalized structures could be analyzed. As the actual geometry in VVERs is hexagonal, we

Table 5. Comparison of k_{inf}, WIMS and DIAMANT results

model		WIMS	DIAMANT 24	DIAMANT 96
supercell, central cell	fuel	1.24305	1.24300	1.24301
	water	1.23141	1.23181	1.23180
	absorber	0.93268	0.91446	0.91557
assembly, control cluster	inserted	0.92979	0.92052	

Note: 24, 96 for DIAMANT means number of triangles per cell

Table 6. Comparison of k_{inf} for assembly, WIMS and HOMOGS

burn-up [MWd/kgU]	control cluster inserted WIMS	HOMOGS regular	HOMOGS actual	with burnable absorber WIMS	HOMOGS regular	HOMOGS actual
0	0.91688	0.91439	0.92315	1.08743	1.08901	1.09202
5	0.88372	0.88161	0.88951	1.07621	1.07740	1.07850
10	0.85111	0.84953	0.85608	1.05618	1.05804	1.05837
15	0.82206	0.82013	0.82503	1.02858	1.03078	1.03081

acquired DIAMANT [8] from the NEA Data Bank to be able to analyze the effects of geometrical simplifications on one side and the effects of diffusion approximation used in HOMOGS, on other side. While the effect of the cylindrical approximation can be regarded negligible for regular lattices, it is of the order of 1% in k_{inf} for assemblies containing absorbers (see Table 5).

2.2.3. HOMOGS.

HOMOGS is a few-group finite difference code derived from MOBY-DICK. At the lattice analysis stage, it serves to the assembly homogenization. It accepts diffusion constanst prepared by WIMS (eventually processed by APPRO) and performs assembly calculations with reflective boundary conditions. Also at the stage of assembly homogenization the method of spectral indices requires homogenized constants not only for asymptotic, but also for disturbed spectrum. The spectrum disturbances are modelled here similarly as in WIMS by adding an extra region to the assembly, applying the boundary condition at the boundary of this extra region and averaging the constanst only over the proper volume of the assembly including the inter-assembly gap.

Results of WIMS and HOMOGS are compared in Table 6. The differences reflect effects of two combined approximations: the geometrical one (cylindrical in WIMS, hexagonal in HOMOGS) and the diffusion difference approximation used in HOMOGS. So called regular geometry is used in WIMS. It differs from the actual one by the shift of control cluster pins so that the

assembly possess a 30 degrees symmetry sector. The differences indicate that the actual geometry should be accounted for in the second stage homogenozation, even if it implies the increase in computing time due to lower symmetry of the problem.

2.2.4. HECON.

HECON is a code computing the heterogeneous constants by collision probability method. It is based on HECS code of Pedersen [9]. For a G-group problem, it generates a GxG matrix γ that couples flux and current on the surface of the element,

$$J = \gamma \Phi .$$

Typically, the calculations are performed in 10 groups with input data prepared by WIMS. Resulting parameter dependent few-group matrices (2 or 4 groups) are stored and later on processed by correlation subsystem.

3. CORRELATION SUBSYSTEM.

The subsystem consists of a single code - APPRO - that process the files created by the lattice analysis subsystem. The code employs the method of the least squares and performs a search for the optimum regression polynomials.

While some parameters are separable, others are correlated and therefore mixed terms appear in resulting polynomials. Up to now, the code haven't been able to determine systematically the degree of the correlations and heuristic approach is used to select the appropriate combinations.

The code is able to perform certain simple manipulations (e.g. select specified values, combine them together by algebraic manipulations etc.) over the input data that are defined by input commands. It can solve the criticality equation, determine the critical buckling and fluxes, that are then used for group collapsing. It determines the sensitivity of k_{inf} to different quantities that is used in the selection of optimum polynomial, where optimum means the simplest polynomial conforming to the criteria of accuracy.

At the output of the code we obtain a list of independent variables and, for each required quantity, the powers of independent variables and corresponding polynomial coefficients.

4. GLOBAL REACTOR ANALYSIS SUBSYSTEM.

4.1. MOBY-DICK.

4.1.1. Overview of the code.

MOBY-DICK [12] is a code system solving few-group diffusion equation. It uses Borresen's modification of the finite difference scheme. The system allows to construct computational paths for two- and three-dimensional calculations with two mesh types:

- triangular mesh with subdivision of the hexagonal mesh element to $6k^2$ triangles, used for coarse-mesh core calculations with a fuel assembly as the basic element;
- hexagonal mesh, used for fine-mesh calculations of the core or its subregion with an equivalent cell as the basic element.

Code allows to describe the wide variety of fuel management schemes: rotation of fuel assemblies, application of burnable absorbers etc. Libraries of parametrized few-group diffusion data in different formats can be easily incorporated. By specialized paths the code allows to perform

- analyses of burn up and transient processes with non-stationary poisoning,
- detailed analysis of characteristics of individual core states, core calculation without feedbacks.

Code results are stored in the code archive and they can be further processed or used as input to other programs.

The Borresen's modification of the finite-difference scheme consists in replacing the conventional averaging of the diffusion coefficient

$$\bar{D}_{ij} = \frac{2}{\frac{1}{D_i} + \frac{1}{D_j}}$$

by the geometric mean,

$$\bar{D}_{ij} = \sqrt{D_i D_j} .$$

Using the transformation

$$\psi_i = \sqrt{D_i}\ \Phi_i ,$$

finite-difference equations can be written in a form allowing substantional reduction of computer memory and time.

Generally, the boundary conditions are expressed by relation

$$J(r) = \gamma(r)\, \Phi(r).$$

Special cases of the boundary conditions are

a) albedo α. Then

$$\gamma = \frac{1}{2} (1 + \alpha)^{-1} (1 - \alpha)$$

and, if nondiagonal elements of α are zeros,

$$\gamma_{ij}^{gg} = \frac{1 - \alpha_{ij}^{g}}{2(1 + \alpha_{ij}^{g})} , \quad \gamma_{ij}^{gh} = 0 \text{ for } h \neq g.$$

b) extrapolated lehgths λ_{ij}^{g} :

$$\gamma_{ij}^{gg} = D_{i}^{g} / \lambda_{ij}^{g} , \quad \gamma_{ij}^{gh} = 0 \text{ for } h \neq g.$$

Any irregularity of finite-difference mesh size strongly deteriorates the effectivity of the corresponding code. MOBY DICK therefore uses the regular mesh. As for the fine-mesh calculations the actual mesh is not regular due to inter-assembly gap, diffusion data for those mesh elements should be modified to account for this effect. Some research has been done in TIC to solve theoretically the problem of the selection of the proper determination of effective constants, but up to now it has not led to conclusive recommendations. Therefore the following approach is used : Dilution coefficient α is determined as the ratio of the actual assembly volume V_{act} to the volume of the regularized assembly V_{reg},

$$\alpha = V_{act} / V_{reg} ,$$

and cross sections of the gap material Σ_{r}^{g} and $\Sigma_{s}^{g->h}$ are then multiplied by this factor. Corresponding diffusion coefficients D^{g} are not modified. The drawback of this method is that for the corner element at the interface among three assemblies the same average dilution is used as for normal interface elements between two assemblies. Mesh regularization implies the increase of the core size. Therefore the radii of reflector zones must be correspondingly modified to preserve their mean thicknesses if radial reflector is to be treated as the diffusion medium.

For inner iterations, conventional successive overrelaxation method is used. Outer iterations are accelerated using the method of Chebyshev polynomials. In special cases (no feedbacks, no criticality search), the method of Ljusternik extrapolation can be applied with advantage.

If the diffusion data are parameter dependent, then the third kind of iterations - feedback iterations - must be performed. In this process, we usually demand the core criticality and therefore criticality search is performed simultaneously. The iteration strategy aims to minimize the overall number of iterations. The low accuracy of inner iterations deteriorates the convergence rate of outer iterations, but there exists some useful limit of sufficient accuracy. If we exceed this limit, we only waste time. In MOBY-DICK the criterion for terminating the inner iterations is the decrease of the error in fluxes in two successive inner iterations to approximately 1% of an error in fission source in the preceding outer iteration,

$$\Delta\Phi^{(\mu,\nu)} \sim 0.01 \, \Delta S^{(\nu\ 1)} ,$$

where μ, ν are indices of inner and outer iterations, respectivelly.

The relation between outer and feedback iterations is more complicated. If the accuracy of outer iterations is relaxed, i.e. their number per one feedback iteration is relatively small, diffusion constants must be recalculated more frequently and, as more than 50% of the overall computational time is spent in these recalculations, it may result in the loss of computational effectivity. On the other side, if the convergence criterion is too stringent, feedback iterations can be oscillatory or even divergent. On the basis of our experience with the calculations of VVER-440 and 1000 we require the reduction of the fission source error in feedback iteration no. ν

$$\Delta S^{(\nu)} \sim c \, \Delta S^{(1)} ,$$

where c = 0.3 for reactor with power and c = 0.1 for reactor without power. The total number of outer iterations is limited to 15. Such strategy ensures in most cases either the monotonous character of iterations or strong dumping of eventual oscillations.

The parameters of the criticality search can be the following:
- critical height in 2-dimensional calculations,
- critical concentration of the boron acid used as a chemical shim control,
- critical level of the insertion of mechanical control elements. This search takes into account the limiting depths of the insertion and the established sequence of control element group insertion or withdrawal.
- critical time step length at the end of the fuel cycle, corresponding to the exhaustion of the available reactivity excess.

The physical and thermohydraulical feedbacks are characterized by
- thermal reactor output determining the local specific power,
  inlet coolant temperature, coolant mass flow and coolant pressure, determining fuel temperature and coolant temperature and density,
  fuel burnup,
- Xe and Sm concentrations,
- spectral indices.

Relatively simple thermohydraulical models and correlations are incorporated to the program. Fuel conductivity is determined by the relation

$$\lambda = \frac{3824}{130 + T} + 4.788 \cdot 10^{-11} T^3 .$$

Coefficient of thermal conductivity fuel - clad is determined by GAPCON-THERMAL3. Thermal convectivity clad - coolant is characterized by the convectivity mode. Two modes are allowed in MOBY-DICK:

convection to sub-cooled coolant. In this case, constant convectivity coefficient is supposed in the core and it is determined by Mac-Adams formula

$$\alpha = 0.023 \frac{\lambda_M(t_{in})}{De} Re^{0.8} Pr^{0.4} .$$

- surface and nucleate boiling. Here, Jens-Lottes correlation

$$t_{sl} - t' + \Delta t, \quad \Delta t = \frac{0.79204}{\exp(p/6.205)} \sqrt[4]{q_{sc}}$$

is used.

The single-channel analysis is applied to determine thermohydraulic characteristics of the coolant. The pressure change along the channel is neglected, homogeneous mixture water - vapour is supposed in two-phase flow, vapour is supposed to be saturated during phase transition and evaporation and condensation are supposed to be immediate.

Osmachkin correlation, which is rather conservative, is used to determine DNBR.

Reactivity coefficients can be calculated either directly by consecutive calculations or using perturbation theory.

4.1.2. Verification of the code.

The ability to predict reliably the performance of the core is the decisive factor of the acceptance of the code system. It can be verified by the follow-up studies based on the operational data. We have seen that the lattice subsystem is able to reproduce k_{eff} with an accuracy of the order of one percent, but even 1% means several days in the fuel cycle length. It means, that it is usually necessary to perform some fitting of the few-group libraries to operational data. Up to now, we don't apply any mathematically rigorous method and use the intuition and trial and-errors method. To estimate the code system performance, two case studies are presented here.

First of them is the study of the ZR-6 cores with absorbers and water gaps. The fitting of the library consisted in multiplying the thermal group diffusion coefficient by factor 0.7. Results of the final calculation are illustrated in Figures 4 and 5, where percent differences between calculated and measured power distributions are presented.

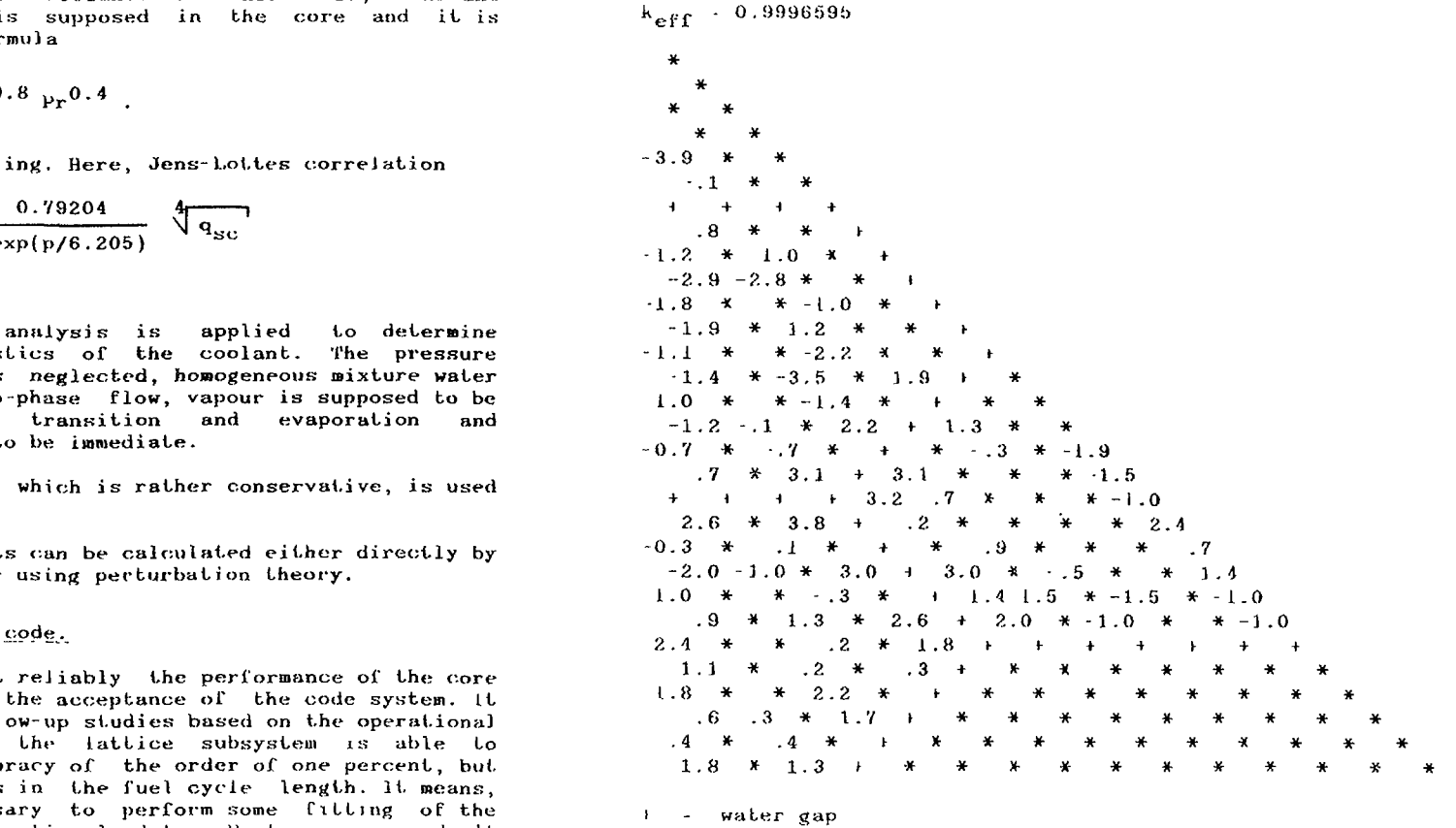

FIG. 4. ZR-6, configuration 101/100.

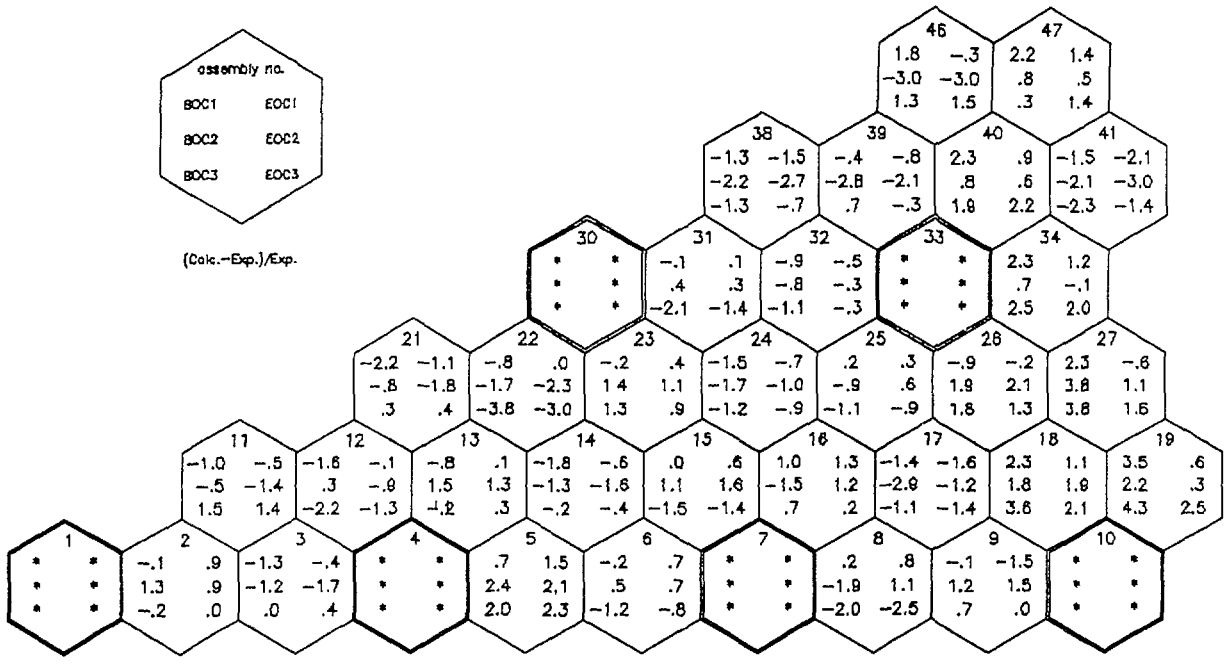

FIG. 6. Differences between power calculations and thermocouple data in Loviisa-1.

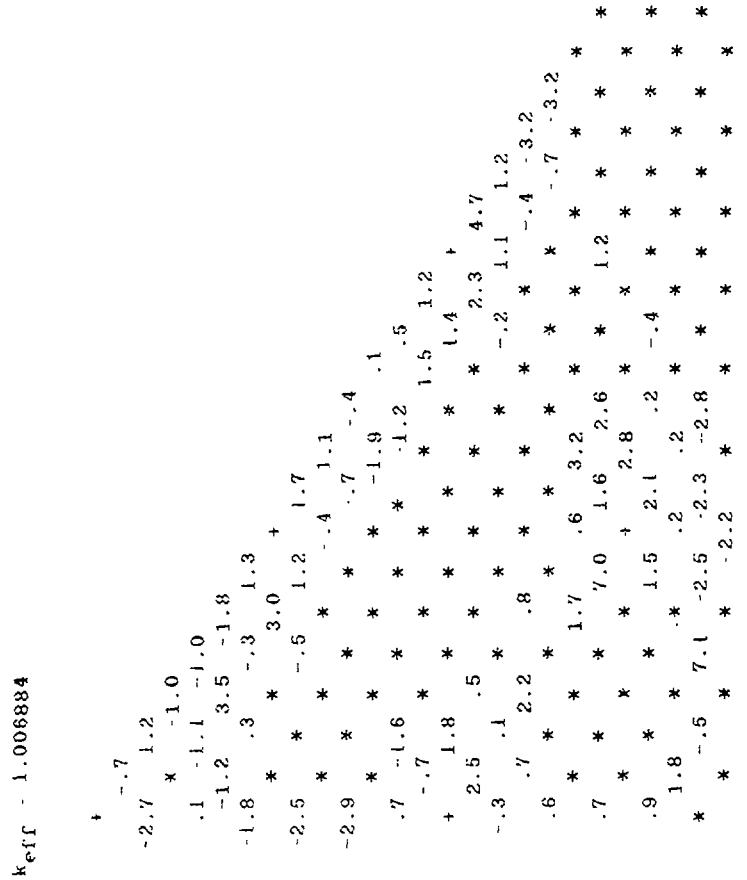

FIG. 5. ZR-6, configuration 57/57.

The second case is the analysis of the Loviisa reactor. This is the widely used case study among the TIC laboratories. The results of the calculations are summarized in Figs. 6 and 7 and Table 7, where the percent differences between calculated and measured specific powers are presented. For Rh self-powered detectors, axial profiles and integrated values are compared. For both sets of detectors, mean values of the differences over the whole core are given together with their standard deviations can be found in Table 7. In Figures 8 - 10, boron letdown curves are given for three cycles of LOVIISA-1.

In this case, the fitting of the library consisted in the multiplication of the diffusion coefficient by the factor 0.7, too. We can see, that the code with the fitted library is able to reproduce the core behaviour - with some exceptional

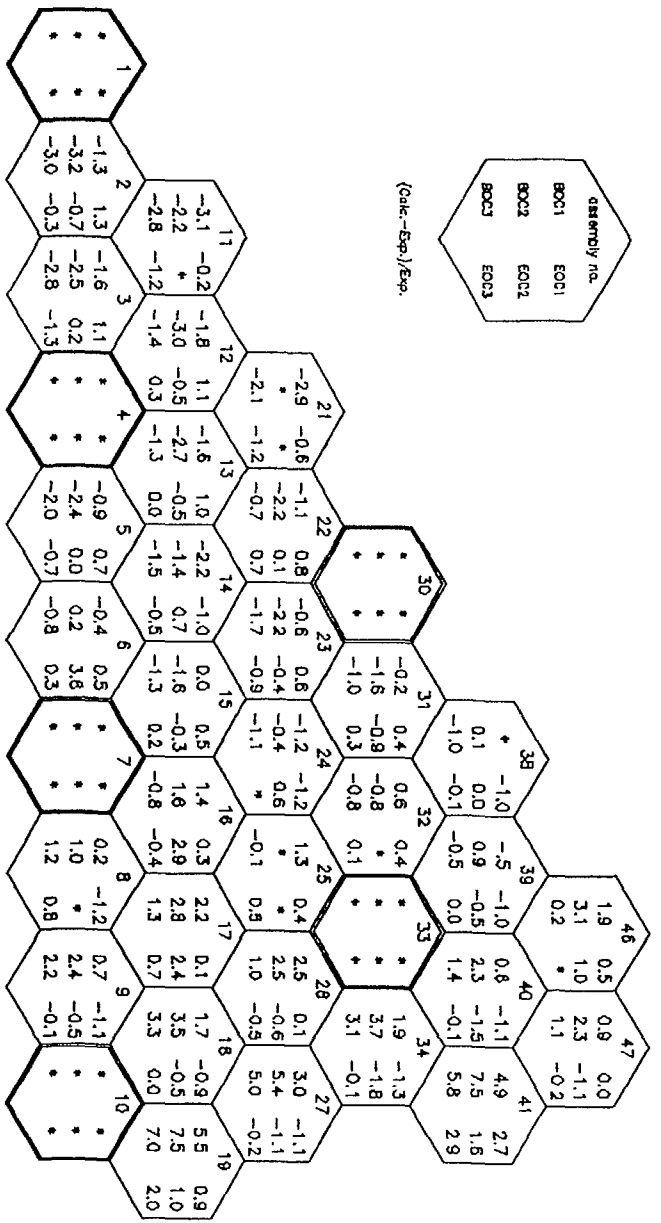

FIG. 7. Differences between power calculations and Rh data in Loviisa-1.

Table 7. Summary of results for Loviisa-1 test problem.

		Rh measurements level					Thermocouple measurements
		50	100	150	200	total	total
BOC1	mean difference	1.6	-0.5	-0.7	-0.5	0.3	0.1
	std. deviation	.9	.7	.7	1.2	1.9	1.5
EOC1	mean difference	-0.8	-1.8	-0.7	3.1	0.1	0.0
	std. deviation	.8	.8	.6	1.0	.9	.9
BOC2	mean difference	3.0	1.0	-1.0	-3.4	0.6	-0.1
	std. deviation	1.1	.8	.7	1.4	2.9	1.7
EOC2	mean difference	-0.7	0.6	0.0	0.1	0.1	-0.1
	std. deviation	.9	.9	.7	1.3	1.3	1.5
BOC3	mean difference	4.8	2.7	-1.1	-7.5	0.2	0.0
	std. deviation	1.0	1.1	0.7	2.0	2.4	2.0
EOC3	mean difference	1.5	0.4	-0.4	1.7	0.1	0.0
	std. deviation	1.0	1.2	.7	1.8	.8	1.5

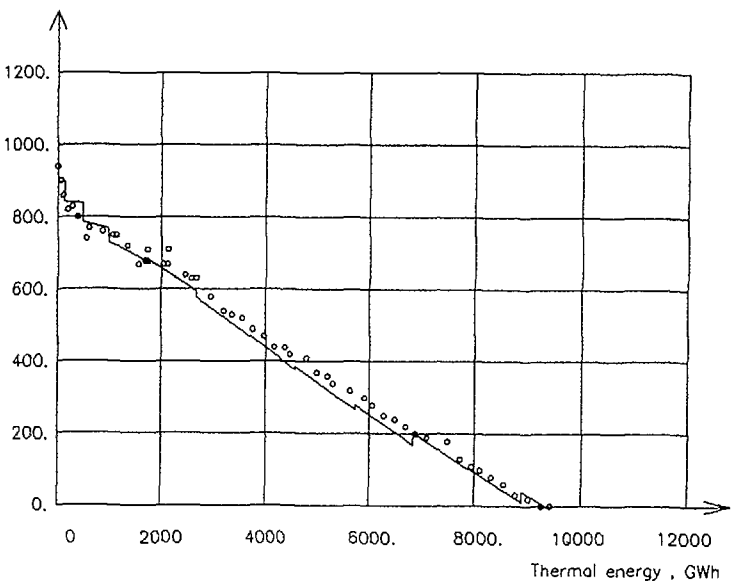

FIG. 8. Boron concentration (ppm) in Loviisa 1, cycle 1.

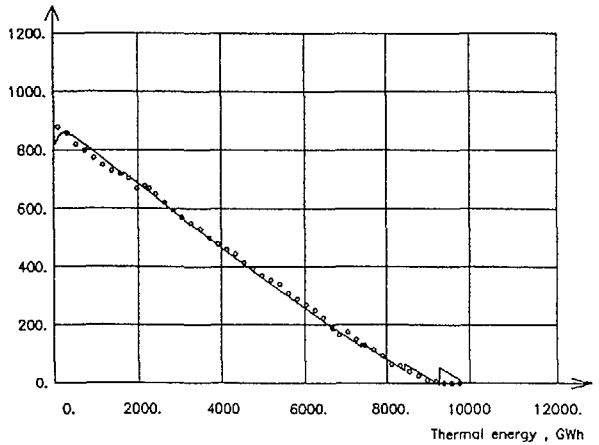

FIG. 9. Boron concentration (ppm) in Loviisa 1, cycle 2.

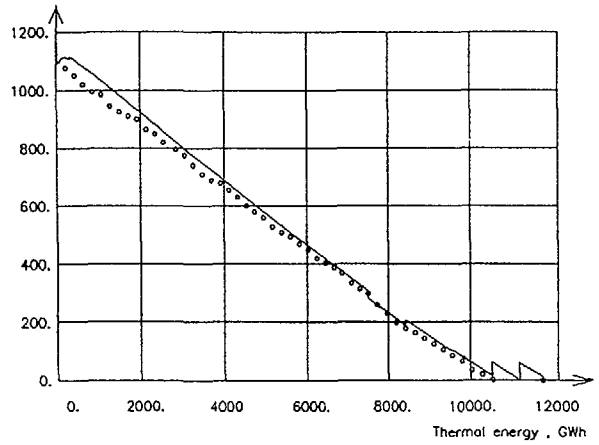

FIG. 10. Boron concentration (ppm) in Loviisa 1, cycle 3.

points - fairly well. The experience is confirmed by the follow-up analyses of start-up and operating states of several others VVER-440 reactors operated in Czechoslovakia. On the basis of these tests, MOBY-DICK with corresponding libraries was authorized by the Czechoslovak Atomic Energy Commission for safety studies and fuel cycle analyses.

At present, the library for the VVER-1000 is being prepared and later on, it will be fitted and tested against available operational data.

4.2. HEXALOK.

Critical assemblies (i.e. the assemblies in which the safety margins could be violated) are usually determined on the basis of the three-dimensional coarse-mesh calculation. Pin-by-pin power distributions can then be determined by the code HEXALOK that performs a fine-mesh diffusion calculation of the selected assemblies. In this case, non-homogeneous boundary problem is solved, boundary conditions being determined on the basis of the preceding coarse-mesh core calculation.

Acknowledgment

The authors would like to acknowledge the assistence of their colleagues Václav Rehoř and Pavel Mach in the preparation of figures presented in this paper.

REFERENCES

[1] J.Vacek, P.Mikoláš: Experience with the WIMS computer code at Škoda Plzeň, A Technical Committee/Workshop on In-Core Fuel Management, IAEA, Vienna, 1989

[2] Experimental Investigations of the Physical Properties of VVER-type Uranium Water Lattices, Final Report of TIC, vol.1, ed. by Z.Szatmary, Akademiai Kiado, Budapest 1985

[3] Consultants Report on Proposed Programme for the CRP on Safe Core Management with Burnable Absorbers in VVERs, IAEA, Vienna, 1988

[4] C.Ahnert, J.M.Aragones: MARIA System: A Code Block for PWR Fuel Assembly Calculation, J.E.N. 543, 1983

[5] C.Maeder, P.Wydler: International Comparison Calculations for a BWR Lattice with Adjacent Gadolinium Pins, EIR-532, 1984

[6] W.L.Zijp: Treatment of Measurement Uncertainties, ECN-194, 1987

[7] C.G. Poncelet: Burnup Physics of Heterogeneous Reactor Lattices, WCAP-6069, 1965

[8] K.Kufner, J.Burkhard, R.Heger : An Updated Fortran-77 Version of the 2-D Static Neutron Transport Code for Regular Triangular Geometry, KfK-4133

[9] J.Pedersen: Calculation of Heterogeneous Constants for Cylinders and Slabs, Riso-M 850, 1969

[10] I.Vidovsky, J.Gazso: Experimental Investigations of VVER type lattices containing Gd absorber rods, IAEA, CRP "Safe Core Management with Burnable Poisons in VVERs", 1989

[11] J. Bárdoš, M.Hron, J.Drexler, P.Veselý: Burnable Absorbers in VVER-type Fuel Lattices, IAEA, CRP "Safe Core Management with Burnable Poisons in VVERs", 1989

[12] V.Krýsl, M.Lehmann, J.Machaček: Theoretical foundations of a Modular Macrocode System "MOBY-DICK", Škoda Internal Report (in Czech)

[13] D.Lutz: Results for the Sidorenko Benchmark, IKE, 1989

THE PROGRAM SYSTEM KARATE

J. GADO, A. KERESZTURI, I. TROSZTEL
Central Research Institute for Physics,
Budapest, Hungary

Abstract

The program system KARATE is being developed for the calculation of the VVER-1000 type reactor. In the first part of the paper the main features of the code system is described. In the second part the first results are presented.

Introduction

In the Central Research Institute for Physiscs the modular code system KARATE is being developed for calculation of the VVER-1000 type reactor. The KARATE system will be finished by the end of 1990. The purpose of the program system is the calculation of the neutron physical and thermal-hydraulic processes in the core at normal, startup and slow transient conditions. The system consists of three calculational levels: the multigroup calculation of the fine-mesh diffusion type constants, the fine-mesh diffusion calculations inside the assemblies and the coarse-mesh global calculation of the reactor. In the first part of this paper the main features of these three levels are described and in the second part the first results are presented. A number of input and output data of calculated and measured benchmark problems are collected in a qualifying system and the calculating programs can be verified against them. Some of the results presented in the second part belong to the verification process.

I. The main features of the KARATE system

1. The multigroup calculations

The aim of the multigroup calculations is the generation of the few-group fine-mesh diffusion type constants for each type of the lattice cells of the further fine-mesh assembly calculations. The obtained cell averaged four-group cross sections are parametrized as a function of burnup, boron concentration, moderator density and temperature, fuel temperature, XE-135, SM-149, PU-239 concentrations. The epithermal-to-thermal flux ratio (abbreviated as SI for Spectral Index) is a further parameter which accounts for the nonasymptotic behaviour of the neutron spectrum.

All the multigroup calculations are performed in 35 epithermal and in 35 thermal groups. The calculations are based on a multigroup library generated from the ENDF/B-IV file. The thermal scattering is described by the Nelkin-model. The cross sections of the three resonance isotopes (U-235, U-238, PU-239) and the Bell factors are tabulated as a function of the dilution cross section of a homogeneous material and the temperature. The equivalence theory is used for the calculation of the shielded multigroup cross sections for the hetrogeneous case, where the Dancoff factor is determined from the first flight collision probabilities.

The following programs can be used for the calculation of the cell averaged few-group constants.

BETTY

The code is applied for the fuel cells. First the cell is homogenized using the multigroup collision probability method with white boundary condition on the edge of the cylindrized cell, after the B-1 equations are solved in order to taking into account the leakage in asymptotic approximation. For the cells with heterogeneous surroundings the nonasymptotic behaviour is assured artifically by means of an extra layer outside the cell. This way the parameter SI can be changed. The obtained few-group constants are parematrized as described above. For further applications the multigroup homogenized macroscopic cross sections of the cells are also stored.

COLA

The code is applied for the cells containing absorber rod or water hole surrounded by fuel cells. The surroundings is described by their homogenized multigroup macroscopic cross sections created by the BETTY calculations. Not only the symmetric solution but also the antisymmetric one is calculated for the determination of the diffusion coefficient. Generalized first-flight collision probabilities are applied in the cylindrical geometry.

CYLAN-SNARE

This pair of progrmmes can be used near to the complicated heterogenities, for example near to the edge of fuel assemblies or to the reflector. The code CYLAN calculates the response matrices for each cell and they are used in the program SNARE to solve the response-matrix equations for a limited number of cells near to the heterogenities. The drawback of this method is that because of its time consuming property the program SNARE works in four groups whereas the program CYLAN performs multigroup calculations. Therefore CYLAN needs four multigroup spectra which must characterize all the possible spectra on the edge of the cells. These spectra can be obtained from the COLA calculations. In the program CYLAN the very similar generalized first-flight collision probability method is used that was applied in the code COLA.

BURN

The fuel pin cell burnup calculations extend to 15 actinide and 73 fission prouduct isotopes, what allows following the burnup upto 50000 MWd/TU. Solving the burnup equations all important xenon and kripton isotopes are determined for the fuel temperature calculation, because they are needed for the determination of the gap and the fuel heat-conductance.

2. Fuel assembly calculations

The fuel assembly characterisitics are calculated by solving the two-group fine-mesh diffusion equation in hexagonal geometry for the given assembly or for the assembly and its surroundings (one third of each neighbour assembly). The irregularity between the assemblies is also taken into account in the difference scheme. The group constants depend on the parameterss listed above at the fuel cell calculations, and the feed-back via the the parameter SI accounts for the nonasymptotic spectrum. The boundary condition may be the traditional white boundary condition on the edge of the fuel assembly or may be a given flux distribution on the boundary of the calculation. The latter possibility allows the determination of the response-matrices for the fuel assembly. In this case it is reasonable not to choose the boundary of the calculation just on the edge of the assembly. This type of the boundary condition leads to an inhomogeneous set of equations (in mathematical sense) with prescribed k-eff instead of the traditional eigenvalue problem.

The aim of the fuel assembly calculations is twofold. In the first type of the calculations one provides the global calculations with two-group homogenized constants or response-matrices, whereas the second one determines the pin power peaking factor using the results from the global calculation in the form of boundary condition.

In the first case only one axial layer is calculated with predetermined thermohidraulic characteristics of the coolant. The burnup and concentrations of the isotopes U-235, U-238, NP-239, PU-239, XE-235, SM-149, I-135 may be calculated pin by pin. The resulting two-group cross-sections are parametrized before using them in the global calculation as in the case of the cell calculations. The response-matrices used only for methodical investigations yet.

The second type assembly calculation obtaines the boundary condition from the global calculation and solves an inhomogeneous problem with a given flux on the boundary. All axial layers are calculated and the third direction is taken into account by an axial buckling originated also from the global calculations. The burnup and the concentrations of the isotopes mentioned above are calculated pin by pin. In this way the complete history of the assembly can be followed in details.

3. Reflector calculations

Reflector regions are represented by albedo matrices in the global calculation and those matrices are deduced from a set of specific fine-mesh diffusion calculations with inhomogeneous boundary conditions. The albedo matrices of diverese reflector types are parametrized as a function of the boron concentration and the water temperature.

4. The global reactor calculations

The functions of the global calculations are as follows.

- Calculation of the state of the reactor core at given assemblywise burnup distribution and at given input flow and temperature. Determination of the k-eff or critical boron concentration or the control rod group position. Calculation of the flux, power and temperature distribution in the core.
- Fuel cycle calculation.
- Xenon transient calculation.
- Refuelling.
- Calculation of reactivity coefficients and kinetic parameters.

The global reactor neutron physics calculations are performad in two energy groups by means of a 3D nodal code in hexagonal geometry. The nodes are the assemblies subdivided into axial layers. The unknowns are the partial currents on each node boundary. In principle the fluxes are already known everywhere in the reactor from the partial currents. The nodes are described either by homogeneous cross-sections either by response-matrices available from the assembly calculation. In the first case the response-matrices coupling the partial currents for a given node are calculated analytically.

The homogenized cross-sections are parametrized in the same way as the fine-mesh diffusion type constants, the only differences are that instead of the fuel temperature the average node power is used and SI is not but k-eff is also a parameter. This parametrization makes it necessary, that during the burnup calculation besides the burnup the concentrations of the isotopes U-235, U-238, NP-239, PU-239, Xe-135, SM-149, I-135 must be also followed for each node.

5 Thermal-hydraulic calculations

The thermal-hydraulic modules of the KARATE system make it possible to calculate the thermal properties of the whole core in detail. The calculations are made on subchannel basis,

preserving the mass, energy and momentum. The mixing between the subchannels are also taken into account.

Because of the relatively high power density in the VVER-1000 core, it is supposed that subcooled boiling may occur in the core especially at abnormal conditions. Therefore KARATE is supplied with options for determination of the two-phase flow conditions. Here first of all the onset of boiling and subcooled void is calculated with care, however the calculation of fully developed boiling is also possible. Determination of the thermal-hydraulic parameters at an acceptable accuracy is reached by the application of VVER specific correlations that are checked to exeperiments of VVER type rod boundles.

The feedback of thermal-hydraulic data into the neutron physics calculations can be made at global and assembly level of the calculation. Preliminary experience shows that - except fast transients - one iteration step in the coupling ensures the necessary accuracy of the results.

II. Calculated results

In this section we are presenting certain results obtained by KARATE. A number of input and output data of calculated and measured benchmark problems is collected in a qualifying system. The first two problems presented here can be found also in this qualifying system, the third one is a special problem, where the thermal-hydraulic feed-back is investigated in the case of the assembly calculation.

1. Calculation of asymptotic lattices

The BETTY program was used to calculate the measured parameters of asymptotic lattices. The comparison of the calculated and the measured values first of all qualifies the multigroup cross-section library generated from the ENDF/B-IV file, because in the case of the asymptotic lattices we are using methodically verified algorithms. Three lattices have been investigated. The first lattice was measured in the BETTIS laboratory [1]. The second and the third lattices are the well-known TRX-1 and TRX-2 lattices [1]. The calculated and the measured values are in good agrrement as it shown in Tables 1-3, only the calculated ρ^{28} parameters related to the U-238 resonance capture are large to a small extent.

2. Calculation of supercell configurations

In the VVER-1000 type reactor the fast reactivity control is achieved by using cluster-type absorber rods. In the absorber assemblies in certain positions either movable absorber rods either water holes can be found. These positions approximately form a superlattice. In the ZR-6 reactor these heterogenities

Table 1. The calculated and measured parameters of the BAPL-1 lattice

Parameter	Measured value	Calculated value
δ^{25}	0.084 ± 0.002	0.0823
δ^{28}	0.078 ± 0.004	0.0731
ρ^{28}	1.39 ± 0.01	1.4366
k_{eff}	1.0	0.9986

Table 2. The calculated and measured parameters of the TRX-1 lattice

Parameter	Measured value	Calculated value
δ^{25}	0.0987 ± 0.001	0.0990
δ^{28}	0.0946 ± 0.0041	0.0941
ρ^{28}	1.320 ± 0.021	1.392
k_{eff}	1.0	0.9949

Table 3. The calculated and measured parameters of the TRX-2 lattice

Parameter	Measured value	Calculated value
δ^{25}	0.0614 ± 0.0008	0.0606
δ^{28}	0.0693 ± 0.0035	0.0679
ρ^{28}	0.837 ± 0.016	0.8653
k_{eff}	1.0	1 0019

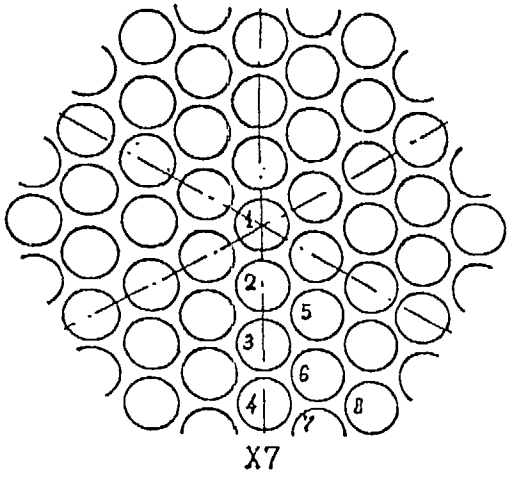

Fig. 1. Positions in the X7 supercell

were modelled by the X7 lattices [2], where the special cells are situated in every seventh lattice position. Apart from the temperatures the cell parameters agree with the VVER-1000 lattice parameters. The obtained supercell and the numbering of the positions can be seen on Fig. 1. Three types of heterogenities were investigated: B_4C absorber rod, water hole and gadolinium rod [3]. The calculations were performed by the COLA program with white boundary condition on the supercell boundary. The calculated and measured energy release distributions are shown in Tables 4-6.

3. The calculation of the fuel assembly with thermal-hydraulic feed-back

The aim of these calcultions was to investigate the influence of the thermal-hydraulic feed-back and the nature of the iteration when subcooled boiling occurs.

For the sake of the simplicity only the 30° sector of a fuel assembly was calculated. The numbering of the cells and the subchannels are shown on the Figs. 2 and 3. The bottom line on the Fig. 3 actually does not exist, it is only because of formal reason to describe the boundary condition. The shaded cells are containing water holes or gaps. All absorber rods were pulled out from the fuel assembly.

Table 4. Intra-supercell energy release distribution in the supercell containing B_4C absorber

Position	Measured value	Calculated value
2	0.880 ± 0.005	0.847
3	0.970 ± 0.007	0.960
4	0.990 ± 0.008	0.995
5	0.961 ± 0.007	0.941
6	0.997 ± 0.014	0.987
7	1.008 ± 0.007	1.000
8	1.000 ± 0.007	1.000

Table 5. Intra-supercell energy release distribution in the supercell containing water hole

Position	Measured value	Calculated value
2	1.115 ± 0.005	1.100
3	1.032 ± 0.005	1.020
4	1.006 ± 0.004	1.002
5	1.034 ± 0.005	1.031
6	-	1.006
7	1.015 ± 0.005	1.000
8	1.000 ± 0.005	1.000

Table 6. Intra-supercell energy release distribution in the supercell containing Gadolinium absorber

Position	Measured value	Calculated value
2	0.906 ± 0.002	0.918
3	0.972 ± 0.002	0.984
4	1.002 ± 0.002	0.998
5	0.973 ± 0.002	0.975
6	0.996 ± 0.002	0.995
7	1.003 ± 0.002	1.000
8	1.000 ± 0.002	1.000

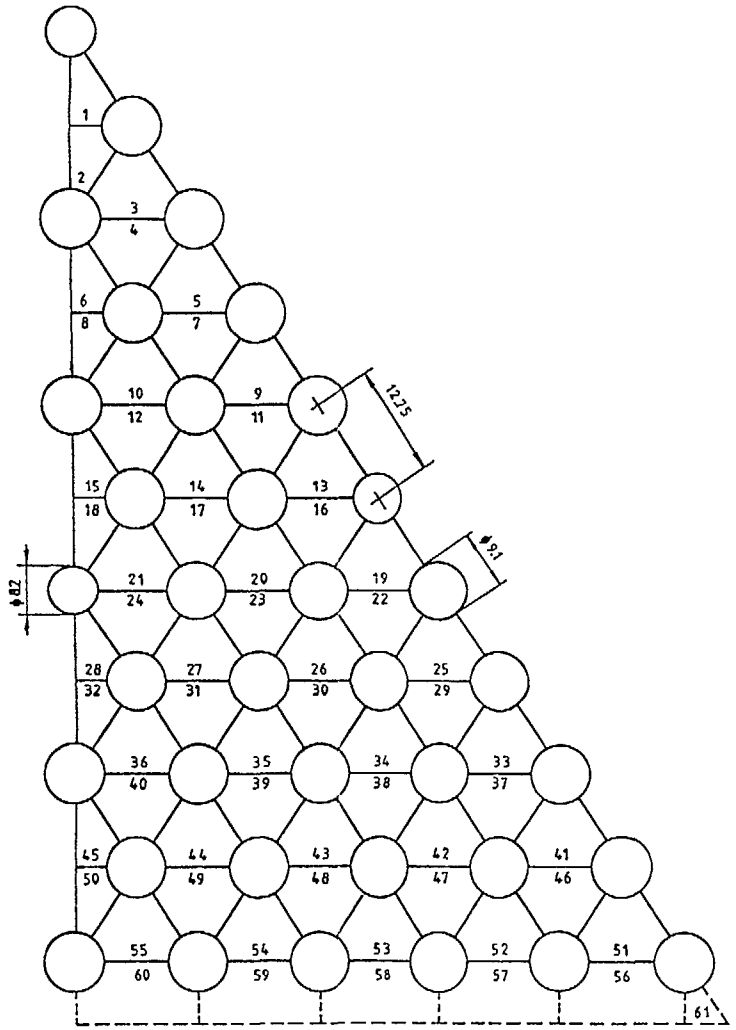

Fig. 2. The numbering of the subchannels

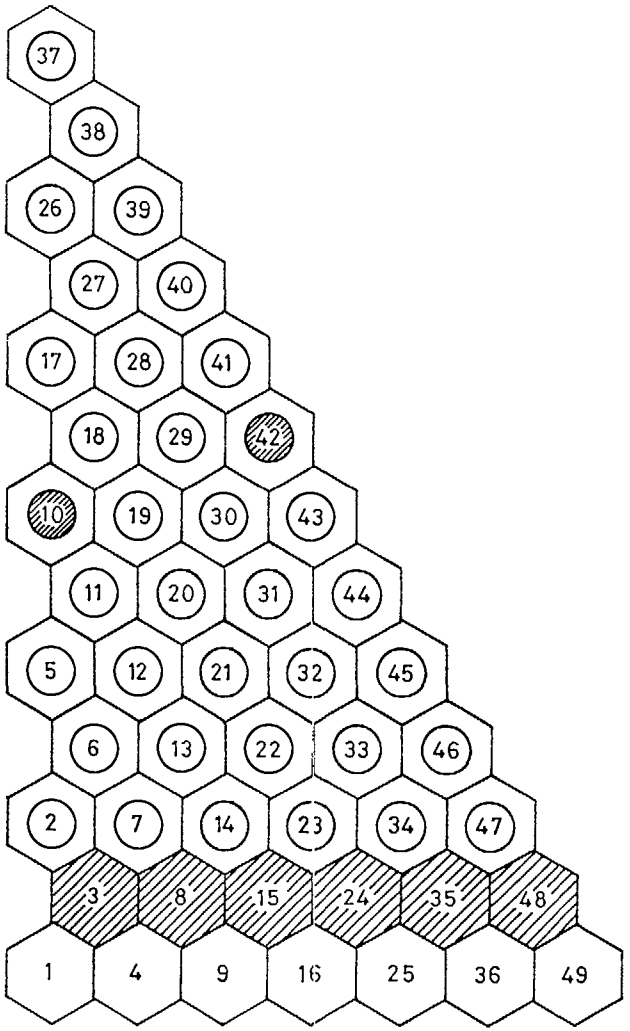

Fig. 3. The numbering of the cells

Table 7. The thermal-hydraulic iteration in the first case: h_0=23.6 cm, k_q=1.7

The weight (X) and volume (α) void contents in the subchannels

the number of the iteration steps	32-th subchannel		51-st subchannel	
	X	α	X	α
1	0.02487	0.1082	0.02186	0.09643
2	0.02572	0.1116	0.01925	0.08610
3	0.02560	0.1112	0.01966	0.08777

The coolant densities in the cells [gr/l]

the number of the iteration steps	5-th cell	47-th cell	46-th cell
1	583.5	639.3	569.5
2	584.2	641.2	573.9
3	584.1	640.9	573.2

The averaged coolant densities at the top of the assembly [gr/l]

the number of the iteration steps	ρ (one-channel model)	Σρ (subcannel model)
1	624.6	607.9
2	624.6	608.1
3	624.6	608.0

Table 8. The thermal-hydraulic iteration in the second case: h_0=24.1 cm, k_q=1.7

The weight (X) and volume (α) void contents in the subchannels

the number of the iteration steps	32-th subchannel		51-st subchannel	
	X	α	X	α
1	0.1709	0.4681	0.2137	0.5281
2	0.1680	0.4635	0.2177	0.5331
3	0.1683	0.4638	0.2177	0.5331

The coolant densities in the cells [gr/l]

the number of the iteration steps	5-th cell	47-th cell	46-th cell
1	487.2	588.4	404.0
2	491.5	587.2	410.6
3	491.2	587.2	410.2

The averaged coolant densities at the top of the assembly [gr/l]

the number of the iteration steps	ρ (one-channel model)	Σρ (subcannel model)
1	624.5	567.6
2	624.5	568.6
3	624.5	568.6

Considering that only the 30° sector of a fuel assembly was calculated the peaking factor between these sectors was taken into account by the increased value of the peaking factor between the fuel assemblies (k_q). The applied k_q was 1.7, which was obtained by supposing the largest gradient in the assembly with the highest power level. This assumption is never met but in this case the void content is already significant The water gap between the assemblies influences the power distribution to a great extent, therefore two cases were investigated; the lattice pitch between the aseemblies was 23.6 cm and 24.1 cm.

Fig. 4. The distribution of the power peaking factor at the top of the assembly
k_q = 1.7, h_o = 23.6 cm

To characterize the change of the power density and temperatures during the iteration three cells and two subchannels are chosen. The 32-th subchannel belongs to the 5-th fuel cell, which takes place next to a water hole. The 51-st subchannel takes place between the 46-th and the 47-th fuel cells. The power density is the highest in the 47-th fuel cell, in the corner of the fuel assembly. The coolant temperature is the highest in the 46-th fuel cell and in the 51-st subchannel.

The weight and volume void contents (X,α) for the subchannels, the coolant densities of the cells and the assembly averaged coolant densities can be found in the Tables 4 and 5. The data shown in these tables belong to the top of the fuel assembly. It can be observed that the inaccuracy of the coolant characteristics is smaller then 1% already after the 2-nd iteration step.

Tables 4 and 5 contain also the result of calculations with a one-channel model used for the whole fuel assembly (as it is in the global calculations) instead of the detailed subchannel model. In this case corresponding to the average heating up of the coolant the void does not appear, while according to the subchannel model the void content is not zero. In the tables the average density from the subchannel model and from the one-channel model are denoted by ρ and $\Sigma\rho$ respectively. The differences in the coolant density are 2.5% and 9% at the top of the assembly.

For the two cases the power densities at the top of fuel assembly are shown on the Figs. 4 and 5. The power density has the maximum at the corner of the fuel assembly. In the case of the greater water gap thickness the power peaking factor increases by 15%.

In the Figs. 6-9 the coolant void content and density distributions are illustrated in the cells and in the subchannels along the axis from the centre to the corner of the fuel assembly at the top. Though the power density is always the highest in the corner, the highest moderator temperature is obtained not in this but in the next cell. It shows that the cooling of the corner fuel cell is better than the cooling of the next one because of the mixing.

References

[1] J. Hardy· CSEWG Thermal Reactor Benchmark Compilation, supplement to BNL-19302 (ENDF-202), Jun 1974

[2] Final report of TIC, Volume 1, Experimental Investigations of the Physical Properties of WWER-type Uranium-Water Lattices, Akademiai Kiado, Budapest, 1985.

[3] I. Vidovszky, J. Gazso Results of the experiments carried out on VVER type lattices containing Gd absorber rods, Material of the Technical Comitte/Workshop on In-Core Fuel Management, 622-I3-TC-676.3 6.4, Vienna, 1989.

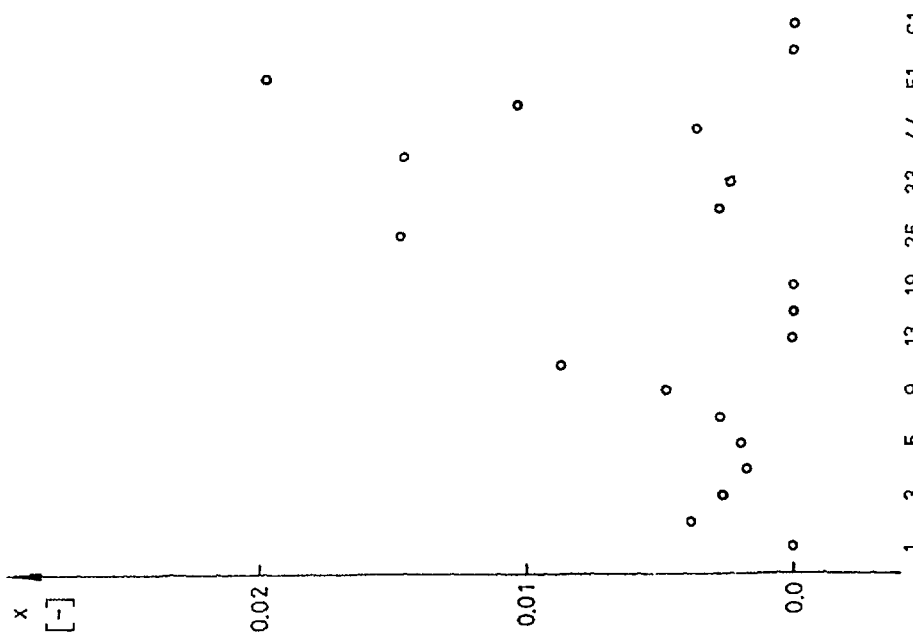

Fig. 6. The coolant void content at the top of the assembly in the subchannels
k_q = 1.7, h_o = 23.6 cm

K-K DISTRIBUTION

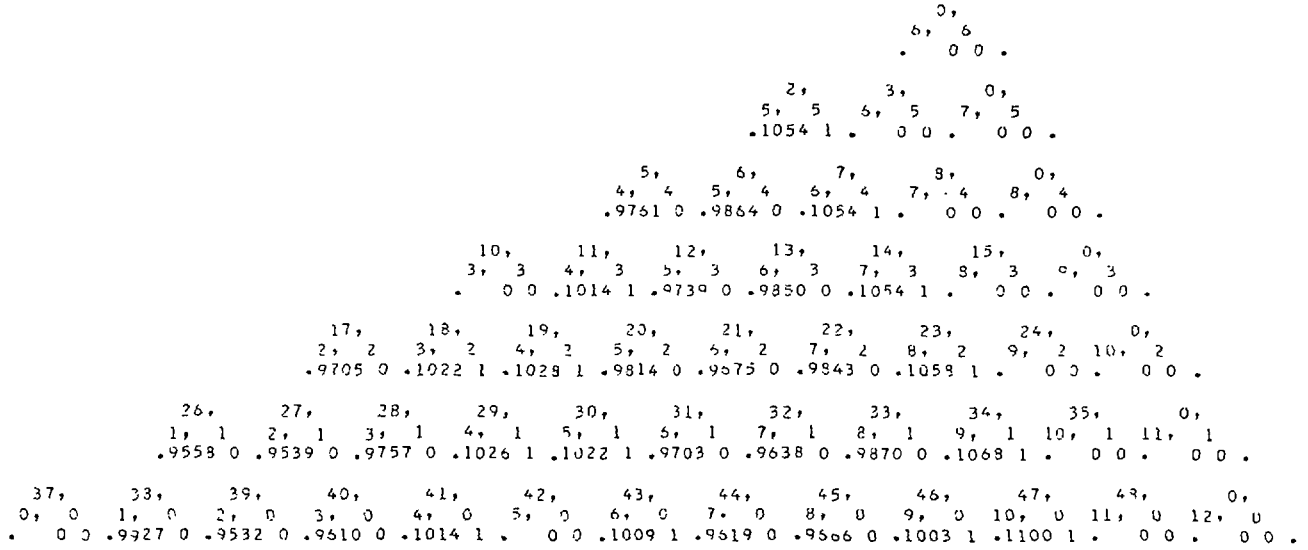

Fig. 5. The distribution of the power peaking factor at the top of the assembly
k_q = 1.7, h_o = 24.1 cm

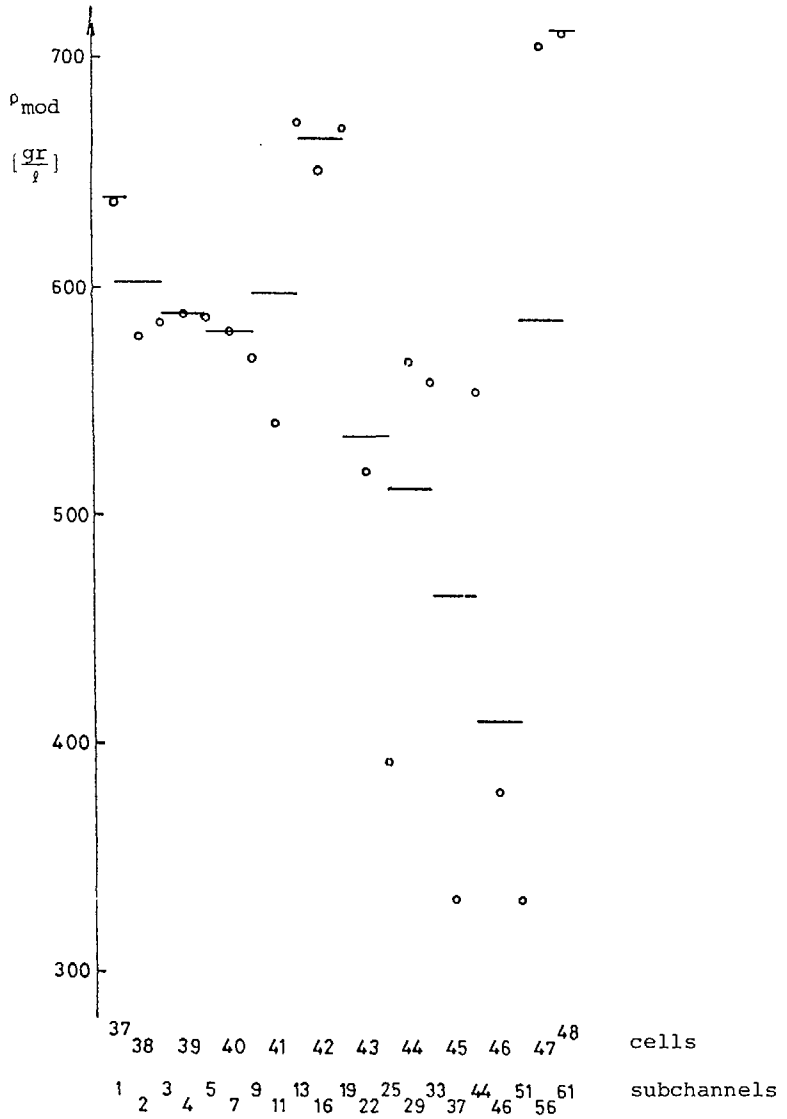

Fig. 7. The coolant density distribution at the top of the assembly
$k_{\sigma} = 1.7$, $h_o = 23.6$ cm

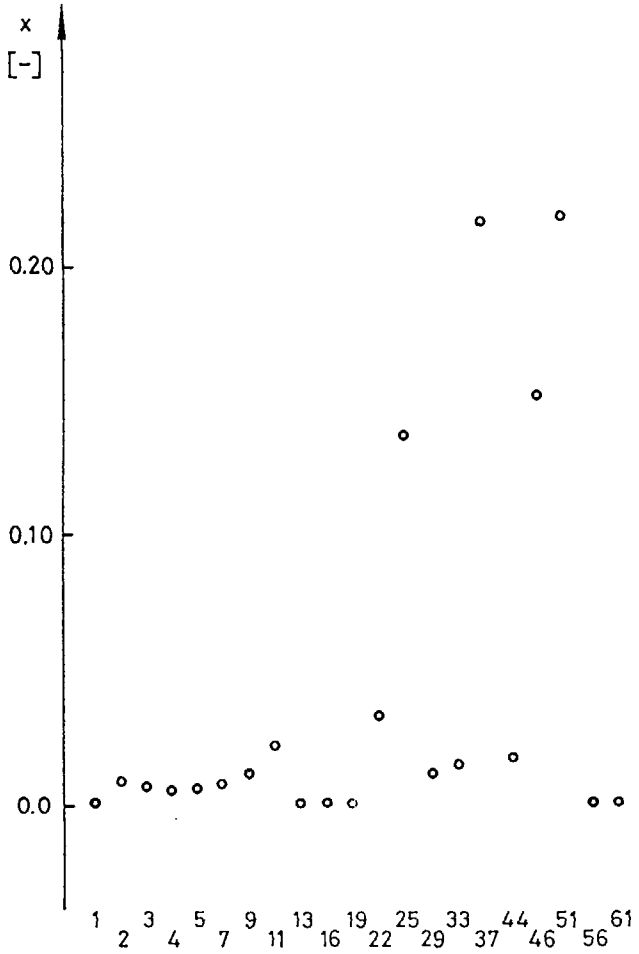

Fig. 8. The coolant void content distribution at the top of the assembly
$k_q = 1.7$, $h_o = 24.1$ cm

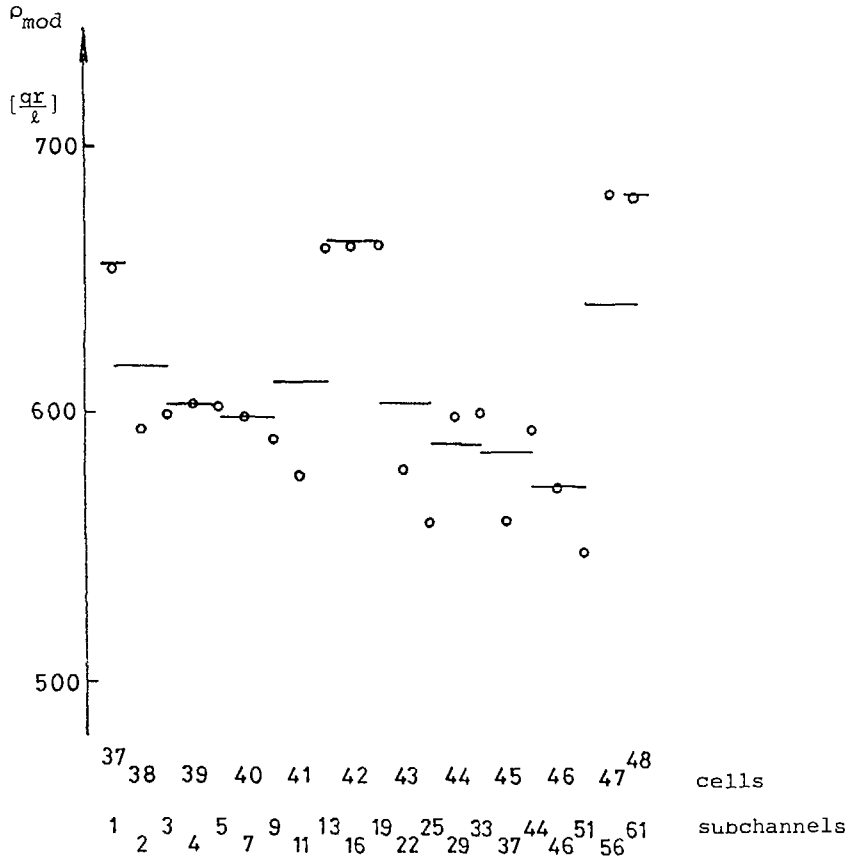

Fig. 9. The coolant density distribution at the top of the assembly
$k_q = 1.7$, $h_o = 24.1$ cm

NODAL METHODS FOR VVER CORE ANALYSIS

M LIZORKIN, V PSHENIN,
A NOVIKOV, A LAZARENKO
I V Kurchatov Institute of Atomic Energy,
Moscow, Union of Soviet Socialist Republics

Abstract

PERMAK is one of the modules of code package for VVER core analyses developed in I.V. Kurchatov Institute This code is used for two-dimensional fine-mesh (mesh step is equal to pins lattice step) few-group (from 1 to 6) calculations Code provides the following possibilities

- single state core calculation. Such calculations are used for codes verification on a base of a comparison of calculated and measured data obtained at zero power critical assemblies,
- calculations of pin by pin fluxes and power release distributions in core layer under burnup with taking into account feedback and reloading patterns. Needed for such type calculations values of axial buclings, full power of layer, water temperature and boron acid concentration are taken from preliminary three-dimensional coarse-mesh calculations. Preliminary prepared elementary cells macro cross sections library is used for such calculations. This library contains information about dependence of macro cross sections on burnup, integral neutron spectrum and others parameters.

Two type of balance equation are realized in PERMAK - finite difference diffusion equation and described in Part I of this paper nodal balance equation. Comparison of calculated and measured data obtained at ZR-6 critica that using of nodal type balance equation provides high accuracy of calculations of pin power release distribution and critical parameters for different nonuniform lattices (the full paper contain the results of such comparison).

Nodal approach similar to described above is used in three-dimensional coarse-mesh simulator BIPR-8 code.

1. Introduction

Calculations of rod by rod power distribution under burnup is necessary stage of VVER design and operational core analysis. Few-group fine-mesh (mesh step is equal fuel rod lattice pitch) diffusion codes are usually used for such calculations. Comparison of measured and calculated data shows that using of a standard finite-difference balance equation leads to a typical unaccuracies of fuel pins power and Keff values. Neutron spectrum deformations near

disturbers of a lattice uniformity (water gaps, reflector, absorbers and so on), unaccuracy of finite-difference approximation and nondiffusion effects are main reasons of mentioned above errors. Increasing of thermal group number from 1 to 3 together with balance equation improving based on representation of group fluxes distributions in a elementary cell as a sum of two functions allows to avoid these errors partially. But such approach leads to a significant increasing of processor time spending and besides this it is not well-founded for calculations of lattices containing very heterogeneous (with strong spatial flux depression) cells. More consistent and rational nodal type algorithm is described below (see also Ref. 1-2). This algorithm allows to increase an accuracy of calculations without rise of energy groups number and to use for its realization slightly modified standard diffusion code.

2. Nodal type balance equation

Mentioned above effects determining of unaccuracies of standard finite-differences few-group approach are the most important in a thermal energy region (correctness of this assumption will be demonstrated in the next section). So assume that thermal neutron flux distribution in an elementary cell "p" of hexagonal lattice can be represented as a sum of two modes - asymptotic (a) and transient (t) :

$$F_{pg}(\bar{r},\bar{\Omega},E) = F_{apg}(\bar{r},\bar{\Omega},E) + F_{tpg}(\bar{r},\bar{\Omega},E) \qquad (1)$$

here g - thermal group number (usually g=4).
Assume that each functions in (1) can be written as a sum of symmetrical (s) and antisymmetrical (a) modes:

$$F_{pg} = F_{aspg} + F_{aapg} + F_{tspg} + F_{tapg} \qquad (2)$$

where

$$F_{aspg} = a_{pg} f_{aspg} \;;$$
$$F_{tspg} = A_{pg} f_{tspg} \;;$$
$$F_{aapg} \simeq \sum_m b_{mpg} \cos[m\varphi + m\pi/3\,(i-1) + \delta^a_{mpg}]\, f_{aampg}$$
$$F_{tapg} \simeq \sum_m B_{mpg} \cos[m\varphi + m\pi/3\,(i-1) + \delta^t_{mpg}]\, f_{tampg} \qquad (3)$$

i - number of cell border (i=1,...,N, N=6)
δ_{mpg} - phase shift;
a, A, b, B - constants;
f - trial function.

Because of curvature of slowing down neutron flux in VVER lattices is not significant it is possible to confine to a first item (m=1) in expression for F_{aapg}. For a simplification let us assume that such approximation can be also used for F_{tapg}. (Index m is missed hereafter). Let us use now conditions of a flux and a current continuity at γ_i - a border between cells p and p_i

$$\tilde{\Phi}^{\gamma_i}_{pg} = \tilde{\Phi}^{\gamma_{i+N/2}}_{p_i g}$$

$$\tilde{J}^{\gamma_i}_{pg} = -\tilde{J}^{\gamma_{i+N/2}}_{p_i g} \qquad (4)$$

p_i - number of neigbouring cell.

According to (3)

$$\tilde{\Phi}^{\gamma_i}_{pg} = 1/\Gamma \int_{\Gamma} F_{pg}\,dE\,d\bar{\Omega}\,d\gamma_i = a_{pg}\,\tilde{f}^{\gamma_i}_{aspg} + b_{pg}\,\tilde{f}^{\gamma_i}_{aapg} + A_{pg}\,\tilde{f}^{\gamma_i}_{tspg} + B_{pg}\,\tilde{f}^{\gamma_i}_{tapg}$$

$$\tilde{J}^{\gamma_i}_{pg} = 1/\Gamma \int_{\Gamma} (\bar{N}_{\gamma_i}\bar{\Omega})\,F_{pg}\,dE\,d\bar{\Omega}\,d\gamma_i = a_{pg}\,\tilde{J}^{\gamma_i}_{aspg} + b_{pg}\,\tilde{J}^{\gamma_i}_{aapg} + A_{pg}\,\tilde{J}^{\gamma_i}_{tspg} + B_{pg}\,\tilde{J}^{\gamma_i}_{tapg} \qquad (5)$$

Condition (4) under consideration of expression (5) contains eight unknown coefficients a_{pg}, A_{pg}, $a_{p_i g}$, $A_{p_i g}$ and others determining amplitudes of corresponding trial functions. Coefficients a_{pg}, $a_{p_i g}$, A_{pg} $A_{p_i g}$ can be easily determined using neutrons balance condition in a cell and trivial properties of antisymmetrical functions:

$$a_{pg} = \bar{\varphi}_{apg}/\bar{f}_{aspg};\quad \bar{\varphi}_{apg} = \frac{\bar{S}_{pg}}{\bar{\Sigma}^a_{apg} + \alpha(\tilde{J}^{\gamma}_{aspg}/\bar{f}_{aspg})};\qquad A_{pg} = (\bar{F}_{pg} - \bar{\varphi}_{apg})/\bar{f}_{tspg}$$

$$\bar{F} = \frac{1}{V}\int F_{pg}\,dE\,d\bar{\Omega}\,dV \qquad (6)$$

$\bar{S}$ and α - source density and cell volume to surface ratio respectively. $\bar{H}$ - cell averaged value of function H. Amplitude of antisymmetrical asymptotic component of current can be expressed in the following form:

$$b^{\gamma_i}_{pg} = \frac{\tilde{J}^{\gamma_i}_{pg-1} - \frac{1}{N}\sum_i \tilde{J}^{\gamma_i}_{pg-1}}{\tilde{J}^{\gamma_i}_{aapg-1}} \qquad (7)$$

In expression (7) $\tilde{J}^{\gamma_i}_{pg-1}$ - currents in epithermal group. Determining two unknown coefficients $B^{\gamma_i}_{pg}$ and $B^{\gamma_i}_{p_i g}$ from system (4-5) and putting them into expression (5) one can arrive to the following formula for current density:

$$\tilde{J}^{\gamma_i}_{pg} = \frac{2}{h}\frac{D_{tpg}D_{tp_ig}}{D_{tpg}+D_{tp_ig}}\left\{(\bar{\Phi}_{p_ig}\, g_{ap_ig}-\bar{\Phi}_{pg}\, g_{apg})+(\bar{\Phi}_{p_ig}-\bar{\varphi}_{ap_ig})\,(g_{tp_ig}-g_{ap_ig})-\right.$$

$$\left.-(\bar{\Phi}_{pg}-\bar{\varphi}_{apg})\,(g_{tpg}-g_{apg})+\left[\tilde{\varphi}^{\gamma_i+3}_{aap_ig}\left(1-\frac{D_{ap_ig}}{D_{tp_ig}}\right)-\tilde{\varphi}^{\gamma_i}_{aapg}\left(1-\frac{D_{apg}}{D_{tpg}}\right)\right]\right\} \quad (8)$$

Balance equation writes as

$$\frac{\Gamma}{V}\sum_i \tilde{J}^{\gamma_i}_{p} - \bar{\Sigma}^{a}_{apg}\,\bar{\varphi}_{apg} - \bar{\Sigma}^{a}_{tpg}\,(\bar{\Phi}_{pg}-\bar{\varphi}_{apg}) + \bar{S}_{pg} = 0 \quad (9)$$

Cell averaged reaction rates as it is seen from (9) are written in the following form:

$$R_{pg} = \bar{\Sigma}^{\beta}_{apg}\,\bar{\varphi}_{apg} + \bar{\Sigma}^{\beta}_{tpg}\,(\bar{\Phi}_{pg}-\bar{\varphi}_{apg}) \quad (10)$$

where

$$\bar{\Sigma}^{\beta}_{apg} = \frac{\int_V \Sigma^{\beta}_{p}\, f_{aspg}\, dE d\bar{\Omega} dV}{V\,\bar{f}_{aspg}} \qquad \bar{\Sigma}^{\beta}_{tpg} = \frac{\int_V \Sigma^{\beta}_{p}\, f_{tspg}\, dE d\bar{\Omega} dV}{V\,\bar{f}_{aspg}} \quad (11)$$

It is possible to show that in a case when contribution of transient mode is negligible equation (9) is transformed to a asymptotic form:

$$\frac{2\Gamma}{hV}\sum_i \frac{D_{apg}\,D_{ap_ig}}{D_{apg}+D_{ap_ig}}\left(\bar{\Phi}_{p_ig}\,\varepsilon_{ap_ig} - \bar{\Phi}_{pg}\,\varepsilon_{apg}\right) - \bar{\Sigma}_{apg}\,\bar{\Phi}_{apg} + \bar{S}_{pg} = 0 \quad (12)$$

where

$$\varepsilon_{apg} = \frac{\tilde{f}^{\gamma_i}_{aspg}}{\bar{f}_{aspg}}\left(1-\frac{\delta_{apg}}{D_{apg}}\right).$$

Definitions of all included into eq. 8,9,12 functionals are given in Appendix 1. Equation of type (9) in principle can be spreaded on epithermal group. But in this case it is necessary to introduce into consideration greater number of trial functions in thermal group. Such more complicate and universal approach has been developed by N. Laletin [3,4]. This approach has also some essential features connected with using more universal than(4) continuity conditions. An expediency of using balance equation of type (9) for epithermal group and corresponding complication of balance equation for thermal group is discussed in the next section.

3. Results of numerical benchmarking for a case of slab geometry

A comparison of benchmark problems solutions obtained using precise code and code realizing algorithm (9) gives most detailed information about accuracy of this algorithm. In this case when functionals of trial functions are also calculated by precise code the results of comparison are interpreted simply. Calculations of typical VVER nonuniform lattices can be performed by codes based on Monte-Carlo method. But it is very difficult to adopt such codes for calculations of some functionals of asymptotic and transient modes. More simple situation takes place in a case of slab geometry when one dimensional transport code provides a possibility of creating the most consistent scheme of verification. In this case it is possible to validate reliability of most important approximations of equation (9). Results of such calculations are described below.

Precise solutions of benchmark problems and needed functionals of asymptotic and transient modes for elementary cells of slab lattice were calculated by one dimensional 61-group (24 thermal group) code AKSKIN [5]. Calculations based on equation (9) and standard finite-difference approach were performed by specially written code MODISN. Calculations by this code were carried out in one group (calculations of thermal neutrons distribution with given from transport calculations neutron source distribution) and four-group approximations. A combination of one and four-group calculations allow to analyze in detail unaccuracies of algorithm (9) under thermal neutron distribution calculations, to estimate a significance of cell heterogeneity and neutron spectrum deformation effects in epithermal group and consequently an expediency of spreading of described approach on epithermal group. Calculations have been carried out for configurations formed by slab cells of different compositions - homogeneous with U^{235} and Pu^{239} as a fissile isotopes and heterogeneous. Main characteristics of cells have been chosen close to corresponding characteristics of real VVER lattices. Calculations of configurations formed by homogeneous cells is a strong test to check a reliability of approach about universality of transient mode functionals. It is explained by an absence of water buffer which makes spectrum of neutrons crossing cell border in heterogeneous cells more universal. Some typical configurations have been considered - "water gap between fuel assemblies", "boundary between core and reflector", "supercell with absorber" and so on. Results of calculations are given in fig.1-4 and tables 1-2.

Results of one group calculations with fixed neutron source distribution for configurations formed by homogeneous and heterogeneous cells are given in fig 1-2 and 3-4 accordingly. It is seen from this figures that algorithm (9) provides a significant reduction of reaction rates calculations unaccuracy. Maximal difference in fission rate for example don't exceed 1.5-1.7%. Results of four-group calculations are given in tables 1-2. In table 1 unaccuracies of Keff and fission rate calculations for configurations with homogeneous cells are presented. In table 2 results for configuration "supercell with strong absorber" formed by heterogeneous cells are given. Data of this tables allow to make a conclusion that applying of algorithm (9) only for thermal group provides in most cases good accuracy of Keff and reaction rates calculations. Performed investigations allow to come to the following conclusions:

- unaccuracy of standard four-group finite-differences diffusion approach is a result of successful compensation of separate components;
- applying of algorithm (9) only to thermal neutron distribution calculations provides significant increasing of accuracy;

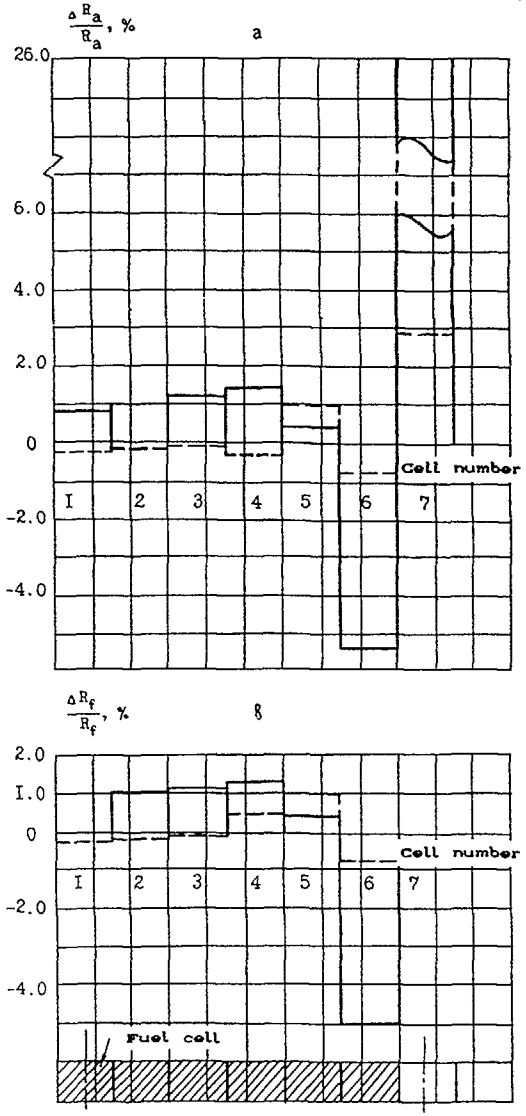

Fig.1 Comparison of absorption (a) and fission (b) reaction rates distributions for configuration "water gap between assemblies" formed by slab homogeneous cells.
—— – standard finite-difference balance eq.;
—— – algorithm (9);
ΔR/R = (Rtr–R)/Rtr·100

- for configurations with strong boron absorbers it is necessary to take into account cell heterogeneity effect in epithermal group;
- functionals of transient mode are enough universal (this means that they only slightly depends on cell position in a core);
- results of calculations are stable under varying of asymptotic and transient modes functionals in limits of their possible unaccuracies.

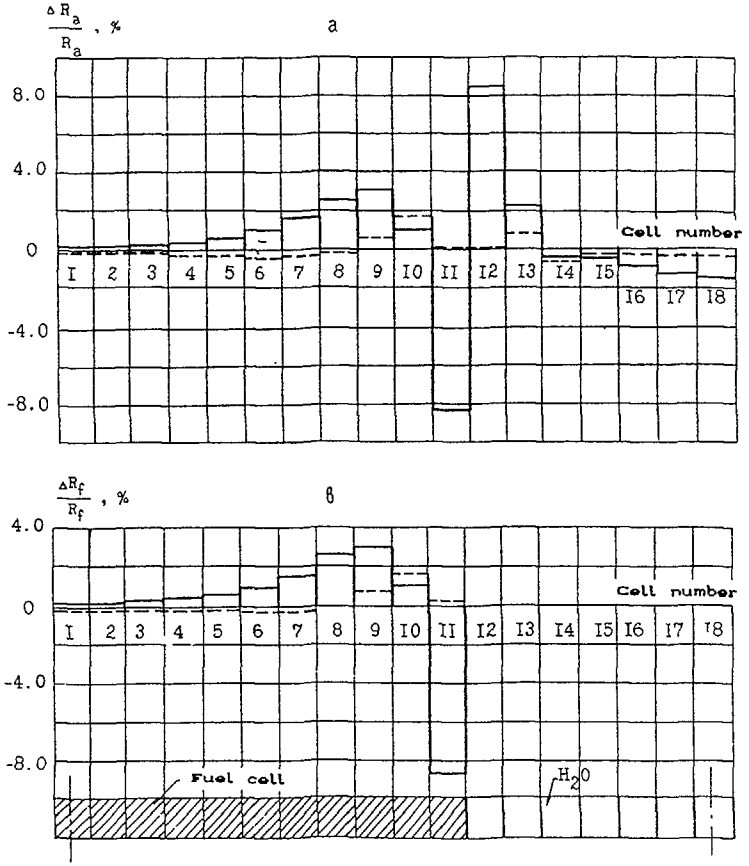

Fig.2 Comparison of absorption (a) and fission (b) reaction rates distributions for configuration "boundary with a reflector" formed by slab homogeneous cells. Conventional signs the same as on Fig.1.

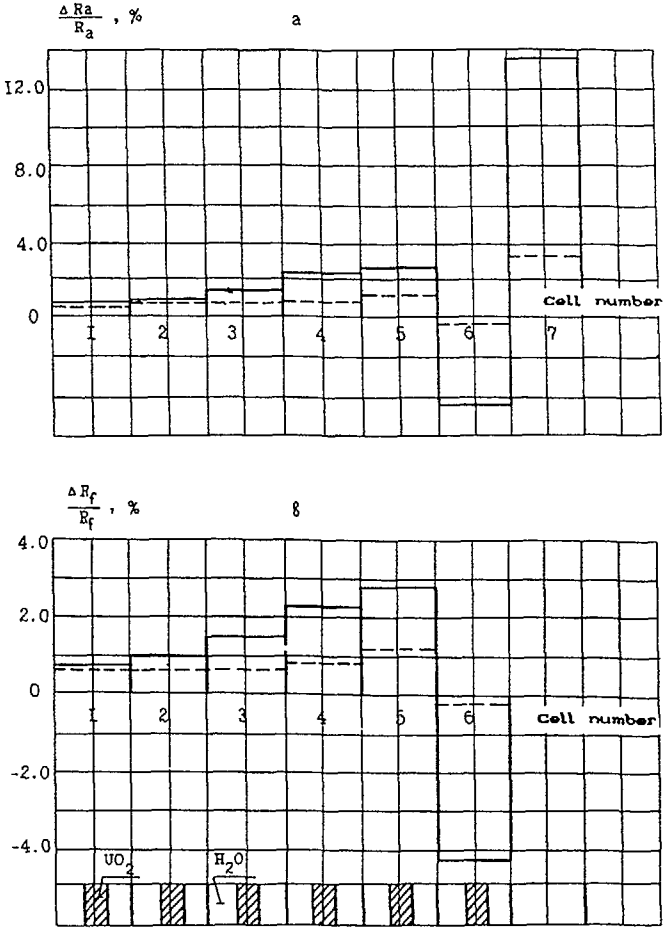

Fig.3 Comparison of absorption (a) and fission (b) reaction rates distributions for configuration "water gap between assemblies" formed by slab heterogeneous cells. Conventional signs the same as on Fig.1.

Mentioned above conclusions have been taken into account under applying of described approach to practical calculations. Results of calculated and measured data comparison demonstrating its accuracy in a case of real hexagonal lattices are discussed in Sect. 7 of this report.

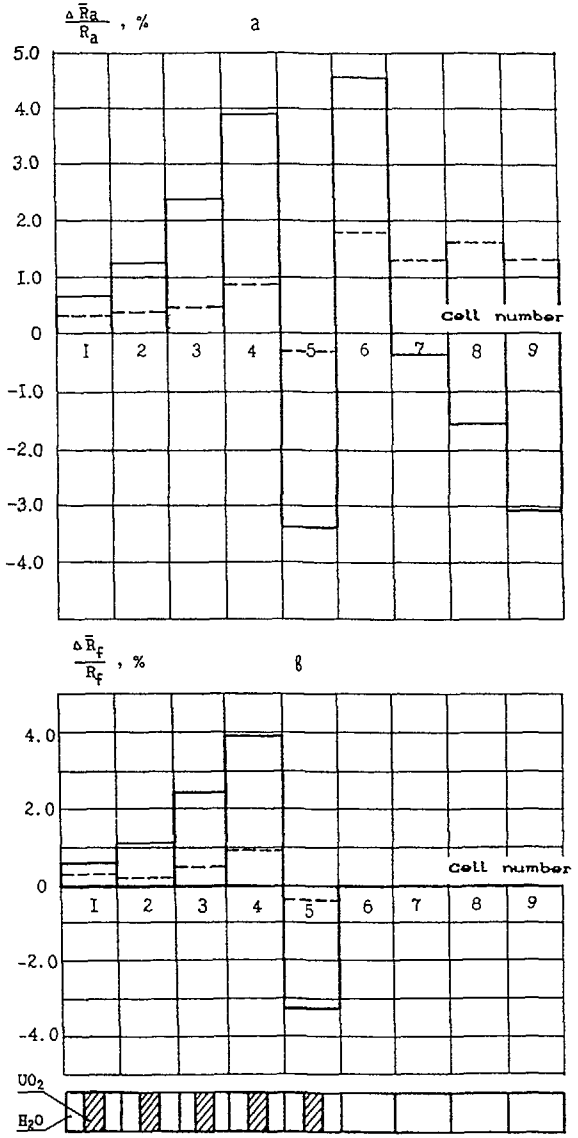

Fig.4 Comparison of absorption (a) and fission (b) reaction rates distributions for configuration "boundary with a reflector" formed by slab heterogeneous cells. Conventional signs the same as on Fig.1.

4. Calculation of asymptotic and transient modes functionals for cells of hexagonal lattices (code RAFORIN)

As it seen from eq.(9) elementary cell is described by set of 12 functionals of asymptotic and transient solutions. Some of them include ratios J^{γ}/Φ^{γ}, $\Phi^{\gamma}/\bar{\Phi}$ which are not usually calculated by standard cell codes based on first collision probabilities method (Pij). Calculations of such and more complex ratios of flux angular moments at a cell boundary can be easily performed on a base of surface pseudo sources method [4]. It should be noted that mentioned above more complex ratios of flux angular moments appear in balance equation if more exact than (4) continuity conditions are used (see [4]). Surface pseudo sources method has also some others advantages in comparison with Pij method Surface pseudo sources method is realized in RAFORIN code which is used for nonuniform lattices characteristics calculations on a base of 38- group approach (2 fast groups, 12 resonance groups and 24 thermal groups). In this code BNAB [6], LIPAR (library of evaluated resonance parameters) and CORT (library of evaluated thermal cross sections) [7] data are used. RAFORIN provides a possibility of supercell burnup calculations in cylinder (with preliminary homogenization of fuel cells surrounding central region of supercell) or cluster (without homogenization) approximations. This code include as modules RACIA

Table 1. Results of four-group calculations for configurations formed by homogeneous cells with U235 fissile isotope.

Configuration	Algorithm of calculation			
	Finite-difference approach		Equation (9)	
	δKeff	(δRf/Rf)max	δKeff	(δRf/Rf)max
"Gap between assemblies"	$1\ 0\ 10^{-2}$	4 6	$3\ 2\ 10^{-3}$	-0 74
"Boundary between core and reflector"	$2\ 7\ 10^{-3}$	8 8	$9\ 0\ 10^{-4}$	-1 3

$\delta Keff = Keff^{tr} - Keff$

Rf - fission in a hole energy region

$(\delta Rf/Rf)max = (Rf - Rf^{tr})/Rf^{tr}\ 100$

Rf^{tr} - result of transport calculation

Table 2. Results of four-group calculations for configuration "supercell with strong absorber" formed by heterogeneous cells.

Algorithm of calculation			δKeff / Keff
1 - 2 groups	3-th group	4-th group	
finite-difference approach	finite-difference approach	finite-difference approach	$3.0\ 10^{-2}$
-	-	eq. (9)	$9.6\ 10^{-3}$
-	eq. (12)	-	$1.0\ 10^{-2}$
-	eq. (12) with taking into account spectrum deformation *	-	$5.7\ 10^{-3}$

$\frac{\delta Keff}{Keff} = Keff^{tr} - Keff$; $Keff^{tr}$-result of transport calculation.

Lower groups energy boundaries are equal: 0.8Mev, 4.65Kev, 0.625ev, 0.
Considered configuration includes strong absorber cell surrounded by three fuel cells from each side.
* Neutron spectrum deformation were taken into account by using removal cross sections depending on cell position.

[8] and KLARA [4] codes which are used for symmetrical and antisymmetrical trial functions functionals calculations. Results of calculations based on RAFORIN data are given in Sect. 7 of this report.

5. Assignment and common characteristics of PERMAK code

PERMAK is one of the modules of code package for VVER core analysis developed in I.V. Kurchatov Institute [9]. This code is used for two-dimensional fine mesh (the mesh step is equal to the pins lattice pitch) few group (from 1 to 6 group) calculations. The code solves the neutron balance equations system in the core transverse cross section (including reflector). Code provides the following possibilities:

a) the neutron fluxes and power distributions calculations for cores with fixed properties of cells and known axial buckling (single state problem). Such calculations are used for codes verification on a base of comparison with zero power core experimental data.

b) calculations of pin by pin power distribution variation under burnup with taking into account feedbacks and reloading patterns. Needed for such type calculations values of axial bucklings, full power of layer, water temperature and boron acid concentration are taken from preliminary coarse-mesh three-dimensional BIPR-7 simulator code [10] calculations as a function of operation time. The library of neutron macro cross sections and their dependencies on cell state is used by PERMAK in this case.

In PERMAK both finite difference method and nodal approach are realized.

The balance equations system is solved by iterational procedure which is divided on accelerated cycles of inner and outer iterations. Full reflection condition is used on core symmetry axis. On outer core surface full reflection, zero flux or other type boundary conditions can be used. Usually in practice four groups calculations are carried out.

In case (b) PERMAK uses spectral parameter to describe neutron spectrum influence on isotopic composition changing under burnup and corresponding changing of fuel cells neutron-physical properties. Spectral parameter is defined as averaged on burnup ratio of local neutron spectrum and asymptotic cell spectrum with taking into account of discount coefficient. Local values of cell macro cross sections are determined by tabulated values interpolation on burnup and spectral parameter. To take into account difference between actual and nominal values of cell state parameters (coolant density and temperature, boron acid concentration, local power, xenon and samarium concentrations, etc.) corresponding sets of derivatives are used.

PERMAK code is applied for:

- design and operational core analysis,
- interpretation of in-core monitoring system data,
- analysis of critical assembles experiments,
- coarse mesh codes verification,
- homogenization of assembles neutron cross sections,
- preparation of boundary conditions for coarse mesh codes calculations.

6. Features of nodal type balance equation in PERMAK

Nodal type equation realized in PERMAK has some features in comparison with approach described in Sect. 2. Main difference between algorithm described in Sect. 2 and algorithm realized in PERMAK is that instead of asymptotic mode a trial function corresponding to neutron distribution in infinite lattice is introduced. In this case all neutron currents which give contribution to cell neutron balance have be considered as transient mode currents.

Taken into account conclusions of paper [2] about slight influence of difference between asymptotic and transient diffusion coefficients on calculational result, their equality in PERMAK algorithm is supposed.

Including definition $\varepsilon_p = \frac{\bar{\Phi}_{sp\infty}}{\bar{\Phi}_p}\varepsilon_{\infty p} + \frac{\bar{\Phi}_{sp\tau}}{\bar{\Phi}_p}\varepsilon_{\tau p}$,

where

$$\bar{\Phi}_p = \bar{\Phi}_{sp\infty} + \bar{\Phi}_{sp\tau}$$

and using connection between boundary averaged flux and current and cell averaged flux

$$\tilde{\Phi}^{\gamma}_{p} - \frac{h}{2D_p}\tilde{J}^{\gamma}_{p} = \bar{\Phi}_p\,\varepsilon_p$$

one can obtain thermal neutron balance equation

$$\frac{4}{3h^2}\sum_{\iota=1}^{6}\frac{D_p D_\iota}{D_p + D_\iota}\left(\bar{\Phi}_p\,\varepsilon_p - \bar{\Phi}_\iota\,\varepsilon_\iota\right) + \Sigma_{ap}\bar{\Phi}_p = S_p, \qquad (13)$$

where $\Sigma_p = \frac{\bar{\Phi}_{sp\infty}}{\bar{\Phi}_p}\Sigma_{p\infty} + \frac{\bar{\Phi}_{sp\tau}}{\bar{\Phi}_p}\Sigma_{p\tau}$, $\bar{\Phi}_{sp\infty} = \frac{S_p}{\Sigma_{ap\infty}}$ (S_p is thermal neutron source, $\Sigma_{ap\infty}$ is infinite lattice thermal absorption cross section).

In epithermal neutron energy region in addition to finite difference method the cell block effect is taken into account, namely

$$\varepsilon = \frac{\bar{\varphi}^{s}_{\gamma}}{\bar{\varphi}^{s}} - \frac{h}{2}\frac{\overline{\nabla\varphi}^{s}_{\gamma}}{\bar{\varphi}^{s}}$$

and neutron balance equation has the same shape as (13).

7. Comparison of measured and calculated data obtained using finite difference and nodal type approaches

Final stage of described in Sect. 3 nodal type approach verification is a comparison of calculated and measured data obtained at critical assembles. Some results of such comparison are given in Fig 2.1-2.6. Measured data has been obtained at ZR-6 [11] zero power critical assemble assigned for VVER lattices physical studying. Few hundred uniform and nonuniform lattices containing fuel rods of different enrichment, absorbers of different types and water gaps have been investigated at this assemble. Some typical lattices have been chose for calculations. These lattices contain 3.6% enrichment fuel rods, absorbers from B_4C and water gaps of different configurations.

Calculated data based on 4-group finite difference approach and on algorithm described above are compared in Fig. 2.1-2.6 with measured data. All needed for calculations 4-group macro cross sections and additional functionals have been obtained by described above RAFORIN code.

It is seen from these figures that under using of finite difference approach maximal difference in pin power (more than 10%) is observed for pins situated near reflector and absorbers. Using of nodal algorithm provides high stability of K_{eff} and significant increasing of accuracy of pin power distribution calculation. Average unaccuracy of pin power calculation don't exceed of measurement error (1-2%). K_{eff} for all cores varies in interval 0.998-1.000

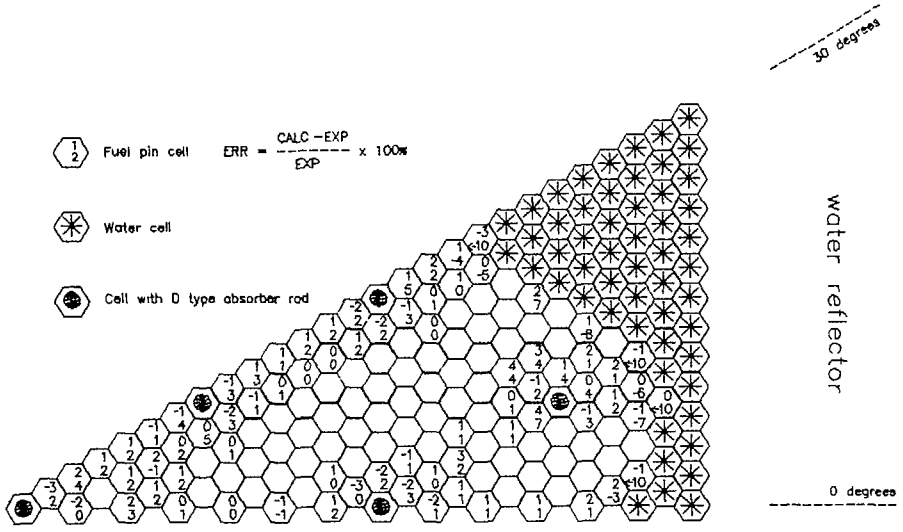

Fig 2 1 CORE CONFIGURATION ZR−6 57(D7) (30 degrees symmetry)
Deviation of calculated pin power distribution from measured data
1 Modified fine mesh method (RAFORIN−PERMAK) Keff=0 9990
2 Finite difference method (UNIRASOS−PERMAK) Keff=1 0125

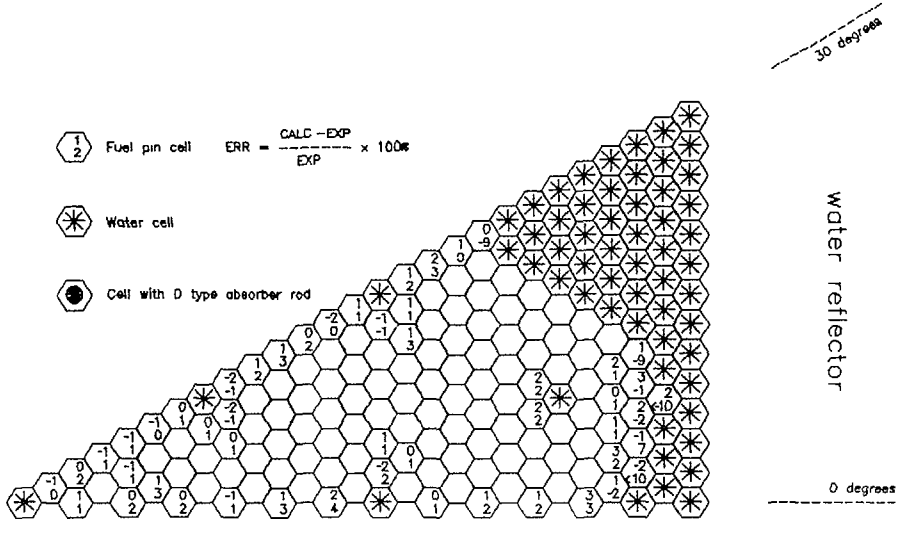

Fig 2 2 CORE CONFIGURATION ZR−6 58(E7) (30 degrees symmetry)
Deviation of calculated pin power distribution from measured data
1 Modified fine mesh method (RAFORIN−PERMAK) Keff=0 9979
2 Finite difference method (UNIRASOS−PERMAK) Keff=1 0054

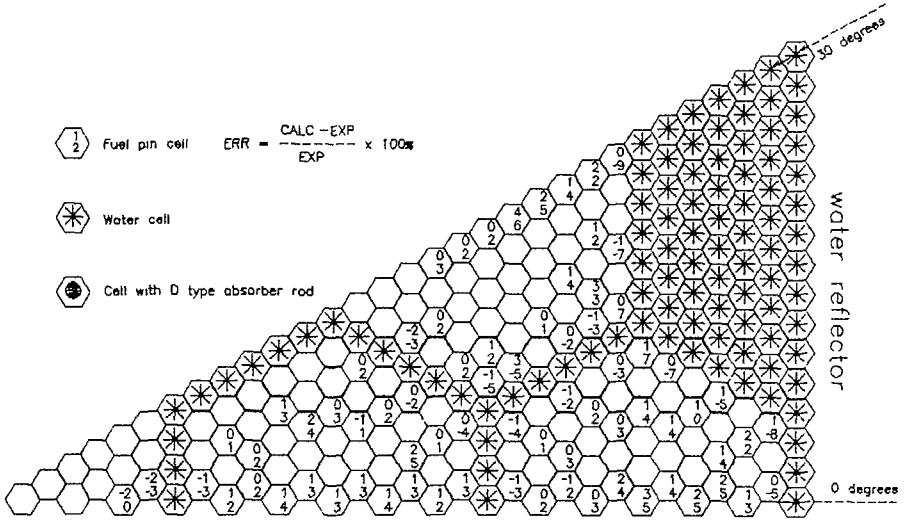

Fig 2 3 CORE CONFIGURATION ZR−6 101 (30 degrees symmetry)
Deviation of calculated pin power distribution from measured data
1 Modified fine mesh method (RAFORIN−PERMAK) Keff=1.0002
2 Finite difference method (UNIRASOS−PERMAK) Keff=0 9980

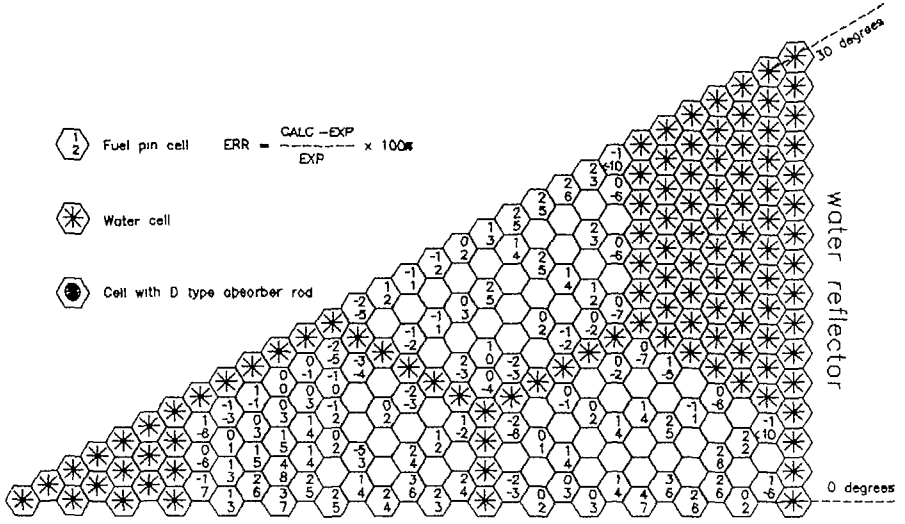

Fig 2 4 CORE CONFIGURATION ZR−6 102 (30 degrees symmetry)
Deviation of calculated pin power distribution from measured data
1 Modified fine mesh method (RAFORIN−PERMAK) Keff=0 9998
2 Finite difference method (UNIRASOS−PERMAK) Keff=0 9978

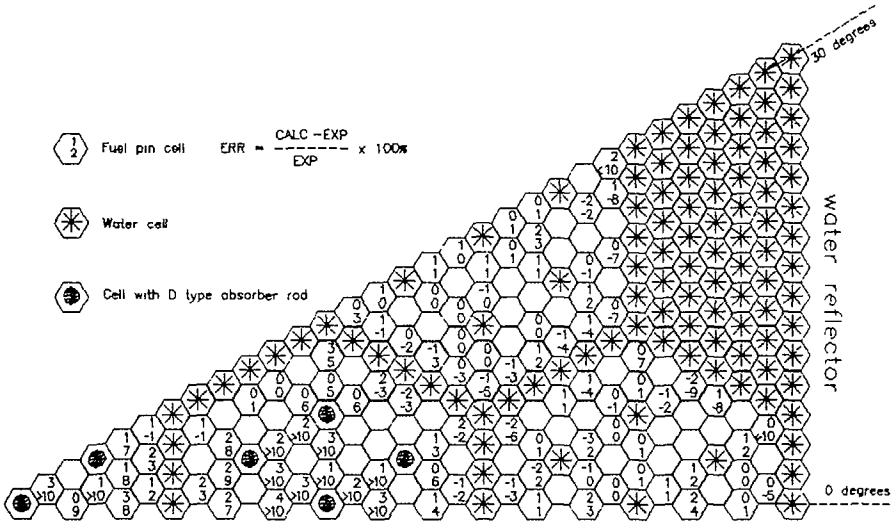

Fig 2 5 CORE CONFIGURATION ZR-6 103 (30 degrees symmetry)
Deviation of calculated pin power distribution from measured data
1 Modified fine mesh method (RAFORIN-PERMAK) Keff=0 9983
2 Finite difference method (UNIRASOS-PERMAK) Keff=0 9988

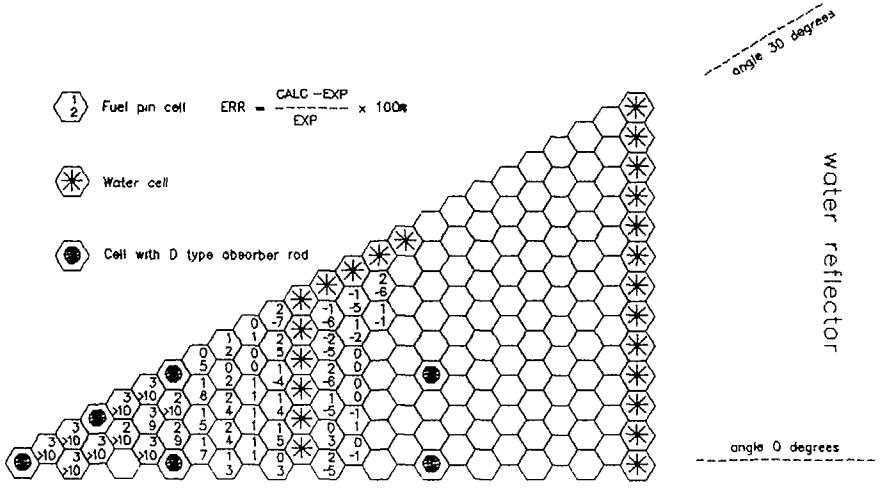

Fig 2 6 CORE CONFIGURATION ZR-6 90 (30 degrees symmetry)
Deviation of calculated pin power distribution from measured data
1 Modified fine mesh method (RAFORIN-PERMAK) Keff=0 9977
2 Finite difference method (UNIRASOS-PEPMAK) Keff=1 0073

8. Nodal type approach for coarse-mesh calculations

In a three-dimensional two-group coarse-mesh nodal code BIPR-8 group neutron flux distribution in a node transverse section is written as

$$\Phi_{gp}(\bar{r}, B_z^2) = A_{gp} f_{gpa}(\bar{r}, B_z^2) + \sum_{m=1}^{M} B_{gp} f_{gpam}(\bar{r}, B_z^2) \cos(m\varphi+\delta_{pm}) + \sum_{i=1}^{\sigma_i} Y_{gpi}(\bar{r})$$

(It is assumed that node has 30^0 azimuthal symmetry). Two first items in this expression describe symmetrical and antisymmetrical components, third - contributions of transient solutions from six node borders. Such representation provides high accuracy of neutron balance in the node and allows openly to take into account its heterogeneity under keeping of differential operator description in a form close to standard finite-difference form. Needed for calculations values of trial functions f_{gps}, $f_{gpam}\cos(m\varphi+\delta_{pm})$ and Y_{gp} functionals are prepared by a special module based on 4-group approximation and described above fine-mesh nodal approach.

An accuracy of BIPR-8 code has been checked on a base of wide set of benchmark problems solutions (precise solution have been obtained by fine-mesh calculations). Results of such verification show that using of three azimuthal harmonics (in this case continuity solutions conditions is provided in average on each node border) provides about 1% accuracy of VVER-440 fuel assemblies power distribution calculations. To provide such accuracy for more large VVER-1000 fuel assemblies it is necessary to increase number of azimuthal harmonics up to 5. In this case continuity conditions are provided in average on each half of node border. Application of described above coarse mesh nodal approach provides also a possibility of rod by rod power distribution reconstruction.

9. Conclusions

Performed investigations allow to come to the following conclusions:

- high symmetry of VVERs hexagonal cells and assembles and closeness of their form to cylindrical form provide good premises for the nodal type approaches realization in fine mesh and coarse mesh codes;
- suggested algorithms ensure sufficient for practical purposes accuracy of calculations.

APPENDIX 1.

1. Definitions of trial functions functionals.

$$D_{apg} = \frac{\tilde{J}^{\gamma}_{aapg}}{\tilde{f}^{\gamma}_{aapg}} \cdot \frac{h}{2}; \qquad D_{tpg} = \frac{\tilde{J}^{\gamma}_{tapg}}{\tilde{f}^{\gamma}_{tapg}} \cdot \frac{h}{2};$$

$$g_{apg} = \frac{\tilde{f}^{\gamma}_{aapg}}{\bar{f}_{aapg}} \cdot \left(1 - \frac{\vartheta_{aapg}}{D_{tpg}} \right); \quad g_{tpg} = \frac{\tilde{f}^{\gamma}_{tapg}}{\bar{f}_{tapg}} \cdot \left(1 - \frac{\vartheta_{tapg}}{D_{tpg}} \right);$$

$$\vartheta_{apg} = \frac{\tilde{J}^{\gamma}_{aapg}}{\tilde{f}^{\gamma}_{aapg}} \cdot \frac{h}{2}; \qquad \vartheta_{tpg} = \frac{\tilde{J}^{\gamma}_{tapg}}{\tilde{f}^{\gamma}_{tapg}} \cdot \frac{h}{2};$$

$$\varphi^{\gamma_i}_{aapg} = \frac{\tilde{I}^{\gamma_i}_{pg-1}}{D_{apg-1}} \cdot \frac{h}{2} \cdot \frac{\tilde{f}^{\gamma}_{aapg}}{\tilde{f}^{\gamma}_{aapg-1}}; \qquad \tilde{I}^{\gamma_i}_{pg-1} = \tilde{J}^{\gamma_i}_{pg-1} - \frac{1}{N} \sum_{i} \tilde{J}^{\gamma_i}_{pg-1};$$

h - lattice pitch.

References

1. Новиков А.Н.
Учет переходных решений в мелкосеточных расчетах.
Материал XIV заседания Научного Совета ВМК, Будапешт, 1983.

2. Пшенин В.В., Новиков А.Н., Сурначева И.И.
Анализ возможностей повышения точности мелкосеточных расчетов ВВЭР на примерах решения модельных задач в плоской геометрии.
Вопросы атомной науки и техники, Сер. "Физика и техника ядерных реакторов", вып.4, 1988.

3. Лалетин Н.И.
Об уравнениях гетерогенного реактора. Вопросы атомной науки и техники. Серия "Физика и техника ядерных реакторов", 1981, вып.5 (18), 1981.

4. N.I. Laletin et. al.
Surface Harmonics and Surface Pseudosources Methods.
Proc. of Int. Conf. on the Physics of Reactors, Marseille, 1990.

5. Пляшкевич В.Ю.
Программа AKSKIN многогруппового расчета потока нейтронов в ячейках плоских реакторных решеток. Препринт ИАЭ-4103/5.

6. Абагян Л.П. и др.
Групповые константы для расчета ядерных реакторов. Москва, Энергоатомиздат, 1981.

7. Майоров Л.В., Юдкевич М.С.
Нейтронно физические константы в расчетах реакторов на тепловых нейтронах. Москва, Энергоатомиздат, 1988.

8. Султанов Н.В.
Аннотация программы РАЦИЯ. Вопросы атомной науки и техники, Сер."Физика и техника ядерных реакторов", вып.2, 1989.

9. A.N.Novikov, V.V.Pshenin, M.P.Lizorkin et al.
Problems of VVERs In-Core Fuel Management. Material of IAEA TC Meeting on In-Core Fuel Management, Vienna, 1989, 622-I3-TC-676.3

10. Д.М. Петрунин, В.Н. Семенов.
Трехмерные программы - компаторы работы ВВЭР. ВАНТ, серия: физика и техника ядерных реакторов, выпуск 9, 1985.

11. Experimental Investigations of the Physical Properties of WWER-type Uranium-Water Lattices. Final report of TIC. Vol. 1. Budapest 1985.

MICRODEPLETION AND EFFICIENCY INVESTIGATIONS OF BURNABLE ABSORBERS IN WWER FUEL ASSEMBLIES

R. BECKER
Kraftwerks- und Anlagenbau AG,
Berlin, German Democratic Republic

Abstract

In the given material validation results of the local burnup and spectrum calculation code NESSEL-4 are summarized. A brief review about basic of the applied calculation model and primary data is included. For estimation of the code accuracy "Numerical Benchmarks", measurements of "Benchmark-Type" and experimental data in WWER typically fuel-arrangements are used. Results of calculational-methodical investigations to study the behaviour of cluster-absorber micro-depletion in WWER fuel assemblies (FA) are presented. The influence of cluster absorber treatment on the calculated efficiency and micro-power release in FA-s is evaluated.
Short remarks to the present quality of gadolinium lattice calculations under the "Coordinated Research Program" (GDR-5775), arranged by the IAEA Vienna, are attached.

1. Introduction

Burnable absorber-materials for a long time are applied for example in boiling water reactors in form of clusters [1] and in pressure water reactors of WWER type they are used as an addition to the fuel jacket [2]. In WWER case as effective absorbing material for thermal neutrons bor in a zirkonium matrix in jackets is usually used.
In WWER 1000 reactor core on the other hand in a large scale fuel assemblies (FA) with cluster-absorbers are charged.
At present the clusters consist of B_4C, BZr_2 and Eu_2O_3 respectively. Recently in connection with large international experiences [3,4] the application of gadolinium as burnable absorbing material in WWER conditions is seriously discussed. In this case to mix fuel with gadolinium for selected fuel pins in FA-s is designed. To this subject from IAEA a "Coordinated Research Programm", on which GDR is taking part, was initiated.
By reason of burnable absorbers charge in WWER-FAs a complex evaluation and validation of calculation codes is necessary. For this reason results of zero power measurements, carried out at ZR-6 critical facility in WWER typically arrangements, are used to estimate the accuracy of calculation codes.
Besides this, extensive calculational-methodical investigations to evaluate the depletion behaviour of cluster absorber are carried out. For fuel-pin lattices, containing gadolinium, benchmarks for square [5,6] and hexagonal lattices [7] are solved.

In the given paper in chapter 2 the calculation model is shortly described. In chapter 3 results of spectrum and diffusion code calculations for numerical benchmarks, benchmark experiments and WWER lattice measurements are summarized. Calculation results of cluster micro-depletion investigations in chapter 4 are presented. An advanced simple method to increase the accuracy in fine-mesh diffusion calculations in the appendix is suggested.

2. Calculation model of NESSEL-4

For calculation of local characteristics (multiplication factor, few-group constants, micro-depletion ...) in KAB the code NESSEL-4 [8] is applied. Calculations on the basis of a more group model (24 epithermal, 10 thermal energy groups) for a selected reactor part - in the following as supercell denoted- are carried out.
In epithermal energy range for spectrum calculation B-1 approximation is used. In the resonance energy range ($0.465\ eV < E < 4.65\ KeV$) the calculation of self-shielded cross-section is based on ABBN f-factors [9] and the equivalence-theorem with specially selected λ_s-parameters to get the evaluated Hellstrand resonance integrals of U-238.
In thermal energy range the neutron transport equation in more group and more zone model on the basis of first collision probabilities (Pij) is solved, using methods applied in the well-known THERMOS S-II computer code [10] and suggested by Bonalumi [11] and Kavenoky [12] respectively.
The necessary primary data of about 60 nuclides (fuel-nuclides, detector-, absorber-, construction-materials, saturation products, moderator-data...) in a 34 group-library are available. In epithermal energy range the data of ABBN-78 [9] are applied. The thermal part in a 10 group structure, basing on ENDF-BIV datas, is described.
The basic idea of homogenisation in NESSEL-4 consist in the following: The calculation of reactor physical parameters of two-dimensional areas (supercell) is reduced by a repeated treatment of one-dimensional cylindrically calculations in the mentioned many-group model. In detail the step by step homogenisation model in papers [8,30] is explained. At boundary of the supercell white boundary condition is assumed. By the aim of more group spectrum of homogenized supercell the condensation to 4 macro-groups is realized.
For local burnup calculation of fissionable nuclides two simplified uranium-plutonium chains, containing (n,γ)-processes and the β-decay, are introduced. The explicite treatment of 6 satturation products (Cd-113, Xe-135, Sm-149, Sm-151, Eu-155, Gd-157) is provided. The remaining fission-products are treated in first draft by the aim of pseudo-fission products. For cluster absorber micro-depletion calculation additional burnup-chains (Gd, Eu, B..) are used.

3 Validation of NESSEL-4

3 1 Undisturbed fuel-pin lattices

For undisturbed fuel-pin lattices the accuracy of NESSEL-4 was evaluated on the one side by analysis of Numerical Benchmarks formulated in paper [13] and on the other side by zero-power measurements of "Benchmark -type [14,15] Besides this the results of measurements for WWER typically configurations at ZR-6 facility were used to check the accuracy of NESSEL-4 code and two-dimensional fine-mesh diffusion code for hexagonal geometries FLEX [16] In the detail all the results are published and discussed in the paper [17,18] Therefore in this material only the most important results in tables 1 - 4 are presented and here summarized

1 For the 'Numerical Benchmark' lattices NESSEL-4 results are in the most cases in a satisfactory agreement with Monte-Carlo calculations (MC) and results of spectral codes EPRI-CELL [19] and CASMO-3 [20] It is necessary to accentuate, that MC calculations were carried out using ENDF-BV datas
2 In table 2 results of RAHAB-OZMA [21], WIMS-D4 [22] and NESSEL-4 for PNL [14] uranium-plutonium mixed fuel lattices are presented The deviations given in this table refer to RAHAB-OZMA calculation results using ENDF-BV data

Table 1 Numerical Benchmark results
(Deviations are given in %)

Lattice	Parameter	CALCULATION METHOD MC	EPRI-CELL	CASMO-3	NESSEL-4
NB-1	Kinf	1 147	-0 2	-0 2	-0 5
	δ_{28}	1 363	-0 2	-1 5	2 1
	δ_{25}	0 0803	1 4	2 2	1 1
	δ_{28}	0 0722	-2 4	1 9	0 0
	CR	0 798	-0 3	-1 6	0 8
NB-2	Kinf	1 175	-0 4	-	-0 5
	δ_{28}	2 612	0 0	-	1 9
	δ_{25}	0 151	0 7	-	0 0
	δ_{28}	0 297	0 0	-	-3 4
	CR	2 148	0 0	-	-1 4
NB-4	Kinf	1 342	-0 1	-0 2	-0 7
	δ_{28}	2 654	-0 8	0 8	3 9
	δ_{25}	0 159	-1 3	-0 1	-0 6
	δ_{28}	0 062	-0 8	3 0	2 3
	CR	0 549	-0 2	-1 3	1 8
NB-5	Kinf	1 146	-0 3	-	0 0
	δ_{28}	0 503	0 4	-	1 9
	δ_{25}	0 548	0 4	-	-4 7
	δ_{28}	0 133	-0 8	-	-1 5
	CR	1 006	0 0	-	-3 1

Results show, that Kinf and spectral parameters, obtained by NESSEL-4, are in satisfactory agreement with the RAHAB-OZMA results

3 In tables 3-4 NESSEL-4 results are compared with experimental values from critical facilities TRX and BAPL For the given experimental buckling NESSEL-4 calculates Keff with an accuracy, comparable with results of international wellknown spectral codes In comparison with experiments - with exception of the tight TRX-lattice a deviation in calculated NESSEL-4 keff-values lower 0 2% is observed For these lattices Keff-values differ until 0 2% in dependence on the used calculation method of P_{ij} in NESSEL-4 (table 5)

Table 2 Results of PNL-lattices
(Deviations in %)

Lattice	Parameter	RAHAB-OZMA	WIMS-D4	NESSEL-4
PNL 31	Kinf	1 253	0 0	0 5
	δ^{25}	0 211	2 4	-1 4
	δ_{49}	0 156	-11 4	5 8
	δ_{25}	0 322	-3 5	1 9
	δ_{28}	5 20	-1 7	-1 0
PNL 33	Kinf	1 179	0 2	-0 1
	δ^{25}	0 220	2 3	-0 4
	δ_{49}	0 085	-11 8	-3 5
	δ_{25}	0 155	-3 3	2 6
	δ_{28}	2 60	-3 6	0 7
PNL-35	Kinf	1 155	0 1	0 3
	δ^{25}	0 228	2 2	-0 4
	δ_{49}	0 062	10 1	3 2
	δ_{25}	0 106	-2 9	2 8
	δ_{28}	1 80	-4 0	1 1

Table 3 Results of WAPD-lattices

Lattice	Parameter	Exper datas	Deviation RSYST-CGM	from experiment RAHAB-OZMA	CASMO-3	NESSEL-4
BAPL-1	Keff	1 000	0 1	0 1	0 1	-0 1
	δ_{28}	1 390±0 010	2 1	1 7	-0 7	1 2
	δ_{25}	0 084±0 002	0 1	1 0	0 1	-2 4
	δ_{28}	0 078±0 004	0 6	-2 4	0 5	-2 1
	MCR	-	0 813	0 810	-	0 806
BAPL-2	Keff	1 000	0 0	0 1	-	-0 1
	δ_{28}	1 120±0 011	-	4 6	2 9	4 6
	δ_{25}	0 068±0 001	-	1 6	1 0	-1 5
	δ_{28}	0 070±0 004	-	-7 0	-4 6	-6 1
	MCR	-	-	0 737	0 707	0 735
BAPL-3	Keff	1 000	0 1	0 2	-	0 0
	δ_{28}	0 906±0 020	-	0 4	0 0	1 5
	δ_{25}	0 052±0 001	-	2 1	1 5	-1 1
	δ_{28}	0 057±0 003	-	-6 3	3 8	-4 8
	MCR	-	-	0 657	-	0 658

Table 4: TRX-lattices

Lattice	Parameter	Exper. datas	RSYST-CGM	RAHAB-OZMA	NESSEL-4	CASMO-3	WIMS-D4
	Keff	1.000	-0.4	-0.5	-0.5	-	0.4
TRX-1	δ_{28}	1.320 0.021	2.8	-0.2	2.9	0.4	-3.9
Vm/Vf=	δ_{25}	0.099 0.001	0.5	2.2	-1.6	1.3	4.3
2.35	δ_{28}	0.095 0.004	5.8	4.4	4.3	4.5	-2.7
	MCR	0.797 0.001	0.2	0.4	-0.4	-1.8	-3.5
	Keff	1.000	-0.3	-0.3	-0.3	-	0.6
TRX-2	δ_{28}	0.837 0.016	0.0	1.2	1.9	-0.4	-5.7
Vm/Vf=	δ_{25}	0.061 0.001	-1.0	0.7	-2.8	0.0	3.2
4.02	δ_{28}	0.069 0.004	3.0	1.0	-2.6	2.0	3.6
	MCR	0.647 0.005	-1.2	-0 8	-0.7	-2.0	-3.2

Table 5 : NESSEL-4 Keff-values in dependence on Pij calculation method

Lattice	BIWA	BONA	ALCO
BAPL-1	0.9988	0.9976	0.9996
BAPL-2	0.9993	0.9975	0.9998
BAPL-3	1.0020	0.9978	1.0008
TRX-1	0.9942	0.9912	0.9947
TRX-2	0.9973	0.9920	0.9979

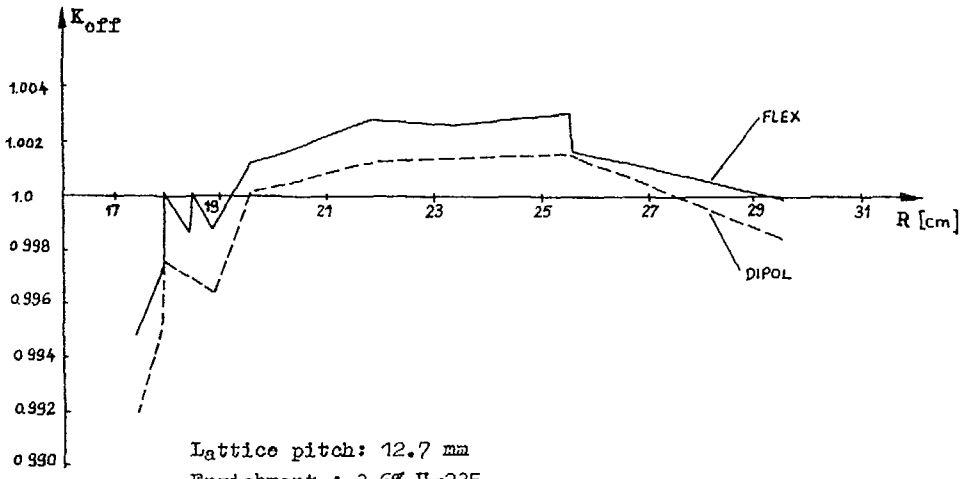

FIG. 1. K_{eff} (R) of ZR-6 lattice (12.7–3.6–0.0).

3.1.1 Accuracy of few-group constants

The calculated NESSEL-4 few-group parameters are analyzed on the basis of diffusion calculations for serial measurements. For this purpose ZR-6 lattices with 3.6% U-235 enrichment, 12.7 mm lattice pitch and two boron acid concentrations (C_B = 0 , C_B = 4.0 g H_3BO_3 /l H_2O) are investigated. The critical water level in dependence on core radius R (variation of fuel-pin numbers in the assemblies) was estimated. Axial leakages of this configurations are taken into account by buckling values. According [23] the axial extrapolation length λ_z depends only on lattice step.

The calculations are carried out by one-dimensional diffusion code DIPOL-1 [24] in cylindrically geometry and by FLEX respectively. The results in figures 1-2 are illustrated. For extremly small values of the core-radius (R < 19 cm) diffusion calculations underpredict Keff of about 0.5%. The deviations in the calculated Keff values in comparison with critical state don't exceed 0.2% for core radius larger 19 cm. Differences for Keff of 0.2% between one and two-dimensional diffusion calculations are observed. At boundary between core and reflector the calculated power release systematically underpredict measured values until 5-10% in dependence on fuel-pin position. A simple method for a particular reduction of this uncertainties in paper [25] is suggested. A summary of this method in the appendix is presented.

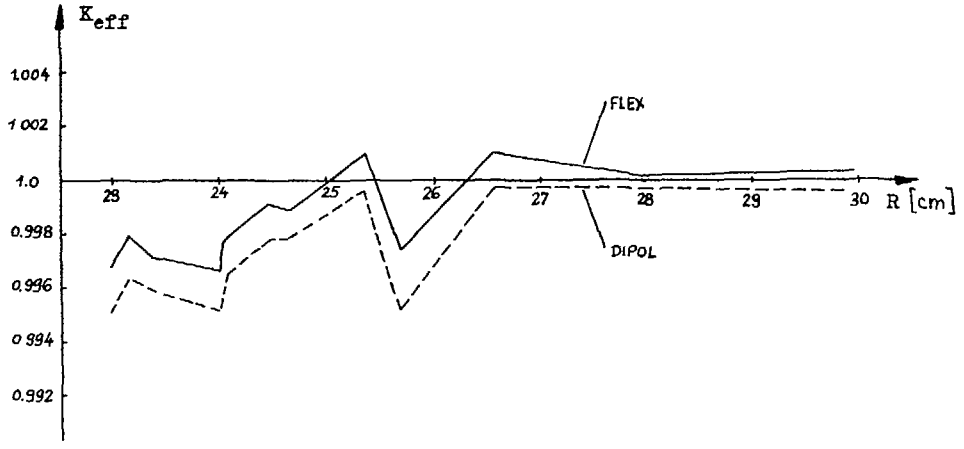

FIG. 2. K_{eff} (R) of ZR-6 lattice (12.7–3.6–4.0).

3 2 Perturbed fuel-pin lattices

For accuracy validation of the used calculation methods for lattice arrangements with WWER-1000 typically disturbances at critical facility ZR-6 large experimental investigations are carried out The perturbations are caused by absorber rods of several material compositions [23] and water gaps (removing of absorber rods) respectively Lattices of type X-n (X means type of perturbance, n distance of perturbance in units of lattice pitch) and arrangements with imitated fuel assembly structures (WWER-440, WWER-1000) were investigated Critical water levels, power release distributions and spectral characteristics (disadvantage factors, spectral indices, epithermal parameters) are measured A complete summary of experimental results is given in I and III volume of TIC [23,26]
Keff values of 23 regulary disturbed fuel-pin lattices on the basis of NESSEL-4/FLEX calculations together with results published in [27] are summarized in table 6 The averaged value of NESSEL 4/FLEX calculations (Keff= 1 0003± 0 0023) demonstrate the satisfactory quality of the calculated few-group constants of NESSEL-4 using the macro-cell model
Keff-values for arrangements with imitated FA-structures in table 7 are summarized For lattices, containing B C absorber rods, a systematically underprediction of Keff from state of criticality is observed

Table 6 Keff-values of ZR-6 macrocell-configurations (mac)

Configuration	X-n	hcrit [cm]	Number of mac	NESSEL-4 FLEX	[27]
64/64	E-5	27 83	73	1 0037	1 0071
65/64	A-5	44 3	73	1 0002	0 9996
66/64	C-5	44 69	73	0 9998	0 9972
70/70	A-5	49 38	67	1 0003	1 0047
71/70	C-5	52 34	67	0 9996	1 0019
73/73	C-5	55 94	61	1 0006	0 9978
76/76	C-5	68 38	52	1 0063	0 9952
59/59	E-6	27 02	55	1 0037	1 0050
60/59	A-6	35 63	55	1 0005	0 9986
61/59	C-6	36 56	55	1 0004	0 9968
62/59	B-6	37 32	55	0 9998	0 9982
63/59	D-6	58 40	55	0 9954	0 9917
67/57	A-7	39 48	31	1 0006	1 0031
68/57	C-7	40 50	31	1 0005	1 0023
54/54	D-7	47 63	37	0 9976	0 9957
55/54	E-7	28 21	37	1 0025	1 0042
156/155	G-7	53 11	31	0 9980	0 9940
310/57	N-7	39 69	31	0 9994	-
57/57	D-7	57 7	31	0 9965	0 9955
58/57	E-7/0 0	31 4	31	1 0037	1 0076
141/138	F-7/0 0	46 51	31	0 9924	-
146/138	F-7/1 8	75 87	31	0 9934	-
147/138	E-7/1 8	40 19	31	1 0031	1 0056

Table 7 NESSEL-4/FLEX Keff-values of FA-s

Configuration	Lattice-description	Keff
87/87	K331/Al 37 D-3	0 9969
88/87	K331/Al 37 E-3	1 0027
89/87	K331/Al -	0 9973
90/87	K331/H_2O 37 D-3	0 9934
144/144	K331/H_2O 13 F-3	1 0002
145/145	K331/H_2O 13 F-3	1 0002
100/100	K91 /H_2O Cb= 4 0	0 9947
101/100	K91 /H_2O Cb= 0 0	0 9934
102/102	K91 /H_2O without centr FA	1 0032
103/103	K91 /H_2O 49 D-3/ 84 E-3	0 9943

The calculated micro power release distributions in macro-cells of type X-7 are in a satisfactory agreement with measured values (table 8) The results demonstrate once more the application of the macro-cell model in the cell calculations, after this the neutron-flux distribution can be separated by a periodical function $\Psi_I(R)$ (micro-flux distribution in the macro-cell I) and the macro-flux $J_o(B\ r)$ according $\Phi(r) = J_o(B_r\ r)\ \Psi_I$
For the lattices D-7, F-7 and E-7 in critical state buckling values B by NESSEL-4 are calculated (tab 9) The realized methods in NESSEL-4 to calculate P_{ij} are applied for this lattices
The corresponding NESSEL-4 calculation is carried out for a cylindrical macrocell of type X-7 with white boundary condition at cell-surface In the calculations the cluster absorber region is subdivided in several mathematically zones. By application of P_{ij} used in THERMOS S-II code (SUBROUTINE BIWA, in the following as BIWA denoted) for B_m^2 a strong dependence on the zone number is observed In this method is suggested, that neutrons at centre of considered zones are starting This assumption is fulfilled much better much smaler the zone is selected By reason of strong flux gradients in the absorber an improvement in the spatial discretization leads to an increasing of the calculated thermal neutron-flux and therefore the absorption rate increase
Investigations have shown, that calculated absorber efficiency by application of P_{ij} on BIWA strong depends on the subdivision of cluster region into mathematically zones Corresponding minimal zone-number for WWER clusters in FA-s are estimated as 8-11

4 Cluster micro-depletion in WWER-1000 FA-s

In the following calculation results of micro-depletion properties of burnable cluster-absorbers in WWER-1000 prototype FA-s are discussed The calculations in each case are carried out for two states In the first case the micro-depletion of cluster absorbers is taken into account in NESSEL-4 calculations, but in second case the micro-depletion is neglected In both cases the number of mathematically zones inside of absorbers is varied

Table 8 Micro distribution in macro-cells of type X-7

Number of cell	Distance from centre	Experiment	NESSEL-4	Lattice
2	1 27	1 1149 ± 0 0045	1 1040	E-7
		0 9009 ± 0 0045	0 8924	F-7
		0 8795 ± 0 0046	0 8665	D-7
3	2 54	1 0323 ± 0 0050	1 0209	E-7
		0 9773 ± 0 0057	0 9634	F-7
		0 9704 ± 0 0072	0 9636	D-7
4	3 81	1 0062 ± 0 0042	1 0025	E-7
		0 9962 ± 0 0068	0 9970	F-7
		0 9895 ± 0 0081	0 9958	D-7
5	2 20	1 0339 ± 0 0052	1 0315	E-7
		0 9667 ± 0 0055	0 9610	F-7
		0 9605 ± 0 0067	0 9440	D-7
6	3 36	-	1 0064	E-7
		0 9951 ± 0 0088	0 9920	F-7
		0 9968 ± 0 0138	0 9889	D-7
7	4 58	1 0150 ± 0 0045	0 9998	E-7
		1 0051 ± 0 0070	1 0003	F-7
		1 0081 ± 0 0072	1 0006	D-7
8	4 40	1 0000 ± 0 0051	1 0000	E-7
		1 0000 ± 0 0067	1 0000	F-7
		1 0000 ± 0 0069	1 0000	D-7

Table 9 Buckling values of X-7 macrocells (in units of $[m^{-2}]$)

Lattice NZ	D-7 BIWA	D-7 BONA	D-7 ALCO	F-7 BIWA	F-7 ALCO	E-7 BIWA	E-7 BONA	E-7 ALCO
2	82 86	69 75	70 28	85 55	79 16	103 58	103 64	104 31
4	77 33	70 02	-	-	-	103 57	103 65	-
8	72 97	-	70 27	-	-	-	-	-
11	71 98	70 04	70 24	79 59	79 17	103 57	103 65	104 31
Exper	70 93 ± 0 20			78 35 ± 0 20		101 26 ± 0 28		

BONA Pij by method of Bonalumi [11]
ALCO Pij by method of Kavenoky [12]
BIWA Pij by method of Stamm'ler [10]

First collision probabilities are calculated by subroutine BIWA The interruption between cluster and fuel-pins in the FA is taken into account during more group spectrum calculation If cluster micro-depletion is neglected in calculations , the burnup of fuel-pins in the neighbourhood of cluster-absorbers is performed in a to harden neutron spectra The total absorption of FA-s - a detailled zone subdivision of cluster-absorber assumed - is therefore generally overpredicted
For several FA-s in tables 10-11 ratios of infinite multiplcation factors δK_{inf} are summarized The definition of δK_{inf} is the following

$$\delta K_{inf} = \frac{K_{inf}^{m.c\,A}}{K_{inf}^{o\,c\,A}}$$

Table 10 δK_{inf}-values of FA with Eu_2O_3

BU [MWd/KgU]	C = 3 0 g/l NZ=1	NZ=3	NZ=8	NZ=17	C = 0 0 NZ=3	NZ=17
0	1 0000	1 0000	1 0000	1 0000	1 0000	1 0000
6	0 9998	1 0021	1 0057	1 0062	1 0019	1 0062
12	0 9999	1 0056	1 0128	1 0137	1 0052	1 0137
18	1 0003	1 0116	1 0223	1 0235	1 0112	1 0237
24	1 0006	1 0215	1 0374	1 0386	1 0212	1 0380
30	1 0007	1 0360	1 0543	1 0554	1 0357	1 0547

Table 11 δK_{inf} of FA-s with B_4C (C = 3 0 g H_3BO_3/(H_2O)

BU [MWd/KgU]	FA-Type 8 NZ=3	NZ=8	NZ=17	FA-Type 2 NZ=3	NZ=17	FA-Type 10 NZ=3	NZ=17
0	1 0000	1 0000	1 0000	1 0000	1 0000	1 0000	1 0000
6	1 0005	1 0030	1 0034	1 0001	1 0046	1 0006	1 0031
12	1 0013	1 0063	1 0072	1 0002	1 0095	1 0012	1 0066
18	1 0025	1 0101	1 0112	1 0002	1 0148	1 0018	1 0102
24	1 0035	1 0137	1 0151	1 0010	1 0206	1 0025	1 0142
30	1 0043	1 0188	1 0199	1 0022	1 0270	1 0032	1 0188

Here it means

m C A - calculation with cluster micro-depletion
o C A - calculation without cluster micro-depletion
BU - burnup in units of [MWd/Kg U]

The results show, that δK_{inf} depends on spatial discretisation of the cluster region and on the 'blackness' of absorber For a roughly subdivision of the cluster region (NZ < 3 for Eu_2O_3, NZ< 5 for B_4C , NZ < 3 for BZr_2) the question of cluster-absorber treatment has only a secondary importance In this case the calculated spatial-energetical spectra in cluster-absorber is practically so wrong, that no difference between the possibilities of cluster-treatment is observed For NZ=12 zones at burnup value BU=30 MWd/Kg U the following differences in reactivity uncertainties of investigated WWER FA-s (table 10-11) are estimated

FA with Eu_2O_3 -rods 5 5%
FA with BZr_2 -rods 3 9%
FA with B_4C -rods 1 9-2 7%

These uncertainties are practically independent from boron acid concentration and from FA enrichment (table 10 and results of paper [28,29])
As the above mentioned results show a neglection of cluster micro-depletion leads to a generally reactivity deficit for FA-s with burnable absorbers
The influence of cluster absorber treatment on the calculated micro-power release distribution in FA-s in fig 3-4 is illustrated Power release calculation is carried out by FLEX code using few-group parameters for two burnup state

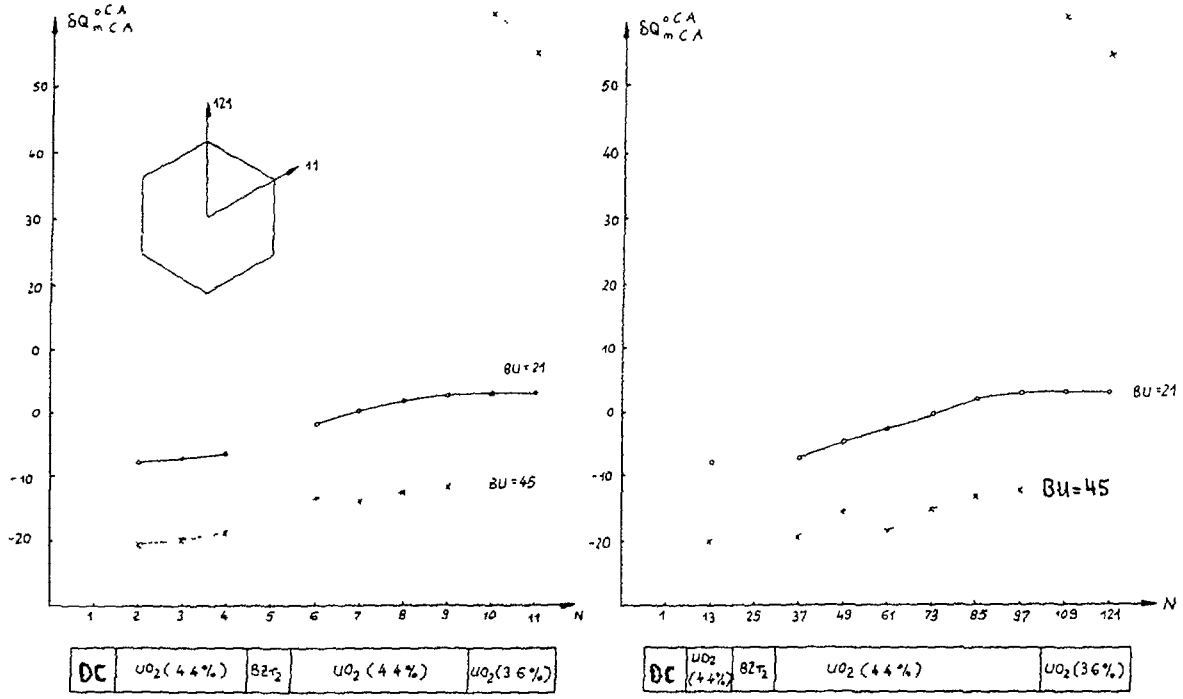

DC: dosimetry channel

FIG. 3. Influence of cluster–absorber treatment on micro-power release distribution in WWER FA.

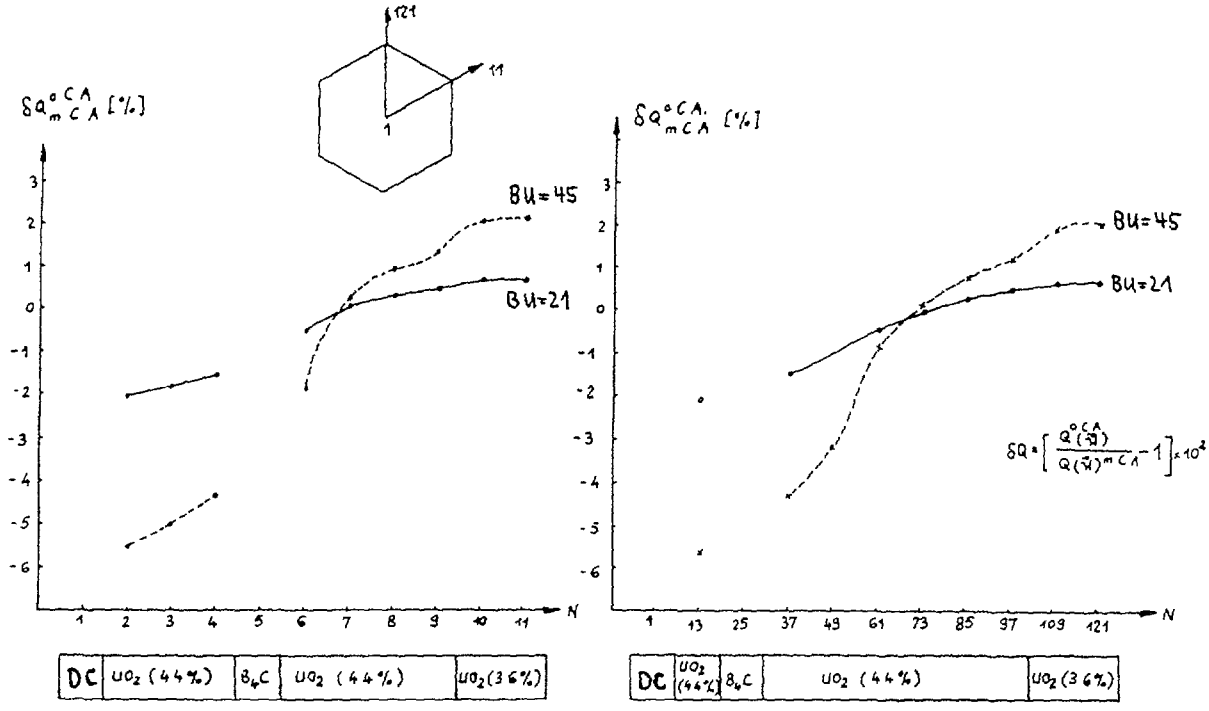

DC: dosimetry channel

FIG. 4. Influence of cluster–absorber treatment on micro-power release distribution in WWER FA.

(BU=21 MWd/Kg U and BU=45 MWd/kg U respectively). For each FA six several sets of few-group parameters in FLEX calculations are used
According to the NESSEL-4 geometry model for WWER FA-s group constants of the following materials are calculated central dosimetry channel, cluster rod cell, fuel-pins neighboured with cluster rods, fuel pins in neighbourhood of assembly jacket rest of fuel-pins in the 'undisturbed' lattice region, assembly jacket
Calculated ratios $\delta Q(\vec{r})$ as a function of pin position in FA two directions in figures 3-4 are given

δQ is defined as

$$\delta Q(\vec{r}) = \left[\frac{Q(\vec{r})^{o\,C.A.}}{Q(\vec{r})^{m\,C.A.}} - 1 \right] \cdot 10^2$$

$Q(\vec{r})$ calculated power release by FLEX

In the case of BZr_2 cluster-absorber deviations in calculated distributions achieve until 20% This circumstance is connected with the relative quickly burnup of BZr_2 rods For FA-s, containing B_4C cluster absorber, uncertainties until 6% in calculated micro-power release in dependence on cluster treatment are expected

4 1 Gadolinium lattice calculations

In table 12 calculated Gd-efficiency values (Kinf), obtained by NESSEL-4, CASMO-HEX [31] and RSYST-CGM [32] for the hexagonal macro-cell of Sidorenko [7] and the square EIR lattice [5], are summarized

Table 12 Δ Kinf-values ('efficiency of Gd)

BU [MWd/KgU]	EIR [19]	EIR NESSEL-4 DIPOL-2	Sidorenko-macrocell CASMO-HEX	Sidorenko-macrocell RSYST-CGM	Sidorenko-macrocell NESSEL-4
0	0 3292	0 3281	0 1151	0 1197	0 1198
1	0 2764	0 2752	0 1052	0 1036	0 1005
2	0 2354	0 2414	0 0953	0 0926	0 0927
3	0 1919	0 1945	-	-	-
4	0 1424	0 1405	0 0727	0 0705	0 0724
5	0 0892	0 0878	-	-	-
6	0 0440	0 0421	0 0473	-	0 0466

Δ Kinf = Kinf (UO_2 fuel-pin) - Kinf (macro-cell)

In comparison with the results of above mentioned codes NESSEL-4 not very large differs Usually, as the investigations in material [30] have shown, NESSEL-4 overpredict the gadolinium absorption and therefore underestimate Keff in dependence on lattice type of about 0 5-1 0%

Appendix

Fine-mesh diffusion calculations with spectral-corrected few-group constants

As it was shown in chapter 3 1 1 at boundary of several media differences of about 5-10% between measured and calculated power-release distributions are observed if asymptotical few group parameters in diffusion codes are used In the following a simple method to reduce this uncertainties, on the basis of spectral-corrected few-group constants in fine-mesh diffusion code FLEX, is suggested
Considering a cylindrical super-cell (fig A1) This cell consists in the inner part of fuel-pin cells of the same type (enrichment, lattice-pitch, temperature,) Around this region a zone is positioned, which affects on the inner district as a disturbance For the so defined super-cell a more-group spectrum calculation by NESSEL-4 is carried out In dependence on thickness and composition of the outer zone the fuel-pin spectrum in the inner part of the super cell is influenced By obvious condensation procedure the few-group constants of the perturbed region are calculated Changing outer disturbances the few group parameters Σ_g in dependence on spectrum value SI are calculated SI is the ratio of epithermal to thermal neutron-flux ($SI = \phi_{epi} / \phi_{th}$) in the fuel-pin region
These dependencies like input datas for FLEX code are used FLEX solves, at first for a given lattice arrangement, the fine-mesh diffusion equation in hexagonal geometry using asymptotical few group constants During outer iteration for all lattice points fluxes are calculated These fluxes are used to calculate a local dependend spectrum ratio $SI(\vec{r})$, defind as

$$SI(\vec{r}) = \phi_{epi}(\vec{r}) \,/\, \phi_{th}(\vec{r})$$

By correlation on basis of interpolation between $\Sigma_g(SI)$ from NESSEL-4 and $SI(\vec{r})$ from FLEX for each point $\vec{r}$ the corresponding spectral-corrected few group constants are calculated Using these parameters the further iteration process is carried out Iteration is finished, if a given accuracy limit for own-value Keff, fluxes and spectral-index value $SI(\vec{r})$ is obtained
The method is realized in FLEX-S code Details about the used method in paper [25] is described For illustration of the code accuracy at figure 5 procentually deviations between calculated and measured power-release distributions using asymptotical and spectral-corrected few-group constants for an investigated ZR-6 assembly (configurations 101/100 and 102/102) are presented

Configuration: 101/100

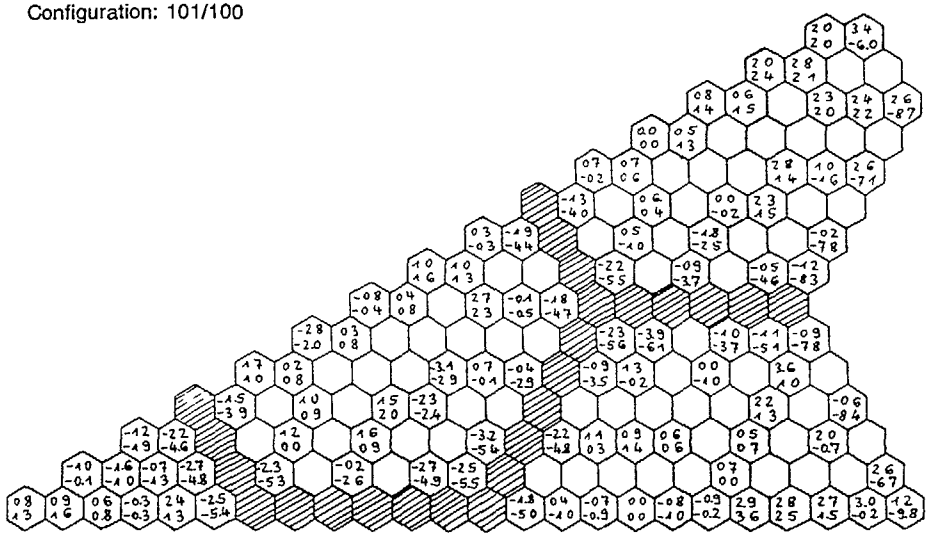

Configuration: 102/102

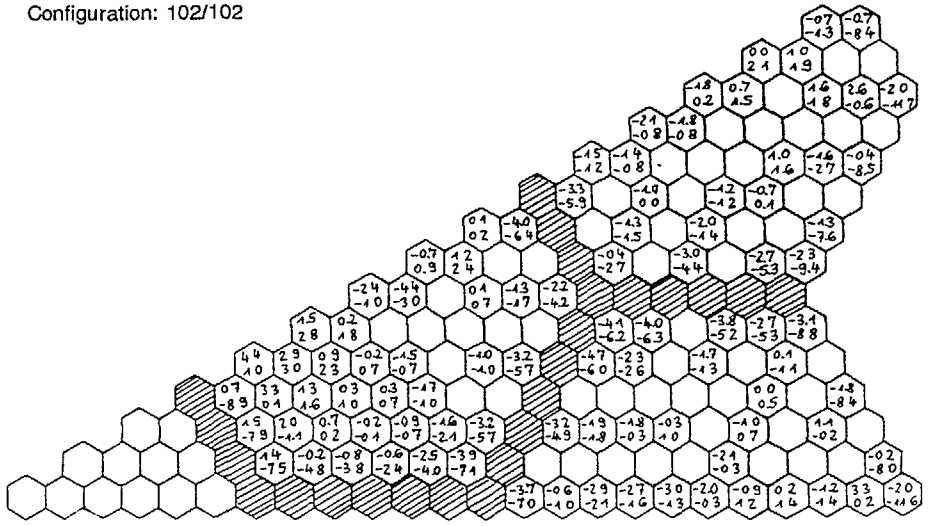

FIG. A1. Deviations between measured and calculated micro-power release distribution (lower numbers: asymptotical few-group parameters in FLEX; upper numbers: spectral-corrected parameters).

REFERENCES

[1] Kessler, Nuclear Fission Reactors, Springer Verlag Wien 1983

[2] И.Н Нигматулин и др., Судовые энергетические установки, Москва, Энергоатомиздат, 1986г.

[3] B.M. Rohleder. Feasibility of Using Gadolinium as a Burnable Poison in PWR cores, EPRI-NP-1663, 1981

[4] L.Goldstein et.al., A Comparison of Gadolinium and Boron for Burnable Poison Applications in Pressurized Water Reactors, Nucl. Techn. 60, p 352, 1983

[5] C. Maeder et.al , International Comparison Calculations for a BWR Lattice with Adjacent Gadolinium Pins, EIR-Bericht Nr. 532, NEACRP-L-271

[6] J J.Arkuszewski, Analysis of the Nine-Cell LWR Gadolinium Benchmark, PSI-Bericht Nr 13, 1988

[7] В.Д. Сидоренко, Тестовая задача для расчета топливных решеток с ТВЭЛами, содержащими гадолиний, Москва, 1988 г.

[8] H Heinrich, Kernenergie 24 (1981), S.465

[9] А.П Абагян и др., Групповые константы для расчета реакторов и защиты, Москва, Энергоатомиздат, 1981г.

[10] R.J.J.Stamm'ler, K-7 THERMOS Neutron Thermalization in a Heterogeneous Cylindrically Symmetric Reactor Cell. Kjeller Report No KR-47 (1963)

[11] R.Bonalumi, Neutron First Collision Probalities in Reactor Physics, Energia nucleare, 8 (1961), Nr.5, p.326

[12] A. Kavenoky, Calcul et utilisation des probabilities de premiere collision pour des milieux heterogenes a une dimension: Les programmes ALCOLL et CORTINA, CEA-N-1077, Centre d'Etudes Nucleaires de Saclay

[13] M.L.Williams et.al., Analysis of Thermal Reactor Benchmarks with Design Codes Based on ENDF/B-V Data, Nuclear Technology, Vol. 71, Nov. 1985

[14] Thermal Reactor Benchmark Compilation CSWC Data Testing Subcomitee

[15] Hardy et.al., Exponential and Critical Experiments, Vol.2, 332-358, IAEA, Vienna (1964)

[16] G. Agthe et.al., Kernenergie 29 (1986), S.413

[17] R. Becker et.al., Kernenergie 32 (1989)8, S.308

[18] R. Becker et.al., Kernenergie 33 (1990)8, S.

[19] Advanced Recycle Methodology Program System Documentation, EPRI-CCM-3, Rp 118-1, Part I, Electric Power Research Institute (1977 Sept.)

[20] A. Ahlin et.al., CASMO, A Fuel Assembly Burnup Program, STUDSVIK AE-RF-76-4158 (1976)

[21] D.S. Craig, Testing ENDF/B-V Data for Thermal Reactors, AECL-7690, 1982

[22] J.R.Askew et.al , A General Description of the Lattice Code WIMS, J Br. Nucl. Energy Soc.,5, 564, 1966

[23] Experimental Investigations of the Physical Properties of WWER-Type Uranium Water Lattices, Final Report of Temporary International Collective (TIC), Volume1, Akademiai Kiado, Budapest 1985

[24] D.Hennig et.al.,Programmbericht DIPOL-1,KKWB-Nr. 11-72-0

[25] R. Becker, Veroeffentlichung Kernenergie (in preparation)

[26] Experimental Investigations of the Physical Properties of WWER-Type Uranium Water Lattices, Final Report of TIC, Volume III (in preparation)
[27] V Jagannathan et al , Validation of Hexagonal Lattice Code System with VVER-Type Uranium-Water Lattice Experiments, Bhabha Atomic Research Centre, Bombay 400085, India, Report 622-13-TC-676, 1989
[28] R Becker, Behandlung von abbrennbaren Clusterabsorbern in Brennstoffkassetten vom Typ WWER-1000, Dissertation A , TH Zittau, 1990
[29] R Becker, Kernenergie 30(1987), 4, S 314
[30] R Becker, GDR-Calculation Results of Gadolinium Fuel-Pin Lattices, CRP-GDR-5775, IAEA Vienna
[31] M Antilla, Finish Results for a VMK Benchmark Problem Concerning Use of Gadolinium in Fuel Rod Lattices, IAEA Vienna 1990
[32] D Luts, Results for the Sidorenko Benchmark, University of Stuttgard, 1990

REFLECTOR MODELING IN ADVANCED NODAL ANALYSIS OF PRESSURIZED WATER REACTORS

E Z. MULLER
Reactor Theory Division,
Atomic Energy Corporation of South Africa Limited,
Pretoria, South Africa

Abstract

Recent progress in the modeling of the reflector regions of pressurized water reactors within the framework of advanced nodal diffusion analysis methods is reviewed Attention is focused on the modeling of the radial reflector of a PWR which is most problematic because of its irregular and heterogeneous structure Numerical results are presented to demonstrate the high accuracy of the methods which are now available for generating nodal reflector parameters and it is shown that errors due to reflector modeling in multi-dimensional nodal reactor analysis can be practically eliminated

INTRODUCTION

The application of advanced nodal diffusion methods[1] to the in-core physics analysis of light water reactors has become quite common in recent years [2-4] These modern nodal methods have at least one basic feature which distinguishes them from the traditional nodal methods,[5] namely that all energy groups and all spatial regions of the reactor (including the reflectors) are treated with the same degree of sophistication Hence, the accuracy of advanced nodal diffusion models is dependent not only on the adequacy of the fuel assembly homogenization methods used to determine equivalent nodal parameters (ENPs) for fuel nodes, but also depends significantly on the methods used to determine ENPs for homogenized reflector nodes [2,6-9] In this regard, the modeling of the radial reflector of a pressurized water reactor (PWR) is singled out as the most challenging because of the heterogeneous structure of this region (This region typically consists of a close-fitting steel baffle around the core followed by a thick water reflector with the steel core barrel and several steel neutron pads interspersed at various distances from the core) The axial reflectors represent less of a problem since they are normally assumed to consist of homogeneous mixtures of water and structural materials

The purpose of this paper is to summarize the principal differences between the methods which are currently available for determining ENPs for PWR radial reflector nodes and to evaluate the accuracy of these methods In particular, numerical results are presented to demonstrate that errors due to reflector modeling in multi-dimensional nodal reactor analysis (i e due to few-group reflector parameters) can now actually be reduced to practical insignificance

NODAL EQUIVALENCE THEORY BASED REFLECTOR MODELS

Several advanced methods for determining nodal reflector parameters (called reflector models) have been reported in recent years [6,10,11,7,8,12,13] Most of these models are based on applications of nodal equivalence theory (NET)[14,15,6,7] involving one–dimensional (1–D) multigroup transport calculations (spectral geometry calculations) which model one or more fuel assemblies, the baffle, and the reflector (and if sufficiently close to the core, the core barrel and neutron pads) to provide the spectral and spatial information necessary to compute reflector ENPs The various NET–type reflector models differ mainly in the manner in which flux discontinuity factors[15] are computed and applied

In Koebke's[6] 1–D simplified equivalence theory (SET) reflector model, for example, discontinuity factors which are identical (per energy group) on the opposite faces of a 1–D homogenized reflector node are determined simultaneously (iteratively) with the group diffusion coefficients for the node These discontinuity factors, which are called heterogeneity factors,[14] are assumed to be valid for all coordinate directions and are thus conveniently divided into the diffusion coefficients and flux–volume weighted (FVW) cross sections for the 1–D node to yield ENPs applicable to a corresponding three–dimensional (3–D) node These ENPs can then be used in standard nodal diffusion codes without the introduction of additional complexities such as the inclusion of flux discontinuities in node interface continuity conditions or the carrying of discontinuity factors as equivalent parameters in cross section tables

Smith[7] applies the generalized equivalence theory (GET)[15] method to determine face–dependent discontinuity factors for a homogenized reflector node However, since 1–D spectral geometry calculations are used for this purpose,[3] discontinuity factors are computed only for those faces which are parallel with the core edge More specifically, Smith utilizes only the discontinuity factors on the coreside face of the 1–D reflector node by assuming that these are valid for all faces of a corresponding two–dimensional (2–D) reflector node[16] (In the axial direction the radial reflector has no structural heterogeneities and unity discontinuity factors are usually assigned to axial node faces However, if axial water density variations within the radial reflector are neglected, then the radial discontinuity factors can also be used in the axial direction) These discontinuity factors are used together with the reflector FVW cross sections and diffusion coefficients in nodal diffusion codes which explicitly account for flux discontinuities

Rathkopf and Liu[12] have described a 1–D GET reflector model in which a single set of coreside discontinuity factors is determined for application to all faces of a 3–D reflector node They utilize a two–group 1–D diffusion theory analytic relationship between core–reflector interface fluxes and net currents for a finite (homogenized) reflector to determine the coreside discontinuity factors Furthermore, they divide these two–group discontinuity factors into the two–group FVW cross sections and diffusion coefficients for the node to obtain a set of ENPs which can be used, just like Koebke's SET parameters, in standard nodal codes

The above two models are strictly speaking applicable only to thick reflector nodes for which neutron transmission through the 1–D reflector node is negligible While this may be the case for assembly–size nodes, neutron transmission becomes significant when homogenization is carried out over quarter–assembly size nodes However, this is of little concern in practice since homogenization for the radial reflector is nearly always applied to assembly–size nodes, even if quarter–assembly homogenization is carried out for fuel nodes

A rather different simplification of a 1–D GET reflector model which achieves the same goal as the Rathkopf–Liu model (i e no discontinuity factors as explicit ENPs), but which is not limited to two energy groups or to thick reflector nodes, has been developed This model, which has been called the normalized GET (NGET) model,[13] utilizes a multigroup analytic method to compute discontinuity factors and a discontinuity factor normalization procedure which starts at the core–reflector interface and proceeds towards the outside of a 1–D array of reflector nodes (retaining the values of the discontinuity factors on the core–reflector interface) to obtain face–independent discontinuity factors for each node These normalized discontinuity factors are divided into the FVW cross sections and diffusion coefficients of the nodes Thus, the NGET method can be used to determine ENPs for reflector nodes of arbitrary thickness as well as for multi–node reflector representations In this respect the NGET method is similar to the SET method The difference is that the NGET method does not require an iterative adjustment of the diffusion coefficients to determine face–independent discontinuity factors In the NGET method, as well as the previously mentioned GET methods, arbitrary diffusion coefficients are allowed, but FVW values are normally used

Utilization of the nodal reflector parameters derived from these 1–D models gives rise to so–called two–dimensional effects in multi–dimensional nodal calculations for PWRs because these reflector parameters do not account for the two–dimensional structure of the baffle at core corners The two–dimensional effects have been estimated[13,17] to be of the order of 1% maximum error in assembly powers accompanied by a core–wide power tilt of 1% to 2% Furthermore, these NET–based models yield radial reflector data which are dependent on core conditions primarily through the use of the flux–volume weighting procedure for spatial homogenization [13] It has been shown[13,17] that this environment dependence might incur even greater uncertainty in power distributions than do the two–dimensional effects However, since two–dimensional and environmental effects often (depending on core conditions) cancel fortuitously, the overall effect is frequently quite small Unfortunately, such cancellation of effects does not provide confidence in the projected accuracy of a particular PWR nodal reflector model, and therefore recent attempts have been directed towards a more consistent elimination or reduction of the individual effects

As far as two–dimensional effects are concerned, these can be eliminated by utilizing simplified two–dimensional calculations, like those used by Hoxie[10] and Khalil,[11] to compute NET parameters for corner reflector nodes Unfortunately, such 2–D NET models are still environment–dependent and are computationally more complex and expensive than the simple one–dimensional models Therefore, the focus has been placed on developing improved one–dimensional models instead

RESPONSE MATRIX BASED REFLECTOR MODELS

The highly asymmetrical structure of the radial reflector and the use of FVW cross sections (together with discontinuity factors) render NET-based reflector data relatively sensitive to core conditions Response matrix (RM) homogenization methods,[18–20] on the other hand, have greater potential (at least in 1–D) of yielding environment-insensitive ENPs Therefore, efforts to obtain less core dependent radial reflector ENPs have been directed towards defining the ENPs in terms of 1–D response matrices Two such reflector models have been reported in the open literature, namely the model of Koebke *et al*[8] and the so– called NGET–RM model [13]

The model of Koebke *et al*,[8] which has also been referred to as the Koebke–RM model,[13] utilizes the results obtained from two separate 1–D multigroup spectral geometry calculations to compute a two–group infinite–reflector flux–current RM and FVW cross sections for a thick reflector node Two–group analytic diffusion theory (presuming zero upscatter) expressions are used to define diffusion coefficients and heterogeneity factors in terms of the elements of this RM and the FVW cross sections The resultant heterogeneity factors are divided into the diffusion coefficients and FVW cross sections to produce the required environment–insensitive ENPs (numerical verification of which is given in Ref 17) This model has one apparent weakness,[13] namely that the ENPs are not uniquely defined since either the epithermal diffusion coefficient (D_1), or the epithermal heterogeneity factor (F_1), must be assigned some *ad hoc* value However, as it turns out, this is actually an advantage (see below) and the real disadvantages of the method are the requirement for two "expensive" spectral geometry calculations and the restriction to two energy groups

The 1–D NGET–RM reflector model[13] has as its basis the observation[13,17] that the environment dependence of NET–based radial reflector data is due almost entirely to the FVW spatial smearing (homogenization) process and not to group condensation, and it utilizes several fundamental properties of partial–current RMs to circumvent the FVW approach in order to homogenize radial reflector nodes Thus, a scheme is devised in which the NGET method is used for energy condensation to produce few–group equivalent diffusion parameters, which are practically environment–independent,[13,17] for each of the component regions of the radial reflector (The SET method could equally well be used for this purpose) These regionwise NGET parameters are then used in the analytic computation and addition of component region (slab) RMs in order to obtain a composite RM for the entire reflector region or parts of it (nodes) In order to define unique ENPs in terms of the elements of the composite RMs of each node, these matrices are symmetrized in such a way that all effects due to this symmetrization are incorporated in an albedo boundary condition computed on the outer edge of the reflector The remaining environment dependence of the NGET–RM ENPs (due to the component region NGET parameters) has been shown to be insignificant and to incur uncertainties in core power distributions of much less than 0 1% [13,17]

Relative to the Koebke–RM reflector model, the NGET–RM method has the advantage that it is a general multigroup model and that it requires only one multigroup spectral geometry calculation to obtain all the necessary information for determining the reflector ENPs However, the latter advantage can be eliminated by modifying the Koebke–RM procedure such that only one spectral geometry calculation is required for it as well This can be done by simply calculating the flux–current transformation of the partial–current infinite–reflector RM which is computed and used in the NGET–RM method (denoted by $\hat{\beta}_0^+$ in Ref 13), in order to obtain the infinite–reflector RM required in the Koebke–RM method Numerical results[13,17] have suggested that this modified scheme should yield practically the same infinite–reflector RM as the original method This approach actually has a second advantage, namely that it allows a consistent elimination of the upscattering element in the two–group infinite–reflector RM (which may not be negligible if computed from the edited results of two spectral geometry calculations) This is achieved by applying the following simple upscatter–correction to the regionwise FVW scattering matrices prior to computing the discontinuity factors for each subregion J (ϕ_G^J being the group G average flux in region J)

$$\Sigma_{GG'}^{J\,*} = \Sigma_{GG'}^{J} - \Sigma_{G'G}^{J}\left[\frac{\phi_G^J}{\phi_{G'}^J}\right] \qquad \forall\ G'<G \quad , \tag{1a}$$

$$\Sigma_{GG'}^{J\,*} = 0 \qquad \forall\ G'\geq G \tag{1b}$$

The subsequently computed NGET parameters then rigorously conserve the integral two–group reaction rates per region and lead to an infinite–reflector RM and a FVW scattering matrix without upscatter

The principal difference between the "modified" Koebke–RM reflector model and the NGET–RM model therefore lies in the manner in which ENPs are defined in terms of the respective composite RMs In contrast to the Koebke–RM model, the NGET–RM method results in ENPs which are uniquely defined Theoretically, this
may be considered an advantage of the NGET–RM model, but from a practical point of view the non–uniqueness of the Koebke–RM ENPs is not an actual disadvantage The reason for this is that both reflector models are 1–D models and consequently they have the same deficiency as the 1–D NET–based models regarding the modeling of the baffle at core corners (2–D effects) However, the Koebke–RM model has the benefit of an extra degree of freedom (i e F_1) which can be used to adjust the equivalent reflector parameters in order to reduce 2–D effects,[21] whereas the NGET–RM method has none A numerical "optimization" experiment[21] has shown that by using a value of $F_1 \approx 2\,0$ for generating ENPs for inner corner reflector nodes (i e nodes wedged into the core) and a value of $F_1 = 1\,0$ for all other reflector nodes, the 2–D effects of the (modified) Koebke–RM reflector model can be reduced dramatically from those obtained by using the standard[8] $F_1 = 1\,0$ for all nodes In fact, the 2–D power distribution errors of the "improved" Koebke–RM model (i e using $F_1 = 2\,0$ for inner corner reflector nodes) are reduced to well below those of the NGET–RM method, which in turn has

much smaller 2–D power distribution errors associated with it than does the standard Koebke–RM model This is evident from the results which are given in Table 1 for two typical (realistic) 2–D PWR problems (PROBLEM 1 is defined in Ref 13 and PROBLEM 2 is defined in Ref 21)

Despite the lack of free parameters in the NGET–RM method, it was recently shown[21] that it is feasible to set up a very simple semi–empirical scheme for reducing the 2–D effects of this reflector model The empirical procedure developed in Ref 21 is based on the transverse leakage concept and an assumed flux separability in corner reflector nodes, and is applied only to inner corner reflector nodes It determines two "optimal" empirical factors which are used to adjust the material buckling matrices (computed from the few–group NGET parameters) of the reflector component regions before proceeding with the calculation and addition of their respective RMs These two empirical factors, which are called the thermal and epithermal factors, facilitate the reduction of 2–D effects in both the thermal and epithermal energy ranges The improved Koebke–RM method, on the other hand, reduces 2–D effects only in the epithermal range and actually increases thermal effects (see Ref 21) Thus, the "improved" NGET–RM reflector model (using the optimized empirical factors[21] to generate ENPs for inner corner reflector nodes) is not only capable of reducing the 2–D errors in the global (nodal) power distribution, but should also reduce local intranode power distribution errors in core peripheral nodes The excellent performance of the improved NGET–RM reflector model relative to the standard NGET–RM model as well as to the improved Koebke–RM model is reflected by the summary of 2–D errors given in Table 1 (see also Fig 1)

It is of practical importance that the optimal empirical factors for the improved NGET–RM reflector model are rather insensitive to core configuration (geometry) and core conditions[21] It is also suggested that these factors should be insensitive to varying reflector conditions (e g soluble boron changes) and to modest changes in reflector configuration (e g realistic changes in baffle thickness) because the applied empirical correction is region–dependent and proportional to the material buckling matrix in each component region Furthermore, since 2–D effects show a distinct separation into thermal and epithermal effects (see Refs 17 and 21) and since two independent factors are used in these two energy ranges, the optimal factors are expected to be valid for multigroup applications as well

The results quoted above demonstrate that both the improved Koebke–RM and the improved NGET–RM reflector models are accurate and practical methods of generating ENPs for PWR radial reflector nodes However, the NGET–RM model has one other feature, namely the non–diagonal nature of its equivalent diffusion coefficient matrix $(\hat{D})$,[13] which may place it at a disadvantage with regard to its utilization within some of the existing nodal reactor calculational systems While modern nodal methods are not in principle restricted to a diagonal $\hat{D}$ treatment[17] and may actually require only modest programming changes to accommodate full D matrices, the alternative would be to find some suitable means of diagonalizing the NGET–RM D matrix without compromising its accuracy It has been found that simply diagonalizing $\hat{D}$ (by whatever means) is inadequate and that such diagonalization should be accompanied by a redefinition of the other ENPs[22] An approximate method based on this approach was proposed in Ref 17 for application to thick reflector nodes The method has been successfully tested[22] and shown to introduce hardly any additional errors in 2–D power distributions (see last row in Table 1) provided a suitable choice is made for the diagonalized D matrix The analysis performed in Ref 22 indicated that the inverse of the sum of the elements in each row of the transport matrix $(\hat{D}^{-1})$ yields a very good diagonalized D matrix

TABLE 1
Summary of 2–D Effects for Two PWR Problems (from Ref. 21)

Reflector Model	PROBLEM 1 $(\Delta P\%)_{max}$	PROBLEM 1 $(\Delta P\%)_{av}$	PROBLEM 1 %Tilt	PROBLEM 2 $(\Delta P\%)_{max}$	PROBLEM 2 $(\Delta P\%)_{av}$	PROBLEM 2 %Tilt
Standard Koebke–RM	–5.0	2.1	+6.2	–4.0	1.1	+3.2
Standard NGET–RM	+1.3	0.7	+2.2	–1.2	0.3	+1.1
Improved Koebke–RM	+1.1	0.3	+0.6	–0.6	0.2	+0.4
Improved NGET–RM	+0.1	0.0	+0.1	–0.1	0.1	+0.2
[a]Improved NGET–RM	–0.2	0.1	+0.2	–0.2	0.1	+0.3

[a]With diagonalized D matrix

TABLE 2
Summary of Nodal Results for Two PWR Problems

Reflector Model	PROBLEM 1 $(\Delta P\%)_{max}$	PROBLEM 1 $(\Delta P\%)_{av}$	PROBLEM 1 %Tilt	PROBLEM 2 $(\Delta P\%)_{max}$	PROBLEM 2 $(\Delta P\%)_{av}$	PROBLEM 2 %Tilt
NGET	+2.7	1.0	–3.1	–0.9	0.1	+0.1
Standard Koebke–RM	–3.2	1.0	+3.1	–4.1	0.7	+2.4
[a]Standard NGET–RM	+1.2	0.4	–1.2	–1.2	0.1	+0.4
Improved Koebke–RM	+2.9	0.9	–2.9	+1.1	0.2	–0.3
[a]Improved NGET–RM	+1.8	1.0	–3.1	+0.7	0.2	–0.5

[a]With diagonalized D matrix

$$(\Delta P\%)_{av} = \frac{1}{V}\sum_{i=1}^{N} V_i|\Delta P_i\%| \quad , \qquad \text{Tilt} = (\Delta P\%)_{centre} - \frac{1}{K}\sum_{k=1}^{K} V_k \Delta P_k\% \quad ,$$

(V = core volume; N = number of fuel assemblies, K = number of peripheral fuel assemblies, $\Delta P_i\%$ = the relative percentage error in the average power of assembly i having volume V_i)

0 1	0 1	0 1	0 1	0 1	0 0	0 0	0 0
0 1	0 1	0 1	0 0	0 0	0 0	0 0	-0 1
0 1	0 1	0 0	0 0	0 0	0 0	-0 1	-0 1
0 1	0 0	0 0	0 0	0 0	-0 1	-0 1	-0 1
0 1	0 0	0 0	0 0	0 0	-0 1	-0 1	
0 0	0 0	0 0	-0 1	-0 1	-0 1	0 1	
0 0	0 0	-0 1	-0 1	-0 1	0 1		
0 0	-0 1	-0 1	-0 1				

Fig 1 Relative percentage errors in the PROBLEM 2 power distribution for the improved NGET–RM reflector model (full D)

IMPACT OF RADIAL REFLECTOR MODELS IN NODAL CALCULATIONS

Thus far the discussion has centred around the accuracy of the various methods available for generating radial reflector ENPs Hence, only results which reflected errors due to reflector modeling alone (i e uncontaminated by spatial truncation errors or fuel assembly homogenization errors) were quoted This unambiguity was achieved (see Refs 13 and 21) by defining 2–D reactor test problems with homogenized assemblies and by performing the reactor diffusion calculations with the 2–D high–order RM code LABANPEL[17] which was used in such a mode as to limit spatial truncation errors to below 0 1% maximum error in assembly powers However, the impact that reflector data generated by the different reflector models would have on the results of actual nodal reactor calculations (for which spatial truncation errors are often significant) has not been considered To investigate this, an analytic nodal diffusion method similar to the QUANDRY[23] method was employed with a one–node–per–assembly mesh structure to perform a series of calculations for the previously defined 2–D two–group PWR problems The results are summarized in Table 2 in terms of the errors relative to the LABANPEL reference (explicit baffle and reflector NGET data) results

Evidently, the use of radial reflector data generated by the more sophisticated reflector models (e g improved NGET–RM) does not necessarily lead to the most accurate nodal results It may therefore appear pointless to generate very accurate nodal reflector data if the eventual nodal results are not much different from those obtained with less sophisticated reflector data However, this is purely due to a fortuituous and unpredictable cancellation of errors, something which is incompatible with the principles of modern nodal reactor analysis The spatial truncation error of the nodal method, of which a good estimate is given by the last row in Table 2, obscures the true performance of the various reflector models Therefore, one should not evaluate the adequacy/inadequacy of a given reflector model on the basis of nodal reactor calculations for which spatial truncation errors may be so large as to prohibit an objective analysis Likewise, one should be cautious about adjusting reflector data to compensate for other reactor modeling errors (such as fuel assembly homogenization errors) since such errors may vary with reactor core conditions (exposure, power distributions) and reactor geometry

CONCLUSION

The characteristics of various modern methods for generating few–group equivalent nodal reflector parameters for the radial reflector of a PWR have been described in this paper Numerical results were presented to demonstrate the high accuracy of the methods which are now available for generating nodal reflector parameters The most advanced nodal reflector models amongst those discussed are the improved Koebke–RM and the improved NGET–RM models It was shown that errors due to reflector modeling can be reduced to practical insignificance (e g corewise power tilts and assembly power errors of no more than several tenths of a percent) if the improved NGET–RM reflector model is used The conclusion is therefore drawn that it is now possible to practically eliminate the contribution of reflector modeling errors to the overall error of advanced nodal reactor analysis It is also concluded that practical nodal reactor analyses should be performed with the best reflector data available without any form of adjustment of such data to compensate for other modeling difficulties

REFERENCES

1 R D LAWRENCE, Prog Nucl Energy, 17, 271 (1986)

2 K KOEBKE *et al*, Atomkernenergie, 46, 224 (1985)

3 M EDENIUS *et al*, "Recent Developments in the MICBURN/CASMO/SIMULATE LWR Analysis Package," Proc Top Mtg Advances in Fuel Management, Pinehurst, North Carolina, USA, 2–5 March 1986

4 K KOEBKE and D H SIMMONS, "Overview of LWR Analysis Methods," Proc Int Reactor Physics Conf, Jackson Hole, Wyoming, USA, 18–22 Sept 1988

5 N K GUPTA, Prog Nucl Energy, 7, 127 (1981)

6 K KOEBKE, "Advances in Homogenization and Dehomogenization," Proc Int Topl Mtg Advances in Mathematical Methods for the Solution of Nuclear Engineering Problems, Munich, FRG, April 27–29, 1981

7 K S SMITH, Prog Nucl Energy, 17, 303 (1986)

8 K KOEBKE *et al*, Nucl Sci Eng, 92, 56 (1986)

9 K S SMITH, Trans Am Nucl Soc, 60, 329 (1989)

10 C L HOXIE, "Application of Nodal Equivalence Theory to the Neutronic Analysis of PWRs," PhD Thesis, Massachusetts Institute of Technology (1982)

11 H S KHALIL, "The Application of Nodal Methods to PWR Analysis," PhD Thesis, Massachusetts Institute of Technology (1983)

12 J A RATHKOPF and Y S LIU, Trans Am Nucl Soc., 53, 247 (1986)

13 E Z MULLER, Nucl Sci Eng., 103, 359 (1989),
see also *E Z MÜLLER*, "Environment-Insensitive Equivalent *Diffusion Theory* Group Constants for PWR Reflector Regions," Proc Int Reactor Physics Conf., Jackson Hole, Wyoming, USA, 18–22 Sept 1988

14 K KOEBKE, "A New Approach to Homogenization and Group Condensation," Proc Technical Committee Mtg Homogenization Methods in Reactor Physics, Lugano, Switzerland, November 13–15, 1978, International Atomic Energy Agency

15 K S SMITH, "Spatial Homogenization Methods for Light Water Reactor Analysis," PhD Thesis, Massachusetts Institute of Technology (1980)

16 K S SMITH, Private Communication (1989)

17 E Z MULLER, "Development of an Environment-Insensitive PWR Radial Reflector Model Applicable to Modern Nodal Reactor Analysis Methods," DSc Thesis, Potchefstroom University for CHE, Potchefstroom, South Africa (1989)

18 A F HENRY *et al*, "Spatial Homogenization of Diffusion Theory Parameters," Proc Technical Committee Mtg Homogenization Methods in Reactor Physics, Lugano, Switzerland, November 13–15, 1978, International Atomic Energy Agency

19 R A BONALUMI, Nucl Sci Eng., 77, 219 (1981),

20 G C PIERINI, "Environment-Independent Homogenized Parameters for Neutron Diffusion in Non-Symmetric Slabs," Proc CNS/ANS Int Conf on Numerical Methods in Nuclear Engineering, Montreal, Canada, 6–9 Sept 1983

21 E Z MULLER, "Improved Pressurized Water Reactor Radial Reflector Modeling in Nodal Analysis," Submitted for publication

22 E Z MULLER, "A Note on the Approximate Diagonalization of the Diffusion Coefficient Matrix of the NGET-RM Nodal Reflector Model,"
Report PEL-297 (1990)

23 K S SMITH, "An Analytic Nodal Method for Solving the Two-Group, Multidimensional, Static and Transient Neutron Diffusion Equations," Engineers Thesis, Massachusetts Institute of Technology (1979)

TREATMENT OF THE REFLECTOR IN TWO-GROUP *DIFFUSION CALCULATIONS FOR LWRs*

W BERNNAT
Institut für Kernenergetik und Energiesysteme,
Universitat Stuttgart,
Stuttgart, Federal Republic of Germany

Abstract

A general method for the treatment of radial or axial reflectors in diffusion calculations for light water reactors will be described The method is based on pre calculated response matrices for the reflector via external bound ary conditions e g in form of space and energy dependent albedos at the core/reflector boundary The response matrices can be calculated with stan dard multigroup or continuous energy Monte Carlo codes and applied for any type of solution method for the two group diffusion equation (e g finite dif ference methods, nodal expansion methods or finite element methods) The advantages of the method are an accurate treatment of neutron transport in the reflector and saving of computer time due to a reduced problem size (no meshes for reflectors are necessary)

1 Introduction

Due to the heterogeneous structure and complicated geometry of the radial and axial reflector of light water reactors an accuarate solution of the neutron diffusion equation in the reflector region can be achieved only if special weighted or adjusted absorption and transport cross sections e g based on equivalence theory [1] or special boundary conditions like space and energy dependent albedos are used If this problem is solved by means of special defined cross-sections, these cross sections depend from the type of numerical solution of the diffusion equation e g by finite difference methods or nodal methods (nodal expansion method [2], finite element method [3]) The use of pre calculated albedos leads to inaccuracies if the albedos are not updated for every actual core composition and power distribution

However, if adequate and updated albedos at the boundary between core and reflector are available, the solution of the diffusion equation for the evaluation of the power distribution can be reduced to the core region with two advantages

- remarkably less nodes are required (up to 30 %),
- the reflector structure (shroud, varying water gap, core vessel etc) can be taken into account accurately in the albedo calculation if an adequate method is used

The calculation of such adequate and updated albedos can be performed by means of a response matrix method based on transport theory The geometry and material composition of the reflector remain practically constant during a reactor cycle (except the boron concentration in PWR), therefore response matrices which define the relation between current directed into reflector at space variable r and energy group i and the returning current of neutrons at space variable r' and group i' depend only from few changeing parameters and hence can be calculated separately from diffusion calculation If the complete response matrix is known, the albedo at every group and at every space point at the boundary between core and reflector can be easily calculated by multiplying the output (from core to reflector) current vector by the response matrix achieving the corresponding input current vector and evaluating the relation between input current and output cur rent This can be done during the iterative solution of the diffusion equation with the most updated fluxes and gradients with negligible computer cost

The calculation of the response matrix may be performed by any adequate transport code In our experience the most convenient and accurate way to calculate such response matrices is the use of a Monte Carlo method By this method the reflector structure can be taken into account as realistic as necessary and the transport equation can be solved with high order of accuracy

A detailled study of the flux spectra at the boundary showed that the form of the energy spectra depend from the assembly type (enrichment etc), burn-up, boron concentration (PWR) and moderator density These dependencies can be taken into account by means of a few parameters The response matrix elements for these parameters can be calculated simultaneously by means of a correlated sampling Monte Carlo technique

With the response matrix method we had very good experiences also in other applications like calculation of SWR assemblies with cruciform absorber elements where the absorber region and water gap was treated by a Monte Carlo response matrix [4] and in (2D and 3D)HTR applications [5,6] where the complete cavity between core and reflector including inserted control rods were treated by means of response matrices (in this case not by external but by internal boundary conditions) The applied theory worked well for both finite difference methods and nodal methods (e g finite element method with isoparametric numerical integrated elements with second order expansion) The method is not only applicable to radial reflectors but also for axial reflectors Using internal boundary conditions instead of external albedos the method can be used to solve diffusion and transport equation in different regions simultaneously

2 Description of the Method

The basic principle is to couple the core region in which the two-group diffusion equation is solved by the reflector region in which the transport equation should be solved (due to the strong gradients in the reflector region) by means of an adequate boundary condition

In a P_L approximation of the transport equation the boundary condition for the neutron flux density between two different media generally can be written in the integral form [7]

$$\int_{(\Omega\ n)>0} Y_l^{m^*}(\vec{\Omega})(\vec{\Omega}\ \ \vec{n})\phi_D(\vec{r},E,\vec{\Omega})d\vec{\Omega} = \int_{(\vec{\Omega}\ \vec{n})>0} Y_l^{m^*}(\vec{\Omega})(\vec{\Omega}\ \ \vec{n})\phi_T(\vec{r},E,\vec{\Omega})d\vec{\Omega} \quad ,$$

where $\phi_D(\vec{r},E,\vec{\Omega})$ and $\phi_T(\vec{r},E,\vec{\Omega})$ are the flux densities in the diffusion region and transport region respectively The above boundary condition requires steadiness of the normal component of the current density along the boundary between two regions

In the region in which the diffusion equation is solved only sufficient conditions for a P_1-approximation (l = m = 0) exist In this case the boundary condition reduces to one equation in which the neutron flux density is approximated by the linear anisotropic term

$$\phi_D(\vec{r},E,\vec{\Omega}) = \frac{1}{4\pi}\left(\phi(\vec{r},E) + 3\vec{\Omega}\ \ \vec{j}(\vec{r},E)\right)$$

The normal component of the current density directed into the diffusion region is then

$$\begin{aligned} j^-(\vec{r},E) &= \frac{1}{4}\phi(\vec{r},E) + \frac{1}{2}D(\vec{r},E)\nabla_n\phi(\vec{r},E) \\ &= \int_{\Omega\ n>0} Y_0^{0^*}(\vec{\Omega})(\vec{\Omega}\ \ n)\phi_T(\vec{r},E,\vec{\Omega})d\vec{\Omega} \end{aligned}$$

The neutron flux density at the boundary between core and reflector region at the phase space coordinates $\vec{r},E,\vec{\Omega}$ is a function of the flux distribution at the surface and the material composition inside this region

$$\phi(r,L,\vec{\Omega}) = \frac{1}{(\vec{\Omega}\ \ n)}\int_{E'}\int_{(\vec{\Omega}\ n)>0}\int_{S} h(\vec{r}\ \ ,E',\vec{\Omega}\ \rightarrow \vec{r},E,\vec{\Omega})$$

$$\phi_D(\vec{r}\ \ ,E',\Omega\ )(\vec{\Omega}\ \ \ n\ )dE'\,d\vec{\Omega}'\,ds$$

where $K(\vec{r}\,', E', \vec{\Omega}' \rightarrow \vec{r}, E, \vec{\Omega})$ is a transport kernel which regards for scattering and absorption in the transport region and $\phi_D(\vec{r}\,', E', \vec{\Omega}')$ can be approximated by the mentioned linear anisotropic term. For the solution of the integral in the above equation a Monte Carlo method can be used for any degree of complexity of the reflector structure.

The principle of coupling exists in calculating the current density directed into the core region $j_g^-(\vec{r})$ (g denotes energy group number) as a function of the angular dependent current density directed into the reflector region. For a discretisized surface the current density j_{gl}^- (l denotes a surface element, e. g. which may be described by any possible surface type of the FE-net generator or a mesh boundary of the FD- or nodal mesh net) can be calculated by means of following equation

$$j_{gl}^- = \sum_{g'l'} \Big(R^0_{g'gl'l} \cdot \Phi_{g'l'} + R^1_{g'gl'l} \cdot \frac{\partial \phi_{g'l'}}{\partial x} + R^2_{g'gl'l} \cdot \frac{\partial \phi_{g'l'}}{\partial y} + + R^3_{g'gl'l} \cdot \frac{\partial \phi_{g'l'}}{\partial z} \Big)$$

The coefficients $R_{g'gl'l}$ are components of a response matrix which describe the neutron exchange between the surface elements. The fluxes $\phi_{g'l}$ and flux gradients $\frac{\partial \phi_{g'l'}}{\partial n}$ can be taken from the diffusion solution at the corresponding surface elements. In the finite element method the flux is approximated by a polynomial expansion

$$\phi_g(\vec{x}) = \sum_i \phi_g^i \cdot \xi_i(\vec{x})$$

where $\xi_i(\vec{x})$ are known functions (e.g. of order two) and ϕ_g^i the fluxes at the nodes of the finite element. In the FE-program DIFGEN /3/ e. g. a general boundary condition of the form

$$\alpha_g(\vec{x})\phi_g(\vec{x}) + \beta_g(\vec{x})\nabla_n\phi_g(\vec{x}) = \gamma_g(\vec{x})$$

can be taken into account at every external or internal side of a finite element (e.g. with pentaedric or hexaedric form). In diffusion approximation the current density from reflector into core region can be described by

$$j_g^-(\vec{x}) = \frac{1}{4}\phi_g(\vec{x}) + \frac{1}{2}D_g(\vec{x})\nabla_n\phi(\vec{x})$$

($D_g(\vec{x})$ is the diffusion coefficient for group g.) This input current vector can be calculated by multiplying the output current vector (into the reflector region) by the response matrix and used as a NEUMANN source term of the gernal boundary condition $\gamma_g(\vec{x}) = j_g^-(\vec{x})$ with $\alpha = \frac{1}{4}$, $\beta_g(\vec{x}) = \frac{1}{2}D_g(\vec{x})$.

The calculation of the average fluxes and gradients at the surface elements along the boundary between transport region and diffusion region can be performed by means of the integration over the functions $\xi_i(\vec{x})$

$$\langle \phi_{gl} \rangle = \sum_{i=1}^{NK0} \phi_g^i \langle \xi_i \rangle_\Gamma$$

$$\left\langle \frac{\partial \phi_{gl}}{\partial n} \right\rangle = \sum_{i=1}^{NK0} \left(\sum_{j=1}^{NK0} \phi_g^j \frac{\partial}{\partial n} \xi_j(\vec{x}_i) \right) \langle \xi_i \rangle_\Gamma$$

where NK0 is the number of nodes at the regarded side of the finite element and NK the total number of nodes of the regarded finite element.

In the nodal expansion method the average flux and gradients at the boundaries can be derived from the basic parameters (average node fluxes and input/output currents at the six node boundaries) of the solution of the nodal equations [8]. The coupling of input/output currents at the boundary between core and reflector can be realized by means of an albedo coefficient

$$\alpha_g(\vec{x}) = \frac{j_g^-(\vec{x})}{j_g^+(\vec{x})}$$

where the input currents $j_g^-(\vec{x})$ can be calculated by multiplying the output currents $j_{g'}^+(\vec{x}')$ by the response matrix again.

For the finite difference method the difference formulas for the fluxes and gradients at the boundary meshes can be used to determine the linear anisotropic flux distribution at every mesh boundary.

The complete solution of the diffusion equation in the core region can be achieved if the system equations corresponding to the FD- , NEM- or FE - method and simultaneously the equations for the determination of albedos or NEUMANN source terms (simple matrix times vector operation) are solved. The diffusion equation has to be solved only for the core region.

3 Calculation of Response Matrices

As mentioned before, the neutron transport in the complex structure of the reflector can be treated most accurately by a Monte Carlo method. A typical geometry for the radial reflector of a PWR is shown in Fig.1 (350 MW plant KWO).

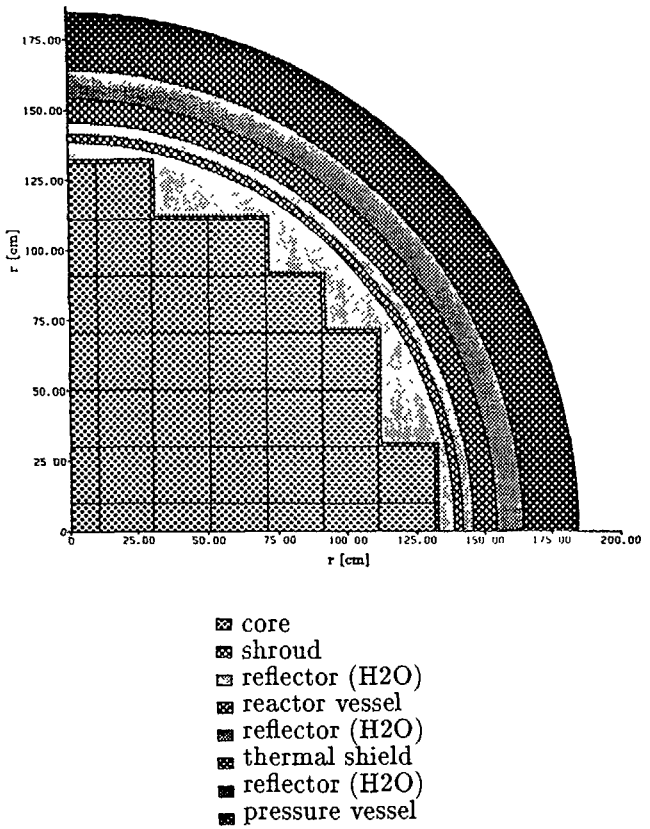

Figure 1: Radial Structure of a 350 MW PWR-Reflector (KWO)

For the calculation of the response matrix elements at every surface element l' of the core/reflector boundary neutrons with energies corresponding to the fast or thermal energy group (index g')have to be started into the reflector region and followed up to their escape from system, absorption (or Russian Roulette killing) or return to the core/reflector boundary. The returning neutrons (at surface element l and energy group g) contribute to the response matrix elements $R^0_{g'gl'l}, R^1_{g'gl'l}$, $R^2_{g'gl'l}$ and $R^3_{g'gl'l}$, respectively.

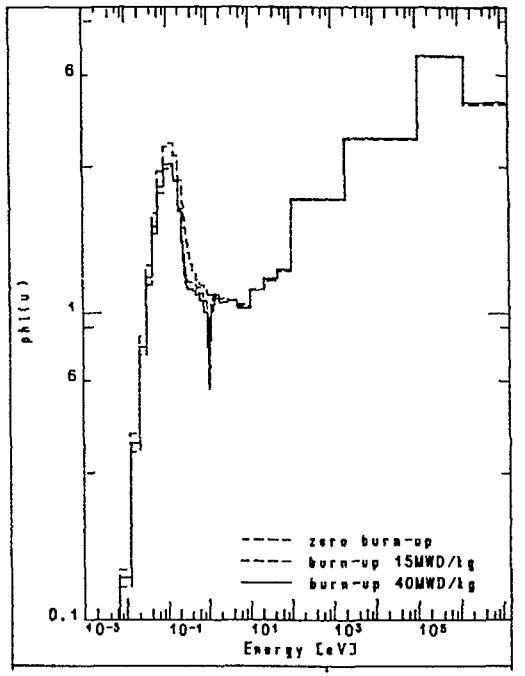

Figure 2: Spectrum at the Radial Core/Reflector Boundary (350MW PWR,KWO)

The spatial distribution of the starting neutrons at the surface element l' can be taken as constant (e.g. if the mesh size is not too large), linear or with higher order depending from degree of approximation of the diffusion solution. The angular distribution is taken cosine shaped in the normal direction of the regarded surface element. With the cosine shaped source distribution the R^0 - term can be calculated directly. The R^1, R^2, R^3 - terms can be calculated simultaneously by multiplying the neutron starting weights (normally 0.5) by the corresponding components $\Omega_x, \Omega_y, \Omega_z$ of the neutron direction Ω. The energy distribution of the starting neutrons can be chosen from typical assembly spectra which mainly depend from assembly type, burn-up, moderator density and boron concentration (PWR). An example of a multigroup spectra at the boundary core/reflector is shown in Fig.2 for different burn-up values. Such assembly spectra may be taken from fundamental mode multigroup assembly calculations (1D or 2D) and interpolated to the group or energy structure which is used in the Monte Carlo transport

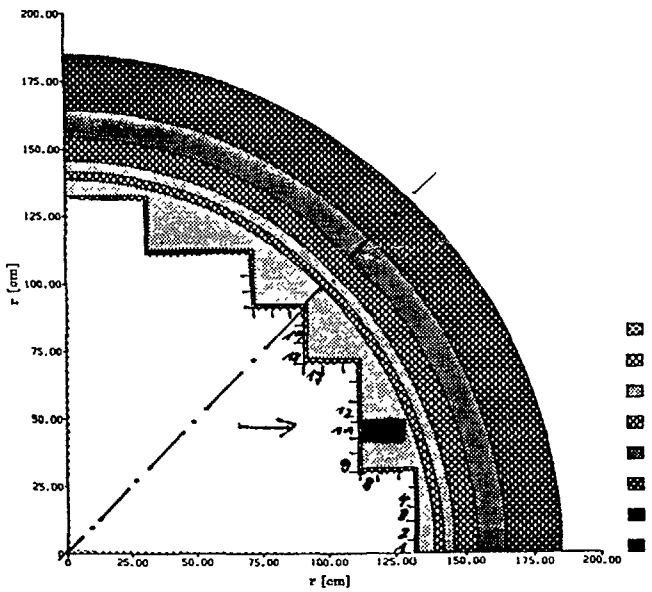

Response function for an input current in surface element No.11

Output element No.	Group 1	Group 2
6	4.0 E-4	6.2 E-4
7	1.8 E-3	1.0 E-3
8	1.5 E-3	7.5 E-4
9	2.1 E-3	8.7 E-4
10	2.4 E-2	9.1 E-3
11	1.7 E-1	2.0 E-2
12	2.6 E-2	3.8 E-3
13	2.4 E-3	1.2 E-3
14	7.9 E-4	5.8 E-4

Input element No.	Group 2
6	2.1 E-6
7	1.9 E-5
8	6.2 E-5
9	1.9 E-4
10	1.6 E-2
11	2.1 E-1
12	1.9 E-2
13	2.2 E-4
14	1.9 E-6

Figure 3: Response Vectors for fast and thermal Group

calculations for the response matrices. The energy structures of assembly calculations and transport calculations must not be identical. The only requirement for the calculation of the response matrix elements is the use of the identical cut-off energy between fast and thermal group as in the two-group structure of the diffusion calculation. Therefore, the transport calculations can be performed also by means of a continuous energy Monte Carlo code e.g. by the well known MCNP-code [9]. In every case a sufficient number of energy groups- or points should be used for the transport calculation.

In a first version we used the multigroup Monte Carlo code MORSE-SGCS [10] for the calculation of reflector response matrix elements. For MORSE-SGCS two user subroutines have to be prepared for the source phase space coordinates selection (subroutine **SOURCE** and a special surface detector routine for the calculation of the response matrix elements (subroutine **BDRYX**) [11]. Of course, The 45^0-symmetry of the reflector structure can be taken into account. The modelling of the reflector geometry by the MORSE-code is no problem even if complex axial structures will be regarded.

4 Examples

As an example the response matrix of a 2D- Problem was calculated by Monte Carlo using the MORSE-code with the special user routines. The surface elements of the core/reflector boundary were subdivided into three meshes/assembly as shown in Fig. 3. The response functions for an input current at surface element 11 is shown in this figure too. In Fig.4 a comparison of a 2D - diffusion solution with a nodal expansion method with different reflector treatment (adjusted reflector cross-sections and albedos from reflector transport calculation) is shown. For the case of a coarse mesh net (for which the reflector cross sections were adjusted to a comparable transport solution) the two solutions are in sufficient good agreement. If these reflector cross-sections are used in fine-mesh calculations the larger discrepancies were observed.

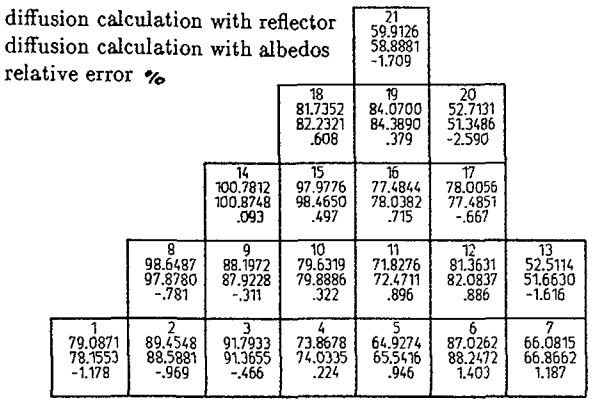

Figure 4: Comparison of Power Distributions from Diffusion Calculations with Reflector Cross-sections and Albedo boundary conditions

5 Conclusions

The coupling of diffusion and transport region via response matrices is an interesting method to treat reflectors in LWR- diffusion calculations. For the test of the accuracy of the method comparisons with multigroup transport solutions are planned. A problem-specific benchmark would be very helpful.

REFERENCES

[1] Y. Chao, C. Suo,"A Two-Dimensional Two-Group Albedo Model for Pressurized Water reactor Reflector",NSE,88,1984, p.103–109.

[2] M. R. Wagner, K. Koebke, H.-J. Winter,"A Nonlineae Extension of the Nodal Expansion Method
,Proc. ANS/ENS Topical Meeting Munich 1981.

[3] F.A.R. Schmidt, R. Fremd and D. Wörner, "DIFGEN – A Program Package for the Solution of the Diffusion Equation by the Finite Element Method", Stuttgart: IKE, 1978 (IKE 4-75)

[4] G. Sibiya,"Application of the Response Matrix Method ffor the Solution of Coupled Diffusion and Transport Problems",Diss. University of Stuttgart,FRG , IKE-Rep. Nr. IKE-6-129 (1980).

[5] K. Neumann, W. Bernnat and D. Emendörfer, "Treatment of Neutron Streaming through Cavities in S_N-Transport and Diffusion Calculations", Int. Top. Meeting on Advances in Reactor Physics, Mathematics and Computation, Paris, France, April 1987.

[6] W. Bernnat, F. A. R. Schmidt, W. Giesser,"Treatment of Cavities in three-dimensional Diffusion Calculations based on the Finite Element Method ",Int. Conf. on the Physics of Reactors: Operation, Design and Computation, Marseille, France, April 1990.

[7] D. Emendörfer, "Randbedingungen für den Neutronenfluß im endlichen Zylinder nach der P_L-Approximation der Transportgleichung", Nukleonik, 9 (1967), p. 285–288.

[8] A. Wörner,"Development and Verification of a Modular Program System for the Calculation of the Long Time Behaviour of Pressurized Water Reactors",IKE-Rep. IKE-6-149, 1984 (in German).

[9] Briesmeister, J.F.; et al.: NCNP – A General Monte Carlo Code for Neutron and Photon Transport. Version 3B. LA-7396-M (1986)

[10] West, J.T.; et al.: MORSE-SGC/S for the SCALE System. NUREG/CR-0200, Vol. 2, Section F9, ORNL/NUREG/CSD-2/V2/R2 (1984)

[11] W. Bernnat,"Calculation of Response Matrices for LWR-reflectors with the Monte Carlo Code MORSE-SGCS", IKE Rep. in preparation 1990.

CALCULATIONAL METHODS FOR PWRs

J KREBS, M.-C. LAIGLE, R LENAIN,
G. MATHONNIÈRE, A. NICOLAS
Direction des réacteurs nucléaires,
Département de mécanique et de technologie,
Commissariat à l'énergie atomique,
Centre d'études nucléaires de Saclay,
Gif-sur-Yvette, France

Abstract

The design procedure for PWR reactors has two main stages the assembly transport calculation (computed by the APOLLO code) and the core calculation, achieved by the diffusion code CRONOS

For rodded or poisoned assemblies, the transport calculation uses the DP00 option (no cell cylinderization and face differenciation) at the very time when the non rodded ones are accurately treated by the ROTH option (cell cylinderization and no face differenciation).

The core calculation in diffusion theory necessitates condensations for cross sections on space (pin-by-pin or per assembly) and energy (2 groups) Different numerical methods have been studied (finite elements and finite differences)

The 3D power transient calculations need more accurate flux precision criterias than fuel depletion studies This comes from the evolution of the axial Xenon distribution

In case of large meshes (homogeneous description of the core), the linear approximations are not precise enough to render the radial flux shape Sufficient results are given by the parabolic finite element with 4 meshes per assembly, with a reduced cost compared to the cubic approximation with 4 meshes, chosen as reference

When taking into account the feedback effects for 2D core calculations, the power shape is more sensible to the heat transfer coefficient than to the thermalhydraulic mesh and to the channel exchange hypothesis

This design procedure has been compared to measures that have been obtained at the begin of life of the CP1 PWR 900 reactors The homogeneous one overestimates the rod efficiency (about 6%) The pin-by-pin calculation is in very good agreement with the measurements

- Introduction

A design procedure for PWR study has to take several points into account

* reflectors calculation [1]
* non-controlled assemblies nuclear properties
* controlled and poisoned assemblies nuclear properties
* feedback effects consideration
* core calculation, with cycle and power transient calculations

Ours has two main steps

* the first one is the calculation in transport theory of a repetitive pattern of the core (pin, assembly or a larger pattern) to find its nuclear properties In our case, this is computed by the APOLLO code [2]
* the second one is devoted to obtain core calculation in multigroup diffusion theory This is done by the CRONOS computer code [3], which solves the multigroup diffusion equation by the finite element method, for steady states and kinetics

Going from the first stage to the second one implies a reduction of the information generated by the detailed transport calculation homogenization in space and energy, and use of a transport-diffusion equivalence

A particular attention should be devoted to the calculation of reflector constants, for which various methods may be used

The matters dealt with the different stages as follows

* transport calculation choices
* diffusion calculation choices (homogeneous or pin-by-pin, selection of flux interpolation polynoms), feedback effects consideration, power transient treatment
* comparison with measure

I - Basic patterns calculation in transport theory.

The APOLLO computer code solves the Boltzmann equation in multigroup approximation with a spatial treatment of collision probabilities It uses a 99 energy group division (47 thermal groups), but for Uranium assembly 37 energy group calculations are quite satisfactory [4] The various isotope self-shielding can be calculated with APOLLO The zones interactions can be considered in two different ways

* direct calculation of collision probabilities in which the exact neutron path is respected , this method produces reference values but is too expensive for design studies
* calculation with a multicell approximation The pairings of different cells are achieved through an interface current formalism Several options are available according to the approximation degree chosen for the integral flux within each cell (uniform or linear) and for the spatial and angular current characteristics at the cell boundaries For design calculation, two options are generally chosen according to the assembly type

To reduce CPU time and memory, cells with the same flux can be calculated as the same calculation point , the choice of "associated cells must be validated A total discretisation of an assembly with a 1/8 th symmetry leads to 45 cells , for a non-rodded one about 12 cells are sufficient , for poisoned or rodded ones, about 20 cells are necessary The CPU time is divided by 6 for rodded assemblies and by 16 for non rodded ones

For non-controlled and poisonless assemblies, ROTH approximation is a good precision/CPU cost compromise (cells cylinderization, going in neutron currents averaged on four faces, consideration of the sole isotropic

Table 1 - ROTH and DP00 effect on rodded assemblies

approximation	DP00	ROTH
K∞	0.86211	0.87308
efficiency	38465 pcm	37200 pcm
M^2	55.1 cm^2	55.0 cm^2
power peak	1.293	1.319
CPU factor	1.	0.37

component of the intercell fluxes). For poisoned or controlled assemblies the use of DP00 approximation is recommended : cells are represented with their differenciated four faces, without regard for the intercell flux anisotropy as major approximation and without cylinderization. This produces a better determination of the power shape and the reactivity of such assemblies. In this case, the use of the ROTH option leads to a slight underestimation of the control rods (-3.3%) and to an approximative determination of the assembly flux gradient, as shown in table 1 and figure 1.

II- Homogenization - Transport diffusion equivalence.

The generation of cross section libraries usable in the diffusion calculation necessarily leads to space and energy condensations. At this stage, calculation methods must be differenciated according to the type of core calculation to be achieved.

* pin-by-pin calculation : a detailed neutronic representation of pins is necessary. To best render the flux level in the pins, mostly in "heterogeneities", (absorbing pins, water cells ...) information generated from the transport calculation must be adapted by a "transport-diffusion equivalence" algorythm. This makes possible the treatment of pin or assembly heterogeneities and spatial discretisation [5] and [6].

* homogeneous calculation : a global neutronic assembly representation is transmitted to the diffusion code. Information from the transport calculation is thus averaged in space and energy.

To generate nuclear datas that can be used in the diffusion code, APOLLO can parametrize cross sections ; burn-up, fuel temperature, moderator density and boron concentration are used as parameters. Typically, we have 5 fuel and moderator values, and 3 boron concentrations [7].

III - Core calculation.

III.1 - Diffusion computer code.

The CRONOS code solves the multigroup diffusion equation through the finite element and finite difference methods. The modular structure of the

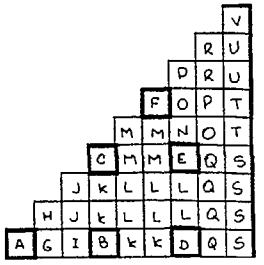

assembly description

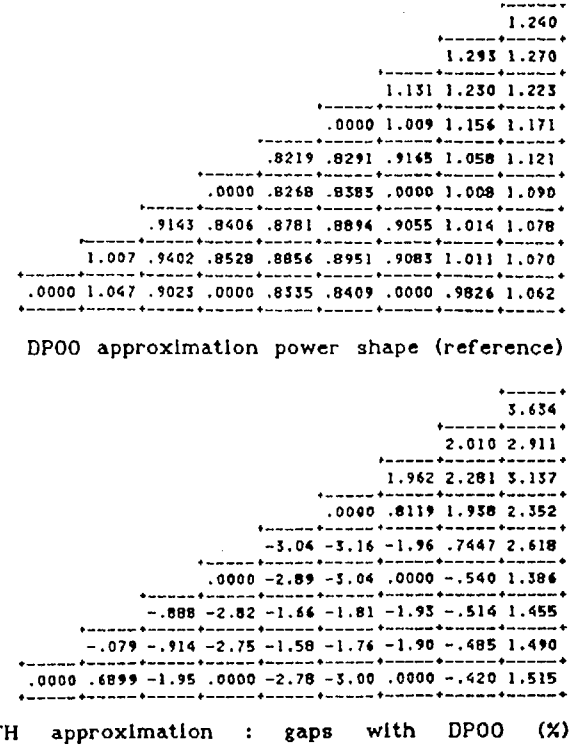

Figure 1 - Power shape in a rodded assembly

code allows the consideration of the feedback effects linked to fuel and moderator either by a simplified pattern or by the FLICA [8] computer code, used as a module of CRONOS. Feedback effects are taken into account through tabulated diffusion cross-section libraries.

The fuel depletion is calculated by a macroscopic method with the burn-up as parameter. Fission products like Xenon and Samarium have a separate evolution to follow power transients. Boron effects can be taken into account by a microscopic modelisation.

Calculation may be made with 1, 2 or 3 dimensions. Calculations can be achieved on any computer (CRAY, IBM, SUN ...). Choosing finite element is possible ; linear, parabolic and cubic approximations are available. The calculation mesh may be different of the assembly physical description in the core.

III.2 - Results.

To treat a 3D power transient, various numerical approximations and flux precision criterias are compared (axial analysis)

To render fuel depletion, a radial analysis is performed We show how the approximation levels are linked to the finite element degree and to the calculation mesh size

Thermalhydraulic representation is also discussed

III 2 1 - Axial aspects

We present the gap variations on the calculated power for different finite elements with a large mesh during a 18-6 power transient (18 hours for full power and 6 hours for 30% full power) [9] So, the axial power is very perturbated (the axial-offset is about 55% and the power peak is 2 1)

The reference calculation is obtained with a cubic element and a flux precision criterion of 10^{-5} It is important to notice that the given gaps are relative deviations

Whatever the approximation may be, the 10^{-3} flux criterion leads to unprecise results , error increases from t = 0 and reachs 40% at t = 6 h

With a sufficient flux precision criterion (10^{-4}) a parabolic approximation gives a very good result , the finite differences method is not adequate with a large calculation mesh (20 cm) , a linear polynom is convenient for the middle part of the reactor, but slightly less precise to treat extremities where the power is very low (see figure 2)

III.2.2 - Radial aspects.

To perform a 2D core calculation, we compare various approximations (cubic "CL16", parabolic "PL9£" and linear "LL4" finite elements, mesh centered finite differences "MCFD" with 1, 2x2, 3x3, 4x4 or 8x8 meshes per assembly The "LL4$" finite element approximation is equivalent to the vertex centered finite differences "VCFD" The studied core is a four-zone equilibrum cycle (begin of life, full power) The chosen reference is achieved with a cubic approximation and 4 meshes per assembly (CL16 - 2x2)

With CL16 and PL9£, eigenvalue is well calculated (30 pcm) The spatial convergence is faster with the LL4 than with the VCFD, but the 8x8 mesh is the sole that can approach the reference (-59 pcm)

The "CL16-1" and the "PL9£-3x3" approximations give very close results With the "PL9£-1" gaps are smaller than 1% The "PL9£-2x2" is the most adequate to make a core calculation with a reduced CPU time

Complete results are given by tables 2 and 3, and figure 3 shows the power shapes and gaps

table 2 - description of the discussed cases

case	1	2	3	4	5	6	7	8	9
method	CL16	PL9£	PL9£	PL9£	PL9£	VCFD	VCFD	MCFD	MCFD
meshes	1	1	2x2	3x3	4x4	3x3	8x8	3x3	8x8

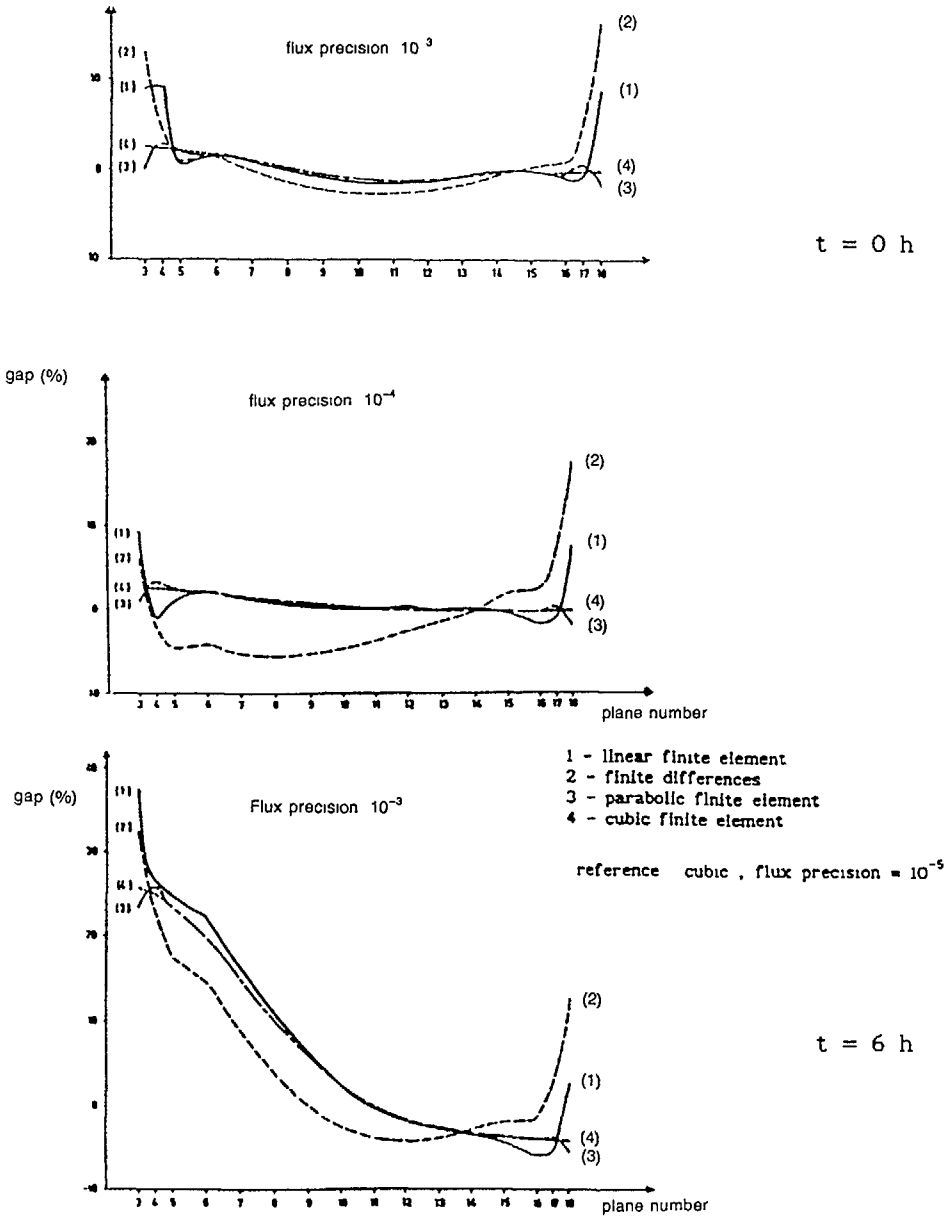

figure 2 - Variation gaps on axial power distributions t = 0 and t = 6 h

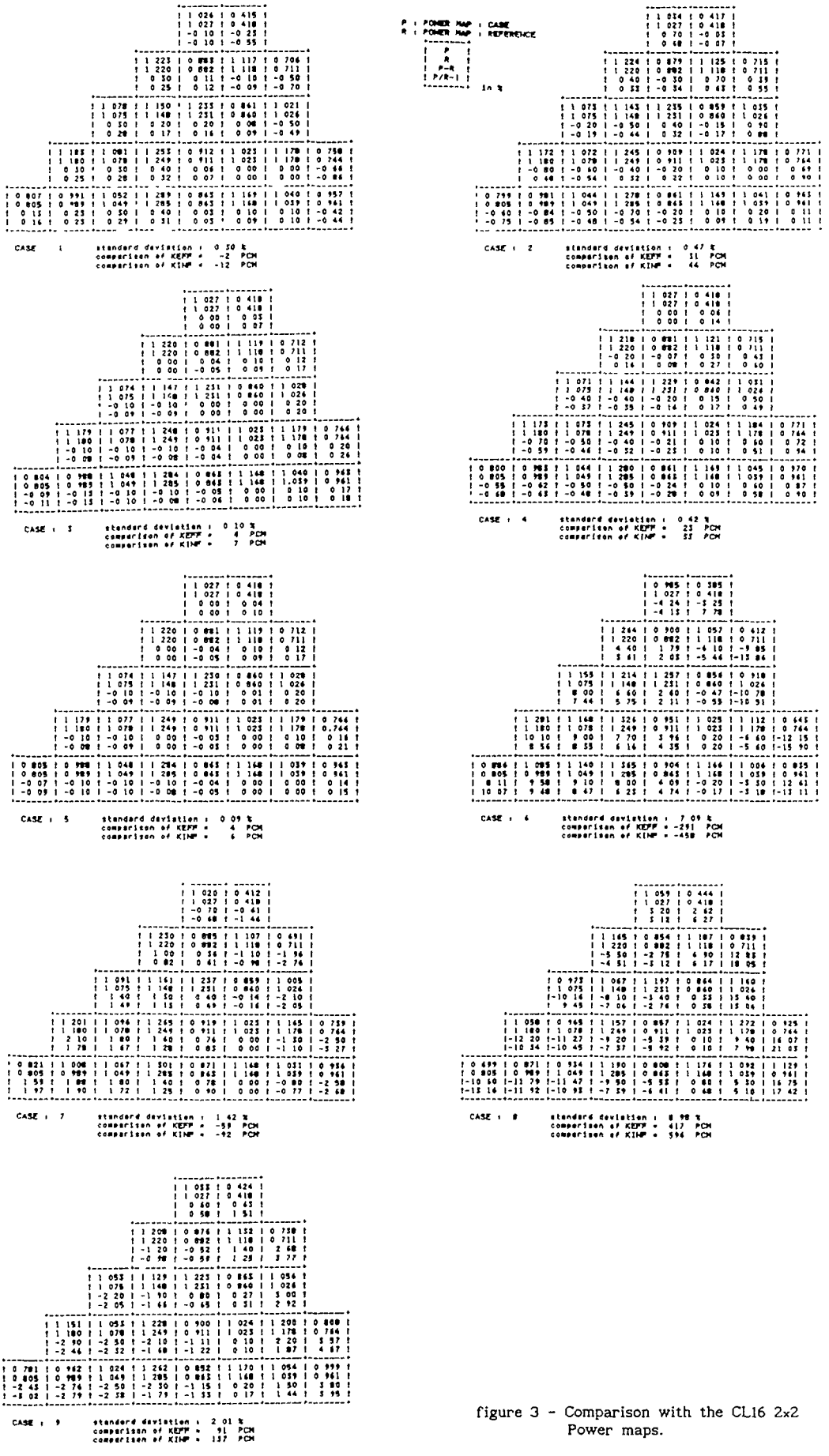

figure 3 - Comparison with the CL16 2x2 Power maps.

table 3 - *Comparison with the "CL16 - 2x2"*

CASE	1	2	3	4	5	6	7	8	9
KEFF	0.99959	0.99992	0.99965	0.99984	0.99965	0.99671	0.99902	1.00379	1.00052
KINF	1.03421	1.03479	1.03440	1.03467	1.03439	1.02960	1.03338	1.04051	1.03575
LEAKAGES	-3405.	-3428.	-3417.	-3425.	-3416.	-3247.	-3382.	-3593.	-3461.
R MAX GAP	0.32	0.90	0.26	0.94	0.21	10.07	1.97	21.03	4.67
R MIN GAP	-0.86	-0.85	-0.13	-0.68	-0.10	-15.90	-3.28	-13.16	-3.02
A MAX GAP	0.40	0.90	0.20	0.87	0.20	10.10	2.10	16.77	3.80
A MIN GAP	-0.66	-0.84	-0.13	-0.70	-0.10	-12.61	-2.58	-12.20	-2.90
STD DEVIATION	0.30	0.47	0.10	0.42	0.09	7.09	1.42	8.98	2.01
KEFF GAP	-2.	31.	4.	23.	4.	-291.	-59.	417.	91.
KINF GAP	-12.	44.	7.	33.	6.	-458.	-92.	596.	137.
LEAKAGE GAP	10.	-13.	-3.	-10.	-2.	168.	33.	-178.	-46.
GAP EXT.	-0.35	0.44	0.12	0.49	0.11	-9.08	-1.79	11.36	2.50
MAX P GAP	0.31	-0.56	-0.08	-0.39	-0.08	6.23	1.25	-1.01	-1.79
MIN P GAP	-0.55	-0.07	0.07	0.14	0.10	-7.80	-1.46	6.27	1.51

Aspects linked to neutronics/thermalhydraulics coupling are also analyzed (channel representation and coupling). Table 4 and figure 4 show that thermalhydraulic hypothesis are also important, especially the value of the heat transfer coefficient between fuel and clad (h).

table 4 - Thermalhydraulic options - Results

	channel number per ass.	h ($W/cm^2/K$)	channel interaction
reference	1	0.44	none
1	4	0.44	none
2	1	0.44	yes
3	1	1. (*)	none

(*) peripherical assemblies only

CASE	1	2	3
KEFF	0.99948	0.99976	1.00005
KINF	1.03434	1.03470	1.03539
LEAKAGES	-3428.	-3435.	-3475.
R MAX GAP	0.68	0.29	1.15
R MIN GAP	-0.85	-0.47	-1.05
A MAX GAP	0.70	0.30	1.02
A MIN GAP	-0.82	-0.38	-1.10
STD DEVIATION	0.39	0.15	0.67
KEFF GAP	-21.	7.	54.
KINF GAP	-29.	6.	72.
LEAKAGE GAP	8.	1.	-39.
GAP EXT	-0.44	-0.03	0.78
MAX P GAP	0.31	0.08	-0.71
MIN P GAP	-0.05	-0.02	0.67

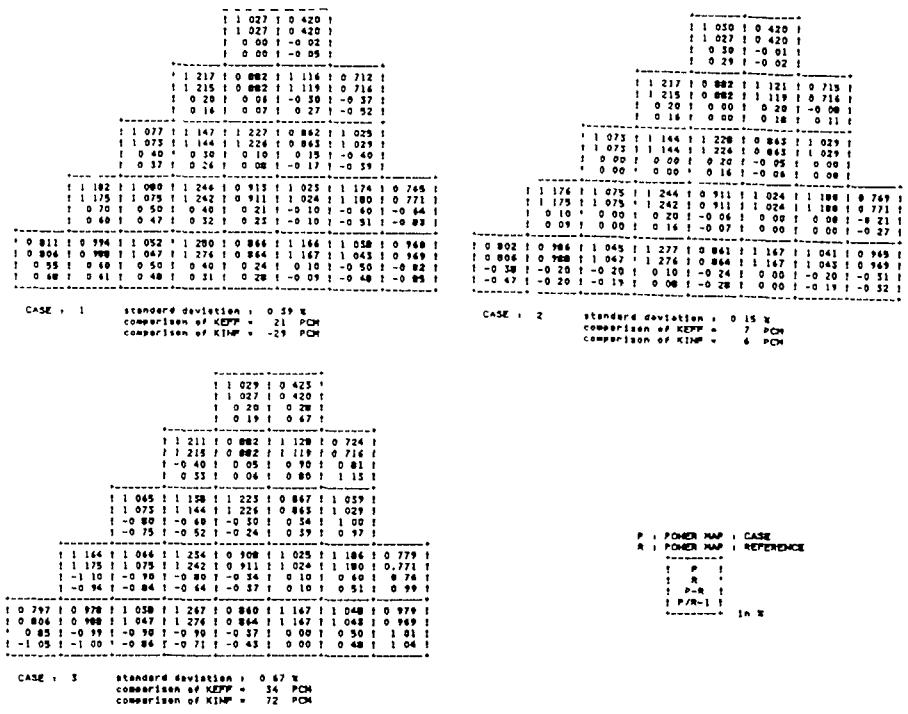

figure 4 - Thermalhydraulic options Power maps

We also compare homogeneous (CL16-2x2) and pin-by-pin (VCFD) design procedures. Power gaps are smaller than 1% ; difference between eigenvalue is 32 pcm. For the pin-by-pin representation, an averaged assembly temperature leads to about the same result as a pin-by-pin temperature calculation. See table 5 and figure 5.

Figure 5 shows the difference between VCFD and MCFD (220 pcm and 1.7% on the power shape). The accuracy of the VCFD result comes from the transport-diffusion calculation, achieved by a VCFD diffusion method.

III.3 - Comparison with measures.

Measures are made at zero power from first PWR 900 cycle (CP1) [10]; see figure 6 and 7. Homogeneous and heterogeneous results are compared ; rod efficiency is quite accurately calculated by a pin-by-pin representation ; an homogeneous calculation overestimates it by about 6%. This comes from the hypothesis of homogenization in infinite medium and from the DP00 option overestimating the flux gradient, particularly in the rodded assemblies.

table 5 - Comparison of pin-by-pin calculations

	numerical method mesh	temperature option
reference	CL16 2x2	4 per ass
1	het VCFD	1 per ass
2	het VCFD	1 per pin
3	het MCFD	1 per ass

CASE	1	2	3
KEFF	0.99993	0.99984	0.99771
KINF	1.03459	1.03441	1.03249
LEAKAGES	-3408	-3399	-3427
R MAX GAP	0.77	0.29	2.45
R MIN GAP	-0.70	-0.49	-1.76
A MAX GAP	0.80	0.30	2.06
A MIN GAP	-0.65	-0.50	-1.70
STD DEVIATION	0.38	0.20	1.08
KEFF GAP	32	23	-190
KINF GAP	25	8	-178.
LEAKAGE GAP	7	15	-12
GAP EXT.	0.29	-0.18	1.26
MAX P GAP	-0.31	0.16	-0.93
MIN P GAP	0.00	-0.29	0.69

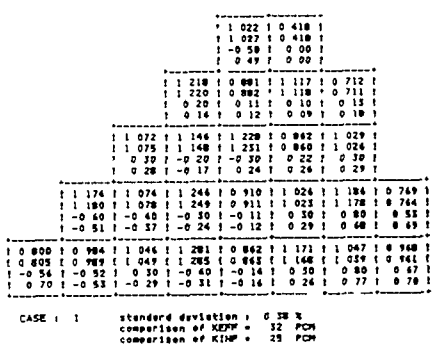

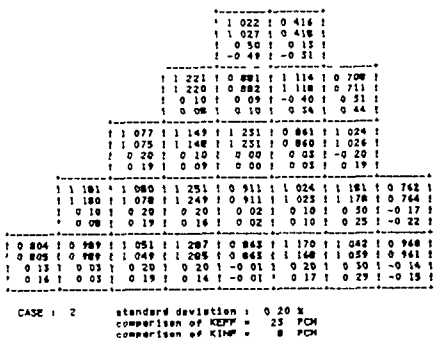

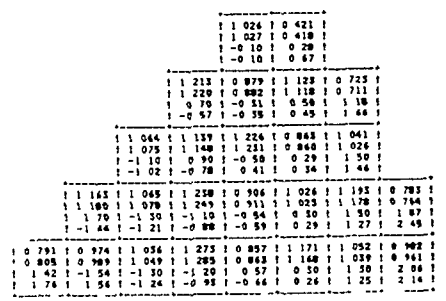

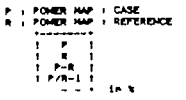

figure 5 - Pin-by-pin calculations
Power maps

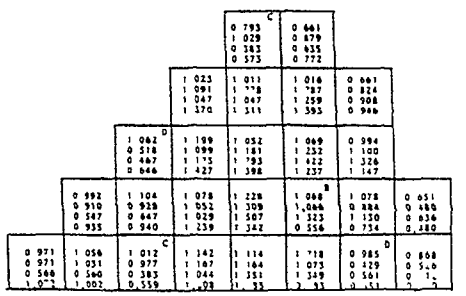

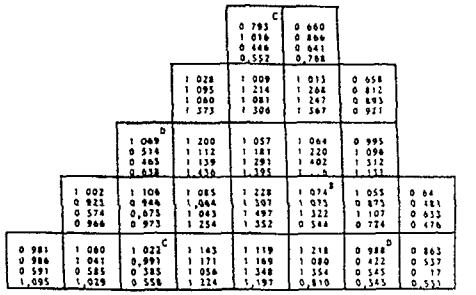

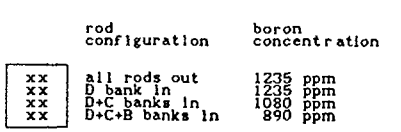

figure 6 :
Homogeneous and heterogeneous results
Power maps

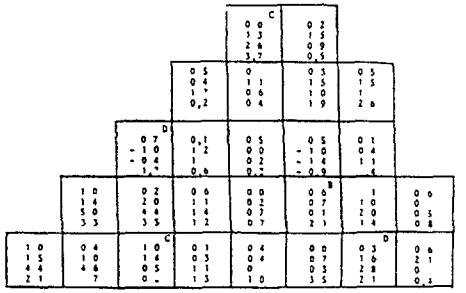

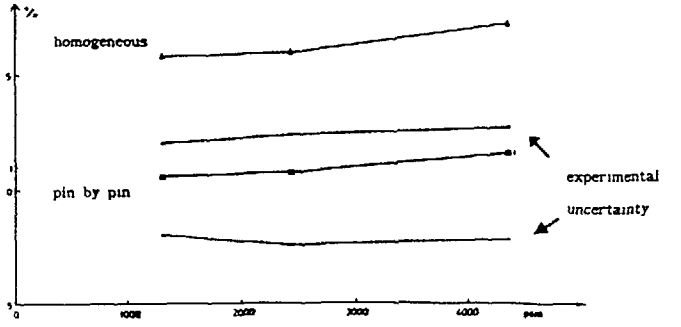

figure 7 - Calculation/measures comparison rod efficiency

- Conclusion

Our calculational method for PWR reactor is based on the computational system SAPHYR : APOLLO, CRONOS and FLICA codes. Among all its possibilities we define a design procedure currently used to study PWR. Its scope extends to the entire normal operation of reactors and accidental situations. Without any external fit, these tools can be used to obtain references or be introduced in industrial procedures.

REFERENCES

[1] J. OLIVERI
Elaboration d'un schéma de calcul des REP qualifié sur les expériences de démarrage des réacteurs du type CP1.
Thèse de 3ème cycle, université Paris XI Orsay

[2] G. MATHONNIERE - Z. STANKOVSKI
The APOLLO1 Assembly Spectrum Code
this meeting

[3] J.-J. LAUTARD - S. LOUBIERE - C. FEDON-MAGNAUD
CRONOS : a Modular Computational System for Neutronic Core Calculation
this meeting

[4] G. MATHONNIERE
Bibliothèque neutronique à nombre restreint pour le calcul des réacteurs à eau.
Thèse de 3ème cycle. Université Paris XI Orsay, Octobre 1980

[5] J. MONDOT
Mise en œuvre de méthodes pour le calcul des poisons consommables dans les réacteurs à eau
Proc. IAEA Specialists Meeting on Homogeneisation Methods in Reactor Physics *Lugano, Nov. 1978*

[6] A. HEBERT
Développement de la méthode SPH : homogénéisation de cellules dans un réseau non uniforme et calcul des paramètres de réflecteur
Thèse de doctorat d'Etat, Paris XI, Orsay

[7] V. BRUN - B. CHANARON - J.-M. DUBOIS
Reactor Calculation Multigroup Parametred Libraries
this meeting

[8] P. RAYMOND
FLICA IV : a Computer Code for Multidimensional Thermal Analysis of Nuclear Reactor Core
International Topical Meeting on Advances in Reactor Physics, Mathematics and Computation *Paris, 1987*

[9] G. MATHONNIERE
Etude de problèmes neutroniques liés à la présence du Xénon dans les réacteurs à eau pressurisée
Thèse de doctorat d'Etat, Paris XI, Orsay

[10] C. MARTIN DEL CAMPO
Contribution à l'élaboration du schéma de calcul neutronique des réacteurs à eau sous pression
Thèse de 3ème cycle. Université Paris XI Orsay, Janvier 1987

PHYSICAL CHARACTERISTICS OF THE CORE OF NUCLEAR DISTRICT HEATING PLANTS

V.S. KUUL', O.B. SAMOJLOV
Experimental Machine Building Design Bureau,
Gorki, Union of Soviet Socialist Republics

Abstract

The main principles of designing the nuclear district heating plant (NDHP) reactor core are formulated. The core neutron-physical characteristics are given. The results of experimental verification of design decisions using the fuel cassettes' model assemblies as well as the main results of full-scale core tests are presented.

I. Main Statements

Nuclear district heating plants (NDHPs) reactor units designed with account of siting in the vicinity of large cities and necessity of providing a qualitatively higher safety level in comparison with NPP. The adopted concept of the NDHP reactor plant safety includes engineering decisions allowing to classify it among enhanced safety systems. These decisions, as applied to the core, include:

- low power density of core and fuel;
- use of all-conditions' natural circulation of the coolant in the reactor;
- absence of boron in moderator and compensation of excess reactivity margin only by mechanically moved absorbers;
- selection of relatively low reactor coolant parameters, determining the quiet run of accidents with reactor circuit loss of tightness;
- low fuel temperature;
- use of materials and decisions shown a good performance in the domestic practice of reactor engineering;
- use of the enlarged diameter (~13.6 mm) fuel element in the core allowing (besides design-technological advantages) to improve the neutrons' balance in the core;
- use of burnable absorber for compensation of part of core reactivity margin;
- use of core profiling along its height by burnable absorber for equalling the energy releases;
- small fuel swelling and reduced gaseous fission products release at fuel burnup depth adopted in the NDHP.

2. Main Core Heat Engineering Characteristics

The NDHP reactor core is located inside the reactor vessel in its lower part. The core consists of hexahedral cassettes (fuel elements' assemblies) with 238 mm across flats forming triangular lattice with 241 mm pitch. The cassettes are spaced by a lower plate and a holddown block plate in which holes the cassettes' ends enter. The core contains 121 cassette. The core cooling down is provided by natural reactor coolant circulation.

The cassettes include individual chimneys which are extensions of core fuel assemblies and allow to provide

TABLE 1. HEAT ENGINEERING CHARACTERISTICS OF CORE AND CIRCULATION CIRCUIT

Parameter	Units	Value
Core power output	MW	500
Core power density	kW/L	27.4
Average linear fuel elements' heat rating	W/cm	97
Coolant parameters		
- pressure	MPa	2.0
- inlet temperature	°C	130
- outlet temperature	°C	208
Coolant flowrate	t/hr	5.500
Average velocity of coolant flow in cassette	m/s	0.7

in the natural circulation conditions the hydraulic coolant flowrate profiling in the cassettes according to their thermal output.

For technically feasible reactor vessel sizes such coolant velocities in the core cassettes and in the built-in heat exchanger are realized, that provide high intensity of heat transfer.

3. Core Neutron-Physical Characteristics

The NDHP reactor cassette contains a bundle of 13.6 mm diameter fuel elements inclosed in of 1.5 mm enclosed hexahedral zirconium jacket, upper and lower head closures.

The bundle is attached to lower head closure by means of steel support grid. The elements' spacing is achieved by 6 intermediate spacing grids placed uniformly along the elements and placed on a central bundle tube, and by an upper end grid.

The fuel element is made of 13.6 x 0.9 mm of zirconium alloy and is filled with sintered uranium dioxide pellets.

For reactor power control there is a regulator in each cassette (except for the central one). It consists of 18 movable absorbing rods, united by a common cross-piece. The rods are located in 17.8 x 0.9 mm zirconium guide tubes spaced in the bundle together with fuel elements.

The absorber rod represents a 12.5 x 1.2 mm stainless steel tube filled with boron oxide.

The cassette cartogram is shown in Fig. 1. For partial compensation of reactivity margin for burnup and for power shaping along the core height the rods with burnable poison are installed in the cassettes instead of 6 fuel elements. They represent 13.6 x 0.9 mm zirconium alloy tube filled with *natural boron in aluminium matrix.*

Special measuring probes are provided for control of core neutron-physical and thermal-engineering parameters. To this aim instead of one fuel element the 13.6 x 0.9 mm zirconium guide tube is installed in the cassettes which tube serves for locating the probe containing thermal transducers. and neutron flux sensors.

Core cartogram is given in Fig. 2.

The movable absorber rods from 3 or 4 cassettes are combined and form a control and protection system (CPS) control

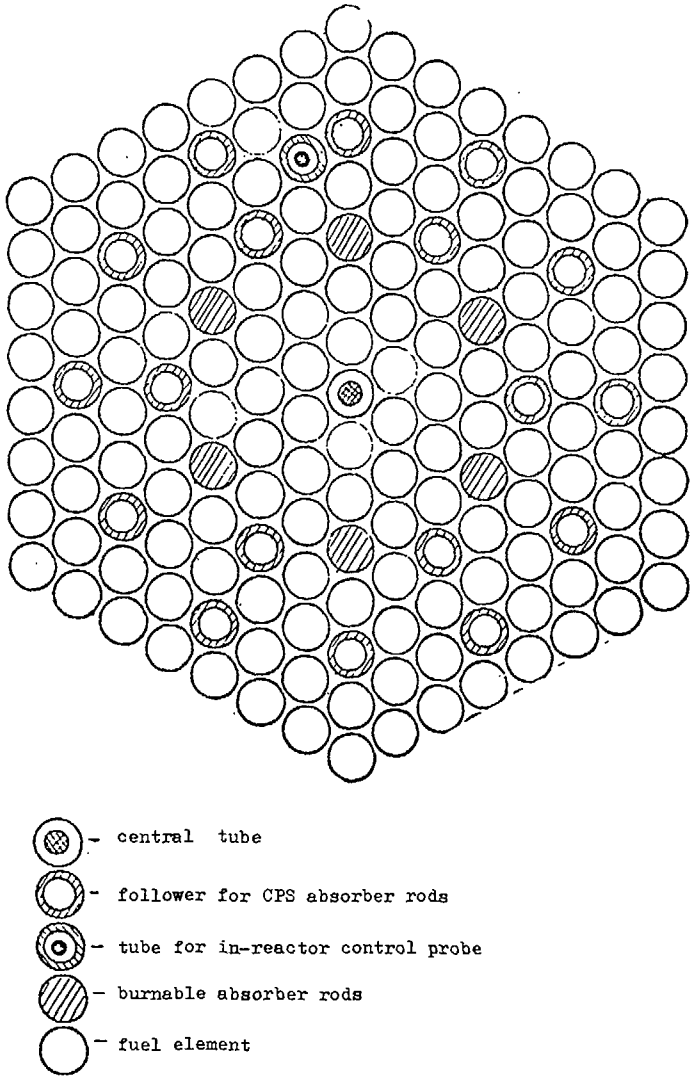

FIG. 1. Cassette cartogram.

member. This system functions as an emergency protection, compensates the excess reactivity necessary for providing the required fuel life, changes reactivity during reactor power control.

Core physical characteristics are given in Table 2.

TABLE 2. CORE PHYSICAL CHARACTERISTICS

Parameter	Units	Value
Core diameter	m	2.8
Core height	m	3.0
Core power density	kW/L	27
Fuel power density	kW/kg	10
Uranium loading	t	49.0
First core:		
First core cycle duration	eff.day	430
Number of cassettes in the core		
with 1.0% enrichment		42
with 1.6% enrichment		55
with 2% enrichment		24
Maximum coefficient of energy release non-uniformity		
in the core cassettes at nominal power	-	1.28
along the core height	-	1.8
Maximum linear heat rating of fuel elements	$W \cdot cm^{-1}$	254

TABLE 2. (cont.)

Parameter	Units	Value
Reactivity margin of cold first core	%	6.9
Reactivity margin for fuel burnup (without burnable poisons)	%	1.6
Reactivity margin for burnup compensated by burnable poison (burnable poison rods worth)	%	4.4
Temperature effect	%	-1.4
Power effect	%	-1.6
Effect of reactor poisoning by Xe-135	%	-2.3
Worth of all control rods	%	20
Steady-state regime of partial reloadings		
Fresh cassettes enrichment	%	1.6;2.0
Fuel life time duration	year	6-8
Fuel burnup in steady state operation regime at:		
- 3-fold reloadings	$\frac{MW \cdot d}{t\ U}$	13.000
- 4-fold reloadings	- -	19.100

4. Experiments on Model Assemblies

Core neutron-physical characteristics were calculated using a code package developed for VVER reactor cores with modified thermal-physical block accounting for the peculiarities of heat exchange under the natural coolant circulation conditions.

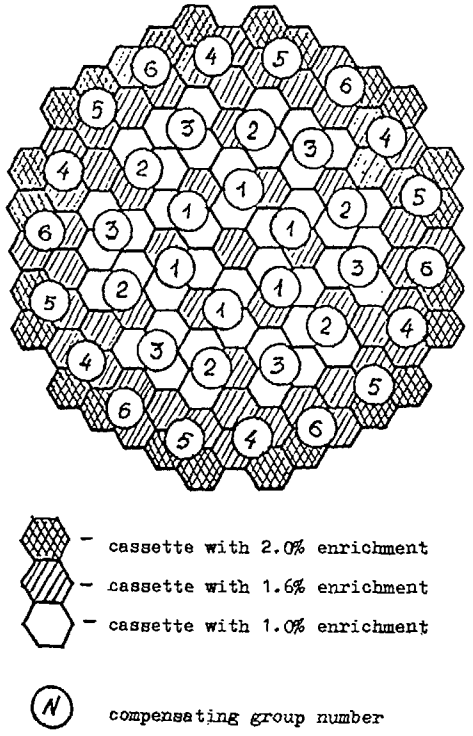

FIG. 2. Cartogram of the first core loading (combining the CPS members into compensating groups).

The investigations of neutron-physical characteristics of NDHP cassettes' model assemblies in "cold" and "hot" conditions were performed for verification of the code package as applied to NDHP cores, as well as for experimental verification of separate design decisions.

The experimental assembly cartogram is given in Fig. 3.

The investigations of neutron-physical characteristics were performed on the critical facilities enabling the experiments with moderator level changes and boric acid reactivity

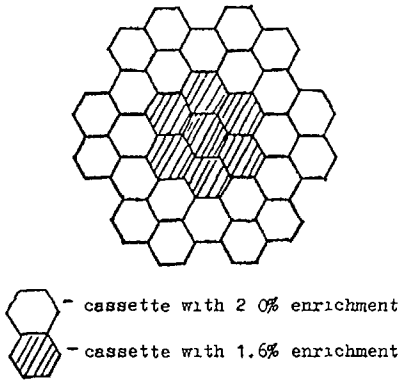

FIG 3 Experimental assembly cartogram

compensation in "cold" state, as well as measurements during heating up and at real core operating parameters.

The investigations performed can be divided into the following main groups:

1. Experiments on determining the parameters of critical states, as well as differential and integral reactivity aspects.

2. Activation experiments for determination of power distribution fields.

3. Experimental studies to assure core subcriticality in the state with maximum multiplication factor at the most effective CPS member stuck in the upper position.

The analysis of a large number of critical experiments different in composition of experimental assemblies, temperature conditions, modelling the composition of standard core, showed the stability of calculated values of the effective multiplication factor for the systems under study. The effective multiplication factor calculation values for critical states

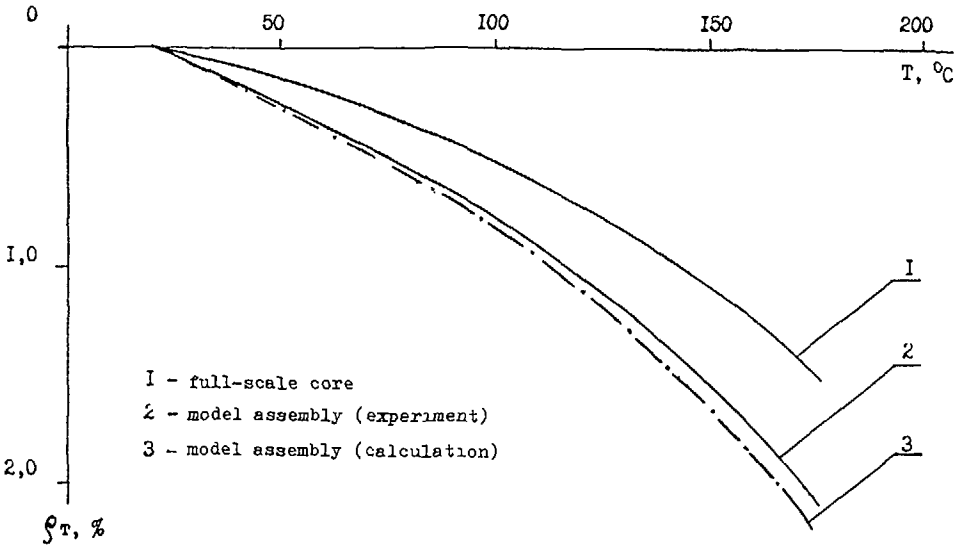

FIG 4 Model assembly and full-scale core temperature reactivity effect

falling in the narrow enough range (K_{eff}= 1 ± 0.005) were used in the standard core design calculations.

In the experiments modelling the core heating up to operating temperatures, the reactivity temperature effect value, as well as the values of reactivity coefficients versus moderator temperature were obtained.

The model assembly reactivity change with temperature and the similar change obtained on its basis for full-scale core are depicted in Fig. 4.

The analysis of the "hot" activation experiments enabled receiving the information on the accuracy of relative cassettes' power calculations (See Fig. 5). The maximum difference in calculation and experimental values does not exceed ~5%.

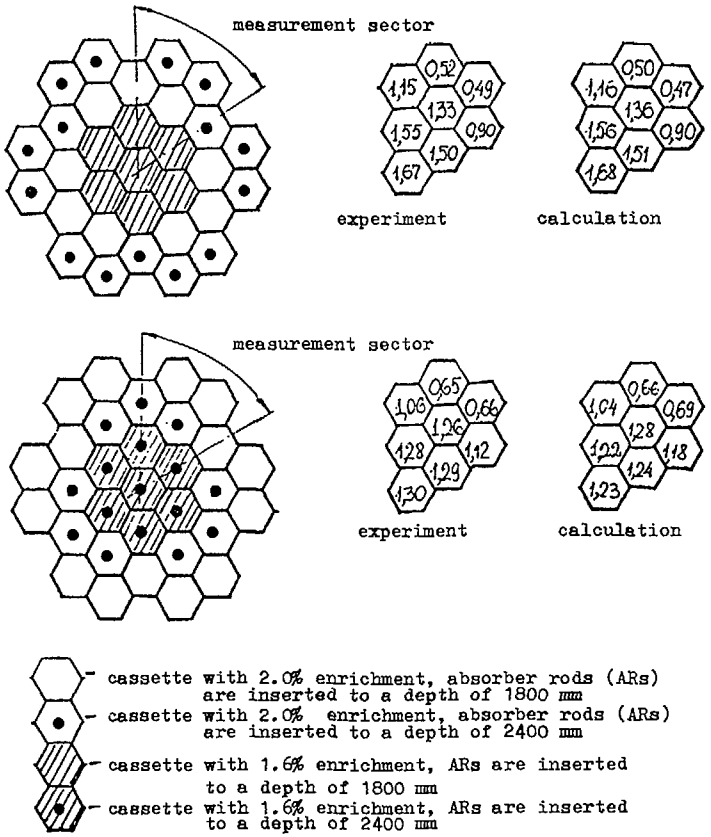

FIG. 5. Experimental and calculation fields of energy releases in the assembly cassettes in the 'hot' state.

Nuclear safety experimental studies included the determination of possibility to provide core subcriticality in the state with maximum multiplication factor at the most effective CPS member stuck in the uppermost position.

The local critical regions consisting of cassettes of different composition simulating in composition and configuration the standard core conditions which gave the possibility to estimate the design margins were studied.

The core critical regions' configuration and subcriticality experimental values obtained are given in Fig. 6.

For the most reactive critical region of a standard core including 2 cassettes with 2% enrichment and 2 cassettes with 1.6% enrichment the experimental subcriticality value amounted to 3.5%.

Thus, the neutron-physical characteristics' investigations performed on the NDHP cassettes model assemblies were the addi-

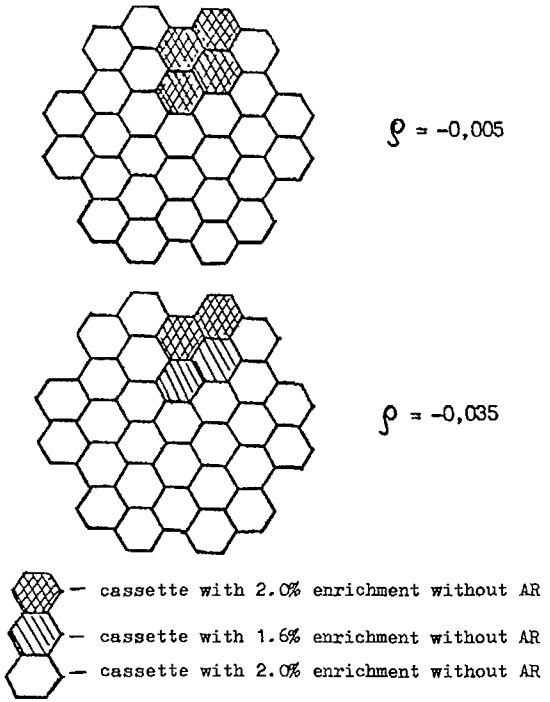

FIG. 6. Core critical region configuration consisting of 4 cassettes.

tional source for verification VVER code package allowed to substantiate the possibility of using it as applied to NDHP reactors, as well as to prove by experiment a number of full-scale core design characteristics.

5. Full-Scale Core Tests

The experimental investigations of neutron-physical charac-characteristics of the first standard core were performed on the full-scale critical facility.

The experimental determination of the core reactivity margin, CPS members' startup positions and their differential effectiveness, emergency protection effectiveness, as well as the verification of fulfilling the requirements on nuclear safety were the objectives of the tests.

Physical non-identity of each cassette was determined by experiments at the initial tests using high-sensitive critical assembly.

The maximum differences in multiplication properties of the cassettes with 1.6% and 2.0 enrichment was 0.1%, with 1.0% enrichment - 0.3%. Measurement results were used for the subsequent core buildup and flattening of energy releases distribution along the core radius and azimuth.

During the experiments the major core characteristics - reactivity margin with withdrawn CPS menbers in the "cold" state was determined which agreed with design value.

The confirmation of the core energy releases absence of non-uniformity was one of the important results of the activation experiments.

During the core tests the effectiveness of each of 120 individual control rods, as well as the effectiveness of standard CPS members were determined.

The measurements results testify to the clusters physical identity and confirm the core azimuth uniformity.

Compensating groups' effectiveness was determined at their sequential insertion into the core at actuation by emergency protection signals.

The results obtained were compared with the design data (see Table 3).

TABLE 3

Number of compensating groups immersed into core (groups' numbers)	Effectiveness of compensating groups immersed into core, %	
	experiment	calculation
1 (no. 2)	2.4	2.3
2 (no. 2; no. 6)	4.6	4.2
3 (no.2; no. 6; no. 1)	5.5	5.4
4 (no.2; no. 6; no. 1; no. 3)	6.0	6.1

During the tests the characteristics important for the subsequent core operation were determined.

They include:

- determination of CPS members' critical positions in the core, differential effectiveness of movable members, as well as experimental verification of standard algorithm of transition to critical state including the investigation of present neutron

flux controllability during transition of the reactor to critical state.

The core subcriticality values obtained at the most effective CPS members stuck in the uppermost position.

Thus, the calculation-experimental investigations performed allowed to verify reliably the main neutron-physical characteristics of the NDHP pilot units' core.

DESCRIPTION AND VALIDATION OF AN APPROXIMATE COARSE MESH SOLUTION METHOD FOR THE DIFFUSION EQUATION IN RZ GEOMETRY

A.Z. TANKER, E. TANKER
Turkish Atomic Energy Authority,
Ankara, Turkey

Abstract

A coarse mesh method based on a nodal method in which the transverse-integrated flux is assumed to have a quadratic shape corrected with discontinuity factors is described and evaluated in this study. The quadratic is required to yield the volume-averaged flux when averaged over its argument and to yield the face-averaged net currents when Fick's Law is applied to it at the nodal interfaces, and its coefficients are determined accordingly. The quadratic is evaluated at the nodal interfaces and the resulting relation is corrected by introducing a discontinuity factor for each face of the node in each energy group.

The equations corrected by discontinuity factors have the capability of reproducing a reference exactly. In routine calculations for which a reference case will not be available, even approximate values for these factors can improve the calculation speed considerably by reducing the number of unknowns.

In the approximate method evaluated in this study the discontinuity factors for 2-D coarse mesh problems are found from 1-D fine mesh calculations. Comparisons with finite difference reference calculations indicate that, for coarse mesh layouts consisting of only a few nodes, this method is faster by a factor of 3 than a fine mesh finite difference calculation of comparable accuracy (about 1% error in k_{eff} and about a maximum error (located at a node producing an insignificant fraction of the total power) of 16% in nodal powers). This method is found applicable to quick survey type calculations that can be performed on a microcomputer.

INTRODUCTION

Nodal methods present fast and accurate means of calculating the global properties of nuclear reactors such as k_{eff} and power distribution. The main goal of these methods is to use coarser meshes than conventional finite difference schemes without loosing accuracy.

This goal is achieved by various methods of estimating or assuming the flux shape within mesh intervals and finding relations between currents and fluxes using this shape. This study is concerned with a nodal method based on a quadratic shape assumption for the transverse-integrated flux corrected by discontinuity factors. A procedure for estimating these factors from auxiliary calculations is described and evaluated using conventional finite difference calculations as reference.

MATHEMATICAL MODEL

For analysis, the reactor is assumed to be made of large, homogeneous (or homogenized) regions called nodes. The neutron balance equation is integrated over the volume of each node to obtain the nodal balance equation which relates nodal leakages to nodal (volume-averaged) fluxes. In cylindrical RZ geometry this balance equation can be written as

$$\Delta z_k[r_{i+1}\bar{J}^k_r(r_{i+1}) - r_i\bar{J}^k_r(r_i)] + \Delta r_i(r_i+\tfrac{1}{2}\Delta r_i)\,[\bar{J}^i_z(z_{k+1}) - \bar{J}^i_z(z_k)]$$
$$+ V^{i,k}[\bar{A}^{i,k}][\bar{\bar{\Phi}}^{i,k}] = V^{i,k}\,\frac{1}{\lambda}\,[\bar{M}^{i,k}][\bar{\bar{\Phi}}^{i,k}] \qquad (1)$$

where $[\bar{A}^{i,k}]$ and $[\bar{M}^{i,k}]$ are GxG matrices of absorption-scattering and fission source cross sections, respectively, of node (i,k); $[\bar{\bar{\Phi}}^{i,k}]$ is the G element vector of nodal fluxes; $[\bar{J}^m_u(u_n)]$ is the net current in u-direction, averaged over the transverse direction and evaluated at the nodal surface u_n; and λ is the eigenvalue. Another relation between the nodal fluxes and the nodal leakages is needed, and nodal methods differ among themselves in these so called spatial coupling equations.

In this study the spatial coupling equations are obtained by assuming a quadratic shape for the transverse-integrated flux in each node. The coefficients of the quadratic are calculated from the requirements that it should yield a) the nodal face-averaged fluxes when evaluated at each face of the node, and b) the nodal flux when averaged over the node. Net currents are introduced using Fick's Law. The resulting quadratic for the r-direction, when evaluated at one side of the node (i,k) is

$$[\bar{\bar{\Phi}}^k_i(r_i)] \approx [\bar{\bar{\Phi}}^{i,k}] + \frac{\Delta r_i}{6}\,[\bar{D}^{i,k}]^{-1}\left\{\left[\frac{r_i+\frac{3}{4}\Delta r_i}{r_i+\frac{1}{2}\Delta r_i}\right][\bar{J}^k_r(r_{i+1})]\right.$$
$$\left. + \left[1+\frac{r_i+\frac{3}{4}\Delta r_i}{r_i+\frac{1}{2}\Delta r_i}\right][\bar{J}^k_r(r_i)]\right\}, \qquad (2)$$

where $[\bar{\bar{\Phi}}^k_i(r_i)]$ is a G-element vector of z-integrated fluxes evaluated at r_i, and $[\bar{D}^{i,k}]$ is a GxG diagonal matrix of the diffusion coefficients for node (i,k). There is a similar equation for the other side of the node (r_{i+1}). Z-direction is treated analogously.

A set of spatial coupling equations are obtained by using the continuity of the fluxes and currents at nodal interfaces and eliminating the surface-flux terms. This yields a relation among three consecutive surface currents and two nodal fluxes of two adjacent nodes. Surface currents can be replaced with leakages by incorporating another neighboring node. Together with (1) and boundary conditions, the problem is well-defined and can be solved numerically to obtain the k_{eff} and nodal fluxes for each energy group.

Equation (2) results from the quadratic shape assumption, and therefore, is inherently inaccurate. For instance, if the fluxes and currents are known from a *more accurate model*, these values will not satisfy (2) and, therefore, cannot be reproduced by the resulting equations of the present model regardless of the solution strategy employed. To make (2) capable of reproducing a known reference, a set of additional parameters, called discontinuity factors, are introduced as follows:

$$[f^{i,k}_{r-}]^{-1}[\bar{\bar{\Phi}}^k_i(r_i)] = [\bar{\bar{\Phi}}^{i,k}] + \frac{\Delta r_i}{6}\,[\bar{D}^{i,k}]^{-1}\left\{\left[\frac{r_i+\frac{3}{4}\Delta r_i}{r_i+\frac{1}{2}\Delta r_i}\right][\bar{J}^k_r(r_{i+1})]\right.$$
$$\left. + \left[1+\frac{r_i+\frac{3}{4}\Delta r_i}{r_i+\frac{1}{2}\Delta r_i}\right][\bar{J}^k_r(r_i)]\right\}, \qquad (3)$$

where $[f^{i,k}_{u\pm}]$ are GxG diagonal matrices corresponding to each face of the node (i,k). The discontinuity factors can be calculated from the known reference, and, using these values the present model can reproduce the average fluxes and the k_{eff} of the reference [1,2]. Detailed derivation of the equations mentioned in this paper can be found in [2].

METHOD

To utilize the freedom introduced to (3) a practical method for calculating the discontinuity factors (without actually performing the reference calculation) is needed. One such method, introduced in [2] and further evaluated in the present study, uses discontinuity factors obtained from fine mesh 1-dimensional calculations in 2-dimensional coarse mesh problems.

First a coarse mesh layout is chosen and each node is partitioned into a number of smaller nodes. A 1-D problem is devised on this fine mesh layout for each direction by assuming zero transverse leakage. Criticality calculations are performed using the material properties of each unique row and column in sequence, and discontinuity factors to be used in the coarse mesh calculations are determined from (3). These discontinuity factors are such that if the 1-D calculations were done on the coarse mesh layout the results would reproduce those obtained from the fine mesh calculations. The coarse mesh 2-D calculation using these discontinuity factors yields k_{eff} and nodal flux values that are presumably more accurate than those obtained from the solution of the original equations, which do not employ discontinuity factors (i.e. those equations derived from (1) & (2)), on the same coarse mesh layout.

The auxiliary 1-D calculations use the same boundary conditions in the specified direction and the same material properties as in the 2-D problem. No correction is done for the transverse leakage, which is taken as zero in 1-D calculations and the value of which will not be known until the 2-D calculation is performed. Therefore, for instance, a column near the core centerline is assigned the same set of z-directed discontinuity factors as another one near the reflector if both columns have the same composition sequence and the same boundary conditions. The auxiliary calculations solve k_{eff} type eigenvalue problems; therefore, discontinuity factors cannot be calculated for non-multiplying rows and columns, and a value of unity is used.

NUMERICAL RESULTS

The effectiveness of the quadratic approximation was evaluated in [2] by comparing 1-D calculations with analytic solutions and with mesh centered finite difference calculations done with the computer code CITATION. It was shown there that quadratic approximation permits the use of two times larger nodes (in 1-D) to obtain the same accuracy as the finite difference calculation. In two dimensions, the approximate discontinuity factor (ADF) method described in the previous section was compared with finer mesh 2-D calculations using unity discontinuity factors (UDF), and found that, with ADF, 10 times larger nodes are sufficient for the same accuracy as fine-mesh UDF.

In this study both UDF and ADF methods are evaluated on coarse mesh layouts in two dimensions and compared to results obtained from CITATION by repeating calculations with increasingly finer meshes and extrapolating the results to zero mesh spacing. All calculations are performed on an Intel 8088 based microcomputer running at 7.16 MHz, having 640k bytes of memory and equipped with an Intel 8087 math coprocessor and a hard disk, therefore, the calculation times given below should be evaluated accordingly. Due to the limitations imposed by the computer used, coarse mesh layouts consisting of only a few nodes could be employed and sufficient detail for spatial convergence could not be incorporated in the finite difference calculations. Consequently, validation efforts for the ADF method is limited to large node survey type problems which do not require much detail and high accuracy.

The first test case presented here is drawn from a fast breeder. There is a core region, a radial blanket, an axial blanket, all surrounded by a reflector. The radii of the regions are 60cm, 112cm and 142cm, respectively. The top reflector is 48cm and the axial blanket is 40cm thick. The core half-height is 22cm. Zero current boundary condition is assumed for the centerline and the bottom, and zero flux condition is assumed for the outer sides of the reflector. Three group cross sections for this problem are taken from a sample problem received in the CITATION package [3].

First a series of finite difference calculations are performed with increasingly finer mesh layouts and the results are extrapolated to zero mesh spacing which serves as reference. The k_{eff} and the fractional nodal powers of the least detailed 3x3 node and the most detailed 30x30 node problems are presented in Fig.1. A UDF nodal calculation using the same coarse mesh layout and an application of the ADF scheme with 7 partitions per node are performed and the results are presented in Fig.2. For the least detailed configuration the UDF method yields better results than the finite difference method as expected (1a and 2a). For ADF, k_{eff} is worse but the nodal powers are better than the most detailed available finite difference (1b and 2b). This

(a)

0.02201 (-47.6)	0.00315 (-69.8)	
0.96378 (+4.51)	0.01106 (-56.4)	

k_{eff} = 0.96232 (+16.5) T = 0.87min

(b)

0.04141 (-1.37)	0.00998 (-4.33)	
0.92506 (+0.31)	0.02356 (-7.09)	

k_{eff} = 0.82930 (+0.39) T = 15.97min

Fig.1 - Fractional nodal powers and percentage errors (in parantheses) for no partition (a) and 10 partition (b) finite difference calculations

(a)

0.03705 (-11.7)	0.00988 (-5.23)	
0.92909 (+0.74)	0.02398 (-5.45)	

k_{eff} = 0.87101 (+5.44) T = 0.63min

(b)

0.04182 (-0.38)	0.01038 (-0.45)	
0.92357 (+0.14)	0.02423 (-4.46)	

k_{eff} = 0.83217 (+0.74) T = 4.17min

Fig.2 - Fractional nodal powers and percentage errors (in parantheses) for UDF (a) and ADF with 7 partitions (b) nodal calculations

suggests that there is a cancellation of errors in the calculation of the nodal powers. The errors in k_{eff} are characteristic of large nodes and can only be improved by using finer nodes in 2-D calculations. The advantage gained in running times is apparent.

As a second test case a small problem with two fuel regions and a reflector is run. The radii of the core nodes are 16cm, 30cm and 46cm; and the reflector thickness is 14cm. About the central symmetry plane there is a homogeneous core region of 18cm half-height. The innermost cylinder of this region extends axially for another 17cm and surrounded annularly by the second fuel region of the same height but of a different enrichment. This second fuel region contains two radial nodes. There is also an 18cm thick top reflector. The boundary conditions are the same as the previous test case. The four group cross sections for this problem are taken from a sample problem for CITATION [3].

Again, a series of finite difference calculations with increasingly finer meshes are performed and the k_{eff} and nodal powers are extrapolated to zero mesh spacing. The results of the least detailed 4x3 node and the most detailed 32x24 node problems are presented in Fig.3. Next, a UDF nodal calculation on the coarse mesh and an ADF calculation with 8 partitions per node are done and the results are presented in Fig.4. It can be seen that both nodal solutions fall between the two limiting finite difference solutions. The ADF method is again seen to be a considerable improvement over UDF, and, though the errors are large for fine-tuning problems they are quite acceptable for survey type calculations. The short calculation times make the ADF method feasible for microcomputer applications.

(a)

0.01569 (-37.7)	0.36530 (+5.96)	0.57393 (+7.42)	
0.00170 (-80.2)	0.01427 (-58.1)	0.02312 (-58.9)	

k_{eff} = 1.07859 (+12.6) T = 1.18min

(b)

0.02480 (-1.54)	0.34636 (+0.47)	0.53661 (+0.44)	
0.00534 (-3.58)	0.03279 (-3.68)	0.05411 (-3.70)	

k_{eff} = 0.96223 (+0.47) T = 10.75min

Fig.3 - Fractional nodal powers and percentage errors (in parantheses) for no partition (a) and 8 partition (b) finite difference calculations

(a)

0.01983 (-21.3)	0.35348 (+2.53)	0.56082 (+4.97)	
0.00346 (-37.5)	0.02702 (-32.4)	0.03939 (-29.9)	

k_{eff} = 1.00536 (+4.97) T = 0.95min

(b)

0.02389 (-5.16)	0.34170 (-0.88)	0.54320 (+1.67)	
0.00466 (-15.9)	0.03251 (-4.48)	0.05403 (-3.83)	

k_{eff} = 0.96767 (+1.03) T = 3.67min

Fig.4 - Fractional nodal powers and percentage errors (in parantheses) for UDF (a) and ADF with 8 partitions (b) nodal calculations

In both of the above cases the coarse meshes consist of only a few nodes. Consequently, the time spent in auxiliary 1-D calculations is rather large compared to the 2-D calculations. In realistic cases where the reactor is represented by a more detailed coarse mesh layout this proportions are reversed and the time spent in auxiliary calculations become a small fraction of the total calculation time [2].

CONCLUSION

In this study a two dimensional nodal method based on a quadratic flux shape corrected with discontinuity factors which are calculated from auxiliary 1-D calculations is evaluated using references obtained from finite difference calculations. Due to the limitations imposed by the computer used for calculations, layouts consisting of only a few nodes can be employed. As a result, the errors in calculated k_{eff} are about 1% and those in nodal powers are about a maximum of 16% located at a node producing an insignificant fraction of the total power. Although a large fraction of the total calculation time is spent in the auxiliary calculations the results indicate that the ADF method is a considerable improvement over UDF, and the time spent in an ADF calculation is at least a factor of 3 shorter than a finite difference calculation of comparable accuracy. This suggests that ADF can be a valuable tool in survey calculations to be performed on microcomputers.

ACKNOWLEDGEMENTS

The authors would like to thank the OECD/NEA Data Bank for providing the computer code CITATION. They also wish to express their gratitude to the Turkish Scientific and Technical Research Council (TUBITAK) Information Technologies Center for allowing Dr. A.Z. Tanker to use their computer facilities for adaptation of CITATION to Intel 8086 class of microcomputers.

REFERENCES

[1] K.Smith, A.F.Henry and R.Loretz, "Determination of Homogenized Diffusion Theory Parameters for Coarse Mesh Nodal Analysis," ANS Topical Meeting, Sun Valley, Idaho, USA, September 1980.

[2] E.Tanker, "A Nodal Analysis of Graphite-Moderated Reactors," Ph.D. Thesis, Department of Nuclear Engineering, M.I.T., Cambridge, Massachusetts, USA, June 1989.

[3] D.R.Vondy, T.B.Fowler, "Job Stream of Cases for the Computer Code CITATION," ORNL-TM-3793, Reactor Division, ORNL, Oak Ridge, Tennessee, USA. July 1972.

EVALUATION OF SAFETY PARAMETERS IN NODAL SPACE-TIME NUCLEAR REACTOR ANALYSIS

H. FINNEMANN, R. BÖER, R. BÖHM, R. MÜLLER
Siemens AG/Unternehmensbereich KWU,
Erlangen, Federal Republic of Germany

Abstract

The integrated program system PANBOX features neutronics models for solving the time-dependent few-group diffusion equations in Cartesian or in hexagonal-z geometry coupled with an advanced version of the well-known thermal-hydraulics code COBRA-III Combined with an accurate and efficient pin power reconstruction module the program is thus capable of performing not only global neutronic / thermal-hydraulic calculations but also to evaluate important safety-related parameters like DNB ratios and centerline fuel temperatures

For the solution of the basic neutronics equations, the nodal expansion and the nodal integration methods are implemented in PANBOX Time-integration is based on a fully implicit Euler method in combination with an exponential transformation technique to reduce truncation errors The reconstruction of pinwise power distributions relies on Cartesian or hexagonal versions of the weak element approximation method

The thermal-hydraulic part of the reactor calculation is based on the program COBRA III-C/P. It allows 3-dimensional steady-state and transient full- or part-core analyses to be performed. The capability to calculate crossflow effects is essential to achieve the high degree of spatial resolution and accuracy aimed at in the coupled system

The present paper gives a description of the coupled neutron kinetics / thermal hydraulics program system PANBOX for steady-state and transient calculation of reactors with rectangular or hexagonal fuel element geometry The underlying physical models, the calculation procedure between neutronics and thermal hydraulics, and the related thermal margin and DNB evaluation methodology are presented in some detail, together with perspectives for further development and refinements

1 Introduction

The numerical analysis and simulation of nuclear reactor phenomena still ranks amongst the most demanding scientific tasks, requiring coupled neutronic / thermal-hydraulic computer programs For the established light water reactors (BWRs, PWRs) such programs have been developed and continuously improved over the last decades, both with regard to mathematical methods and physical modeling For calculating PWR behaviour under steady-state and transient conditions, solving the few-group neutron diffusion equations by the nodal expansion method (NEM) /1/ and/or the analytic nodal integration method (NIM) /2/ coupled with a thermal-hydraulic model has proved to combine high accuracy of the results with acceptable computing times. This approach has recently been extended /3, 4/ to also allow evaluations for hexagonal geometries as encountered in VVER type and pressurised water high converter reactors (PWHCRs) These nodal methods are the basis of the neutronic part of the PANBOX code system for space-time reactor analysis The computational efficiency of PANBOX was improved by an order of magnitude compared with earlier implementations of NIM / NEM by exploiting their high vectorization potential in a multi-level iteration process

The thermal-hydraulic part of PANBOX makes use of the open-channel methods as implemented in COBRA III-C/P /10,11/ Coupling between subchannels is modeled for the net diversion crossflow resulting from flow redistribution and for turbulent mixing without net mass exchange. The diversion crossflow is considered to be small compared with the axial mass flow rate. In the case of boiling, a one-dimensional homogeneous two-phase slip flow is assumed to exist in each affected subchannel.

The time derivatives of the neutronic equations are approximated by a fully implicit differencing scheme rendering the solution procedure for the time-dependent problem similar to that for a static source problem. The fluid conservation equations are converted to a system of linear equations by a differencing scheme implicit both in space and time Control of the overall coupled steady-state and transient iteration and calculation procedure includes examination of local truncation errors as well as of the behaviour of relative changes of the neutronic and thermal-hydraulic solutions between time steps

2 Cartesian and Hexagonal Nodal Methods

2.1 Basic Equations

Consistent nodal methods enjoy widespread computational use because they are easy to program and very accurate even on a coarse mesh The nodal expansion method NEM /1,5/ and the nodal integration method NIM /2/ are consistent higher-order nodal methods which can be derived by converting the P_1-form of the neutron diffusion equation into a set of nodal equations and equivalent one-dimensional diffusion equations for the average flux in each space direction. The nodal equations are obtained by formally integrating the diffusion equation over each volume element (box, hexagonal prism) into which the nuclear assembly is partitioned In matrix notation, the system consists of the nodal balance equations

$$\frac{1}{v}\frac{d\Phi}{dt} + M\Phi = \frac{1}{\lambda}(1-\beta)\,\chi_p\,F^T\Phi + B\,J^{in} + \sum_{i=1}^{I}\lambda_i\chi_d C_i + G, \quad (1)$$

the outgoing current equations

$$J^{out} = D\Phi + E\,J^{in} + H \quad , \quad (2)$$

$$J^{in} = A\,J^{out} \quad , \quad (3)$$

the precursor equations

$$\frac{dC_i}{dt} = -\lambda_i C_i + \beta_i\frac{1}{\lambda}F^T\Phi \quad , \quad (4)$$

and a set of transverse-integrated 1-D diffusion equations, with

Φ	flux density vector,
J	partial current vector,
C	precursor density vector,
F	fission vector,
λ_i	decay constants,
M	absorption and scattering matrix,
λ	eigenvalue
χ_p, χ_d	prompt, delayed emission spectrum vector
A	generalized Albedo matrix which describes coupling to neighbours and

B, D, E, G H — matrices whose elements are functions of the diffusion coefficient and parameters dependent on the method by which the 1-D diffusion equations were solved

The matrix M contains as a nonlinear contribution the coupling coefficients defined as the ratio of outgoing currents to average fluxes

The nodal integration method NIM is practically restricted to two-group problems whereas NEM is an efficient multigroup technique A procedure which combines the merits of both methods was recently implemented in the PANBOX code system for space-time analysis of nuclear reactors This method relies on the fact that the 1-D diffusion equation can be solved analytically if the scattering and fission source is represented by a parabolic or higher-order polynomial It turns out that a parabolic approximation of the source is already sufficiently accurate if the coefficients are determined iteratively by a suitable weighted-residual method The method was therefore termed NIM-WR The NIM-WR method is equally well applicable to Cartesian and hexagonal problems Introducing some additional simplifying assumptions /3 4/ nodal methods, originally developed for Cartesian geometry, can readily be transferred to hexagonal geometry For a hexagonal prism, however, three 1-D equations for the transverse-averaged flux in the three directions perpendicular to the hexagon faces are needed, and solved by NIM-WR Thus the system of equations is formally identical for both geometries With a proper ordering for the unknowns, the coefficient matrices of the flux and current equations have a regular sparse structure, and highly vectorizable solution algorithms can be used These are explained in more detail in the next subsection

2.2 Efficient Solution Algorithms

In order to solve equations (1) through (4) the time derivative term $\frac{d\phi}{dt}$ has to be approximated This is done by the application of the implicit first order Euler method combined with the frequency transformation /5/

$$\frac{d\phi}{dt} = \omega\,\phi(t) + \left(\phi(t) - e^{\omega \Delta t}\,\phi(t_0)\right) / \Delta t$$

It has been shown /5/ that the resulting system of equations describing the solutions ϕ (t) and J (t) has the same structure as that for the stationary problem The fundamental principles for an efficient solution technique are therefore exemplified for the stationary system of equations The nodal balance equation reduces now to

$$M\Phi = \frac{1}{\lambda}\,\chi_t F^T \Phi + B J^{in} \qquad (1a)$$

where χ_t is the total spectrum vector The outgoing current equations (2) and (3) remain valid also in the stationary case

The system of equations (1a), (2) (3) can be solved by an iterative Gauss-Seidel method for neutron fluxes and partial currents Efficient solution techniques for this iteration process include both the application of acceleration techniques and an appropriate formulation of the algorithms to gain the most possible profit on modern high speed vector computers

Firstly, multi-level adaptive techniques are applied to accelerate the convergence process These techniques solve adapted simplified equations on a hierarchy of successively coarser grids Appropriate restriction operators transform the fine-mesh solutions to the coarser grid whereas prolongation operators interpolate the fine mesh solutions from the coarse mesh solution /6/

Secondly, indexing of the calculational nodes by a red-black checkerboard scheme allows a vectorized formulation of the Gauss-Seidel iteration process for equations (1a), (2), (3) For this purpose the matrices and the vectors ϕ J and C can be split and ordered into "red" or "black" components (index c, where c = red or black) as follows

$$M_c\Phi_c = \frac{1}{\lambda}\,\chi_t F_c^T \Phi_c + B_c J_c^{in} \qquad (1b)$$

$$J_c^{out} = D_c\Phi_c + E_c J_c^{in} + H_c \qquad (2a)$$

$$J_c^{in} = A_c J_c^{out} \qquad (3a)$$

Flux and current solution vectors are now determined by a loop over all red and all black nodes This ensures typical vector lengths of at least N/2 where N is the total number of nodes to be calculated In consequence, a substantial computational speedup on computers equipped with vector facilities is obtained The iteration is formulated as a multigrid cycle to accelerate the convergence process

It should be noted that the complete algorithm is highly vectorizable Indeed, the bulk of the calculation of matrix coefficients needed for the multi-level process and of the iterative solution on all grids can be performed in vectorized form Furthermore, it was demonstrated that the described algorithms can efficiently be parallelized on multiprocessor systems by applying the principle of domain splitting /7/ Efficiencies of about 80 % can be reached Therefore, these algorithms are also well suited for multi-CPU vector computer architectures

3 Thermal Hydraulics and Coupling to Neutronics

The thermal-hydraulic part of the PANBOX code system for the analysis of space-time effects in nuclear reactors is based on the program COBRA III-C/P It allows 3-dimensional steady-state and transient pressurised and boiling water reactor analyses to be performed The capability to calculate crossflow effects is essential to achieve the high degree of spatial resolution and accuracy aimed at in the coupled neutronics - thermal hydraulics system Geometry specification for the reactor core is flexible, relying on information about flow areas and lateral interconnections, i e no particular coordinate system is defined This allows application to Cartesian and hexagonal problems The underlying conservation equations for the fluid have been given in /4/ and need not be reproduced here

The calculation scheme of the coupled reactor core simulation in PANBOX is as described in /4/ for the hexagonal option The modules for neutron kinetics (HEX-CART) and thermal hydraulics (COBRA) now represent the pure calculation parts of the formerly independent programs In the coupled system, their internal solution procedures have remained unchanged, i e suitable convergence criteria and iteration step limits can still be specified individually However, coupling of the modules introduces the need for an additional outer iteration loop which also contains the interface routines for updating cross sections and power density in dependence of thermal-hydraulic conditions and nuclear fission rate, respectively

4 Pin Power Reconstruction Schemes

The solution of nodal balance and currents equations yields volume- and surface-averaged fluxes and currents for each energy group. The nodal averages can further be used to construct corner values by linear extrapolation and a subsequent smoothing step. This method can be used in Cartesian and hexagonal geometry:

Geometry

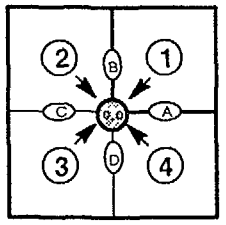

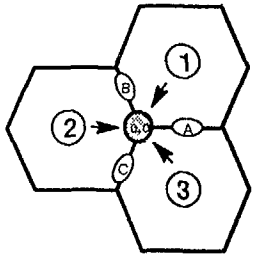

Extrapolation

$$\phi^1_{oo} = \psi_A + \psi_B - \bar{\phi}^1$$
$$\phi^2_{oo} = \psi_B + \psi_C - \bar{\phi}^2$$
$$\phi^3_{oo} = \psi_C + \psi_D - \bar{\phi}^3$$
$$\phi^4_{oo} = \psi_D + \psi_A - \bar{\phi}^4$$

$$\phi^1_{oo} = \frac{2}{3}\psi_A + \frac{2}{3}\psi_B - \frac{1}{3}\bar{\phi}^1$$
$$\phi^2_{oo} = \frac{2}{3}\psi_B + \frac{2}{3}\psi_C - \frac{1}{3}\bar{\phi}^2$$
$$\phi^3_{oo} = \frac{2}{3}\psi_C + \frac{2}{3}\psi_A - \frac{1}{3}\bar{\phi}^3$$

Smoothing

$$\phi_{oo} := \sum_{i=1}^{4} w_i \, \phi^i_{oo} \qquad \phi_{oo} := \sum_{i=1}^{3} w_i \, \phi^i_{oo}$$

According to the above formulae the extrapolated node values ϕ^i_{oo} at the corner under consideration are averaged to get a smoothed flux estimate ϕ_{oo} . Both arithmetic and diffusion coefficient weighting ($w_l = D_l / \Sigma D_l$) have proved to yield sufficiently accurate results. Further boundary values like gradients in the corner or average values on subsurfaces can be estimated. Weak element approximations /8/ to the diffusion equation can then be used to match point and average values on the boundary of the fuel assembly. Though the proposed method is also applicable in three dimensions we assume that the intra-nodal flux distribution is separable in the axial and radial directions. Thus after having obtained suitable boundary values the interpolation problem is reduced to the solution of a two-dimensional inhomogeneous diffusion problem for each node. For the construction of this solution the buckling B^2 is calculated by the condition that the determinant of the multigroup diffusion equation system with $\Delta\Phi$ replaced by $-B^2\Phi$ is zero. Denoting the solutions of this algebraic equation by κ_g^2 (g = 1,...,G) the flux solution is a linear combination of the corresponding solution functions η_g

$$\Phi_g = \sum_{g'=1}^{G} \beta_{gg'} \, \eta_{g'} \qquad g=1,\ldots,G$$

where $\beta_{gg'}$ are the group coupling constants. The elementary functions η_g are solutions of the Helmholtz equation

$$\Delta \eta_g + \kappa_g^2 \eta_g = 0$$

and chosen as follows

$$\eta(x,y) = \sum_{j=1}^{J} \left(c_j^{+} \cosh \kappa \xi_j + c_j^{-} \sinh \kappa \xi_j \right) \qquad \kappa^2 < 0, \quad \kappa = \sqrt{-\kappa^2}$$

$$\eta(x,y) = \sum_{j=1}^{J} \left(c_j^{+} \cos \kappa \xi_j + c_j^{-} \sin \kappa \xi_j \right) \qquad \kappa^2 > 0$$

where

$$\xi_j = x \cos \alpha_j + y \sin \alpha_j \qquad \text{and} \qquad \alpha_j \text{ arbitrary .}$$

The coefficients of the symmetric (c_j^{+}) and the asymmetric (c_j^{-}) solution functions have to be determined by the 2*J boundary conditions. The choice of the arbitrary parameters α_j is suggested by symmetry considerations. If we use only corner and surface-average fluxes as boundary conditions we have J = 4 for Cartesian and J = 6 for hexagonal geometry. The following α_j for point and integral conditions can be chosen :

Cartesian geometry: Point/Integral: α = 45°, 135° / 0°, 90°
Hexagonal geometry: Point/Integral: α = 30°, 90°, 150° / 0°, 60°, 120°

Given the parameters α the further evaluation of point and integral conditions is a somewhat tedious but elementary task. In two-group problems, the matrix to be evaluated in Cartesian geometry splits up into two 4x4 systems which can easily be inverted. In hexagonal geometry we correspondingly have two 6x6 systems. Thus the proposed method can be made very efficient with respect to computation. This is a necessary prerequisite for an extensive use of on- and off-line pin power reconstruction methods. The resulting interpolating flux functions fulfill the two-dimensional diffusion equation in the interior of the node. Experience has shown that for large nodes this approximation is superior to polynomial interpolation both with respect to accuracy and computational efficiency. This is especially true in case of steep flux gradients as they occur under off-nominal conditions. It should be noted

that the procedure outlined is applicable for steady-state and transient problems. In time-dependent 3-D problems a buckling and a time absorption term have to be added to the removal cross section. For the precursors an approximation similar to that made in the derivation of the equivalent one-dimensional diffusion equation of NEM can be used. The behaviour of the solution at the boundary of the node can be improved by using more than the discussed minimum of boundary conditions. If at all, this is only necessary for the thermal flux in strongly absorbing nodes or fuel assemblies at the core-reflector boundary and thus does not impair computational efficiency /9/.

5 Local Evaluation of Coupled Neutronic / Thermal-Hydraulic Calculations

5.1 Basic Methodology

The coupled neutronics / thermal hydraulics steady-state and transient nodal reactor calculations yield thermal-hydraulic results for each flow channel node. These results reflect the influences of neutronic feedback and of crossflows between neighbouring channels. For safety-related analyses, they must be checked against the maximum permissible values in order to determine thermal margins. One of the most important safety criteria is the departure from nucleate boiling ratio (DNBR). It is defined as the ratio between critical heat flux and local heat flux at any particular position on the surface of a fuel rod. Some of the most widely used critical heat flux (CHF) correlations available are those of W-3-L/R-Grid, B&W, and the KWU CHF Tables.

In standard nodal space-time kinetics applications, reactor core subdivision in the horizontal plane is based on the actual fuel assembly arrangement, i.e. both the neutronic and the thermal-hydraulic modules will treat the problem in a comparatively coarse full assembly geometry rather than performing more detailed subchannel analyses. This implies that each of the flow channels is calculated as though containing only one fuel rod which then represents an average of all the rods actually present. Therefore in such fuel element based calculations only average values of thermal-hydraulic conditions (for instance quality, enthalpy) of the coolant and of heat flux can be determined.

In DNB evaluations, however, maximum local (or pin) values of the thermal-hydraulic quantities would be needed. In order to estimate these values without expensive pin-based subchannel analysis local neutron flux and pin power reconstruction methods must be applied, as described in the previous section. In current methods the resulting average and maximum nodal neutronic power formfactors serve as multipliers to the average nodal heat flux. The maximum heat flux within a node thus determined is then used in the DNB analysis.

In the following a refined methodology for hot channel analysis will be presented. It is suitable for on-line local safety margin evaluation and applicable to both Cartesian (pressurised water reactor PWR) and hexagonal (pressurised water high converter reactor PWHCR) geometries.

The method relies on the identification and explicit re-calculation of relevant hot channels in the reactor core. The module for this on-line local safety margin evaluation is integrated into the normal neutronic / thermal-hydraulic calculation procedure. Its details are given in Fig. 1. To start with, the thermal-hydraulic results of the assembly based nodal calculation are available. As already mentioned, these results are average values. However, they allow recognition of channels in which maximum values of selected quantities (for instance exit quality, local heat flux, enthalpy increase) occur. These criteria can be used to identify one or more channels ("hot channels") to be examined in more detail. For each axial level of the hot channel the local pin power values must be calculated applying the corresponding Cartesian or hexagonal methods discussed in section 4. If these local power factors are already available (they might have been calculated for other purposes) they can serve as another criterion for hot channel identification.

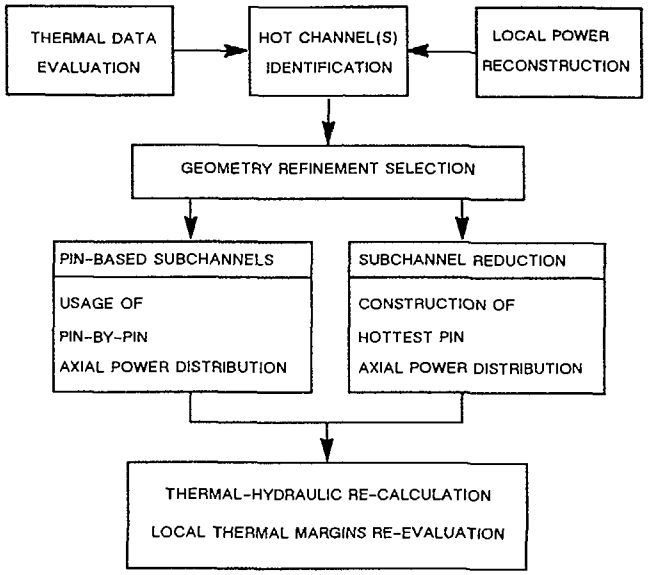

Fig. 1: Integrated Local Safety Margin Evaluation

Next, the grade of geometric refinement of the hot channel must be defined. The first branch (cf. Fig. 1) with the option to generate a very detailed subchannel layout based on the actual fuel pin arrangement will be described in section 5.3. At present, the second branch giving a one-zone, one-rod representation of the hot channel is implemented. It corresponds to a refined methodology for hot channel analysis which has been proved efficient for nodal reactor calculations in Cartesian geometry /12/. In the normal channel calculation the average nodal rod power was used. In contrast, for the improved safety margin evaluation now a "hottest" pin condition has to be examined. The axial power distribution of this hottest pin is constructed by selecting the maximum power value from each axial layer of the hot channel. As this maximum is not necessarily encountered in always the same pin, the resulting "hottest pin" axial power distribution is kind of fictitious and therefore represents a conservative "worst case" when re-calculating thermal hydraulics.

In both steady-state and transient applications, the next step is to re-calculate the hot channel thermal hydraulics. This implies re-calculation of heat conduction in the individual fuel pins, of heat transfer to the coolant, of thermal-hydraulic channel conditions, and of coolant crossflow between subchannels. After this procedure, exact maximum values for the safety-related quantities are available. In the final step, these quantities are used to realistically re-evaluate local thermal margins, for instance with regard to centerline fuel temperatures and DNB ratios.

This methodology for realistic thermal margin re-evaluation applies to steady state as well as to each transient time step. In particular, it solves the problems encountered in transient calculations (where neutronic and thermal-hydraulic quantities are not directly coupled any more due to their different time constants) by identification and explicit re-calculation of the relevant hot channels in the core.

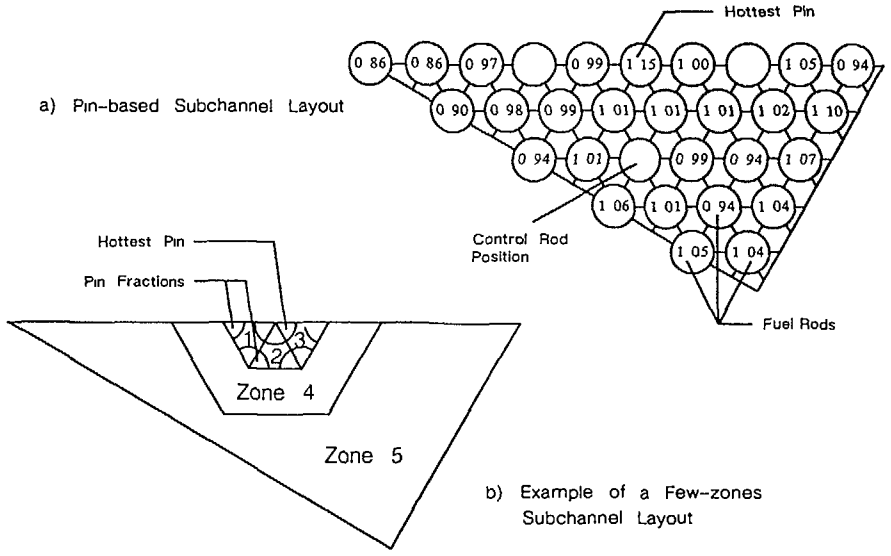

Fig 2 Local Safety Margin Evaluation

Consequently, both maximum rod surface heat flux and hot subchannel thermal-hydraulic conditions are calculated instead of estimated, and hence correctly used in the CHF correlations and in the DNB and thermal margin evaluation

5.2 Sample Results

A typical case well-suited for PANBOX application is the analysis of a main steam line break at zero load During this accident, a substantial core subcooling takes place due to the live-steam outflow. Under conservative assumptions and boundary conditions (e g end of cycle, stuck rod), the reactor may temporarily return to power in the course of the transient, in spite of the reactor trip initiated at accident onset In this case it is sufficient to demonstrate that neither DNB nor fuel centerline melting occur This is a difficult task, since the thermal-hydraulic properties of the core are far-off-nominal (low coolant inlet temperature, low pressure, low mass flow), and the power density distribution resulting from the return to power is highly skewed in axial and radial direction

In this section, results of a steam line break analysis carried out for the SIEMENS PWR 1300 MW with 18x18 FA are presented The analysis was performed according to the SIEMENS methodology (concept of fictitious supercriticality at zero load, $\Delta\rho_{FUEN}$ /13/) in which the important variables of the core after return to power are correlated with the excess reactivity – to be compensated by power generation – at the instant of maximum core subcooling The analysis was carried out in a cycle-overlapping way, considering different reload cores with different contents of MOX-FA

Results of centerline fuel temperature vs $\Delta\rho_{FUEN}$ obtained via local evaluation of the coupled neutronic / thermal-hydraulic calculations are given in Fig 3a (pure UO_2 core) and Fig 3b (core with 50% MOX-FA) For comparison, results obtained by a simple extrapolation procedure (based on pin power interpolation and local peaking factors assumed identical between hot pin and node-averaged results with respect to power and temperature rise within the fuel rod) are plotted, too Centerline fuel temperatures were evaluated at two nodes, corresponding to the location of the local maxima according to the explicit hot channel calculation (loc 1) and to the extrapolation model (loc 2)

In the case of the pure UO_2 core (Fig 3a) loc 1 and loc 2 are identical almost over the whole $\Delta\rho_{FUEN}$ regime The node-averaged values of centerline fuel temperature are rather high, thus long-distance extrapolation is not required, and the discrepancies between the results are below 100 °C, even at the highest (and safety-relevant) temperatures close to the fuel melting temperature

The situation completely changes in the case of mixed UO_2/MOX cores (Fig 3b), where the harder neutron spectrum leads to an increased local peak of the axial power density distribution at the reflector At high $\Delta\rho_{FUEN}$ values (> 3%), with resulting high power generation and coolant temperature rise, the local maximum of power density distribution is located directly at the lower core edge, and the local peaking factor between hot pin and node-averaged value is in the order of 2 to 3 In this case the extrapolation model fails because long-distance extrapolation at loc 1 leads to an underestimate of maximum centerline temperature by several hundred degrees, the maximum value is found at a different location (loc 2) in another axial layer with higher node-averaged results and lower local peaking factors This maximum value according to the extrapolation model may be up to 300 °C lower than the maximum value resulting from the explicit hot channel analysis model, thus leading to an error in the determination of an allowable $\Delta\rho_{FUEN}$ limit of several 10^{-3} $\Delta\rho$

These results demonstrate the necessity of an explicit neutronic / thermal-hydraulic hot channel analysis, especially under far-off-nominal conditions and for cores with large flux gradients within single nodes, e g cores containing MOX-FA

5.3 Further Development

Further development of the hot channel analysis method presented above concerns the geometric refinement of the hot channel The first option in Fig. 1 , namely to generate a very detailed subchannel layout based on the actual fuel pin arrangement, will be provided Alternatively, a reduction in the number of subchannels leading, in extreme, back to only one zone (as discussed above) can be chosen

The pin-based approach is illustrated in Fig 2a For a 30 degree section of a hexagonal fuel assembly, it shows results of a pin-by-pin power reconstruction in a particular axial plane As indicated, the flow zone definition treats each subchannel between fuel rods individually. On this basis, and using the known axial power distributions of all the fuel rods, the fuel assembly can be re-calculated in a very detailed manner The boundary conditions for pressure, inlet mass flow and inlet enthalpy are the same as in the previous global calculation for this fuel assembly

Using the same boundary conditions, the fuel assembly can also be subdivided in a coarser way Fig 2b depicts a layout where only the immediate vicinity of the hottest pin is represented by detailed subchannels This region is surrounded by a zone (number 4) in which the fuel rods are not modeled individually any more, but averaged (or "smeared") Similarly, all the rest of the fuel assembly is included in zone 5 Such a subchannel layout allows for crossflow from the hottest subchannel It is still accurate but obviously much less expensive to calculate than the first option It should be noted that this approach is also in accordance with the common practice of reactor core thermal-hydraulic design and safety analysis, but now directly integrated into the coupled neutronic / thermal-hydraulic calculation sequence

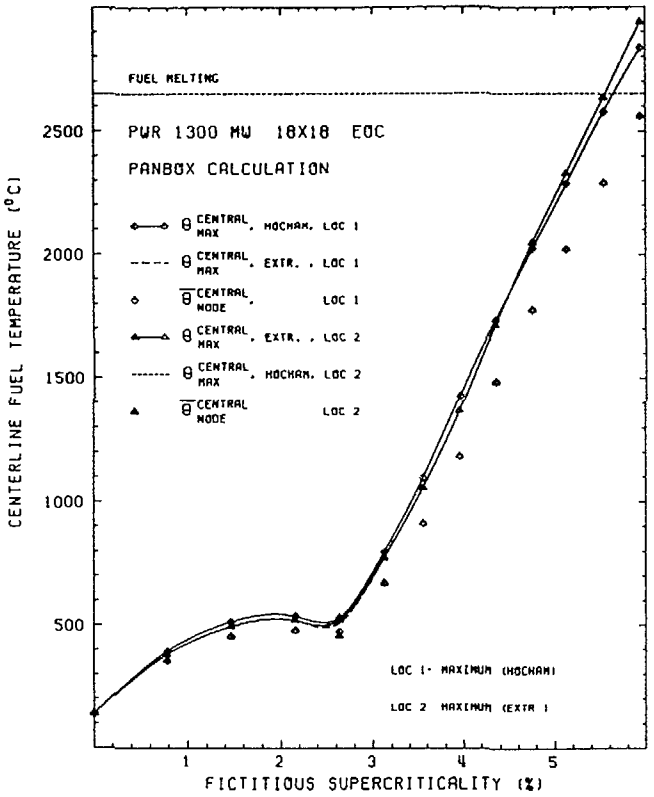

FIG. 3A CENTERLINE FUEL TEMPERATURE AFTER MAIN STEAM LINE BREAK AT ZERO LOAD CORE CONTAINING 0 % MOX-FA

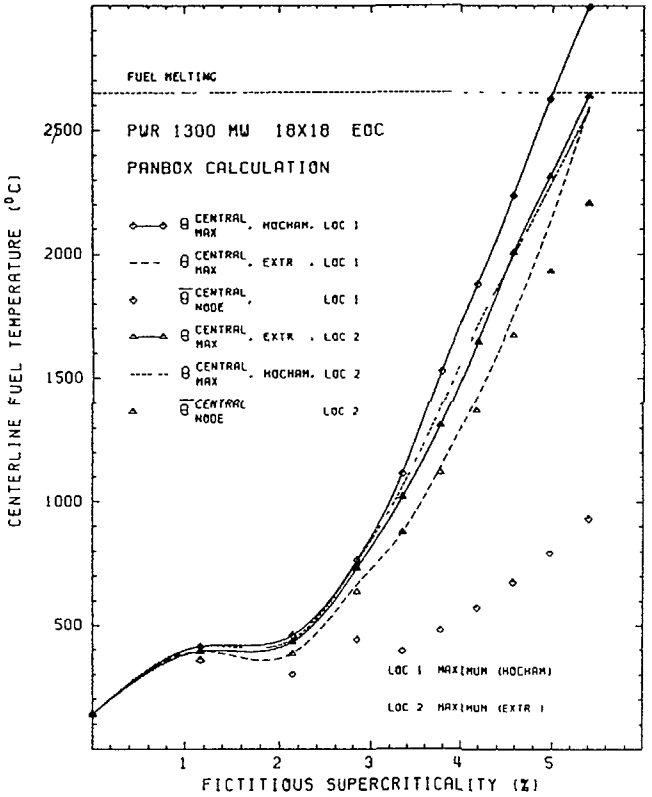

FIG. 3B CENTERLINE FUEL TEMPERATURE AFTER MAIN STEAM LINE BREAK AT ZERO LOAD CORE CONTAINING 50 % MOX-FA

6 Conclusions

The integrated program system PANBOX offers important achievements in four areas vital to future reactor design and analysis. Firstly, it couples neutron kinetics and thermal hydraulics, thereby directly taking into account their respective feedback mechanisms. Secondly, it allows 3-dimensional calculation of the reactor core on the basis of fuel assemblies or finer subchannels, also with regard to fluid flow. Thirdly, its equations are formulated and solved including time-dependence, i.e. both steady-state and transient analyses can be performed. Finally, PANBOX features flexible options for direct evaluation of safety-related parameters such as centerline fuel temperatures and DNB ratios.

PANBOX is designed for the calculation of reactor core behaviour under conditions ranging from close-to-nominal to far-off-nominal. It may be applied to any light water reactor with Cartesian or hexagonal fuel rod lattice.

The capability to calculate crossflow effects is essential to achieve the high degree of spatial resolution and accuracy aimed at in the coupled calculation. PANBOX thus can serve for high accuracy core design applications, achieving economically efficient reload strategies. Its capability to evaluate thermal safety margins based on local hot channel fuel pin values is especially valuable in safety analyses for events resulting in highly non-uniform power density distributions and/or low mass flow through the core.

References

/1/ H Finnemann, F Bennewitz, M R Wagner
Interface Current Techniques for Multidimensional Reactor Calculations
Atomkernenergie/Kerntechnik 30 (1977), pp 123-128

/2/ H D. Fischer, H Finnemann
The Nodal Integration Method - A Diverse Solver for Neutron Diffusion Problems
Atomkernenergie/Kerntechnik 39 (1981), pp 229-236

/3/ M R Wagner
Three-Dimensional Nodal Diffusion and Transport Theory Methods
for Hexagonal-z Geometry
Nuclear Science and Engineering 103 (1989), pp 377-391

/4/ H Finnemann R Böhm, J Hüsken, R. Müller J Mackiewicz
HEXTIME A Hexagonal Space-Time Kinetics Code for the
Analysis of PWHCR Transients
IAEA Technical Committee Meeting on Technical and Economic Aspects
of High Converters Nuremberg, FRG, 26-29 March 1990

/5/ H Finnemann, H Raum
Nodal Expansion Method for the Analysis of Space-Time Effects in LWRs
Proceedings of a Specialists' Meeting on
The Calculation of 3-Dimensional Rating Distributions in Operating
Reactors, Paris, 26-28 November 1979, NEA/OECD 1980

/6/ A Brandt
Multi-Level Adaptive Solutions to Boundary-Value-Problems
Math Comp 31, p 333-390, 1977

/7/ R Müller, R Boer, H Finnemann
Software Development for Reactor Simulation on Multiprocessor Systems
Proceedings of the ANS Topical Meeting on Advances in Nuclear
Engineering Computation and Radiation Shielding, Santa Fe, New
Mexico, USA, April 9-13, 1989

/8/ M. E. Rose
Weak-element Approximations to Elliptic Differential Equations
Numer Math 24 (1975) pp 185-204

/9/ R Böer, H Finnemann
MSS-AS A Pin Power Reconstruction Method Based on Weak Element
Approximations to the Neutron Diffusion Equation
to be published

/10/ D S Rowe
COBRA III C A Digital Computer Program for Steady State and
Transient Thermal Analysis of Rod Bundle Nuclear Fuel Elements
BNWL-1695 Battelle-Pacific Northwest Laboratories (1973)

/11/ R. E Masterson, L Wolf
COBRA III P An Improved Version of COBRA for Full Core
Light Water Reactor Analysis
Nuclear Engineering and Design 48 (1978),p 293

/12/ R Muller
The Hot Channel Analysis Model for Improved Local Safety Margin Evaluation
Proceedings Jahrestagung Kerntechnik 88, Travemunde, FRG
May 17-19, 1988, pp 97-100

/13/ R Bohm, H Finnemann H Roth-Seefrid
Cycle-Overlapping Analysis of Faults in Pressurized Water Reactors with Assumed
Recriticality of the Reactor Core
VGB Kraftwerkstechnik 59 (1984) English edition pp 86-93

PWR CORE PHYSICS CALCULATIONS USING THE COCCINELLE CODE

C. BANGIL, F. BLANCHON, P. HEMMERICH,
J. PLANCHARD, D. VERWAERDE, J.P. WEST
Direction des études et recherches,
Electricité de France
Clamart

A. FERRIER, V. JOURDAN
Service Etudes et projets thermiques et nucléaires,
Electricité de France
Villeurbanne

J.C. BARRAL
Service de la production thermique,
Electricité de France
Paris-La Défense

France

Abstract

In France, the large share of Nuclear (PWR) power plants in the installed electricity generation capacity has, for economic reasons, led to consider different operation modes, as well as different fuel management strategies. As a matter of fact, load follow, strech-out, together with four batches fuel management and plutonium recycling are part and parcel of EDF's nuclear reactor operation situations.

In this context and in order to improve the PWRs productivity and flexibility, calculation routes as well as surveillance systems have to take into consideration such situations that require detailed core calculations (3D, Pin power distribution...).

Therefore, EDF is developing its own core calculation tools including neutronics diffusion and thermalhydraulics codes.

As regards Neutronics, the COCCINELLE software is beeing developed for light water reactor static and kinetic calculations, mainly devoted to the following applications : Core Design, Fuel Management, Safety, Off line Monitoring, On-line Surveillance.

Major efforts of development were recently devoted to 3D space time kinetics calculations using detailed thermal hydraulics. (THYC code for 3D core thermalhydraulics and CATHARE for overall NSSS thermalhydraulics). First applications were obtained for such accidental situation as a control rod ejection or a steam line break which put forward the feasibility of such internal or external code coupling.

The paper also presents a specific module that was developed for neutron data parameters adjustment based upon 3D importance calculation. A first series of tests is presented in the case of core monitoring calculations which put forward the applicability of such a module.

INTRODUCTION

The COCCINELLE code is developed in EDF for light water reactor, 3D, static and kinetic calculations, mainly devoted to the following applications : core design, fuel management, safety analysis, off line monitoring and on line surveillance.

An overview of the COCCINELLE performances was given in reference/1/ which put forward its capabilities in terms of numerical solution methods and modellings, computing time performances and accuracy. Reference /2/ details the extensive validation work performed during an on-line PWR core monitoring using the CAROLINE system derived from COCCINELLE.

The present paper is devoted to the following core physics calculations :

- adjustment of neutronic data using 3D inverse calculations.
- 3D Space time Kinetics, with emphasis on the accident situations we have modelized by coupling COCCINELLE calculations with 3D thermalhydraulics THYC and CATHARE calculations.

2 - ADJUSTMENT OF NEUTRONIC DATA AND INVERSE PERTURBATIONS

A specific module was developed in cooperation with INRIA aimed at neutron data adjustment using 3D importance calculations.(Reference /3/). On the basis of experimental data recorded and on the comparison with calculated values, neutron data parameters may be calibrated by :

- evaluating the gradient of an error function between the predicted and measured fluxes with respect to model parameters,
- minimizing this error function with an optimization method.

The computation of the gradient is based on the Generalized Perturbation Theory, which leads to an adjoint diffusion system (which has a singular matrix) with a nonzero source term. The solution of this adjoint system, the so-called "importance" function, is obtained via a power iteration method.

A first series of tests were run using experimental data from CRUAS 2 power plant aimed at calibrating neutron reflector diffusion parameters in a coarse mesh nodal calculation.

Table hereafter and Figure 1 summarize the major results we have obtained in terms of radial power distribution, with an adjusted set of neutron coefficients:

CRUAS 2 - cycle 4 - Flux map analysis

BURN UP	103 MWD/T		5500 MWD/T	
E/C Discrepancies	Max Error	Standard Deviation	Max Error	Standard Deviation
Initial Set	11.2 %	4.5 %	8.9 %	3.4 %
Adjusted set	8.8 %	2.9 %	6.0 %	2.4 %

Such results put forward the ability of the module to improve the accuracy of the calculations. Such tests have to be pursued by considering other neutron parameters.

This module may also be used for fuel shuffling optimization.

3 - USE OF COCCINELLE FOR ACCIDENT CALCULATIONS

As regards space time kinetics calculations, efforts of development in the framework of the COCCINELLE code are devoted to the following aspects :

- Numerical methods and acceleration techniques for fast and slow transients.
- Coupling with the 3D thermalhydraulics code THYC (See Reference/1/) and concatenation of COCCINELLE and CATHARE calculations (overall NSSS thermalhydraulic code developed by CEA/FRAMATOME/EDF - Reference /4/).

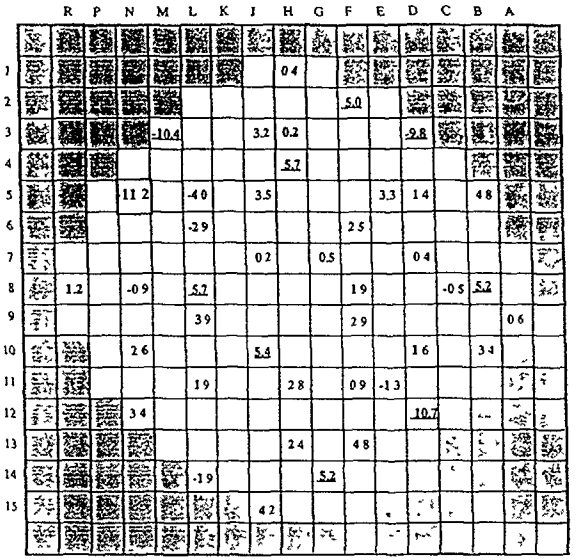

INITIAL E/C DISCREPANCIES

E/C DISCREPANCIES AFTER ADJUSTMENT OF THE REFLECTOR DIFFUSION COEFFICIENTS

FIGURE 1 : Experiment/calculation comparison on radial flux distribution

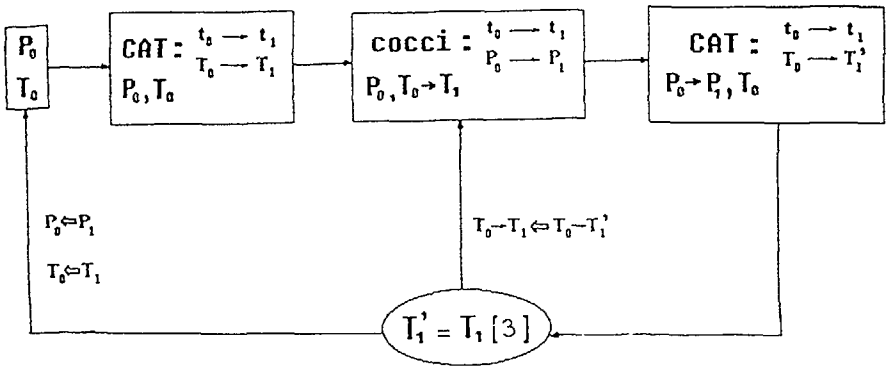

Pi : CORE POWER AT THE INSTANT i

Ti : CORE INLET CONDITIONS

Assembly temperature and pressure,
Boron concentration

FIGURE 2 : COCCINELLE/CATHARE External coupling

From the basic methodology of a steam line break accident calculation using a point kinetic model, new studies and developments are undertaken aimed at using 3D COCCINELLE space time kinetics in association with CATHARE calculations. The following sequence has been implemented (see Figure 2) :

- Overall operation conditions analysis of the reactor with the CATHARE code, using COCCINELLE results, via an external "coupling" :
  - . CATHARE provides COCCINELLE with core inlet conditions (Assembly Temperature and Pressure, Boron Concentration)
  - . COCCINELLE produces the core power distribution.
- 3D fine core power distribution assessment (COCCINELLE) at the most penalizing time.
- DNBR assessment using the COBRA core thermal hydraulic code.

The first results we have obtained so far show the feasibility of such an external coupling.

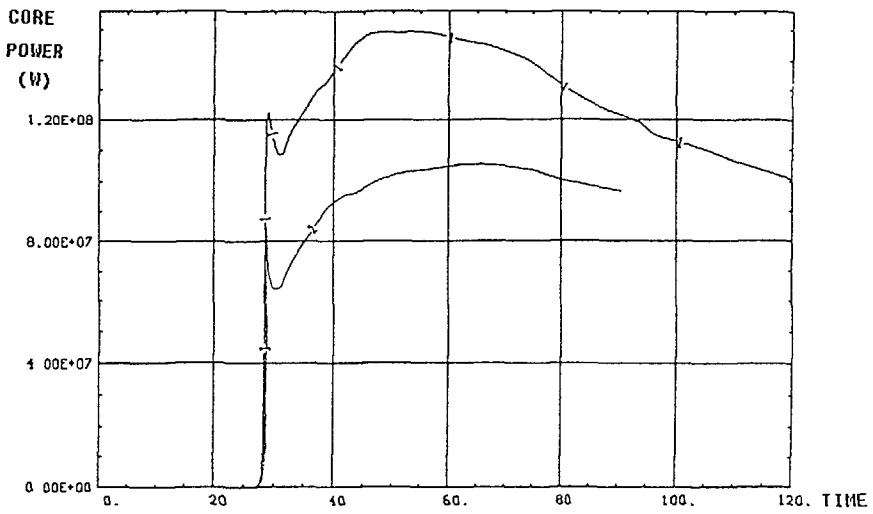

1. "Disconnected" Methodology
2. CATHARE - COCCINELLE calculations (external coupling)

FIGURE 3 : Power evolution during a steam line break accident.

A comparison is given on Figure 3 with values produced by a standard "disconnected" methodology, in terms of core power evolution during the accident.

Present developments and studies are devoted to :

- further analysis of these preliminary results to quantify conservatism of the previous "disconnected" methodology,
- optimization of the coupling methodology aimed at reducing computing times.

4 - CONCLUSION

In the present stage of development, the COCCINELLE code covers the major needs for standard PWR calculations, with a wide range of applications and capabilities.

As regards design static calculations, an extensive validation programme was performed aimed at assessing COCCINELLE's accuracy on the different core parameters, which

has evidenced the ability of the code to reproduce the different core configurations.

The present paper put forward the efforts devoted to the analysis of core accidental situations using 3D space time kinetics with detailed thermalhydraulics.

Studies are now undertaken by EDF to introduce COCCINELLE in the standard calculation route for fuel management.

Major efforts are also devoted to the following aspects : pin by pin calculations, neutron feed-back, as well as COCCINELLE's extension to hexagonal geometries in multigroup theory.

REFERENCES

/1/ COCCINELLE : a consistent software for light water reactor physics calculations ; Design, Safety, Management, Monitoring and Surveillance
International Conference on the Physics of Reactors : Operation, Design and Computation
PHYSOR 90 - April 23-27 1990 Marseille

/2/ CAROLINE : On - line 3D Surveillance System for 900 MWe PWR's
International Conference on the Physics of Reactors : Operation, Design and Computation
PHYSOR 90 - April 23-27 1990 Marseille

/3/ An off - line calibration method to improve the accuracy of a PWR reactor diffusion model.
CMEM (Computational Methods and Experimental Measurements - conference) Capri - May 89.

/4/ Assessment results of the French advanced safety code CATHARE
4 th International ENS/ANS Conference - juin 86.

CONTROLLED PORTABILITY OF FUEL MANAGEMENT SOFTWARE

S. ALTOMARE, T.M. CAMDEN, A.L. CASADEI
Westinghouse Commercial Nuclear Fuel Division,
Pittsburgh, Pennsylvania,
United States of America

Abstract

An important aspect in the transfer of technology is for design computer software to be operational on a number of computer platforms In order for Westinghouse to make its technology transfers in an efficient, controlled and timely manner to any computer system, Westinghouse adopted a set of control procedures and combined this with a set of portable software standards while still preserving the software quality assurance basis

With the dynamic changes occurring with computer hardware, computer intensive engineering calculations can now be performed on mini- computers and engineering workstations at substantially reduced hardware costs This is demonstrated by a set of Westinghouse benchmarks that were executed on several computer systems from supercomputers to engineering workstations

1. INTRODUCTION

The current trend in the nuclear industry of nuclear utility owners acquiring independent engineering analysis capability for reload core analysis requires that software be operational on a number of computer platforms. In addition, the evolution of computer hardware makes it possible to have nuclear, thermal-hydraulics and accident analysis computer codes operate efficiently on a variety of hardware with significant improvement on cost/performance ratio over mainframe computers. This is only possible if the corresponding software strategy can provide the necessary portability while preserving the software quality assurance basis.

This paper reviews the Westinghouse approach and experience in delivering its design computer programs in a controlled software environment, and presents running time benchmarking results for a number of different computer hardware

2. SOFTWARE APPROACH

Strict quality standards are required in order to generate error free software operational on a variety of computer hardware. The software delivery procedure adopted at Westinghouse maximizes portability and maintains the integrity of

the Quality Assurance basis of its software. The procedure adopted considers two key elements. Software Development Life Cycle and software standards.

The software life cycle provides a systematic approach to the development, use, and operation of all production software from initial request to final product release, and provides the framework for the evolution of the software in a controlled environment. The explicit phases of this software lifecycle include:

- Evaluation and Planning
- Functional Specification
- Software Design
- Software Implementation
- Software QA Testing
- Software Release

The software life cycle provides a framework for controlled evolution of software applications, with emphasis on upfront planning, design and testing. Extensive testing prior to software release includes the execution of a comprehensive test matrix, exercising most of the software options and comparison with reference solutions. The adoption of a software life cycle methodology is receiving increasing regulatory attention.

The Westinghouse software standards were developed in order that Westinghouse software products could execute on multiple target computer systems using a single version of the source code. The strategy employed was to organize the software into a three (3) level hierarchy:

- Application Software
- Utility Packages
- System Dependent Utilities

For the portable application code the objective was to develop guidelines that would enable the application code to be highly portable to multi-target computers The portable application code guidelines address such portability requirements as conformance to the ANSI 1977 FORTRAN Full Language Standard, naming conventions, variable initialization, FORMAT statements, data packing, etc The general purpose portable utility routines are used across all applications to perform general purpose functions. The system dependent utility routines serve to interface between the application codes and general purpose portable utilities, and the target computer system hardware and operating system

The software process adopted at Westinghouse has evolved over the years as a result of Quality Improvement initiatives. The experience obtained in delivering fuel management software to external customers indicates that these approaches are successful in minimizing installation and maintenance costs.

3 COMPUTER HARDWARE

The rapid evolution of computer hardware is forcing some changes in computer configurations for engineering calculations from mainframe supercomputers to desktop engineering workstations. These changes are coming because some of the minicomputers/workstations currently available offer necessary power and speed, and can provide the capability to support highly computer intensive applications at decreasing prices. In addition, the physical equipment is small, and is installed and operated without any significant investments in facilities and operations support

Hardware performance is usually established with the help of standard benchmarking tests, a set of controlled problems. A typical parameter of interest, MIPS (Million Instructions Per Second) can be used to rank hardware. Shown in Figure-1 are the corresponding MIPS for a host of engineering workstations varying from 1 5 MIPS to 100 MIPS. Another important consideration in ranking hardware is the cost/performance ratio ($/MIPS). The computer hardware shown in Figure-1 varies in cost from about $ 5K to $ 100K with a cost/performance ratio variation of 0 6 $K/MIPS to 2.5 $K/MIPS.

Performance benchmarks have also been established using a more representative application, 3D ANC[1] model depletion, from CPU and I/O demands. Figure-2 shows the results (running time relative to the CRAY-1S) for several different

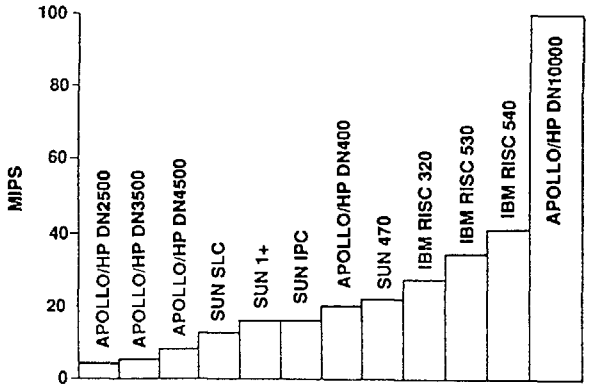

FIG 1 Workstation performance benchmarks

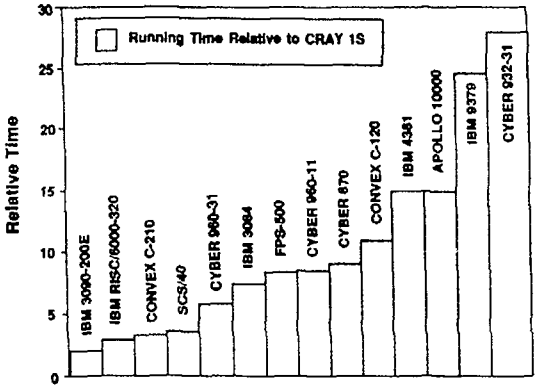

FIG 2. 3D ANC computer running time benchmarks

platforms. As can be seen, there is a wide spread on performance with a range of acceptable results for intermediate minicomputers to workstation ranges, with very favorable relative performance times. Such results are useful in guiding the definition of appropriate computer architecture for each organization according to specific requirements on computer turnaround, investment, number of users, capacity for emergency situations, and expansion capability. Other requirements that must be considered in selecting a software/hardware configuration are disk, memory, word size, compilers, network communications, etc

4. CONCLUSIONS

Fuel Management computer codes presently reside on a number of different computer systems which range from mainframe supercomputers (CRAY, IBM 3090), minicomputers (SCS 40) to APOLLO worstations. The technology transfer agreements in place provide a variety of commercial arrangements for the transfer of fuel management technology, including, computer program, design methods, and training to meet specific customer requirements. The software approach used enable the portability of design software to a variety of computer hardware hosts in a controlled fashion that preserves the qualification basis of each computer program.

The development of powerful workstations enables the availability of fuel management software to be operational effectively on dedicated workstations, with significant cost performance improvement compared to mainframes. These alternatives clearly depend on the user global computational requirements

REFERENCE

1. Y.S. Liu et al, "ANC - A Westinghouse Advanced Nodal Computer Code", WCAP-10966 NP, December 1985.

WESTINGHOUSE ADVANCED FUEL MANAGEMENT SYSTEM

Y.A. CHAO, T.Q. NGUYEN, A.L. CASADEI
Westinghouse Commercial Nuclear Fuel Division,
Pittsburgh, Pennsylvania,
United States of America

Abstract

The Westinghouse Incore Fuel Management analysis methodology has been qualified and implemented for a broad range of fuel management strategie and operating conditions Monitoring of the performance and additions to the qualification database provide a continuous process for methodology upgrades Additions to the experience database include performance for other NSSS and fuel assembly designs, including large guide thimble and off-center assembly core configuration, Mixed-Oxide reload design, and Gadolinia burnable absorber Several other functional interfaces are required for the design, safety evaluation, licensing, operation support and core monitoring of PWR cores In-core fuel management methods need to provide the data required for these interfaces in a consistent manner (format and accuracy) so as to avoid unnecessary conservatisms that penalize operational margins This paper reviews recent results in the Westinghouse Incore Fuel Management methodology

1. INTRODUCTION

The need for accurate and efficient methods for design and licensing of PWR fuel has become more important as more complex fuel assembly concepts and core designs are placed into operation. Current emphasis on plant license extension, power uprating, and high burnups introduce additional fuel management constraints that make core designs more difficult. This increased complexity requires accurate three-dimensional models for most of the analysis to avoid unnecessary conservatisms in design, safety analysis and monitoring of PWR cores.

The design, safety analysis, licensing, operational support, and core monitoring require integrated methodologies in several key areas. These areas, including Incore Fuel Management, Thermal-Hydraulics, System Transient Analysis, and analysis of incore instrumentation These methodologies require a high level of integration, in order to meet licensing requirements and Utility Customers needs

2. INCORE FUEL MANAGEMENT SYSTEM

The design, licensing, and operational support of PWR fuel requires a design system composed of computer programs and methodology that provide high level of accuracy and flexibility to meet a variety of fuel management strategies, licensing requirements, and scheduler needs.

■ PHOENIX-P/ANC Methods

The qualification of a code system requires extensive data comparison that covers a broad range of applications. Considering the initial philosophy of no empirical model adjustments, the Westinghouse system provides a quality controlled basis for methods evolution from its initial qualification [1]

Code enhancements were introduced in PHOENIX-P/ANC recently to address specific user needs. In addition, a processing code ALPHA was implemented to automate core model development, thus enhancing quality assurance basis by eliminating manual preparation of input data and processing of data files Consistent collapsed 1D or 2D models from the referenced three-dimensional model has also been completed.

The system's performance was also established for other NSSS core design and fuel features, including large guide-thimble fuel assembly designs, core layout with off-center assemblies in the periphery, Gadolinia, and MOX core designs. Core modeling benchmarked for the first two features were completed for a Combustion Engineering reactor design (133 assembly core, 14x14 fuel array). Figure 1 shows Critical boron concentration compared to measurements and Table 1 provides summary information of key startup parameters. The performance for these fuel/core configurations are consistent with the extensive database for Westinghouse reactors and fuel assembly designs

Performance for mixed-oxide fuel was included in the original qualification database of PHOENIX-P/ANC. More recent design results, including a large fraction

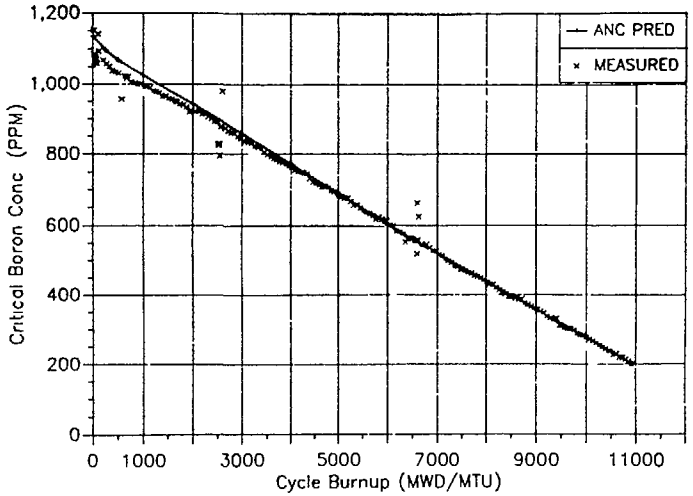

FIG 1 large guide thimble, off-center assembly core design, 133 assembly core, 14 X 14 fuel assembly

Table 1 : Large Guide Thimble, Off-Center Assembly Core Design 133 Assembly Core, 14x14 Fuel Assembly BOL HZP Physics Measurements

		Meas	Pred	Delta	
C_B ARO	(ppm)	1575	1568	-7.0	
ITC ARO	(pcm/°F)	3.1	3.7	-0.6	
Rodworth	(pcm)				
Bank 4		450	439	2.5	(%)
Bank 3		730	785	-7 4	
Bank 2		1120	1084	3.3	
Bank 1		580	609	-5 0	
S_A		1780	1755	1.4	
S_B		1580	1586	-0.4	
Total		6240	6258	-0.3	

of MOX assemblies were obtained at a two loop European plant. The critical boron concentration compared to measurement is presented in Figure 2, indicating excellent agreement. Power distribution and startup parameters showed very high level of accuracy (Figure 3 and Table 2, respectively) These results are also consistent with the overall database performance of the PHOENIX-P/ANC design system.

■ SPNOVA Methodology

The SPNOVA methodology represents the next generation of advanced nodal method to provide accurate and very fast computational capability. This methodology has been developed and qualified for PWRs applications, including static and kinetic applications [2] SPNOVA is being implemented in several different applications in a manner consistent with ANC designed-based cores.

As part of the qualification of the kinetic capability, a severe rod ejection case was analyzed. SPNOVA results were compared to those of TWINKLE, presently licensed code using a finite-difference coarse-meshed approach. The results shown in Figure 4 indicate the excellent performance and stability of SPNOVA methodology. In terms of running time, the SPNOVA case was two orders of magnitude faster than the TWINKLE's solution with a much higher level of accuracy.

■ Loading Pattern Optimization

Loading Pattern optimization is an area of focused effort, considering the benefits on fuel economics that can be achieved through optimized fuel management strategies. Enhancements added to the Loading Pattern Computer Optimization Program (LPOP) provide enhanced consistency in cross sections representation

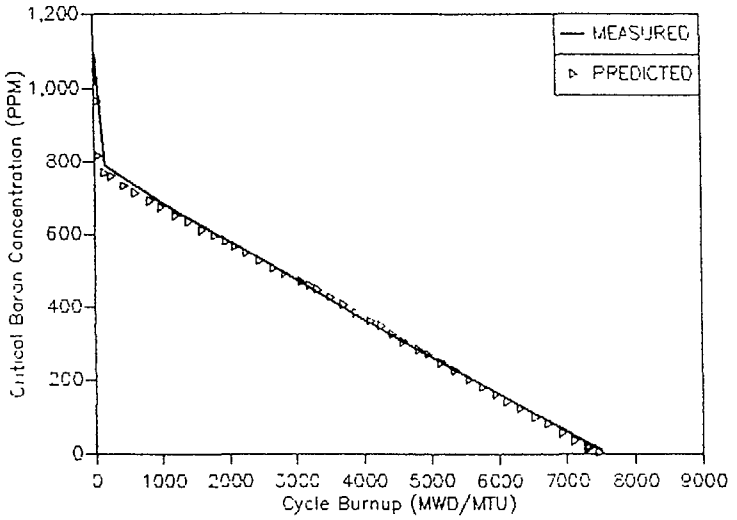

FIG 2. MOX core design — critical boron concentration, 2 loop core, cycle 19.

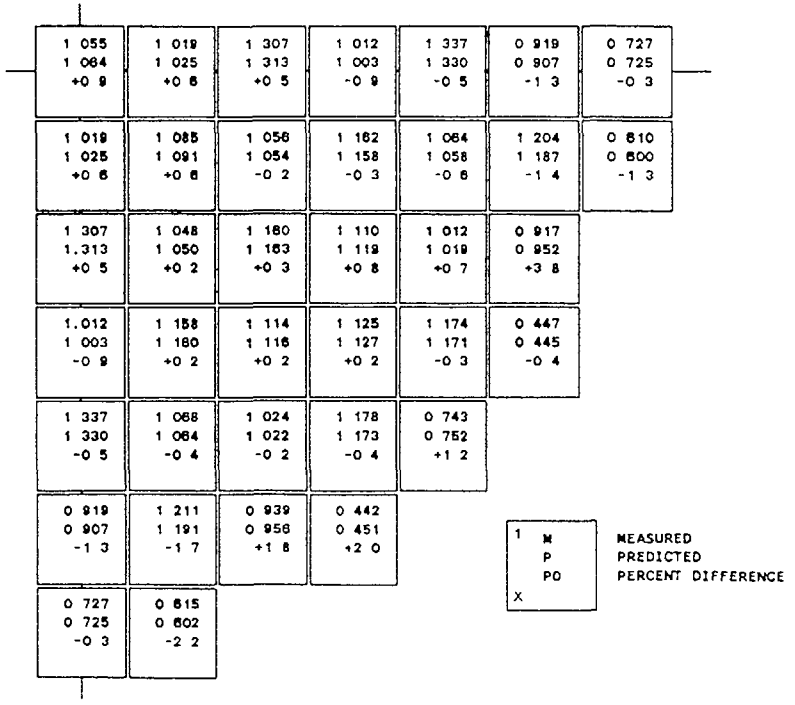

FIG. 3 MOX core design — assembly average power distribution, 2 loop core, cycle 19

Table 2 : MOX Core Design - 2 Loop Core, Cycle 19
BOL HZP Physics Measurements

		Meas	Pred	Delta
C_B ARO	(ppm)	1286	1279	7 0
ITC ARO	(pcm/°C)	-12.0	-12.1	0 1
Bank 1	(ppm)	200	198	2.0
Bank 2	(ppm)	195	200	-5 0

with ANC, and minimizes any differences in reactivity prediction The performance, compared to several cores, shows that the differences in reactivity are small and within the target band desirable for a scoping tool Therefore, it maximizes the number of acceptable loading pattern candidates that are confirmed to be acceptable with design pedigree analysis.

3. CORE MONITORING METHODS

Instrumentation systems available for core monitoring in existing plants includes moveable or fixed in-core detectors. Plant technical specifications for monitoring of limiting condition of core operations depend on the detector system available, as well as the design analysis, licensing philosophy, and core control strategy.

With the increasing need for additional margin to safety limits for plan availability and operation flexibility, improvements in core limits and operating strategies are becoming more important. Simulator based on-line systems are now being developed to provide enhanced monitoring and operational margins for existing plants. The BEACON System provides integrated core operation support capabilities which includes on-line power distribution monitoring, predictive functions, instrumentation analysis, and core follow functions.[3] The consistency between design and core operation is achieved by the use of SPNOVA as the neutronics module This approach provides a totally integrated system that minimizes model inconsistencies and at the same time, provides exceptional computational efficiency After an extensive qualification and demonstration program, this system is now being installed at two Westinghouse plants, with plans for delivery and installation in several other plants.

The qualification of this system followed a detailed plan which included the 3D core model predictions and its coupling with the on-line signals from plant instrumentation for the range of conditions covered in the plant operation Figure 5 shows a typical example of the excellent performance of the BEACON system in predicting core performance for severe load maneuvering conditions

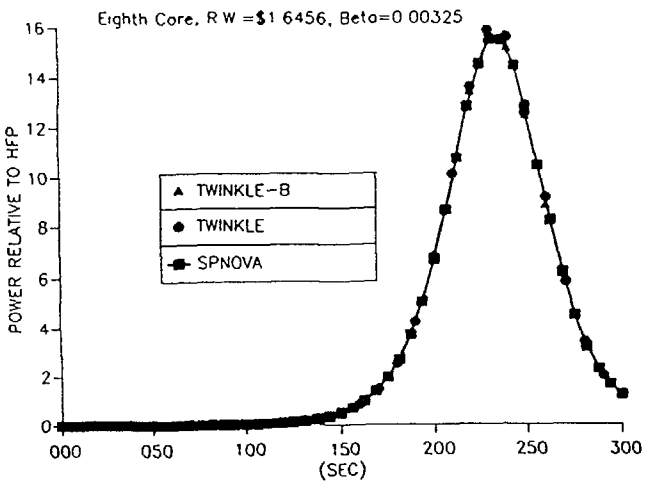

FIG 4 SPNOVA/TWINKLE rod ejection comparison, BOL, HZP conditions

4 CONCLUSIONS

The ultimate objective of the fuel management activities is to provide a strategy for fuel utilization that meets economics, operation and safety requirements. As such, Reactor Physics has to be integrated with Thermal-Hydraulics, Transient Analysis, and instrumentation systems methodologies Therefore, it is imperative that the incore fuel management tools provide information consistent with the requirements of other functional areas methodology, format and accuracy Inconsistencies in the interfaces may require conservatisms to be added with direct negative impact on operational margin

The development of Best Estimate Safety Analysis methodologies will make the interface between fuel management and safety analysis more tightly coupled The development of on-line core monitoring and predictive systems will require increased accuracy for In-core fuel management methods as they will have significantly more visibility in plant operation These trends will demand a lot more of Incore Fuel Management methods, which will require broader scope of benchmarking data and qualification efforts than presently used

The direction at Westinghouse is to achieve complete integration of reactor physics methods With the SPNOVA methodology, Westinghouse has enabled the utilization of accurate and self-consistent core models for all phases of engineering applications These applications range from core design, safety analysis, core monitoring, operations support to operations training This integration will set the framework for new applications that will provide enhanced operational and safety margins to existing plants

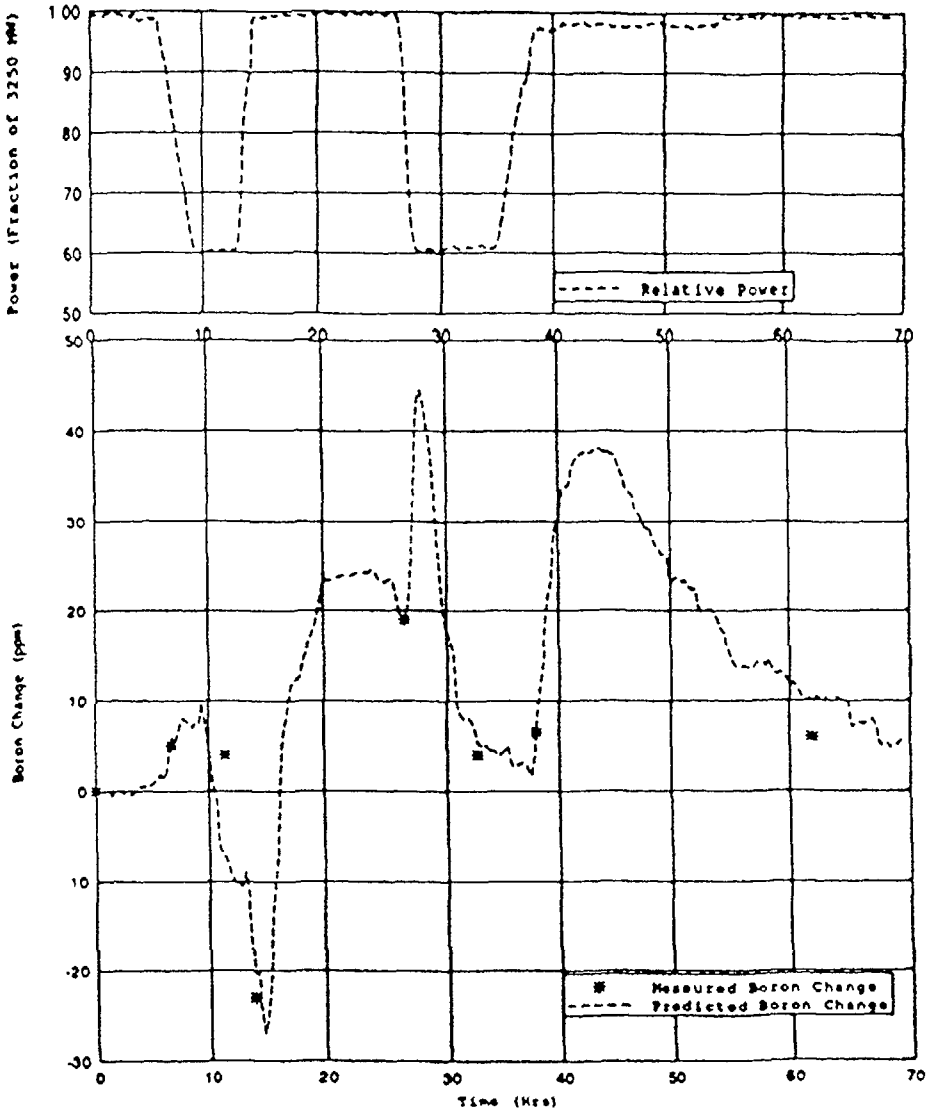

FIG 5 BEACON core monitoring system performance load follow test

REFERENCES

1. K.C. Hoskins et al., "Implementation of the Westinghouse Nuclear Design System for In-core Fuel Management Analysis", *Proceedings of the International Conference on the Physics of Reactors: Operation, Design and Computation*, Marseille, France, V.130-138,1990.

2. Y.A. Chao et al, "Theory and Qualification of SPNOVA - A Multidimensional Static and Transient PWR Core Analyzer", *Proceedings of the International Conference on the Physics of Reactors· Operation, Design and Computation*, Marseille, France, V.55-64, 1990

3 C.L. Beard et al, "BEACON Core Monitoring System: Load Follow Qualification", *Proceedings of the International Conference on the Physics of Reactors Operation, Design and Computation*, Marseille, France, XIII.51-57, 1990.

THE RITME METHOD: BASIC PRINCIPLES AND OVERVIEW OF THE LOGARITME CONCEPT

J.M. BOHLER, P. DUFOUR,
J.P. FERRERO, L. SAUVAGE
Direction des réacteurs nucléaires,
Département d'études des réacteurs,
Commissariat à l'énergie atomique,
Centre d'études nucléaires de Cadarache,
Saint-Paul-lez-Durance, France

Abstract

This paper dicusses the basic principles of the RITME method of 3-dimensionnal reactor core flux and power calculations, and briefly describes the LOGARITME development environment for implementing and managing applications based on the RITME method .

RITME is a nodal method for solving the neutron transport equation; it obtains an integral solution in which the fluxes are related to the source terms by precalculated Green functions .

The mean flux value per mesh and point flux values are calculated using a library of Green functions computed once and for all by a reference transport code . The carrier and microscopic power distributions can be determined from these flux values .

LOGARITME is a computerized environment based on software case (object-oriented analysis aid software utilities) and ADA language . It provides a consistent framework for applications using the RITME method . The general specifications of this environment are described, and potential applications are noted .

1 INTRODUCTION

RITME is a nodal method for solving the transport equation that is suitable for a wide variety of reactor cores . The possibility of performing 3-dimensionnal flux and power calculations quickly and accurately on a standard workstation makes the method available to a variety of core calculation applications .

This paper presents the method formalism through a solution to the steady-state transport equation . The LOGARITME development environment is then described .

2 THE RITME METHOD : BASIC PRINCIPLES

2.1 Flux Equations

2.1.1 Initial Equation

For the sake of clarity, the method is applied to the steady-state neutron transport equation expressed in integral-differential form .

The initial equation is :

$$-\mathrm{Div}\,(\Omega\,.\,\varphi(r,E,\Omega)) - \Sigma_t(r,E)\,.\,\varphi(r,E,\Omega) + S(r,E,\Omega)$$

migration — disappearance — sources

$$+\int\iint \Sigma_s(r,E'\rightarrow E,\Omega.\Omega')\,.\,\varphi(r,E,\Omega)\,dE'\,d^2\Omega' = 0 \qquad (1)$$

transferred

The neutron medium is assumed to be isotropic and is characterized by macroscopic cross sections noted Σ .

The fission sources $S(r,E,\Omega)$ are isotropic and associated with a fission spectrum $\kappa(E)$,

$$S(r,E,\Omega) = \kappa(E) * S(r) \qquad (2)$$

2.1.2 Notations and Definitions

By definition, the actual medium is considered to be the superposition of a "zero medium" and a "prime medium" :

* the **"zero medium"**, designated "0" is isotropic and independent of the space variable (r) . This homogeneous medium is independent of local variations affecting the neutron parameters, including boron concentration, fuel and moderator temperatures, xenon concentration, burnup, subassembly type, etc .

* the **"prime medium"**, designated "'" and dependent on the space variable describes local variations in neutron properties relative to the "zero" medium .

Symbolically, the neutron medium is then :

Actual medium (r) = "Zero medium" + "Prime medium (r) "

The macroscopic cross sections and fluxes are expressed in the following forms :

$$\Sigma(r) = \Sigma^0 + \Sigma'(r) \qquad (3)$$

$$\varphi(r,E,\Omega) = \varphi^0(r,E,\Omega) + \varphi'(r,E,\Omega) \quad \text{(angular fluxes)} \qquad (4)$$

$$\Phi(r,E) = \Phi^0(r,E) + \Phi'(r,E) \quad \text{(scalar fluxes)} \qquad (5)$$

2.1.3 Φ^0 and Φ' Flux Equations

The fluxes $\varphi^0(r,E,\Omega)$ and $\varphi(r,E,\Omega)$ are solutions to the transport equation **(1)** ; allowance for expressions **(2)** , **(3)** , **(4)** and **(5)** yields the following equations :

$$\begin{cases} -\mathrm{Div}\,(\Omega\,.\,\varphi^0(r,E,\Omega)) - \Sigma_t^0(r,E)\,.\,\varphi^0(r,E,\Omega) + \kappa(E)\,.\,S(r) \\ +\int\iint \Sigma_s^0(r,E'\rightarrow E,\Omega.\Omega')\,.\,\varphi^0(r,E',\Omega')\,dE'\,d^2\Omega' = 0 \\ \Phi^0(r,E) = \iint \varphi^0(r,E,\Omega)\,d^2\Omega \end{cases} \qquad (6)$$

$$\begin{cases} -\mathrm{Div}\,(\Omega\,.\,\varphi'(r,E,\Omega)) - \Sigma_t(r,E)\,.\,\varphi'(r,E,\Omega) - \Sigma_t'(r,E)\,.\,\varphi^0(r,E,\Omega) \\ +\int\iint \Sigma_s(r,E'\rightarrow E,\Omega.\Omega')\,.\,\varphi'(r,E',\Omega')\,dE'\,d^2\Omega' \\ +\int\iint \Sigma_s'(r,E'\rightarrow E,\Omega.\Omega')\,.\,\varphi^0(r,E',\Omega')\,dE'\,d^2\Omega' = 0 \\ \Phi'(r,E) = \iint \varphi'(r,E,\Omega)\,d^2\Omega \end{cases} \qquad (7)$$

hypotheses : Flux $\varphi'(r,E,\Omega)$ and media are assumed to be isotropic and to meet the following criteria :

$$\Sigma_s(r,E'\rightarrow E) = \iint \Sigma_s(r,E'\rightarrow E,\Omega.\Omega')\,d^2\Omega \qquad (8)$$

$$\Sigma_s'(r,E'\rightarrow E) = \iint \Sigma_s'(r,E'\rightarrow E,\Omega.\Omega')\,d^2\Omega \qquad (9)$$

$$\Phi'(r,E) = \iint \varphi'(r,E,\Omega)\,d^2\Omega = 4\pi\,.\,\varphi'(r,E,\Omega) \qquad (10)$$

Given hypotheses **(8)** , **(9)** and **(10)** , and after integrating equation **(7)** over $d^2\Omega$, the scalar flux $\Phi'(r,E)$ is the solution to the following equation :

$$-1/4\pi\,.\iint \mathrm{Div}\,(\Omega\,.\,\Phi'(r,E))\,d^2\Omega - \Sigma_t(r,E)\,.\,\Phi'(r,E)$$

$$+\int \Sigma_s(r,E'\rightarrow E)\,.\,\Phi'(r,E')\,dE' + S'(r,E) = 0 \qquad (11)$$

where ,

$$S'(r,E) = -\Sigma_t'(r,E) \cdot \Phi^0(r,E) + \int \Sigma_s'(r,E' \rightarrow E) \cdot \Phi^0(r,E')\, dE' \qquad (12)$$

2.2 Solving the Flux Equations

The A^0 and A' operators associated with equations (6) and (11) , defined by $A^0\Phi^0 = S$ and $A'\Phi' = S'$ are linear and thus integral . Consequently, fluxes Φ^0 and Φ' may be expressed as integrals over space, for a given source term neutron emission spectrum .

The kernel of operator A^0 (or A') is known as a Green function, noted Ψ^0 (or Ψ') . The scalar fluxes $\Phi^0(r,E)$ and $\Phi'(r,E)$ are expressed as follows :

$$\Phi^0(r,E) = \iiint_{core} \Psi^0(r,r',E) * S(r') * d^3r' \qquad (13)$$

$$\Phi'(r,E) = \iiint_{core} \Psi'(r,r',E) * S'(r',E) * d^3r' \qquad (14)$$

2.3 RITME - Specific Green Functions

2.3.1 Définitions

$\Psi^0(r,r',E)$ (or Ψ') is the flux at r of energy E due to one neutron/second emitted at r' , in the form of a Dirac distribution, with the spectrum of source S (or S') in the "zero" medium (or actual medium) .

2.3.2 Procedure for $\Phi^0(r,E)$

$\Phi^0(r,E)$ is by definition a flux in a homogeneous medium, therefore :

- $\Phi^0(r,E)$ will have a "clean" spatial form (no interface between different neutron media); it involves "long-range" migration, and can be calculated with a coarse mesh consistent with the migration properties of the selected "zero" medium . The "zero" medium corresponds in fact to the average neutron medium of the configuration in question .

- the Ψ^0 functions depend only on the distance between r and r' , and thus involve geometrical symmetries . For a given "zero" medium and neutron emission spectrum, they may be calculated once and for all to constitute a compact function library .

2.3.3 Procedure for $\Phi'(r,E)$

The Green functions necessary to calculate Φ' depend on the S' source spectrum as well as the r and r' media, which generally have different neutron properties .

Flux $\Phi'(r,E)$ results from "short-range" neutron effects; neutron variations between the actual medium and the "zero" medium generally take place in the thermal and epithermal energy ranges . Compared with $\Phi^0(r,E)$ it is generally a low-amplitude flux , and its accuracy is primarily related to the quality of the cross sections in the r medium . The Ψ' functions are tabulated according to sensitive parameters of the S' spectrum (e.g. the moderator density) and to characteristic neutron migration parameters (e.g. absorbers in intermediate energy ranges) .

2.3.4 Calculating the Green Functions

The Green functions for a given application are calculated once and for all using multigroup transport code . The energy discretization is fine enough to provide an accurate description of neutron migration in the high-energy ranges; these values are then condensed to a smaller number of groups for flux calculations in the application .

3 APPLICATION TO CORE CALCULATIONS

3.1 General

The RITME method yields an integral solution to the neutron transport equation with approximations concerning the isotropism of the media and flux φ' , and possible allowance for simplifying hypotheses in constituting the Green function library . It is therefore suitable for a wide variety of cores, and has been extensively qualified for PWR cores /1/ /2/ .

This section discusses the approach used to calculate a 3D flux distribution in a reactor core, with attention to some aspects of the algorithms and calculation meshes . The results are described in part 3.5 for an actual application : PRO-RITME /3/ .

3.2 Discrete Formulation of Φ^0

After dividing the core (and reflector) into meshes (subscript j), equation (13) becomes the following, for a resolution with G energy groups :

$$\Phi^0_{jg} = \sum \Psi^0_{kjg} * V_k * S_k \qquad (15)$$

where :

S_k is the neutron source density in the "emitting" mesh k

V_k is the volume of mesh k

Ψ^o_{kjg} is the flux in mesh j, of group g, due to a neutron/second emitted in mesh k according to fission spectrum $\kappa(E)$.

The Green function Ψ_{kjg} , also known as the coupling function between meshes j and k at energy g, is calculated by integrating the characteristic function of the kernel of integral operator A^o over the spatial mesh of Φ^o .

- **Mesh Characteristics**

Φ^o involves "long-range" migration in a homogeneous medium, and is calculated over the most regular possible coarse mesh for symmetry reasons, to minimize the coupling function library and the run time .

- **Calculating Φ^o for every point**

The integral formalism of RITME makes it possible to determine Φ^o at every point from the source distribution Sk and precalculated "local" Green functions :

$$\Phi^o_{j(x,y,z)g} = \sum \Psi^o_{kj(x,y,z)g} * V_k * S_k \qquad (16)$$

The emitting meshes k are meshes in which the mean flux Φ^o and sources have been calculated . The smooth shape of flux Φ^o makes it possible to interpolate the result throughout the core from a few suitably selected points depending on the type of core and application . This approach makes it possible to calculate the source term S' in order to calculate Φ' for an irregular mesh .

3.3 Calculating Φ'

Flux Φ' results from local variations in the neutron properties of the actual medium relative to the "zero" medium . It is thus advantageous to adapt the Φ'_{jg} calculation mesh to the neutron heterogeneities of the configuration . The RITME method is well suited to this type of solution using the following approach :

- Φ^o is first calculated using the Φ' mesh based on the carrier form determined from the point Φ^o flux values
- the source term S'(r,E) is then computed
- at last, Φ'_{jg} is computed from the sources S' and tabulated Green functions precalculated on the Φ' mesh .

The ability to use different,irregular meshes for Φ^o et Φ' makes it possible to use simple algorithms for a precise assessment of neutron heterogeneities such as absorber assemblies or mixed oxide assemblies, without any significant run time penalty .

3.4 Total Flux calculation

The total flux ,

$$\Phi_{jg} = \Phi^o_{jg} + \Phi'_{jg} \qquad (17)$$

is obtained after iteration of the fission sources . The procedure is carried out on the Φ' mesh; from the mean flux distribution, a carrier form (flux in homogenized medium) is obtained throughout the core by interpolation .

The microscopic flux (i.e. the flux on elementary items :cells, pins, etc.) is factorized in so far as the infinite-medium microscopic fluxes were stored in the neutron library associated with the RITME calculation .

3.5 The PRO-RITME Application

A version of the RITME code /1/ /2/ applied to a 900 MW PWR has been qualified with a coarse mesh (regular meshes 20 cm on a side).

This version is used for on-line monitoring of a PWR core as part of the PRO-RITME application .

PRO-RITME is a software package for 3-dimensionnal power reconstitution of a PWR core. The program is installed at the CRUAS 2 site , and was used to monitor the entire 4th campaign in an open-loop configuration .

This experimentation showed that the 3D RITME code can be implemented on a commercial workstation (HP9000/350 running under UNIX) for on-line core monitiring purposes, and demonstrated the code execution speed : a 3D power distribution for 2669 meshes was calculated in 3 seconds on the site using a MOTOROLA MC680320 microprocessor; the same calculation required only about 1 second in a laboratory setting with a MC68030 microprocessor .

An off-line accuracy study was conducted with static and transient tests during the experiment . Table 1 summarizes the statistical investigation for 25 static maps; similar results were obtained for normal operating transients .

Table I
Estimated Nuclear Uncertainty Factor based on a comparison between PRO-RITME and Measurements .

(%)	FUN Systematic Component	Stand. Dev calculation / measurement	FUN Random Component
Fq	-2.6	2.4	8.6
FΔHmax	-2.4	2.5	8.8
FΔH 2D	-0.1	2.3	7.3
P > 1.	-1.2	3.7	8.7

4 THE LOGARITME ENVIRONMENT

4.1 Introduction

The wide range of applications and the speed and accuracy of the RITME method make it potentially applicable for a number purposes, including on-line reactor applications (core monitoring system), on-site control aid or laboratory studies, design calculations and core control parameter studies for future reactor cores .

Work now in progress with RITME /3/ includes a workstation PWR core simulation study and control rod reactivity measurements . Each of these studies uses an application-specific RITME version . This raises problems for code maintenance and management, and prompted the implementation of a software development environment to design RITME applications efficiently with suitable quality management : this environment is known as LOGARITME .

4.2 Specifications

The wide range of applications possible within the LOGARITME environment make it indispensable to ensure portability on the hardware in use by the CEA and its partners : HP, SUN and DEC workstations, IBM and CRAY mainframes . Stringent quality assurance for the resulting applications implies that quality must be implemented by the application generator . Moreover, the model and data libraries must meet strict quality criteria regarding reliability, coupling, maintenability, and reutilization .

4.3 Methods

From a methodological standpoint, LOGARITME is based on the following :

- the Shlaer and Mellor method of modeling the problem as an entity-relation diagram ,
- the De Marco analysis method of representing the problem by data flows consistent with the entity-relation diagram ,
- the Buhr method for designing ADA program outlines from the preceding analysis .

These methods are supported by the facilities of the TEAMWORK software engineering unit, and are particularly well suited to development in ADA, the selected design and programming language .

5 CONCLUSION

The RITME method, by virtue of its simple and flexible formalism, is capable of executing flux and power calculations for a variety of cores . It has already been qualified for PWR cores in the PRO_RITME application .

Qualification of the method for other types of cores and irregular meshes will be carried out in the LOGARITME development environment .

REFERENCES

/1/ P.BERNARD - H.GIRARD - JP.FERRERO - L.SAUVAGE
Principles of the fast computing 3D PWR core power calculation method RITME .
International topical meeting on Advances in reactor physics,mathematics and computation . PARIS April 1987

/2/ P.BERNARD - H.GIRARD - JP.FERRERO - L-SAUVAGE - JC.BARRAL - A.VASSALLO
Testing and on-line applications of the fast 3D PWR core power distribution model RITME .
OECD Meeting "Incore Instrumentation and nuclear power plant core assessment " CADARACHE June 1988

/3/ L.SAUVAGE - Ph.DUFOUR - P.BERNARD - J-CRAY - M.PEYTIER - A.VASSALLO - JC.BARRAL - S.GHATTAS - B.GUESDON
Development of the RITME fast 3D core power calculation and application for reactor operation and control .
International conference on the Physics of Reactors : Operation, design and computation . MARSEILLE April 90

VERIFICATION OF ADVANCED METHODS IN TARMS BOILING WATER REACTOR CORE MANAGEMENT SYSTEM

M. TSUIKI, T. IWAMOTO
Nuclear Engineering Laboratory,
Toshiba Corporation,
Kawasaki

I. TOYOSHI
Toshiba Corporation,
Yokohama

Japan

Abstract

The TARMS (Toshiba Advanced Reactor Management System) software package was developed as an effective on-line, on-site Boiling Water Reactor (BWR) core operation management system It covers almost all the functional requirements to the current process computer to increase on-site core management capability, capacity factors, thermal margins, fuel reliability, and so on, by supporting application functions for monitoring the present core power distribution, and for aiding site engineers in making the core operation plans, by predicting future core performance

It is based on a three dimensional, 1 5 energy group, coarse mesh nodal diffusion theory code "LOGOS02", and includes advanced methods to increase the accuracy of core power distribution calculations as well as a local peaking factor calculation method by which the effect of neighboring nodes on intra-nodal power distribution can be considered TARMS has been installed in eight BWR plants and was verified to be an effective BWR core operation management tool This paper describes its advanced methods and the results of verifications with actual plant data

1 Introduction

The TARMS (Toshiba Advanced Reactor Management System) software package was developed as an effective on-line, on site Boiling Water Reactor (BWR) core operation management system It covers almost all the functional requirements to the current process computer to increase on-site core management capability, capacity factors thermal margins, fuel reliability, and so on, by supporting application functions for

-monitoring the present core power distribution, and
-aiding site engineers in making the core operation plans, by predicting future core performance

It is based on a three dimensional, 1 5 energy group, coarse mesh nodal diffusion theory code "LOGOS02", and includes advanced methods to increase the accuracy of core power distribution calculations as well as a local peaking factor calculation method by which the effect of neighboring nodes on intra nodal power distribution can be considered

To increase the accuracy of power distribution calculations by utilizing in-core neutron detector signals, a method (named "adaptive learning") was developed and implemented in TARMS The main part of the adaptive learning is automatically triggered following the whole-core TIP (Traversing In core Probe) scanning, which is performed about once in 30 through 60 days The best estimated TIP readings are then obtained from LOGOS02 simulated results, and the measured TIP readings by minimizing possible errors in the measured ones, that are caused mainly by the dislocations of the detectors Then, the best estimated nodal power is obtained by correcting LOGOS02-calculated nodal power, so that it becomes consistent with the best estimated TIP readings The accuracy of the best estimated nodal power so obtained was verified by comparing the data to gamma-scanning experiments results

Biasing factors to correct the LOGOS02 nodal power deviation from the best estimated value are obtained at the same time In the core monitoring calculations performed hourly, where LPRM (Local Power Range Monitor) readings are available, or in the predictive core simulation, where no detector signals are available, the nodal power calculated by LOGOS02 is corrected by such biasing factors "experienced" above The factor was observed to be almost independent from core operating parameters However, its axial shape was found to be weakly dependent on the coolant flow rate The biasing factor correction method was verified by core follow calculations that emulate the core monitoring and the predictive simulations

The linear heat generation rate of an individual fuel rod in a node has to be calculated to monitor fuel integrity Since nodal methods are based on node by-node homogenized diffusion equations, the local peaking factors are not straightforwardly obtained by nodal methods In the present work, a method was developed to accurately calculate local peaking factors within reasonable computing time, and was verified by comparing the factors to those obtained by multigroup, multi assembly, heterogeneous (rod-by-rod) diffusion theory calculations

2. System Overview

Figure 1 shows an overview of TARMS functional linkage The user can operate the core monitoring, and the core prediction modules via the man-machine interface It is easy to use the core monitoring module, because its function - monitoring the present core power distribution - is quite simple and requires almost no data input from the user The core prediction calculations, on the other hand, require many complicated input data Also, it is sometimes difficult to determine at what time point the three-dimensional (3D) core simulator should be run To minimize the user's operating effort, the TARMS core prediction module includes input generators and the automatic 3D core simulator drivers for typical predictive calculation patterns for, e g ,

- Haling calculations,
- control rods pattern search calculations,
- subcycle predictions,
- core startup plannings,
- scram recovery plannings,
- control rods pattern adjustment plannings

The adaptive learning is accomplished by the adaption, and the power distribution best estimate modules, fully automatically without any interaction to the user The biasing factors obtained by these modules are stored and supplied to the core monitoring, and the core prediction modules to increase the accuracy of the 3D core simulator outputs Core status data, such as the coolant flow rate, the control rod positions, and the in core detector signals, are transferred automatically from the core to TARMS via process I/O modules

3. Methods

This section presents the adaptive learning method, and the local peaking factor calculation method used in TARMS

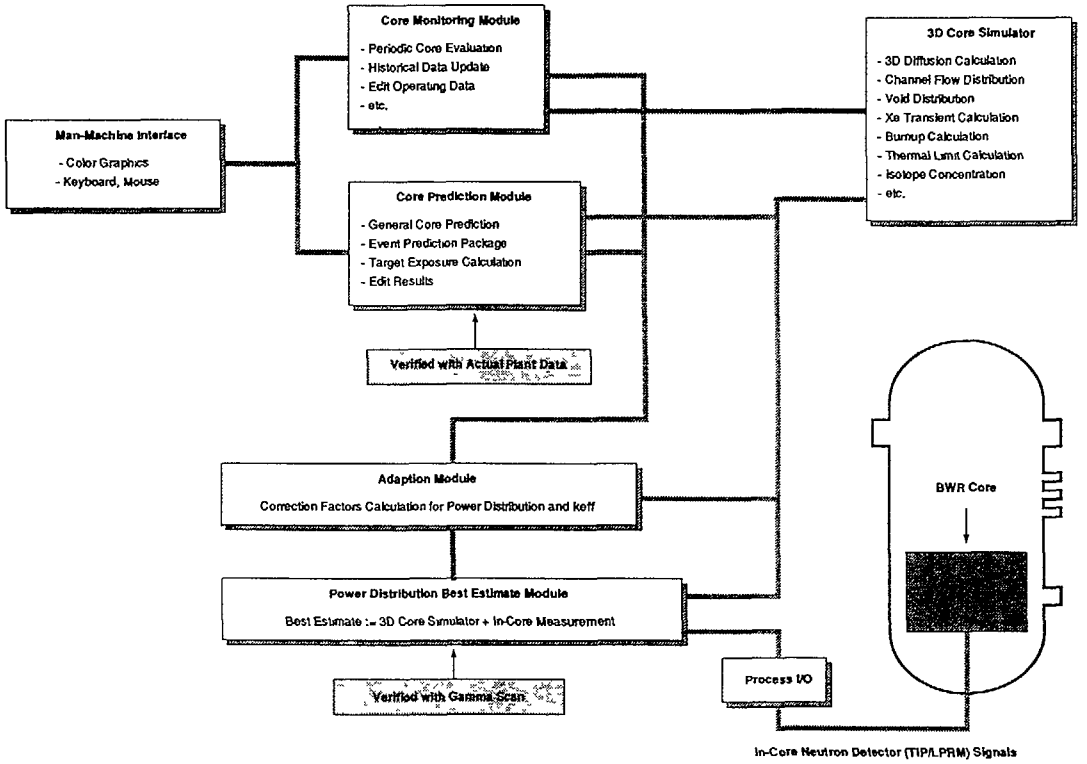

Fig. 1 TARMS functional linkage Overview.

3.1 Adaptive Learning Method

The purpose of the adaptive learning is to obtain correction factors to increase the accuracy of LOGOS02-calculated nodal power distribution. It is implemented in two phases. Phase 1 is executed following the whole-core TIP scannings (about once in 30 through 60 days). Phase 2 is accomplished in the periodic (almost hourly) core monitoring calculation.

3.1.1 Best Estimate of Nodal Power

In the first half of Phase 1, the best estimated nodal power is calculated by using the 3D core simulator and the measured TIP readings.

The 3D core simulator LOGOS02 first calculates nodal power, PC(k,j), taking into consideration core operating condition, specified by the total coolant flow rate, the core pressure, the control rod pattern, the inlet temperature, and so on. Here, (k,j) indicates a node of axial position index k in fuel assembly j. From the nodal power, one readily obtains simulated TIP readings, TC(k,i), for an axial position k of a TIP string i, by, e.g.

$$TC(k, i) = \mathrm{Sum}_j\, C(k, j)\,.\, PC(k, j) \,/\, \mathrm{Sum}_j\, 1.0, \qquad (1)$$

Sum_j : summation over fuel assemblies surrounding TIP string i,

where C(k,j) is a conversion coefficient from nodal power to the thermal neutron flux at the TIP position, obtained by the infinite lattice calculations.

Let TM(k,i) be the measured TIP readings for the same core operating condition. The simulated and measured TIP readings are generally different from each other. This is mainly because of the errors in PC(k,j) caused by approximations included in the physical model of the 3D core simulator, and due to the errors in TM(k,i) caused by the dislocations of the detectors. By comparing the results to the data obtained from gamma scanning experiments, it was found that the radial component of TM(k,i) includes a greater error than that for TC(k,i). On the contrary, the axial component of TM(k,i) agrees with gamma scanning experiments much better than that

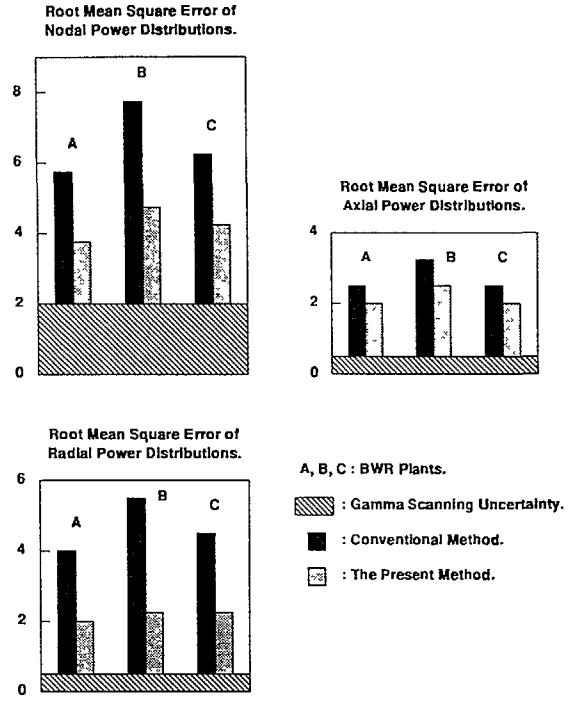

Fig. 2 Error indices of nodal power distributions to gamma scanning experiments.

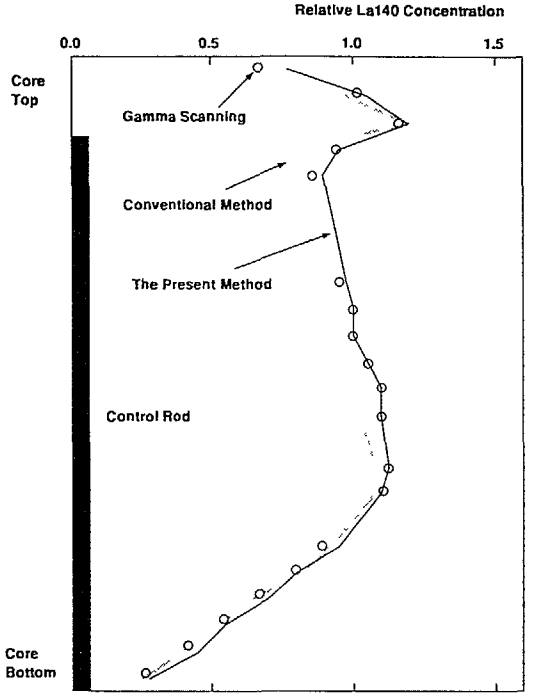

Fig. 3 Relative nodal La140 concentration comparison along a fuel assembly which was adjacent to a deep control rod, (La140 concentration represents nodal power distribution at the end of a cycle.)

for TC(k,i). Therefore, the best estimated TIP readings, TB(k,i), can be obtained by taking the axial part of TM(k,i) and the radial part of TC(k,i), namely:

$$TB(k, i) = TMa(k, i) \cdot TCr(i), \quad (2)$$

where

$$TMa(k, i) = TM(k, i) / TMr(i), \quad (3)$$

$$TMr(i) = Sum_k\, TM(k, i) / Sum_k\, 1.0, \quad (4)$$

$$TCr(i) = Sum_k\, TC(k, i) / Sum_k\, 1.0, \quad (5)$$

$$TCa(k, i) = TC(k, i) / TCr(i), \quad (6)$$

Sum_k : summation over k.

The best estimated nodal power, PB(k,j), values are obtained by correcting LOGOS02-calculated nodal power, PC(k,j), so that it becomes consistent with the best estimated TIP readings.

The accuracy of the best estimated nodal power, PB(k,j), obtained by the present method, was verified by comparing it to gamma-scanning experiments. Figure 2 shows error indices for the nodal power distributions, obtained by the present method, to those by the gamma scanning experiments for three BWR plants. This figure also shows the error indices for nodal power distributions obtained by the conventional process computer method, where nodal power is calculated directly from the measured TIP readings. As can be seen from the figure, the error in nodal power distributions, obtained by the present method, decreased to about 1/2 those obtained by the conventional method. Figures 3 and 4 show the node-by-node comparison of power obtained by the gamma scannings, by the present method, and by the conventional process computer method. In these figures, the conventional process computer method has larger errors than average, because of abnormally large radial dislocation for TIP strings. The present method gives quite accurate nodal power, in spite of such dislocation. From these comparisons, it can be concluded that the agreement of the present method with the gamma scanning experiments is much better than that for the conventional process computer method, mainly because the errors included in the radial component of the measured TIP readings are rejected in the present method.

3.1.2 Biasing Factors

In the latter half of Phase 1 in the adaptive learning, biasing factors to correct nodal power by the 3D core simulator will be calculated.

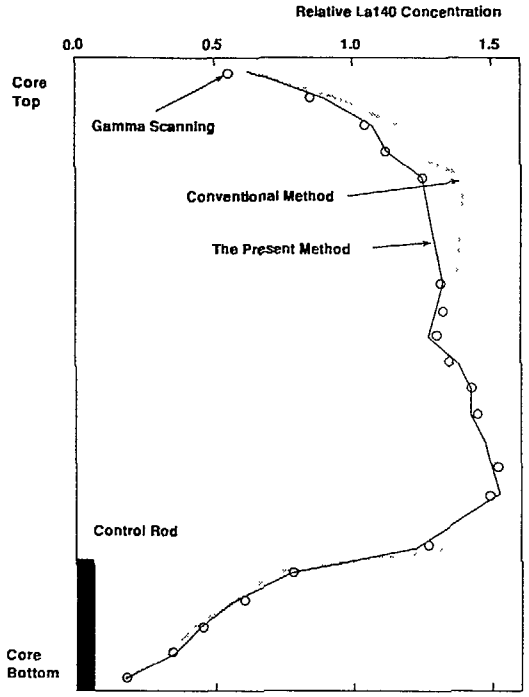

Fig. 4 Relative nodal La140 concentration comparison along a fuel assembly which was adjacent to a shallow control rod, (La140 concentration represents the nodal power distribution at the end of a cycle.)

The nodal power biasing factor, Y*(k,j), is defined by:

$$Y^*(k, j) = PB(k, j) / PC(k, j). \quad (7)$$

The factor Y*(k,j) was observed to be almost independent from core operating parameters, except that its axial shape was found to be weakly dependent on the coolant flow rate. Therefore, it is assumed that:

$$Y^*(k, j; w) = Y(k, j) \cdot A(k; w). \quad (8)$$

Where Y*(k,j;w) means the value of Y*(k,j) at coolant flow rate of w, Y(k,j) is the constant part of Y*(k,j), and A(k;w) represents the dependence of the axial shape of Y*(k,j) on the coolant flow rate.

To correct LOGOS02-calculated nodal power later in the core monitoring, and in the core prediction calculations (Eq.(10) below), the factors Y*(k,j;w) and

$$A^*(k; w) = \mathrm{Sum}_j\, Y^*(k, j; w) \quad (9)$$

Sumj : summation over all the fuel assemblies in the core.

are stored. (The factors Y* and A* should be initialized with appropriate values at the beginning of a cycle.)

3.1.3 Core Monitoring Calculation

Phase 2 of the adaptive learning is a part of the core monitoring calculation for TARMS, where the best estimate of nodal power, PB'(k,j), is to be evaluated.

In this phase, LOGOS02-calculated nodal power, PC(k,j), is corrected by the nodal power biasing factor:

$$PC'(k, j) = PC(k, j) \cdot Y^*(k, j; w0) \cdot A^*(k; w1) / A^*(k; w0)$$
$$(= PC(k, j) \cdot Y^*(k, j; w0) \cdot A(k; w1) / A(k; w0)) \quad (10)$$

where w0 is the coolant flow rate at the last adaptive learning of Phase 1, where Y*(k,j;w0) is calculated and stored, while w1 is the present coolant flow rate. As in Phase 1, simulated TIP readings, TC'(k,i), are readily obtained from PC'(k,j) by Eq.(1). At this time the measured TIP readings are not available. Instead, the measured LPRM readings, LM(k',i), are obtained for the axial LPRM position k' of TIP string i. Let TC'(k',i) be the simulated LPRM reading at position (k', i). Then, the difference between TC'(k',i) and LM(k',i) is smaller than that between TC(k,i) and TM(k,i), because TC'(k',i) is calculated from the corrected nodal power. Therefore, it is a good approximation to inter/extrapolate the ratio R(k',i) = LM(k',i) / TC'(k',i) along this LPRM string, in order to obtain an approximate value for R(k,i) = TM'(k,i) / TC'(k,i), where TM'(k,i) is an approximation for the measured TIP readings. Then, from R(k,i), one obtains:

$$TM'(k, i) = R(k, i) \cdot TC'(k, i), \quad (11)$$

The best estimated TIP readings, TB'(k,i), and nodal power, PB'(k,j), are obtained from TM'(k,i) and TC'(k,i) in the same way as in Phase 1. Here PB'(k,j) is output as the present core power distribution.

The ratio:

$$Y^*(k, j; w1) = PB'(k, j) / PC(k, j) \quad (12)$$

includes the effects of the inter/extrapolation of the ratio R(k',i). Therefore, the data are not stored as the nodal power biasing factors. However, the factor:

$$A^*(k; w1) = \mathrm{Sum}_j\, Y^*(k, j; w1) \quad (13)$$

is stored for later use, because the value of A*(k,w) is needed for a wide range of the coolant flow rate.

3.1.4 Predictive Calculation

In predicting the future core power distribution, no detector signals are available. Therefore, the best estimated nodal power values in this case are calculated by Eq.(10). The accuracy of this method was verified by making core follow calculations. Figure 5 shows the root mean square errors for TARMS-predicted nodal power and the core eigenvalue errors, compared to actual values. As shown in the figure, within the prediction period of one through two months, the TARMS predicted nodal power had an average error of 3%, and the maximum eigenvalue prediction error was observed to be less than 0.1%.

3.2 Local Peaking Factor Calculation

To certify the integrity of fuels in core performance evaluation, the linear heat generation rate, HGR(m,n), of a fuel rod m in a node n, which is defined by:

$$HGR(m, n) = C \cdot LPF(m, n) \cdot P(n) \quad (14)$$

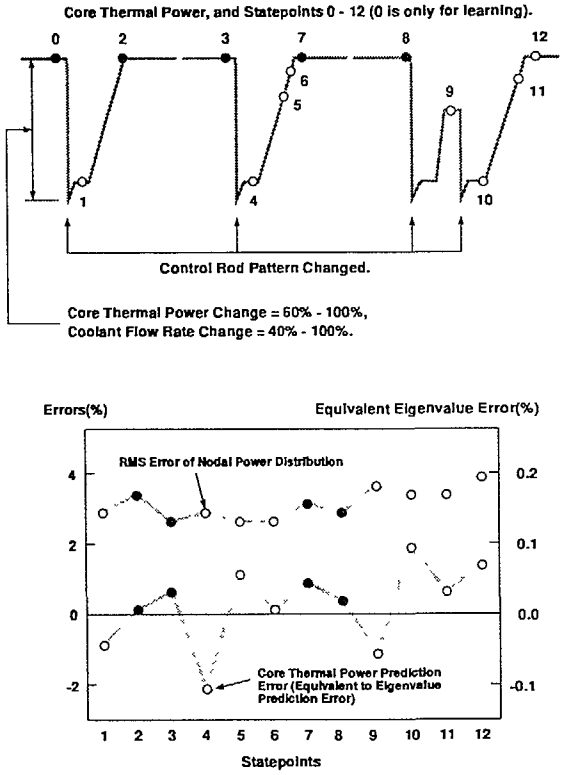

Fig. 5 Root mean square (RMS) error of TARMS-predicted nodal powers, and the core eigenvalue prediction error, observed in core follow calculations.

has to be calculated. Here, P is the average power density of node n, LPF is the local peaking factor of fuel rod m in node n, and C is the unit conversion constant (watt/cc to watt/cm). The average power density can readily be obtained from the nodal power. However, the local peaking factors are not straightforwardly obtained by nodal methods, which are based on node-by-node homogenized diffusion equations. The lowest level approximation for local peaking factors in a node is obtained by the infinite-lattice calculations of the node. However, it does not include the effect of neighboring nodes of different compositions on local peaking factors, because infinite-lattice calculations are usually carried out with zero-current boundary conditions. Several methods have already been proposed to accurately calculate LPF[1], [2], [3].

In TARMS, the local peaking factors are calculated with sufficient accuracy within reasonable computing time by a method described below. Here, the point is to take into account the effect of radially neighboring nodes on the intra-nodal power distribution. Let Q(r) be the intra-nodal power distribution, and adopt the 2-group diffusion model, then

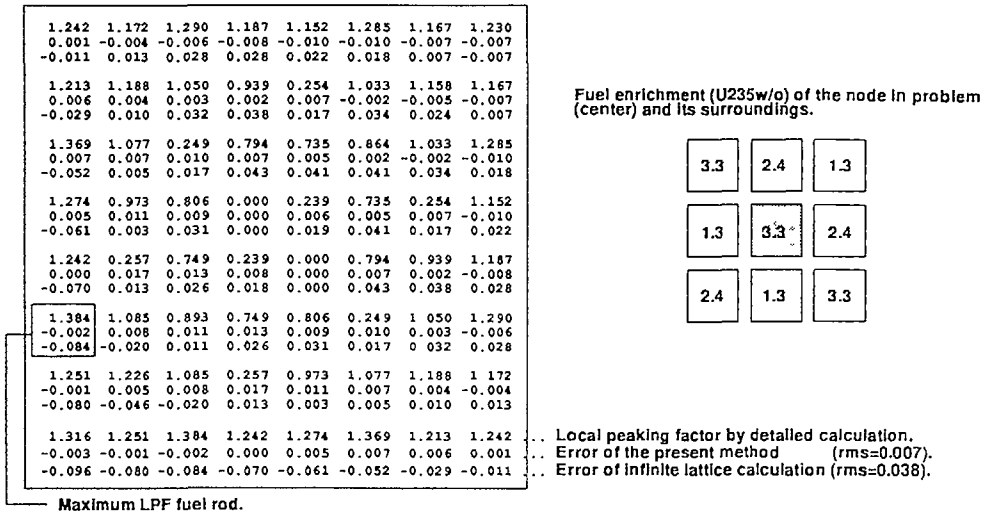

Fig. 6 Local peaking factor comparison.

$$Q(r) = Sf1(r) \cdot F1(r) + Sf2(r) \cdot F2(r), \qquad (15)$$

where r is intra-nodal spatial coordinate, Sfg(r) is the g-th group macroscopic fission cross section, and Fg(r) is g-th group neutron flux. Because the 1st (fast neutron) flux distribution F1(r) is much flatter than the 2nd (thermal neutron) flux F2(r), F1(r) can be well approximated by the infinite-lattice solution. Only the effect of neighboring nodes on thermal neutron flux will be considered. The thermal neutron flux F2(r) can be separated into:

$$F2(r) = Finf(r) + Ftr(r). \qquad (16)$$

Here, Finf(r) is the infinite-lattice solution for the thermal neutron flux, obtained by the lattice calculation. Function Ftr(r) represents the deviation in the thermal neutron flux from the infinite lattice value caused by the non-zero thermal neutron current at the node boundary. In the present method, Ftr(r) is approximated by an analytic solution of a 2-dimensional node-by-node homogeneous diffusion equation with asymptotic boundary conditions. By using the approximate solutions for thermal neutron flux and Eq.(13), one finally obtains local peaking factors in a node. The accuracy of local peaking factors so obtained was verified by comparing them to those obtained by multigroup, multi-assembly, heterogeneous (rod-by-rod) diffusion theory calculations. Figure 6 shows comparisons of local peaking factors for a node obtained by (1) multigroup, multi-assembly, heterogeneous diffusion theory calculations, (2) by the present method, and (3) by the infinite-lattice calculation. Here (2) and (3) are represented by the difference from (1). In this case, the average fuel enrichment (3.3w/o) for the node in problem (containing eight by eight fuel rods, including two water rods at the center) is relatively higher than those for its surrounding nodes. Therefore, the thermal neutrons flow into this node from the surrounding nodes, especially from the lowest enriched (1.3w/o) ones. This makes the local peaking factors of fuel rods at the lower-left part of this node larger than those of the infinite lattice calculation. As can be seen from the figure, such effects can be taken into account very well by the present method .

4. Conclusions

The TARMS *on-line, on-site* BWR core operation management system was developed, and is now in use in eight BWR plants The adaptive learning method for TARMS was tested by using actual plant data, including gamma scannings, and was verified to be effective to increase the accuracy of power distribution evaluations, both in the core monitoring, and in core predictive calculations A method for calculating the local peaking factors for fuel rods was also developed and tested by detailed heterogeneous calculations, and was verified to be sufficiently accurate It can be concluded that TARMS, with such advanced methods, can be a great aid for the operators and site engineers to manage BWR core operations.

References

[1] I Mitsuhashi "Local power peaking monitor", Japanese patent document, Tokkaisho-62-106396, 1987 (In Japanese)

[2] K R Rempe et al. "SIMULATE-3 Pin Power Reconstruction Methodology and Benchmarking", N S E , 103, 1989.

[3] T. Iwamoto et al "A method to calculate local power distribution in fuel segments", Japanese patent document, to be published (In Japanese)

THE PROBLEM OF CREATING A FULL SCALE COMPUTER SIMULATION CODE COMPLEX FOR NPPs WITH RBMK REACTORS

E.N. DANILOVA, N.K. ZINOV'EVA, L.N. PODLAZOV,
S.V. SMIRNOV, V.E. TREKHOV
R&D Institute of Power Engineering,
Moscow, Union of Soviet Socialist Republics

Abstract

At the present time one of decisive factors both in creating a new generation of reactors with improved safety and in safety of the now operating NPP's is oreation of qualitively new mathematical models and programs capable of modelling processes truly enough as well as capable of taking into account the whole complex of processes characteristic for normal NPP operation and emergency conditions.

The creation of the full scale computer code complex for NPP with RBMK is a multispectral task which requiers joint efforts of the specialists of different specialities. This task covers the choice and the justification of mathematical models of specified processes or reactor facility equipment, the choice and adjustment ("calibration") of algorithmes for digital realisation of these models, verification of computer codes and on the basis of these programs creation of programming complexes that enables NPP researchers and development engineers to carry out all necessary investigations in ease interactive form and obtain informative images of the investigations. It is obvious that each of the above-mentioned trends represents by itself a serious and large scale research work and must be the subject of a special discussion.

The present paper reviews the problem of choice and just- ification of digital solution algorithms of spatial model

and its realization on computers, as well as research technical problems which deal with the creation of the full scale modelling complex and special dialog system of communication with this complex, system that will be applicable to NPP reactors of the channel-type.

I. GENERAL ASSUMPTIONS

At the present time one of decisive factors both in creating a new generation of reactors of improved safety and in increasing a safety of now operating NPPs is the creation of qualitatively new mathematical models and computer codes capable to reproduce the processes truly enought as well as capable of taking into account the whole complex of process characteristics for normal NPP operation and emergency conditions.

In spite of this it is necessary to stipulate exactly the types of both the models and the simulation that should be mentioned in this paper.

For the total safety analysis we want to have not only the models but the models of NPPs processes and components that combines both the features of pure "mathematical" models as also the features of so-called "computer simulation" models. The models of last type now are widely spread in the NPP's training simulators and research simulators, but for the safety analysis their speed is not very important. Therefore, we must effectively combine the either.

The following main features of safety simulation models are of the most importance:

- information-object space for processes and components of the system to be modelled although does not copy the physical 3D (or more) images of its elements, but must be constructed according to the popular ideas because of extremely large value of information that excludes or brings to minimum the "training" or "getting used" function;

- the modelling a situation is a machine experiment and its organization and analysis are imposible without less or more automatized data base because of a lot of parameters to be given, calculated and analysed;

- code complex for the model must be "mobile" (that is it must be transferable from one machine to another) in corresponding computer class (mainly "main-frame" or higher), and all its components, including the data input-output, must be written in high level international standard computer language what is now the Fortran-77.

That's why the creation of full-scale code complex for NPPs with RBMK is a multispectral task which requiers joint efforts of the specialists of different specialities.

In this list of tasks are:

- the choice and the ground of different processes or equipment mathematical models of a reactor unit;

- models numerical realization methods choice and refinement;

- code verification;

- code complex creation on the ground of these codes allowing to NPP's research and development personnel to get all the necessary images of the results and to carry out their studies in friendly interactive form.

Apparently, that every of listed above areas is itself a serious and large-scale scientific work and must be the subject of special discussion [3,4,5].

Now in the institutes connected to the RBMK design and safety analyses (NIKIET, IAE, NPPRD) there are some experience of RBMK processes and component adequate models creation.

There are the mathematical models of:

- one- or two-group 3D diffusion core neutron kinetics;
- heat transfer in the reactor core graphite laying;
- two-phase time-dependent thermohydraulics of the core channels;
- primary loop, including safety systems;
- RCS logic (especialy LAR, LAZ, AZ, BAZ, plant on-line computer);
- turbine and electrical systems.

As the mathematical models being improved, the numerical realization problems being promoted to the first plan. It is especially illustrated by the comparison of requirements for algorithms fast running and modern computer industry capacity.

The present paper reviews the problems of choice and algorithms justification of digital solution of the reactor spatial model and its realization on computers, as well as researoh technical problems which deal with the creation of full-scale modelling complex and special dialog system of communications with this complex, that will be applicable to NPPs with channel-type reactors.

II. THE COMPARISON OF SOME NUMERICAL LITTLE-GROUP SPATIAL NEUTRON DYNAMICS PROBLEMS SOLVING METHODS USED FOR THE CODE COMPLEX "TROJA"

The choice of effective numerical equations solving methods is one of the most complicated problems in spatial kinetics full-scale modelling complex creation.

Now there is developed the complex problem studying technology based on the creation and computer-aided analysis of the mathematical models of the object to be investigated. This method is called a computer experiment.

It is naturally to treat a calculation algorithm like a necessary component of a computer experiment.

The same mathematical task can correspond to a number of different discrete models. However far from the all of them are suitable for a practice realization. Calculation algorithms must satisfy the contradictory requirements: the adequacy and the computer feasibility. The memory value and performance limits usualy are the main obstacle for a correctly developed algorithm computer realization.

The task specifics is in the complex transient consideration necessity in a large geometric size area and the calculation time even for the modern fast computers may be about of a number of hours. This makes important the fast running of a numerical algorithm.

The other important requirement for the numerical scheme is its absolute stability (at any $\tau>0$) and "unconditional approximation", that is the source equation acceptable

approximation with some difference scheme independently from the time step (τ) and the space step (h) corellation.

These requirements for the numerical method are connected first to the full-scale reactor core model development and it leads not only to the calculation nodes number increase (about 2000 plane points and a number of dozens hight levels) but even to the large scale diffusion equation coefficients change.

Now the implicit schemes for the spatial kinetics equations solving are of most eficiency but it does not exclude the other methods applying.

The matematical model discription

The mathematical modelling of the neutron flux behavior usualy is carried out in diffusion approximation and it leads to the parabolic nonlinear equations system solving having the zero conditons at a border. In the one-group approximation the process is described in partial derivatives equation:

$$l\frac{\partial\Phi}{\partial t} = d_r^{(1)}(D\, d_r^{(1)}\Phi) + (K_\infty - 1)\Phi - K_\infty\beta\Phi + K_\infty\Sigma \sum_{i=1} \beta_i C_i + Q_{nr} \qquad (1)$$

$$\frac{dC_i}{dt} = \lambda_i(\Phi - C_i)\,, \qquad i = 1,6 \qquad (2)$$

where: $D = D\{Dx, Dy, Dz\}$

Dx, Dy, Dz - diffusion coefficients accordingly in X-,Y-,Z-directions.

$d_r^{(1)}$ - space derivatives vector,

$$d_r^{(1)} = \left(i\frac{\partial}{\partial x}, j\frac{\partial}{\partial y}, k\frac{\partial}{\partial z} \right)$$

$$\beta = \sum_{i=1}^{6} \beta_i$$

Q_{nr} - neutron sources.

Equations coefficients D and K_∞ are functions of feedback parameters: burnup P, xenon concentracion X, fuel temperature T_f, graphite temperatureT_c, coolant density γ, the adsorber, follower or water presence (for RCS channels).

All the conventionals in eq. 1,2 are of commonuse. The equations are reduced to the finite-difference mode. In the case of implicit scheme using we can solve then both by the direct or the iterational methods.

The numerical methods

Now there are widely spread the iterational methods, in particulary the "over-relaxation" method. Those iteration methods (or succesive approximations methods) are that the decision x of the system Ax=f can be found like the limit at n going to ∞ for the succesiive approximations$x^{(n)}$, where n- iterations number. As a rule, we cannot reach this limit in finite number of iterations. Usually we set a small quantity $\varepsilon>0$ and continue our calculations while is not fulfilled the condition $|x^{(n)}-x| < \varepsilon$. We can compare the different iterational processes quality using the necessary number of iterations $n(\varepsilon)$.

The "over-relaxation" method

The "over-relaxation" method is the generalization of Seidel method and can be writen as:

$$(D + \omega A_1)\ 1/\omega\ (x^{(n+1)} - x^{(n)}) + A\ x^{(n)} = f \qquad (3)$$

where $D = diag[a_{11}, a_{22}, \ldots, a_{mm}]$ - a diagonal matrix whith the same main diagonale that is the A matrix;

A_1 - lower triangular matrix with zero main diagonals;

$\omega > 0$ - a given numerical parameter.

The method converges at $0<\omega<2$ .At the optimal choice of parameter ω the necessary number of iterations needed to obtain a given accuracy ε is of magnitude $O(h^{-1})$,but not $O(h^{-2})$ like in Jacoby and Seidel methods that is the main advantage of "over-relaxation" method to the other mentioned iterational methods.

The over-relaxation method was used in the code "TRIADA" for the 3D spatial kinetics calculations with maximun 540 plane nodes.

We firstly assumed to use the code "TRIADA" like a component of the code complex "TROJA" that includes the spatial kinetics calculations like a subsystem together with the thermohydraulics model, tne neutron physics constants calculation and the outer primary equipment model.

But after changing to the full-scale reactor model we had met the requirement to rise abruptly the number of the nodes that leads to the considerable increase the computer runtime.

Besides that the runtime, if we use this method, essentialy depends on the inserted perturbation value and this can essentialy made difficult its using.

The using of the local-one-dimensional difference schemes

According to the mentioned above assumptions it seems possible the using of implicit schemes together with the "economical" methods where the number of arithmetical operations for getting the solution is proportional to the number of nodes. Among these methods there are: variable directions method, brokenup steps method and local-one-dimensional methods.

From the special methods of accuracy $O(\tau + h^2)$ the local-one-dimensional scheme is of most economical matter. The calculations with this scheme reduces to the succession of drives in different directions. Because of the accuracy $O(\tau+h^2)$ is not sufficient for fast transients calculations it seems reasonable to use the "predictor-corrector" Yanenko scheme together with the local-one-dimensional one, that provides the accuracy $O(\tau^2 + h^2)$.

In the neutron kinetics calculation code used the local-one-dimensionals (LOS) there are realized the following economical difference schemes:

A. The Douglas-Rachford scheme:

$$\frac{U_1 - U}{\tau} = \Lambda_1 U_1 \qquad (4)$$

$$\frac{U_2 - U_1}{\tau} = \Lambda_2 U_2 \qquad (5)$$

$$\frac{U_3 - U_2}{\tau} = \Lambda_3 U_3 \qquad (6)$$

$$\hat{U} = U_3 + \tau f \qquad (7)$$

Б. The Yanenko "predictor-corrector" scheme:

$$\frac{U_1 - U}{0.5\tau} = \Lambda_1 U_1 \qquad (8)$$

$$\frac{U_2 - U_1}{0.5\tau} = \Lambda_2 U_2 \qquad (9)$$

$$\frac{U_3 - U_2}{0.5\tau} = \Lambda_3 U_3 \qquad (10)$$

$$\frac{\hat{U} - U}{\tau} = (\Lambda_1 + \Lambda_2 + \Lambda_3)U_3 + f^* \qquad (11)$$

Λ_1, Λ_2, Λ_3 -difference (variational-difference) operators correspondong to the three spatil components of the operator,

$U = U (t, x, y, z)$ - the function to be found,

$\hat{U} = U (t+\tau , x, y, z)$

$f^* = f (t + 0.5\tau ,x, y, z)$

U_1, U_2, U_3- intermediate grid functions without the independent physical meaning.

For the applying the local-one-dimensional schemes we calculate for every direction the difference three-diagonal matrix of coefficients.

Diffusion coefficient D and K_α can vary in every active element, and the D coefficient can depend on the direction, so it is the vector D = (Dx, Dy, Dz) .

Let's consider the diffusion operator:

$$LU= \frac{\partial}{\partial x} (D (r,t) \frac{\partial U}{\partial x}) + \frac{\partial}{\partial y} (D(r,t) \frac{\partial U}{\partial y}) + \frac{\partial}{\partial z} (D(r,t) \frac{\partial U}{\partial z}) \qquad (12)$$

At every fixed t in every direction this operator is approximated by the following difference expression :

$$\Lambda(t)y_i = \frac{1}{h^*} [a(x_{i+1},t) \frac{y_{i+1} - y_i}{h_{i+1}} - a(x_i,t) \frac{y_i - y_{i-1}}{h_i}] \qquad (13)$$

where the difference coefficient a(x ,t) is set like

$$a(x_i,t) = 0.5 (D_1(x_i,t) + D_1(x_{i-1},t)) \qquad (14)$$

The local-one-dimensional schemes using leads to the following two errors :

I) discretization error ;

2) error of the method, i.e. the substitution of the operator $(1 - \tau L_1 - \tau L_2 - \tau L_3)$ by local-one-dimensional reverse $(1 - \tau L_1)(1 - \tau L_2)(1 - \tau L_3)$ for a complitely implicit scheme.

Theoretical considerations show that both errors are of magnitude $O(\tau + h^2)$ or $O(\tau^2 + h^2)$ depending on the method being used

The Du Fort - Frankel three-layer scheme

The three-layer schemes sometimes are used to icrease the approximation order and to improve the stability.

The Du Fort and Frankel scheme ("rhomb") looks :

$$\frac{y_i^{n+1} - y_i^{n-1}}{2\tau} = \frac{y_{i-1}^{n} - y_i^{n+1} - y_i^{n-1} + y_{i+1}^{n}}{h^2} \qquad (15)$$

and is derived from the Richardson's explicit scheme by means of substitution in the right pert $2y_i^n$ to the $y_i^{n+1} + y_i^{n-1}$. The scheme remains explicit for y_i^{n+1} and is absolutly stabil (at any h and τ) . We can write the "rhomb" scheme like:

$$y_t^0 + \frac{\tau^2}{h^2} y_{\bar{t}t} = \Lambda y \qquad (16)$$

where: $$y_{\bar{t}t} = (y_i^{n+1} - 2y_i^n + y_i^{n-1})/\tau^2 \qquad (17)$$

The term $\frac{\tau^2}{h^2} y_{\bar{t}t}$ provides the stability . The scheme has the conditional approximation of the order $O(h^2)$ at $\tau = O(h^2)$.

So, if we put, for example, $\tau = h$, then the equation(13) will approximate the hyperbola-type equation.

The main advantage of the Du Fort and Frankel scheme is its realization simplicity. The necessity to use the small time step (in order of 0.001) is compesated by the possibility of comlete vectorization for matrix-CPU computers.

To compare the effectivities of different numerical methods we take in capacity of base variant the variant with the number calculation nodes 540*43 (540 points in plane, 43 - in hight). The calculation yields that the runtime per 1 node per 1 time step is for the:

over-relaxation method - $4.2*10^{-3}$ - $7.2*10^{-3}$ s for $\Delta\rho$ = 0.5 - 1.5 correspondingly;

local-one-dimesional scheme - $8.3*10^{-5}$ s

.Du Fort - Frankel scheme - $4.8*10^{-5}$ s.

This characteristics show that we can use the over-relaxation method for the calculation slowly changing processes allowing the time step of magnitude 0.1 s and higher. In the same time, the time step for fast transients (taking to account the RCS features simulation) can not be more than 0.01 s.

III. THE CODE COMPLEX STRUCTURE AND THE OPERATIONAL PRINCIPLES

The code complex "TROJA" is written on Fortran-77 and consist of the following main parts:

- the leading code (main);
- the neutron diffusion equation solving code (flux);
- the code for initial input from the reactor data base (cyltran);
- the control system simulation code (rcs);
- the hydrostatics and hydrodinamics boiling channels code (xfz0,sdyn);
- the diffusion equation coefficients calculation code (kcl);
- the three-dimensional distribution calculations of graphite temperature, fuel temperature and xenon concentration (termoxen);
- the data acquisition code for displaying and control the simulation (specout).

These codes works under the management of the leading code "main" as shown on fig.1

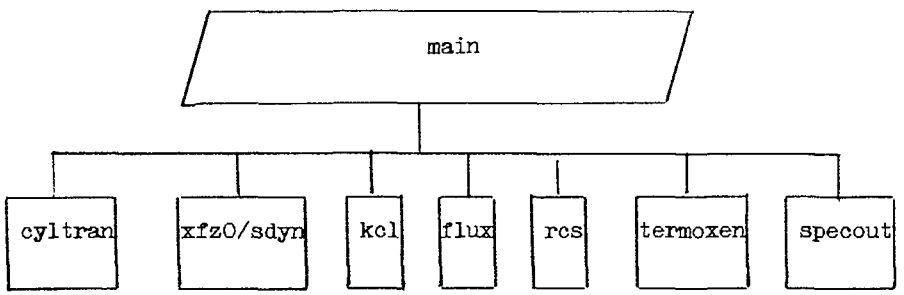

Fig.1 Complex TROJA subroutines controlled by leading code "main".

Besides that we have the data displaying codes that works in asynchronous regime of information exchange with the the mentioned above codes:

- the code to yield the "pancake-type" images, power trends and the other time-dependent graphics(z4);
- the code to yield height distributions of the oore parameters(v2);
- the code to yield isometrical images(z6).

Both z4,v2 и z6 codes interact with the main calculation code complex using the file system as shown on fig.2.

The files "foto1","foto2",... are the "snapshots" of modelled object and, using them we can make an arbitrary quantity images produced dy codes z4,v2 and z6.

The amount of simultaneosly made displays is restricted only by the needs of the research work and by the quantity of soreens available.

We have a practical experience in simulataneous usage of 15 terminals, to which the RBMK state was yielded during the control rod self-moving experiments and Chernobyl-like accident computer simulation.

The examples of yielded images are shown on the slides 1,2,3,4,5,6,7,8,9,10, applied to the report.

The file "control" contens the control information to set the simulation regime. Research-operator can, at arbitrary time, using the orbitrary screen editor, to set the change of reactor internal and external parameters at any current or future time, for example:

- to move or to stop a control rod or a group of control rods;
- to increase or to decrease the inlet coolant flow for a channel or a group of channels;
- to change the inlet enthalpy for channel or a group of channels;
- to change the steam-drum pressure.

This given parameters' set was used in practice during the RBMK accident simulation, but we can enlarge it arbitrary. Including this, according to the testing interests, we can enter the local or total flux or reactivity perturbatuions at any time.

To monitor the perturbations the results are displayed in file "inf" which cab be read using an ordinary screen editor.

The file "ixjy.p" is used for on-line changes in data lists for files "foto1","foto2",...

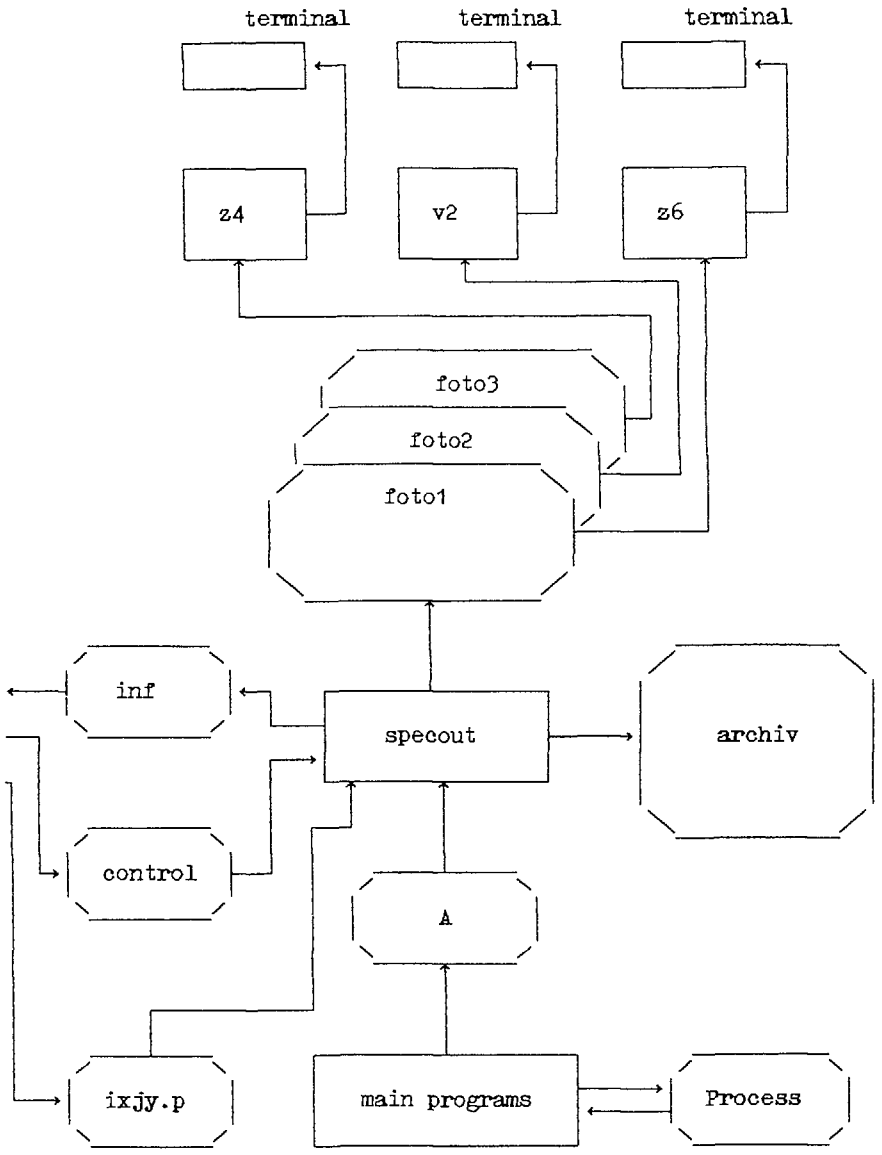

Fig.2 Asynchronous interaction calculation and reflection programs in TROJA complex

The file "A" is a set of all the necessary display parameters and is renewed per every time step.

We assume the all internal model parameters and variables gathered in file "Process".

And at list, the file "archiv" is an ordinary "history" of modelled process and includes the most informative parameters.

IV. THE ON-LINE DISPLAYING PRINCIPLES

The on-line information display task can be formulated by the following way:

- the choice of the optimal value of information to be displayed;
- the simplification of displayed information perception;
- the displaying operativity level rising.

The succes depends on the every above mentioned tasks solving.

The codes for operative displaying of the 3D NPP dynamics calculations' results are written in Fortran-77 with some possibility to use the Regis-language commands. The data transfer between display codes and calculation codes is carried out in asynchronous mode through direct access files that allows us to separate the calculation and display processes. In the case when the display code has no time for take the data from the exchange file, the data would be overwritten by the next time step data. If calculation code has no time to renew the exchange file, the display code goes to the *information waiting regime*.

We desided to use a traditional way of graphic representation of 3D-field with the three mutual-supplement components:

- the height-averaged coloured map of a field or the one-level map (vertical or horizontal) for the current or previous time step together with process trend for integral and local reactor power;
- the height functioins graphics in an arbitrary plane point at the current time step;
- the isometrical field image with user-guided colour scale at a given time step.

The mentioned above is realized by the three codes z4,v2,z6.

The code z4 outputs on a screen the two coloured maps of NPP power field. The one shows the current reactor state and the other - the previous (initial) one. For every map it also displayed the model time of the data generation, the colour scale and the graphic of two parameters, one of which is integral power and the other is arbitral. The frequency of the information renovation depends on:

- the data renovation speed;
- the quality and the magnitude of data changes considerable to the previous step, but in any case it can be regulated taking into account the ergonomical and computer experiment tasks requirements.

The code z6 outputs on a terminal screen the coloured isometrical power field image, obtained at a current time step from the calculation code. We can turn around the image on 0^0, 90^0,$I80^0$, and 270^0 .

To the same screen we output the model time, obtained from the calculation code, the colour scale and the isometrical angles marks.

Note that the colour scale in z4-code is fixed and in the z6-code is variable. This is made for z4 to simplify the maps comparison and for z6 to use the all colour range.

The code v2 outputs to the screen the hight functions graphics that describes the reactor core, for example:

- the height profile of initial neutron flux $U^{(N)}(Z)$,
- the height profile of current neutron flux U(Z),
- the local manifolding factor $K_\infty(Z)$,
- the diffusion factor $M^2(Z)$ or $L^2(Z)$,
- the coolant density $\gamma(Z)$,

for the two arbitrary choosed channels (z is the height)at current time step.

We output to the same screen the model time obtained from the calculation code, the channels coordinates and the colour scale.

We consider that the described above information value being displayed by the mentioned graphics mode is enough for operational displaying of the simulated process, but some extension can be made, for example, the control rods positioning etc.

V. THE CONCLUSION

Now in the RDIPE it is constructed the code complex TROJA that allows to solve full-scale simulation task for RBMK-type reactors. The complex has intellegent means for calculation results displaying and also the computer experiment control during the simulation that allows one to make operative decision during the modelling.

The solved tasks scope covers complicated tramsients and accidents without the core damage.

The complex TROJA is written in Fortran-77 and can be used at any computer having a Fortran-77 compiler without any modifications.

The creation of this complex required the thorough analysis, choise and improving firstly the numerical methods of neutron kinetics tasks solving.

All the methods was specially tested using the reactor neutron flux behavior criteria under the conditions of inserted flux and reactivity perturbations. And also there were choosed or specially developed the methods and the software means for operational calculation results displaying that allows to make the computer experiment analysis in an acceptable time.

Now we use the complex TROJA to carry out the comprehensive analysis of the Chernobyl accident.

LIST OF PARTICIPANTS

M.J. ABBATE
Gerencia Area Investigación
y Desarrollo
Avenida del Libertador 8250
1429 - Buenos Aires
Argentina

U. ADALIOGLU
Cekmece Nuclear Research
and Training Center
P.K. 1
Navaalani/Istanbul
Turkey

K.J. ANDRZEJEWSKI
Institute of Atomic Energy
Swierk
05-400 Otwock
Poland

C. BANGIL
EDF/DER
1, Av. du Général de Gaulle
F-92141 Clamart Cedex
France

R. BECKER
VEB Bergman-Borsig
Stammbetrieb des Kombinates Kab
Abt. NI-4
Petersplatz 9
Allee der Kosmonauten 32
D-1140 Berlin
Germany

P. BERGEONNEAU
CEA
DER/SPRC/LEDC. BT.212
CEN CADARACHE
F-13108 St. Paul-lez-Durance Cedex
France

P. BERNARD
C.E.A., Centre d'Etudes Nucléaires
de Cadarache, DRP/SPRC - Bldg. 230
F-13108 St. Paul-lez-Durance Cedex
France

W.E.O. BERNNAT
Universität Stuttgart
Institut für Kernenergetik
und Energiesysteme
Pfaffenwaldring 31
D-7000 Stuttgart 80
Germany

P. BIOUX
EDF/DER
1, Av. du Général de Gaulle
F-92141 Clamart Cedex
France

T. BISIAUX
Tour Fiat, Cedex 15
F-92084 Paris - La Défense
France

F. BLANCHON
EDF/DER
1, Av. du Général de Gaulle
F-92141 Clamart Cedex
France

G.B. BRUNA
FRAMATOME
Tour Fiat, Cedex 15
F-92084 Paris - La Défense
France

A.L. CASADEI
Westinghouse Electric Corp.
Commercial Nuclear Fuel Division
P.O. Box 3912
Pittsburgh, PA. 15230
USA

B. CHANARON
C.E.N. - Cadarache
CEA/DRN/DEC/SCOS
F-13108 St. Paul-lez-Durance Cedex
France

M. CHOUHA
FRAGEMA/FRAMATOME
10, rue Juliette Récamier
F-69006 Lyon
France

P.L. CORNILUS
Tour Fiat, Cedex 15
F-92084 Paris - La Défense
France

M.J. CRIJNS
International Atomic Energy Agency
Division of Nuclear Power
Nuclear Power Technology Section
P.O. Box 100
A-1400 Vienna
Austria

A.S. ERK
Faculty of Sciences and Arts
Yildiz University
80270 Sisli, Istanbul
Turkey

H. FINNEMANN
Siemens AG, KWU, B3/B313
Hammerbacher Str. 12 + 14
D-8520 Erlangen
Germany

E. FIORINO	ENEL Direzione Studi e Ricerche - Vice Direzione Nucleare G.B. Martini 3 I-00198 Rome Italy
M.J. HALSALL	AEA Technology Winfrith Technology Centre Dorchester, Dorset United Kingdom
K.N. IVANOV	Institute for Nuclear Research and Nuclear Energy Boulevard Lenin 72 Sofia 1784 Bulgaria
V. JAGANNATHAN	Bhabha Atomic Research Centre Theoretical Physics Division Bhabha Atomic Research Centre Trombay, Bombay 400085 India
A. KAVENOKY	Commissariat a l'Energie Atomique C.E.N. Saclay F-91191 Gif-sur-Yvette Cedex France
A. KERESZTURI	Central Research Institute for Physics Konkoly Thege Ut 29-33 Budapest XII Hungary
T. KULIKOWSKA	Institute of Atomic Energy Swierk 05-400 Otwock Poland
V.S. KUUL	Experimental Machine Building Design Buereau Gorky Russia
J.J. LAUTARD	C.E.A. DRN/DMT/SERMA/LENR Centre d'Etudes Nucléaires de Saclay F-91191 Gif-sur-Yvette Cedex France
R. LENAIN	C.E.A. DRN/DMT/SERMA/LENR Centre d'Etudes Nucleaires de Saclay F-91191 Gif-sur-Yvette Cedex France
M. LIZORKIN	I.V. Kurchatov Institute of Atomic Energy I.V. Kurchatov Sq.1 Moscow 123182 Russia
D. LUTZ	Institut für Kernenergetik und Energiesysteme (IKE) Universität Stuttgart Pfaffenwaldring 31 Postfach 801140 D-7000 Stuttgart 80 Germany
G. MARLEAU	Institut de Génie Energétique Ecole Polytechnique de Montréal Case Postale 6079, Succursale A Montreal, Quebec H3C 3A7 Canada
R. MARTINELLI	ENEA - CRE CASACCIA S.P. Anguillarese, 301 I-00060 Rome Italy
G. MATHONNIERE	C.E.N./Saclay DMT/SERMA F-91191 Gif-sur-Yvette Cedex France
G. MINSART	CEN/SCK KRO Reactor Physics (BRI) Boeretang 200 B-2400 Mol Belgium
J. MONDOT	C.E.A. Centre d'Etudes Nucléaires de Cadarache DRN/DER/SPRC/LEPh F-13108 St. Paul-lez-Durance Cedex France
E.Z. MUELLER	Atomic Energy Corporation of South Africa Ltd. P.O. Box 582 Pretoria 001 South Africa
Gérard NAUDAN	C.E.A. Centre d'Etudes Nucléaires de Cadarache DRN/DEC/SECA F-13108 St. Paul-lez-Durance France

S. NISAN
Commissariat à L'Energie Atomique
DER/SIS
Bât. 211
CEN/Cadarache
F-13115 St. Paul-lez-Durance
France

B. PETROVIC
Ruder Boskovic Institute
Materials Research and
Electronics Dept. (OOUR IME)
Bijenicka C.54
P.O. Box 1016
41001 Zagreb
Yugoslavia

I. PETROVIC
C.E.A., Centre d'Etudes Nucléaires
de Saclay, DRN/DMT/LENR/SERMA
F-91191 Gif-sur-Yvette Cedex
France

D. PEVEC
Faculty of Electrical Engineering
Department of Physics
Unska 3, P.O. Box 170
41001 Zagreb
Yugoslavia

J. PLANCHARD
E.D.F.
Direction des Etudes et Recherches
1, avenue du Général de Gaulle
F-92141 Clamart Cedex
France

V.V. PSHENIN
I.V. Kurchatov Institute of
Atomic Energy
I.V. Kurchatov Sq.1
Moscow 123182
Russia

B. ROULIER
E.D.F./SEPTEN
12-14 Avenue Dutrievoz
F-69628 Villeurbanne Cedex
France

M. SALVATORES
C.E.A., Centre d'Etudes Nucléaires
de Cadarache, DRP/SPRC - Bldg. 230
F-13108 Saint-Paul-lez-Durance Cedex
France

E. SARTORI
OECD/NEA Data Bank
F-91191 Gif-sur-Yvette
France

L. SAUVAGE
DER/SSAE
CEN Cadarache
F-13115 Saint-Paul-lez-Durance
France

J. SLOBBEN
Netherlands Energy Research
Foundation ECN
P.O. Box 1
1755 ZG Petten
Netherlands

T. SMUC
Ruder Boskovic Institute
Bijenicka C.54, P.O. Box 1016
OOUR IME
41001 Zagreb
Yugoslavia

Z. STANKOVSKI
C.E.N./Saclay
DMT/SERMA
F-91191 Gif-sur-Yvette Cedex
France

E. TANKER
Turkish Atomic Energy Authority
Alacam Sokak no.9
Kavaklidere-06690
Ankara
Turkey

J.-B. E. THOMAS
C.E.N./Saclay
DMT/SERMA
F-91191 Gif-sur-Yvette Cedex
France

V.E. TREKHOV
R&D Institute of Power Engineering
(RDIPE)
Moscow, 101000
Russia

A. TRKOV
Jozef Stefan Institute
Jamova 39
P.O. Box 100
61111 Ljubljana
Yugoslavia

M. TSUIKI
Toshiba Corporation
Nuclear Engineering Lab.
4-1, Ukishima-cho, Kawasaki-ku,
Kawasaki 210
Japan

J. VACEK
Power Machinery Plant
Skoda Plzen, Concern Enterprise
316 00 Plzen
Czechoslovakia

A. VALLEE
FRAMATOME
Tour Fiat, Cedex 15
F-92084 Paris La Defense
France

J.P. WEST

EDF/DER
1, Av. du Général de Gaulle
F-92141 Clamart Cedex
France

L. WILK

Ontario Hydro
700 University Avenue
Toronto, Ontario
M5G 1X6
Canada

Next page(s) left blank

TECHNICAL COMMITTEE MEETING AND WORKSHOP ON LWR CORE DESIGN PARAMETERS

ŘEŽ, CZECHOSLOVAKIA, 7-11 OCTOBER 1991

SUMMARY OF THE TECHNICAL COMMITTEE MEETING AND WORKSHOP

Session 1 - Benchmarks

Chairman: Mr. T.Q. Nguyen
Rapporteur: Mr. J. Vacek

Six papers concerning the reactor core benchmark calculations were presented in this session. Most of them analyze benchmarks for lattices containing Gd as a burnable absorber. The performance of simpler codes (SUPERB 1D transport, 2D-diffusion, LWRBOX 2D transport) was compared with Monte-Carlo (MONALI and MCNP) and was shown to be satisfactory. While the initial Gd worth in SUPERB was lower than that in LWRBOX, Gd depletion burns at a fasten rate. The application of RSYST to Gd-containing lattice was presented with stressing the importance of homogenization procedure and proper treatment of fission products. The results in various cases for BWR benchmark with adjacent Gd pins were near to target accuracies, but substantial differences exist between individual codes even in the case of the uniform lattice. A comparison of performance of NEA Data Bank and ANSWERS code and library versions was reviewed. The use of "1986 ANSWERS" library results in increase of k_{inf} and its slower decrease during burnup for uniform lattice and in decrease of k_{inf} for Gd cells. The application of WIMS to both calculational and experimental benchmarks was also presented in this session.

Highlights of the discussion were as follows:

1. WIMS and its library are widely used. Therefore all the library development is relevant to broad range of participants.

2. Simple methods are often successfully used in the analysis of experiments and operating data thanks to the cancellation of errors at different stages of the calculation.

3. To analyze some effect in more detail, it seems to be necessary to include into intercomparison more detailed data, e.g., microscopic cross sections or reaction rates of individual isotopes.

4. Attention should be paid to the proper treatment of Gd isotopes and fission products.

5. In advanced codes homogenization based on conservation of reaction rates is better than just flux volume weighted approach. Effective diffusion coefficient for cells with strong absorber, based on the conservation of leakage can be used to link transport and diffusion theory. The discontinuity factor should be used more widely.

6. Influence of time step length in integration of burn-up equations and of the radial pin subdivision for Gd absorbers were investigated. The analysis shows that steps of the order of hundreds of MWd/tU and 4 zones in the pin are satisfactory.

7. Data for diffusion codes can be based on the calculation of fuel assemblies with reflective boundary conditions. In more complicated lattices (MOX) and on the boundary with the reflector, more sophisticated methods should be applied.

8. The dispersion of results even for uniform lattices suggests that for the codes to be successfully applied in core analysis it is necessary to validate the computing system against the broad database of operational data.

Session 2 - Methods for Core Parameters Calculation

Chairman: Mr. M.J. Halsall
Rapporteur: Mr. V. Lelek

There were six presentations in the framework of the Session 2, concerning basic theoretical concepts, comparison with experimental data and the simulation of strong absorbers. Most of them used variational approaches to connect the experimental data with the theoretical models and to find the reasons for the differences between models and reality. It is clearly possible to use theoretical methods and experimental information together in such a way that the computer codes will smooth out random and even systematic uncertainties in experimental measurements, and will reject measurements that are definitely in error.

A new theoretical approach was formulated on the interpretation, computation, and use of the adjoint function. Further theoretical analyses are necessary to be sure that the new formulations will keep the mathematical and physical properties of adjointness. Demonstration on simplified examples would be desirable.

In the context of theory and its verification by means of benchmarks, it is necessary to formulate more explicitly what the precise targets are and within which bands the results are acceptable. Such bands or targets would add useful information to the sets of curves which are the results of benchmark calculations and code intercomparison. The use of high quality experimental data is necessary to provide the final evidence about errors and computational accuracy.

Session 3 - Core Monitoring and Experiment

Chairman: Mr. L. Sauvage
Rapporteur: Mr. O. Hrazdil

Session 3 consisted of two topics
(a) Core Monitoring
(b) Experiment

Core Monitoring:

Three papers were presented in this part of the Session 3. The PC controlled system of CAMAC units used for the measurement and for the evaluation of the basic safety and reactor physics parameters of the experimental reactors in NRI at Rez was described. This system has been used for the measurement of the critical height, reactivity, reactivity coefficients, buckling, radial and axial neutron flux distributions on the LR-0 and LVR-15 experimental reactors. An overview of the use of the RITME method for on-line applications and studies based on 3-D PWR core simulation was presented. The simulator is used in a testing facility for PWR core monitoring and instrumentation optimization. An advanced core monitoring and operational support system, BEACON, was also presented with an outline of the numerical scheme, hardware requirements and applications of the system to improve plant operational flexibility and availability.

Experiment:

Three papers were presented, all concerning experiments on the LR-0 reactor in NRI at Rez. An outline of recent experimental programmes for WWER core parameters estimation was presented. The versatility of LR-0 reactor for experimental studies of core parameters was demonstrated on a study concerning the interpretation of a self-powered detector response. WWER reactor dosimetry and pressure vessel exposure monitoring is a programme which is aimed to increasing the pressure vessel life. Model experiments performed on LR-0 in connection with this programme were presented and the PC experimental data base and the evaluation programmes were described and discussed. For years the LR-0 reactor has played a significant role in the verification of the accuracy of calculation methods. Some examples of this testing were also presented.

Session 4 - Fuel Management

Chairman: Mr. H. Moldaschl
Rapporteur: Mr. J. Rocek

Many of technical and economic features of a nuclear plant are cross-coupled and partially nonlinear. Thus, when calculating energy costs the complete set of all influences should be considered. While complex computer programs can improve precision for design, they do not necessarily foster understanding of fundamental interrelations. Therefore a rather simple plant model ("COMO") developed at Siemens and based on existing results and experiences is under preparation, which considers all important design parameters and process variables, e.g. water side corrosion with temperature correction, optimization of the power history or the RPV fluency. Since fuel expenses are an important component of total nuclear power costs, the first module of the above mentioned code deals with the core and the fuel cycle. A set of examples is given. Another modules for the steam generator and the whole secondary loop are under preparation.

Results of analysis of the departure from nucleate boiling ratio (DNBR) for an equilibrium cycle of an advanced PWR core with prolonged nuclear fuel burnup carried out at VINCA were presented. The analysis and the results given indicate that increasing the total discharge burnup and introducing advanced refueling schemes require more sophisticated safety analysis, i.e. more detailed both physical and thermal-hydraulic calculation models and methods.

Activities in Turkey concentrate on one step from the in-core fuel management of PWR, which includes: (i) a criterion to select the best reload pattern; (ii) power and depletion calculations on trial patterns to check the safety constraints; (iii) an optimization method to determine the best pattern. Strong dependence on initial guess pattern was observed, so that the method generates and calculates final patterns for each of the distinctly different initial guesses. The optimization method was found suitable for sifting through a large number of possible patterns, to select a few to be analyzed more accurately.

The advancement of powerful engineering workstations has made it possible to have thermal-hydraulics and accident analysis computer programs operating efficiently with a significant performance/cost ratio compared to large mainframe computer. Recognizing these trends Westinghouse adopted a software development life cycle process for the software development activities which strictly controls the development, testing and qualification of design computer codes. In addition, the results of comprehensive test matrices establish the Quality Assurance basis and consistency for the same software operating on different computer platforms.

The KARATE program system of the Hungarian Atomic Energy Research Institute has been constituted to calculate WWER-1000 units. Test results obtained for the first fuel cycle of NPP Kalinin are given. The calculated boron concentrations agree fairly well with the measurements. The k_q distributions are also in accord with the measurements, though there the experimental values are sometimes contradicting. As to the axial shapes, they suit fairly well, but some corrections of the extrapolation distances at the top and bottom of the core should be introduced.

The FUMACS code package developed at the University of Zagreb enables in-core fuel management analysis of PWR core. Its validation was performed by comparison of FUMACS results with design parameters for the first eight reload cycles of NPP Krsko core. The differences between obtained results and reference data show that the FUMACS code package is the fast and reliable code system suitable for repetitive and numerous in-core fuel management calculations.

Conclusions of the session were as follows:

1. The development effort on the one hand and the large amount of knowledge available, offer the chance of performance of optimization procedures for the whole power plant on a work station.

2. The large amount of nuclear energy installed, asks for a perfect calculation of all important parameters and variables to decrease uncertainties.

3. The wide-spread of nuclear energy also asks for coupled treatment of neutronic-thermohydraulic problems for quasi-stationary and fast dynamics calculation.

Session 5a - Core Design of WWER

Chairman: Mr. M. Makai
Rapporteur: Mr. J. Svarny

The presentations indicate a tendency in WWER using countries to verify their core design and operational codes. The presentation pointed out the need for an up-to-date safety analysis of WWERs. The verification is done by benchmark calculations and by comparison to experiments. Extended measured data on critical facilities (ZR-6, LR-0) are available and help the verification. As to the benchmark problems, they are just being set out. The first calculations of the Kalinin-1 benchmark revealed contradictions in the benchmark data.

In conclusion the following recommendations can be formulated:

1. The endeavor of WWER users to reassess safety analysis requirements should be assisted by recommendations concerning the structure and methodology of SAR.
2. The verification of core calculation raises such problems as software documentation, quality assurance, verification standards etc. IAEA assistance in this field is desirable.
3. The effort to define benchmark problems should be countinued. The benchmark data should be revised taking into account the remarks above.
4. Those having capabilities of WWER calculations are encouraged to calculate the proposed benchmarks.

Session 5b - Core Design for PWR, BWR, HWR

Chairman: Mr. M. Nurdin
Rapporteur: Mr. P.D. Krishnani

In this session papers on various aspects of core design sight from the design of the core to the design of spent fuel pool and thermal hydraulics for studying, hot spots were presented.

The experimental reactors of early design were having 93% enriched U-235. In order to prevent the proliferation of such a highly enriched fuel (HEU) it is being suggested to use low enriched uranium (LEU) with enrichment less than 20%. The design of small LWRs using LEU and SEU fuel developed in Argentina were presented. The particular case of HEU to LEU fuel conversion was also considered. Finally, he discussed the optimization of the fuel management by taking into account the radioisotope production requirement of RAS.

In order to improve the accuracy of calculation for Th-core fuel management, a new Indonesian procedure to overcome the over-estimation of the worth of the control fuel assembly was discussed. It was interesting to see the corrections applied depending upon the environment and the equivalence of homogeneous transport and diffusion calculations.

A paper presented the results under various conditions for a 300 MW(e) PWR calculated using the lattice code WIMS D-4 and 2-D diffusion code EXTERMINATOR-2.

A physical and mathematical model used in the Romanian thermal hydraulic code COBRA-VI-I for hot spot analysis of fuels for both LWRs and PHWRs was discussed. Included were some results obtained in assessing the degree of conservatism of the hot spot factors evaluation during the LWR core thermohydraulic design.

Workshop Session 1 - IFM Code Package Validation for PWR

Chairman: Mr. D. Pevec
Rapporteur: Mr. V. Jagannathan

Under the CRP on In-core Fuel Management (IFM) Code Package Validation for PWRs, the present status was reviewed and future plan of action by different participants was discussed.

During the previous RCM in Vienna (December 1989), there were only participants present from Spain, Yugoslavia and India. South Africa, Turkey and the IBK Institute from Belgrade have joined later in this CRP. The country status is given below:

Spain: Calculations for cycle-1 follow-up have been completed. Cycle-2 results are to be provided.

Yugoslavia (Zagreb): Revised calculations following some changes in input data will be completed in 3-4 months.

India: Results of a 2-D code (Level-2) for the two cycle follow-up analysis were submitted in March 1991. Revised reformatted data can be provided in about 6 months.

South Africa: All results have been received.

Turkey: Calculations are to be started. All possible results of level-2 codes will be provided by about 6 months.

Yugoslavia (Belgrade): Similar to Turkey.

The participants have been provided with a specific format for submitting the results of lattice analysis. Additional temperature points have also been included.

Workshop Session 2 - IFM Code Package Validation for WWER

Chairman: Mr. M. Makai
Rapporteur: Mr. S. Thomas

Workshop session 2 discussed the problems of WWER benchmarks, which form part 3 of the CRP on In-core fuel management. The WWER benchmarks consist of two parts:

- first six fuel cycles of WWER-440, Kozloduy unit 2, submitted by Mr. T. Apostolov;
- first six fuel cycles of WWER-1000, Kalinin unit 1, submitted by Mr. V. Saprikin.

The CRP participants began solving the benchmarks and presented the first results at the TCM. The session concluded that the WWER-440 benchmark was well documented, the minor errors could easily been corrected. However, major errors and discrepancies were found in the WWER-1000 benchmark. The participants could not clarify them and they proposed to contact Mr. Saprikin for eliminating the discrepancies in the benchmark.

In addition to the WWER-1000 benchmark, Mr. T. Apostolov presented a benchmark problem and solution for Kozloduy unit 5, a WWER-1000 unit. The benchmark was based on the first two fuel cycles. The operational history was specified and the assembly features are the same as in the Kalinin unit 1 benchmark. Some participants volunteered to perform also a calculation on this benchmark.

The participants were sorry that the submitted benchmarks did not include reliable experimental data for comparison thus creating a physical benchmark. Benchmark parameters were discussed and suggestions were made for values of needed input parameters.

Workshop Session 3 - Homogenization Techniques/Cross Section Representation

Chairman: Mr. M.J. Halsall
Rapporteur: Mr. T.G. Nguyen

1. Homogenization Techniques

Dr. Halsall began by giving an overview of the cross section generation process for core model calculation.

Some discussion arose as to the need for such a topic as it was pointed out that there are many publications/references available. Overall, the audience reached a consensus that this topic is worthwhile and they would like to hear what is being done by others.

Dr. Nguyen discussed the fundamentals of homogenization as to why it is needed. Comments were given by Dr. Nguyen and supplemented by Dr. Halsall as to the strengths and weaknesses of various approaches (flux-volume weighted constants vs. reaction rate matching etc). The concepts of discontinuity factors and diffusion coefficient adjustment were discussed. Specific examples were given for both lattice and baffle/reflector region homogenization schemes in the PHOENIX-P and WIMS codes. The discussion was supplemented by several questions from the audience.

2. Cross-section Representation

Both Westinghouse and Winfrith cross section representation approaches were presented. In general, a macroscopic cross section model is used in core calculations. Feedback mechanisms (such as water, doppler, boron, xenon, samarium) are treated either microscopically or by interpolation of tabulated data. History effect treatments were discussed and the general consensus is that this effect is relatively small and can be ignored or treated in a simple manner by tracking fast to thermal flux ratios.

COMPARISON OF DIFFERENT WIMS LIBRARY VERSIONS

J VACEK
Nuclear Engineering Plant,
Škoda Plzeň,
Plzeň, Czechoslovakia

Abstract

This year Skoda has rented the authorized version of WIMS from the ANSWERS service. This version of the code is accompanied by the 1986 version of the multigroup library. Employing different versions of the code and its library now available at SKODA Nuclear Engineering Plant, we aim to evaluate the differences in results caused by the use of different library versions and to assess their effects on the core characteristics

Basically, the use of the new library results in the increase in the multiplication factor for experimental lattices and initial core states and, due to the modificatiuon of fission product cross sections, to its slower decrease during burn-up. While the latter property seems to have an favorable effect on results for VVER analyses, the overall improvement of multiplicative properties has to be carefully analyzed, as it is directly reflected in such basic core characteristics as the boron acid concentration and the cycle length.

This year Skoda has rented the authorized version of WIMS from the ANSWERS service. This version of the code is accompanied by the 1986 version of the multigroup library. At the time being, we have at our disposal several versions of the code and its libraries. Currently in use is the WIMS-D/4 version acquired from NEA Data Bank (NEA 0329/13) with associated library received on July 2, 1990, and the WIMSD2A version rented from ANSWERS service with "1986' data library (AEEW-R 2133), which has been in use since February 1991. Both versions are operated on IBM-4341 mainframe, adapted NEA version also on the IMB-PC compatible personal computer. Both versions can use either version of the library.

Comparison of NEADB and ANSWERS versions performance with different multigroup libraries is presented In Table 1. It can be concluded that not the version of the program, but the version of the library makes a substantial difference

What troubles us a bit is a remarkable difference between 8-group and 2-group values of k-inf in NEADB version It is probably connected with incorrect interpretation - while k-inf in 8 groups is computed using corresponding leakage spectrum, k-inf in two groups is determined using zero leakage spectrum When

TABLE 1. WIMS - Test Case 4

Program version Library version	NEA NEA	NEA ANSWERS	ANSWERS NEA	ANSWERS ANSWERS
k-inf, SPECTROX	1.305346	1.320454	1.305343	1.320462
PIJ Dancoff, inner	0 49836	0.50344	0.49836	0.50344
k-inf, SPECTROX	1.306369	1.322803	1.306366	1.322808
k-inf, CHAIN 14	1.294323	1.310701	1.294332	1 310734
k-eff, Benoist	1 218156	1.233064	1.218174	1.233126
Pu-239 w/%, 500MWd/t	2.763E-2	2.367E-2	2.730E-2	2.374E-2
Pu-239 siga-epi	14.98	17 10	15 11	17 26
Pu-239 siga-th	1167.0	1174 7	1165.3	1173 2

Program version = NEA, library version = NEA

	input bucklings	buckling search ratio	radial	axial
k-inf 8 groups	1.289212	1.272370	1.271955	1.272552
k-inf 2 groups	1.293813	1.292195	1.292238	1 292176

ZADOC option is used with NEADB version, values of fission cross sections are not correct and ZADOC option is not compatible with MOMOD. Test case considered corresponds to standard WIMS Test Case no. 4.

At the end of the last year, a new WIMS Library Update Project has been initiated by the IAEA, coordinated by J.Stefan Institute. As we have been using WIMS for many years and intend to use it further on, we are naturally interested in any WIMS development and therefore we would like to take part in the cooperation proposed. We will not be able to participate in generation of WIMS multigroup libraries from basic nuclear data files, as we have no financial support for such an activity, but we are prepared to participate in solution of selected problems using available libraries. The solution of numerical benchmarks suggested for the first stage of the Project is presented in Table 2.

To assess an influence of the library version on the burnup, we re-solved a widely used Yankee burnup problem. Results are presented in Figure 1.

An influence of the new library version on the results for lattices containing Gd absorbers is illustrated in Figs. 2 and 3 Results presented here under WIMS correspond to [4], WIMS86 are new results with ANSWERS library, Lutz correspond to [5], Lutz-2 to [6], Psenin to [7] and Prodanova to [8] Fig. 3 suggests that the inclusion of complete Gd chain (present in 1986 WIMS library) results in decrease in k_{inf}. The discrepancies between the results of different codes are still remarkable

TABLE 2. TRX and BAPL Lattices

ANSWERS version + library

	TRX-2	TRX-1	BAPL-1	BAPL-2	BAPL-3
k-eff	0.9980	0.9959	0.9975	0.9974	0.9988
k-inf	1.1727	1.1880	1.1476	1.1516	1.1378
B**2	53.92	55.58			
delta 25	0.0601	0.0977	0.0825	0.0674	0.0519
ro 28	0.8377	1.3369	1.1429	1.1767	0.9249
delta 28	0.0728	0.1017	0.0791	0.0682	0.0561
MCR	0.6369	0.7876	0.8078	0.7367	0.6588

NEA version + library (IAEA-TECDOC-567)

	TRX-2	TRX-1	BAPL-1	BAPL-2	BAPL-3
k-eff	0.9965	1.0011	1.0039	1.0017	0.9999
k-inf	1.1643	1.1833	1.1461	1.1484	1.1328
B**2	53.37	57.39			
delta 25	0.0612	0.0996	0.0840	0.0686	0.0529
ro 28	0.8000	1.2719	1.3395	1.1187	0.8821
delta 28	0.0688	0.0962	0.0758	0.0656	0.0541
MCR	0.6329	0.7769	0.7939	0.7267	0.6528

Experiment

	TRX-2	TRX-1	BAPL-1	BAPL-2	BAPL-3
delta 25	0.0614	0.0987	0.084	0.068	0.052
+-	0.0008	0.0010	0.002	0.001	0.001
ro 28	0.837	1.320	1.39	1.12	0.906
+-	0.016	0.021	0.01	0.01	0.01
delta 28	0.0693	0.0946	0.078	0.070	0.057
+-	0.0035	0.0041	0.004	0.004	0.003
MCR	0.647	0.717			
+-	0.006	0.008			

Basically, the use of the new library results in the increase in the multiplication factor for experimental lattices and initial core states and, due to the modificatiuon of fission product cross sections, to its slower decrease during burn-up. (compare Figs. 2 and 3). This conclusion is in good agreement with comparison of both data libraries performed by Halsall in [2] and others, e.g. [3]. While the slower decrease in multiplicative factor seems to have an favorable effect on results for VVER analyses, the overall improvement of multiplicative properties has to be carefully analyzed, as it is directly reflected in such basic core characteristics as the boron acid concentration and the cycle length. All few-group diffusion data libraries generated for VVER-440 and VVER-1000 reactors in Skoda are based on the older WIMS library and the

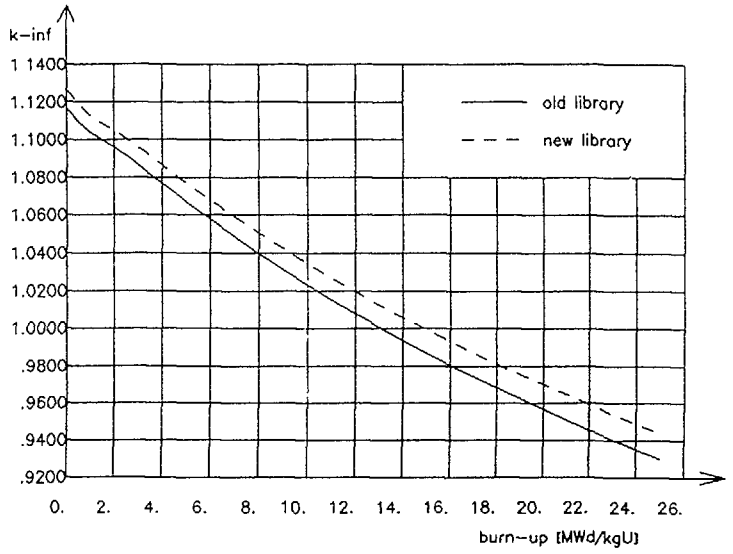

Fig. 1. Yankee – burnup

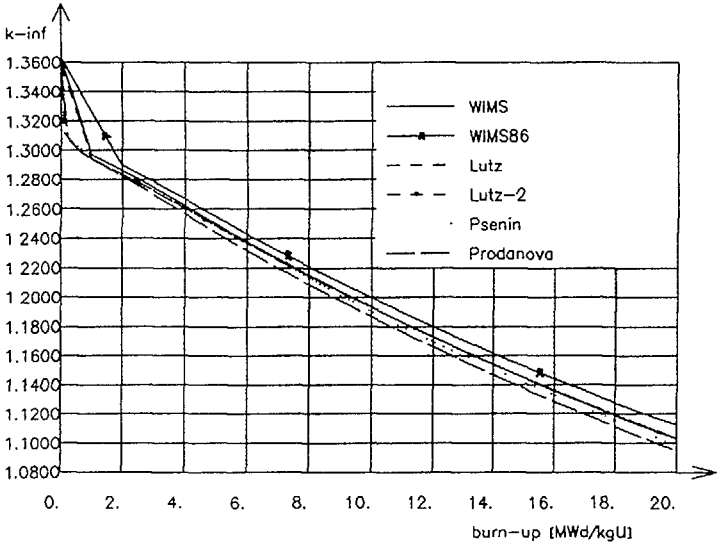

Fig. 2. Sidorenko benchmark – cell

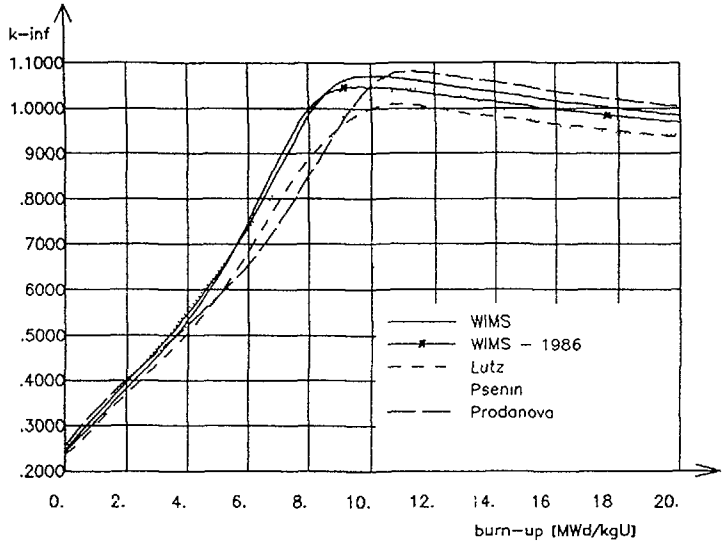

Fig. 3. Sidorenko benchmark – Gd cells

library change would imply re-evaluation of all core follow results and adjustment of new few-group diffusion library to operational data. The effect of the library change confirms a necessity to establish a comprehensive data base of operational data which can be used to validate and adjust libraries of few-group diffusion data.

REFERENCES

[1] WIMS Library Update Project, IAEA, 1991
[2] M.J. Halsall: Recent Adjustments to the WIMS Nuclear Data Library, AEEW-R 1492, May 1982
[3] W.Oosterkamp: EPRI Pin Cell Calculations Using Different Code Packages in the Netherlands, ANSWERS 1991 Reactor Physics Seminar, May 1991
[4] J.Vacek, P.Mikolas: Experience with the WIMS Computer Code at Skoda Plzen, in: In-Core Fuel Monagement Practices, IAEA-TECDOC-567, IAEA, Vienna, 1990
[5] D.Lutz: Results for the Sidoreko Benchmark, IKE, 1989
[6] D.Lutz: Results for the Sidoreko Benchmark, 2nd version, IKE, 1990
[7] V.V.Psenin et al.: Calculation Results for Gadolinium in Fuel Rod Lattices, CRP on Safe Core Management with Burnable Absorbers in VVERs, IAEA, Vienna, 1989
[8] R.Prodanova: Some Results on Benchmark Problem Calculations under Research Contract no. BUL-5599, CRP on Safe Core Management with Burnable Absorbers in VVERs, IAEA, Vienna, 1989

ANALYSIS OF THE ARKUSZEWSKI BENCHMARK BY 1-D SUPERCELL, 2-D COLLISION PROBABILITY AND MONTE CARLO METHODS

V. JAGANNATHAN, P.D. KRISHNANI, H.C. GUPTA
Bhabha Atomic Research Centre,
Trombay, Bombay,
India

Abstract

The Arkuszewski benchmark is a square lattice assembly with 8 uranium pins surrounding a Gd loaded fuel pin. For this problem details of K-infinity, absorption and production rates at zero burnup alone are required to be computed. Results from Monte Carlo method using a cross section library based on ENDF/B-V data are available which can be treated as reference values.

We have used 69 group WIMS library. Cross sections for Gd isotopes were generated here from their resonance parameters. The above benchmark was solved by a 1-D supercell approach, a 2-D collision probability method and a Monte Carlo method. This paper discusses the results obtained using these three methods.

1. INTRODUCTION

Due to the very high absorption occuring in the Gd-loaded fuel pins, the applicability of the standard light water spectral codes to Gd lattices is questionable and requires profound verification. For this reason a calculational benchmark [1] was suggested for the analysis in the RCM on safe core management with burnable absorbers in VVERs [2]. It consists of 8 unpoisoned fuel pins surrounding a poisoned pin (3*3 assembly). The results of the Monte carlo simulation using an ENDF-B/V based cross section library have also been presented which can be considered as a preliminary reference analysis [1]. These results can also serve to check the cross section data base.

We have analysed this benchmark using three methods (i) 1-D supercell approach [3], (ii) 2-D collision probability method [4] and (iii) Monte Carlo method [5] The latter two analyses have been performed using 69 group WIMS cross section library In the first method a condensed 28-group WIMS library was used

A brief description of the three methods used in the analysis is given in Section 2 Section 3 gives problem specifications for the benchmark Results of the analysis are summarised in Section 4

2 CODES USED IN THE ANALYSIS

The calculations were performed using the computer codes SUPERB, LWRBOX and MONALI The computer codes SUPERB and LWRBOX are used for latticeburnup analysis of LWR lattice cells and MONALI is a general geometry Monte Carlo code A brief description of these codes is given below

2 1 METHOD IN SUPERB

In the computer code SUPERB the calculations are performed in three steps In the first step, various pincell types according to their enrichment and Dancoff factors are identified in the lattice cell The multigroup transport calculations are performed by interface current method in 1-D cylindrical geometry for these pincells and the multigroup cross sections for these lattice cell are spatially smeared

In the second step, a series of supercell calculations in multigroups are performed in 1-D cylindrical geometry by interface current method for assembly lattice cell, and for various heterogeneities such as water rod, poisoned pin or an absorber rod We consider a water rod, a poisoned pin or an absorber rod at the centre of the supercell, surrounded by rings of fuel pincell paste regions Multiple rings are considered for the poisoned fuel pin The presence of other water rod or other absorber materials in the surrounding rings is ignored in this calculation The cross sections are collapsed to few (five) groups by using the appropriate supercell ring spectra For fuel isotopes microscopic cross sections are condensed after multiplying with respective flux advantage factors of pincell calculations For non-burnable regions macroscopic cross sections are condensed after multiplying with disadvantage factors For water rod and absorber rods the homogenisation and group collapsing are done upto the equivalent area of a pincell by normal flux and volume weighting procedure

In the third step, the 2-D fuel assembly cell is analysed by few group diffusion theory Reflective boundary condition is used Five point centre-mesh finite differencing of the diffusion equations is used The eigenvalue or K_∞, flux and power distribution are obtained from this calculation

2 2 METHOD IN LWRBOX

The computer program LWRBOX has been developed to calculate lattice parameters as a function of burnup for rectangular assemblies of LWRs In this code, the multigroup integral transport equation is solved by the combination of small scale collision probability (CP) method and large scale interface current technique In this method, the whole lattice cell is divided into several connected cells which can further be subdivided into homogeneous zones The interaction between various zones within a cell and their contribution to outgoing currents at cell interfaces are directly calculated by the CP method Each cell is connected to neighbouring cells by interface currents At these interfaces, the angular flux in the incoming and outgoing direction is separately expanded in terms of spherical harmonics The simplest assumption is that of isotropic angular flux or popularly known as cosine current approximation (i e , one term expansion) This approximation has been found to be adequate for normal calculations However, at present, upto six terms can be considered in the code LWRBOX Another basic assumption of the method is that

the scalar flux is constant in each zone of the region (i e , flat flux approximation)

2 3 COMPUTER CODE MONALI

The computer code MONALI is a Monte Carlo code primarily written for calculating nuclear parameters associated with thermal reactors The parameters calculated by the code include multiplication factor, neutron flux, material absorptions, and leakage from outermost surfaces Treatment of anisotropy is possible upto the first order The geometry module can handle any region which can be enclosed by a set of quadratic surfaces Six special forms including planes, cylinders and spheres are also present Any number and combination of the surfaces can enclose a region The outermost surface can also be any combination of these surfaces Any of the three boundary conditions, namely, reflective, white or vacuum boundary condition can be applied on the outermost surfaces Neutron absorption is accounted by reducing the weight at each collision When the weight reduces below a user defined value the neutron history is terminated by Russian Roulette Fluxes are calculated by any of the three estimators, namely, track-length, collision, or expected track-length estimators Frequency distribution of the multiplication factor is also found The Shapiro and Walk normality test is optionally applied to the batch estimates of the multiplication factor Application of the test gives an indication about the adequacy of the batch size The code has restart option also

3 PROBLEM SPECIFICATIONS

The Arkuszewski benchmark [1] is a square lattice LWR assembly with 8 uranium pins surrounding a gadolinium loaded fuel pin Fig 1 gives the cell numbering after taking into account the symmetry of the problem The cell geometry specifications are given below

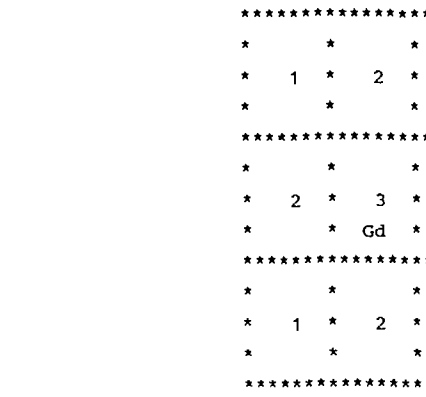

Fig 1 Numbering of cells

Fuel pellet radius	0 41135	cm
Inner clad radius	0 4215	cm
Outer clad radius	0 4815	cm
Lattice pitch	1 35	cm
The generic material specifications are		
Regular fuel enrichment (U-235)	3 19	w/o
Regular fuel density	10 126	g/cm^3
Gd fuel enrichment (U-235)	3 48	w/o
Gd fuel density	10 106	g/cm^3
Gd_2O_3 fraction	2 99	w/o
Clad density	6 55	g/cm^3
Water density	0 9983591	g/cm^3
Temperature of medium	20	^0C

4 RESULTS

In the following results, 69-group WIMS library has been used with identifiers 235, 2238, 3239 for U-235, U-238 and Pu-239 The cross sections for Gd-155 and Gd-157 have been obtained from their resonance parameters The resonance table numbers 235 4, 2238 4 and 3239 1 respectively, have been used for the three isotopes mentioned above However, the calculations by the computer code SUPERB were performed by a condensed 28 group WIMS library

The calculations by LWRBOX have been performed by considering 1 zone each in the fuel and clad and 2 zones in the water in the radial direction and 4 divisions in the azimuthal direction in the cells containing unpoisoned fuel pins and 5 zones in fuel, 1 in clad and 2 in water in the radial direction and 1 division in the azimuthal direction in the cells containing poisoned fuel pins 1 term has been considered in the expansion of angular flux at cell interfaces

The results for this benchmark using the MCNP code have also been provided [1] The code MCNP is Monte Carlo code and these results have been obtained using a cross section library based on ENDF/B-V data These results are also given in the following tables

The Tables 1 and 2 give the different eigenvalues and the power, flux and absorptions in the three cells Unit absorption in the entire solution domain is assumed for flux normalisation The eigenvalue calculated by the computer code LWRBOX compares well with the MCNP value However, the k_∞ calculated by SUPERB and MONALI are higher by approximately 1 8% and 1 1% respectively The absorptions in the Gd cells are underpredicted by SUPERB code and relative pin powers as calculated by different codes compare well The one-group integrated flux as calculated by the three codes compare well except in the Gd cell in which the SUPERB value is approximately 3 % larger compared to other codes

Table 1 Eigenvalues for the Arkuszewski Benchmark

Computer code	Eigenvalue
SUPERB	1 1182
LWRBOX	1 1018
MONALI	1 1119 ± 0 0023
MCNP	1 1010 ± 0 0022

Table 2 Local distributions of power flux and absorption

Computer code	U-Cell 1	U-Cell 2	Gd-Cell
	Relative power density		
SUPERB	1 122	1 059	0 279
LWRBOX	1 120	1 060	0 281
MONALI	1 120	1 060	0 283
MCNP	1 0885		0 2916
	One Group Flux integral		
SUPERB	3 908	3 860	3 624
LWRBOX	3 900	3 841	3 544
MONALI	3 924	3 856	3 537
	Relative absorption distribution		
SUPERB	0 100	0 0953	0 219
LWRBOX	0 0985	0 0941	0 2297
MONALI	0 0992	0 0947	0 224
	± 0 0087	± 0 0083	± 0 0451

Table 3 gives the absorption and production rates of the Gadolinium and Uranium isotopes in the 3 different pincells for two energy groups with cutoff energy at 0 625 ev and for single group

In general, the results of LWRBOX and SUPERB are on opposite sides of MONALI results and they are within 1 % of MONALI values The absorption in Gd isotopes is more in the LWRBOX results and less in SUPERB results compared to the Monte Carlo values As a result of this, the K_∞ calculated by LWRBOX is low compared to SUPERB

Tables 4 and 5 give the one and two group microscopic cross sections of U, Pu and Gd isotopes In Table 4 they have been calculated using the following definition

$$\sigma_{xGn} = \sum_{i \in f} V_i \sum_{g \in G} \sigma_{xgn} * \phi_{ig} \Big/ \left(\sum_{i \in f} \sum_{g \in G} V_i \phi_{ig}\right) \qquad (1)$$

Table 3: Absorption and Production rates 1 and 2 Groups
(cutoff 0.625 ev)

		U-Cell 1			U-Cell 2			Gd-Cell 3		
		SUPERB	LWRBOX	MONALI	SUPERB	LWRBOX	MONALI	SUPERB	LWRBOX	MONALI
	A 1/2	-	-	-	-	-	-	5 57-3	5.52-3	5.48-3
Gd-155	A 2/2	-	-	-	-	-	-	3 03-2	3.24-2	3.13-2
	A 1	-	-	-	-	-	-	3 59-2	3.79-2	3.68-2
	A 1/2	-	-	-	-	-	-	2 71-3	2.69-3	2.68-3
Gd-157	A 2/2	-	-	-	-	-	-	1.40-1	1.50-1	1 44-1
	A 1	-	-	-	-	-	-	1.43-1	1.52-1	1.47-1
	A 1/2	8.60-3	8.55-3	8 59-3	8 67-3	8.53-3	8 56-3	8.99-3	8 80-3	8.95-3
	A 2/2	5.67-2	5.56-2	5.62-2	5.30-2	5.25-2	5.27-2	6 62-3	6 92-3	6.91-3
U 235	A 1	6 54-2	6.42-2	6 48-2	6.17-2	6.10-2	6.12-2	1.56-2	1.57-2	1.59-2
	P 1/2	1 45-2	1.44-2	1.44-2	1.45-2	1.43-2	1.44-2	1 50-2	1.48-2	1.50-2
	P 2/2	1.17-1	1.15-1	1.16-1	1.09-1	1.08-1	1.09-1	1 35-2	1.41-2	1 41-2
	P 1	1 32-1	1.29-1	1.30-1	1.24-1	1.23-1	1 23-1	2.85-2	2.89-2	2.91-2
	A 1/2	1.87-2	1.85-2	1 86-2	1 87-2	1.84-2	1.86-2	1 78-2	1 74-2	1 77-2
	A 2/2	7 24-3	7.08-3	7.16-3	6.76-3	6.69-3	6.72-3	8.55-4	8.89-4	8.87-4
U-238	A 1	2.59-2	2 56-2	2.58-2	2 54-2	2.51-2	2.53-2	1.87-2	1.83-2	1.86-2
	P 1/2	7.54-3	7.45-3	7.46-3	7.52-3	7.31-3	7.33-3	6.76-3	6.39-3	6.41-3
	P 2/2	0.0	0.0	0.0	0 0	0.0	0.0	0.0	0.0	0.0
	P 1	7.54-3	7.45-3	7.46-3	7.52-3	7.31-3	7.33-3	6.76-3	6.39-3	6.41-3

The computer code LWRBOX treats the fuel pin explicitly whereas many codes first homogenise the unit cells and then perform the 2-D calculations Therefore, in order to compare the microscopic cross sections with such codes, they have also been calculated using the following definition.

$$\sigma_{xGn} = \sum_{i \in f} V_i \sum_{g \in G} \sigma_{xgn} * \phi_{ig} / (V_f * \phi_{avG}) \qquad (2)$$

$$\phi_{avG} = \sum_{i \in cell} V_i \sum_{g \in G} \phi_{ig} / V_{cell}$$

Table 4. Microscopic absorption and production cross sections in b
(Using definition 1)

		U-Cell 1			U-Cell 2			Gd-Cell 3		
		SUPERB	LWRBOX	MONALI	SUPERB	LWRBOX	MONALI	SUPERB	LWRBOX	MONALI
	A 1/2	-	-	-	-	-	-	4 061+1	4 093+1	4 045+1
Gd-155	A 2/2	-	-	-	-	-	-	4 900+3	5.107+3	4 916+3
	A 1	-	-	-	-	-	-	2 502+2	2 685+2	2 593+2
	A 1/2	-	-	-	-	-	-	1 863+1	1 872+1	1 871+1
Gd-157	A 2/2	-	-	-	-	-	-	2 131+4	2 217+4	2 136+4
	A 1	-	-	-	-	-	-	9 371+2	1 014+3	9 764+2
	A 1/2	1.243+1	1 215+1	1 218+1	1 245+1	1 223+1	1 225+1	1 259+1	1 253+1	1 267+1
	A 2/2	4 215+2	4 227+2	4 209+2	4 183+2	4 197+2	4 173+2	2 057+2	2 096+2	2 082+2
U-235	A 1	7.857+1	7 684+1	7 721+1	7 495+1	7 420+1	7 421+1	2 092+1	2 138+1	2 144+1
	P 1/2	2 081+1	2 043+1	2 047+1	2.083+1	2 055+1	2 057+1	2 106+1	2.103+1	2 130+1
	P 2/2	8 702+2	8 728+2	8.689+2	8 635+2	8 665+2	8 615+2	4 196+2	4 273+2	4 241+2
	P 1	1 581+2	1 547+2	1 555+2	1.506+2	1 492+2	1 492+2	3 825+2	3 928+2	3 938+1
	A 1/2	8 940-1	8 780-1	8 822-1	8 951-1	8 820-1	8 880-1	9 120-1	9 070-1	9.174-1
	A 2/2	1 793+0	1 798+0	1 790+0	1 781+0	1 786+0	1 778+0	9 694-1	9.830-1	9 758-1
U-238	A 1	1 039+0	1 023+0	1 027+0	1 031+1	1 019+1	1 024+0	9 145-1	9 110-1	9 200-1
	P 1/2	3 605-1	3 540-1	3 531-1	3 602-1	3.500-1	3 501-1	3 455-1	3 320-1	3 313-1
	P 2/2	0 0	0 0	0 0	0.0	0 0	0 0	0 0	0 0 0	0 0
	P 1	3 022-1	2 980-1	2 969-1	3 048-1	2 970-1	2 965-1	3 306-1	3 170-1	3.164-1
	A 1/2	1 519+1	1 371+1	1.374+1	1 521+1	1 380+1	1 381+1	1 543+1	1.418+1	1 417+1
	A 2/2	1 110+3	1 113+3	1.117+3	1.118+3	1 121+3	1 117+3	1 532+3	1 536+3	1 567+3
Pu-239	A 1	1.922+2	1.870+2	1 892+2	1 850+2	1.821+2	1 826+2	8 085+1	8.255+1	8 388+1
	P 1/2	2.749+1	2 443+1	2 445+1	2 752+1	2 456+1	2.458+1	2 785+1	2 513+1	2 518+1
	P 2/2	2.126+3	2 133+3	2 138+3	2.138+3	2 144+3	2 136+3	2 704+3	2.712+3	2.763+3
	P 1	3.669+2	3.566+2	3.607+2	3.525+2	3.468+2	3.476+2	1 433+2	1 458+2	1.480+2

In formulae (1) and (2), the subscripts x, g and G stand for the reaction type, fine group and condensed group indexes and n stands for an isotope

The results in the Table 5 have been calculated using the definition (2) It can be seen from these tables that the cross sections for all the isotopes except Gd-155 and Gd-157 compare reasonably well In the case of Gd cells there is slightly more deviation in one group cross sections of Gd isotopes

Table 5 Microscopic absorption and production cross sections in b
(Using definition 2)

		U-Cell 1			U-Cell 2			Gd-Cell 3		
		SUPERB	LWRBOX	MONALI	SUPERB	LWRBOX	MONALI	SUPERB	LWRBOX	MONALI
	A 1/2	-	-	-	-	-	-	4 056+1	4 104+1	4 073+1
Gd-155	A 2/2	-	-	-	-	-		1 746+3	1 754+3	1 752+3
	A 1	-	-		-	-	-	2 319+2	2 478+2	2 413+2
	A 1/2	-	-	-	-	-	-	1 861+1	1 877+1	1 884+1
Gd 157	A 2/2	-		-	-	-	-	7 595+3	7 614+3	7 610+3
	A 1	-	-	-	-	-	-	8 685+2	9 358+2	9 087+2
	A 1/2	1 268+1	1 249+1	1 251+1	1 269+1	1 255+0	1 258+1	1 257+1	1 256+1	1 275+1
	A 2/2	3 842+2	3 837+2	3 797+2	3 816+2	3 811+2	3 772+2	7 331+1	7 198+1	7 418+1
U-235	A 1	7 862+1	7 732+1	7 757+1	7 508+1	7 465+1	7 463+1	1 939+1	1 973+1	1 996+1
	P 1/2	2 122+1	2 098+1	2 101+1	2 125+1	2 108+1	2 112+1	2 104+1	2 109+1	2 145+1
	P 2/2	7 932+2	7 922+2	7 838+2	7 877+2	7 868+2	7 787+2	1 495+2	1 467+2	1 511+2
	P 1	1 582+2	1 558+2	1 562+2	1 509+2	1 501+2	1 501+2	3 545+1	3 626+1	3 665+1
	A 1/2	9 120-1	9 020-1	9 058 1	9 130-1	9 050-1	9 117-1	9 110-1	9 100-1	9 237-1
	A 2/2	1 635+0	1 632+0	1 615+0	1 625+0	1 622+0	1 607+0	3 450-1	3 380-1	3 477-1
U-238	A 1	1 040+0	1 029+0	1 031+0	1 033+0	1 025+0	1 030+0	8 470-1	8 410-1	8 562-1
	P 1/2	3 680-1	3 630 1	3 625-1	3 670 1	3 590-1	3 594-1	3 450-1	3 330-1	3 336-1
	P 2/2	0 0	0 0	0 0	0 0	0 0	0 0	0 0	0 0	0 0
	P 1	3 020-1	3 000-1	2 983-1	3 050-1	2 990-1	2 982-1	3 060-1	2 930-1	2 945-1
	A 1/2	1 549+1	1 380+1	1 411+1	1 551+1	1 416+1	1 418+1	1 542+1	1 421+1	1 427+1
	A 2/2	1 012+3	1 121+3	1 007+3	1 020+3	1 018+3	1 010+3	5 460+2	5 276+2	5 585+2
Pu-239	A 1	1 923+2	1 821+2	1 901+2	1 853+2	1 832+2	1 836+2	7 493+1	7 620+1	7 806+1
	P 1/2	2 804+1	2 456+1	2 511+1	2 807+1	2 520+1	2 524+1	2 781+1	2 520+1	2 535+1
	P 2/2	1 938+3	2 144+3	1 928+3	1 950+3	1 947+3	1 931+3	9 638+2	9 314+2	9 845+2
	P 1	3.671+2	3 468+2	3 624+2	3 531+2	3 489+2	3 496+2	1 328+2	1 346+2	1 378+2

REFERENCES

[1] J J Arkuszewski, 'MCNP Analysis of the Nine-Cell LWR Gadolinium Benchmark', Wuerenlingen PSI, 1988

[2] Research Coordination Meeting to discuss the CRP on Safe Core Management with Burnable Absorbers in VVERs, IAEA, Vienna, Dec 11-14, 1989

[3] V Jaganmathan et al , Ann nucl Energy, 7, 641, 1980

[4] P D Krishnani, Ann nucl Energy, 14, 463, 1987

[5] H C Gupta, Report BARC-1529, 1990

ANALYSIS OF BENCHMARK ON INTERACTIVE EFFECTS OF GADOLINIUM PINS IN BWRs

V JAGANNATHAN, P D KRISHNANI, H C GUPTA
Bhabha Atomic Research Centre,
Trombay, Bombay,
India

Abstract

Presently, fuel assemblies with adjacent poison pins are employed in BWRs In order to check the capability of various calculational methods used for calculating lattice parameters of such assemblies, the Nuclear Energy Agency Committee on Reactor Physics (NEACRP) suggested a benchmark which consists of a simple 4*4 fuel assembly with two adjacent gadolinium rods In this report, the results of the burnup calculations for this benchmark as calculated by the computer codes SUPERB (1 D supercell) and LWRBOX (2-D collision probability) are presented At zero burnup a Monte Carlo analysis by MONALI code has also been made The analysis by SUPERB code used a condensed 29 group WIMS library while for the other two methods the analyses have been carried out with 69 groups WIMS library The comparison of results with these three codes is presented in this paper

1 INTRODUCTION

In boiling water reactors (BWRs), the gadolinium fuel pins are used to control the reactivity changes due to fuel burnup Earlier, fuel assemblies of BWR contained two isolated gadolinium fuel rods Now, fuel elements with adjacent poisoned fuel pins have been introduced in BWRs to enhance the performance of the fuel It has to be checked, whether the calculational methods used in BWRs can adequately predict the resulting mutual shielding of the pins and, in particular, its effect on the depletion of the burnable poison

The Swiss Federal Institute for Reactor Research (EIR) in 1980 proposed a new gadolinium benchmark for a simplified BWR fuel assembly with 14 unpoisoned and 2 adjacent poisoned fuel rods [1] The intention was to investigate whether calculational methods used for isolated Gd pins are capable of treating this more complex geometry with sufficient accuracy

The Nuclear Energy Agency Committee on Reactor Physics (NEACRP) provided an organizational basis for this benchmark The participants were asked to use their own cross section libraries and group structures and to perform burnup calculations upto 10 GWD/T In addition, a reference solution for the regular unpoisoned pin was requested, allowing checks on basic data and calculational methods to be made

This calculational benchmark in square lattice was suggested for the analysis in the RCM for CRP on safe core management with burnable absorbers in VVERs [2] (Though this CRP is essentially engaged in improving nuclear data and methods for use of Gd in hexagonal cores like VVERs, it was cosidered worthwhile to analyse parellelly some square lattice benchmarks for which many intrnational solutions are available)

In this paper, the results of the burnup calculations for this benchmark as calculated by the computer codes SUPERB (1-D supercell) and LWRBOX (2-D collision probability) are presented At zero burnup a Monte Carlo analysis by MONALI code has also been made Section 2 describes the calculational methods as used in SUPERB, LWRBOX, MONALI The Section 3 gives the problem specification and in Section 4 the results are presented

2 CODES USED IN THE ANALYSIS

The calculations were performed using the computer codes SUPERB, LWRBOX and MONALI The computer codes SUPERB and LWRBOX are used for lattice burnup analysis of LWR

lattice cells and MONALI is a general geometry Monte Carlo code A brief description of these codes is given below

2 1 METHOD IN SUPERB

In the computer code SUPERB the calculations are performed in three steps In the first step, various pincell types according to their enrichment and Dancoff factors are identified in the lattice cell The multigroup transport calculations are performed by interface current method in 1-D cylindrical geometry for these pincells and the multigroup cross sections for these lattice cell are spatially smeared

In the second step, a series of supercell calculations in multigroups are performed in 1-D cylindrical geometry by interface current method for assembly lattice cell, and for various heterogeneities such as water rod, poisoned pin or an absorber rod We consider a water rod, a poisoned pin or an absorber rod at the centre of the supercell, surrounded by rings of fuel pincell paste regions Multiple rings are considered for the poisoned fuel pin The presence of other water rod or other absorber materials in the surrounding rings is ignored in this calculation The cross sections are collapsed to few (five) groups by using the appropriate supercell ring spectra For fuel isotopes microscopic cross sections are condensed after multiplying with respective flux advantage factors of pincell calculations For non-burnable regions macroscopic cross sections are condensed after multiplying with disadvantage factors For water rod and absorber rods the homogenisation and group collapsing are done upto the equivalent area of a pincell by normal flux and volume weighting procedure

In the third step, the 2-D fuel assembly cell is analysed by few group diffusion theory Reflective boundary condition is used Five point centre-mesh finite differencing of the diffusion equations is used The eigenvalue or K_{∞}, flux and power distribution are obtained from this calculation

2 2 METHOD IN LWRBOX

The computer program LWRBOX has been developed to calculate lattice parameters as a function of burnup for rectangular assemblies of LWRs In this code, the multigroup integral transport equation is solved by the combination of small scale collision probability (CP) method and large scale interface current technique In this method, the whole lattice cell is divided into several connected cells which can further be subdivided into homogeneous zones The interaction between various zones within a cell and their contribution to outgoing currents at cell interfaces are directly calculated by the CP method Each cell is connected to neighbouring cells by interface currents At these interfaces, the angular flux in the incoming and outgoing direction is separately expanded in terms of spherical harmonics The simplest assumption is that of isotropic angular flux or popularly known as cosine current approximation (i e , one term expansion) This approximation has been found to be adequate for normal calculations However, at present, upto six terms can be considered in the code LWRBOX Another basic assumption of the method is that the scalar flux is constant in each zone of the region (i e , flat flux approximation)

2 3 COMPUTER CODE MONALI

The computer code MONALI is a Monte Carlo code primarily written for calculating nuclear parameters associated with thermal reactors The parameters calculated by the code include multiplication factor, neutron flux, material absorptions, and leakage from outermost surfaces Treatment of anisotropy is possible upto the first order The geometry module can handle any region which can be enclosed by a set of quadratic surfaces Six special forms including planes, cylinders and spheres are also present Any number and combination of the surfaces can enclose a region The outermost surface can also be any combination of these surfaces Any of the three boundary conditions,

namely, reflective, white or vacuum boundary condition can be applied on the outermost surfaces Neutron absorption is accounted by reducing the weight at each collision When the weight reduces below a user defined value the neutron history is terminated by Russian Roulette Fluxes are calculated by any of the three estimators, namely, track-length, collision, or expected track-length estimators Frequency distribution of the multiplication factor is also found The Shapiro and Walk normality test is optionally applied to the batch estimates of the multiplication factor Application of the test gives an indication about the adequacy of the batch size The code has restart option also

3 PROBLEM SPECIFICATION

The simplified fuel element consists of 14 initially identical unpoisoned fuel rods and 2 Gd rods Taking the symmetry into account, the 16 pins can be reduced to 5 different unpoisoned pins and a single Gd pin Reflective boundary conditions are prescribed on the four surfaces The material properties are as follows

Fuel	Material UO_2, density=10 g/cm^3, diameter = 1 cm, temperature = 600 ^{0}C, U-235 enrichment = 3 w/O, The Gd pin contains 3 w/O of Gd_2O_3
Clad	Material = zircaloy-2, density = 6 55 g/cm^3, temperature = 300 ^{0}C, inside diameter - 1 cm, outside diameter = 1 2 cm
Moderator	Material = H_2O, void content=0 %, saturated at a temperature of 286 ^{0}C, (pressure = 70 06 bar), square lattice pitch = 1 6 cm

The assembly average power density is 20 W per gram of the uranium metal in the fresh fuel In addition, a burnup calculation has also to be performed for a regular lattice without burnable poison rods The regular lattice is equivalent to a single unpoisoned fuel pin with a UO_2 density of 10 g/cm^3 and associated cladding and moderator

4 RESULTS

The calculations by the computer code SUPERB were performed by a condensed 28 group WIMS library 69-group WIMS library has been used in LWRBOX and MONALI Element identifiers 235, 2238, 3239 for U-235, U-238 and Pu-239 and the pseudo-fission product scheme for burnup calculation The resonance table numbers 235 4, 2238 4 and 3239 1 respectively, have been used for the three isotopes mentioned above The cross sections for Gd-155 and Gd-157 have been obtained from their resonance parameters

In LWRBOX, the calculations have been performed by considering 4 azimuthal zones in the cells containing unpoisoned fuel pins and 1 azimuthal zone in the cells containing poisoned fuel pins and 1 term has been considered in the expansion of angular flux at cell interfaces However, for the purpose of comparing the results with Monte Carlo method we have taken 8 azimuthal zones instead of 4

Table 1 compares the multiplication factors of the two lattices, the absorptions in different materials and relative pin power distribution in the poisoned lattice as calculated by the three methods at zero burnup In the Monte Carlo results, percent fractional deviations (psd) are also given It is seen from this table that the K_∞ and absorption rates for regular lattice compare very well For poisoned lattice the Monte Carlo K_∞ value lies in between those of SUPERB and LWRBOX SUPERB overpredicts K_∞ by 0 4% The LWRBOX K_∞ is slightly less compared to the Monte Carlo value This trend may be due to the fact that the absorptions in the Gd pin as calculated by LWRBOX is more compared to MC value This can be further improved by taking more subdivisions but the memory requirement increases to a very large value The power in the Gd pin as calculated by SUPERB is more compared to MC value Because of 1-D approximation the Gd cell absorption and Gd pin power are expected to deviate more compared to LWRBOX from the MC values and is also seen from Table 1 A detailed comparison

Table 1 Comparison of Results of SUPERB, LWRBOX and MONALI at 0 Burnup

Multiplication factors

	SUPERB	LWRBOX	MONALI
Regular lattice	1 3395	1 3409	1 3404 ± 0 0029
Poisoned lattice	1 0163	1 0086	1 0122 ± 0 0023

Absorption in each material in regular lattice cell

Material	SUPERB	LWRBOX	MONALI	psd
Fuel	9 360-1	9 354-1	9 353 1	0 3
Sheath	1 388-2	1 387-2	1 379-2	0 5
Moderator	5 020-2	5 076-2	5 094-2	0 3

Absorption in each material in poisoned lattice cell

Material	LWRBOX	MONALI	psd
Fuel-reg	7 005-1	7 049-1	0 2
Fuel-Gd	2 470-1	2 425-1	0 8
Sheath	1 263-2	1 259-2	0 3
Moderator	3 988-2	4 001-2	0 2

Relative pin powers in poisoned lattice

Pin no	SUPERB	LWRBOX	MONALI	psd
1	1 118	1 114	1 118	0 64
2	1 061	1 059	1 060	0 44
3	1 111	1 116	1 120	0 46
4	1 163	1 167	1 166	0 62
5	1 000	0 998	0 988	0 64
6 (Gd-pin)	0 374	0 368	0 366	0 55

of flux distribution between LWRBOX and MONALI is given in the reference [6]

Now we shall give the results as a function of burnup In LWRBOX burnup steps were taken to be 500 MWD/T for the regular lattice and 200 MWD/T for poisoned lattice cell initially (upto 6000 GWD/T burnup) which was increased to 500 MWD/T afterwards In SUPERB the burnup steps were

Table 2 Reactivity and Poison Worth for Regular and Poisoned Lattices

Burnup GWD/T	K-infinity Regular		ϱ-Reg (E)		K-infinity Poisoned		Gd - Worth	
	SUPERB	LWRBOX	SUPERB	LWRBOX	SUPERB	LWRBOX	SUPERB	LWRBOX
0 No Xe	1 3395	1 3409	--	--	1 0163	1 0077	0 241	0 248
1	1 2629	1 2836	--	--	1 0179	1 0040	0 207	0 218
2	1 2685	1 2691	0 011	0 011	1 0489	1 0320	0 173	0 187
3	1 2542	1 2553	--	--	1 0763	1 0637	0 142	0 153
4	1 2403	1 2417	0 033	0 033	1 1041	1 0996	0 110	0 114
5	1 2265	1 2283	--	--	1 1325	1 1404	0 077	0 072
6	1 2133	1 2151	0 054	0 053	1 1646	1 1750	0 040	0 033
7	1 1993	1 2022	--	--	1 1791	1 1902	0 017	0 010
8	1 1867	1 1896	0 075	0 073	1 1829	1 1887	0 003	0 001
9	1 1743	1 1772	--		1 1757	1 1794	0 001	0 002
10	1 1623	1 1652	0 094	0 092	1 1651	1 1680	-0 002	-0 002

200,300,500, 9*1000 MWD/T for regular lattice and 200,300, 6*250, 8*500 and 4*1000 MWD/T for poisoned lattice

Table 2 gives the variation of multiplication factor K_∞, with burnup for regular and poisoned lattices In this table we also give $\varrho_{reg}(E)$ for regular lattice and ϱ_{Gd} worth for poisoned lattice $\varrho_{reg}(E)$ is the reactivity loss above 1 GWD/T for the regular lattice calculated as follows

$$\varrho_{reg}(E) = [K_{reg}(1\ 0) - K_{reg}(E)]/K_{reg}(1\ 0)$$

$\varrho_{reg}(E)$ compares well for the two methods The total reactivity loss at 10 GWD/T as calculated by SUPERB is 94 mk while that of LWRBOX is 92 mk

ϱ_{Gd} is the reactivity worth of Gd isotopes at any burnup defined by

$$\varrho_{Gd}(E) = [K_{reg}(E) - K_{pol}(E)]/K_{reg}(E)$$

$\varrho_{Gd}(E)$ differ substantially which can explain the different trends in the calculated K_∞, values of SUPERB and LWRBOX

Table 3 gives the number densities for U-235, Pu-239 and Pu-240 for the regular lattice and Table 4 gives the same for the poisoned pin of the poisoned lattice cell

Table 3 Number Densities of U,Pu Isotopes for regular lattice(1 O/barn*cm)

Burnup	U-235*10^{-4}		Pu-239*10^{-5}		Pu-240*10^{-6}	
(GWD/T)	SUPERB	LWRBOX	SUPERB	LWRBOX	SUPERB	LWRBOX
0	6 776	6 776	0 000	0 000	0 000	0 000
2	6 258	6 256	2 214	2 087	0 941	0 870
4	5 769	5 776	4 024	3 822	3 224	3 016
6	5 328	5 330	5 450	5 229	6 145	5 864
8	4 901	4 913	6 651	6 375	9 574	9 111
10	4 516	4 522	7 593	7 312	13 100	12 586

Table 4 Number Densities of U,Pu Isotopes for poisoned lattice(1 O/barn*cm)

Burnup	U-235*10^{-4}		Pu-239*10^{-5}		Pu-240*10^{-6}	
(GWD/T)	SUPERB	LWRBOX	SUPERB	LWRBOX	SUPERB	LWRBOX
0	6 573	6 573	0 000	0 000	0 000	0 000
2	6 349	6 355	2 245	2.141	0 599	0 553
4	6 057	6 067	4 120	3 999	2 333	2 264
6	5 704	5 702	5 595	5 441	5 032	5 001
8	5 307	5 290	6 728	6 539	8 423	8 367
10	4 903	4 884	7 623	7 414	12 100	11 984

SUPERB over-predicts the Pu isotopes even in the regular lattice cell case Table 5 gives the number densities of Gd-155 and Gd-157 This table also gives the Gd destruction in the poisoned pin defined by,

$$D_{Gd}(E) = [d_{Gd}(O) - d_{Gd}(E)]/d_{Gd}(O)$$

where $d_{Gd}(E) = d_{155}(E) + d_{157}(E)$

d gives the number density of an isotope of Gd There is significantly large diffrence in the two results for the

Table 5 Number Densities of Gd Isotopes for poisoned lattice(1 O/barn*cm)

Burnup	Gd-155*10^{-4}		Gd-157*10^{-4}		Gd-Destruction	
(GWD/T)	SUPERB	LWRBOX	SUPERB	LWRBOX	SUPERB	LWRBOX
0	1 470	1 470	1 560	1 560	--	--
2	0 890	0 987	0 514	0 554	0 537	0 492
3	0 634	0 707	0 287	0 269	0 696	0 678
4	0 417	0 450	0 129	0 093	0 820	0 821
5	0 248	0 237	0 034	0 013	0 907	0 918
6	0 115	0 090	0 002	3 27-4	0 961	0 970
7	0 044	0 025	0 000	1 84-6	0 985	0 992

Table 6 Radial distribution of Gd isotopes at 2 GWD/T (1 O/barn*cm)

Radius	Gd-155*10^{-4}		Gd-157*10^{-4}	
cm	SUPERB	LWRBOX	SUPERB	LWRBOX
0 13	1 327	1 290	1 178	1 089
0 30	1 196	1 210	0 762	0 820
0 39	0 806	0 979	0 146	0 320
0 47	0 269	0 500	0 001	0 002

gadolinium isotopes SUPERB underpredicts the destruction of Gd isotopes and hence the over-prediction of K_∞ at burnups below 5 GWD/T Table 6 gives the radial distribution of Gd isotopes at 2 GWD/T SUPERB underpredicts the depletion of Gd isotopes at the centre and highly overpredicts the same at the outer layer of the poisoned pin

Table 7 Relative pin powers in pin 4 and Gd pin for poisoned lattice

Burnup (GWD/T)	Power in pin 4		Power in Gd pin	
	SUPERB	LWRBOX	SUPERB	LWRBOX
0	1 163	1 166	0 374	0 369
2	1 112	1 119	0 562	0 538
4	1 064	1 065	0 745	0 740
6	1 017	1 012	0 928	0 944
8	0 994	0 993	1 017	1 021
10	0 991	0 991	1 027	1 026

Tables 7 compares the pin power for the pin with highest rating (pin 4) and the poisoned pin (pin 6) The peak power is predicted within 1 % by the two codes However, the power in poison pin varies by about 5 %

REFERENCES

[1] C Maeder and P Wydler, "Benchmark on Interactive Effects of Gadolinium Poisoned Pins in BWRs', Status report prepared for the 26 th meeting of NEACRP, Oak Ridge, USA, October 17-21, 1983, Report NO NEACRP-A-567

[2] Research Coordination Meeting to discuss the CRP on Safe Core Management with Burnable Absorbers in VVERs, IAEA, Vienna, Dec 11-14, 1989

[3] V Jagannathan et al , Ann nucl Energy, 7, 641, 1980

[4] P D Krishnani, Ann nucl Energy, 14, 463, 1987

[5] H C Gupta, Report BARC-1529, 1990

[6] P D Krishnani, "Analysis of Benchmark on Interactive Effects of Gadolinium Poisoned Pins in BWRs by the Computer Code LWRBOX', Note No ThPD/36, 1991

POLISH EXPERIENCE WITH APPLICATION OF THE RSYST MODULAR SYSTEM

B. SZCZESNA
Institute of Atomic Energy,
Otwock-Świerk,
Poland

Abstract

The higher requirement in both safety operation and optimal fuel management cause that more accurate computing technics must be used in reactor analysis The gadolinium bearing or high enriched fuel or tight fuel lattice needs more detailed treatment The code which can be used successfully in analyses of that non-standard fuel lattices is the modular system RSYST [1,2]

With RSYST the case dependent multigroup microscopic cross section library can be generated as well as the transport, diffusion and burnup calculations can be performed. The fact that RSYST is able to create its own microscopic library cause that the real material composition and geometry as well as the heterogeneous structure and overlapping of resonances for defined fuel lattice are taken into account It makes that the library is always adequate to the fuel lattice under consideration.

In this paper the results of two benchmark problems are analysed the Arkuszewski benchmark problem [3] for square lattice with gadolinium bearing fuel and the Sidorenko benchmark problem [4] for hexagonal fuel lattice with gadolinium as a burnable poison

The microscopic library generation

The RSYST system does not have its own microscopic library It cause that analysis of new type of fuel lattice must begin with calculations of this data. The general method of the library generation has been developed in IKE [6,7] According to that the detailed method has been prepared Three sets of nuclear data based on the ENDF/B-IV data file have been used 99 group data in the fast and epithermal energy range, 8500 group data in the resonance energy range and 122 group data in the thermal energy range

For both benchmarks the 45 group microscopic cross sections libraries have been prepared for most important isotopes in the fuel cell including all gadolinium isotopes. The geometrical and material data have been taken from [4,5]. In both cases two geometrical models have been used: the pin cell case for unpoisoned fuel cell and the supercell case for the poisoned one. The overlapping of resonances for isotopes U-235, U-238 and Pu-239 as well as the heterogeneous structure of the pin cell have been taken into account. The 1-dimensional transport calculation in 99 groups and 122 groups separately provided neutron spectra which have been used for coupling and condensation of microscopic cross sectins to 45 group structure. The cutoff energy was 0.625 eV. Depending on the considered fuel lattice the goemetrical model and calculational method can be modified.

The Arkuszewski benchmark problem

The Arkuszewski benchmark for the LWR square lattice with gadolinium poisoned fuel (Fig. 1) has been calculated by the RSYST modular system in 45 groups and then by the CITATION

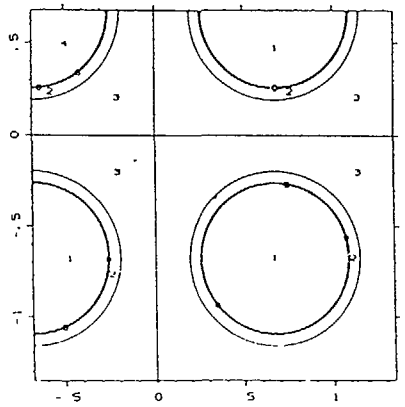

Figure 1. The Arkuszewski Benchmark case.

diffusion code [8] in 2 groups. The 45 group microscopic cross sections have been prepared according to the above described model.

Based on 45 group microscopic data the 1-dimensional transport calculation for the supercell has been performed by the RSYST/ISOSTO module which solves the multigroup multizone transport problem using the first flight collision probability method. The supercell consisted of cylindricalized heterogeneous poisoned fuel cell surrounded by two annular zones. Each of those zones contained 4 homogenized unpoisoned fuel cells. Then homogenization and collapsing of macroscopic cross sections to 2 groups for 3 types of fuel cells (Gd-cell, UO2-cell 1, UO2-cell 2) have been made to get 2 group macroscopic data for farther calculation. It is well known fact that the volume-flux homogenization is not sufficient treatment for strong absorbers. Therefore the homogenization of gadolinium poisoned fuel cell has been realized by special procedure [9]. In this procedure macroscopic cross sections have been evaluated to get the same reaction rates in the cell as in heterogeneous case. The partial current on the surface were not conserved. With those 2 group macroscopic data the 2-dimensional diffusion calculation have been performed by the CITATION code. The reflected boundary condition has been used.

Results are shown in table 1. The influence of the homogenization method is very expressive in term of k_{inf} obtained in 2-dimensional calculations. The homogenization with the reaction rate conservation effects in better estimation of the power and absorption distributions. This results shows good agreement with results presented in [12], which were obtained by 2-dimensional nodal the ICM2D code.

The Sidorenko Benchmark Results

The Sidorenko Benchmark for LWR hexagonal lattice with gadolinium as a burnable poison (fig. 2) has been analysed by

Table 1. Results for the Arkuszewski Benchmark

Infinite multiplication factor:			
MCNP [4]			1.1010+0.0022
2-D,45-gr, ICM2D [12]			1.0999
1-D, 45-gr, RSYST			1.10361
2-D, 2-gr, CITATION			
with volume-flux homogenization			1.06764
with reaction rate conservation			1.10082
Relative power density:	Gd-cell	U-cell 1	U-cell 2
MCNP [4]	0.2916	1.0885	
2-D ICM2D [12]	0.2905	1.0658	1.1116
1-D RSYST	0.28908	1.06396	1.11377
2-D CITATION			
volume-flux homogen.	0.31375	1.05612	1.11545
reaction rate cons.	0.29194	1.06558	1.11144
Relative absorption distribution:			
2-D ICM2D [12]	0.2308	0.0945	0.0978
1-D RSYST	0.22640	0.09487	0.09853
2-D CITATION			
volume-flux homogen.	0.24884	0.07680	0.09599
reaction rate cons.	0.22801	0.09484	0.09816
Flux integral, 1 group:			
2-D ICM2D [12]	3.6179	3.8033	3.8576
1-D RSYST	3.55136	3.81956	3.86750
2-D CITATION			
volume-flux homogen.	3.59200	3.77441	3.82079
reaction rate cons.	3.58110	3.73390	3.77571

the RSYST modular system and by the CITATION diffusion code. The 45-group microscopic cross sections for most important isotopes in the fuel have been calculated according to previous described method and the microscopic library for fission products had been prepared by Dr D. Lutz from IKE in Stuttgart.

The 1-dimensional transport calculation of the cylindricalized supercell, homogenization and collapsing of macroscopic cross sections to 2 groups have been done by the RSYST/ISOSTO . The volume-flux homogenization has been made only because the application of the homogenization with reaction rate conservation does not influence significantly on results (Tab. 2).

The burnup calculation have been performed by the RSYST/ABBRAND module using 2 group model with 16 fissionable isotopes and with 74 fission products including all gadolinium isotopes [10]. In the supercell the gadolinium rod has been divided into 7 equal volume zones depleted independently. Three rings of unpoisoned fuel cells have been smeared together and depleted as a one zone. The burnup calculations have been performed up to Bu_{max}= 20 MWd/kgU starting with Xenon concentration equal zero. The average power density was equal 39.86 W/gUO_2.

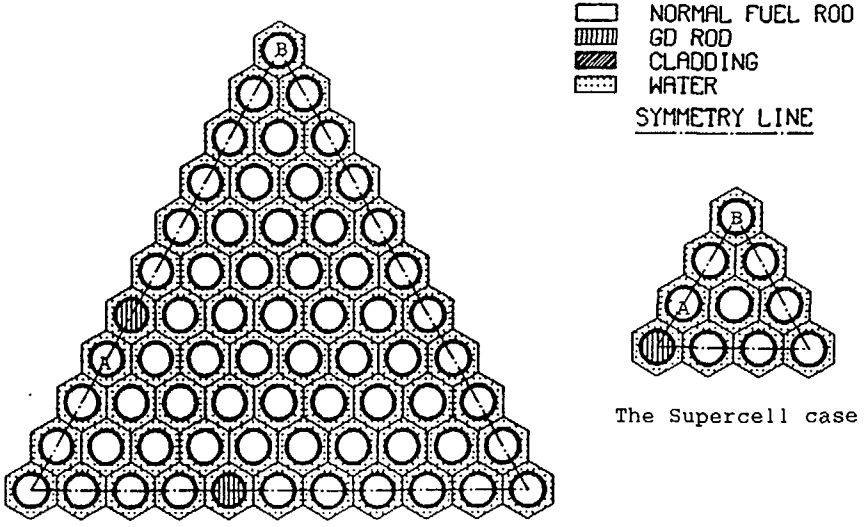

Figure 2. The Sidorenko Benchmark cases.

Table 2. Results for the Sidorenko Benchmark Problem
The supercell case, Bu= 0.0.

Infinite multiplication factor:				
CASMO-HEX [11]			1.20597*	
2-D, -gr, CITATION				
with volume-flux homogenization			1.24376	
with reaction rate conservation			1.24930	
	Gd-cell	U-cell A	U-cell C	U-cell B
Relative power density:				
CASMO-HEX [11]	0.23	0.98	1.04	1.05
1-D RSYST	0.22320	0.9900	1.03875	1.04645
2-D CITATION				
volume-flux homogen.	0.22246	0.98802	1.04247	
reaction rate cons.	0.21843	0.99474	1.04065	

* - with Xe - equilibrium

Table 3. Results for the Sidorenko Benchmark Problem

Infinite multiplication factor for the pin cell:		
	RSYST	MICBURN-3 [11]
Bu=0.0 MWd/kgU	1.36570	1.36355
Bu=20.0 MWd/kgU	1.11750	1.10621
Bu=20.0 MWd/kgU with fissionable isotops only		
the number densities according to RSYST results		1.23365
the number densities according to MICBURN-3 results		1.23123

The 2-dimensional calculations in hexagonal geometry have been performed by the CITATION code for the supercell and the assembly cases. The multiplication factors in a function of burnup are shown in a table 4.

Those results have been compared with Finnish results obtained by the CASMO-HEX code [11], (Tab 6, 7). The comparison showed a big discrepancy in term of k_{inf} for high depleted fuel. In spite of this the densities of of uranium and plutonium isotopes

Table 4. Infinite multiplication factor as a function of burnup

Burnup [MWd/kgU]	1-D RSYST UO2-cells	1-D RSYST Supercell	2-D CITATION Supercell	2-D CITATION Assembly
0.	1.36572E+00	1.24217E+00	1.24366E+00	1.30080E+00
4.97847E-02	1.32232E+00	1.20758E+00	-	-
1.00022E-01	1.31636E+00	1.20301E+00	1.20441E+00	1.25689E+00
2.49829E-01	1.31184E+00	1.20029E+00	-	-
5.00110E-01	1.30603E+00	1.19745E+00	1.19859E+00	1.24903E+00
9.99995E-01	1.29860E+00	1.19528E+00	1.19618E+00	1.24433E+00
1.49988E+00	1.29293E+00	1.19468E+00	-	-
1.99976E+00	1.28743E+00	1.19427E+00	1.19479E+00	1.23848E+00
2.49965E+00	1.28181E+00	1.19375E+00	1.19398E+00	1.23548E+00
2.99953E+00	1.27606E+00	1.19312E+00	-	-
3.49942E+00	1.27023E+00	1.19243E+00	-	-
3.99930E+00	1.26437E+00	1.19174E+00	-	-
4.49918E+00	1.25850E+00	1.19109E+00	-	-
4.99907E+00	1.25267E+00	1.19052E+00	1.19091E+00	1.22049E+00
5.49895E+00	1.24689E+00	1.19004E+00	-	-
5.99884E+00	1.24118E+00	1.18967E+00	-	-
6.49872E+00	1.23554E+00	1.18941E+00	-	-
6.99860E+00	1.22999E+00	1.18927E+00	-	-
7.49849E+00	1.22453E+00	1.18919E+00	1.19030E+00	1.20725E+00
7.99837E+00	1.21917E+00	1.18908E+00	-	-
8.99837E+00	1.20864E+00	1.18742E+00	-	-
9.99836E+00	1.19852E+00	1.18429E+00	1.18628E+00	1.19312E+00
1.12483E+01	1.18629E+00	1.17762E+00	-	-
1.24983E+01	1.17454E+00	1.16851E+00	1.17091E+00	1.17381E+00
1.37482E+01	1.16320E+00	1.15812E+00	-	-
1.49999E+01	1.15224E+00	1.14749E+00	1.15003E+00	1.15231E+00
1.62499E+01	1.14167E+00	1.13708E+00	-	-
1.74998E+01	1.13145E+00	1.12697E+00	1.12959E+00	1.13173E+00
1.87498E+01	1.12156E+00	1.11718E+00	-	-
1.99998E+01	1.11197E+00	1.10768E+00	1.11036E+00	1.11242E+00

Bu=0.0[MWd/kgU]

The assembly without BA	1.36759E+00
The assembly with XE-equilib.	1.26789E+00
The assembly without BA with XE-equilib.	1.33044E+00

seems to be closed to each other. To find out the reason of this discrepancy the transport calculation of the pin cell with the depleted fuel, but including the uranium and plutonium isotopes only has been performed. Fission products have been neglected.

Table 5a Number densities of actinidies in the pin cell burnup case as a function of burnup, (1-D RSYST calculation)

Burnup [MWd/kg]	k-inf	U-235	U-236	U-238
0	1 36570E+00	9 00000E-04	0	2 03000E-02
4 52574E-02	1 32510E+00	8 98822E-04	2 23144E-07	2 02994E-02
9 05147E-02	1 31854E+00	8 97646E-04	4 47501E-07	2 02989E-02
2 26287E-01	1 31454E+00	8 94122E-04	1 11970E-06	2 02971E-02
4 52574E-01	1 30947E+00	8 88278E-04	2 23399E-06	2 02942E-02
0 99962E-01	1 30173E+00	8 74322E-04	4 89264E-06	2 02871E-02
1 99992E+00	1 29139E+00	8 49478E-04	9 61625E-06	2 02741E-02
2 99989E+00	1 28056E+00	8 25410E-04	1 41804E-05	2 02610E-02
4 99981E+00	1 25783E+00	7 79368E-04	2.28603E-05	2 02345E-02
7 49974E+00	1 22989E+00	7 25278E-04	3 29627E-05	2 02008E-02
9 99966E+00	1 20383E+00	6 74579E-04	4 23144E-05	2 01662E-02
1 24996E+01	1 17980E+00	6 26943E-04	5 09686E-05	2 01308E-02
1 49995E+01	1 15759E+00	5 82124E-04	5 89668E-05	2 00946E-02
1 74994E+01	1 13690E+00	5 39924E-04	6 63439E-05	2 00576E-02
1 99994E+01	1 11750E+00	5 00181E-04	7 31300E-05	2 00199E-02
2 24993E+01	1 09917E+00	4 62756E-04	7.93526E-05	1 99814E-02

Table 5b Number densities of actinidies in the pin cell burnup case as a function of burnup, (1-D RSYST calculation)

Burnup [MWd/kg]	Pu-238	Pu-239	Pu-240	Pu-241	Pu-242
0	0	0	0	0	0
4 52574E-02	-2 77556E-17	6 83219E-08	1 26089E-10	2 46435E-13	2 77556E-17
9 05147E-02	2 22045E-16	2 50710E-07	6 14990E-10	2 37711E-12	1 11022E-15
2 26287E-01	2 50772E-14	1 23071E-06	5 34118E-09	5 06349E-11	5 56222E-14
4 52574E-01	6 05155E-13	3 49009E-06	2 71326E-08	5 17905E-10	1 13332E-12
9 99962E-01	1 77561E-11	9 42792E-06	1 57480E-07	6 86783E-09	3 39775E-11
1 99992E+00	2 58622E-10	1 96986E-05	6 46233E-07	5 82662E-08	5 94445E-10
2 99989E+00	1 10330E-09	2 91312E-05	1 38952E-06	1 89851E-07	7 96310E-09
4 99981E+00	6 17853E-09	4 57367E-05	3 40998E-06	7 70894E-07	2 06783E-08
7 49974E+00	2 27635E-08	6 31562E-05	6 53149E-06	2 12896E-06	8 88112E-08
9 99966E+00	5 59724E-08	7 77100E-05	1 00120E-05	4 08586E-06	2 35862E-07
1 24996E+01	1 11031E-07	8 99405E-05	1 36821E-05	6 49093E-06	4 84438E-07
1 49995E+01	1 92683E-07	1 00242E-04	1 74414E-05	9 20140E-06	8 49565E-07
1 74994E+01	3 05145E-07	1 08920E-04	2 12233E-05	1 20976E-05	1 33987E-06
1 99994E+01	4 52080E-07	1 16217E-04	2 49808E-05	1 50839E-05	1 95892E-06
2 24993E+01	6 36571E-07	1 22334E-04	2 86783E-05	1 80854E-05	2 70635E-06

Table 6. Infinite multiplication factor as a function of burnup, [11]

Burnup (MWd/kgU)	CASMO Pin cell	MICBURN-3 Pin cell	Program/case Supercell	CASMO-HEX (Supercell without BA)	Assembly	MICBURN-3/supercell Burnup (MWd/kgU)	
0.0	1.31938	1.36355*	1.20597	1.31765	1.26399	0.0	1.20530
0.1	1.31681	1.31703	-	-	-	0.1	1.20368
0.5	1.30697	1.30735	1.19755	1.30389	1.25251	0.5	1.19926
1.0	1.29930	1.30051	1.19574	1.29702	1.24768	1.1	1.19761
2.0	1.28783	1.28903	1.19452	-	1.24034	2.0	1.19678
2.5	-	-	1.19412	1.27988	1.23677	2.4	1.19645
3.0	1.27624	1.27720	1.19379	-	1.23322	3.0	1.19579
4.0	-	-	1.19375	-	1.22639	4.0	1.19492
5.0	1.25260	1.25323	1.19426	1.24995	1.22000	5.2	1.19383
7.5	1.22373	1.22409	1.19639	1.22086	1.20625	7.5	1.19215
10.0	1.19683	1.19700	1.18689	1.19389	1.19051	9.9	1.18516
12.5	1.17191	1.17192	1.16586	1.16893	1.16886	13.0	1.16010
15.0	1.14875	1.14862	1.14333	1.14574	1.14627	14.6	1.14571
17.5	1.12707	1.12681	1.12180	1.12402	1.12469	17.8	1.11809
20.0	1.10660	1.10621	1.10147	1.10352	1.10428	20.3	1.09791

Isothermal calculations (T = 293 K)

Burnup (MWd/kgU)	Supercell case	Assembly case
0	1.29394	1.35028
20	1.18478	1.18827

* without Xe-135

Table 7. Number densities of the most important uranium and plutonium isotopes as a funktion of burnup in the pin cell case, [11].

POWER DENSITY (W/G FUEL) = 39.670
NOMINAL MODERATOR TEMPERATURE (C-DEG.) = 302.000
NOMINAL FUEL TEMPERATURE (C-DEG.) = 827.000
NOMINAL BORON CONCENTRATION (PPM) = 0.000

A) MICBURN-3 CALCULATION

BURNUP MWD/KGU	U-235	U-236	U-238	PU-238	PU-239	PU-240	PU-241	PU-242
0.0	$9.000\cdot10^{20}$	0.	$2.030\cdot10^{22}$	0.	0.	0.	0.	0.
.1	$8.974\cdot10^{20}$	$4.947\cdot10^{17}$	$2.030\cdot10^{22}$	$6.291\cdot10^{12}$	$1.101\cdot10^{18}$	$1.989\cdot10^{15}$	$8.580\cdot10^{12}$	$4.680\cdot10^{9}$
.5	$8.870\cdot10^{20}$	$2.470\cdot10^{18}$	$2.029\cdot10^{22}$	$1.728\cdot10^{14}$	$5.511\cdot10^{18}$	$4.941\cdot10^{16}$	$1.094\cdot10^{15}$	$2.992\cdot10^{12}$
1.0	$8.742\cdot10^{20}$	$4.902\cdot10^{18}$	$2.029\cdot10^{22}$	$7.411\cdot10^{14}$	$1.082\cdot10^{19}$	$1.906\cdot10^{17}$	$8.492\cdot10^{15}$	$4.660\cdot10^{13}$
2.0	$8.492\cdot10^{20}$	$9.641\cdot10^{18}$	$2.027\cdot10^{22}$	$3.324\cdot10^{15}$	$2.075\cdot10^{19}$	$7.059\cdot10^{17}$	$6.290\cdot10^{16}$	$6.967\cdot10^{14}$
3.0	$8.250\cdot10^{20}$	$1.422\cdot10^{19}$	$2.026\cdot10^{22}$	$8.246\cdot10^{15}$	$2.987\cdot10^{19}$	$1.467\cdot10^{18}$	$1.952\cdot10^{17}$	$3.270\cdot10^{15}$
5.0	$7.787\cdot10^{20}$	$2.293\cdot10^{19}$	$2.024\cdot10^{22}$	$2.686\cdot10^{16}$	$4.592\cdot10^{19}$	$3.513\cdot10^{18}$	$7.632\cdot10^{17}$	$2.173\cdot10^{16}$
7.5	$7.243\cdot10^{20}$	$3.307\cdot10^{19}$	$2.020\cdot10^{22}$	$7.081\cdot10^{16}$	$6.274\cdot10^{19}$	$6.656\cdot10^{18}$	$2.076\cdot10^{18}$	$9.127\cdot10^{16}$
10.0	$6.732\cdot10^{20}$	$4.246\cdot10^{19}$	$2.017\cdot10^{22}$	$1.432\cdot10^{17}$	$7.678\cdot10^{19}$	$1.015\cdot10^{19}$	$3.966\cdot10^{18}$	$2.403\cdot10^{17}$
12.5	$6.253\cdot10^{20}$	$5.118\cdot10^{19}$	$2.013\cdot10^{22}$	$2.491\cdot10^{17}$	$8.856\cdot10^{19}$	$1.382\cdot10^{19}$	$6.292\cdot10^{18}$	$4.916\cdot10^{17}$
15.0	$5.801\cdot10^{20}$	$5.926\cdot10^{19}$	$2.010\cdot10^{22}$	$3.926\cdot10^{17}$	$9.846\cdot10^{19}$	$1.756\cdot10^{19}$	$8.917\cdot10^{18}$	$8.607\cdot10^{17}$
17.5	$5.376\cdot10^{20}$	$6.673\cdot10^{19}$	$2.006\cdot10^{22}$	$5.775\cdot10^{17}$	$1.068\cdot10^{20}$	$2.132\cdot10^{19}$	$1.172\cdot10^{19}$	$1.356\cdot10^{18}$
20.0	$4.976\cdot10^{20}$	$7.363\cdot10^{19}$	$2.002\cdot10^{22}$	$8.070\cdot10^{17}$	$1.138\cdot10^{20}$	$2.503\cdot10^{19}$	$1.462\cdot10^{19}$	$1.981\cdot10^{18}$

B) CASMO-3 CALCULATION

BURNUP MWD/KGU	U-235	U-236	U-238	PU-238	PU-239	PU-240	PU-241	PU-242
0.0	$9.000\cdot10^{20}$	0.	$2.030\cdot10^{22}$	0.	0.	0.	0.	0.
.1	$8.974\cdot10^{20}$	$4.985\cdot10^{17}$	$2.030\cdot10^{22}$	$7.024\cdot10^{12}$	$3.027\cdot10^{17}$	$3.784\cdot10^{14}$	$1.285\cdot10^{12}$	$5.592\cdot10^{8}$
.5	$8.870\cdot10^{20}$	$2.480\cdot10^{18}$	$2.029\cdot10^{22}$	$1.854\cdot10^{14}$	$4.025\cdot10^{18}$	$2.881\cdot10^{16}$	$5.389\cdot10^{14}$	$1.260\cdot10^{12}$
1.0	$8.743\cdot10^{20}$	$4.918\cdot10^{18}$	$2.029\cdot10^{22}$	$7.885\cdot10^{14}$	$9.484\cdot10^{18}$	$1.449\cdot10^{17}$	$5.760\cdot10^{15}$	$2.818\cdot10^{13}$
2.0	$8.494\cdot10^{20}$	$9.668\cdot10^{18}$	$2.027\cdot10^{22}$	$3.512\cdot10^{15}$	$1.984\cdot10^{19}$	$6.208\cdot10^{17}$	$5.167\cdot10^{16}$	$5.296\cdot10^{14}$
3.0	$8.252\cdot10^{20}$	$1.426\cdot10^{19}$	$2.026\cdot10^{22}$	$8.674\cdot10^{15}$	$2.936\cdot10^{19}$	$1.358\cdot10^{18}$	$1.716\cdot10^{17}$	$2.708\cdot10^{15}$
5.0	$7.790\cdot10^{20}$	$2.300\cdot10^{19}$	$2.023\cdot10^{22}$	$2.813\cdot10^{16}$	$4.623\cdot10^{19}$	$3.389\cdot10^{18}$	$7.039\cdot10^{17}$	$1.919\cdot10^{16}$
7.5	$7.247\cdot10^{20}$	$3.318\cdot10^{19}$	$2.020\cdot10^{22}$	$7.385\cdot10^{16}$	$6.394\cdot10^{19}$	$6.585\cdot10^{18}$	$1.959\cdot10^{18}$	$8.317\cdot10^{16}$
10.0	$6.737\cdot10^{20}$	$4.261\cdot10^{19}$	$2.016\cdot10^{22}$	$1.487\cdot10^{17}$	$7.866\cdot10^{19}$	$1.019\cdot10^{19}$	$3.799\cdot10^{18}$	$2.228\cdot10^{17}$
12.5	$6.258\cdot10^{20}$	$5.136\cdot10^{19}$	$2.013\cdot10^{22}$	$2.577\cdot10^{17}$	$9.094\cdot10^{19}$	$1.400\cdot10^{19}$	$6.091\cdot10^{18}$	$4.616\cdot10^{17}$
15.0	$5.806\cdot10^{20}$	$5.946\cdot10^{19}$	$2.009\cdot10^{22}$	$4.049\cdot10^{17}$	$1.012\cdot10^{20}$	$1.792\cdot10^{19}$	$8.702\cdot10^{18}$	$8.157\cdot10^{17}$
17.5	$5.381\cdot10^{20}$	$6.696\cdot10^{19}$	$2.005\cdot10^{22}$	$5.943\cdot10^{17}$	$1.098\cdot10^{20}$	$2.185\cdot10^{19}$	$1.151\cdot10^{19}$	$1.295\cdot10^{18}$
20.0	$4.980\cdot10^{20}$	$7.388\cdot10^{19}$	$2.002\cdot10^{22}$	$8.290\cdot10^{17}$	$1.169\cdot10^{20}$	$2.575\cdot10^{19}$	$1.443\cdot10^{19}$	$1.904\cdot10^{18}$

Two sets of number densities for uranium and plutonium isotopes have been taken from RSYST (tab. 5) and MICBURN-3 (tab. 7) results corresponding to burnup equal 20.0 MW/kgU. Results of multiplication factors are shonw in table 3. Good agreement of k_{inf} leads to assumption that besides of fissionable isotopes the fisson product data or/and the model of the burnable chain have a significant influence on the burnup results.

REFERENCES

1. R.Ruhle, RSYST- An Integrated Modular System with a Data Basis for Automated Calculations of Nuclear Reactor, IKE-BNR-4-12, Stuttgart, 1973.
2. R.Ruhle, RSYST- Kurtzbeschreibung der Moduln, IKE 4-5, Stuttgart, 1983.
3. L.Bordzan, Implementation of RSYST Modular System on the CDC CYBER-72 Computer, Int. Rep. 18/E-II/89, Swierk, 1989.
4. J.Arkuszewski, MCNP, Analysis of the Nine-Cell LWR Gadolinium Benchmark, Wuerenlingen, PSI, 1988.
5. Consulting Report on Proposed Programme for the CRP on Safe Core Manegement with Burnable Absorbers in VVERs, IAEA, Viena, 1988.
6. R. Wartmann, W. Bernnat, Nachrechnung einer Kritischen Anordung von Siedewassrreaktorbrennelementen auf der Basis von ENDF/B-IV Daten, IKE 6-118, Stuttgart, 1978.
7. J. Keinert, Therm-126, a Thermal Neutron Cross-section Library Including Scattering Matrices, Part A, Part B, IKE6-105, Stuttgart, 1978.
8. H.Tomecki, The CITATION Code - The Reference of the Version for the CDC CYBER-72 Computer, Rep IBJ 0-199, Swierk, 1974.
9. D. Lutz, personal communication.
10. D.Lutz, ABBRAND 98 eine Abbranddatei fur 19 Aktinide und 79 Spaltprodukte fur Gadolinimhaltinge Brennstoffe, Interne IKE-Notiz, Stuttgart, 1978.
11. M. Anttila, Finnish Results for a VMK Benchmark Problem Concerning Use of Gadolinium in Fuel Rod Lattices, CRP on Safe Core Management with Burnable Absorbers in VVERs, IAEA, Viena, 1989.
12. D. Lutz, Results for the Arkuszewski Benchmark Problem, IKE, University of Stuttgart, 1990.

COMPARISON CALCULATIONS FOR A BWR LATTICE WITH ADJACENT GADOLINIUM PINS

N. MARINKOVIĆ
Nuclear Engineering Laboratory,
Boris Kidrič Institute of Nuclear Sciences,
Belgrade, Yugoslavia

Abstract

Within the frame of the Coordinated Research Program (CRP) SAFE CORE MANAGEMENT WITH BURNABLE ABSORBERS IN VVERs the BWR simplified fuel element with two adjacent gadolinium pins was chosen as the square lattice benchmark problem. The input calculation data, the format and the comparison of the results of the CRP participants were defined according to the NEACRP comparison as previously done at Eidg. Institute fur Reaktorforschung, Wurenlingen (EIR).
The results were received from the following CRP participants: Skoda Czechoslovakia; Technical Research Center of Finland (VTT); VEB Bergman-Borsig Stammbetrieb des Kombinates Kab, Germany; Institut fur Kernenergetik Universitat Stuttgart, Germany; Bhabha Atomic Research Center, India and Boris Kidric Institute of Nuclear Sciences, Yugoslavia. Besides the comparison of these six CRP available data sets, an analysis was performed taking into account the 10 NEACRP data sets, which when added to the results of CRP participants gave the totasl of 16 sets all together. This is a number with more significance from statistical point of view. To illustrate the significance of the number of data sets taken into account, both treatments were compared to NEACRP results.
Variation coefficients of the most important parameters were compared to typical target accuracies for power reactors recommended by IAEA. The variations of most CRP results are in good agreement with the target accuracies except for the lifetime and Pu-239 build-up for the poisoned lattice. The variations of NEACRP+CRP and NEACRP results are larger than target accuracies for both the regular and the poisoned lattice.
On the whole, an acceptably good agreement is obtained for the results suupplied by CRP participants when treated separately. Smaller variations are observed in treating 16 sets of results (NEACRP+CRP) than in NEACRP comparison.

INTRODUCTION

Since no data for a suitable PWR square lattice with burnable absorber were available, a simplified BWR lattice was adopted for comparison as benchmark within the CRP on SAFE CORE MANAGEMENT WITH BURNABLE ABSORBERS IN VVERs. Comparison of the results, as well as the format, were the same as the previously adopted ones in the NEACRP comparison[2] This paper summarizes the most important comparison results and draws conclusions concerning the influence of gadolinium burnable absorber on the neutronic lattice parameters Comparison of all the available results is shown in detail in the report COMPARISON CALCULATIONS FOR A BWR LATTICE WITH ADJACENT GADOLINIUM PINS performed at the Nuclear Engineering Laboratory of the Boris Kidric Institute of Nuclear Sciences[10]

The mean values, standard deviations and variation coefficients were computed for the obtained as well as for the calculated parameters Besides the comparison of six CRP data sets, an analysis was performed taking into account the CRP data added to those of ten NEACRP participants (marked NEACRP+CRP in Tables). The sixteen sets of results were considered as more significant from statistical point of view. To illustrate the significance of number of data sets which are taken into account, both treatments were compared to NEACRP results[2]

The list of all the participants including those of NEACRP International comparison is shown in Table 1 with the most important relevant data concerning the calculations applied.

PROBLEM SPECIFICATION

The benchmark BWR fuel element consists of 16 fuel pins, 14 initially identical UO_2 fuel cells and 2 gadolinium poisoned ones Taking into account the lattce symmetry 6 different cell types were defined The input data applied were the same as those adopted in Ref [2] Fuel pins 1 cm in diameter were made of UO_2,

Table 1 List of participants with main relevant data

No	Participant	Data Library	Code name	Ref
		N E A C R P		/2/
1	AEEW	WIMS	LWR-WIMS	
2	AMN	ENDF/B-4	BLA	
3	CEA	ENDF/B-3+ENDF/B-4	APOLLO	
4	CISE	MUFT-IV+TEMPEST	NUOVO,AUTOBUS	
5	EIR	ENDF/B-4	BOXER	
6	ENEA	ENDF/B-4+UKNDL	KIM	
7	JAERI	ENDF/B-4	SRAC	
8	NAIG	ENDF/B-4+ENDF/B-5	TGBLA	
9	OSAKA	WIMS + ENDF/B-3	RESPLA	
10	RISO	UKNDL	CRS+CDB	
		C R P		
11	SKODA(CSR)	WIMS	WIMS	/3/
12	VTT(FIN)	ENDF/B-4	MICBURN-3 CASMO-3G	/4/
13	VEB(GERM)	ENDF/B-4	NESSEL-4,DIPOL-2	/5/
14	IKE(GERM)	JEF-1	RSYST ICMD KENO	/6/
15	BARC(INDIA)	WIMS	LWRBOX	/7/
16	IBK(YU)	WIMS+UKNDL	WIMSD-4	/8/

having density 10g/cm³, at temperature 600°C, and U-235 enrichment was 3 weight-%. Gadolinium pins consisted of 0.3 g/cm³ Gd_2O_3 and 9.7 g/cm³ UO_2. Cladding was Zirkaloy-2 having density 6.55 g/cm³, at temperature 300°C, inside diameter 1 cm, and outside diameter 1.2 cm. Water was the moderator, at temperature 286°C and void content 0%. Lattice pitch was 1.6 cm. Average power density was 20 W/g U.

The following parameters were requested for assembly average burn steps of 1000 MWd/t up to 10000 MWd/t:

- Burnup dependent infinite multiplication factor;
- Burnup of fuel pins;
- Relative power distribution of the 6 different fuel pins normalized to an average of 1;
- Gd pin average densities of Gd-155, Gd-157, U-235, Pu-239, Pu-240 in atoms/barn.cm;
- Spatial distribution of the Gd isotopes at 2000 MWd/t

Two cases were defined for calculatng the regular lattice parameters: single UO_2 fuel pin and fuel assembly without absorber rods. At this stage of the CRP only the case of single fuel pin was treated in the comparison because data for the second case were not available, except for one participant (IBK)[10].
From the available infinite multiplication factors and number densities of the most important isotopes, the following parameters were derived:
- reactivity deviations from mean values for both the regular and the poisoned lattice,
- gadolinium reactivity worth,
- gadolinium destruction,
- reactivity gain in the poisoned assembly dependent on burnup and Gd destruction,
- plutonium ratio,
- reactivity loss in the regular lattice dependent on burnup, U-235 destruction and Pu-239 number density,
- reactivity gain or loss at given values of Gd destruction, U-235 destruction and Pu-239 number density.

RESULTS OBTAINED

Comparisons of the most important neutronic parameters are shown in Tables 2-6. In order to separate the problem of fuel element modelling from the influence of the burnable absorber, the results concerning fresh regular lattice must be analyzed. Variation coefficients of the multiplication factors for the fresh regular lattice (Table 2) obtained by comparison of the 16 sets of results are lower in comparison to the NEACRP values as expected. It may be considered that the CRP results are in a good agreement, the variation being 0.5% One may see that the k-infinity results of CEA, CISE, EIR, JAERI, NAIG, SKODA, VTT,

Table 2. Infinite multiplication factor

		REGULAR LATTICE						POISONED LATTICE					
	BURNUP (MWd/TU)	0 no Xe	1000	2000	3000	4000	5000	6000	8000	10000	0 no Xe	1000	2000	3000	4000	5000	6000	8000	10000
No.	Participant																		
1	AEEW	1.3514	1.2926	1.2773	1.2630	1.2489	1.2349	1.2213	1.1951	1.1703	1.0093	1.0024	1.0295	1.0625	1.1042	1.1516	1.1866	1.1939	1.1715
2	ANN	1.3400	1.2794	1.2681	1.2563	1.2445	1.2329	1.2214	1.1986	1.1781	1.0140	1.0036	1.0316	1.0631	1.1002	1.1412	1.1747	1.1891	1.1727
3	CEA	1.3298	1.2742	1.2623	1.2495	1.2369	1.2240	1.2111	1.1865	1.1633	.9970	.9991	1.0314	1.0658	1.1035	1.1433	1.1731	1.1756	1.1546
4	CISE	1.3278	1.2752	1.2613	1.2488	1.2357	1.2238	1.2111	1.1876	1.1652	1.0164	1.0058	1.0286	1.0531	1.0884	1.1196	1.1501	1.1788	1.1621
5	EIR	1.3316	1.2744	1.2626	1.2501	1.2373	1.2245	1.2119	1.1875	1.1645	1.0110	1.0093	1.0403	1.0727	1.1083	1.1477	1.1754	1.1861	1.1657
6	ENEA	1.3390	1.2869	1.2692	1.2618	1.2449	1.2354	1.2226	1.2000	1.1740	.9965	.9935	1.0187	1.0504	1.0846	1.1250	1.1595	1.1811	1.1705
7	JAERI	1.3285	1.2723	1.2617	1.2506	1.2393	1.2279	1.2167	1.1951	1.1747	.9983	.9973	1.0270	1.0596	1.0964	1.1399	1.1745	1.1901	1.1728
8	NAIG	1.3340	1.2767	1.2646	1.2515	1.2381	1.2246	1.2114	1.1860	1.1621	1.0004	1.0044	1.0368	1.0699	1.1051	1.1419	1.1714	1.1803	1.1595
9	OSAKA	1.3060	1.2537	1.2424	1.2301	1.2172	1.2040	1.1908	1.1652	1.1410	.9899	.9895	1.0162	1.0439	1.0742	1.1105	1.1465	1.1850	1.1466
10	RISOE	1.3180	1.2637	1.2538	1.2427	1.2310	1.2192	1.2074	1.1845	1.1625	.9815	.9798	1.0093	1.0435	1.0855	1.1379	1.1739	1.1837	1.1642
11	SKODA	1.3328	1.2757	1.2637	1.2507	1.2373	1.2240	1.2102	1.1858	1.1621	1.0000	1.0121	1.0460	1.0745	1.1032	1.1333	1.1642	1.1838	1.1646
12	VTT	1.3359	1.2821	1.2701	1.2576	1.2447	1.2317	1.2189	1.1942	1.1707	1.0004	1.0007	1.0305	1.0646	1.1015	1.1393	1.1705	1.1847	1.1649
13	VFB	1.3235	1.2678	1.2556	1.2433	1.2306	1.2180	1.2057	1.1818	1.1590	.9954	.9926	1.0142	1.0488	1.0901	1.1302	1.1636	1.1805	1.1629
14	IKE	1.3349	1.2778	1.2658	1.2530	1.2399	1.2267	1.2138	1.1888	1.1653	1.0006	.9938	1.0235	1.0563	1.0913	1.1256	1.1551	1.1771	1.1609
15	BARC	1.3409	1.2836	1.2691	1.2553	1.2417	1.2283	1.2151	1.1896	1.1652	1.0077	1.0040	1.0320	1.0637	1.0996	1.1404	1.1750	1.1887	1.1680
16	IBK	1.3287	1.2724	1.2600	1.2468	1.2332	1.2198	1.2046	1.1814	1.1575	.9896	.9841	1.0129	1.0461	1.0876	1.1346	1.1699	1.1773	1.1561
	NEACRP MEAN	1.3306	1.2749	1.2623	1.2504	1.2374	1.2251	1.2126	1.1886	1.1656	1.0014	.9985	1.0269	1.0585	1.0950	1.1359	1.1686	1.1824	1.1640
	VAR.	.009	.009	.007	.008	.007	.007	.008	.008	.009	.011	.009	.009	.010	.010	.012	.011	.007	.007
	NEACRP+CRP MEAN	1.3314	1.2755	1.2630	1.2507	1.2376	1.2250	1.2122	1.1880	1.1647	1.0005	.9983	1.0268	1.0587	1.0952	1.1351	1.1677	1.1822	1.1636
	VAR	.008	.007	.006	.006	.006	.006	.007	.007	.008	.009	.009	.010	.010	.009	.009	.009	.006	.006
	CRP MEAN	1.3327	1.2766	1.2641	1.2511	1.2379	1.2247	1.2117	1.1869	1.1633	.9990	.9979	1.0265	1.0590	1.0956	1.1339	1.1664	1.1820	1.1629
	VAR	.005	.004	.004	.004	.004	.004	.004	.004	.004	.006	.009	.011	.009	.006	.004	.005	.004	.003

Table 3. Gadolinium worth and Gadolinium destruction in the poisoned pin (1.E-04/barn cm)

No.	Participant	BURNUP (MWd/TU) 0 no Xe	1000	2000	3000	4000	5000	6000	7000	8000	9000	10000	2000	3000	4000	5000	6000	7000
1	AEEW	.253	.225	.194	.159	.116	.067	.028	.008	.001	-.001	-.001	.507	.699	.842	.933	.978	.995
2	AMN	.243	.216	.186	.154	.116	.074	.038	.017	.008	.005	.005	.495	.681	.823	.919	.969	.990
3	CEA	.250	.216	.183	.147	.108	.066	.031	.015	.009	.008	.007	.523	.710	.850	.935	.979	.995
4	CISE	.235	.211	.184	.157	.119	.085	.050	.023	.007	.003	.003	.457	.636	.781	.884	.950	.983
5	EIR	.241	.208	.176	.142	.104	.063	.030	.008	.001	-.001	-.001	.501	.691	.834	.928	.973	.994
6	ENEA	.256	.228	.197	.168	.129	.089	.052	.020	.016	.007	.003	.537	.701	.822	.909	.962	.988
7	JAERI	.249	.216	.186	.153	.115	.072	.035	.012	.004	.002	.002	.495	.682	.825	.921	.972	.992
8	NA18	.250	.213	.180	.145	.107	.068	.033	.013	.005	.003	.002	.508	.693	.832	.923	.972	.992
9	OSAKA	.242	.211	.182	.151	.117	.078	.037	.011	.000	-.003	-.005	.487	.669	.810	.910	.967	.991
10	RISOE	.255	.225	.195	.160	.118	.067	.028	.008	.001	-.001	-.001	.508	.701	.846	.933	.978	.994
11	SKODA	.250	.207	.172	.141	.108	.074	.038	.011	.002	-.001	-.002	.488	.665	.803	.902	.962	.989
12	VTT	.251	.219	.189	.153	.115	.075	.040	.017	.008	.005	.005						
13	VEB	.248	.217	.192	.156	.114	.072	.035	.011	.001	-.002	-.003	.451	.623	.754	.853	.925	.968
14	IKE	.250	.222	.191	.157	.120	.082	.048	.023	.010	.005	.004	.475	.657	.798	.896	.955	.984
15	BARC	.248	.218	.187	.153	.114	.072	.033	.010	.001	-.002	-.002	.491	.678	.821	.917	.970	.992
16	IBK	.255	.227	.196	.161	.118	.070	.030	.010	.003	.002	.001	.511	.704	.845	.933	.978	.995
NEACRP	MEAN	.247	.217	.186	.154	.115	.073	.036	.013	.005	.005	.004	.502	.686	.826	.919	.970	.991
	ST.DEV	.007	.007	.007	.008	.007	.009	.008	.005	.005	.003	.002	.022	.021	.020	.016	.009	.004
NEACRP+CRP	MEAN	.249	.217	.187	.154	.115	.073	.037	.013	.005	.003	.003	.496	.679	.819	.913	.966	.989
	ST.DEV	.006	.007	.007	.007	.006	.007	.008	.005	.004	.002	.002	.023	.025	.026	.022	.014	.007
CRP	MEAN	.250	.218	.188	.154	.115	.074	.037	.014	.004	.003	.003	.483	.665	.804	.901	.958	.985
	ST.DEV	.003	.007	.008	.007	.004	.004	.006	.005	.004	.002	.001	.017	.023	.027	.025	.018	.010

Table 4. Reactivity loss from 1000 MWd/t for regular lattice and reactivity gain for poisoned lattice

No.	Participant	BURNUP (MWd/TU) 2000	4000	6000	8000	10000	2000	3000	4000	5000	6000	7000
1	AEEW	.012	.034	.055	.075	.095	.027	.060	.102	.149	.184	.196
2	AMN	.009	.027	.045	.063	.079	.028	.059	.096	.137	.170	.185
3	CEA	.009	.029	.050	.069	.087	.032	.067	.104	.144	.174	.182
4	CISE	.011	.031	.050	.069	.086	.023	.047	.082	.113	.143	.165
5	EIR	.009	.029	.049	.068	.086	.031	.063	.098	.137	.165	.179
6	ENEA	.014	.033	.050	.068	.088	.025	.057	.092	.132	.167	.191
7	JAERI	.008	.026	.044	.061	.077	.030	.062	.099	.143	.178	.194
8	NA18	.009	.030	.051	.071	.090	.032	.065	.100	.137	.166	.178
9	OSAKA	.009	.029	.050	.071	.090	.027	.055	.086	.122	.159	.177
10	RISOE	.008	.026	.045	.063	.080	.030	.065	.108	.161	.198	.211
11	SKODA	.009	.030	.051	.070	.089	.033	.062	.090	.120	.150	.168
12	VTT	.009	.029	.049	.069	.087	.030	.064	.101	.139	.170	.185
13	VFB	.010	.029	.049	.068	.086	.022	.057	.098	.139	.172	.190
14	IKE	.009	.030	.050	.070	.088	.030	.063	.098	.133	.162	.181
15	BARC	.011	.033	.053	.073	.092	.028	.059	.095	.136	.170	.185
16	IBK	.010	.031	.052	.072	.090	.029	.063	.105	.153	.189	.201
NEACRP	MEAN	.010	.029	.049	.068	.086	.029	.060	.097	.138	.170	.186
	ST.DEV	.002	.003	.003	.004	.006	.003	.006	.008	.013	.015	.013
NEACRP+CRP	MEAN	.010	.030	.050	.069	.087	.029	.061	.097	.137	.170	.186
	ST.DEV	.003	.004	.005	.007	.008	.003	.005	.007	.012	.014	.012
CRP	MEAN	.010	.030	.051	.070	.089	.029	.061	.098	.136	.169	.185
	ST.DEV	.001	.001	.002	.002	.002	.004	.002	.005	.010	.012	.010

Table 5. Reactivity gain and gadolinium destruction

Gd-DESTRUCTION (%)		50	60	70	80	90	100
No.	Participant						
1	AEEW	.026	.043	.060	.080	.123	.200
2	AMN	.029	.046	.064	.086	.125	.192
3	CEA	.029	.046	.064	.081	.120	.185
4	CISE	.027	.042	.062	.088	.121	.176
5	EIR	.031	.047	.065	.084	.120	.183
6	ENEA	.021	.038	.057	.082	.127	.202
7	JAERI	.030	.048	.067	.088	.129	.200
8	NAIG	.031	.049	.067	.088	.123	.183
9	OSAKA	.029	.044	.062	.082	.116	.184
10	RISOE	.029	.047	.065	.080	.133	.216
11	SKODA	.035	.051	.069	.089	.119	.175
12	VTT						
13	VEB	.032	.049	.076	.113	.162	.196
14	IKE	.034	.049	.063	.084	.126	.184
15	BARC	.029	.040	.044	.059	.121	.187
16	IBK	.027	.045	.062	.081	.126	.205
NEACRP	MEAN	.028	.045	.063	.084	.124	.192
	ST.DEV	.003	.003	.003	.003	.006	.012
NEACRP+CRP	MEAN	.031	.049	.068	.090	.135	.205
	ST.DEV	.004	.005	.008	.012	.014	.018
CRP	MEAN	.032	.047	.063	.085	.131	.189
	ST.DEV	.003	.004	.012	.019	.018	.011

Table 6. Rectivity loss dependent on U-235 destruction (%) and Pu-239 density (1.E-5 barn cm) for regular lattice

U-235 DESTRUCTION		8	14	20	26	32	Pu-239 DENSITY	2.8	3.9	5.0	6.1	7.2
No.	Participant											
1	AEEW	.013	.032	.051	.071	.092		.020	.035	.052	.071	.092
2	AMN	.010	.026	.043	.061	.078		.011	.021	.032	.044	.059
3	CEA	.011	.028	.046	.065	.085		.015	.028	.043	.059	.075
4	CISE	.012	.028	.046	.063	.082		.018	.032	.047	.063	.085
5	EIR	.010	.027	.045	.064	.084		.015	.028	.042	.059	.074
6	ENEA	.015	.031	.046	.062	.084		.022	.035	.049	.067	.094
7	JAERI	.008	.023	.038	.054	.072		.013	.025	.038	.053	.069
8	NAIG	.010	.028	.047	.066	.086		.015	.028	.043	.060	.075
9	OSAKA	.009	.026	.045	.065	.086		.013	.024	.039	.055	.074
10	RISOE	.009	.024	.041	.059	.078		.014	.026	.040	.056	.076
11	SKODA	.010	.027	.047	.059	.085		.014	.028	.044	.061	.073
12	VTT	.010	.027	.046	.064	.084		.016	.029	.044	.063	.079
13	VEB	.010	.027	.044	.063	.082		.015	.028	.042	.059	.075
14	IKE	.011	.028	.047	.066	.086		.016	.030	.045	.064	.084
15	BARC	.012	.030	.049	.068	.089		.019	.034	.050	.069	.087
16	IBK	.010	.028	.047	.066	.086		.015	.029	.044	.062	.077
NEACRP	MEAN	.011	.027	.045	.063	.083		.016	.028	.042	.059	.077
	ST.DEV	.002	.003	.003	.004	.006		.003	.005	.006	.007	.010
NEACRP+CRP	MEAN	.011	.027	.045	.064	.084		.016	.029	.043	.060	.078
	ST.DEV	.002	.002	.003	.004	.005		.003	.004	.005	.006	.009
CRP	MEAN	.011	.028	.047	.064	.085		.016	.030	.045	.063	.079
	ST.DEV	.001	.001	.002	.003	.002		.002	.002	.003	.003	.004

IKE and IBK agree well, the variation coefficient being 0.2% at the most for the fresh lattice. In the case of the fresh poisoned lattice (Table 2), the variation is somewhat lower in treating all the 16 participants than in the NEACRP case, but the CRP results may be considered to be in good agreement, since the variation coefficient is 0.6%. Results of CEA, ENEA, NAIG, JAERI, SKODA, VTT, VEB and IKE are in good agreement, variation not exceeding 0.2%.

According to what has been said the, values of Gd reactivity worth for the fresh lattice shown in Table 3, are in good agreement for the CRP values compared to those of NEACRP, the standard deviation being 0.3% and 0.7% respectively. On the whole the agreement of results is acceptable (standard deviation is 0.6%), considering that variation of k-infinity values of the fresh lattice is 0.9%.

Further analysis of data in Table 2 shows that, in comparison to the values of the regular lattice, the variations of multiplication factors for the poisoned lattice somewhat increase during burnup. The largest fluctuations of results are at burnup values from 1000 MWd/t to 3000 MWd/t and they decrease towards the end of the cycle. This is caused probably by different Gd destructions and Gd reactivity worth as shown in Table 3. Influence of gadolinium is diminished at the end of the cycle, since it has burned out. The same is true for both comparisons of all the available data sets and for CRP participants separately.

In order to separate the burnup effects from the reactivity effects for the fresh lattice, reactivity losses for the regular lattice from 1000 MWd/t and reactivity gains for the poisoned lattice above 1000 MWd/t were calculated and they are shown in Table 4. By comparing Table 4 with Table 5 which shows reactivity gain and Gd destruction, one may conclude that Gd destruction affects the reactivity gain more than burnup. Burnup of 1000 MWd/t is taken as referent value to avoid the xenon effect,

Table 7. Variation of the main results

Parameter	VARIATION			Target accuracy (%)
	NEACRP	NEACRP + CRP	CRP	
Multiplication factor for regular lattice				
0 MWd/t	0.9	0.8	0.5	0.25-0.5
5000 MWd/t	0.7	0.6	0.4	
10000 MWd/t	0.9	0.8	0.4	
Multiplication factor for poisoned lattice				
0 MWd/t	1.1	0.9	0.6	0.25-0.5
5000 MWd/t	1.2	0.9	0.4	
10000 MWd/t	0.7	0.6	0.3	
Reactivity life time for regular lattice(*)	6.1	7.4	2.1	2-5
Reactivity life time for poisoned lattice(*)	13.2	10.3	10.1	2-5
Changes in isotope densities -regular lattice/10/				
U-235 depletion	0.8	0.7	0.5	2
Pu-239 build-up	5.8	4.7	1.9	2
Pu-240 build-up	3.6	3.0	2.2	-
Changes in isotope densities -poisoned lattice/10/				
U-235 depletion	1.2	1.2	1.3	2
Pu-239 build-up	4.6	4.4	4.4	2
Pu-240 build-up	6.9	5.5	2.1	-
Pin power relative to lattice/10/				2
Pin No. 4	0.8	1.3	2.5	
Gd pin	3.6	3.3	3.1	

(*) Deduced from the standard deviation of the reactivity loss between 1000 and 10000 MWd/t (Table 2) and assuming a reactivity swing of 1% per 1000 MWd/t at end of cycle.

although it has been shown/10/ that the magnitude of xenon effect seems insensitive to gadolinium poisoning and it may be neglected in treatment of burnup dependent solutions. Reactivity loss is correlated with U-235 destruction and Pu-239 build-up presented in Table 6. It may be seen that the Pu-239 build-up does not affect significantly the reactivity loss.

Summary of the variations of the most important parameters is shown in Table 7. Since experimental values for this benchmark are not known, the computed variations are compared to the typical target accuracies for power reactors recommended by IAEA/7/. The variations of CRP results are in good agreement with the target accuracies except for the lifetime and Pu-239 build-up in case of the poisoned lattice.

The NEACRP and NEACRP+CRP variations are somewhat larger than target accuracies for the regular lattice except for the U-235 concentrations. Particularly large is the variation of Pu-239 concentration. Variation of the multiplication factor for the poisoned lattice is somewhat larger, but the variation of the deduced reactivity lifetime is rather large compared to the target accuracy. The pin power variations are acceptable in comparison to the target accuracies/10/.

CONCLUSION

From the obtained comparison results one may conclude that the uncertainties of calculating the important parameters for both the regular and the poisoned lattice are due to different reaction rates for U-235, Pu-239 and gadolinium isotopes. This results from different data libraries applied. Results of the participants applying ENDF/B-4 library show much better agreement. Taking into account the complexity of the problem, the values of initial gadolinium worth are in quite a good agreement. Variations of the reactivity loss and reactivity gain above 1000MWd/t lead to higher uncertainties of the reactivity lifetime, particularly in the case of the poisoned lattice. The fact that the variation of the Pu-239 build-up is large suggests that it may be influenced by the spectrum effect.
On the whole, an acceptably good agreement is obtained for the CRP results treated separately although their number is rather small. Smaller variations are observed in treating 16 sets of results (NEACRP+CRP) than in the NEACRP comparison.
The analysis would be complete if a larger number of results were available. It could be suggested to the participants to repeat calculations by applying the same cross section library to separate the effect of data base from the computational methods.

REFERENCES

/1/ Report of the Research Coordination Meeting on Safe Core Management with Burnable Absorbers in VVERs, IAEA, Vienna, Dec.1989.

/2/ C.Maeder, P.Wydler, International Calculations for a BWR Lattice with Adjacent Gadolinium Pins, EIR-Bericht Nr.532 NEACRP-L-271, Wurenlingen, 1984.

/3/ J.Vacek, P.Mikolas, Experience with WIMS Computer Code at Skoda Plzen, A Technical Committee Workshop on In-Core Fuel Management IAEA, Vienna, Dec. 1989, 622-I3-TC-676.3

/4/ M.Anttila, Co-ordinated Research Project on Safe Core Management with Burnable Absorbers in VVERs. Finnish Results for the Benchmark problem 4.2.,VTT Report No. RFD-5/90, 1990.

/5/ R Becker, GDR-Calculation Results of Gadolinium Fuel-Pin Lattices, CRP-GDR-5775, 1990
/6/ D Lutz, Results for the Square Lattice Benchmark of Maeder and Wydler, Private communication, 1990
/7/ P D Krishnani, Analysis of Benchmark on Interactive effects of Gadolinium Poisoned Pins in BWRs by the Computer Code LWRBOX, Note No ThPD/336, Bhabha Atomic Research Center, Trombay, Bombay, 1991
/8/ N Marinkovic, Use of Burnable Poisons in Prolonged VVER Fuel Cycles, Annual Report IAEA Contract No 5330/RB, Dec 1989
/9/ Reactor Burnup Physics, Proc of IAEA panel, 12-16 July 1971, p 278, Vienna, 1973
/10/N Marinkovic, COMPARISON CALCULATIONS FOR A BWR LATTICE WITH ADJACENT GADOLINIUM PINS performed at the Nuclear Engineering Laboratory of the Boris Kidric Institute of Nuclear Sciences, IAEA Contract No 5330/RB, July 1991

CALCULATIONAL MODELS FOR GADOLINIUM EFFECTS IN VVER LATTICES

C ALVAREZ-CARDONA, R GUERRA-VALDES,
D LOPEZ-ALDAMA
Centro de Estudios Aplicados al Desarrollo Nuclear,
La Habana, Cuba

Abstract

The advantage of gadolinium as burnable absorber in LWR have been practically demonstrated

Nowadays experimental and theoretical studies on the effect of the introduction of gadolinium as burnable absorber in VVER type reactors are in progress

This work presents calculational models developed for the description and analysis of the physical characteristics of VVER type hexagonal lattices containing gadolinium based on the WIMS-D/4 code

In the first part of the work the models are applied to experimentally studied lattices of the critical assemblies ZR-6M at KFKI, Budapest and LR-0 at Rez, Czechoslovakia The integral lattice parameters K_∞ and the spectral indexes as well as the power rate distribution were calculated Our calculational results show fair agreement with the experimental results

The second part deals with the description of the effects due to the presence of gadolinium during the reactor cycle To this end four infinite lattices proposed in the Sidorenko's task were calculated by means of WIMS-D/4 code

As main results the dependencies of K_∞, nuclear densities for the U, Pu and Gd isotopes and power rate distribution on the burnup were obtained

This work was under the International Atomic Energy Agency research contract 5701/RB

1 Introduction

In the frame of CRP Safe Core Management with Burnable Absorbers in VVERs, altogether with numerical benchmarks ,two experimental benchmarks and an operational one were investigated

The present paper shows the obtained results in VVER lattices calculations containing Gd_2O_3 in different w/O in the fuel at zero power, experimentally investigated in ZR-6 critical assembly in CRIP, Budapest, Hungary and in the LR-0 critical assembly, in Rez, Czechoslovaquia and also presents the solution of the operational benchmark designed as Sidorenko task

2. Calculational results for ZR-6 critical assembly experiments

The calculations were performed using the spectral code WIMS-D/4 and the diffusion code SNAP-3D, and were focused to the core integral parameters, spectral indexes, fission rates and thermal fluxes bidimensional distributions determination.

The calculations were carried out according to experimental conditions and specifications described in papers [1, 2]. Nuclear densities and geometrical dimensions for normal fuel in ZR-6 (3.6 at % enrichment) were assumed as in reference [3].

Spectral code used was the WIMS-D/4 code [4]. Multicell option was used with the aim of obtaining effective cross sections and reaction rates in configurations X7.

A FEWGROUPS structure of 36 groups was employed and from these 11 were thermal groups. This feature allows a 4 or 8 groups VECTOR structure for condensation.

Four mesh points were used for transport calculations inside fuel rods. In the case of Gd_2O_3 absorber rods eight points were used.

For leakage corrections corresponding to experimental bucklings B_1 approximation was used.

2D-Diffusion calculations were performed with SNAP-3D code [5], using effective cross sections previously obtained through the spectral code calculations.

Experimentally measured material and axial bucklings for spectral and criticality calculations were taken from [1] and are given in table 1.

Table 1.

Recommended material and axial bucklings for the investigated configurations.

Configuration	$B^2[m^{-2}]$	$Bz^2[m^{-2}]$
I7	97.84	47.95
J7	91.88	42.84
K7	89.03	39.27
L7	88.03	37.66
M7	85.38	35.89
N7	84.25	35.25

Table 2.

Supercell calculations results.

Case	K_∞	$M^2[cm^2]$	$K_{eff}(B^2_{exp})$	$B^2_{exp}[m^{-2}]$
I	1.411376	39.98	1.008829	97.84
J	1.386899	39.82	1.010539	91.88
K	1.368344	39.73	1.006433	89.03
L	1.363005	39.70	1.005779	88.03
M	1.356877	39.64	1.009781	85.38
N	1.354011	39.62	1.011292	84.25

Table 3.

2D-Diffusion calculations.

Case	$K_{eff}(Bz^2_{exp})$	$Bz^2_{exp}[m^{-2}]$ (recommended)
I	1.011597	47.95
J	1.010211	42.84
K	1.008336	39.27
L	1.009602	37.66
M	1.011096	35.89
N	1.011374	35.25

In table 2, K_∞, M^2 and $K_{eff}(B^2_{exp})$ values are given. For WIMS-D/4 calculations it is neccesary to provide material bucklings as $Bm^2=Br^2+Bz^2$. In our case the value equal to $1/2*Bm^2$, for both radial and axial bucklings was assumed.

In table 3, results for 2D criticality diffusion calculations are shown. Bz^2 recommended values are not the experimental measured ones. They were obtained from the corresponding critical heights for each configuration as $Bz^2=(\pi/Hcrit+\delta z)^2$, where δz=13.24 cm is the recommended value for the axial reflector saving in the case of 12.7 mm lattice pitch configurations.

In 2D-Diffusion calculations for fuel cells, different four group effective cross sections obtained from spectral code WIMS-D/4 values were used, depending on their relative position in the X7 supercell.

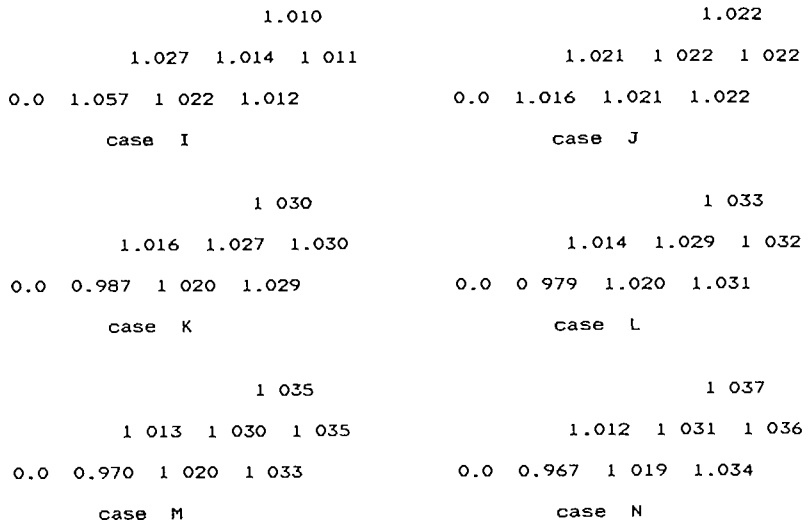

Fig 1

Fission rate distributions

WIMS-D/4 calculation with K_∞ spectrum.

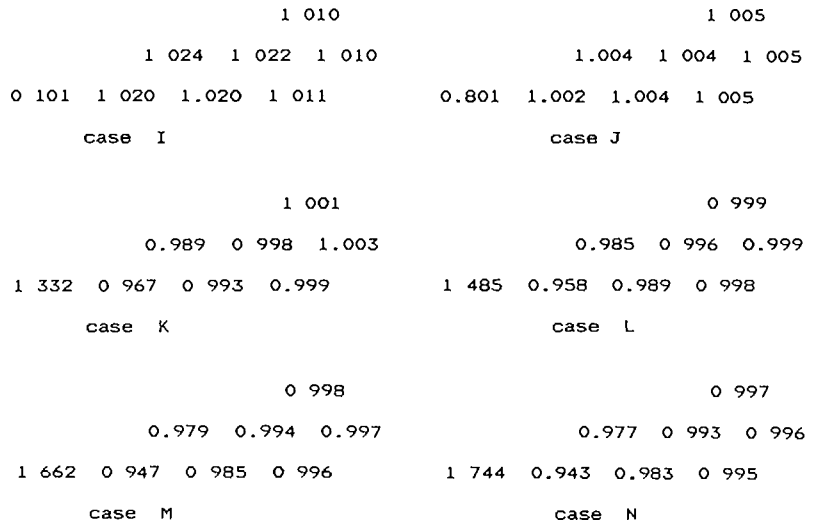

Fig. 2

Absorption rate distributions.

WIMS-D/4 calculation with K_∞ spectrum

In the case of reflector, four group effective cross sections were obtained from a developed calculational model for an equivalent 20 cm radius core with several edition zones in the 20 cm thick water reflector region.

Afterwards, several attempts were made in order to achieve better agreement between calculational and experimental results Nevertheless K_{eff} maximum deviation from experimental value remains about 1%. Best agreement corresponds to cases K and L in both approximations from spectral and 2D-Diffusion codes.

Fission rate and absorption rate distributions are given in figs. 1 and 2 for K_∞ spectrum as they were obtained from WIMS-D/4 code

Thermal flux and fission rate distributions were obtained from SNAP-3D four group flux distribution by using adequate weighting factors by means of the CDF transformation module [6]

In figs 3 and 4 thermal flux and fission rate distributions for fuel elementary cells from 2D-Diffusion calculations are shown

In table 4 spectral indexes for specified positions in the supercell are given (positions 2, 3 and 8)

In table 5 comparisons between calculated and measured results for spectral index SI(Np/Ce) are made

3. LR-0 Experimental Benchmark

The aim of this task was the calculation and comparison of the energy release distributions in fuel assemblies with burnable absorbers, performed at the LR-0 critical assembly in Rez, Czechoslovaquia.

The burnable absorber rods composition is an homogeneous mixture of UO_2 and Gd_2O_3 with different contents of gadolinium A detailed description for the LR-0 experimental facility, as well as a description for the research plan carried out may be found in paper [8]

Our calculations were realized using the CLUSTER and MULTICELL options of WIMS-D/4 code [4], with the aim to perform the comparisons with the experimental results given in [8]

CALCULATED DATA FILE

THERMAL FLUX DISTRIBUTION

TASK 3.2 ZR-6 LATTICE CRITICALITY CALCULATION. CASE I

0	0												
1	1980												
2	1911	1897											
3	1869	1857											
4	1841	1838	1829										
5	1814	1813	1812										
6	1784	1786	1798	1834									
7	1749	1759	1808	0									
8	1705	1707	1720	1757	1731								
9	1655	1655	1655	1642	1604								
10	1603	1601	1593	1578	1553	1517							
11	1551	1541	1525	1503	1475	1441							
12	1509	1499	1477	1453	1429	1402	1375						
13	1487	1437	1404	1378	1355	1339	1340						
14	0	1418	1356	1325	1301	1286	1299	0					
15	1350	1299	1266	1242	1223	1215	1229	1207					
16	1233	1222	1201	1180	1161	1148	1144	1146	1149				
17	1138	1129	1115	1100	1088	1087	1107	1161	1254				
18	1058	1055	1048	1039	1031	1035	1072	1174	1387	1692			
19	985	983	982	982	988	1030	1164	1486	0	0			
20	924	924	929	952	964	989	1126	1484	0	0	0		
21	884	885	911	0	965	1076	1424	0	0	0	0		
22	895	887	879	902	936	1032	1348	0	0	0	0	0	
23	1011	957	926	934	1023	1294	0	0	0	0	0	0	
24	0	1257	1151	1082	1116	1331	0	0	0	0	0	0	0
25	0	0	0	1386	0	0	0	0	0	0	0	0	0
H2/H1	12	11	10	9	8	7	6	5	4	3	2	1	0

Fig. 3

CALCULATED DATA FILE

FISSION RATE DISTRIBUTION

TASK 3.2 ZR-6 LATTICE CRITICALITY CALCULATION. CASE I

0	0												
1	2013												
2	1943	1930											
3	1901	1890											
4	1875	1871	1862										
5	1847	1844	1844										
6	1816	1817	1829	1865									
7	1780	1790	1838	0									
8	1735	1736	1748	1786	1760								
9	1685	1684	1684	1670	1632								
10	1632	1630	1621	1605	1580	1544							
11	1578	1569	1553	1530	1501	1467							
12	1535	1526	1502	1480	1454	1426	1400						
13	1513	1461	1429	1403	1379	1361	1362						
14	0	1441	1380	1348	1324	1308	1319	0					
15	1372	1320	1288	1264	1243	1232	1243	1216					
16	1253	1243	1221	1201	1180	1163	1155	1149	1142				
17	1157	1148	1134	1117	1102	1094	1103	1139	1206				
18	1076	1073	1065	1054	1043	1040	1063	1139	1305	1548			
19	1000	997	996	991	991	1017	1120	1377	0	0			
20	934	933	937	959	963	973	1076	1363	0	0	0		
21	885	887	910	0	946	1026	1302	0	0	0	0		
22	878	871	864	885	909	978	1228	0	0	0	0	0	
23	958	912	886	889	957	1172	0	0	0	0	0	0	
24	0	1145	1056	996	1020	1192	0	0	0	0	0	0	0
25	0	0	0	1230	0	0	0	0	0	0	0	0	0
H2/H1	12	11	10	9	8	7	6	5	4	3	2	1	0

Fig. 4

The nuclear densities used for calculations are given in table 6 and the geometrical description for fuel elementary cells and absorber rod cells are shown in table 7.

In the CLUSTER option it was used a simplified one dimensional model without consideration of the water hole in the fuel assembly center. In this model several fuel elements are allowed to be allocated in the same annulus in spite of the different distances from their centers to the absorber rod positions.

With the aim of obtaining the expected results for positions 1, $\sqrt{3}$, 2, $\sqrt{7}$, 3, 4, 5, $\sqrt{31}$, $\sqrt{37}$, 7, $\sqrt{52}$ (in lattice pitch units), it was neccesary to calculate using MULTICELL option in WIMS-D/4 code. It allows to differenciate several cells in the same hexagonal annulus, but with different distances to the absorber rod position (see table 8).

In table 9 results obtained by CLUSTER and MULTICELL options, using an energy structure of 36 energy groups in FEWGROUPS directive, are compared with experimental and calculational results from paper [8] as a function of Gd w/o (c) for the different fuel rings surrounding the absorber rod.

The comparisons with the results obtained by the program CELLPAR and with experimental results [8], allow us to say that using our models the best results for energy release distributions were obtained for regions near the absorber rod. For regions far enough from the absorber rod the energy release is overestimated more than it is done by calculational CELLPAR model. From the two used models, the MULTICELL option gives a better agreement with the experimental results.

Table 10 and figures 5 and 6 show the calculational results for energy release distribution and the function F(x,c) experimentally fitted defined in [8] for the lower Gd contents in absorber rods.

Table 4.

Case	SI(Np/Ce) cell 2	SI(Np/Ce) cell 3	SI(Np/Ce) cell 8
I	3.321	3.390	3.419
J	3.450	3.428	3.429
K	3.555	3.460	3.439
L	3.584	3.469	3.443
M	3.614	3.478	3.445
N	3.628	3.483	3.446

Table 5.

Comparisons between calculated and experimental values for SI(Np/Ce).

		Position		
Case		Cell 2	Cell 3	Cell 8
J7	exp.	3.450±0.056	3.340±0.056	3.348±0.055
	cal.	3.450	3.428	3.429
N7	exp.	3.668±0.060	3.393±0.055	3.371±0.059
	cal.	3.628	3.483	3.446

4. Sidorenko's benchmark problem for hexagonal lattices

This task consists in the study of four infinite lattices generated by repetition of one of the following elements:

i. Fuel cell without gadolinium.

ii. Fuel cell with gadolinium.

iii. Supercell with a gadolinium bearing central cell.

iv. Fuel assembly imitator with 6 gadolinium bearing cell.

In all cases first collision probability theory (PERSEUS) [4] was applied for the transport calculations. In the cases iii. and iv. MULTICELL approximation was used.

A 34-group FEWGROUPS energy structure was used which adequately describes the gadolinium isotopes absorption cross section energy

Table 6.

Composition data.

FUEL				
U-235	7.9704-4			
U-238	2.1343-2			
O-16	4.4280-2			
CLAD				
Zr	3.8217-2			
Hf	5.9030-6			
Nb	3.8637-3			
BAF	0.5 w/o	1.0 w/o	1.5 w/o	2.0 w/o
U-235	7.81148-4	7.77223-4	7.73298-4	7.69372-4
U-238	2.10386-2	2.09329-2	2.08272-2	2.07214-2
O-16	4.38845-2	4.39102-2	4.39358-2	4.39615-2
Gd-155	2.41687-5	4.83374-5	7.25062-5	9.66752-5
Gd-157	2.55568-5	5.11135-5	7.66704-5	1.02227-4
BAF CLAD				
Zr	3.44313-2			
Hf	5.31825-6			
Nb	3.48101-3			
MODERATOR (T=21° C)				
H-1	6.6729-2			
O-16	3.3364-2			

Table 7.

Geometrical data.

$h_{ij} = 1 - (r_i/r_j)^2$

Radii [cm]	FUEL	BAF
r_1	0.0700	0.0725
r_2	0.3765	0.3665
r_3	0.3855	0.3855
r_4	0.4575	0.4575
$r_5 = r_{eq}$	0.6405	0.6405
Pitch [cm]	1.22	1.22
h_{12}	0.9654	0.9609
h_{34}/h_{24}	0.8985	0.8095

Table 8

MULTICELL option data.

Cell position x [pitch]	LR-0 cell type number	MULTICELL type number	Number of cells N	Total fuel volume V_f [cm^3]
0	0	1	1	0 421985
1	6,7,13,14,19,20	4	6	2 671964
√3	3,5,8,18,21,23	16	6	2 671983
2	2,12,24,15	5	6	2 671963
√7	1,4,22,25,26,17	17	12	5 343971
3	11,27	6	6	2 671962
4	10,28	7	6	2 671962
5	9,29	8	6	2 671961
√31	16,30	21	12	5 343973
√37	31,37	25	12	5 343971
7	34 32,36	10	6	2 671962
√52	33,35	12	6	2 671974

Table 9

Experimental and calculated values of relative energy release in the BAF pin and its neighbouring fuel pins

c [w/o]	x [pitch]	exp	CELLPAR	DSN/CLUSTER	MULTICELL
0 5	0	0 4094	0 4692	0 4480	0 4237
	1	0 9255	0 9430	0 9420	0 9418
	2	0 9820	0 9846	0 9860	0 9853
	3	1 0000	1 0000	1 0000	1 0000
1 0	0	0 3344	0 3935	0 3714	0 3482
	1	0 9181	0 9336	0 9357	0 9335
	2	0 9802	0 9821	0 9838	0 9829
	3	1 0000	1 0000	1 0000	1 0000
1 5	0	0 3034	0 3538	0 3360	0 3136
	1	0 9065	0 9291	0 9298	0 9290
	2	0 9765	0 9808	0 9826	0 9816
	3	1 0000	1 0000	1 0000	1 0000
2 0	0	0 2755	0 3350	0 3143	0 2924
	1	0 9074	0 9264	0 9270	0 9257
	2	0 9769	0 9799	0 9818	0 9807
	3	1 0000	1 0000	1 0000	1 0000

Table 10

MULTICELL option results

$P(x,c) = \nu\Sigma_f \Phi V_f$

$P'(x,c) = P(x,c)/N$

$p(x,c) = P'(x,c)/\max[P'(x,c)]$

$P(x,c) = P'(x,c)$ for $x \leq 4$

$= (1/5)\ \Sigma\ [P'(x,c)]$ for $x > 4$

$P^*(x,c) = P(x,c)/\max[P(x,c)]$

$F(x,c) = 1-[1-\exp(-b\ c)]\ g\ \exp(-a\ \sqrt{x})$, [2]

c = 0 5 w/o of Gd_2O_3

$F(x, 0\ 5) = 1-0\ 5049\ \exp(-1\ 944\ \sqrt{x})$

Cell position x [pitch]	P(x c) [1/s]	P (x c) [1/s]	p(x c)	P*(x c) [1/s]	P'(x c)	F(x c)
0	3 04354 3	3 04354 3	0 4188	3 04354 3	0 4192	0 4951
1	4 05901 2	6 76502 3	0 9308	6 76502 3	0 9317	0 9277
√3	4 21831 2	7 03052 3	0 9673	7 03052 3	0 9682	0 9606
2	4 24653 2	7 07755 3	0 9738	7 07755 3	0 9747	0 9677
√7	8 58870 2	7 15725 3	0 9847	7 15725 3	0 9857	0 9786
3	4 31007 2	7 18345 3	0 9883	7 18345 3	0 9893	0 9826
4	4 33705 2	7 22842 3	0 9945	7 22842 3	0 9955	0 9897
5	4 35069 2	7 25115 3	0 9977			0 9935
√31	8 71014 2	7 25845 3	0 9987			0 9949
√37	8 71413 2	7 26178 3	0 9991	7 26124 3	1 0000	0 9958
7	4 36088 2	7 26813 3	1 0000			0 9971
√52	4 36001 2	7 26668 3	0 9998			0 9973

dependence and the plutonium isotopes resonances at thermal energies [9].

The transport calculations were done taking 6 material regions in the gadolinium bearing rod and 1 material region in other rods Later calculations considering 8 material regions in the gadolinium bearing rods had shown no significant differences

The number of mesh intervals was taken as follows

Cases i, ii and iii . 18 mesh intervals in the gadolinium bearing cells and 10 mesh intervals in the other ones cells

Case iv 18 mesh intervals in the gadolinium bearing cells, 9 mesh intervals in the 8 cells as well as in the nearest neigboring cells of the gadolinium bearing cells, and only 5 mesh intervals in the other one cells

The number of different cell types considered was 6 in the supercell case and 25 in the fuel assembly case, respectively In the later case a higher number of different cells was not used due to the prohibitively large main memory and CPU time required

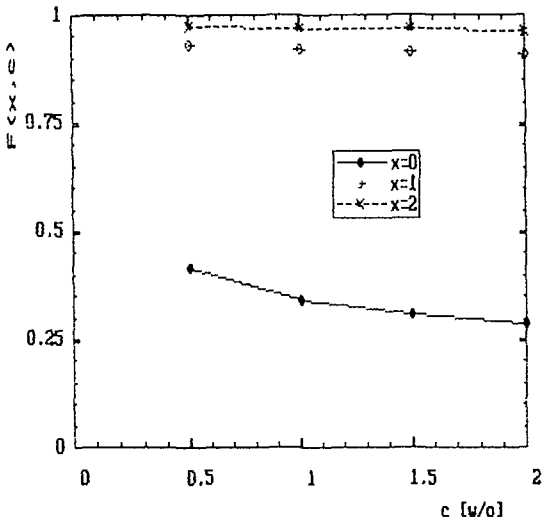

Fig. 5. Energy Release Distribution

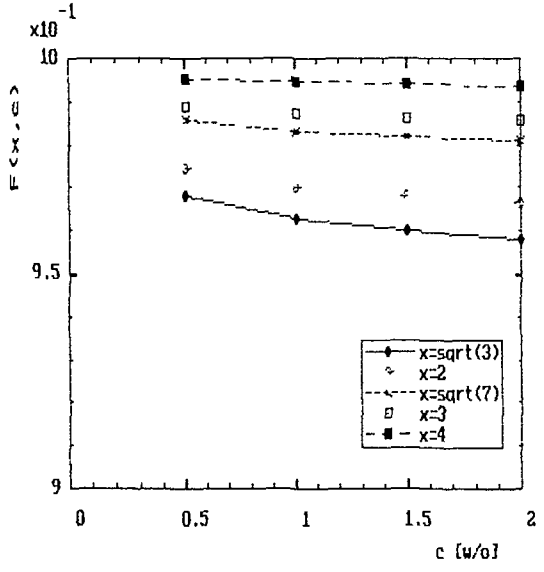

Fig. 6. Energy Release Distribution

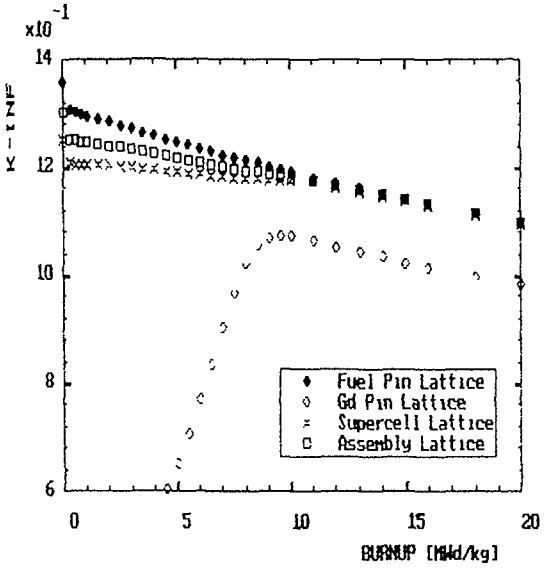

Fig. 7. K-inf vs Burnup.

Nevertheless, the description used is well suited to study the particularities of this configuration. According to the literature available to us this is the problem of largest dimensions solved using the WIMS-D/4 MULTICELL approximation in a burnup calculation.

In all cases the burnup calculation ranged from 0 to 20000 MWd/tU with the following lattice calculation frequency:

Each 250 MWd/tU for the interval from 0 to 1000 MWd/tU.
Each 500 MWd/tU for the interval from 1000 to 10000 MWd/tU.
Each 1000 MWd/tU for the interval from 10000 to 16000 MWd/tU.
Each 2000 MWd/tU for the interval from 16000 to 20000 MWd/tU.

Calculational results were:

- K_∞ (fig 7), τ, L^2, M^2 as functions of burnup.

- Nuclear number densities of the isotopes of gadolinium, uranium and plutonium as functions of burnup for each of the specified cells (figs. 8, 9, 10, 11).

- One-group constants as functions of burnup for the specified cells

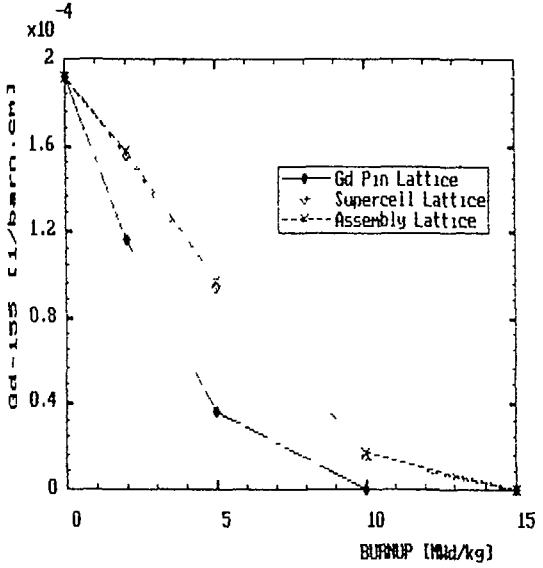

Fig. 8. Gd-155 Number Density vs Burnup.

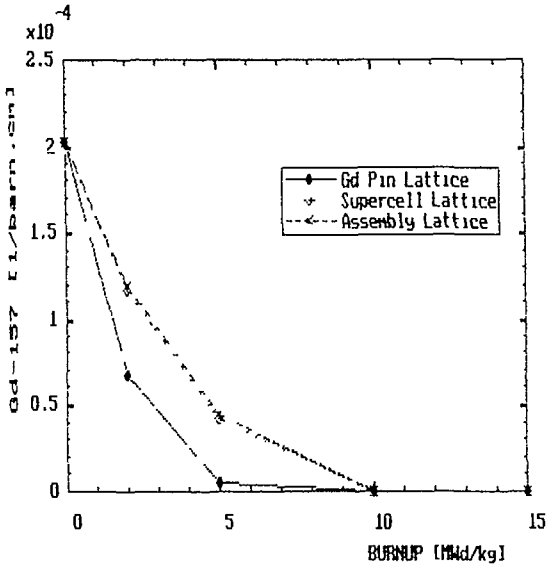

Fig. 9. Gd-157 Number Density vs Burnup.

- One-group constants as functions of burnup for the supercell an for the assembly (figs. 12, 13).

- Power spatial distribution for the supercell and for the assembly as a function of burnup.

- Number density spatial distribution of the gadolinium isotopes in the fuel rod as a function of burnup (figs. 14, 15, 16).

- K_∞, τ, L^2, M^2 at 293 K cold state for burnup 0 and 20000 MWd/tU.

A comparison of our results with those by other authors from Bulgaria [11], Czechoslovakia [10, 12], Finland [13], India [14], Poland [15], USSR [16] and Yugoslavia [17] allows us to state that the MULTICELL approximation if properly used gives an adequate description of the fuel burnup in the range of gadolinium concentrations typical for PWRs

5. Conclusions

From these results one may conclude that the 34-group as well as the 36-group structures provide adequate descriptions of lattices bearing gadolinium and plutonium isotopes.

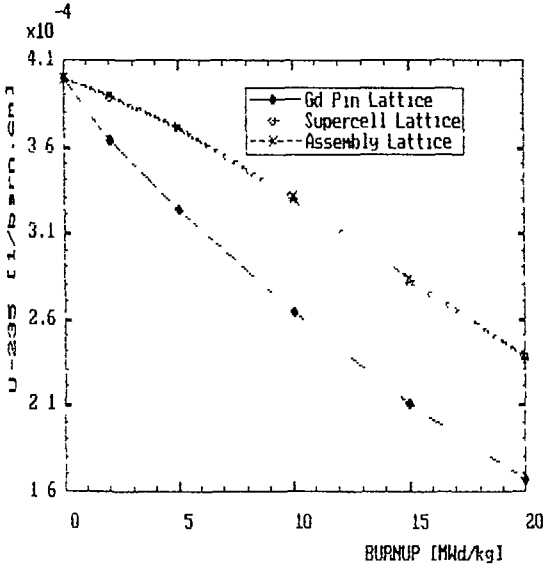

Fig. 10. U-235 Number Density vs Burnup.

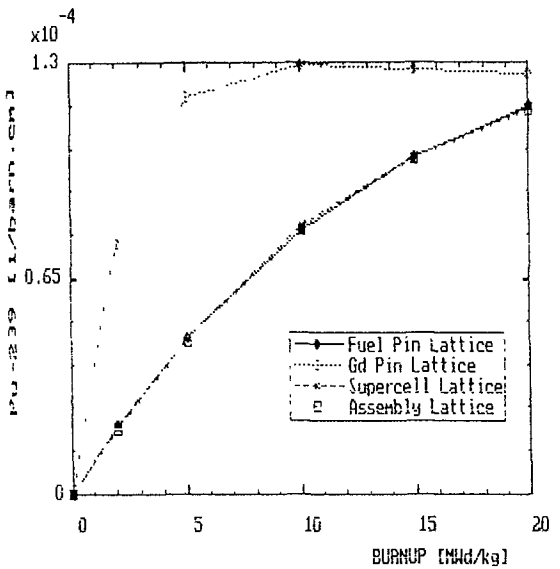

Fig. 11. Pu-239 Number Density vs Burnup.

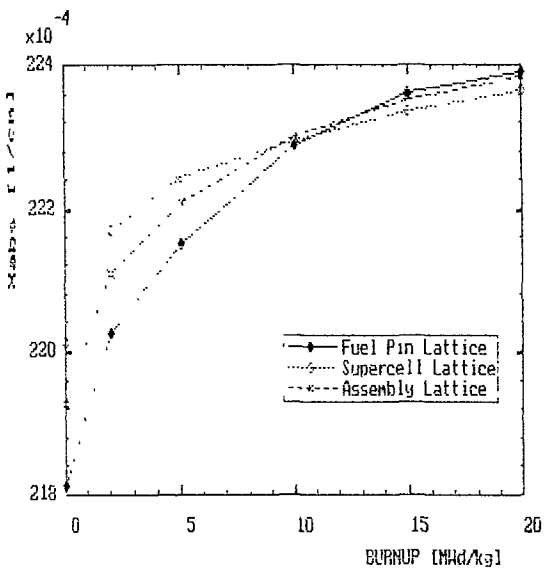

Fig. 12. Absorption Cross Section (Xabs) vs Burnup

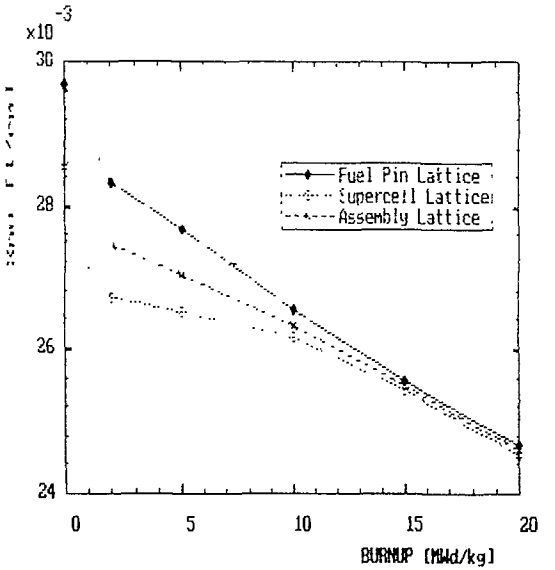

Fig. 13. Neutron Production (Xnu) vs Burnup

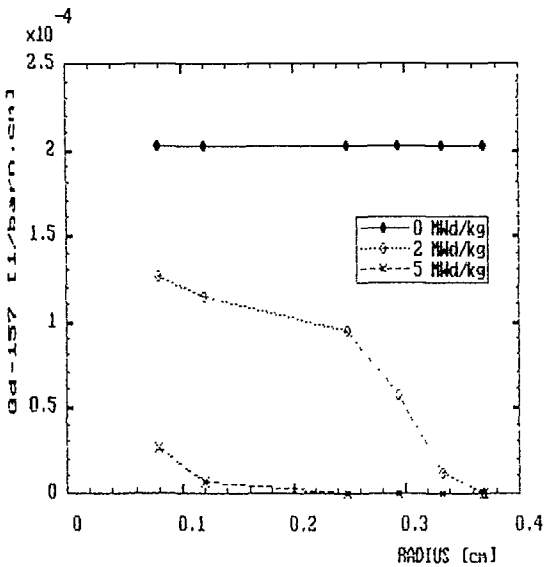

Fig. 14. Gd-157 vs Radius. Gd Pin Lattice

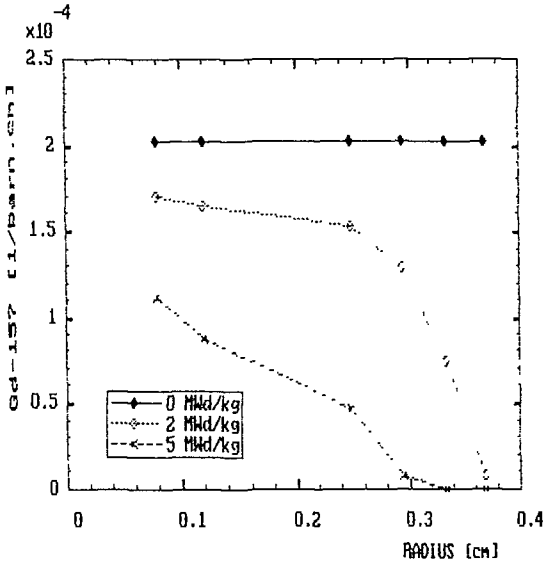

Fig. 15. Gd-157 vs Radius. Supercell Lattice

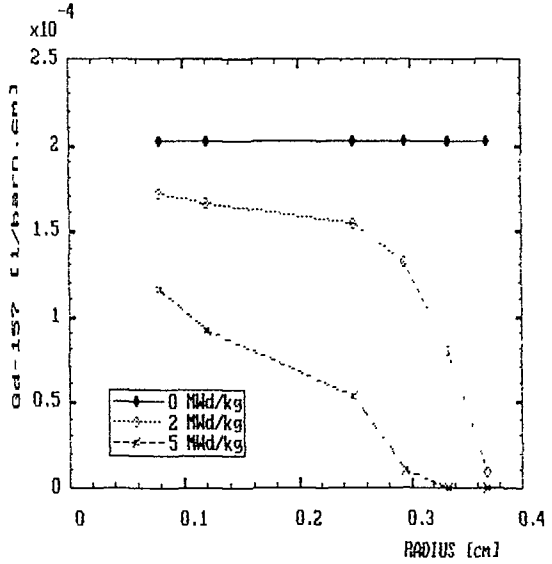

Fig. 16. Gd-157 vs Radius. Assembly Lattice

The possibility of applying the WIMS-D/4 code MULTICELL approximation not only to zero power but also to burnup calculations up to 20000 MWd/tU in order to obtain a satisfactory description of the fuel assembly is thus proved. This approximation brings out the differences among the cells and makes thus possible the calculation of few-group constants and isotopic composition for each of the indicated cells as required by the problem at hand. Other WIMS-D/4 code options do not describe the supercell and assembly geometries as satisfactorily as the MULTICELL option.

The partition of the fuel region of the gadolinium bearing cells in 6 material zones and the subdivision of the entire cell in 18 mesh intervals permit good results in the burnup calculations. At the same time, the frequency of lattice calculations used in the burnup calculation has proven adequate to describe the changes of the isotopic composition of the lattices investigated.

It is necessary to use the directive ODDS to determine the spectral indexes by means of the MULTICELL approximation, since the directive REACTION is no longer adequate in this case.

Among all posed problems, the Sidorenko's benchmark for hexagonal lattices was the task of higher computer storage and CPU time requirements. Case iv needed 4352 Kbytes and took about 13 hours CPU in an EC-1061 computer.

References

1. I. Vidovszky and J. Gadó, Results of experiments carried out on VVER type lattices containing Gd absorber rods. Paper no. 622-I3-TC-6763/6.4 presented at Technical Committe/Workshop on IFM, IAEA, Vienna, 4-7 December 1989.

2. Lattice description of critical experiments at ZR-6 of KFKI, Budapest. Task 3.2. Document of CRP on Safe Core Management with Burnable Absorbers in VVER, IAEA, 1989.

3. Final Report of TIC, volume 1, Experimental Investigations of the Physical Properties of WWER-type Uranium-Water Lattices, Akadémiai Kiadó, Budapest 1985.

4. Halshall, M. J. A summary of WIMS-D/4 input options. AEEW-M1-327/1980.

5. C. W. J. McCallien. SNAP-3D A Three-Dimensional Neutron Diffusion Code, TRG Report 2677(R), UKAEA.

6. J. Gadó. Private Communication.

7. I. Vidovszky. Definition of the quantities to be calculated for the comparisons of VVER lattice calculations. Internal CRP document.

8. J. Bárdos, M. Hron, J. Drexler, P. Vesely. Fuel pin energy production in a core with Gd-poisoned fuel. Technical Committee/Workshop on In-Core Fuel Management. IAEA, Vienna, 4-7 December 1989.

9. Stamm'ler R. J. J., Abbate M. J., Methods of Steady State Physics in Nuclear Design. Academic Press, London, 1983.

10. Vacek J., Test Problems Resolution Results by Using WIMS-D/4 Code, Paper presented at the 18th Simposium of TIC, Prachatice, Czechoslovakia, 1989, (in Russian).

11. Prodanova R., Some Results on Benchmark Problem Calculations. IAEA Research Contract No. Bul 5599 Progress Report, IAEA Sofia, Bulgaria, 1989.

12. Vacek J., Mikolas P., Experience with the WIMS-D/4 Computer Code at Skoda, Plzen. Paper presented at Technical Committe Workshop on IFM, IAEA, Vienna, 4-7 December, 1989.

13. Anttila M., Finnish Results for a VMK Benchmark Problem Concerning Use of Gadolinium in Fuel Rod Lattices. Part II. Calculations with an ENDF/B-IV Based Data Library. 891002 Ref 133004 Doc:(89)11.

14. Jamnathan V., et al, Indian Results of the Benchmark on the Use of Gd as Burnable Poison in VVERs. Paper presented at Technical Committe Workshop of CRP on Safe Core Management with Burnable Absorbers in VVERs, IAEA, Vienna, December, 1989.

15. Kulikowska T., et al, Safe Core Management with Burnable Poison in VVERs. IAEA Research Contract No 5329/RB, Progress Report No 1, IAE Swierk, Poland, 1989.

16. Pshenin V. V., Sidorenko V. D., Calculation Results for Gadolinium in Fuel Rod-Lattices. Paper presented at Technical Committe Workshop on IFM, IAEA, Vienna, 4-7 December, 1989.

17. Marinkovic N., Use of Burnable Poisons in Prolonged VVER Fuels Cycles. IAEA Research Contract No 5330/RB, Final Report. Boris Kidric Institute of Nuclear Sciences, Yugoslavia 1989.

CORRECTION OF EQUATIONS BASED ON MEASUREMENTS AND APPLICATION TO THEORY AND EXPERIMENT ANALYSIS

V. LELEK, M. PECKA, L. VRBA
Nuclear Research Institute,
Řež, Czechoslovakia

Abstract

Problems of comparison between theory and experiment can be solved. Two mathematical methods are used: generalized Lagrange multipliers and direct calculation of flux derivatives. For both approaches it is necessary to develop methods for solving the equations of these new functions (Lagrange multipliers or derivatives), which are of the same type as fluxes, and approximately the same effort on computers as for flux calculations is needed.

From the measurements on critical assemblies ZR-6 and LR-0 data bases were composed and the diffusion program SVATOPLUK enables to use these data bases for finding the minimum of deviation of theory and experiment.

There are methods developed how to transfer the results from critical assemblies to power reactors, which enables for example to correct libraries for cell parameters at high temperature, specific burn up etc.

Because it is possible to calculate the accuracy of the parameters and their correlation matrix, one can derive the accuracy of the local flux calculations.

The algorithm for correcting the coefficients based on measurements for burn up, power feed-back and temperature is applied in the modified version of the code CRIT(BIPR-6)-CS.

Traditional treating of experiments involves theoretical calculations, comparison with measurements and analyses of differences found. If the agreement is not sufficient we look for ways of the improvement, partially in experiments, partially in calculations. It is possible to reach better agreement using calculations based on a new model, for example taking into account basic libraries of nuclear data, transport microcalculation of cells and the diffusion macrocalculation (for the critical assemblies obviously four-group net equations). The macrocalculations are then compared with measurements in the local (power of chosen rods) and integral (criticality, reactivity coefficients) quantities.

New model supposes changes not only in the input parameters, but also changes in the corresponding equations. Nevertheless, this way is not applicable in every case - for example, various libraries of nuclear data could give a multiplication factor differing up to 1%. At present, in spite of the fact that the computers make so great progress, it is not possible to perform two or three dimensional transport macrocalculations and demand precision at about 1% in the local powers. So the calculation is performed by the series of approximations and using input information with various precision. So as a result differences arise between measurements and calculations. This is really one of the reasons why the experimental testing equipments are built - otherwise only the calculations would be sufficient for the project and operation of power stations.

Existence of considerable differences between calculations and measurements is a challenge for developing better methods and performing additional measurements to have broader and more precise description of reality.

When we try to prepare more precise description, we can also take the position: the model is all right, only input parameters (i.e. coefficients of equations) are not precise. Using such an approach, the analyses of results could be considerably simplified. In most cases the calculation for critical assembly is performed in the four group net diffusion equations. If we formulate the agreement between calculations and measurements as a functional we obtain a complicated but exactly defined variational problem - to minimize the functional with supplementary conditions (fulfillment of the system of partial differential equations with given eigenvalue). The parameters we are looking for are the coefficients in the equations, which we have as supplementary conditions.

Briefly, we can describe this problem in the next steps. We write a group diffusion equation for neutron fluxes in the following form:

$$- \nabla D_k \nabla \Phi_k + \left(\Sigma_k + \frac{\pi^2}{H^2} D_k \right) = \Sigma_{k,k-1} \Phi_{k-1} + \frac{1}{\lambda} \chi_k \sum_{l=1}^{4} (\nu \Sigma_f)_l \Phi_l \qquad (1)$$

where Φ_k - neutron flux in the group k

D_k - diffusion coefficient in the group k

Σ_k - removal cross-section in the group k

χ_k - fission spectrum

ν - number of neutrons per one fission

$\Sigma_{f,l}$ - fission cross-section in the group l

H - height of the reactor

λ - maximum eigenvalue (k_{ef})

In equation (1) we can show or choose some of the coefficients (obviously connected with one type of material) as unknown or not precisely known, known with errors. Unknown parameters, characterizing used materials and constructional elements, are limited and naturally the number of experimental data must be sufficient to have a chance to determine correspodings coefficients. This means that the number of terms in the functional must be sufficient

$$I^{exp} = \sum_{\{p\}} \left(A_p^{exp} - N \sum_{l=1}^{4} \Sigma_{fl}^{e}{}_p \, \Phi_{l,p} \right)^2 \Big/ \chi_p^2 + \left(1 - \frac{1}{\lambda}\right) \Big/ \chi_\lambda^2 + \left(H^{exp} - H \right)^2 \Big/ \chi_H{}^2 + \sum_{r,s=1}^{K} w_{rs} \frac{(x_r - x_{r0})(x_s - x_{s0})}{x_{r0} \, x_{s0}} \qquad (2)$$

where p - place of the measurements

N - normalization factor

λ - eigenvalue

A_p^{exp} - experimental measurements in the place p

χ_λ - artificially chosen error of the eigenvalue (0.001)

x_r - unknown parameters

x_{r0} - initial estimation for x_r

w_{rs} - correlation matrix of x_r

If we also take into account reactivity measurements, functional (2) has more complicated form and include also adjoint solution. To minimize (2) two methods were developed: generalized Lagrange multipliers and the least square method, based on the direct calculation of flux derivatives.

The generalized Lagrange multipliers lead to the changing I^{exp} by L

$$L = I^{exp} + \int dV \, \Psi^* \left(R - \frac{1}{\lambda} S \right) \Phi + q_\phi \int dV \, \Sigma_f \, \Phi \qquad (3)$$

where $\left(R - \frac{1}{\lambda} S \right)$ is the symbolically written equation (1).

Minimization of L leads to the singular equation for Ψ^* which must be orthogonal to Φ (equation for q). Having Ψ^* and q , partial derivatives of L over x_k give direction to the minimum of I^{exp}. A big practical advantage is that we solve the equation only for one function Ψ^*, independently of the number of unknowns. The disadvantage is that we have only the direction but not the distance to the minimum. This method has been proved also for the case when we do not know fully which coefficients should be changed.

Direct calculation of derivatives leads to the equations for $\partial\Phi/\partial x$

$$R\frac{\partial\Phi}{\partial x} - \frac{1}{\lambda} S \frac{\partial\Phi}{\partial x} = \\ = -\left(\frac{1}{\lambda}\frac{\partial\lambda}{\partial x} S\Phi + \frac{\partial R}{\partial x}\Phi - \frac{1}{\lambda}\frac{\partial S}{\partial x}\Phi\right) \quad (4)$$

which have formally the same structure and properties as those for Ψ^+ . Using (4) in the process of minimizing (2) we obtain equations for x_r which are often nearly singular equations due to correlations between unknowns and small influence of unknowns on the results.

This negative features and also time consuming calculations of all $\partial\Phi/\partial x$ favor the treatment by the method of generalized Lagrange multipliers.

Lagrange multipliers treat also very simply the tolerances of fuel fabrication parameters which can lead to remarkable changes in fluxes for a large reactor where the solution of equations is not stable.

Both methods are included in the program SVATOPLUK [1] which was developed from the program BRETISLAV [2]. In this new program new developed iteration schemes were included for singular equations for Ψ^+ and $\partial\Phi/\partial x$.

The last version of this code was implemented on the personal computers AT-286 and AT-386, using operating systems DOS 3.30 and OS/2.

For the PCs, a system of some special programs for operating with input data and with output files was developed. User can operate directly with all of the input files that contain physical parameters of reactor cores and experimental data from the measurements on critical assemblies. In this time the input files describe more than 20 different experiments (which could be openly distributed) realized on assemblies ZR-6 (KFKI Budapest) and LR-0 (NRI Rez) and contain a lot of different sets of diffusion constants.

With the help of the special graphic program user can evaluate results of calculations more easily and quickly. It is possible to show on the screen - in color graphic mode - neutron fluxes in all groups, power distribution, differences between measured and calculated values etc.

All results can be saved on the disk in the binary form. User can simply modify this binary files and use them as an input for new calculations. All the system of the input and output files can be expanded and modified by the programs.

Suitable experimental data were the collection of measurements done on ZR-6 [3] critical assembly in Budapest which was in the technical and physical conception forerunner to the LR-0 critical assembly.

A lot of calculations based on various sets of four group parameters were performed in which various subsets of these were corrected. Initial differences between measurements and calculations were practically the same. Results obtained with corrected parameters were dependent on chosen subset of group parameters which were corrected.

The quantities of a special attention are diffusion coefficients. Using them for minimization, it is possible to reach the best results.

Table 1 demonstrates the simultaneous minimization of a series of experiments. Methods were developed how to transfer these results from critical assemblies to power reactors, which enables us, for example, to correct libraries of cell's parameters for states with higher temperature, burn-up, etc. [4].

Tests and controls were performed on the experimental data not included in the minimization algorithm. From all these calculations we can conclude that it is possible completely exclude systematic character of errors and differences near the water holes, reflector and absorbers. Survey of chosen results cannot fully show the degree of improvements because lot of measured cores are pure (only with fuel elements of the same type) with small amount of measurements near the reflector. Results could be demonstrated on color pictures which have been from results painted by special software.

The fact that the diffusion term in the equation (1) is necessary to formulate in a new way, taking into account explicitly non-zero currents on the cells boundaries is also demonstrated by the last works of soviet authors [5]. We have tested results also comparing them with the Monte-Carlo calculation of subregions with the zero currents boundary conditions. Resulting mean absorption cross sections for cells with absorber rods are nearer after correction. It is clear because in the lattices with studied materials and composition we are trying to reach transport accuracy with corrected diffusion approximation.

In the framework of our corrected equation we can conclude, that even higher precise of calculation could be reached than that of experiments. Generally it is explainable· the corrected equation are composed from the two parts - theory and experiment - on the same level and so they carry more information that alone each of their components (equations have been learned by experience).

Because we are able to calculate the accuracy of our parameters and their correlation matrix, we can find the accuracy of the local flux calculation, concepts which are one of the greatest interest for power reactor.

The above mentioned algorithm, for corrections of coefficients on the basis of measurements for equations with burn-up and both power and temperature feedback, was used for the correction of some coefficients in the computing code BIPR-6. The modified version of this code CRIT (BIPR-6)-CS [6] was created. The parameters which are looked for are the coefficients of approximations which reflect dependencies on the reactor state (burn-up, power, etc.) in the equations describing the reactor.

In the present version of the code, the algorithm of a correction based on the method of generalized Lagrange multipliers for a reactor on

Table 1. Improvement in the description of local power densities of various cores. Measurements from the critical assembly ZR-6 are used. Great errors in effective multiplication factor (denotes by *) are due to underestimation of extrapolated lengths.

Number of groups 4		Results taken using initial data (UNIRASOS) corrected data(SVATOPLUK)				
Control number	Temp. [°C]	Effective mult. factor	Value of Func.	Average deviation [%]	Maximum deviation positive [%]	negative [%]
188/188	20	0.9954 0.9976	2912 609	1.32 0.91	+ 2.70 + 1.69	- 17.4 - 5.74
188/188	80	0.9954 0.9975	2832 741	2.65 1.64	+ 4.86 + 3.48	- 20.3 - 8.87
188/188	130	0.9947 0.9968	8359 1158	2.15 1.14	+ 3.64 + 3.16	- 18.1 - 4.91
154/154	20	0.9971 1.0013	164 69	1.67 1.30	+ 5.03 + 4.32	- 5.58 - 2.54
154/154	80	0.9981 1.0023	74 E+6 40 E+6	1.18 1.13	+ 3.40 + 3.09	- 4.59 - 2.23
154/154	130	1.0001 1.0040	826 323	1.09 0.84	+ 3.01 + 1.90	- 5.91 - 3.09
161/161	20	0.9986 1.0006	1487 964	1.20 1.09	+ 4.43 + 3.99	- 7.72 - 3.24
161/161	80	0.9983 1.0006	31 E+6 15 E+6	1.31 1.16	+ 4.91 + 4.57	- 7.43 - 3.45
161/161	130	0.9971 0.9997	84 E+6 42 E+6	1.32 1.18	+ 3.27 + 2.50	- 8.04 - 3.14
163/161	20	1.0020 1.0040	121 E+6 60 E+6	1.35 1.12	+ 3.34 + 2.67	- 9.01 - 3.97
163/161	80	1.0030 1.0052	145 E+6 62 E+6	1.16 0.95	+ 2.12 + 2.01	- 8.84 - 3.78
163/161	130	1.0040 1.0063	73 E+6 33 E+6	0.93 0.83	+ 1.99 + 2.02	- 6.87 - 2.28
58/57	20	0.9970 1.0003	550 165	2.15 1.31	+ 4.17 + 5 06	- 10.4 - 4.32
147/138	20	0.9975 1.0004	5616 2090	2.17 1.48	+ 5.97 + 4.57	- 8.95 - 4.19
57/57	20	0.9938 0.9964	768 238	2.33 1.52	+ 4 82 + 5 51	- 16.2 - 8.11
100/100	20	0.9877 * 0.9885 *	1159 334	3.20 1.53	+ 7.64 + 5.32	- 6.08 - 3.95
101/100	20	0.9934 0.9981	1391 169	3 22 1.00	+ 5.73 + 3.33	- 10.1 - 3.90
103/103	20	0.9808 * 0.9836 *	7829 2101	3.98 2.00	+ 11.4 + 6.48	- 10.2 - 5.83
90/87	20	0.9863 * 0.9893 *	789 90	3.10 1.02	+ 5.02 + 2 50	- 8.02 - 2.25

power is used. For the time being, it is possible to perform the correction according to measurements of thermocouples or according to relative powers in assemblies, which are obtained by a reconstruction of power distribution from measurement of self-powered detectors.

The functional

$$I = \sum_{\{N_{TC}\}} \int_0^T \left[\frac{P_l(t') - \tilde{P}_l(t')}{\chi(t')\tilde{P}_l(t')} \right]^2 dt' + \sum_{\{N_{SPD}\}} \int_0^T \left[\frac{p(x_j,t') - \tilde{p}(x_j,t')}{\chi(x_j,t')\,\tilde{p}(x_j,t')} \right]^2 dt' + \sum_{t_i} \left[\frac{C_B(t_i) - \tilde{C}_B(t_i)}{\chi C_B(t_i)} \right]^2 + \left[\frac{T_{EOB} - \tilde{T}_{EOB}}{\chi T} \right]^2 + \left[\frac{T_{EOC} - \tilde{T}_{EOC}}{\chi T} \right]^2 \quad (5)$$

is minimized,

where (~ denotes experimental values)

- P_l - relative assemblywise power according to thermocouple measurement in assembly l
- p - relative power according to self-powered detector measurement
- N_{TC} - number of thermocouples
- N_{SPD} - number of self-powered detectors
- χ - relative error
- C_B - boron concentration
- T_{EOB} - part of operating lifetime, in which reactor was controlled by boric acid
- T_{EOC} - full operating lifetime of a cycle

The work of the code was tested by calculations of the VVER-440 reactor on the basis of mean relative power in assemblies according to thermocouple measurements from the 1st, 2nd and 3rd fuel cycle of the 4th unit of the Jaslovske Bohunice Nuclear Power Plant (NPP).

Considerable differences of relative power in assemblies on the core edge led to a correction of boundary conditions on the boundary with radial reflector. In case there are great differences with opposite sign in adjacent assemblies a better agreement can be reached by correction of local boundary coefficients only. These coefficients correct local values of boundary conditions of a single abscissa of the interface core - radial reflector. Their correction (on the base of measurements from the beginning of the 1st cycle) led to the decreasing of relative errors in boundary assemblies.

Table 2 An improvement of relative assemblywise powers description
J.Bohunice-4 NPP, 1st, 2nd, 3rd cycle
(O - original data set, C - corrected data set)

		Deviation			Functional		
		mean	maximum positive	maximum negative	rel. power	cB	total
1	O	1.9	7.30	-8.76	1725	392	2117
	C	1.4	4.03	-3.51	707	439	1146
2	O	4.1	9.00	-11.59	4913	67	4980
	C	2.9	8.54	-7.79	2672	55	2727
3	O	3.2	15.86	-7.86	3700	12	3712
	C	2.8	12.72	-8.14	2817	11	2828

All coefficients for an approximation of the diffusion length were corrected (for all fuel types) on the data from the 3rd fuel cycle (the reason is to consider the whole interval of burn-up) for the decreasing of relative errors in internal assemblies.

The comparison of calculational results with original input data and with a data set with corrected diffusion length coefficients and local boundary coefficients is presented in Table 2. The comparison of relative errors at one time point is demonstrated in Figure 1. Experimental data in the sector of symmetry 60° for a fuel charge with symmetry 30° were given. Relative great differences of measured values for some assemblies in symmetric position influence error distribution after the correction, too, and speaks about the quality of measurements or about the other sources of differences (manufacturing, geometry).

The general validity of corrected data was tested by experimental data from the 2nd fuel cycle, which were not used for the correction.

Later the code was tested by experimental data from the 1st cycle of the Loviisa-1 NPP, which had a different initial loading pattern. It is not possible to use for this reactor the data set corrected on the base of measurements from the J.Bohunice-4 NPP. An influence of correction of the same groups of coefficients (diffusion length approximation was corrected in spite of little burn up) on the measurements from this reactor and comparison with results of HEXBU-3D and BIPR-7 codes [7] is presented in Tab. 3 and on Fig. 2, 3.

The experimental data for this reactor were given in the 30° sector of symmetry. An influence of measured values differences in symmetric positions is eliminated in this case.

Most of all it is necessary to test widely the code by measurements from other reactors. According to up to now obtained results from the measurements which were at our disposal it can be supposed, that corrected data set can be probably used for other cycles of the same reactor to reach better agreement at least. It can be supposed, that this situation is partly caused by the fact, that the described

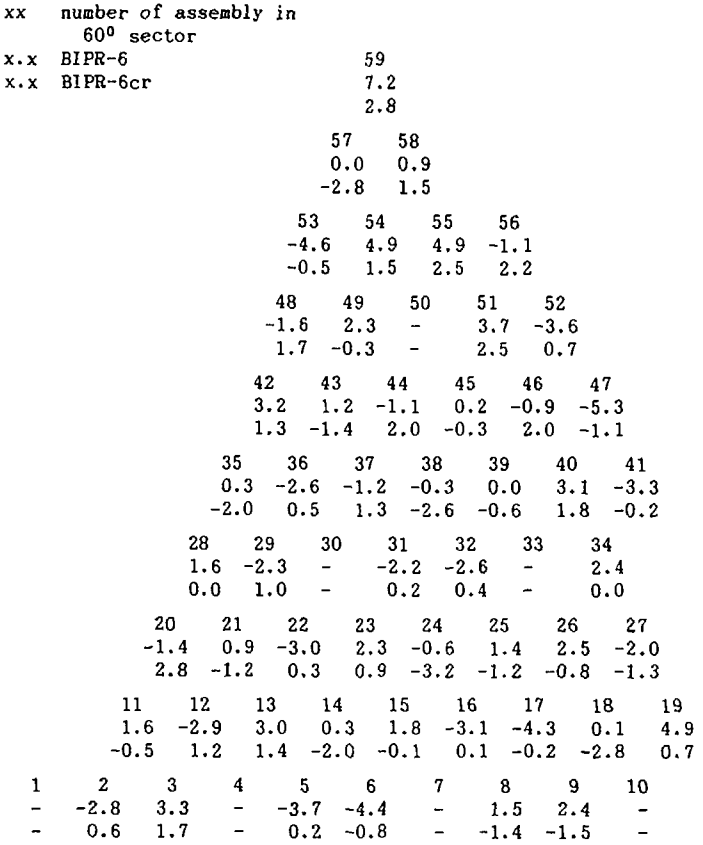

Fig.1 An improvement in relative assemblywise power description
(cr - corrected data set)
J.Bohunice-4, 1st cycle, 13 EFPD

correction can reduce systematic differences between the results of calculations and measurements, which can be different for different reactors (units) or for different loading patterns of the same unit, too. The reduction of systematic errors is estimated about 30 - 50 % and for the calculated examples practically vanish. But the experience from various calculation should be greater to support such statements.

Table 3 An improvement of relative assemblywise powers description and comparison with BIPR-7 and HEXBU-3D codes
(cr - calculation with corrected data set)

Loviisa-1 NPP, 1st cycle

	37 EFPD			285 EFPD			Oper. life time
	Deviation			Deviation			
	mean	maximum positive	maximum negative	mean	maximum positive	maximum negative	mean
BIPR-6	1.52	3.2	-5.7	1.81	2.9	-5.2	1.67
BIPR-6cr	0.99	1.8	-2.1	0.91	1.5	-2.8	0.95
BIPR-7	1.15	2.8	-2.8	1.50	3.5	-3.4	1.33
HEXBU-3D	1.40	4.8	-2.7	1.36	4.6	-2.1	1.38

xx	number of assembly in 60⁰ sector									
								46	47	
x.x	BIPR-6							-0.4	-2.7	
x.x	BIPR-6cr							-0.7	-0.6	
x.x	BIPR-7							1.0	-1.3	
x.x	HEXBU-3D							1.4	4.8	
						38	39	40	41	
						-2.6	-2.3	-1.7	-5.7	
						-1.4	-0.9	-1.5	-1.3	
						-1.6	-0.4	1.6	-2.7	
						-0.3	0.8	3.4	-2.6	
				30	31	32	33	34		
				-	0.6	-0.8	-	0.5		
				-	-0.8	-2.1	-	0.7		
				-	-0.5	-1.4	-	2.8		
				-	-0.8	-1.7	-	3.2		
			21	22	23	24	25	26	27	
			-2.1	0.8	1.5	-1.6	0.8	-0.3	0.5	
			-0.6	-0.7	0.0	0.0	-0.2	1.6	0.2	
			-2.8	-0.7	-0.6	-1.7	0.2	0.8	1.3	
			-1.1	-1.2	-0.7	-0.9	-1.1	0.9	2.9	
		11	12	13	14	15	16	17	18	19
		-0.3	0.5	0.9	-1.5	2.6	3.3	-0.6	-0.8	-0.3
		1.3	-1.1	-0.6	0.1	1.2	1.8	-2.1	-2.1	-0.6
		-1.0	-1.0	-0.7	-1.7	0.5	1.3	-1.5	1.2	0.3
		0.0	-1.6	-1.1	-1.0	-0.9	-0.2	-2.7	2.2	2.3
1	2	3	4	5	6	7	8	9	10	
-	3.3	0.9	-	2.6	2.8	-	0.7	-1.1	-	
-	1.7	-0.6	-	1.1	1.3	-	1.7	-0.1	-	
-	1.0	-1.3	-	1.2	0.3	-	0.9	0.5	-	
-	-0.5	-1.5	-	0.2	-0.8	-	0.5	0.0	-	

Fig.2 An improvement in relative assemblywise power description and comparison with BIPR-7 and HEXBU-3D codes
(cr - corrected data set)
Loviisa-1, 1st cycle, 37 EFPD

xx	number of assembly in 60⁰ sector									
								46	47	
x.x	BIPR-6							1.5	0.0	
x.x	BIPR-6cr							3.5	2.1	
x.x	BIPR-7							-0.3	3.4	
x.x	HEXBU-3D							2.1	-1.7	
						38	39	40	41	
						-2.0	-1.1	-1.3	-5.2	
						-0.9	0.1	-1.3	-1.3	
						-0.7	1.1	2.6	-2.8	
						-0.8	0.0	1.9	-2.1	
				30	31	32	33	34		
				-	1.9	1.5	-	0.4		
				-	0.5	0.2	-	0.5		
				-	0.1	0.5	-	3.5		
				-	-0.9	-1.1	-	4.6		
			21	22	23	24	25	26	27	
			-3.1	1.7	1.9	-2.7	1.7	-0.4	-1.8	
			-1.3	0.3	0.5	-0.9	0.8	1.4	-2.1	
			-3.0	-0.9	-0.2	-1.4	0.9	2.2	0.1	
			-1.3	-1.1	-0.7	-0.7	-0.5	0.8	4.2	
		11	12	13	14	15	16	17	18	19
		-2.9	1.0	1.7	-2.7	1.5	2.2	0.0	-1.6	-2.6
		-1.1	-0.4	0.3	-0.9	0.2	0.7	-1.4	-2.8	-2.8
		-3.4	-2.0	-1.2	-1.9	-0.1	0.4	-0.9	1.8	-2.6
		-0.8	-1.7	-1.1	-0.7	-0.7	0.1	-2.1	2.0	3.2
1	2	3	4	5	6	7	8	9	10	
-	1.1	0.7	-	2.9	1.5	-	-1.1	-2.3	-	
-	-0.2	-0.6	-	1.5	0.1	-	0.0	-1.2	-	
-	-2.0	-2.5	-	0.0	-0.9	-	0.9	0.4	-	
-	-1.0	-1.8	-	0.3	-0.7	-	1.1	-0.5	-	

Fig.3 An improvement in relative assemblywise power description and comparison with BIPR-7 and HEXBU-3D codes
(cr - corrected data set)
Loviisa-1, 1st cycle, 285 EFPD

CONCLUSION

The aim of this work is to evaluate experiments and measurements which can bring information about the neutron fluxes in the critical assemblies and cores of power reactors. It is shown when we take into account all experimental data and the whole problem of comparison with theory is formulated as a variational functional we are able to find better description of measurements and through the model of description (equations) we are able to transfer corrected models to the situations in which possibility of measurements are very limited. In our definite examples the differences of the fuel elements power distributions in the neighborhood of material heterogeneities between the theory and experiments were about three times lower and the systematic character of errors has left.

Special software enables us not only to solve new equations but also to work with the libraries of experimental data and to evaluate calculations and experiments quickly.

REFERENCES

[1] Lelek, V.. A Code for Correction of Coefficients of Few-Group Diffusion Equations Based on Measurements (in Russian) (Report UJV 8249 - R,A). NRI Rez 1987 . 76 pp.

[2] Lelek, V.. BRETISLAV - A Net Code for Calculation of a Reactor in Hexagonal Geometry (in Russian) (Report UJV 7771 - R,A). NRI Rez 1986 . 40 pp.

[3] Final Report TIC. Vol.1. Akadémiai Kiadó, Budapest 1984

[4] Lelek V., Pecka M.: The Use of Results from Critical Experiments to the Correction of Exploitational Parameters of Reactor Cores 1st Symposium of AER, Rez, Czechoslovakia, 23-27 September 1991

[5] Laletin N.P., Novikov A.N.· Final Report TIC. Vol.2. Akadémia Kiado, Budapest (at press)

[6] Vrba L.: Correction of Coefficients Based on Measurement in the Code CRIT(BIPR-6)-CS (Report UJV) (to be published)

[7] Styrin J.A.· personal information

NUMERICAL SOLUTION OF THE CRITICALITY PROBLEM FOR VVER FUEL ASSEMBLIES BY THE MONTE CARLO CODES MOCA AND MOCA 2

J. KYNCL
Nuclear Research Institute,
Řež, Czechoslovakia

Abstract

The codes MOCA and MOCA 2 serve to detailed solution to the problem for transport equation in case of three-dimensional hexagonal geometry and energy group description They have been implemented to personal computer In MOCA code, the problem is solved by method of successive generations Different way of the solution is used in MOCA 2 code It is based on theory of positive operators and it enables to avoid the problem of bias which frequently occurs in the method of successive generations In this contribution, information concerning input and output of the codes, their possible applications and some results are presented

THE PROBLEM SOLVED

The codes have been developed to numerical solution of the criticality problem for steady state linear Boltzmann equation They are designated for calculation of detailed neutron flux distribution in a reactor and they are composed in such a way to model correctly a real situation Nevertheless, the following conditions are assumed to be satisfied

a) Region of fuel assembly is considered which is placed either in vacuum or in infinite regular hexagonal lattice Next, existence of 30° - or 60° - sector of symmetry of the assembly is supposed (Fig 1 and 2)

b) The assembly is composed of cells which, in transversal (i e x - y) direction have shape of regular hexagons filling up regular hexagonal lattice and of an envelope

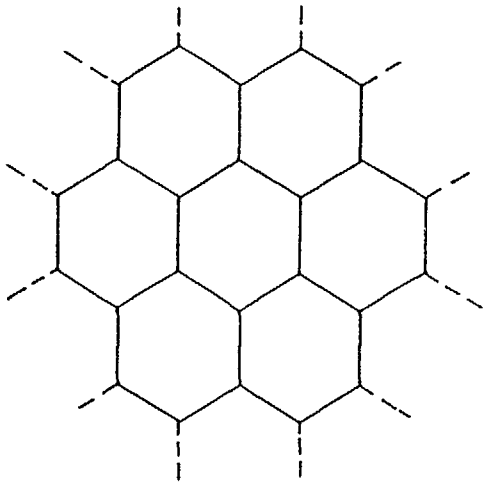

FIG 1 Infinite hexagonal lattice

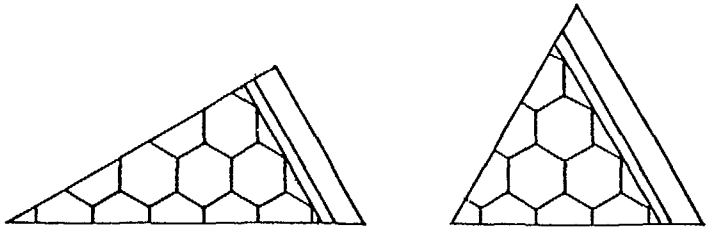

FIG 2 Permissible sectors of symmetry

consisting of triangles and quadrangles The cells have geometrical structure as shown at Fig 3

c) The problem has form

$$\mathbb{A}\varphi = \mathbb{B}\varphi + \mathbb{C}\varphi/\lambda \quad , \qquad \lambda = k_{eff} \quad , \qquad \varphi \in m(D) \tag{1}$$

where D is the spatial sector of symmetry considered, m(D) a lineal space of complex functions which are defined on the set $M \equiv D \times E_3$ and

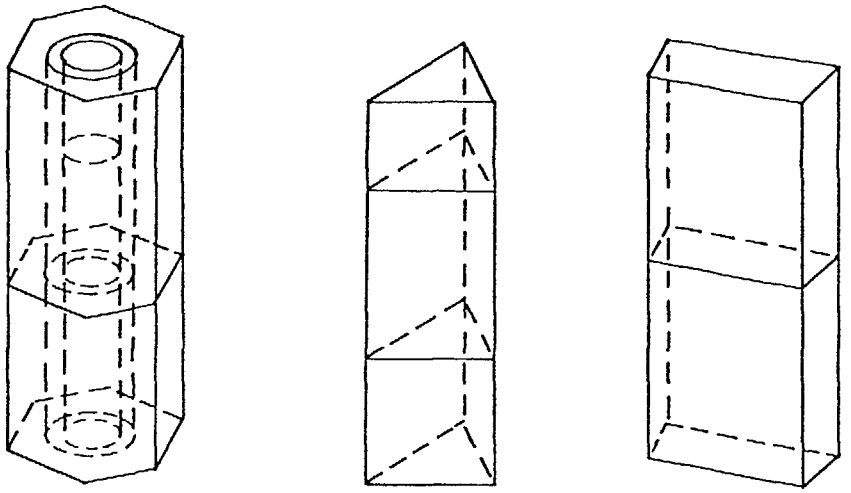

FIG 3 Permissible geometrical structure of cells

$$\mathbb{A}\varphi \equiv \vec{\omega}\,\vec{\nabla}\,\varphi + \Sigma_t(\vec{x},E)\,\varphi(\vec{x},E,\vec{\omega}) \quad ,$$

$$\mathbb{B}\varphi \equiv \int_0^\infty dE' \int_\Omega d\vec{\omega}'\; \Sigma_s(\vec{x},E'\to E,\vec{\omega}'\to\vec{\omega})\;\varphi(\vec{x},E',\vec{\omega}') \quad ,$$

$$\mathbb{C}\varphi = \int_0^\infty dE' \int_\Omega d\vec{\omega}'\,\varphi(\vec{x},E',\vec{\omega}')\{\chi_f(E)\nu(E')\Sigma_f(\vec{x},E') + 2\chi_n(E)\Sigma_n(\vec{x},E')\}/4/\pi$$

Next, $\vec{x}$, E, $\vec{\omega}$ mean the spatial coordinate, energy and the angular vector, Ω the surface of unit sphere, Σ_t the total macroscopic effective cross-section, Σ_s, Σ_f and Σ_n the macroscopic cross-sections for scattering, fission and (n,2n) reaction, χ_f and χ_n the energy spectrum of neutrons from the fission and (n,2n) reaction, $\nu(E')$ the number of fission neutrons corresponding to energy E' of impinging neution, k_{eff} the effective multiplication factor and φ is the differential neution flux

d) Problem (1) is solved in energy group formalism assuming that scattering cross-section is known as a decomposition to Legendre polynomials in angular variable.

The main result of numerical solution to problem (1) is the multiplication coefficient and integral neutron flux

$$\Phi(\vec{x},E) = \int_{\Omega} d\vec{\omega}\ \varphi(\vec{x},E,\vec{\omega})$$

in individual energy groups and spatial zones. This flux computed serves as a basis for evaluation of another physical quantities: power in any of zones, mean power density per fuel rod, mean neutron flux per cell, the mean flux in the assembly, activation rate, mean effective cross-sections per cell and reductions of groups and the mean diffusion constants for the assembly in reduced energy groups /1/.

METHOD OF THE SOLUTION

In both codes, the problem is solved by monte Carlo method. Specifically, method of successive generations is used in MOCA code:
Problem (1) is transformed to the integral form

$$\lambda\varphi = (\mathbb{I} - \mathbb{A}^{-1}\mathbb{B})^{-1}\mathbb{A}^{-1}\mathbb{C}\varphi \equiv \mathbb{T}\varphi\ , \qquad \varphi \in D(\mathbb{T}) \equiv m(D) \qquad (2)$$

and iterative scheme

$$\varphi_{i+1} = \mathbb{T}\varphi_i\ ,$$

$$\lambda_i = (\varphi_{i+1},g)/(\varphi_i,g)\ , \quad i=0,1,\ldots$$

$$\lambda = \lim_{i\to\infty} \lambda_i\ , \qquad \varphi = \lim_{i\to\infty} \varphi_i\ /(\varphi_i,g)$$

is employed. Here, g is a function and (φ_i,g) means scalar product, e.g.

$$(\varphi_i,g) = \int g\varphi_i d\vec{x}d\vec{\omega}dE.$$

In any generation i, scalar product (φ_i, g) is simulated by means of results of N_i mutually independent trials in a process of random collisions. Unfortunately, such a computation leads to a bias. It has been shown that the error depends on the number N of trials per one generation and it does not decrease with the number of generations used (see e.g. /2/).
To avoid this difficulty we have employed rather different idea of computation in code MOCA 2:
By appropriate choice of the domain $D(\mathbb{T})$ operator $\mathbb{T}$ gains these properties:

a) $\mathbb{T}$ is linear and positive .
b) $\mathbb{T}^2$ is compact.
c) Spectral radius $r(\mathbb{T})$ of $\mathbb{T}$ is positive

(see e.g. /3/). Then, according to theory of positive operators /4/, there is one and only one nonnegative eigensolution φ_o to the problem (2) eigenvalue λ_o corresponding to it being positive and

$$\lambda_o = r(\mathbb{T}).$$

Next, for any function $\chi \in D(\mathbb{T})$ and for any positive integer n, relation

$$\mathbb{T}^n\chi = \lambda_o^n\ \varphi_o\langle\psi_o,\chi\rangle + \mathbb{T}_1^n\ \chi \qquad (3)$$

holds. Here, ψ_o is a positive eigensolution to the problem adjoint to (2) and $\mathbb{T}_1$ is a linear operator such that

$$r(\mathbb{T}_1) < \lambda_o.$$

Clearly, by (3)

$$\lambda_o = \lim_{n-m\to\infty} ((\mathbb{T}^n\chi,g)/(\mathbb{T}^m\chi,g))^{1/(n-m)}\ . \qquad (4)$$

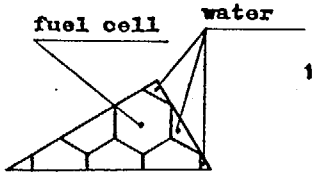

FIG. 4a. Structure of cassette.

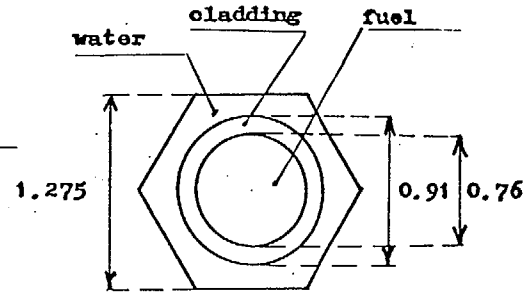

FIG. 4b. Details of fuel cell.

In the code MOCA 2, scalar product $(\Gamma^n\chi,g)$ is simulated by means of special random process and $\lambda_o = k_{eff}$ calculated according to expression (4) for n, m sufficiently great. Accuracy $\varepsilon_{m,n}$ corresponding to eigenvalue λ_o is computed from expression

$$\varepsilon_{m,n} = ((1 + \varepsilon_n)/(1 - \varepsilon_m))^{1/(n-m)} - 1$$

where ε_k denotes the accuracy of product $(\Gamma^k\chi,g)$ determined by Monte Carlo method. In this way, using MOCA 2 code, we obtain numerical results bias of which can be made arbitrarily small (for some details, see /5/).

APPLICATIONS

The codes MOCA and MOCA 2 are written in FORTRAN and recently they have been implemented also to personal computers AT-286 and AT-386 using operating system DOS 3.30 and OS/2. They consist of 2313 and of 2523 statements and they need about 400 kB of the computer memory. Under OS/2, history of a particle takes about 0.1 sec.

MOCA code has been utilized to the computations connected with the project "Compact Spent Fuel Storage". Three-dimensional four-group calculations of a fuel assembly of the VVER type with an absorbing envelope have been carried out with the code. In this way, preparation of the mean diffusion constants for such assemblies was evaluated. Also, the utilization of diffusion codes to more detailed calculations in the case of complicated fuel assembly geometry has been tested. In this case, remarkable differences frequently appeared between the results computed by transport and by diffusion codes.

Several problems were computed also by MOCA 2 code and results of two of them are shown from the table. Problem 1 (a) - d)) corresponds to the case of fuel assembly VVER-1000 being placed in infinite regular hexagonal lattice of the same assemblies. Absorbing rods are in and the height of the assembly is considered as infinite. Formulation of second problem is the same but the absorbing rods are replaced by water. The computations were performed in two steps: Resulting particle distribution from the first step served as a starting point in the next one of computation (see variants a), b) and c), d), respectively). In both steps, we have put n = 100 and m = 5. For comparison, the same problems were computed by the method of successive generations (code MOCA).

In this case we have considered 100 particles per one generation, 5 initial generations were omitted.

Table
Results of two test problems

	MOCA 2			MOCA		
Var.	N. hist.	k_{eff}	Err.(%)	N.hist.	k_{eff}	Err.(%)
1a)	600	0.9585	0.19			
1b)	1100	0.9610	0.11			
1c)	400	0.9650	0.11	124500	0.9517	0.31
1d)	900	0.9643	0.1			
2a)	700	1.1547	0.16			
2b)	800	1.1533	0.15			
2c)	400	1.1528	0.15	177400	1.1434	0.24
2d)	1100	1.1522	0.12			

REFERENCES

/1/ Kyncl J., The code MOCA, ÚJV 6487 R (1983)

/2/ Zolotukhin V.G. and Mayorov L.V., Estimate of reactor criticality parameters by Monte Carlo method, Moscow (1984), (Russian)

/3/ Shikhov S.V., Problems of mathematical theory of reactors, Moscow (1973), (Russian)

/4/ Krein M.G. and Rutman M.A., Linear operators leaving invariant a cone in a Banach space, Usp. mat. nauk III, N.1, pp.3-95 (1948), (Russian)

/5/ Kyncl J., Numerical solution to the problem of criticality by Monte Carlo method, ÚJV 8727-R (1989)

AN EQUIVALENCE PRINCIPLE FOR THE ADJOINT NEUTRON FLUX IN LATTICE CELL

M. NASR
Atomic Energy Authority,
Cairo

H. ROUSHDY
Faculty of Engineering,
Alexandria University,
Alexandria

Egypt

Abstract

The adjoint flux calculated by multigroup effective cross sections generated by considering the conservation of reaction rates in the direct flux has a noticable error specially in the resonance energy range. In this work an equivalence principle for adjoint flux is developed for the calculation of multigroup effective cross sections to be used in adjoint flux calculation. These multigroup effective cross sections can be tabulated as functions of two independent parameters, namely: the equivalent cross section and the total macroscopic cross section of the moderator medium. The numerical calculations showed a linear dependence of the multigroup effective cross sections with the second parameter.

1. Introduction

The equivalence principle [1] is widly used in reactor cell calculation codes [2], [3], for generating the effective multigroup cross sections which are tabulated as functions of a parameter named equivalent cross section [4], and are stored in the code library.

In most of the cell calculation codes the effective multigroup cross sections are generated considering the conservation of reaction rates in the direct flux, they are used in calculation of both direct and adjoint multigroup flux distribution. It is evident that the adjoint flux calculated by this method is erroneous. The error is small in energy regions in which the spectrum is slowly varying with energy, such as in thermal energy range. In the resonance energy range the error is significant [5]. In fact, in direct flux weighting, the reaction rates are conserved, what is required in the adjoint flux calculation is not to conserve the reaction rates but to conserve the integral of the neutron importance function multiplied by the cross section. In case of homogeneous medium this error was estimated numerically using very fine group width [6]. To our knowledge there is no published estimation of this error in case of heterogeneous reactor lattice cell calculations.

In the present work, a trial is made to derive an equivalence principle applicable for generating the effective multigroup cross sections in the resonance energy regions suitable for adjoint flux calculations in reactor lattice cells.

2. Derivation of Adjoint Spectrum Equation

The equation describing the neutron adjoint spectrum for the fuel zone can be written in the form:

$$\Sigma_0 \Phi_0^* = P_{00} R^*_0 \Phi_0^* + P_{01} R_1^* \Phi_1^* \qquad (1)$$

where

Φ^*: Adjoint flux

Σ: Total macroscopic cross section

P_{ij}: Probability that a neutron born in zone (i) has its first collision in zone (j)

$P_{00} + P_{01} = 1$

R^*: Adjoint slowing down operator

Equation (1) can be written as

$$\Sigma_0 \Phi_0^* = P_{00} R_0^* \Phi_0^* + \Sigma_1 (1-P_{00}) \frac{R_1^* \Phi_1^*}{\Sigma_1} \qquad (2)$$

Now define a Green's function such that

$$\Sigma_0(u)\ \phi^*(u,u_0) = P_{oo}\ R_o^*\ \phi^*(u,u_o) + \Sigma_1\ (1-P_{oo})\ \delta(u_c) \quad (3)$$

where $\phi^*(u,u_c)$ is the adjoint flux inside the absorber at lethargy (u) due to a unit source at lethergy u_0, δ is the Dirac delta function.

Now, define the function

$$\psi(u) = \frac{R_1^*\ \Phi_1^*}{\Sigma_1} \quad (4)$$

which describes the contribution of the moderator. The adjoint flux spectrum in fuel region can be described by:

$$\Phi_0^*(u) = \int_{-\infty}^{u} du_0\ \phi^*(u,u_0)\ \psi(u_0)$$

If we consider that $\psi(u)$ is a slowly varying function of lethargy, we can write that

$$\Phi_0^*(u) = \psi(u)\ \phi_0^*(u) \quad (5)$$

where

$$\phi_0^* = \int_{-\infty}^{u} du_0\ \phi(u,u_0) \quad (6)$$

In order to get ϕ_0^*, equation (3) is integrated over u_0 from $-\infty$ to u, then

$$R_o^*\ \phi_0^*(u) - (\Sigma_e+\Sigma_0)\ \phi_0^*(u) + \frac{\Sigma_e}{\Sigma_0}\ \Sigma_1 = 0 \quad (7)$$

where, Σ_e is the equivalent cross section given by:

$$\Sigma_e = \Sigma_0\ \frac{1 - P_{oo}}{P_{oo}} \quad (8)$$

ϕ_0^* describes the fine structure of the adjoint spectrum inside a particular resonance. It can be seen from equation (7) that the value of ϕ_0^* depends only on two independent parameters: Σ_e and Σ_1 whatever the physical structure of the lattice cell is. This means that an effective cross section tabulation for the adjoint calculation can be realized as function of the two parameters Σ_e and Σ_1.

In the following section the narrow resonance approximation will be considered.

3. Narrow Resonance Approximation

$R_o^*\ \phi_o^*$ is given by

$$R_o^*\ \phi_o^* = \Sigma_s(u) \int P(u \longrightarrow u')\ \phi_o^*(u')\ du'$$

where $P(u \longrightarrow u')$ is the scattering kernel. If the lethargy width of the resonance is small compared to the average lethargy decrement by collision, narrow resonance approximation is applicable and $\phi_o^*(u')$ must take its asymptotic value outside the resonance, i.e. $\phi_o^*(u')=1$,..

so that

$$R_o^*\ \phi_o^* = \Sigma_s\ (u)$$

Substituting in equation (7), then

$$\phi_0^* = \frac{\Sigma_s(u) + \frac{\Sigma_e}{\Sigma_0(u)}\Sigma_1}{\Sigma_3(u) + \Sigma_e} \qquad (9)$$

4. Numerical Applications

The multigroup effective cross sections weighted by the adjoint flux are calculated for the most important resonances of U-238 and the corresponding resonance integral for the energy range from 3.928 up to 454ev for thermal light water reactor lattics. The United Kingdom Nuclear Data Library (UKNDL) [7] is used. The collision probability (P_{oo}) is calculated using a method developed by (A. KAVENOKY) [8]. Uranium oxide fuel moderated with light water lattices are used. The moderator to fuel volume ratios are 2.7, 1 and 0.7. For each of these cases the fuel radius is 0.5cm. The fuel is UO_2 containing natural uranium at a density of $0.0233x10^{24}$ molecules/cm^3. The clad is of 0.6mm thickness zirconium. The density of the light water used is 0.71gm/cm^3.

In table 1 the effective cross sections weighted by adjoint flux (denoted by SA) are compared with those

Table 1
Comparison of multigroup effective cross sections weighted on direct and adjoint flux

Energy range (ev)	SI	Vm/Vf=2.7		Vm/Vf=1		Vm/Vf=0.7	
		SD	SA	SD	SA	SD	SA
6.476-8.315	515.64	16.244	35.943	13.341	35.662	12.259	35.4
17.600-22.60	247.26	10.053	64.703	8.62	64.698	8.083	64.654
37.270-47.85	179.97	5.514	95.011	4.754	95.234	4.523	95.311
61.440-78.87	47.896	2.802	23.867	2.326	23.983	2.185	24.017
101.30-130.0	41.553	2.661	26.995	2.175	27.194	2.030	27.26
Ieff		14.566	71.473	12.278	71.501	12.022	71.433

weighted by direct flux using LIVOLANT-JEAN PIERRE method [4] (denoted by SD). The infinite dilution cross sections (SI) are presented also in the same table. The effective resonance integrals (denoted by I_{eff}) are represented also in the same manner.

5. Discussion of Results

The comparison between the values of the effective cross sections weighted by the direct flux spectrum (SD) and those weighted by the adjoint flux spectrum (SA) in Table (1) indicates the following:

- The self shielding effect is much more significant in case of (SD) than in case of (SA) since the value of the latter is much higher than that of the first for all resonances.

- There is a strong dependence of the value of (SD) for a given resonance on the moderator to fuel volume ratio (V_m/V_f), where (SD) increases significantly with increased value of (V_m/V_f). At the same time the value of (SA) increases very slightly with increased value of (V_m/V_f) and their dependence is practically insignificant.

These phenomena can be explained as follows:

The fine structure of the direct flux spectrum for the fundamental mode in the narrow resonance approximation can be described by [4]

$$\phi_o = \frac{\Sigma_p + \Sigma_e}{\Sigma_o(u) + \Sigma_e} \qquad (10)$$

where Σ_p is the potential scattering cross section in fuel region.

Comparing expressions (9) and (10) it can be seen that inside a resonance region the depression in the direct flux spectrum distribution should be much more important than the depression in the adjoint flux spectrum distribution. In fact, in the latter case, the existance of $\Sigma_s(u)$ in the numerator, compensates considerably the effect of $\Sigma_o(u)$ in the denomenator, since $\Sigma_s(u)$ has a resonance structure comparable practically to that of $\Sigma_o(u)$. This explains the weak self shielding of (SA). In other hand it can be seen from expression (10) that the value of ϕ_o for a given resonance increases with increased values of Σ_e, this means lower self shielding effect, and an increased values of (SD), while, in expression (9) Σ_e in the numerator is multiplied by the fraction $\Sigma_1/\Sigma_o(u)$ which is usually a very small fraction. Hence the dependence of (SA) on Σ_e is weak (for a given fuel radius Σ_e increases with (V_m/V_f)).

It can be seen clearly that the difference between the effective cross sections for direct and adjoint flux weighting is significant. This means that the adjoint flux calculated using direct flux weighting cross sections can have a great error particularly in the resonance region.

6. Effective Cross Section Tabulation

It needs more computation effort to calculate the effective cross sections weighted on adjoint flux using two parameters Σ_e and Σ_1 (double tabulation), for this reason analysis is made for the influence of the second parameter (Σ_1). In table 2 the percentage change in Σ_1 (denoted by D_1) (in case of $V_M/V_F=2.7$) and the corresponding percentage change in effective cross sections (denoted by DS) as well as the percentage change in the effective resonance integral (DI)

Table 2
The effect of the moderator total macroscopic cross section on the effective cross sections weighted on adjoint flux

Energy range (ev)	D1=-50%	D1=-25%	D1=25%	D1=50%
	DS	DS	DS	DS
6.476-8.315	-10.7%	- 5.9%	4.9%	9.8%
17.600-22.60	- 3.6%	- 1.8%	1.8%	3.6%
37.270-47.85	- 0.8%	- 0.4%	0.4%	0.8%
61.440-78.87	- 2.1%	- 1.1%	1.1%	2.1%
101.30-130.0	- 2 %	- 1 %	1 %	2 %
DI	- 6.4%	- 3.3%	3 %	6.1%

for the energy ranges considered in table 1 are represented. It can be concluded that the effective cross section value is approximately a linear function of Σ_1. Then the tabulation procedure is considerably facilitated, since we can use only two values for linear interpolation.

7. Conclusion

In this work an equivalence principle is derived for the calculation of multigroup effective cross sections to be used for adjoint flux calculations. It was verified that they can be tabulated as functions of two independent parameters, namly the equivalent cross section (Σ_e) and the macroscopic total cross section of the moderator (Σ_1). However the numerical calculations showed that the effective multigroup cross sections have a linear dependence on Σ_1 which considerably facilitate the tabulation procedure.

REFERENCES

[1] Bell G. I. and Glasstone S. 1970 "Nuclear reactor theory".

[2] Hoffmann A. et al. 1973 "APOLLO, code multigroupe de resolution de l'equation du transport pour les neutrons thermiques et rapides," CEA. N. 1610, Commissariat, a l'Energie Atomique.

[3] Halsal M. J. 1980 "A summary of WIMSD4 code", AEEW-M 1327.

[4] Livolant M. and Jeanpierre F. 1974 "Autoprotection des resonances dans les reacteurs nucleaires: application aux isotopes lourds", CEA. R. 4533, Commissariat a l'Energie Atomique.

[5] Greenspan E. and Karni Y. 1979 *Nucl. Sci. Eng.*, 69, 169-190.

[6] Wade D. C. and Bucher R. G. 1977 *Nucl. Sci. Eng.*, 64, 517-538.

[7] UKNDL (United Kingdom Nuclear Data Library), 1973, given by IAEL (NDS) 1978.

[8] Kavenoky A. 1969 "Calcul et utilisation des probabilites de premiere collision pour des milieux heterogenes a une dimension" Note CEA., N1077.

EVALUATION OF PERTURBATION IN THE RESONANCE REGION

M. NASR
Atomic Energy Authority,
Cairo

M. NAGY
Faculty of Engineering,
Alexandria University,
Alexandria

Egypt

Abstract

In the present work the mathematical expressions for the direct and adjoint flux in fine structure and in multigroup formalisms are analyzed. A mathematical correlation between the values of the reactivity effect calculated by each formalism is established. The discrepancy in multigroup calculation is estimated and analyzed for different categories of perturbations in light water reactor systems.

NOMENCLATURE

H : integro differential operator in Boltzmann neutron balance equation
H^* : the adjoint operator of H
ϕ, ϕ^* : direct and adjoint neutran flux fine structure distribution
$\Sigma_t(E)$: macroscopic total cross section for a neutran of energy E
$\Sigma_s(E)$, $\Sigma_f(E)$: macroscopic scattering and fission cross sections for a neutron of energy E.
$P(E' \rightarrow E)$: the probability that a neutron suffering a collision at initial energy E' to have a final energy E.
υ : A verage number of neutrons emmitted per fission.
χ : Distribution function of fission neutrons energy spectrum.

INTRODUCTION

Reactivity effects resulting from cross section variations can be evaluated by using the perturbation theory.[1] This can be formulated as follows:
Consider the balance equation for the direct and adjoint flux in the unperturbed situations:

$$H\phi = 0 \tag{1a}$$
$$H^*\phi^* = 0 \tag{1b}$$

The reactivity effect ($\delta\rho$) due to a variation δH in H is given by the equation.[2]

$$\delta\rho = \frac{1}{D} < \phi^* . \delta H \tilde{\phi} > \tag{2}$$

- $\tilde{\phi}$ is the perturbed flux, D is the total importance.
- $< >$ signify integration over space and energy variables.

In the resonance region both $\tilde{\phi}$. ϕ^* and δH have a fine structure as function of energy variable.

The effective multigroup cross section data in the resonance region are calculated with consideration of the fine structure effect on the direct flux only [3]. If these cross sections data are used-as it is the usual practice-in evaluating the reactivity effect (equation 2); it is not evident that the result will be exact. By the word exact we mean that the solution agrees with the result which can be obtained when using the exact fine structure distribution for both the cross-section data, the direct flux and the adjoint flux.

The aim of this work is to clarify some aspects of this problem.

2. Fine structure of direct and adjoint flux

In an infinite homogeneous medium, the neutron flux must statisfyes the equation.

$$\Sigma_t(E)\phi(E) = \int_0^{\infty} \Sigma_s(E') . P(E' \rightarrow E) \phi(E')dE' + \chi(E)\int_0^{\infty} \nu \Sigma_f(E')\phi(E')dE' \tag{3}$$

Since $\chi(E)$ and $P(E' \rightarrow E)$ are independant of the cross section value at E, the right hand side of equation (3) does not have an energetic fine structure correlated to the cross section at E. Again if the hypothesis of narrow resonance is assumed, it will be a slowly varying function of energy; which can be considered as constant over some resonances situated within an energy group around the energy E [4]. Equation (3) can then be written as:

$$\Sigma_t(E)\,\phi(E) = F(E) \tag{3a}$$

$$\phi(E) = F(E) / \Sigma_t(E) \tag{3b}$$

where F(E) is a slowly varying function of E representing the right hand side.
This show that the direct flux have a fine structure similar to that of $1/\Sigma_t(E)$.

The adjoint flux is given by the adjoint version of Equation (3), namely:

$$\Sigma_t(E)\phi^*(E) = \Sigma_s(E)\int_0^{\infty} P(E \rightarrow E')\phi^*(E')dE' + \nu\Sigma_f(E) \int_0^{\infty} \chi(E')\phi^*(E')\, dE' \tag{4}$$

In the same way the two integrals in the right hand side of equation (4) do not have fine structures correlated to that of the cross section at E. The second integral is constant by normalisation and is denoted by $\overline{H^*}$, while the first one is a slowly varying function in energy; denoted by $\overline{G^*}(E)$

Then we can write:

$$\Sigma_t(E)\phi^*(E) = \Sigma_s(E).\bar{G}(E) + \nu\Sigma_f(E).\bar{H} \quad (4a)$$

$$\phi^*(E) = \frac{\Sigma_s(E)}{\Sigma_t(E)}\bar{G}(E) + \frac{\nu\Sigma_f(E)}{\Sigma_t(E)}\bar{H} \quad (4b)$$

It can be seen that the adjoint flux has a fine energy structure related to these of the fission, scattering and total cross sections. However it can be observed that this fine structure is more smooth than that of the direct flux due to the presence of $\Sigma_t(E)$ in the denomenator of the expressions $\Sigma_s(E)$ and $\nu\Sigma_f(E)$.

3. Multigroup flux and Multigroup cross sections

The multigroup effective cross section $\tilde{\Sigma}_x(E)$ for any type of reaction χ around an energy E in any one group of energy extending from E_1 to E_2, such that E is the mean value of E_1 and E_2; is defined by the equation.

$$\tilde{\Sigma}_x(E).\int_{E_1}^{E_2}\phi(E')dE' = \int_{E_1}^{E_2}\Sigma_x(E')\phi(E')dE'$$

This can be written in the form

$$\tilde{\Sigma}_x(E).[\phi(E)] = [\Sigma_x(E).\phi(E)] \quad (5)$$

where $[\phi(E)]$ is the average flux in the interval E_1 to E_2 and is given by:

$$[\phi(E)] = \frac{1}{E_2 - E_1}\int_{E_1}^{E_2}\phi(E)\,dE$$

and

$$[\Sigma_x(E).\phi(E)] = \frac{1}{E_2 - E_1}\int_{E_1}^{E_2}\Sigma_x(E)\phi(E)\,dE$$

using equations (3a) and (3b) and substitute in (5) we get:

$$\tilde{\Sigma}_x(E).\int_{E_1}^{E_2}\bar{F}(E).\frac{1}{\Sigma_t(E)}\,dE = \int_{E_1}^{E_2}\bar{F}(E')\,\frac{\Sigma_x(E')}{\Sigma_t(E')}\,dE'$$

Since $\bar{F}(E)$ is a slowly varying function, it can be considered as constant in the interval E_1 to E_2 Then we can write

$$\tilde{\Sigma}_x(E) = \frac{[\Sigma_x(E)/\Sigma_t(E)]}{[1/\Sigma_t(E)]} \quad (6)$$

It is easily to verify that :

$$\tilde{\Sigma}_t(E) = \frac{1}{[1/\Sigma_t(E)]} \quad (6a)$$

Then

$$\frac{\tilde{\Sigma}_x(E)}{\tilde{\Sigma}_t(E)} = [\Sigma_x(E) \,/\, \Sigma_t(E)] \quad (6b)$$

integrating equation (3b) and (4b) from E_1 to E_2 and substitute from (6a) and (6b), we obtain:

$$[\phi(E)] = F(E) \,/\, \tilde{\Sigma}_t(E) \quad (7a)$$

$$[\phi^*(E)] = \bar{G}(E)\frac{\tilde{\Sigma}_s(E)}{\tilde{\Sigma}_t(E)} + \bar{H}\frac{\nu\tilde{\Sigma}_f(E)}{\tilde{\Sigma}_t(E)} \quad (7b)$$

4. Multigroup equation of the direct and adjoint flux

In the multigroup formalism, the direct flux is given by the equation:

$$\tilde{\Sigma}_t(E).[\phi(E)] = \sum\tilde{P}(E'\!\to\!E).\tilde{\Sigma}_s(E')[\phi(E')]\Delta E' + \chi(E).\sum\nu\Sigma_f(E')[\phi(E')]\Delta E' \quad (8)$$

This equation gives the average flux in each group, using a multigroup effective cross section values

The multigroup adjoint flux $\varphi^*(E)$ is defined by taking the adjoint of equation (8) using the same multigroup effective cross section values.

$$\tilde{\Sigma}_t(E)\varphi^*(E) = \Sigma_s(E).\sum\tilde{P}(E\!\to\!E')\varphi^*(E')\,\Delta\,E' + \nu\tilde{\Sigma}_f(E)\sum\chi(E')\varphi^*(E')\,\Delta\,E' \quad (9)$$

It is clear that the multigroup average flux values given by equation (8) are identical to those given by equation (7a) or (3) but it is not evident that the adjoint flux values given by equation (9) are identical to those given by equation (7b). or (4b). However $\varphi^*(E)$ can satisfy an equation similar to (7b)

$$\varphi^*(E) = \bar{G}'(E).\frac{\tilde{\Sigma}_s(E)}{\tilde{\Sigma}_t(E)} + \bar{H}\frac{\nu\tilde{\Sigma}_f(E)}{\tilde{\Sigma}_t(E)} \quad (7c)$$

where

$$\overline{G'(E)} = \sum\tilde{P}(E\!\to\!E')\varphi^*(E')\Delta E', \quad (10a)$$

which is a slowly varying function of E
and

$$\bar{H}' = \sum\chi(E')\varphi^*(E')\Delta E' \quad (10b)$$

which, by normalization, takes a constant value

5. Evaluation of Reactivity effect

For a cross section perturbation $\delta\Sigma(E)$, equation (2) will be used to evaluate the reactivity effect using the fine structure and the multigroup formulations

It will be considered that both direct and adjoint fluxes are normalized in the following manner

$$\int \upsilon\, \Sigma_f\, \phi\,(E)\, dE = 1 \tag{11a}$$

$$\int \chi(E)\, \phi^*\,(E)\, dE = 1 \tag{11b}$$

$$\sum_{\upsilon} \upsilon\, \Sigma_f\,(E)\, [\,\phi\,(E)]\, \Delta E = 1 \tag{11c}$$

$$\sum \chi(E)\, \varphi^*\,(E) \Delta E = 1 \tag{11d}$$

For convenience,, equation (2) will be formulated as

$$\delta\rho = \langle \phi, H^* \phi^* \rangle \tag{2a}$$

where δH^* is the adjoint operator to δH
1/D is omitted by normalisation
In fine structure formulation $\delta\rho_f$ is given by

$$\delta\rho_f = \int_0^{\bar{}} dE \;.\; \phi(E) \;.\; [\nu\delta\Sigma_f(E) - \phi^*(E)\delta\Sigma_t(E) + \delta\Sigma_s(E) \int P(E\to E')\phi^*(E')dE' \,] \tag{12a}$$

In multigroup formulation the change of reactivity $\delta\rho_m$ is given by

$$\delta\rho_m = \sum \Delta E \;.\; [\phi(E)] \;.\; [\nu\delta\bar{\Sigma}_f(E) - \varphi^*(E)\delta\Sigma_t(E) + \delta\bar{\Sigma}_s(E) \;.\; \sum P(E\to E')\varphi^*(E')\Delta E' \,] \tag{12b}$$

It is required to identify the difference between $\delta\rho_f$ and $\delta\rho_m$, taking into consideration the relations obtained previously and considering the normalizations in equations (11a, 11b, 11c and 11d).

The integration in equation (12a) can be expressed as a summation of individual integrations, each one is carried out over an energy group corresponding to the same devision as in the multigroup case·

$$\delta\rho_f = \sum \int dE\phi(E) \quad [\nu\delta\Sigma_f(E) - \phi^*(E)\delta\Sigma_t(E) + \delta\Sigma_s(E) \int P(E\to E')\phi^*(E')dE' \,]$$

Each term can be defined separately whichs is pertained to the group substituting equations (3b) and (4b) for $\phi\,(E)$, $\phi^*(E)$ We get

$$\delta\rho_f = \sum \int dE \frac{\bar{F}}{\Sigma_t} [\nu\delta\Sigma_f - \bar{G}\frac{\Sigma_s}{\Sigma_t}\,\delta\Sigma_t - \frac{\nu\Sigma_f}{\Sigma_t}\,\delta\Sigma_t + \bar{G}\,\delta\Sigma_s \,]$$

$\bar{F}$ and $\bar{G}$ are considered constant in each group
To simplify writting, the energy variable is omitted as

$$\delta\rho_f = \sum \bar{F} \int dE[\nu(\frac{\lambda\Sigma_f}{\Sigma_t} - \frac{\Sigma_f}{\Sigma_t^2}\,\delta\Sigma_t) + \bar{G}(\frac{\delta\Sigma_s}{\Sigma_t} - \frac{\Sigma_s}{\Sigma_t^2}\,\delta\Sigma_t)]$$

$$\delta\rho_f = \sum \bar{F} \int dE[\nu\delta(\frac{\tilde{\Sigma}_f}{\tilde{\Sigma}_t}) + \bar{G}\delta(\frac{\tilde{\Sigma}_s}{\tilde{\Sigma}_t})]$$

It can be easily verified that

$$\int dE\, \delta(\frac{\Sigma_f(E)}{\Sigma_t(E)}) = \delta(\frac{\bar{\Sigma}_f(E)}{\bar{\Sigma}_t(E)}) \tag{13a}$$

and

$$\int dE.\delta(\frac{\Sigma_s(E)}{\Sigma_t(E)}) = \delta(\frac{\bar{\Sigma}_s(E)}{\bar{\Sigma}_t(E)}) \tag{13b}$$

$$\delta\rho_f = \sum \bar{F} \quad [\nu\delta(\frac{\bar{\Sigma}_f}{\bar{\Sigma}_t}) + \bar{G}\delta(\frac{\bar{\Sigma}_s}{\bar{\Sigma}_t})]\Delta E$$

$$\delta\rho_f = \sum \bar{F}[\nu(\frac{\delta\bar{\Sigma}_f}{\bar{\Sigma}_t} - \frac{\bar{\Sigma}_f}{\bar{\Sigma}_t^2}\,\delta\bar{\Sigma}_t) + \bar{G}(\frac{\delta\bar{\Sigma}_s}{\bar{\Sigma}_t} - \frac{\tilde{\Sigma}_s}{\bar{\Sigma}_t^2}\,\delta\bar{\Sigma}_t)]\Delta E$$

rearranging, one gets

$$\delta\rho_f = \sum \frac{\bar{F}}{\bar{\Sigma}_t}[(\nu\delta\bar{\Sigma}_f + \bar{G}\delta\bar{\Sigma}_s) - (\frac{\nu\bar{\Sigma}_f + \bar{G}\bar{\Sigma}_s}{\bar{\Sigma}_t})\,\delta\bar{\Sigma}_t]\Delta E$$

$$\delta\rho_f = \sum [\phi] \quad [(\nu\delta\bar{\Sigma}_f + \bar{G}'\delta\bar{\Sigma}_s) - (\frac{\nu\bar{\Sigma}_f + \bar{G}'\bar{\Sigma}_s}{\bar{\Sigma}_t})\delta\bar{\Sigma}_t]\Delta E$$

$$+ \sum [\phi]\,[\bar{G} - \bar{G}'] \;.\; [\delta\bar{\Sigma}_s - \frac{\bar{\Sigma}_s}{\bar{\Sigma}_t}\,\delta\bar{\Sigma}_t]\Delta E$$

$$\delta\rho_f = \delta\rho_m + \sum [\phi] \;.\; \bar{\Sigma}_s[\bar{G}' - \bar{G}][\frac{\delta\bar{\Sigma}_t}{\bar{\Sigma}_t} - \frac{\delta\bar{\Sigma}_s}{\bar{\Sigma}_s}]\Delta E \tag{14}$$

The second term in the right hand side side of equation (14) represents a correction term which is denoted by R We can see that the error in reactivity effect calculated by a multigroup formalism depends only on the error in evaluating the total importance of slowed down neutrons This error can be minimized by reducing the value $[\bar{G}-\bar{G}']$.

6 Special case Correction term in the resonance region

The correction term R (equation 14) is written in the form

$$R = \sum [\phi(E)]\,\Delta E\,\bar{\Sigma}_s(E)\,[\bar{G}(E) - \bar{G}'(E)]\,[\frac{\delta\bar{\Sigma}_s}{\bar{\Sigma}_s} - \frac{\delta\bar{\Sigma}_t}{\bar{\Sigma}_t}] \tag{15}$$

Now considering the value of $\bar{G}'(E)$

$$\bar{G}'(E) = \sum \tilde{P}(E \to E')\varphi^*(E') \quad \Delta E' \tag{10 a}$$

where $\tilde{P}(E \to E')$ is calculated in most calculation codes by the formula

$$\tilde{P}(E \to E') = \frac{1}{\tilde{\Sigma}_s(E)} \quad \frac{\iint \Sigma_s(E) \quad P(E \to E')\phi(E)dE\, dE'}{\int dE \int \phi(E)dE}$$

where $\int$ signifies integration over the energy interval of the corresponding group

For the resonance region which is generaly situated in the slowing down range, the scattering kernel can be represented as a seperable functions, then we can write [5]

$$P(E \to E') = Z(E) \quad Y(E') \tag{16}$$

it follows that

$$\tilde{P}(E \to E') = \frac{\int \Sigma_s(E) \,.\, Z(E) \quad \phi(E)dE \int Y(E')dE'}{\tilde{\Sigma}_s(E) \quad \int \phi(E)dE \int dE'}$$

Then we can write

$$\tilde{P}(E \to E') = \tilde{Z}(E)\, \bar{Y}(E') \tag{17}$$

where $\tilde{Z}(E)$ and $\bar{Y}(E')$ are given by

$$Z(E) = \frac{\int \Sigma_s(E) Z(E) \phi(E)dE}{\int \Sigma_s(E)\phi(E)dE}, \qquad \bar{Y}(E') = \frac{\int Y(E')dE'}{\int dE'}$$

Substituting in (10 a), we obtain

$$\bar{G}'(E) = \tilde{Z}(E) \quad \sum \bar{Y}(E')\varphi^*(E') \quad \Delta E \tag{18 a}$$

Getting use of equation (16), the value of $\bar{G}'(E)$ in equation (15) can be obtained by

$$G(E) = Z(E) \int_0^{\bar{}} Y(E')\phi^*(E')dE' \tag{18 b}$$

substituting into equation (15) one gets

$$R = \sum [\phi(E)] \quad \Delta E\, \tilde{\Sigma}_s(E) \quad [Z(E) \int_0^{\bar{}} Y(E')\phi^*(E)dE$$
$$- \tilde{Z}(E) \sum \bar{Y}(E')\varphi^*(E)\Delta E'] \quad \left[\frac{\delta \tilde{\Sigma}_s}{\tilde{\Sigma}_s} - \frac{\delta \tilde{\Sigma}_t}{\tilde{\Sigma}_t} \right] \tag{19}$$

In the slowing down region the up scattering is neglected and the scattering kernel can be obtained from the following relation

$$\Sigma_s(E \cdot E') = \Sigma_s(E) \frac{1}{(1 - \alpha)E} \qquad \text{for} \quad E > E' > \alpha E$$
$$= 0 \qquad \text{elsewhere}$$

from equation (16) it can be seen that the function Y (E) can be represented by a constant value Substituting in equation (4) and comparing with equation (9) we conclude that $[\varphi^*(E)]$ is equivalent to $[\phi^*(E)]$ and hence

$$\bar{G}(E) = \bar{G}'(E)$$

7 - CONCLUSIONS

We conculude that the reactivity effects in infinite homogeneous medium for narrow resonances can be calculated precisely by multigroups cross sections.

In some situations such as U_{238} resonances situated at energies higher than 80 ev the over all result could be exact, although a term by term correspondance does not exist In other situations a correct result can be obtained if the importance of slowed down neutrons is correctly evaluated The case of wide resonances needs further analysis

REFERENCES

1 J Bussac and P REUSS, Traite de neutronique, Hermann PARIS (1978)
2 A. GANDINI , J Nucl, Energy 21, 755 (1967)
3 J PORTA etal, Nucl Sci & Eng 95, 266 (1987)
4 P REUSS, Nucl Sci & Eng 92, 261 (1986)
5 M M R WILLIAMS, Slowing down & thermalization of neutrons, North Holland pubishing company - AMSTERDAM

APPLICATION OF DEPLETION PERTURBATION THEORY TO IMPROVING DEPLETION CODE BIPR5-AK USING MEASURED PERFORMANCE PARAMETERS

L. KORPÁS
Paks Nuclear Power Plant,
Paks, Hungary

Abstract

This paper presents the formulation of the adjoint depletion equations for BIPR5-AK depletion code This code is used in NPP of Paks to calculate the performance parameters of the VVER-440 core The adjoint depletion equations are developed using Depletion Perturbation Theory

Perturbation expressions are used to define sensitivity coefficients for responses that depend on the coupled interaction between the neutron end the special depletion fields

For the solution of adjoint depletion equations and for the determination of sensitivity coefficient is developed the TAROK code Results obtained from direct calculations and from the coupled perturbation theory are compared

The derived sensitivity coefficients are used to modify input parameters of BIPR5-AK The modification is taken place by the minimalization of squared deviation of measured end calculated performance parameters In the presented example the appointed performance parameter is the assemblywise power distribution

1 INTRODUCTION

The purpose of this paper is the presentation of a calculational method with the help of which one can improve a Depletion Code the BIPR-5AK The improvement is carried out with the utilisation of measured performance parameters

The main task of the Depletion Codes used in NPP is the determination of the performance parameters or operational characteristics of the core These parameters are very important and must be known precisely to ensure safe and economic reactor performance

These parameters are for example the length of cycle, assemlywise power distribution and various reactivity coefficients etc The above mentioned parameters are measurable quantities, but for the case of burnup analysis or depletion code these parameters are integrals of the flux and nuclide fields that is it is mathematically a functional of both fields

The accuracy of depletion code is proven if we can calculate these performance parameters with satisfactory exactness From the operational point of view these calculated and measurable parameters are crucial but it seems very useful an another utilisation of measured data This is the 'feed back of this data to the Depletion Code to improve it The improvement means the modification of input data with respect to measured parameters

To achieve the modification of input parameters we have to know the sensitivity coefficients of functional to given input parameters For the determination of the sensitivity coefficients we used the Depletion Perturbation Theory The Depletion Perturbation Theory is a special case of Generalised Perturbation Theory In our work we use it in approximative form developped by M L Williams Ref (1) and enriched by others Ref(2-4) This is the so called quasi-static approximation This formulation is consistent with the computational methods used for depletion analysis

This method provides a very good and fast way for the determination of sensitivity coefficients The sensitivity coefficient have been used to determine the optimal value of input parameters minimizing the squared deviation

between the calculated and measured performance parameters with gradient method

The BIPR-5AK is a suitable depletion code for fitting ,because it's a simple 1 5 groupe diffusion code with previously fitted k_{inf} formula This doesn't contain cross-sections, the coefficients in k_{inf} were obtained by fitting procedure Oubviosly an another fitting based on performance parameters is understandable

2 DERIVATION OF ADJOINT DEPLETION EQUATIONS

The governing equations in BIPR-5AK are the followings

$$(A^i - \lambda^i B^i)\ \Psi = 0 \qquad 1$$

$$\frac{dK}{dt} = c\ p^i \qquad 2$$

$$[\ \Psi^i \quad 1^i\ ] = T^i \qquad 3$$

The Eq (1) is the eigenvalue equation for Ψ^i at t_i.

where $A^i\ \Psi^i$ the diffusion and absorption term

$B^i\ \Psi^i$ the source term

The very simple Eq (2) describes the change of depletion with only one variable. The equation for K the depletion variable. substitues the nuclide transmutation equation (Bateman equation) The p^i is the power of the volume element

The last equation is the flux normalization equation obtained from the power constraint at t_i

where T^i is the reactor power at t_i,

1^i is unambiguous function of p^i

Let be P^{I+1} the functional measured and calculated at $t=t_{I+1}$ For the derivation of sensitivty coefficients we use a variational technique With this method the quasi-static burnup equations Eq (1-3) are treated as constraints on the functional P^{I+1} and as such are appended to functional using Lagrange multipliers

The problem of sensitivity analysis for quasi-static burnup equations reduces to finding the appropriate stacionary conditions on F following functional

$$F = P^{I+1}(i) - \sum_{i=1}^{I+1} [\ \Gamma^i\ (\ A^i - \lambda^i B^i)\ \Psi^i\ ]$$

$$+\sum_{i=1}^{I} \int_{t_i}^{t_{i+1}} dt\ [\ L(t), (c\ p^i - \frac{dK}{dt})\ ]$$

$$+ \sum_{i=1}^{I+1} Z^i\ (\ [\Psi^i, 1^i] - T^i) \qquad 4$$

Consider first the functional derivative with respect to Ψ^{I+1}

$$(\ A^{I+1} - B^{I+1})\ \Gamma^{I+1} = \frac{\partial P^{I+1}(i)}{\partial \Psi^{I+1}} + Z^{I+1}\ 1^{I+1} \qquad 5.$$

At this point it should be noted that Eq (5) and Eq (1) demand that the flux function must be orthogonal to the adjoint source

$$[\ (\frac{\partial P^{I+1}(i)}{\partial \Psi^{I+1}} + Z^{I+1}\ 1^{I+1}),\ \Psi^{I+1}] = 0 \qquad 6$$

For the most cases of practical interest the first term in Eq (6) is zero

$$[\ \frac{\partial P^{I+1}(i)}{\partial \Psi^{I+1}} \quad \Psi^{I+1}] = 0 \qquad 7$$

Because of the Eq (7) on the right side of Eq (6) remains only one expression

$$(A^{I+1} - \lambda^{I+1}B^{I+1})^T \Gamma^{I+1} = \frac{\partial P^{I+1}(t)}{\partial \Psi^{I+1}} \qquad 8$$

On the same way we can determine the equation for Γ^l at an arbitrary point at t_l

$$(A^l - \lambda^l B^l)^T \Gamma^l = [c \int_l^{\bar{l+1}} L(t)\, dt \quad - \frac{\partial p^l}{\partial \Psi^l}] \qquad 9$$

The condition corresponding to a variation in K is slightly more complex than for other variables

$$\delta F_{\delta K} = [\frac{\partial P^{l+1}(t)}{\partial K^{I+1}}, \delta K^{I+1}] - \sum_{l=1}^{I+1} [\Gamma^l, \delta K^l (\partial (A^l - \lambda^l B^l)/\partial K^l) \Psi^l]$$

$$+ \sum_{l=1}^{I} \int_l^{\bar{l+1}} [\delta K(t), \frac{dL}{dt}]\, dt - [L_-^{I+1} \quad \delta K_-^{I+1}]$$

$$+ [L_+^I , \delta K_+^I] - [L_-^I \quad \delta K_-^I] \qquad + [L_+^1 , \delta K_+^1] \qquad 10$$

This condition will be stationary if the following conditions are met

$$\frac{dL(t)}{dt} = 0 \qquad 11$$

$$L_-^{I+1} = \frac{\partial P^{I+1}(1)}{\partial K^{I+1}} - [\Gamma^{I+1}, \partial (A^{I+1} - \lambda^{I+1} B^{I+1})/\partial K^{I+1}) \Psi^{I+1}] \qquad 12$$

$$L_-^l = L_+^l - [\Gamma^l \quad \partial (A^l - \lambda^l B^l)/\partial K^l \Psi^l]$$

$$+ c\Delta T_l^{l+1} [L^l \frac{\partial}{\partial} \frac{p^l}{K^l}] \qquad 13$$

Eq (11) is valid for open interval $(t_l \; t_{l+1})$ Eq (12) and Eq (13) describe the behavior of L at the boundaries of intervals

This development has provide the adjoint field equation for quasi-static approximation We have found that there exist adjoint equations corresponding to the depletion equation and to the flux shape equation

We now can establish a suitable computational algorithm for numerical solution of the adjoint quasi-static equations

1 Solve Eq (8) for Γ^{I+1}

2 Use Eq (12) for det final value of L at t_{I+1}

3 Because Eq (11) L is constant in intervals we can solve Eq (9)

4 With the application of Eq (13) we can det the new value of L

5 Etc

This marching procedure is followed backward through all the time intervals until the values at t=0 are obtained, at which time the adjoint calculation is complete

We have to take into consideration that Eq (8) and Eq (9) are heterogeneous equations This means that general solution has the following form

$$\Gamma = \Gamma_p + b\,\Psi \qquad 14$$

Γ_p is the particular solution of Eq.(8) and Eq (9) and b is an arbitrary constant The Ψ appears in (14) expression is the fundamental solution to the (1) homogeneous equation This comes from the self-adjoint properties of operators A end B To unambiguous solution of Eq (8) and Eq(9) we have to determine the value of b

There are two possibilities to achieve this goal

In the case in which there is no λ reset (it is that λ is allowed to change with data perturbation) we have to evaluate $\partial F/\partial\lambda^l = 0$ It is easy to show that inthis case b=0

For the case in which λ is made invariant by adjusting a control variable C, it is easily shown that the proper conditions are the following

$$b^{I+1} = \frac{\frac{\partial P^{I+1}(\iota)}{\partial C^{I+1}} - [\Gamma^{I+1}, \frac{\partial}{\partial C^{I+1}}(A^{I+1} - \lambda^{I+1}B^{I+1})\Psi^{I+1}]}{[\Psi^{I+1}, \frac{\partial}{\partial C^{I+1}}(A^{I+1} - \lambda^{I+1}B^{I+1})\Psi^{I+1}]} \qquad 15$$

$$b^l = \frac{-[\Gamma^l, \frac{\partial}{\partial C^l}(A^l - \lambda^l B^l)\Psi^l] + c\,\Delta T_l^{l+1}[L^l, \frac{\partial P^l}{\partial C^l}]}{[\Psi^l, \frac{\partial}{\partial C^l}(A^l - \lambda^l B^l)\Psi^l]} \qquad 16$$

When all the adjoint values have been obtained, the sensitivity coefficient for data variations can be easily computed

$$S_\alpha(P^{I+1}) = \frac{\alpha}{P^{I+1}(\iota)}\left(\frac{\partial P^{I+1}(\iota)}{\partial\alpha} - \sum_{l=1}^{I+1}[\Gamma^l \frac{\partial}{\partial\alpha}(A^l - \lambda^l B^l)\Psi^l]\right.$$

$$\left. + \sum_{l=1}^{I} c\Delta T_l^{l+1}[L^l \frac{\partial P}{\partial\alpha}]\right) \qquad 17$$

The solution of the adjoint depletion equations and the determination of sensitivity coefficients is carried out by the TAROKK code. The computational time is the same as in the case of the original depletion code BIPR-5AK

3 SELECTION OF PARAMETERS FOR THE CORRECTION

As we have mentioned above the parameters for correction in our case are the coefficiets of k_{eff} in BIPR-5AK

The chosen functional is the squared deviation of measured and calculated assemblywise power distribution

This functional only represent the fitness of the method for determination a better input parameters We have to emphasize that improved input values only mean better parameters and not the optimal values

With mathematical statistical analysis (main factor analysis) we were able to chose those input parameters which cause the main deviations between the calculated and measured assemblywise power distribution It turned out that the main factors are the coefficients which describe the dependence of k_{inf} with repect to enrichment and depletion So we have chosen the coefficients of enrichment end of depletion term in k_{inf} as coefficiets for correction This means 27 input parameter altogether for correction

The result of adjoint calculation for the above described functional and for the 27 input parameters are given in Table I The first column of Table I shows number of input parameters The columns from 2 to 4 regard to terms in expression (17) respectively

Table II shows results from perturbation theory and from direct calculation The direct calculation means the actual variation of input parameters and the calculation of effect on the functional The results show good agreement

TABLE Ia Sensitivity coefficients of squared deviation of measured end calculated assemblywise power distribution to input parameters The chosen distribution regard to Unit 2 Cycle 3 at 15 full day

N	1 column	2 column	3 column	4 column
1	- 881	385	- 324	000
2	099	045	053	000
3	000	000	000	000
4	6 887	- 517	2 702	- 001
5	14 092	- 959	6 905	- 003
6	-47 128	3 094	-25 911	011
7	71 432	-4 608	42 050	- 017
8	-60 081	3 829	-37 153	014
9	28 264	-1 780	18 229	- 007
10	-6 836	425	-4 589	002
11	642	- 039	642	000

TABLE Ib Sensitivity coefficients of squared deviation of measured end calculated assemblywise power distribution to input parameters The chosen distribution regard to Unit 2 Cycle 3 at 15 full day

N	1 column	2 column	3 column	4 column
12	- 243	012	010	000
13	-4 342	209	144	000
14	20 084	- 975	- 569	- 002
15	-45 529	2 211	1 165	004
16	57 496	-2 779	-1 381	- 004
17	-40 947	1 965	946	003
18	15 357	- 730	- 347	- 001
19	-2 357	111	052	000
20	000	000	000	000
21	000	000	000	000
22	000	000	000	000

TABLE Ic Sensitivitv coefficients of squared deviation of measured end calculated assemblvwise power distribution to input parameters. The chosen distribution regard to Unit 2 Cycle 3 at 15 full day

N	1.column	2.column	3 column	4 column
23	000	000	000	.000
24	000	000	000	000
25	000	000	000	.000
26	000	000	000	000
27	000	000	000	000

4. THE ACTUAL MODIFICATION OF INPUT PARAMETERS

The actual modification of input parameters is fulfiled by minimizing the squared deviation of assemlywise power distribution The gradient method is used to find a minimum On an average it requires ten production of sensitivity coefficients In the iterational process the advantage of fast and easv determination of sensitivity coefficient is very usefull The modification algorithm of the input parameters is the following

$$\alpha_k^{n+1} = \alpha_k^n - \delta^n S_k^n \alpha_\nu^n / sqr\left(\sum_{k=1}^{K} (S_k^n)^2 / K \right) \qquad 18$$

where n the number of iteration and k number of input parameter The value of 'step' δ^n was determined by trial

TABLE II

Sensitivity coefficients calculated with DPT and with direct way

Data referring Unit 2 Cycle 4 at 21 full day

B(1,4)*E-5	SC(direct way)	SC(with GPT)
-.70522018	-54.4686	-53.6590
-.70562018	-21.9737	-25.9905
- 70602018	-4 8993	-5.1745

Data referring Unit 3 Cycle 3 at 34 full day

B(1,5)*E-6	SC(direct way)	SC(with GPT)
.23767601	-17.1829	-15.9875
.23787601	-5.9610	-4.9674
.23807601	14.9290	14 1783

We have examined 15 different assemblvwise power distribution. These distributions refer to different loading end different moment of the cycle of different unit. Only data from NPP of Paks Unit 1 to 4 were used. The procedure led to different input values We accepted the average value of these different impoved parameters. The mean values have provided better agreement between calculated and measured assemblywise power distribution in the examined 15 cases We consider these results temporary. The temporary, improved parameters are given in Table III.

5 CONCLUSION

A very effective and exact algorithm was developped to estimate the effect of input parameter changes on functionals calculated by BIPR-5AK This algorithm is suitable to carry out the task of "feed back" of measured performance parameters to depletion code. A temporary input modification was given

TABLE III

Original values of input parameters referring coefficients of depletion in k_{eff}

```
AI=-0.968159293E-2.-0.856568852E-3.0.118534481E-3.-0.712786942E-5.
    0.231642377E-6.-0.413938684E-8.0.375863649E-10.-0.131442461E-12.
     -0.490779047E-2.-0.318866792E-2.0.568645887E-3.-0.497046766E-4.
    0.241892849E-5.-0.663018899E-7.0.955305312E-9.-0.562013399E-11.
    0.222674103E-2.-0.488970123E-2.0.909228031E-3.-0.904532820E-4.
    0.522137542E-5.-0.174774438E-6.0.315014498E-8.-0.236555413E-10.56*0..
```

Modified values of input parameters referring coefficients of depletion in k_{eff}

```
AI=-0.966531000E-2.-0.850329000E-3.0.120428000E-3.-0.706657000E-5.
    0.230427000E-6.-0.417128000E-8.0.374730000E-10.-0.131490000E-12.
     -0.489871000E-2.-0.314850000E-2.0.581250000E-3.-0.491222000E-4.
    0.240447000E-5.-0.670303000E-7.0.950402000E-9.-0.562497000E-11.
    0.222674103E-2.-0.488970123E-2.0.909228031E-3.-0.904532820E-4.
    0.522137542E-5.-0.174774438E-6.0.315014498E-8.-0.236555413E-10.56*0..
```

REFERENCES

[1] M.S.Williams: Development of Depletion Perturbation Theory for Coupled Neutron/Nuclide Fields, Nucl.Sci.Eng.70,20(1979)

[2] T.Takeda, T.Umano: Burnup Sensitivity Analysis in a Fast Breeder Reactor- Sensitivity Calculation Method with Generalized Perturbation Theory, Nucl.Sci.Eng.91,1 (1985)

[3] W S.Yang, T.,J.,Downar: Generalized Perturbation Theory for Constant Power Core Depletion, Nucl.,Sci.Eng.99,353 (1988)

[4] W S.Yang, T.,J.,Downar Depletion Perturbation Theory for the Constrained Equilibrium Cycle, Nucl.,Sci.Eng.102,365 (1989)

SIMULATION OF CRUCIFORM CONTROL RODS IN THE COMPUTER CODE LWRBOX

P.D. KRISHNANI
Bhabha Atomic Research Centre,
Trombay, Bombay,
India

Abstract

The BWRs employ cruciform type control rods. It consists of B_4C granules (poison pins), its stainless steel cladding and the interspersed water kept in another sheath. The pitch between poison pins is usually small compared to lattice pitch. Due to this, it is not possible to treat this geometry exactly. This problem is solved by homogenising the region of control blade. We have introduced an option in the code LWRBOX for homogenising the control rod based on preserving the blackness of neutrons at the surface of control cell as is done in the code LWR-WIMS of UK. We have introduced two options for solving the integral transport equation for getting the flux distribution within the control cell with its exact geometry. In the first option, the spectrum of incoming neutron current at the surface of the control blade is supplied and then integral transport equation is solved within the control cell. In the second option, the original cell problem is approximated to an equivalent cell problem in which control rod with exact geometry is surrounded by homogeneous slab regions. The cross sections of the homogeneous slab regions are calculated by first doing the single pin cell calculations. Then the multigroup integral transport equation is solved for this geometry. This paper discusses the homogenisation procedure and the method for calculating the flux distribution within the control cell followed by the results obtained for a simple problem.

I INTRODUCTION

We have developed an efficient computer code LWRBOX [1] for calculating lattice properties of fuel assemblies used in light water reactors (LWRs) It solves the multigroup integral transport equation by a method based on a combination of interface current technique and collision probability (CP) method However, it was not capable to handle cruciform control rods used in BWRs Recently, the computer code LWRBOX was modified to calculate the lattice parameters of BWR fuel assembly with control rod

The cruciform control rod consists of B_4C granules (poison pins), its stainless steel cladding and the interspersed water kept in another sheath The pitch between poison pins is usually small compared to lattice pitch Due to this, it is not possible to treat this geometry exactly This problem is solved by homogenising the region of control blade We have introduced an option in the code LWRBOX for homogenising the control rod based on preserving the blackness of neutrons at the surface of control cell as is done in the code LWR-WIMS of UK [2] We have introduced two options for solving the integral transport equation for getting the flux distribution within the control cell with its exact geometry In the first option, the spectrum of incoming neutron current at the surface of the control blade is supplied and then integral transport equation is solved within the control cell In the second option, the original cell problem is approximated to an equivalent cell problem in which control rod with exact geometry is surrounded by homogeneous slab regions The cross sections of the homogeneous slab regions are calculated by first doing the single pin cell calculations Then the multigroup integral transport equation is solved for this geometry

In order to check the implementation of the methodology in LWRBOX, we chose a simple problem of 2 by 2 fuel rods with a cruciform control rod having the poison pin pitch within the control rod equal to the fuel pin pitch The two pitches were taken to be same because then the LWRBOX can directly solve this problem without making any approximation This problem was solved by both the approximate methods introduced in the LWRBOX to treat the cruciform control rod Both the methods were found to give results which were very close to the exact results

The paper discusses the homogenisation procedure and the method for calculating the flux distribution within the control cell followed by the results obtained for above mentioned problem

II METHOD USED IN LWRBOX

In this method, the whole lattice cell is divided into several connected cells which can further be subdivided into homogeneous zones The interaction between various zones within a cell and their contribution to outgoing currents at cell interfaces are directly calculated by the CP method Each cell is connected to neighbouring cells by interface currents We shall consider only one group integral transport equation The extension to multigroups is straight forward For the isotropic scattering and sources, the one group steady state integral transport equation can be written using standard notation

$$\Psi(\underline{r},\underline{\Omega}) = \Psi(\underline{r}_s,\underline{\Omega})\, e^{-\tau} + \int_0^{Rs} q(\underline{r}')\, [e^{-\tau}/4\pi]\, dR \qquad (1)$$

$\underline{r}'=\underline{r} - R\underline{\Omega}$ and $\underline{r}_s=\underline{r} - R_s\underline{\Omega}$

where $\underline{r}'$ is any point on the line drawn from $\underline{r}$ in the direction of $-\underline{\Omega}$, $\tau(\tau_s)$ is the optical path length between the point $\underline{r}$ and $\underline{r}'$ ($\underline{r}_s$) and $q(\underline{r})$ is the emission density and in one group it is given by

$$q(\underline{r}) = \mathcal{S}(\underline{r}) + \Sigma_s(r)\, \phi(r)$$

It is assumed that the source $\mathcal{S}(\underline{r})$ and scalar flux $\phi(r)$ are constant in each zone of the cell and the incoming (-)/ outgoing (+) angular flux at a surface can be expanded as

$$\psi^{\pm}_{s}(\underline{r}_{s},\underline{\Omega}) = [1/\pi S] \sum_{\varrho=1}^{N_t} J^{\varrho}_{\pm,s}\ \psi^{\varrho}_{\pm,s}(\underline{\Omega}) \qquad (2)$$

where N_t is the number of terms retained in the expansion, $J^{\varrho}_{\pm,s}$ are the expansion coefficients, S is the surafce area and $\psi^{\varrho}_{\pm,s}(\underline{\Omega})$ are the properly orthonormalized linearly independent functions and are known as representation functions They satisfy the following orthonormalization condition

$$\int_S \int_{\Omega} \psi^{\varrho}_{\pm,s}(\underline{\Omega})\ \psi^{\nu}_{\pm,s}(\underline{\Omega})\ (\underline{n}_{\pm}\ \underline{\Omega})\ dS\ d\underline{\Omega} = \pi\ S\ \delta_{\varrho\nu}$$

where $\delta_{\varrho\nu}$ is the Kronecker delta function With this normalisation, the first component of the coefficient J gives the total number of neutrons crossing the surface

With these assumptions, the collision density in a zone and the expansion coefficients of the outgoing currents can be given by

$$\Sigma_j V_j \phi_j = \sum_s \sum_{\varrho} P^{\varrho}_{sj}\ J^{\varrho}_{-,s} + \sum_i P_{ij}\ Q_i \qquad (3)$$

and

$$J^{\varrho}_{+,s} = \sum_{s'} \sum_{\nu} P^{\nu\varrho}_{s's}\ J^{\nu}_{-,s'} + \sum_i P^{\varrho}_{is}\ Q_i \qquad (4)$$

with $Q_i = V_i(S_i + \Sigma_{si}\phi_i)$ The coefficients P's are known as probabilities These obey conservation and reciprocity relations

III HOMOGENISATION PROCEDURE

A typical BWR control blade consists of a shrouded row of cooled absorber pins The basic problem is to convert this heterogeneous system consisting of B C granules, its stainless steel cladding and the interspersed water into an equivalent homogeneous slab region The method adopted in the code LWRBOX is similar to the CRUX procedure used in the code LWR-WIMS of UK [2] The homogenisation method is based on the conservation of outgoing neutron current for the two types of assemblies

Fig 1 illustrates the internal row of pins constituting a typical BWR cruciform control rod blade Let us assume that the cell is divided into N homogeneous zones If the angular flux of the incoming neutrons at the surface of the control blade is expanded as in Eq (2) then the collision rate in a zone j for any group g can be written as

$$\Sigma_{jg} V_j \phi_{jg} = 2 \sum_{\varrho} P^{\varrho}_{sjg}\ J^{\varrho}_{in,g} + \sum_i P_{ijg}\ Q_{ig} \qquad (5)$$

with

$$Q_{jg} = V_j \sum_{g'} \Sigma_{j,g'g}\ \phi_{jg'} \qquad (6)$$

where $J^{\varrho}_{in,g}$ are the expansion coefficients and $\phi_{jg'}$ is the scalar flux of neutrons of energy group g' in zone j

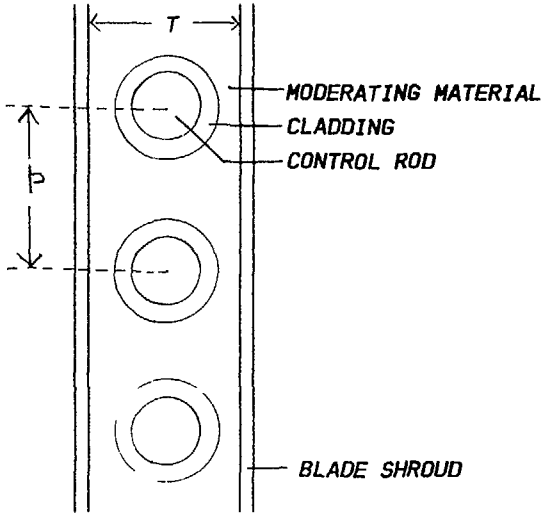

FIG 1

The coefficients of outgoing current from each surface of the cell in group g is given by

$$J^{\varrho}_{out,g} = \sum_{\nu} P^{\nu\varrho}_{ssg}\, J^{\nu}_{in,g} + \sum_{i} P^{\varrho}_{isg}\, Q_{ig}$$

The first component of the coefficient J gives the total number of neutrons going out of the surface

$$J_{out,g} = J^{1}_{out,g} = \sum_{\nu} P^{\nu 1}_{ssg}\, J^{\nu}_{in,g} + \sum_{i} P^{1}_{isg}\, Q_{ig} \qquad (7)$$

Using the conservation relations

$$P^{\nu 1}_{ss,g} = \delta_{1\nu} - \sum_{i} P^{\nu}_{sig}$$

$$2P^{1}_{isg} = 1 - \sum_{j} P_{ijg}$$

We have

$$J_{out,g} = J^{1}_{in,g} + \sum_{i} Q_{ig}/2 - \sum_{i} \Sigma_{ig}\, V_i\, \phi_{ig}\, /2 \qquad (8)$$

Eqs (5) and (8) give the collision rate and outgoing neutron current from a surface of the cell for the heterogeneous system

For homogeneous system, the equations for collision density and outgoing neutron current from a surface can be written as:

$$V\, \phi_g\, \Sigma_g = P_{VV,g}\, Q_g + 2 \sum_{\varrho} J^{\varrho}_{in,g}\, P^{\varrho}_{SV,g} \qquad (9)$$

$$J_{out,g} = J^{1}_{in,g} + Q_g/2 - V\, \phi_g\, \Sigma_g/2 \qquad (10)$$

with

$$V = \sum_{i} V_i \quad , \qquad Q_g = V \sum_{g'} \Sigma_{g'g}\, \phi_{g'}$$

The total cross sections Σ_g and transfer cross section $\Sigma_{g'g}$ refer to homogeneous cell These cross sections are calculated so that they preserve the blackness, β, derived for the heterogeneous problem in each group Now, $\beta=(J_{in}-J_{out})/J_{in}$, and since J_{in} is same for both models of control blade it is required that J_{out} be preserved Comparing Eqs (8) and (10), two physically reasonable sufficient conditions for equality of out leakage are apperent

$$Q_g = \sum_{i} Q_{ig} \qquad (11)$$

and

$$V\, \phi_g\, \Sigma_g = \sum_{i} V_i\, \phi_{ig}\, \Sigma_{ig} \qquad (12)$$

There are no slowing-down sources for energy group 1 so that condition of Eq (11) imposes equality of within group scatterers and condition (12), in turn requires equal neutron removals from the group In general, therefore, we require the following equalities

$$V\, \phi_g\, \Sigma_{gg} = \sum_{i} V_i\, \Sigma_{igg}\, \phi_{ig} \qquad (13)$$

$$V\, \phi_g\, \Sigma_{gg'} = \sum_{i} V_i\, \Sigma_{igg'}\, \phi_{ig} \qquad (14)$$

$$V\, \phi_g\, \Sigma_{ag} = \sum_{i} V_i\, \Sigma_{aig}\, \phi_{ig} \qquad (15)$$

where Σ_{ag} is the absorption cross section.

Returning to Eq (12) and using Eq.(9) gives

$$P_{VV,g}\, Q_g + 2 \sum_{\varrho} J^{\varrho}_{in,g}\, P^{\varrho}_{sv,g} = \sum_{i} V_i\, \phi_{ig}\, \Sigma_{ig}$$

Since

$$P^{\varrho}_{SV,g} = \delta_{1\varrho} - P^{\varrho 1}_{SS,g}$$

$$P^{11}_{SS,g} = 2\, E_3(\tau_g)$$

$$P_{VV,g} = 1 - P^{1}_{SV,g}/(2\tau_g) = 1 - (1 - P^{11}_{SS,g})/(2\tau_g)$$

where

$$\tau_g = T\,\Sigma_g$$

T is the thickness of the cell (control blade without sheath) containing control rod We obtain,

$$(1-P^{11}_{SS,g})(2J^{1}_{in,g}-Q_g/2\tau_g) - 2\Sigma\, P^{o1}_{SS,g}\, J^{o}_{in,g} + Q_g - \Sigma\, V_i\, \phi_{ig}\, \Sigma_{ig} = 0 \qquad (16)$$

This is the condition which should be satisfied by the equivalent homogeneous system in order to preserve the blackness in each group First, the integral transport equation is solved by either of the two methods mentioned below from which we obtain the flux distribution (ϕ_{ig}) in the control cell From this, we obtain the Q_g using Eq (11) Then Eq (16) is solved for Σ_g using the Newton-Raphson iterative procedure, converged to 10^{-4} precision in Σ_g As a first guess for the iterations, $\Sigma_g = \Sigma\,\Sigma_{ig}\,V_i\,\phi_{ig} / \Sigma\,V_i\phi_{ig}$ is applied

IV CALCULATION OF FLUX DISTRIBUTION IN CONTROL CELL

Fig 1 illustrates the internal row of pins constituting a typical BWR cruciform control rod blade The basic problem is to calculate the flux distribution within the control blade There are two options for it In the first option (ICONTR=2) the spectrum of the incoming neutron current at the surface of the inner shroud is provided (which can be obtained from 2-D box calculations in an iterative manner) and then multigroup integral transport equation is solved within the control cell In the code LWRBOX, this problem is converted to a single pin cell as shown in Fig 2 with zero net current (reflective) boundary condition at the two surfaces and a given spectrum of incoming neutrons at the remaining two surfaces The program has been suitably modified to take account of such mixed

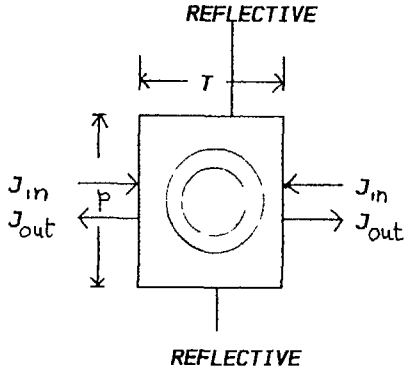

FIG 2

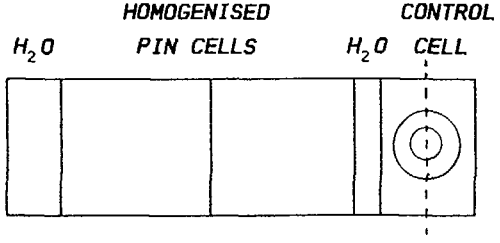

FIG 3

boundary condition The multigroup integral equation within the control cell is solved by the CP method and the angular flux at the cell surface is expanded in terms of half space angular representation functions as explained in the method of LWRBOX

In the second option (ICONTR=3), the reaction rates and flux distribution in the control cell are calculated by considering an equivalent problem shown in Fig 3 In this method, the whole lattice cell is converted into an equivalent homogeneous slab cell However, the geometry of the control rod is accurately represented Therefore, the calculations are performed in two stages In the first

stage, the single pin cell calculations are performed for different type of pin cells which are then spatially smeared. In the second stage, the control cell is surrounded by different layers of different materials. The cross sections of the layers containing fuel are obtained by mixing the smeared cross sections of various pin cells obtained in the first stage in proper proportion which is given in the input. Then in the second stage, the integral transport equation is solved for the geometry shown in Fig. 3 by the method based on combination of interface current and CP method normally used in the code LWRBOX. The reflective boundary condition is applied at the three surfaces and at the center of the control cell. Therafter, the equivalent homogenised cross sections of the control cell are obtained by preserving the blackness of the neutrons as explained above.

V. RESULTS

In order to check the implementation of the methodology in LWRBOX, we chose a simple problem of 2 by 2 fuel rods with a cruciform control rod having the poison pin pitch within the control rod equal to the fuel pin pitch. The two pitches were taken to be same because then the LWRBOX can directly solve this problem without homogenising the control rod. For the sake of bravity, the shroud sheath has not been considered. The lattice cell is shown in Fig. 4. The material properties are as follows :

Fuel: Material UO_2, density = 10 g/cm^3, temperature = 600 ^{0}C, U-235 enrichment = 3 w/O, diameter = 1 cm.

Clad: Material = zircaloy-2, density = 6.55 g/cm^3, temperature = 300 ^{0}C, inside diameter = 1 cm, outside diameter = 1.2 cm.

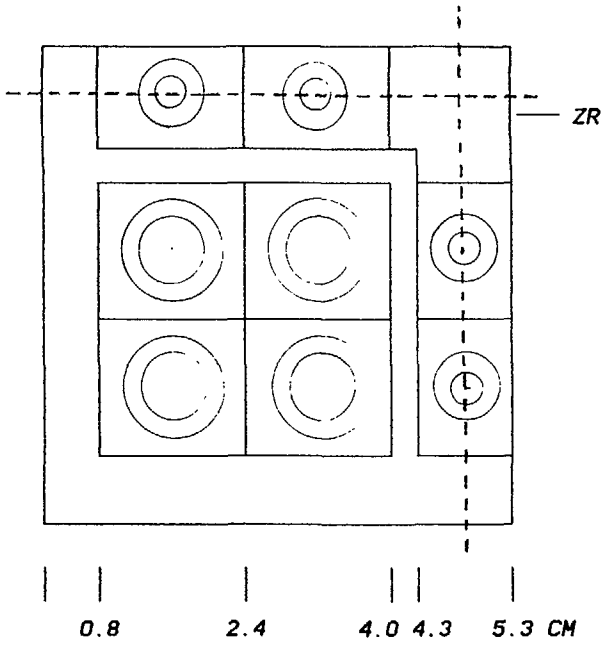

FIG. 4

Moderator: Material = H_2O, void content = 0 %, temperature = 286 ^{0}C, density = 0.7358 g/cm^3, lattice pitch = 1.6 cm.

Control rod: Material = B_4C, density = 1.761 g/cm^3, temperature = 286 ^{0}C, diameter = 0.6 cm having S.S. sheath (density = 8.03 g/cm^3) with outside diameter 0.8 cm and temperature 286 ^{0}C.

The calculations have been done in 27 groups and only 1 term has been considered in the expansion of angular flux at region interfaces to save the computer time. Though, more number of terms should be considered but the aim here is to inter compare the two methods under the same approximation. In fuel cell, 3 zones have been considered whereas in the control cell 4 zones (corresponding to 2 zones in poison

tube, 1 in sheath and 1 in the moderator) have been considered In the approximate method, in which control cell has been homogenised, only 1 zone has been considered

In the exact method, the calculations were done in the exact geometry taking control rod exactly In rest of the calculations, the control rod along with its sheath and the interspersed moderator was homogenised first and then the calculations were done using the homogenised cross sections for the control cells In the second method, the control rod parameters (homogenised cross sections) were generated by giving the current spectrum of the incoming neutrons at the surface of the cell in the input (ICONTR=2) which was taken from the exact calculations done in the case 1 Ideally speaking, the results of this case should match with the case 1 The difference in the results of the two cases is due to the fact that 4 zones were considered in the control cell in case 1 whereas only 1 zone was considered in the second case Therefore, the difference in the results of the two cases is due to the poor representation of flat flux approximation in the second case In the third method, the control rod parameters were generated by approximating the whole lattice cell in slab geometry in which the geometry of the control cell was preserved and the fuel cell was spatially smeared (ICONTR=3) The control rod parameters were generated by preserving the blackness of the neutrons at the surface of the cell as in the case 2 In order to see the difference in the results if the control rod parameters are generated by usual volume and flux weighting instead of preserving the blackness of neutrons, we repeated the generation of control rod parameters as in case 2 but the usual flux and volume weighting was used to generate them The results of these calculations are given in the case 4

Table 1 gives the K-infinity for the 4 cases mentioned above The results of first three methods agree well within the approximation mentioned above However, the results of case 4 are far away from the case 2 and 3 and this indicates the superiority of these methods which preserve the blackness of the neutrons The lower value of K-infinity in case 4 indicates that there are more absorptions in the control rod

Table 1 Comparison of K-infinity

Method	K-infinity
Exact Method	0 6596
ICONTR=2	0 6538
ICONTR=3	0 6541
Flux,Volume weighting	0 6314

Table 2 Power Distribution

	0 837	Exact
	0 835	ICONTR=2
	0 836	ICONTR=3
	0 826	ϕV Weighting
1 165	0 999	
1 166	0 999	
1 166	0 999	
1 177	0 999	

Table 2 gives the power distribution (normalised to 4) as calculated by the four methods There is hardly any difference in the first three methods In the fourth method, the fuel pin near the control rod produces less power due to depression of flux caused by relatively more absorptions in the control rod

VI. CONCLUSIONS

The two options to generate control rod parameters in the computer code LWRBOX are working properly The method based on preserving the blackness of neutrons to generate homogenised parameters of the control cell has been found to be more accurate compared to the usual flux-volume weighting procedure.

REFERENCES

[1] P.D. Krishnani, Ann Nucl. Energy, 12, 675(1985).

[2] F.J. Fayers et al , AEEW-R 785 Part 1, 1972

BASIC CORE PARAMETERS IN ON-LINE MEASUREMENT FOR NRI EXPERIMENTAL REACTORS

J. BROULÍK, B. ENDT, J. HOLEČEK,
V. RYPAR, Z. TURZÍK
Nuclear Research Institute (NRI),
Řež, Czechoslovakia

Abstract

The PC (XT/AT) controled system of CAMAC units used for the measurement and for the evaluation of the basic safety and reactor physics parameters of the experimental reactors in N.R.I. Řež is described. The has been used for the measurement of the critical height, reactivity, reactivity coefficints, buckling, radial and axial neutron flux distributions on LR-0 and LVR-15 experimental reactors.

INTRODUCTION

Personal computer based systems for the measurement of the basic core parameters have been developed in the Reactor physics division, NRI Řež . The systems have been used on the LR-0 reactor (critical assembly VVER 1000) and on the experimental reactor LVR-15 (LWR, 15 MWt) for the start-up experiments, for the measurements of space and time - space dependent neutron flux distribution, for reactivity measurement and for basic macro parameters measurement. Previously hardware of all these experiments used the special single purpose equipments consisting of the analog part for detector signal processing (HV supply, amplification, discrimination, AD conversion, etc.), the analog and digital units for the sampling of signal pulses (scalers, real time pulse clock, etc.) and data output devices (punch tape or printers). Recently with the HW and computers development as well as with the standardisation of the analog and digital units (NIM, CAMAC) we have transferred old experimental systems to the general PC based experimental system, where for the different measurements only special CAMAC units are to be changed in the controlled CAMAC crate . The block diagram of the experimental system is on the Fig 1. One part of the experimental hardware are analog electronics units providing detectors high voltage supplies as well as detectors signal adjustment and amplification. The second part of the system are CAMAC units for signals sampling and if necessary for the absorption cluster or fuel element movement control.

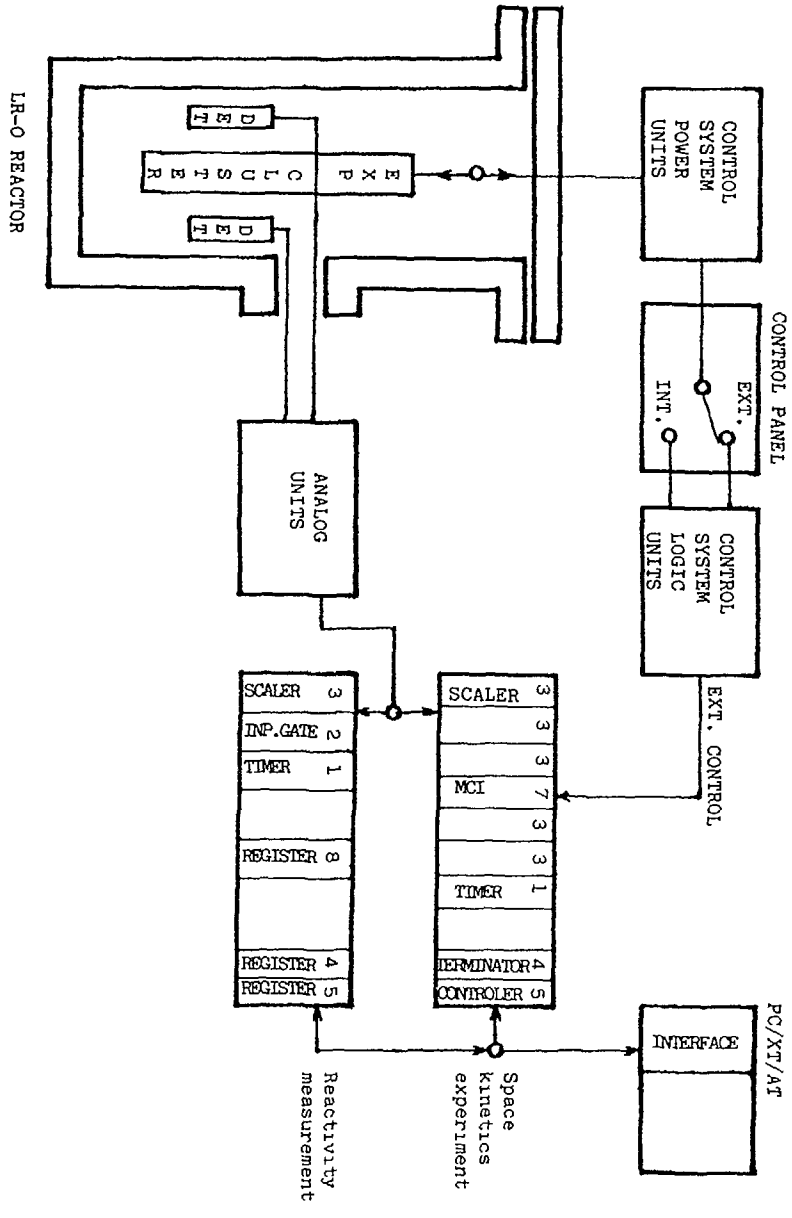

FIG. 1 - Basic configuration of the experimental system

Specification of CAMAC units is following : No 1-clock pulse generator CAM 5.01 used as programmable unit for sampling interval selection (RTCL), No. 2-input gate CAM 321 used for reading of BCD coded moderator height from the standard reactor control system, No.3-quad scalers CAM 401 (NL 2305) for the measurement of count from the detection lines, No.4- highway terminal CAM 1.40-3, No.5-crate controller (e.g. CAM 1.40-1, NL 2106, CLANP, CAM 1.22- PDP11 to CAMAC), No.6- PC interface card (e.g. CAM 1.40-2), No.7- motor control interface CAM 2.13, No.8-interrupt register CAM 303.

The start-up experiments are covered with two special data acquisition software (STRT90, BLB15C) depending on the necessity to obtain the estimation of the critical mass and k_{eff} or only the critical moderation water height and to measure reactivity. Space or time and space dependent neutron flux distribution is covered with two software codes VOJTA and DROP. For the macro parameters measurement the special code (SCAN) was written in FORTRAN, which control CAMAC step motor controller unit.

Start-up experiment, reactivity measurement and space -time neutron flux distribution measurement can be characterised as the measurement of the time distribution of the counts from neutron detectors in selected time intervals (sampling intervals or time resolution of the signal). According to the the methodology of the different experiments the counts representing neutron flux value in the sampling intervals are measured and the desired statistical parameters of the time distribution are evaluated The experimental data are analysed in the first period of the analysis to obtain the estimation of the immediate value in the interval or the estimation of the mean value used for the following analysis. In this second period of the analysis we obtain desirable core parameters

START UP EXPERIMENTS

The measurement for the start-up experiments on LR-0 and LVR-15 reactors have been covered with two versions of code STRT90 for PC/XT/AT. The code control the data acquisition as well as the data analysis and the determination of start-up parameters (the critical mass, k_{eff} and critical moderator height). The simple method for the count mean value estimation and the outliers exclusion is used in the code. There is possibility using up to 4 neutron detectors, to change outputs to the display, to the printer or to the hard disk and to set all experimental parameters (sampling interval, number of sampling interval for mean value estimation, statistical precision for cumulative count estimation) In this experiment all measurements are done in the subcritical condition All changes in the core building (increasing the number of fuel assemblies, the change of absorbing cluster insertion or change of the moderator height) result after some transient period in stable neutron flux This fact al-

lows to sum up the counts from the single time intervals. Firstly to see if there is stable neutron flux we estimate the reactor period from monitored counts.

At the beginning of the experiments in the table of the interrupt vectors the address of standard interrupt 1C hex is overwritten to the address of procedure covering time sampling (TimeIntr). Interrupt procedure is called app. every 20 ms and it controls data acquisition. After finishing data sampling procedure ETIME renew previous values for interrupt 1C hex. In the data sampling and analysing we have used active control for the data acquisition from the keyboard.

The output parameters are:
on-line · estimated reactor period, filtered count rate
off-line predicted critical mass and keff, the graph of 1/counts (critical mass, H).

REACTIVITY MEASUREMENT

The code BLB15C is devoted for the measurement of the reactivity and/or for the measuring of the critical moderator height in the start-up experiment on LR-0 reactor. The code estimates also the reactor period used to determine the core critical state. The output of the code is the experimental data file containing the measured values of the reactivity, moderator level and estimation of the errors. Reactivity measurement is based on the inverse kinetics method. The old versions of the code, written in FORTRAN and ALGOL, was previously used on the HP 21MX and PDP 11/4 computers for the same purpose. New code version for PC is written in TurboPascal 6.0 and its most frequently used procedures and functions was rewritten to assembler. The code is working on PC/XT/AT286/AT386 with or without the coprocessor. The choice of the fastest sampling rate depends on the real time clock frequency and on the type of PC : AT286/10 + 287 coprocessor works already with dt=0.05 s and with 4 measured lines. The same configuration without coprocessor works only with dt=0.1s. We have used 16 bits counters with SW correction on 17th after overflow. There are two basic possibilities for the time synchronisation of the measurement control:

- active waiting in the loop,
- passive waiting for the interrupt.

In the last version of BLB15C code we have used the active waiting in the loop and at the end of sampling interval reading and erasing of the scaler :

```
repeat
until TestLAM(CAM 5 01 position)  {end of sampling interval}
clear LAM                         {CAMAC function F10,A15  }
read+erase scaler                 {CAMAC function F2       }
read  CAM 321                     {moderator height        },
```

where TestLAM is the procedure for the testing LAM signal from RTCL (CAM 5.01). Time consumption in the waiting loop and asynchronous character of HW routines in DOS kernel results in the fluctuation around mean value of measured frequency which was bellow true value from RTCL. DOS kernel routines could not be influenced. We have to change the code itself to increase the precision of the measurement influenced by the time scale uncertainty. The first method to overcome this inherent uncertainty was to apply the coprocessor with data type Real Extended and the second one was to use assembler part in the procedure NAFD, which provide the complex communication between PC and CAMAC crate. NAFD procedure works at every experimental data transfer from the crate to the PC (read), at every control of CAMAC units (write) as well as in the special operations on the crate Using assembler part in TurboPascal code we have decreased time in the waiting loop (decrease the time uncertainty of the time synchronisation). The up described methods minimise the discrepancy between true and measured frequency from RTCL.

SPACE DEPENDENT NEUTRON FLUX DISTRIBUTION

NRI Řež and ZfK Rossendorf have jointly prepared and performed neutron detectors response measurement due to reactivity perturbation on LR-0 reactor /1,2/. Space-time neutron flux distribution was measured in 31 and 55 fuel assemblies core configurations. Experimental data files have been used for the verification of kinetics codes for VVER-1000 type core. Time dependent local reactivity perturbation induced by the movement of the one experimental cluster was used in the first period of experiment. Cluster deposition has responded to the ramp negative reactivity perturbation from the critical state and back with hold on in the subcritical state in the first period of experiments, followed by cluster drop measurements in the second period. The second type of reactivity perturbation has been the absorption cluster drop. The experimental hardware is based on a computer controlled CAMAC system for simultaneous data acquisition of 20 spatially distributed neutron detectors and for absorption cluster control. HV supply units and the amplifiers are in analog units crates, which are placed in well shielded metal box. To minimise electromagnetic disturbances on low level neutron detector signal the box is as close to the core as possible and it is grounded to the vessel. Signal amplifiers are galvanicaly isolated from following crate with impulse discriminators, which are placed 20 m apart in the control room. PC controlled CAMAC system has been used in the all described experiments. PC sets real time sampling of measured detectors signal and it control fuel element or absorption cluster depositions with the CAMAC step motor interface CAM 2.13. The real time clock module sets the time axis of experiments. Neutron detectors signals are sampled by 5 quad scalers. CAMAC crate controller represents interface between

PC used for experiment control as well as for the data acquisition system, and the controlled CAMAC crate. To set all experimental parameters as well as to control the measurement the codes VOJTA and DROP was written. Sampled counts are stored on floppy diskettes or to the hard disk. Software package has been written in FORTRAN or TurboPascal to evaluate primary experimental data files, to check detectors reliability, to correct and to accumulate primary data files, to calculate the inverse kinetics reactivity and to analyse final data files. All codes use the same experimental data files.

The space-kinetics experiments have been measured in 1986-1989 with PDP 11/4 computer. The data acquisition and control system were based on code VOJTA to provide the desired changes of reactivity perturbation or DROP for the experimental absorbing cluster drop. The codes were recently rewritten to TurboPascal for PC/XT/AT. Sampling time interval, cluster down and/or up motion start the velocity and the direction of the motion, the end of the data sampling, total numbers of the motor steps (the amplitude of reactivity perturbation) and the address of CAMAC units in the crate are set in the codes To identify the experiment we have also to write the critical height, the initial and final position of the cluster as necessary information. The code use following procedure for sampling time loop

```
if TestLAM(CAM 5.01) then          {end of sampling interval}
begin
read + erase scaler                  {CAMAC function F2     }
write data to hard disk
erase LAM (CAM 5.01)                 {CAMAC function F10,A15}
until index >N                       {Number of intervals   }
```

MACRO PARAMETERS MEASUREMENT

One of the basic tasks being solved on each LR-0 reactor core is finding its spatial neutron flux distribution. The method used for this purpose is based on the measurement of the induced gamma activity of U235 fission products. A set of the fuel elements which are designed to be used for the measurement are pulled out from the core after the irradiation and transported to the laboratory. There they are scanned at the same axial coordinate in order to determine the radial part of the spatial distribution. The axial part of the distribution is derived from the scanning of several single fuel elements along their longitudinal axis. In both cases gamma rays in the energy range 600-900 keV are taken into account. HPGe detector in connection with CANBERRA Series 80 multichannel analyser is used to measure fuel elements' activity in the radial direction. Axial distribution profile is scanned using the device consisting of two independent channels equipped with NaI(Tl) scintillation detec-

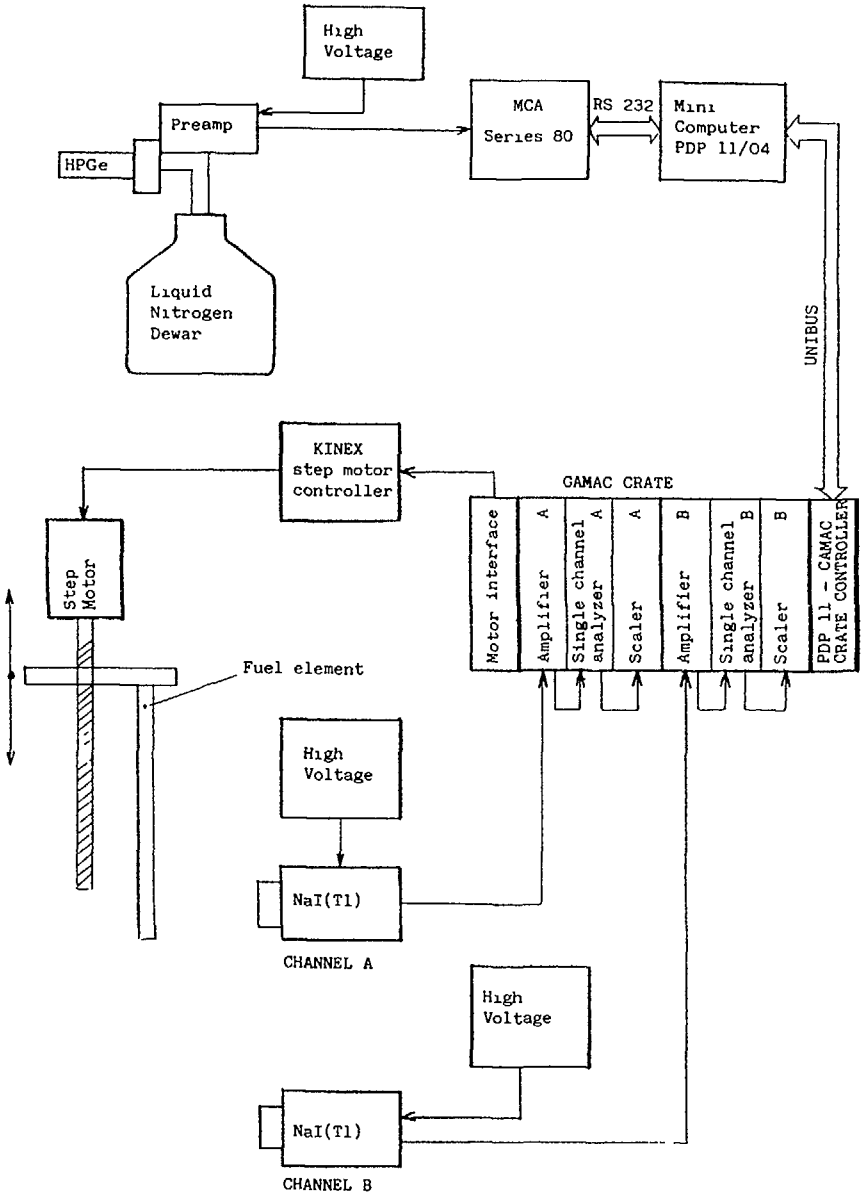

Fig. 2 - Block diagram of macro parameters system.

tors and standard analogue part (HV power supply, amplifier and single channel analyser) of CAMAC modules. The whole system is schematically shown on Fig. 2. The PDP 11/04 computer provides the control over the whole system. This consists in the control of the CANBERRA analyser measuring cycle for the radial part of the distribution measurement and simultaneous scanning of single fuel elements to find the axial part. In the latter case one of the measuring channels is equipped by the device consisting of KINEX step motor controlled by the computer via special CAMAC interface providing automatic motion of the scanned fuel element in front of the detector. The other channel is used for fission products radioactive decay monitoring. To control the device a code called SCAN was written in FORTRAN. The program provides the control of the CAMAC crate using special interrupt service routines, data acquisition and their record into floppy diskettes files. The further data evaluation is done by the complex of codes calculating the standard corrections of the measured data (e.g. dead time, radioactive decay, calibration and background correction). The obtained results are then related to the fission density distribution. The above described method has not been applied to define the spatial distribution only. Basic macro parameters such as material buckling and multiplication factor can be also estimated as a function of spatial distribution. This approach has been used recently to estimate the subcriticality of various spent fuel compact configurations, for example. With recent experiences with PC control of CAMAC crate SCAN code is under transferring to above described general PC/AT based system.

REFERENCES

/1/ V. RYPAR, J. RACEK, K.H. FAHRMANN,
U. GRUNDMANN, D. ZIEGENBEIN
Neutron Kinetic Investigation at the Zero Power Reactor LR-0.
Nucl.Sci. and Eng. 105,3,218,1990

/2/ E. NOVÁK, J. RACEK
Technical arrangement of the experiment space kinetics on reactor LR-0 in 1987 (in Czech)
ÚJV 9104 R,A , 1990

RITME: A FAST AND SIMPLE COMPUTING CODE FOR PWR CORE CALCULATIONS AND MONITORING

L. SAUVAGE
Direction des réacteurs nucléaires,
Département d'études des réacteurs,
Centre d'études nucléaires de Cadarache,
Commissariat à l'énergie atomique,
Saint-Paul-lez-Durance, France

Abstract

This paper discusses an overview of the use of the RITME method for on-line applications and studies based on PWR core simulation .

Section I outlines the basic principles of the method; some equations are given in order to illustrate the simplicity of the method .

Section II discusses the PRO-RITME application, PRO-RITME is a software package for 3-dimensional power reconstitution of a PWR core. Neutronic parameter 3D distributions (fuel and moderator temperature, xenon concentration, burnup) and synthetic factors such as axial-offset, hot peaking factors are also performed by the PRO_RITME system . The run time performances and the qualification results are also given in this section .

The last section describes the 3D PWR core simulator RITME . The main features, and particularly the graphic interface developed with an advanced graphic software, are presented .

INTRODUCTION

This paper discusses an overview of the use of the RITME method for on-line applications and studies based on PWR core simulation .

The basic principles of the method and the main equations are presented in the first section .

The RITME method is a close solution to the neutron transport and thus, this makes it well adapted to a variety of core calculation applications . In this paper, we present two software systems based on the RITME method .

Section II discusses the PRO-RITME application . It is a software package for 3-dimensional power reconstitution of a PWR core . The principal features and performances are presented .

The last section describes the 3D PWR core simulator RITME and particularly its graphic interface developed using an advanced graphic software .

I. PRESENTATION OF THE RITME METHOD

I.1. Introduction

RITME is a nodal Green's function method for solving the neutron transport equation . In this section, only the main characteristics and the methodology to calculate fluxes per mesh on PWR cores are discussed ; the detailed formulations are given in reference /1/ .

For the sake of clarity, the method is applied here to the steady-state neutron transport equation expressed in integral-differential form.

The initial equation is the following :

$$\underset{\text{migration}}{-\mathrm{Div}\,(\Omega\,.\,\varphi(r,E,\Omega))} \;\underset{\text{disappearance}}{-\Sigma_t(r,E)\,.\,\varphi(r,E,\Omega)} \;\underset{\text{sources}}{+S(r,E,\Omega)}$$

(Eq: 1)

$$+\int\!\!\iint \Sigma_S(r,E'\rightarrow E,\Omega.\Omega')\,.\,\varphi(r,E',\Omega')\,dE'\,d^2\Omega' \;=\; 0$$

transferred

The neutron medium is assumed to be isotropic and is characterized by macroscopic cross sections (Σ) . The fission sources S (r,E,Ω) are isotropic and associated with a fission spectrum κ (E) ,

$$S(r,E,\Omega) = \kappa(E)\times S(r) \qquad \text{(Eq: 2)}$$

I.2. Notations and definitions

By definition, the actual medium is considered to be the superposition of a "zero medium" and a "prime medium" :

* the **"zero medium"**, designated "0" is isotropic and independent of the space variable (r) . This homogeneous medium is independent of local variations affecting the neutron parameters, including boron concentration, fuel and moderator temperatures, xenon concentration, burn-up, etc .

* the **"prime medium"**, designated "'" and dependent on the space variable describes local changes in neutron properties relative to the "zero" medium .

Symbolically, the neutron medium is then :

Actual medium (r) = "Zero medium" + "Prime medium (r)"

The macroscopic cross sections and fluxes are expressed in the following forms :

$$\Sigma(r) = \Sigma^{\circ} + \Sigma'(r) \qquad \text{(Eq: 3)}$$

$$\varphi(r,E,\Omega) = \varphi^{\circ}(r,E,\Omega) + \varphi'(r,E,\Omega) \qquad \text{(Eq: 4)}$$

$$\Phi(r,E) = \Phi^{\circ}(r,E) + \Phi'(r,E) \qquad \text{(Eq: 5)}$$

I.3. Calculating the flux Φ^o

• Theory

Writing Φ^o is solution to the transport equation (Eq: 1) and using the linearity of the operator A° associated with equation (Eq:1) , one obtains without approximations :

$$\Phi^{\circ}(r,E) = \iiint \Psi^{\circ}(r,r',E)\times S(r')\times d^3r' \qquad \text{(Eq: 6)}$$

where Ψ^o is known as a Green function .

Ψ^o (r,r',E) is the flux at r of energy E due to one neutron/second emitted at r' , in the form of a Dirac distribution, with the spectrum of source S in the "zero" medium .

• Application

Φ^o(r,E) is by definition a flux in a homogeneous medium, therefore :

- Φ^o(r,E) will have a smooth spatial form (no interface between different neutron media); it involves "long-range" migration, and can be calculated with a coarse mesh consistent with the migration properties of the selected "zero" medium . The "zero" medium corresponds in fact to the average neutron medium of the configuration in question .

- the Ψ^o functions depend only on the distance between r and r' , and thus involve geometrical symmetries . For a given "zero" medium and neutron emission spectrum, they may be calculated once and for all to constitute a limited function library .

After dividing the core (and reflector) into meshes (subscript j), equation (Eq: 6) and for a resolution with G energy groups, the discrete formulation of Φ^o is the following :

$$\Phi^{\circ}_{jg} = \sum_k \Psi^{\circ}_{kjg}\times V_k\times S_k \qquad \text{(Eq: 7)}$$

where :

S_k is the neutron source density in the "emitting" mesh k

V_k is the volume of mesh k

Ψ^o_{kjg} is the Green function between meshes j and k at energy g .

I.4. Calculating the flux Φ'

• Theory

Writing the total flux defined by equation (Eq: 5) and considering the following hypotheses :

1/ the media are isotropic

2/ the angular flux φ' (r,E,Ω) is isotropic

the scalar flux Φ' (r,E) is solution to the simplified equation :

$$A'\Phi' = S' \qquad \text{(Eq: 8)}$$

where

A' is a linear operator (thus integral) associated with the developed equation giving Φ' (r,E) (see reference /1/)

and,

S' is a source term function of the flux Φ^o(r,E) and cross sections of the "prime medium" .

Thus, the scalar flux Φ' (r,E) can be expressed as follows :

$$\Phi'(r,E) = \iiint \Psi'(r,r',E) \times S'(r') \times d^3r' \qquad \text{(Eq: 9)}$$

where Ψ' is a Green function in an heterogeneous medium, it depends on both the S' source spectrum and the neutron media in r and r'.

• Application

Flux Φ' results from local changes in the neutron properties of the actual medium relative to the "zero" medium . It is thus advantageous to adapt the Φ' calculation mesh to the neutron heterogeneities of the core calculated .

For PWR cores, the neutron variations will affect the thermal and epithermal ranges, thus the migration term concerning Φ' will be small . That means:

- the accuracy on Φ' is mainly related to the quality of the cross sections in the r medium

- the coupling area necessary to calculate Φ' is reduced .

The RITME method enables the users to define different meshes for Φ' and Φ^o. This allows us to obtain a precise assessment of neutron heterogeneities (absorber , mixed oxide assemblies ...) saving the computational time .

I.5. Remarks concerning the Green functions

The Ψ' functions are tabulated according to sensitive parameters of the S' spectrum (e.g. the moderator density) and to characteristic neutron migration parameters (e.g. absorbers in intermediate energy ranges) .

The Green functions for a given application are calculated once and for all using multigroup transport code . The energy discretization is precise enough to provide an accurate description of neutron migration in the high-energy ranges; these values are then condensed to a smaller number of groups for flux calculations in the application .

I.6. Total flux calculation

The total flux $\Phi_{jg} = \Phi^o_{jg} + \Phi'_{jg}$ is obtained, on the Φ' mesh, after "outer" iterations on the fission sources in order to obtain the critical flux form and the effective multiplication factor .

A carrier flux (flux in homogenized medium) is calculated throughout the core by interpolation . The microscopic flux is reconstructed by a factorization of the carrier form with the pin-by-pin infinite medium flux stored in the neutron library .

II. THE PRO-RITME ON-LINE SYSTEM

II.1. General description

PRO-RITME /2/ is a software package for 3-dimensional flux and power reconstitution of a 900 MWe PWR core . The flux calculation is based on the RITME method, thus the use of a transport method makes PRO-RITME well suited to a wide variety of cores .

PRO-RITME allows for a fast and an accurate core performance assessment consistent with a use in an on-line monitoring system . The input measured core parameters for the 3D calculation are the following :

- inlet and outlet primary loop temperatures
- primary pressure and flow rate
- control rod positions
- two stage excore detector signals to adjust the axial power distribution using a measured axial offset /3/ .

Fluxes per energy-group, power and the neutron parameters (fuel and moderator temperature, burn-up, xenon concentration) are performed throughout the entire core over a 21.5 cm edge regular mesh .

From the 3D distributions, synthetic factors are generated :

- average power per assembly
- average axial power with axial offset
- hot peaking factors : FΔHmax , FQ , Plin_max(kw/ft)

The responses of the core instrumentation (thermocouples , moveable or fixed chambers) can be simulated and compared with the measured values .

II.2. Principle of the flux calculation - Equations

The flux is calculated using the RITME method for quasi-static conditions including an approximation well justified for the homogeneous PWR core .

In this fast computing version, the treatment of the migration of Φ' is performed using a simple convolution .The total flux Φ is obtained from very simple formulas .

Fluxes are performed for 2 energy groups without up-scattering, the PRO-RITME formalism yields the following expressions :

$$\Phi_{j1} = \alpha_j \times \Phi^{\circ}_{j1} \text{ (fast group)} \qquad \text{(Eq: 10)}$$

$$\Phi_{j2} = \beta_j \times \Phi^{\circ}_{j1} + \Gamma_j \times \Phi^{\circ}_{j2} \text{ (thermal group)} \qquad \text{(Eq: 11)}$$

where α, β,Γ are functions of cross sections of the neutron medium in mesh j

and Φ° is calculated from the equation (Eq: 7) taking exchanges with 26 neighbouring meshes into account .

These simple equations explain the high performances of the system related to the computational time . The approximation used in PRO-RITME has been qualified on various French PWR cores ; synthetic results are presented in the next paragraph .

II.3. Performances

The PRO-RITME system was installed at the CRUAS 2 site to monitor, in an open-loop configuration, the entire 4th operation campaign . The software version was implemented on a commercial workstation : HP9000/350 under UNIX operating system with MOTOROLA MC68020 microprocessor .

For this experimentation, an off-line accuracy study was carried out for the first four cycles of CRUAS 2 . This study includes a comparison between calculated and measured 3D power distributions for 25 static states . During the experiment, various transient tests were also studied . The measured distributions are the periodic core maps deduced from in-core moveable chamber signals .

Table I summarizes the statistical investigation for 25 3D static maps .

This experiment showed that the RITME method can be implemented for on-line core calculations on standard workstations . The run time performances are about 3 seconds for calculating a 3D power distribution (2669 meshes) during a normal operating transient on MOTOROLA MC68020 ; the same calculation required only 1 second on MC68030 .

TABLE I

Estimated Nuclear Uncertainty Factor based on a comparison between PRO-RITME and Measurements .

(%)	FUN Systematic Component	Stand. Dev calculation / measurement	FUN Random Component
Fq	-2.6	2.4	8.6
FΔHmax	-2.4	2.5	8.8
FΔH 2D	-0.1	2.3	7.3
P > 1.	-1.2	3.7	8.7

III. PRESENTATION OF THE 3D CORE SIMULATOR RITME

III.1. General description

A 3D core simulator has been developed for PWRs using the RITME computing code and advanced graphic interfaces . This simulator, operational on 32 bit workstations, benefits from the advantages of the RITME method : accuracy and high run-time speed .

This is an interesting and easy-to-use tool for core control and monitoring studies ; it is integrated in the BEST-RITME facility /4/ whose purpose concerns the PWR core control and instrumentation optimization .

• Input parameters :

An acquisition process yields the dynamic input parameters according to two possibilities :

1- reactor conditions are read from data files recorded on an actual PWR plant

2- reactor conditions are calculated with a simplified reactor simulator . In this case, the simulator is linked to the MISTRAL PWR reactor simulator which represents, for operating transients, the dynamic evolution of the reactor parameters and the actions initiated by the reactor's automatic controls .

• Output parameters :

All the parameters calculated by RITME are avalaible; the 3D distributions can be displayed using an output graphic interface .

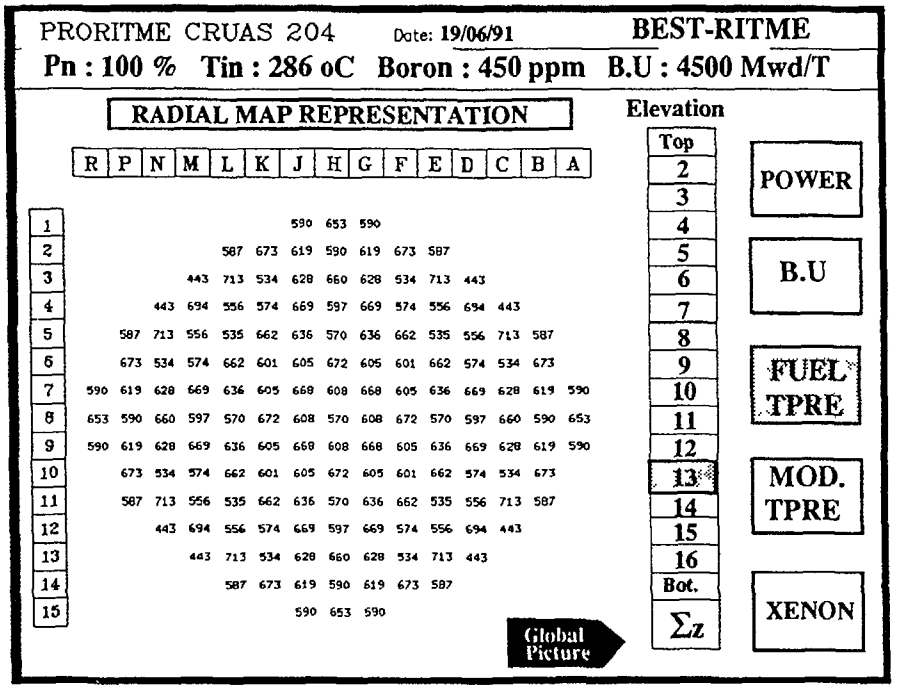

FIGURE 1 : Radial representation of the core state .

III.2. The graphic interfaces

A colour graphic interface has been carried out using DATAVIEWS advanced graphic software .

Several displays, belonging to a fully interactive process, have been developed to represent the core state . One gives a synthetic view that contains the values of the operating parameters, the average power per assembly and the average power axial form . The others concern the radial (example given in figure 1) and axial detailed representation in order to follow parameters such as power, burn-up, xenon concentration , fuel and moderator temperature .

The operating parameters can also be initialized or modified using an interactive input graphic interface .

CONCLUSION

The RITME method allows researchers to perform flux and power calculations for a variety of cores . Up to now, it has been used for 900 PWR studies related to core control and monitoring such as improvement of core protection systems, instrumentation optimization ....

At present, future applications including other types of cores and based on parametrable RITME versions are carried out within the framework of LOGARITME project /5/ .

REFERENCES

/1/ J.M. BOHLER, Ph. DUFOUR, J.P. FERRERO, L. SAUVAGE
"The RITME method: Basic principles and presentation of the LOGARITME concept"
Specialists meeting on advanced methods of calculations for power reactors - AIEA - Cadarache, September 1990 .

/2/ P. BERNARD, H. GIRARD, L. SAUVAGE
"Principles of the fast computing 3D PWR core power calculations method RITME"
International topical meeting on advances in reactor physics, mathematics and computation - Paris, April 1997 .

/3/ P. BERNARD, H. GIRARD, J.P. FERRERO, L. SAUVAGE, J.C. BARRAL, A. VASSALLO
"Testing and on-line applications of the fast 3D PWR core power distribution model RITME"
Incore instrumentation and nuclear power plant core assessment - OCDE - Cadarache, June 1988 .

/4/ M. GUEVARA, L. SAUVAGE
"BEST-RITME : A versatile testing facility for PWR core control and instrumentation optimization"
Specialists meeting on in-core instrumentation and reactor core assessment - OCDE - Pittsburgh, October 1991 .

/5/ L. SAUVAGE, Ph. DUFOUR, P. BERNARD, J. CRAY, M. PEYTIER, JC. BARRAL, A. VASSALLO, S. GHATTAS, B. GUESDON
"Development of the RITME fast 3D core power calculation and application for reactor operation and control ."
International conference on the physics of reactors : operation, design and computation - Marseille, April 90 .

OPERATION FLEXIBILITY AND AVAILABILITY IMPROVEMENTS USING BEACON, AN ADVANCED CORE MONITORING SYSTEM

T.Q. NGUYEN, R.W. MILLER,
A.L. CASADEI, P.K. DOSHI
Westinghouse Commercial Nuclear Fuel Division,
Pittsburgh, Pennsylvania,
United States of America

Abstract

In response to utilities needs in improving plant operation flexibility and plant availability, Westinghouse introduced the advanced core monitoring and operational support system, BEACON, two years ago. Since then, the continuous development of the BEACON system has led to significant advances in further reducing utilities Operation and Maintenance (O&M) costs. The development of the BEACON system is made possible by two breakthroughs: 1) advanced numerical method to solve the diffusion equations extremely fast and 2) development of cost effective, state-of-the-art computing system, workstation. This paper presents the numerical scheme used in the neutronic solution and how BEACON uses the core instrumentations to provide the continuous three-dimensional (3D) core power distribution. Once the state of the core is known on a continuous basis, several indirect surveillance and/or Technical Specifications on core power distribution can be relaxed or totally eliminated. Section 1 outlines the numerical scheme used in BEACON for solving the diffusion equations and to provide the 3D continuous power distribution. Section 2 describes the hardware requirements. Section 3 discusses applications of BEACON to improve plant operation flexibility and plant availability. Examples of actual BEACON usage to demonstrate its effectiveness are presented in Section 4 and the paper is closed with a summary of future directions.

1. BEACON POWER DISTRIBUTION INFERENCE METHODOLOGY

BEACON uses a combination of incore instrumentation (e.g., movable detectors, thermocouples) and excore detectors in conjunction with an advanced nodal method to provide continuous 3D core power distribution. The advanced nodal method employed by BEACON is based on an innovative concept called Diffusive Homogeneity(1). Simply speaking, this concept is based on the recognition that the coupling between assemblies in light water reactor environment is dominated by fast group diffusion which has long diffusion length. As such, the core can be considered homogeneous in diffusion, although heterogeneous in reactivity. Mathematically, the fast group (in conventional two-group equations) flux can be expressed as follows:

$$\phi_1 = (1/\mu)*(G)*(k^*)*\phi_1$$

where: G represents the transit probability of a neutron from one node to another

k* represents an effective fast group multiplication factor with thermal leakage correction

Once the fast flux is calculated, the thermal flux is constructed with the higher order leakage term included. The instrumentation tube flux is reconstructed by a combination of an homogeneous intranodal flux shape superposed with a heterogeneous instrumentation tube flux calculation from a transport-based lattice code, PHOENIX-P(2). Once the assembly flux is calculated, the assembly power is easily obtained via conventional method. This advanced nodal method is embodied in the SPNOVA computer code used by BEACON. The continuous power distribution provided by BEACON is obtained via the following process:

a. The BEACON 3D SPNOVA model is calibrated against the incore flux trace measurements. By using the calibrated power distribution, the excore detectors and thermocouples are cross-calibrated. These calibration factors are used until the next flux map is taken.

b. The BEACON model is updated following the actual reactor operation as closely as possible. Typically, once every fifteen minutes, the model is updated by integrating the actual core operating history (power, rod position, temperature) using the calibrated power in step (a) as the basis.

c. The continuous power distribution is provided by applying thermocouple and excore detector measurements which are available virtually on a continuous basis. The thermocouple measurements are not applied on an absolute basis. Rather, the deviation of the continuous thermocouple measurements from the cross-calibrated values (taken at the flux map) is used. During normal operation, the deviation is very small as expected. In abnormal condition, such as dropped rod, the deviation will be larger and this methodology enables the reactor operator to detect anomaly and know precisely what is happening in the reactor core.

A two-dimensional surface spline fitting technique is used to fit the adjusted information from the incore flux map and the thermocouple readings. Flexibility to properly weight the individual measurement is available to account for the quality of the individual reading. Extrapolation to uninstrumented assemblies is performed by the surface spline fitted values from the instrumented assemblies in conjunction with the up-to-date core model power distribution for the uninstrumented assemblies.

2. HARDWARE REQUIREMENTS

To effectively develop a continuous core monitoring and operational support system, it is a must to have a computer which allows multi-task operation, be compact without special environment requirements and with good computational speed for multidimensional calculations. The advent of the workstation addresses all of these requirements. The capability to link multiple workstations in a network enables the users to receive information from a single data source to address each user's specific needs. BEACON presently is configured with an HP/APOLLO workstation with the following characteristics:

- A 25MHz 32-bit Motorola 68040 central processor
- A 24 MB of RAM

- A 19 inch color display with a 1280x1024 pixel resolution
- A 660 MB formatted Winchester disk drive
- A 60 MB 1/4 inch cartridge tape for disk backup, system updates and data transfer
- Ethernet/IEEE-803 network for communication protocol

BEACON can be configured to access the plant data directly through the plant process computer or linked to a network. The capability to link BEACON in a network enables multiple users to access consistent core information and to perform core operation support functions.

3. PLANT OPERATION FLEXIBILITY AND AVAILABILITY IMPROVEMENTS WITH THE BEACON SYSTEM

Traditionally, Westinghouse Pressurized Water Reactor employs movable incore and excore detectors as a mean to monitor the core power distribution. Technical Specifications and surveillance requirements are in place to assure that the core is operating within analyzed limits. The power distribution related limits typically consist of indirect measure of core power distribution and thermal margins, such as axial flux difference, quadrant power tilt ratio. Detailed power distribution is measured once a month to confirm peaking factors limit. With BEACON, the detailed core power distribution is available on a continuous basis which is analogous to having a fixed incore detector system or a continuous movable incore detector system. In addition, with the extremely fast neutronic model using actual measured parameters, BEACON provides analysis of actual thermal margins in terms of kw/ft and DNBR. Directly monitoring these parameters enable the users to determine the impact of anomaly without having to take drastic action, such as reduction in power, unless absolutely necessary.

With kw/ft and DNBR monitoring capabilities, the need for axial flux difference is eliminated. This significantly improves the utility operator ability to return to power quickly. An example of this benefit is illustrated in Figure 1. In a core with conventional monitoring devices and employing the Constant Axial Offset Control (CAOC) strategy, the reactor operator is required to keep the axial offset within the CAOC limit. This necessitates movement of the control rod frequently and slowly to assure that the axial power distribution is within limit. If the axial power distribution is outside of the prescribed limit, penalty minutes are taken which limit future operation flexibility. With BEACON kw/ft and DNBR calculation on an essentially continuous basis, the core thermal margin is known at all times. This allows the reactor operator to capitalize on operating margin, in particular at low power, to trade-off with more relaxed operating space. Actual plant data shows that operation of a more relaxed operating space (RAOC) can result in a saving of eight effective full power hours relative to a conventional +/- 5% delta-I CAOC band.

Another benefit of having an up-to-date neutronic model is the ability to "know" the xenon distribution in details to devise strategy to control it. In BEACON, the xenon mode (XeMode) display enables the operator to determine the appropriate rod movement to control xenon distribution very effectively in preventing xenon oscillation or dampening one if one is in progress (3). The XeMode represents the latest advancement in core control strategy in that it

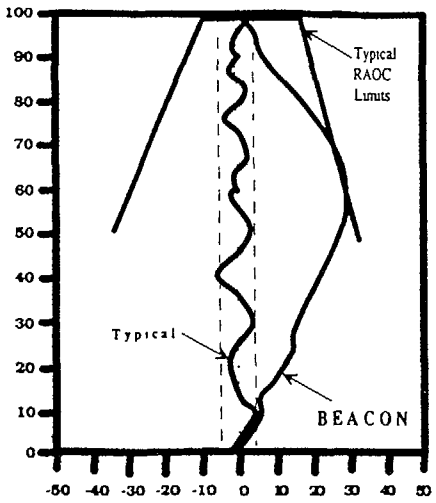

Figure 1: Startup With and Without BEACON

allows the projection of the future core axial power distribution based on action taken by the reactor operator at a particular instant. Future axial power distribution is really determined by the iodine and xenon distribution which is created due to a certain control rod, core power and axial power distribution intermix during a plant maneuvering. In BEACON, two new quantities are invented to describe the movement of the xenon distribution(4).

$$\Delta\, Xe = \int_{L/2}^{L} Xe(z)\,dz - \int_{0}^{L/2} Xe(z)\,dz$$

A free running xenon oscillation can be approximated by:

$$\Delta Xe(t) = \Delta Xe_o\, e^{At}\, Sin(w\pi t)$$

For a stable xenon oscillation, the time derivative is defined by:

$$\partial \Delta Xe(t)/\partial t = w\pi\, \Delta Xe_o\, COS\ (w\pi t)$$

A parameter r can be defined which determines the rate of change of the xenon skewness as a function of time. A phase diagram can be constructed to pictorially see the behavior of xenon due to plant maneuvering. An example of such a diagram is shown in Figure 2.

This phase diagram provides invaluable information for the reactor operator to control the axial power distribution. For example, a stable xenon condition would have the derivative equal to zero and the delta xenon at the nominal equilibrium value. To effective dampen a xenon oscillation, action via

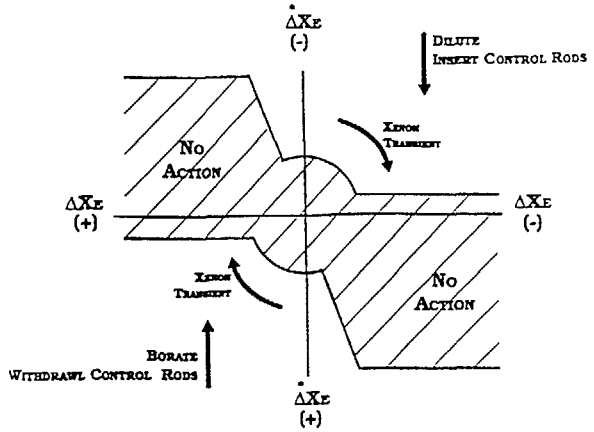

Figure 2: Xenon Mode Control Actions

control rod movement and associated boration/dilution should be taken when the delta xenon is near the equilibrium value and by forcing the r value to zero at this time.

4. FIELD EXPERIENCE WITH THE BEACON SYSTEM

BEACON has been installed at several reactors in the United States and one unit in Korea. Actual plant data have been collected and analyzed to reaffirm the accuracy of BEACON continuous power distribution methodology and global reactivity calculation such as Estimated Critical Condition. Direct comparison against INCORE based system showed that the BEACON-based reaction rate integral and inferred power distribution are essentially the same as those of the INCORE system. Several Estimated Critical Condition calculations, performed by the utilities for startups as well as power maneuvers, showed the BEACON results are typically within 150 pcm from actual core condition.

To demonstrate the usefulness and importance of having the XeMode control strategy, a simulation was made of an actual return to power maneuver by an US utility. By a combination of rod movement and power level, the utility initiated a xenon oscillation which was further compounded by inappropriate xenon dampening strategy. Consequently, the utility was forced to stay at low power for two days to allow a separate engineering organization to model the maneuver and to provide an operating strategy to dampen the xenon. The same maneuver was simulated in BEACON at the onset of the xenon transient. By using the XeMode control strategy, the xenon was dampened quickly. Figure 3 shows the actual plant axial offset and rod position as a function of time during the xenon oscillation. The xenon oscillation can be clearly illustrated via the XeMode diagram in Figure 4 with the spiral moving outward indicating a) the xenon distribution is further skewed by the operator's action and b) the rate of change of the xenon skewness is accelerated due to inappropriate rod movements.

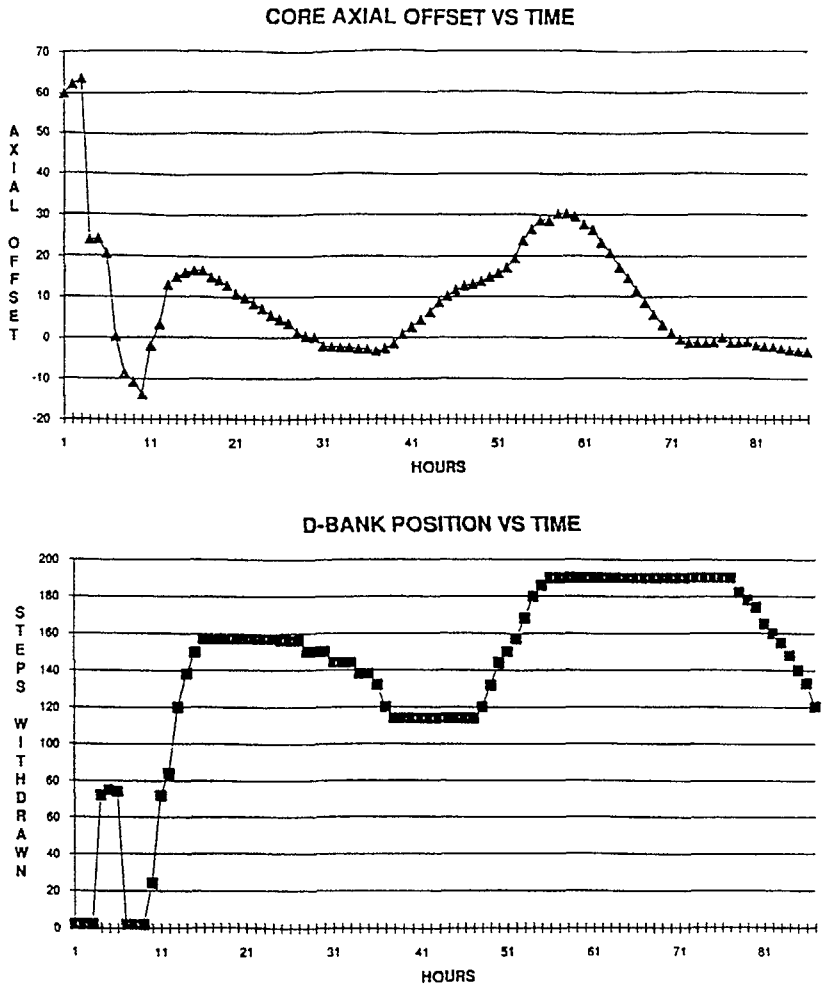

Figure 3: Poorly Controlled Xenon Transient Time Plot

Figure 5 demonstrates the effectiveness of the XeMode operating strategy. At the initiation of the xenon oscillation, the control rod is kept at 160 steps withdrawn at a slightly longer period and further inserted (rather than withdrawn) afterward using the XeMode plot guidance. The result of the maneuver is a spiral moving inward rapidly indicating the xenon has been dampened. Figure 6 shows the behavior of the axial offset and rod positions in this maneuver.

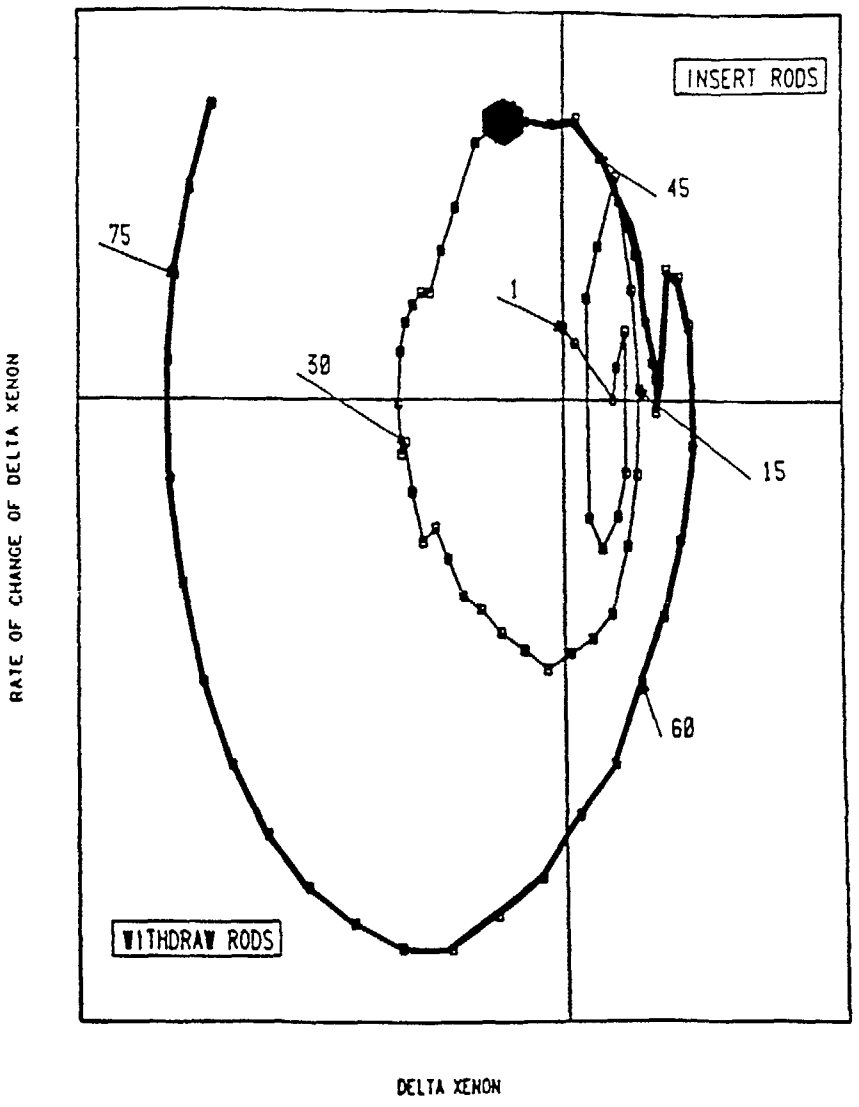

Figure 4: Poorly Controlled Xenon Transient Phase Plane Diagram

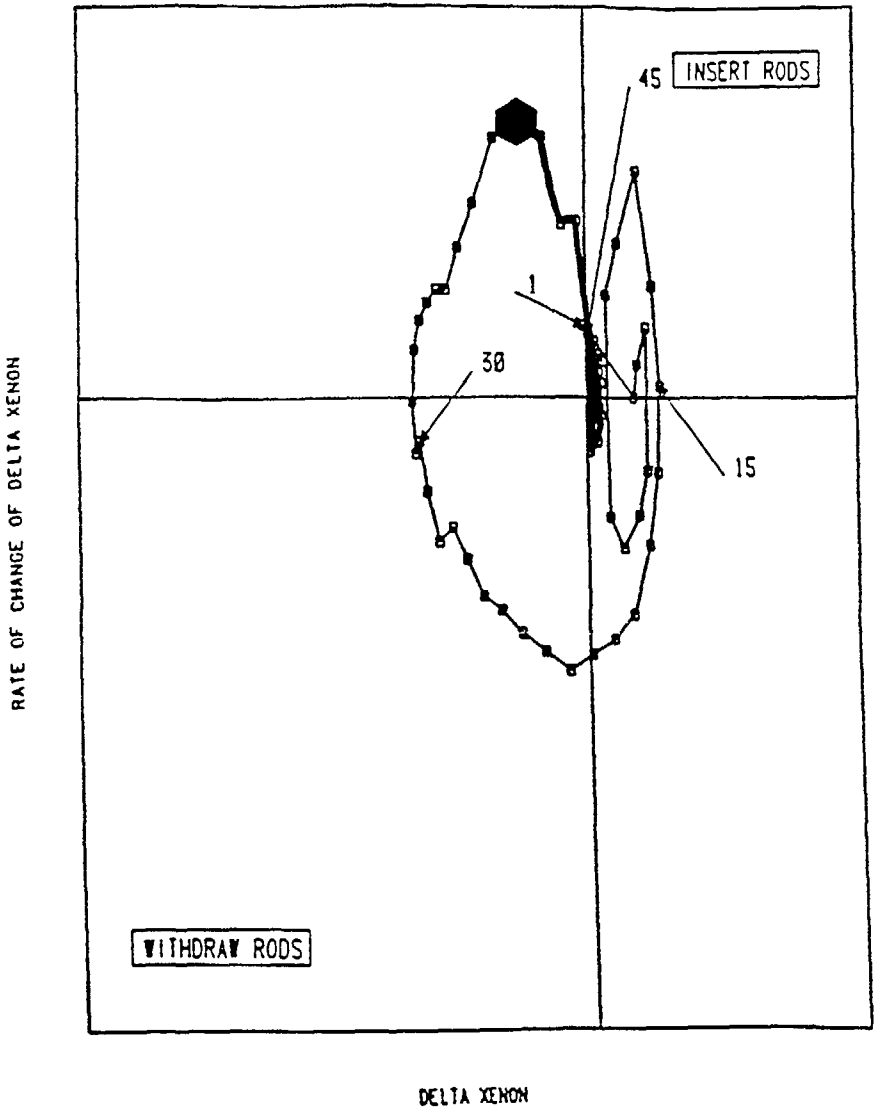

Figure 5: Phase Plane Diagram for Xenon Transient with Xenon Mode Control

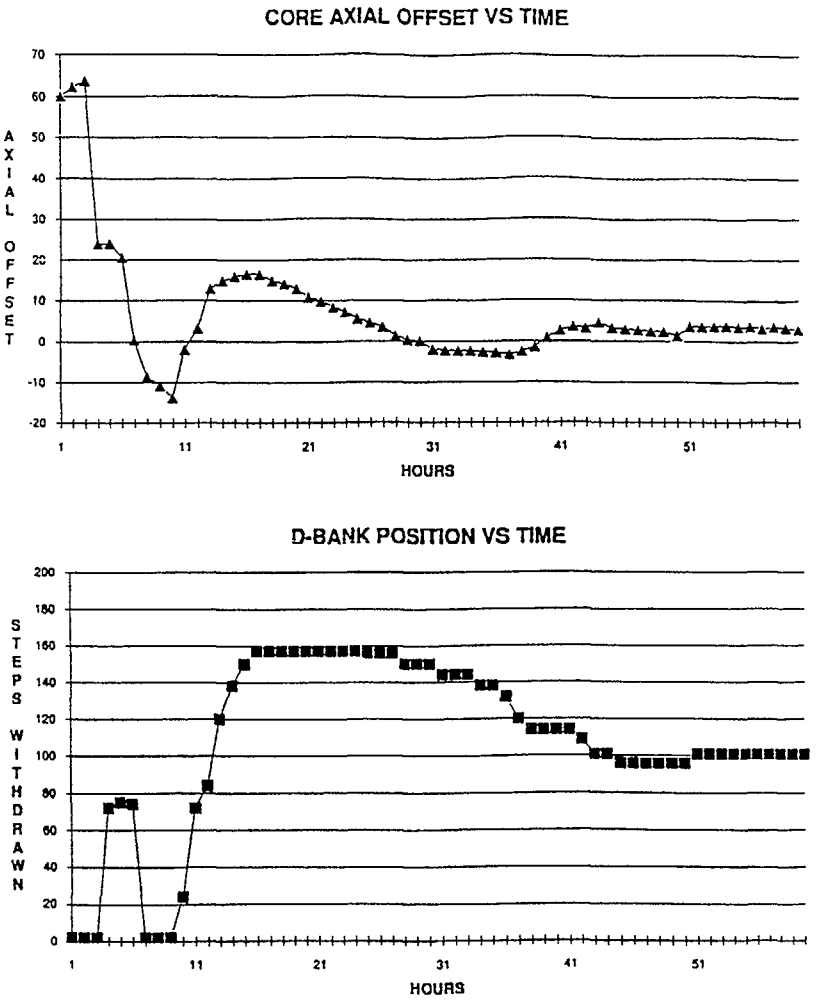

Figure 6: Time Plot of Xenon Transient with Xenon Mode Control

5. SUMMARY

The state-of-the-art advanced core monitoring and operational support system BEACON has evolved over the past few years to further improving the plant operation flexibility and availability. By direct monitoring of true thermal margin parameters, kw/ft and DNBR, several existing Technical Specifications and surveillance requirements can be relaxed or eliminated. In addition, with the fast evolution of workstation technology, realistic 3D calculation can be done in less than one minute which allows accurate prediction of core behavior to optimize plant operation strategies.

REFERENCES

1. Chao, Y.A. and Penkrot, J.A., "Diffusive Homogeneity - The Principle of the Superfast Multi-Dimensional Nodal Code, SUPERNOVA", Trans. Am. Nucl. Soc., 55, Pg. 583 (1987).

2. Nguyen, T.Q. et al., "Benchmarking of the PHOENIX-P/ANC Advanced Nuclear Design System", Proc. Int. Reactor Physics Conf., Jackson Hole, Wyoming (1988).

3. Beard, C.L. et al., "Operational Impact of Xenon Mode Control", Proc. Int. Topical Meeting on M&C and Reactor Physics, Pittsburgh, PA, USA (1991).

4. Impink, A.J., "Anticipatory Control of Xenon in a Pressurized Water Reactor", U.S. Patent 4,642,213, February 1987.

USE OF THE LR-0 EXPERIMENTAL REACTOR FOR VVER CORE PARAMETERS ESTIMATION

O. HRAZDIL
Nuclear Research Institute,
Řež, Czechoslovakia

Abstract

The outline of recent experimental programs for VVER core parameters estimation is introduced. The versatility of the LR-0 reactor for an experimental study of core parameters is emphasized and new ways in experimental research of LWR cores are outlined.

1. INTRODUCTION

More than eight years have elapsed since the first critical state of the LR-0 reactor in the Nuclear Research Institute at Řež near Prague. Within this period reactor became one of the most important experimental facilities of the Institute, around of which almost all activity concerning the physics of nuclear reactors has been concentrated. The LR-0 reactor was designed for research of neutron physical parameters of active zones of the pressurized water reactors of VVER type. Nuclear power engineering of nearly all East-European countries and Finland was built up on the basis of these light water reactors. In addition, Czechoslovakia for years has played a significant role in constructing nuclear power plants of East-European countries where it delivers key components, e.g. the complete bodies of nuclear reactors. The operation of nuclear power plants with VVER-440 reactors the construction and operation of power plants with VVER-1000 reactors as well as the manufacture of nuclear power instalation components put questions to the research in the field of neutron physics, the solution of which considerably increases nuclear safety and economy.

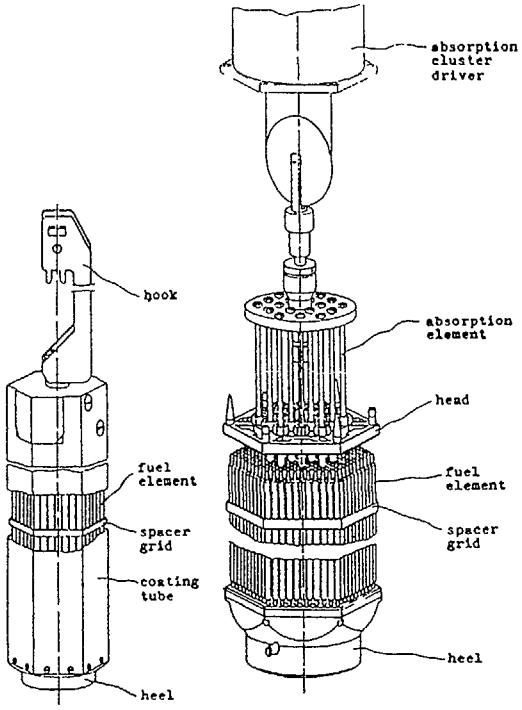

Fig. 1 Fuel assemblies

2. THE LR-0 REACTOR

During more than eight years of operation the LR-0 reactor has been modified to satisfy all experimental and operational demands. The mean features are summarized as follows:

(1) The basic type of fuel assemblies used are the shortened dismountable models of the VVER-1000 and VVER-440 assemblies. All LR-0 assemblies are loaded with fuel elements of one type (Fig. 1).

(2) The fuel enrichment varies from 1.6 to 4.4% of ^{235}U and includes the following nominal values: 1.6, 2.0, 2.4, 3.0, 3.3, 3.6 and 4.4% of ^{235}U.

(3) A small part of fuel elements of each enrichment is dismountable, which enables, e.g., to place activation detectors between fuel pellets or experimental devices into the zirconium coating tube.

(4) Fuel elements containing Gd were prepared for experiments. A set of fuel elements containing a homogeneous di-gadolinium-tri-oxide admixture has the following nominal values: 3605, 3610, 3615, 3620, 4401, 4403, 4420 and 4460, where the first group of two digits gives the fuel enrichment with the ^{235}U isotope and the second one means the weight content of Gd_2O_3 in fuel pelets (e.g. 4460 designates a fuel element with 4.4% enrichment and 6.0 w% of Gd_2O_3).

(5) The main part of the technology equipment is the reactor core (Fig. 2) located on the supporting system in the reactor vessel.
This system consists of

- the standard supporting plate, which enables to set various configurations with fuel assemblies of VVER-1000 type with a pitch of 236 mm (Fig. 3),
- the auxiliary inserted plate, which makes it possible to place 7 fuel assemblies of VVER-440 type with a pitch of 147 mm into the central part of the core, while the standard coatless assemblies of VVER-1000 type are placed in the periphery of the core (Fig. 4),
- the special plate with radial grooves, which enables to change continuously the assembly pitch (Fig. 5).

(6) The H_3BO_3 concentration in the moderator may vary from 0 to 12 g per 1 l H_2O.

(7) The moderator may be heated up to 70°C.

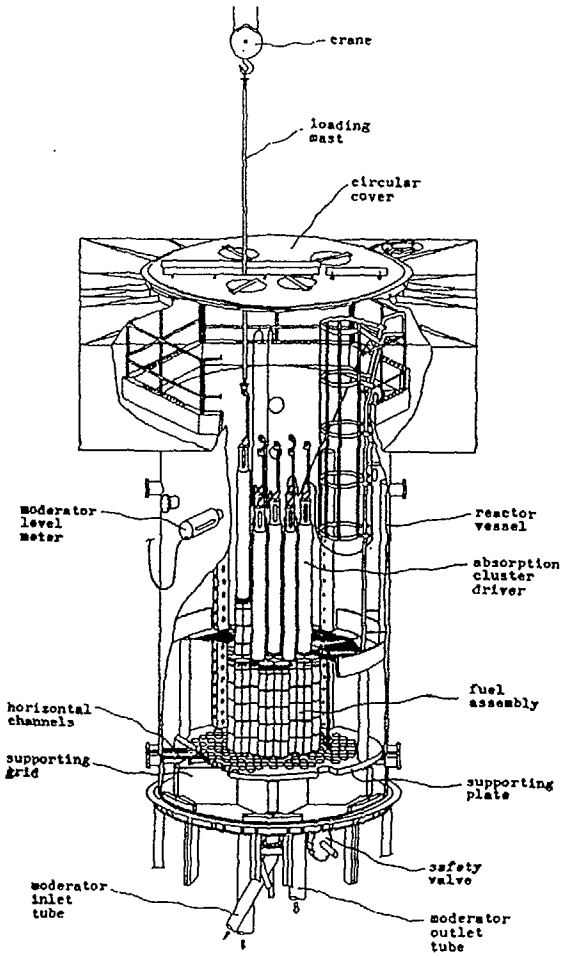

Fig. 2 Reactor vessel and its equipment

(8) The thermal power of the reactor is limited to 5 kW for 1 hour and the thermal neutron flux density in the centre of the reactor core to 10^{13} $m^{-2} . s^{-1}$.

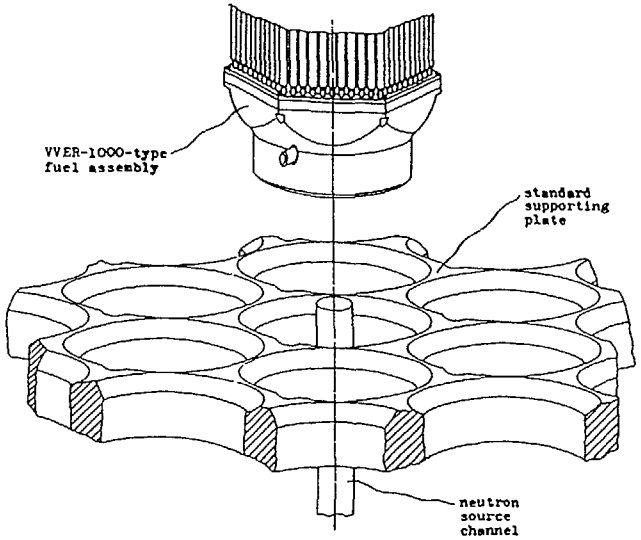

Fig. 3 Standard supporting plate

The reactor equipment is closely connected with its experimental program and is continuously modified and refined to meet requirements of design specialists, suppliers and operators of nuclear power plants.

3. THEORETICAL RESEARCH

An experimental program on the LR-0 reactor involves a number of calculations that are performed to support the design and evaluation of experiments. The elaborated methods and codes create a library and programme equipment, which involve

- generating of multigroup cross.section libraries,
- calculation of microparameters and condensed four-group constants,
- macroscopic calculations,

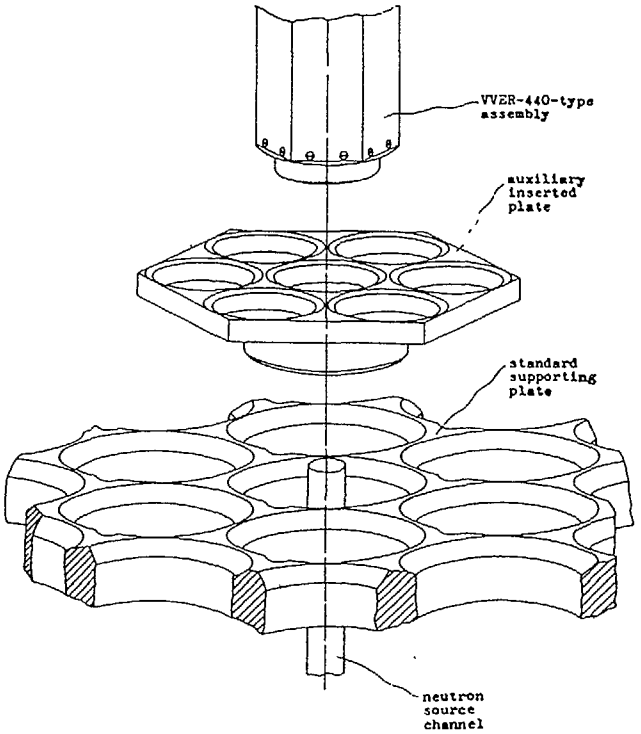

Fig. 4 Auxiliary inserted plate

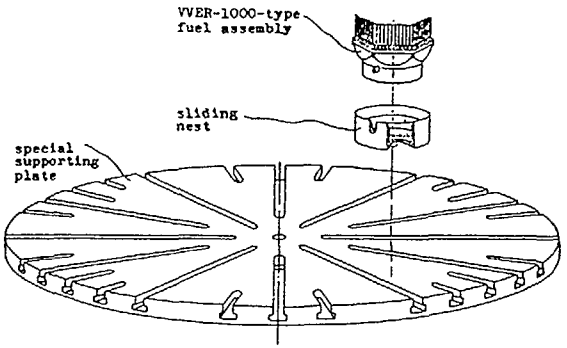

Fig. 5 Special supporting plate with grooves

- Monte-Carlo calculations,
- kinetic calculations,
- special calculations.

Detailed information about the theoretical research on the LR-0 reactor is not a purpose of this paper and a short overview was introduced only to complete an integral research activity on this facility.

4. EXPERIMENTAL RESEARCH

Experimental and theoretical research in physics of VVER-type nuclear reactors in last years has been concentrated on solution of the following problems:

- study of nuclear fuel utilization improvement, especially research of nuclear fuel with burnable poison,
- VVER pressure vessel neutron exposure evaluation in the context with solution of problems concerning the pressure vessel life increasing,
- spent fuel storage investigation,
- experimental research in space kinetics.

A research programme with the nuclear fuel containing gadolinium is aimed at
- experimental verification of the influence of gadolinium-bearing fuel elements on fission sources distribution in a model reactor core,
- verification on an accuracy of computer codes and programme libraries for a description of VVER cores containing fuel elements with burnable poison,
- obtaining a physical basis for safety analyses, with a tendency to ensure a reliable manipulation of nuclear fuel containing a burnable poison in VVER systems.

For VVER pressure vessel neutron exposure evaluation the model experiments have been performed with models of reactor periphery of both type - VVER-440 and VVER-1000 - as well. The precise physical model makes it possible to obtain direct experimental estimation of some quantities for the power reactors, such as fast neutron spectra at "crucial points", which are very important for a pressure vessel radiation damage estimation. The research programme will be closed by elaboration of operational rules for VVER-440 reactor operation with shielding fuel assemblies.

A research programme concerning the nuclear safety aspects of the spent nuclear fuel storage of the VVER-1000 type has been closed recently. This programme has covered a series of experiments aimed at the obtaining of the physical foundation for nuclear safety evidence of nuclear fuel repositories, based on the utilization of hexagonal absorption tubes from the boron steel with a minimum content of natural boron of 0.8 w%. The subcriticality greater then 0.95 ($k < 0.95$) has been proved both experimentally and theoretically, even with fresh fuel of 4.4% enrichment and with pure moderator. The results of this research are realized in a compact spent fuel storage of our own conception, which covers the boron steel production, the boron steel sheets rolling and the production of hexagonal absorbing tubes and storage construction system.

The LR-0 is a versatile facility, where a wide spectrum of experiments with various kinds of light water lattices can be performed. An experimental verification of an effect of asymmetry of rhodium self-powered detector (SPD) could be mentioned as an example of a nonstandard experiment.
From Fig.6 it results that an emitter of the SPD is placed in the fuel assembly asymmetrically with regard to the assembly axis. As the azimutal orientation of a channel with SPD is unknown, a systematical error in the interpretation of the SPD signal arises when such a SPD is placed in the gradient of the neutron flux. Both theoretical and experimental research of this effect were performed and results were in-

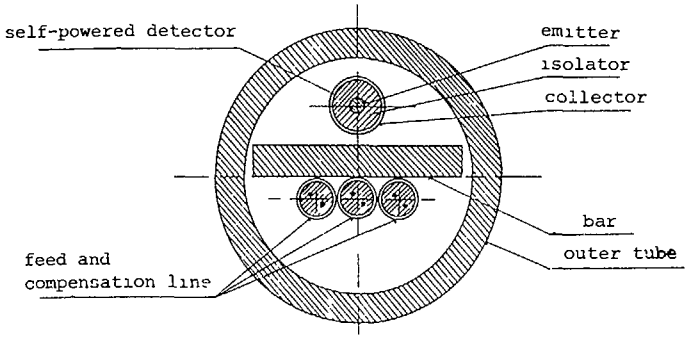

Fig. 6

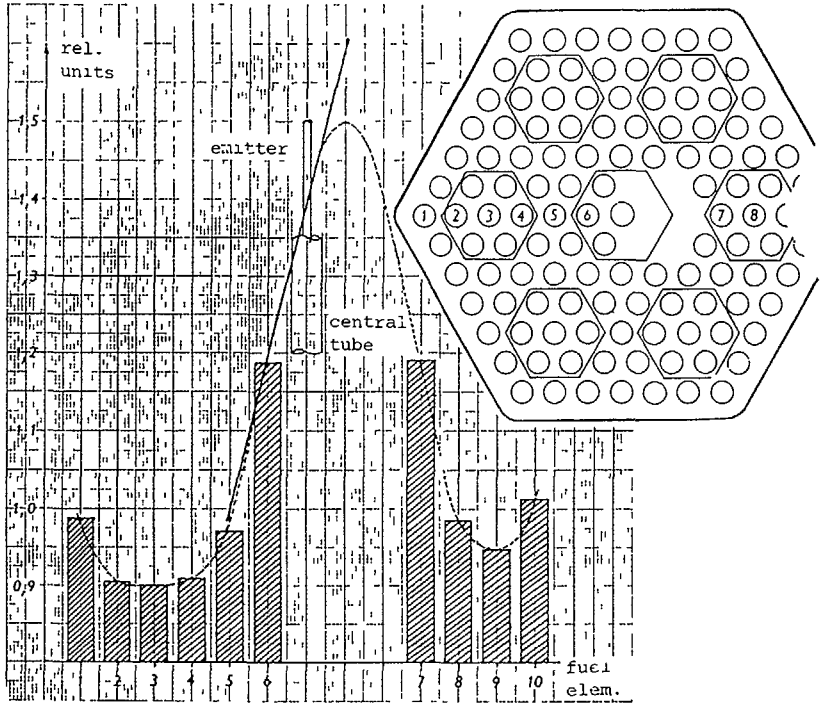

Fig. 7 Experimental and calculated neutron flux density distribution in a fuel assembly with a water gap

volved in the software of the control system HINDUKUSH on the NPP V-2 at Jaslovské Bohunice [1,2].

A brief description of the experimental arrangement:
A gradient of the neutron flux was created in the central fuel assembly by means of a water gap and neutron flux distribution was measured along the main diagonal in the assembly (Fig. 7). An effect of asymmetrical placement of an SPD emitter was estimated by means of the SPD response in two opposite positions - in the maximum and minimum of neutron flux. The orientation of the SPD was changed by remote control without changing the reactor output. Experimental results were compared with calculation and a good agreement was chosen. This result enabled to confirm an analytical expression which was derived for the dependence of an SPD-emitter activation on its eccentricity and on the gradient of the neutron flux (Fig. 8).

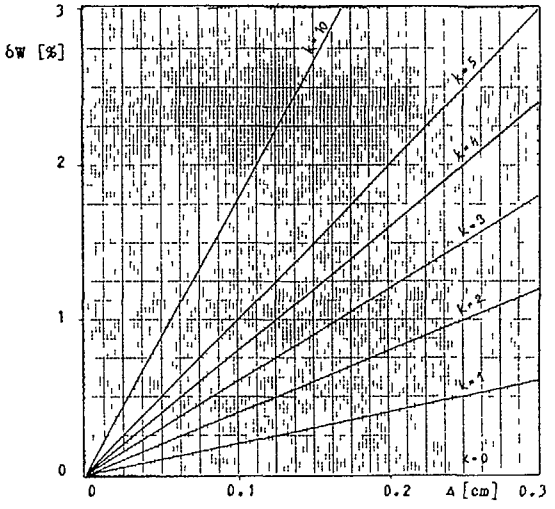

Fig. 8 Dependence of the relative change of SPD response on the SPD eccentricity (Δ) and on the gradient of neutron flux density (k[%])

REFERENCES

[1] O. Hrazdil
Impact of a measuring channel asymmetry on the interpretation of a SPD signal. (In Czech)
UJV 8107 R, 1987

[2] O. Hrazdil, J.V. Ushakov, S.A. Cimbalov
Experiments with a model of the diagnostic fuel assembly. (In Russian)
ÚJV 8304 R,T, 1987

[3] Q. Sochor, R. Starý
The experimental reactor LR-0 after five years' operation.
Nucleon, A special issue, 1988

VVER REACTOR DOSIMETRY AND PRESSURE VESSEL EXPOSURE MONITORING

Č. SVOBODA, B. OŠMERA
Nuclear Research Institute,
Řež, Czechoslovakia

Abstract

The pressure vessel exposure is determined by means of surveillance neutron monitors and by the ex-vessel monitoring. The dosimetry data of ČSFR VVER-440 reactor have been callected in order to reevaluate them using the new IRDF-90 cross section library. The PC experimental data base and the evaluation programmes are described and discussed.

Introduction

The pressure vessel exposure is determined by means of surveillance neutron monitors and by ex-vessel monitoring The surveillance chains are equipment with Nb, Cu and 54Fe detectors (Fe for the 1st fuel cycle only) The acceleration of the specimen (the ratio between fluxes in the its position to the fluxes on the pressure vessel) is about 10 and the last chain is pulled out after 5 fuel cycles

The present standard surveillance evaluation procedure requires the fluence above 0,5 MeV with target accuracy 20 % This accuracy corresponds to the determination of the material characteristics changes with accuracy better than 5 %

The neutron exposure evaluation is based on the following data

- measured activity of the surveillance specimens monitors and ex-vessel monitors

- neutron spectra at critical locations measured in mock-up
- reactor dosimetry cross-section data libraries (DOSCROSS-81, IRDF-90)
- power history of the corresponding power units

The neutron spectra have been obtained as the results of the mock-up experiments carried out by the proton recoil spectrometers in a physical model (mock-up) in the LR-0 experimental reactor

Schema of evaluation procedure

The schema of the evaluation procedure is briefly shown on the Fig 1. The programme BLB24EX evaluates the integral cross sections according to the users options using reactor dosimetry cross section data libraries (DOSCROSS-81 or IRDF-90 respectively) and spectra library in 3 positions (surveillance specimens chain radial position, inner and outer pressure vessel surfaces) User must select the detector reaction, data library, detector position and the energy range

The programme BLB23 evaluates fluxes and fluences (above 0 1, 0 5 and 1 0 MeV respectively) according to the users option by means of the effective cross sections, measured activities and the data file of power history User also select the power station unit and the set of irradiated detectors

The file of the measured activities and the result file of the fluxes and fluences are DBF type ones The structures of this files are shown on the Fig 2

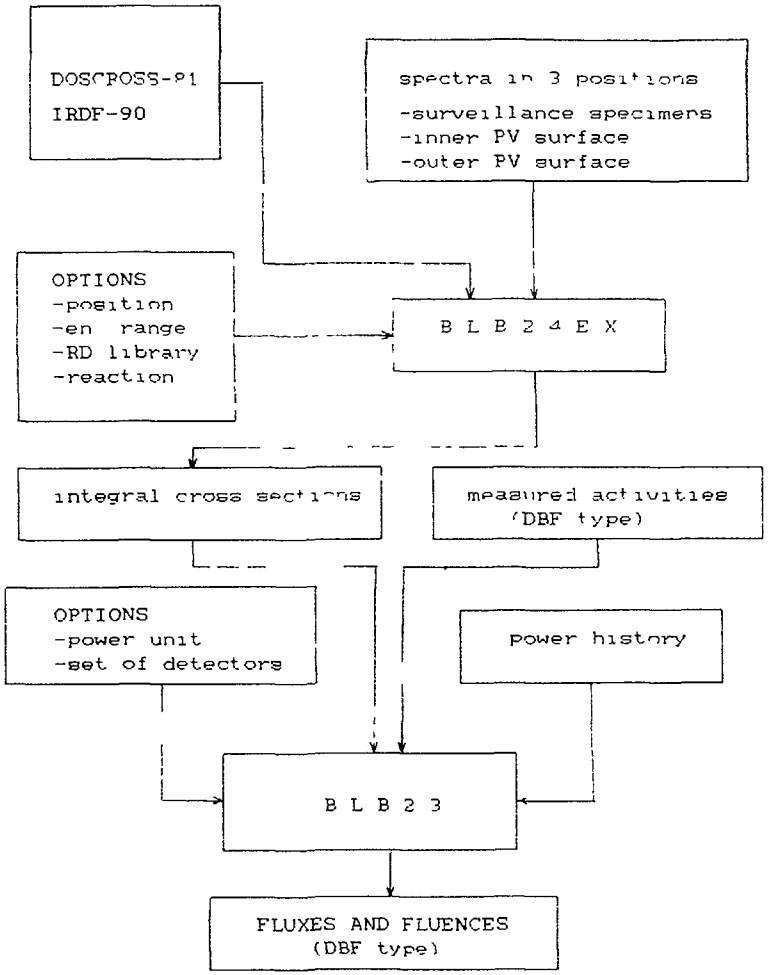

Fig. 1

Conclusions

The error propagation could be based on the experimental neutron spectra uncertainties and the cross section covariance matrices The solving of this problems is in progress

Structure for database: C:\FOX\ZAZ1DU.DBF
Number of data records: 108
Date of last update : 06/17/91

Field	Field Name	Type	Width	Dec
1	RETEZEC	Numeric	4	
2	DATUM	Character	26	
3	MONITOR	Character	7	
4	CAPS	Numeric	4	
5	HMOTA_MG	Numeric	8	5
6	ACT_KBQ	Numeric	9	3
7	F01	Numeric	10	
8	F05	Numeric	10	
9	F1	Numeric	10	
10	FLUENCE01	Numeric	10	
11	FLUENCE05	Numeric	10	
12	FLUENCE1	Numeric	10	
** Total **			115	

Structure for database: C:\FOX\1DUF.DBF
Number of data records: 109
Date of last update : 09/03/91

Field	Field Name	Type	Width	Dec
1	RETEZEC	Character	1	
2	STARTDAY	Date	8	
3	ENDDAY	Date	8	
4	EVALDAY	Date	8	
5	MONITOR	Character	2	
6	CAPS	Character	2	
7	HMOTNOST	Numeric	7	4
8	AKTIVITA	Numeric	8	3
9	FLUENCE	Numeric	7	1
** Total **			52	

Fig. 2

Supposing the mock-up spectra are the best estimation of these quantities it is possible to test the consistency of the measured reactions rates and the corresponding cross section data We have compared the DOSCROSS-81 and IRDF-90 cross sections data libraries The 93Nb(n,n') and 63Cu(n,alpha) dosimeter results for both libraries were compared with the 54Fe(n,p) result (dosimetry standard, identical cross section in both libraries) We have found improvment of the detector Cu consistency for the outer PV wall position (for IRDF-90). Similar conclusion for the surveillance position was obtained, but there are some unbelievable exceptions which could be probably caused by the impurities As concern this detector, there are also some troubles with the integral cross section evaluation because the spectra were measured up to 10 MeV only and the contribution above this energy is not negligible and an extrapolation is needed

The different conclusion should be done for Nb detectors, the DOSCROSS data provide evidently better consistency

Reference

Ošmera,B.,Holman,M Surveillance neutron dosimetry and cavity neutron flux monitoring at Czechoslovak VVER-440 power reactors 7th ASTM-EURATOM Symp on Reactor Dosimetry, Strasbourg, August 1990

PRIMARY EXPERIMENTAL AND CALCULATIONAL STUDY OF THE WWER-1000 CORES OF THE LR-0 REACTOR

J. VANÍČEK
Nuclear Research Institute,
Řež, Czechoslovakia

Abstract

During last years a number of essential experiments were performed on the reactor LR-0 with fuel assemblies of the WWER-1000 type. The critical height of moderator level and the height coefficient of reactivity were always measured as basic integral characteristics of all arrangements. Efficiency of control rods (clusters) made from different absorbing materials and particular distribution of fission rate important especially in the vicinity of all irregularities were experimentally evaluated and theoretically calculated. Some calculations were also carried out to determine the influence of the input data deviation on the criticality of a reactor. The temperature coefficient of reactivity was measured and calculated in the limited range of temperatures.

These experiments implied results which enabled us to appreciate used calculational methods and accuracy of codes for calculations of the WWER type cores.

Introduction

The LR-0 experimental reactor was designed for physical research of reactor cores with WWER reactor type fuel. A multi-purpose design of the technology equipment allows accomplishment of experiments with WWER-1000 or WWER-440 type fuel assemblies in symmetric or asymmetric arrangements with the standard or variable triangular lattice pitch.

The control of a fission chain reaction is provided mainly by changing the moderator level in the reactor vessel and/or inserting clusters of absorbers into the fuel assemblies. Thus "clean" core arrangements, i.e. cores without inserted absorption elements, may be simulated.

The H_3BO_3 concentration in the moderator may be from 0 to 12 g H_3BO_3 per liter H_2O, the moderator may be externally heated up to 70°C. The heat from uranium fission in fuel elements is dissipated into the moderator. The thermal power of the reactor is limited up to 5kW for 1 hour and the thermal neutron density in the centre of the core to $10^{13}m^{-2}s^{-1}$.

Fuel assemblies contain fuel elements arranged in triangular lattice, filled with sintered UO_2 pellets. The height of the fuel filling in the element is 1250 mm, fuel enrichment varies from 1 6 to 4.4% of U235 The hexagonal coatless fuel assembly of the WWER-1000 type used in LR-0

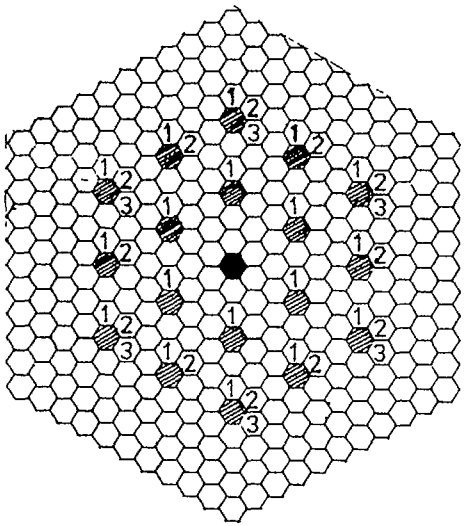

Fig. 1.: Fuel assembly with the distribution of absorption elements of the clusters used.

may be equipped with an absorption cluster of several absorption elements. (Fig 1)

During last years a number of essential experiments were performed on the reactor LR-0 and it is possible to compare their experimental results with the results of our codes with aim to verify the codes and cross section data as well as the results of experiments. In this paper basic critical experiments, measurements and calculations of cores with burnable absorbers, efficiency of control clusters, temperature coefficient of reactivity and some calculations performed to support the evaluation of experiments are described

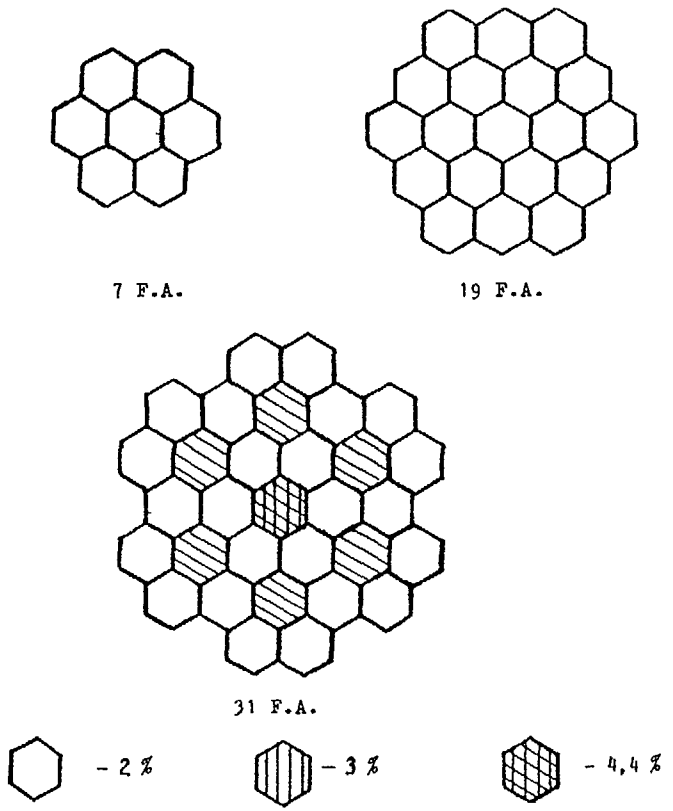

Fig. 2.: Configurations of the LR-0 cores with 7, 19 and 31 fuel assemblies

Other areas of research programme performed on the LR-0 reactor concerning spent nuclear fuel storages subcriticality investigation, space kinetics, experiments for WWER pressure vessel neutron exposure evaluation and experiments with Gd poisoned fuel for WWER reactors are processed separately.

Basic Critical Experiments

Measurements of basic physical parameters of the LR-0 reactor were realized on three fundamental configurations of the core with 7, 19 and 31 fuel assemblies (Fig. 2) at the physical start-up of the reactor. The critical state of a given core arrangement is attained and successive power control is performed by changing the height of moderator level or by inserting clusters of absorbers into the fuel assemblies. A preliminary estimation of a critical height of moderator level, height coefficient of reactivity and knowledge of cluster efficiency are necessary for preparation of all experiments with different reactor core configurations.

The measurements of the critical height of moderator level and of the height coefficients of reactivity were performed by an inverse kinetics method [1]. A special effect caused by interaction of water with the surface of fuel elements in the case of close lattice was recorded and quantitatively evaluated. The level of moderator in close proximity of the fuel elements does not correspond with the moderator level measured with the moderator level meter and the shape (convex or concave) depends on the previous history of a level movement, so that the special operational procedure and evaluation method were used.

Typical results of this measurement are shown in Fig.3, from where it is obvious and was also experimentally checked that there is a region of heights (width of span of about 1.5 mm) at which the reactor can be critical. The actual critical height must lie in this region and depends on the previous history of a moderator level movement.

The next important effect was caused by dry lattice of fuel elements over the moderator level. The reactor "feels" the cluster practically when the lower end of the cluster is about 30 cm above the moderator level. When the lower end of the cluster touches the moderator level, the worth of the cluster is about 5% of the worth of the fully inserted cluster.

The final results of the critical heights (H_{exp}) and the height coefficients of reactivity for three basic configurations are presented in Table 1 together with results of theoretical calculations [2]. For the calculations of these quantities the code Břetislav [3] (solution of diffusion equations by finite-difference method with one mesh-point per elementary cell) was used, the irregularities at the boundaries of fuel assemblies being taken into account. Four-group diffusion constants for all different elementary cells were prepared by the programme Microbe [4].

At all configurations the critical height (H_{calc}) of the moderator level was calculated including the reflector savings and the influence of a dry lattice (ΔH_{calc})

$$H_{calc} = H_{exp} + \Delta H_{calc} .$$

With the help of a perturbation theory the height coefficient of reactivity $\partial\rho / \partial H$ was found

The difference of the calculated critical height H_{calc} and the measured height H_{exp} increases with decreasing a critical height. To make the thing clear it will be necessary to find extrapolation distances experimentally for all cores and to involve spacing grids material in calcula-

Tab. 1.. Critical heights and height coefficients of reactivity

Core No of F.A.	H_{exp} [cm]	H_{calc} [cm]	ΔH_{calc} [cm]	$\partial\rho/\partial H$ experim. [pcm/cm]	$\partial\rho/\partial H$ calcul. [pcm/cm]	Relat. deviation of calc. and exp. $\partial\rho/\partial H$ [%]
7	61.76	72.26	10.50	169.1±8	183.8	+ 7.9
19	34.36	49.27	14.91	532.7±6	581.3	+ 8.4
31	23.81	41.00	17.19	968.5±16	967.3	- 0.1

Tab. 2.: Influence of a fully inserted cluster into the central fuel assembly

Core No of F.A.	k_{eff}	H_{calc} estimated [cm]	Experim. worth of cluster [pcm]	Calc. worth of cluster [pcm]	Deviation of calc. and exper. worth of cluster [%]
7	0.9478	143.3	5122±232	5063	- 1.2
19	0.9790	53.3	1983±53	2085	+ 5.1
31	0.9805	43.2	1676±63	1801	+ 7.4

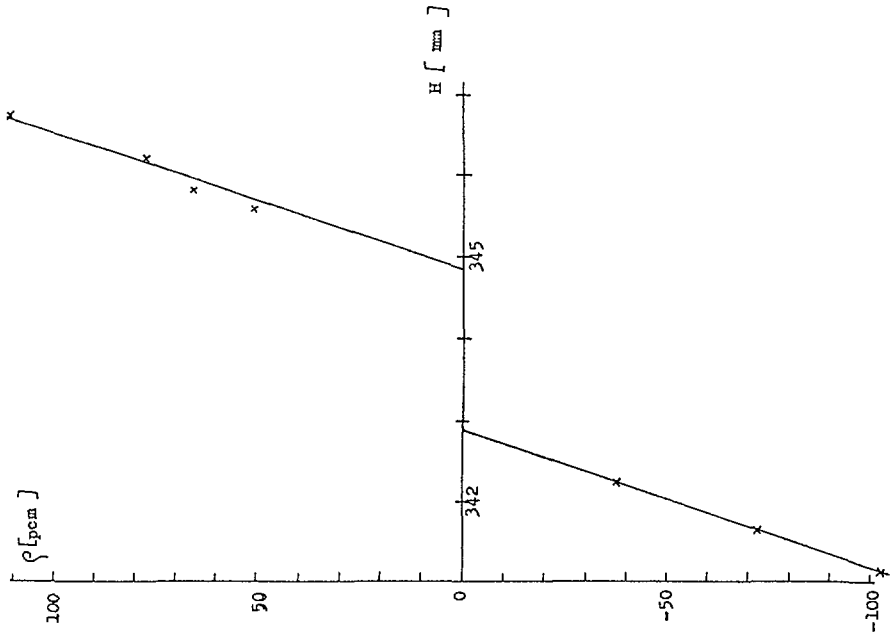

Fig. 3.: The measurement of the height coefficient of reactivity

tions. Agreement in experimental and calculated values of the height coefficient of reactivity is good.

Calculations of the effect of a fully inserted cluster into the central fuel assembly on core criticality were also performed for each core. The results (k_{eff} for core with inserted central cluster, an estimation of critical height H_{calc} (incl. ΔH_{calc}), and the worth of cluster) are shown in Tab. 2 together with the experimental worth of clusters measured by an inverse kinetics method.

Efficiency of Clusters Containing Burnable Absorbers

For safe and optimal control of the WWER reactors the experiments with control clusters composed of different number of elements containing burnable absorber CrB_2 and with standard cluster composed of 18 absorption elements containing B_4C were performed on the LR-0 reactor. Together with experimental finding of basic neutron - physical characteristics of cores (critical height of the moderator level, efficiency of clusters, distribution of power in the core, height coefficient of reactivity) the corresponding theoretical calculations were carried out.

The experiments were performed on the core in configuration with 7 fuel assemblies, the fuel enrichment being 2% of U235. Standard cluster (SC) or cluster with burnable absorbers CrB_2 (BAC) was inserted into the central or peripheral fuel assembly and its worth was measured by the inverse kinetics method and by the method using the critical height measurement with the fully inserted cluster [5]. Cluster BAC was composed from 18, 12 or 6 burnable elements. The results are shown in Tab. 3.

For the core without clusters the height coefficient of reactivity has been measured $\partial\rho/\partial H$ = 161.2 ± 1.6 pcm/cm.

Macroscopic calculations of criticality, neutron flux distribution and power density were carried out by programme Břetislav, four-group diffusion constants were prepared again with programme Microbe. The influence of an axial reflector and of a dry lattice was taken into account by increasing the height of the core by the reflector savings ΔH = 14 cm.

In these calculations the critical height of the core without cluster was found at first, then the decreasing of k_{eff} caused by inserting the cluster into the core with that moderator level was calculated and at last the new critical height of the core with inserted cluster was determined. The efficiency of the cluster was calculated as difference of reactivities or difference of critical heights [6,7]. The results of calculations are shown in Table 4. Calculated height coefficient of reactivity of the core without clusters $\partial\rho/\partial H$ = 158.47 pcm/cm agrees well with measured one.

Good results were also obtained from criticality calculations of cores with clusters where measured critical heights were taken as input data.(Table 5).

Particular distribution of fission rate, which is important especially in the vicinity of all irregularities was measured by means of the gamma activity of the fission products of uranium in irradiated fuel elements. These measurements were performed on multichannel analyser with HPGe detector. The maximum relative difference of experimental and calculational values of power density did not exceed 10%.

The use of the code which is based on diffusion theory is problematic with respect to the considerable heterogenous structure of investigated cores. But for practical calculations we are still limited to diffusion codes. Even those are time - consuming because of the number of necessary net points (e.g. 3560 net points for case with peripheral cluster).

Tab. 3.: Experimental critical heights and the worth of the clusters
ρ_1 ... the worth of cluster measured by an inverse kinetics method
ρ_2 ... the worth of cluster determined by the change of the critical height caused by an insertion of cluster

Type of cluster	Position	H_{crit}[cm] without cluster	t[°C]	H_{crit}[cm] cluster inserted	ρ_1[pcm] worth of the cluster	ρ_2[pcm] worth of the cluster	worth of the cluster in Δ H [cm]
SC	central	63.1	20.5	-	5022 ± 130	-	-
BAC-18	central	63.2	21.1	119.444	3395 ± 100	3822 ± 40	56.24
BAC-12	central	62.9	20.6	92.595	2520 ± 100	2980 ± 30	29.70
BAC-6	central	62.898	20.6	74.382	1582 ± 60	1577 ± 17	11.48
SC	peripheral	62.925	20.5	74.605	1602 ± 50	1599 ± 16	11.68
BAC-18	peripheral	62.888	20.5	71.081	1117 ± 42	1147 ± 12	8.19
BAC-12	peripheral	62.942	20.5	69.092	880 ± 25	899 ± 10	6.15
BAC-6	peripheral	62.938	20.6	66.408	511 ± 15	564 ± 7	3.47

Tab. 4.: Calculated critical heights and the worth of clusters

Type of cluster	Position	H_{crit}[cm] without cluster	k_{eff} for H = 67.88 cm cluster inserted	H_{crit}[cm] cluster inserted	ρ [pcm] worth of the cluster	worth of the cluster in Δ H [cm]
SC	central	67.88	0.9481	~ 309	5187	241
BAC-18	central	67.88	0.9664	119.66	3359	51.78
BAC-12	central	67.88	0.9758	96.34	2419	28.46
BAC-6	central	67.88	0.9870	79.96	1296	12.08
SC	peripheral	67.88	0.9858	81.43	1441	13.55
BAC-18	peripheral	67.88	0.9902	76.57	994	8.69
BAC-12	peripheral	67.88	0.9925	74.26	756	6.38
BAC-6	peripheral	67.88	0.9958	71.32	426	3.44

Tab. 5.: Calculated k_{eff} of configurations with cluster in central fuel assembly for measured critical heights of cores

Configuration	without cluster	BAC-18	BAC-12	BAC-6
H_{exp}[cm]	63	119.444	92.595	74.382
k_{eff}	0.9930	0.9999	0.9978	0.9946

Sensibility Analysis

In some experiments which were repeated with different fuel assemblies but with the same number of fuel assemblies of the same nominal enrichment of uranium (i e. with the same type of fuel elements) in the core, some deviations in critical height were found. To reveal the reason a number of experiments and calculations were performed to verify the influence of technological tolerances and input data deviations on neutron-physical properties of fuel assemblies.

In these experiments always one central fuel assembly out of the collection of 18 assemblies investigated was successively inserted into the ring-shaped core compound of 6 assemblies with an enrichment of 2% and the influence on the core reactivity was studied

Experimental dependence of the critical height on the fuel enrichment was formed by using data from the fuel certificate. Another experiment was performed where certain number of fuel elements with 2% enrichment in the central assembly were replaced by fuel elements with 3% enrichment and nonstandard mean enrichment in the central assembly was reached.

To find out the influence of the enrichment deviation by theoretical way, the possibility of calculations with non-standard enriched fuel, for which diffusion constants were not calculated in advance, was included into the programme Břetislav.

Obtained dependence of the critical height and of reactivity on fuel enrichment showed, that the mean reason for difference in nuclear qualities of the fuel assemblies investigated is their difference in the U235 content. However, some fuel assemblies showed another deviation in reactivity than would correspond to the fuel certificate data and further investigations had to be done.

To separate the influence of temperature the temperature coefficient of reactivity was calculated. The influence of a water gap between fuel assemblies, the influence of the cladding tube diameter deviation and that of fuel density were also contemplated. This sensibility analysis is very important for better understanding of technological tolerances influence on neutron-physical properties of fuel assemblies.

The Temperature Coefficient of Reactivity

The influence of possible unequal temperature of the core on the reactivity when experiments were performed successively was determined in the range of temperatures from 18 to 32 °C both calculationally and experimentally. Further reason was safe operation of a reactor with inserted absorption elements, it was necessary to verify that the temperature coefficient is not positive.

Calculations were made for temperatures 20, 25 and 30°C for two arrangements of the core with seven fuel assemblies. First core (C1) without absorbers had critical height 61.23 cm, second core (C2) contained in each of 6 peripheral fuel assemblies 13 inserted absorber rods so that the critical height was increased up to 103.83 cm [8]. The fuel enrichment was 2% of U235 in both cores.

Calculated values of the temperature coefficient of reactivity are presented in Table 6 from where it is possible to see that the temperature coefficient of the LR-0 core is in the interval of temperatures considered negative and that it remains negative for core with inserted absorbers as well [9].

These theoretical results were very well confirmed experimentally [8]. For core C2 the mean temperature coefficient in the temperature interval 18 - 28 °C has been measured $\partial\rho/\partial t$ = - 12.65 ± 0.67 pcm/ °C, for the core C1 experiment was not performed but for the core where the central fuel assembly in core C1 was replaced by fuel assembly with 4.4% enrichment has been measured in interval of temperatures 18 - 32 °C $\partial\rho/\partial t$ = - 11.53 ± 0.42 pcm/°C. These values are in good agreement with calculated ones.

Conclusion

In this report several experiments performed on the LR-0 reactor were described together with brief mention of calculational methods used for theoretical determination of basic characteristics of the core. Calculational and experimental results were always compared which enabled us to appreciate used calculational methods and cross section data,

Tab. 6.: Temperature coefficient of reactivity in pcm/°C

Core	Temperature interval [°C]		
	20 - 25	25 - 30	20 - 30
C1	- 10.2	- 12	- 11.1
C2	- 12.5	- 14.3	- 13.4

accuracy of codes for calculations of the WWER type cores and credibility of experimental results as well

The results of comparison drew our attention to what is necessary to calculate with more precision, what is possible to neglect and on the contrary what requires to be taken into account This information was always included in further calculations to improve their accuracy

References

1 Rypar V., Hudec F., Svoboda Č The Results of the Basic Experiments on the LR-0 Reactor Report UJV 6885-R, Řež 1984, (in Czech)

2 Vaníček J . Calculations of Criticality and Neutron Flux Distribution of Selected LR-0 Cores for Reactor Start-up and Design of Experiments In Results of Research on WWER-1000 NPPs, ČSVTS ZES, k p Škoda Plzeň, Plzeň 1984, (in Czech)

3 Lelek V. Finite-Difference Code Břetislav for Calculation of a Reactor in Hexagonal Geometry Report UJV 7771-R,A, Řež 1986, (in Russian)

4. Zaleský K.. Programming Handbook for Microbe-02 Code to Calculate Local Burn-up Report ÚJV 6880-R,A, Řež 1984, (in Czech)

5. Svoboda Č., Hudec F.. Experiments on the Core Containing Absorption Elements of the WWER-1000 Type. Report ÚJV 9221-R,T, Řež 1990, (in Czech)

6. Vaníček J., Vrba L. Macroscopic Calculations of the Reactor LR-0 Cores with Burnable Absorbers Report ÚJV 8870-R, Řež 1989, (in Czech)

7 Vaníček J. et al. A Study of Neutron-Physical Characteristics of the WWER-Type Cores with Absorbers Report ÚJV 9159-R,A, Řež 1990, (in Russian)

8 Hudec F et al · An Experimental Verification of Physical Identity of WWER-1000 Fuel Assemblies on the Reactor LR-0 Report ÚJV 8879-R,T, Řež, 1989, (in Russian)

9. Vaníček J. The Temperature Criticality Coefficient of the Reactor LR-0 Report UJV 8867-R, Řež 1989, (in Czech)

COMO: A CORE MODEL FOR PARAMETRIC FUEL CYCLE COST EVALUATION

H MOLDASCHL
Siemens AG/Unternehmensbereich KWU,
Erlangen, Federal Republic of Germany

Abstract

Many of the technical and economic features of a nuclear plant are cross coupled and partially nonlinear Thus, when calculating energy costs the complete set of all influences should be considered While complex computer programs can improve precision for design, they do not necessarily foster understanding of fundamental interrelations

Therefore a rather simple plant model based on existing results and experiences is under preparation, which considers all important design parameters and process variables

Since fuel expenses are an important component of total nuclear power costs, the first module of the above mentioned code deals with the core and the fuel cycle A set of examples is given

1 Problem description

Fuel expenses are an important component of nuclear power costs In fact, since costs can be reduced by improving both fuel cycle technology and fuel design during the lifetime of a plant, the analysis of fuel cost is of continuing interest to the electric utility, whereas fixed charges of the plant do not change after the plant has been built The primary objectives have to be to identifiy the principal cost components and to examine how they are affected by changes in the reactor design

The technical and economic features of a nuclear power plant are defined by a lot of technical parameters and system variables Many of them are cross- coupled, and there are several nonlinear parameters among them Therefore the analysis of the fuel cycle expenses is complicated, however, since a number of operations are involved and economic factors are sensitive to burnup as well as to numerous financial and process variables

The energy cost component attributable to the fuel can be determined in principle by sophisticated computer programs, which include the fine structure of present worth and other second order effects But as in so many other fields of endeavour, complex computer programs sometimes combersome and slow are normally used to carry out state of the art design calculations While this improves precision, it does not necessarily foster understanding and ability to integrate it into optimization procedure

Thus there is a chance as well as the necessity for simpler models describing nuclear power reactor behaviour in a very fast way by the aid of personal computers or work stations Those methods are very useful for illustrating the principles involved and the influence of changes in design parameters and at least can also be used within optimization procedures based e g on the method of steepest descent or on a trial and error strategy

2 Core Model

At Siemens KWU there is a plant model under development (Fig 1), consisting of several modules which can describe all important systems and processes, influencing economy The first module of them is the core module which will be described herein

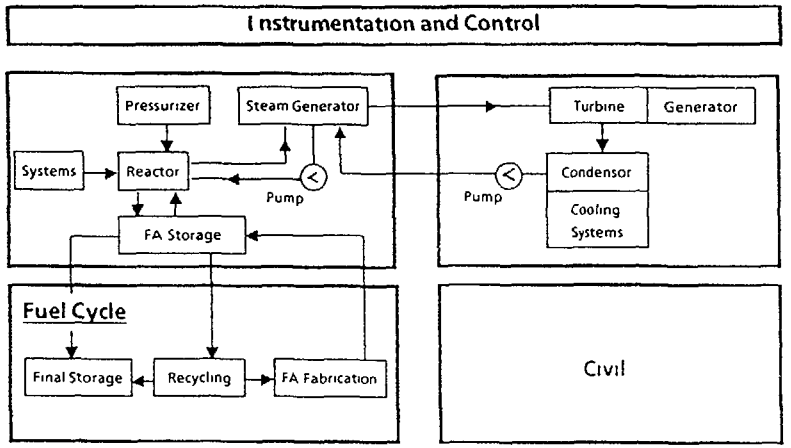

Fig 1: COPAS: Principle schedule

During the last decades of reactor design and operation a large amount of knowledge has been collected as an available data base Those date stam from many design calculations, formerly performed with very sophisticated tools We fitted them while we employed our knowledge about reactor physics By that we can calculate all parameters which mainly influence fuel cycle costs, e g batch burnup, reload enrichment, fuel cycle length and load factor under boundary conditions, for example given by waterside corrosion or RPV fluence

2.1 Input table

All parameters and process variables which are necessary to perform quantitative relevant results are taken into account The input table contains

	Fuel assembly (FA) data	active core height, FA type, number of rod positions, number of guide tubes, pitch, rod outer diameter, thickness of the cladding, fuel density etc
-	Core data	number of FA or maximum outer radius of the core, position of control assemblies (CA)
	RPV data	thickness of the shroud, size of the core barrel size of the RPV
	Operational data	thermal and electric reactor power, load factor, operation mode of the reactor (U or Pu, with or without reprocessing), fuel shuffling characteristing reload burnup/cycle length/batch size
	Economic data	plant investment, natural uranium FA fabrication, reprocessing, waste disposal

2.2 Output table

The output table contains the following variables and parameters of the core

-	Geometry, masses	number of FA if maximum radius of the core is given, moderation ratio with and without CA, FA width over flats, mass of heavy metal in the FA
-	Average thermodynamic values	linear heat rate, heat flux, rating
	Neutron physics	neutron fluence at the RPV, reload burnup/cycle length/batch size, fissile mass recovery rate, reload enrichment, waterside corrosion oxide layer
	Fissile mass balance	inventory, mass flow
	Fuel cycle and energy cost	

3 Description of important modules

3.1 Geometry, average thermodynamic values

A module calculates the maximum number and pattern of fuel assemblies from the maximum radial distance R_{max} of the outermost FA edge in the core given (Fig 2) and the most common thermodynamic values, like the average linear heat rate, the heat flux and the fissile material rating

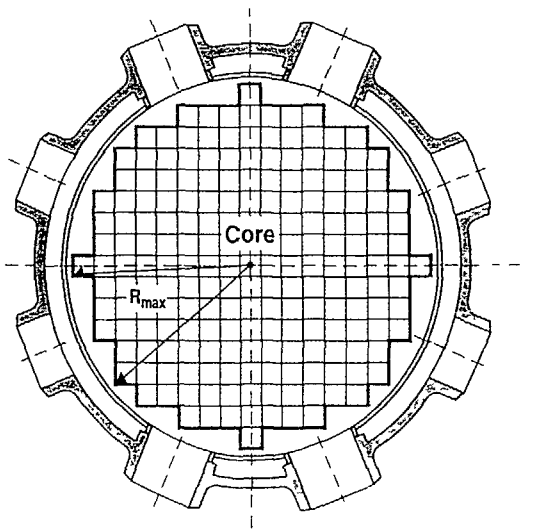

Fig 2 Determination of the FA Pattern

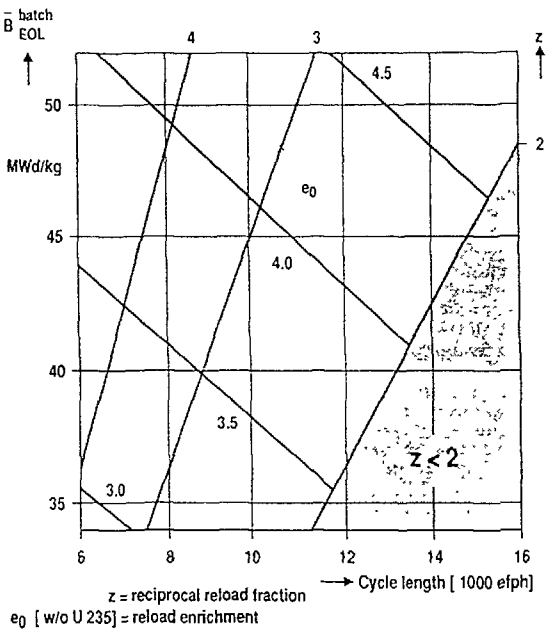

Fig. 3: Average Discharge Burnup vs. Cycle Length for the Equilibrium Cycle of a 1300 MWe PWR.

3.2 Cycle length, reload burnup, enrichment, batch size

The dependence between cylce length, reload burnup, enrichment and batch size is shown in Fig. 3 for a 3765 MWth plant with full Zirconium FA

Those data were condensed by a 2D interpolation The error of the interpolation is < 1.5 %

3.3 Waterside clad corrosion

3.3.1 Basis polynome

The waterside corrosion process of the cladding depends - among other rather small influences - on the residence time, the burnup history, the power peaking factor, the heat conductance in the cladding and the temperature of the moderator

The dependence of the corrosion process on the residence time and the radial power peaking factor is shown in Fig. 4 The accuracy of the 2D interpolation is approx $\pm$ 4 µm for the corrosion layer thickness.

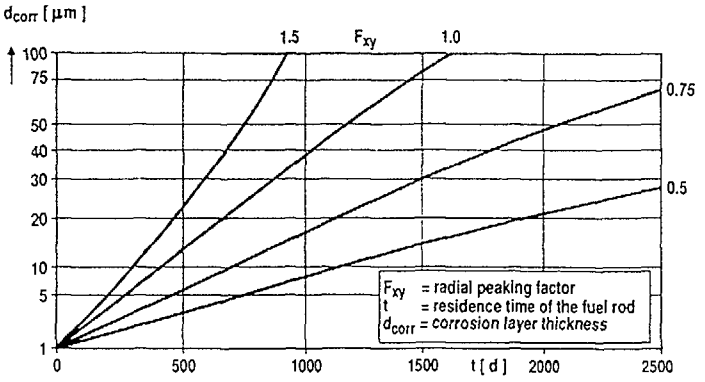

Fig. 4: Oxyde Layer Nomogram

3.3.2 Temperature correction

The correction of the corrosion layer thickness d_{corr} to the given temperature, if it is different from the reference temperature, is performed by the Arrhenius equation.

$$(\partial/\partial t)\ d_{corr} = a_1\ e^{a_2 (T_{clad} + q''/\lambda\ d_{corr})}$$

The exact solution of this equation can be easily given :

$$d_{corr} = -\frac{1}{a_2} \ln (1 - a_2\beta_1 t)$$

$$a_1 = a_2 T_{clad}$$

$$a_2 = a_2 \frac{q''}{\lambda}$$

$$\beta_1 = a_1 e^{-a_1}$$

T_{clad} - cladding outside temperature
q'' - heat flux
t - irradiation time
λ - heat transfer coefficient

3.3.3 Optimization of the fuel power history

Since waterside corrosion can restrict the reload burnup from the technical point of view, one may be interested in an optimization procedure to minimize corrosion layer thickness d_{corr} Among other important parameters which cannot be influenced, the "power history" of the FA, that means F_{xy} (t) (F_{xy} - power peaking factor) is one of the important parameters to reduce d_{corr} , i e. by an adequate fuel shuffling scheme

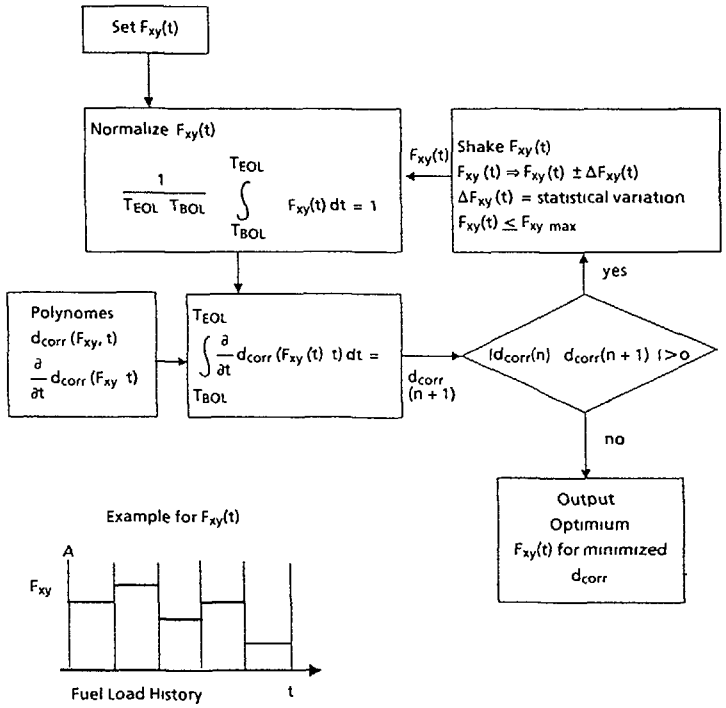

F_{xy} power peaking factor

Fig 5 **Minimization Procedure for the Oxide Layer Thickness by Optimizing the Fuel Assembly Load History**

Since the problem is of the functional kind and the basic corrosion behaviour as well as the Arrhenius equation for the temperature correction are highly nonlinear, we developed a stochastic optimization procedure to do the job we called it "Shake procedure", since the basic idea is to shake the F_{xy} function, which is to be optimized, by a stochastic variation around the actually best solution, as long as the functional value, i e the corrosion layer thickness d_{corr} decreases (Fig 5)

$$\int_{T_A}^{T_E} \left(\frac{\partial}{\partial t}\right) d_{corr}(F_{xy}(t))\,dt = d_{corr} = \underset{F_{xy}(t)}{\text{Min!}}$$

Two examples for such an optimization procedure are given in Figs 6a and 6b, for two different upper limits for $F_{xy}(t)$

4 Calculation of the RPV fluence

The dependency of the RPV fluence from the thickness of the shroud, the water gaps between shroud and core barrel and the core barrel itself (see Fig 7) can be calculated using the results of existing Monte Carlo calculations for several geometries The following approximative equation for the shielding effect was established

$$\frac{\Phi_{RPV}}{\Phi_{Core}} \simeq \exp\left(\sum_{i=1}^{4} b_i \Delta x_i\right) \qquad b_i \text{ constants}$$

The error of the estimate compared to a precise calculation is smaller than 10 %

5 Results

Fig 8 shows for example the fuel cycle cost (FCC) for 5 cases (reference case and 4 variations) as a function of the parameters

core height
number of fuel assemblies
fuel assembly type

One should mind that changes of one of these parameters cause changes of several others, as it is shown in the table

Comments to the results (referred to the reference case)

Variation 1 — Reduction of the core height

The linear heat rate and the heat flux increase, as a consequence also the corrosion rate and the RPV fluence do, the reload enrichment requested to gain the given cycle lenght is higher than in the reference case, also is the reload burnup, despite the fact that due to the higher enrichment effort the specific fuel cost increase, the fuel cycle cost decrease since burnup is enlarged and fissile mass inventory is smaller

Variation 2 — Enlargment of the FA cross section, FA number reduced

Only the RPV fluence will be increased markedly due to the more protruding core

Variation 3 — Smaller number of FA

This case is similar to variation 1, but the FCC and the RPV fluence are markedly reduced, unfortunately at the expense of waterside corrosion layer thickness

Variation 4 — Less FA with the same FA cross section and reduced core height

Compared to variation 3 the FCC are reduced at the expense of clad corrosion as it was for variation 3

SHAKE Procedure for Fuel Sharing Optimization
SIEMENS KWU V231 (C) H. Moldaschl 07.91

JS - iteration number
Fxy - power peaking factor
SP - kind of shuffling [1 out-in, 0 in-out]
SS - corrosion layer thickness
Cycle Number = 5
Residence times TA - in, TE - out [fpd]

JS	Fxy						SP	SS[µm]
MAX	1.00,	1.20,	1.30,	1.20,	1.20,	0.00,		
TA	0	250	500	750	1,000	0		
TE	250	500	750	1,000	1,250	0		
1	0.81,	1.01,	1.09,	1.04,	1.06,	0.00,	0.68,	75.21
4	0.87,	0.97,	1.06,	1.04,	1.07,	0.00,	0.66,	74.34
5	0.93,	1.02,	1.06,	1.00,	0.99,	0.00,	0.54,	64.41
6	0.98,	1.03,	1.04,	0.90,	1.06,	0.00,	0.50,	63.45
7	0.98,	1.04,	1.09,	0.92,	0.98,	0.00,	0.46,	59.84
11	0.98,	1.04,	1.16,	0.88,	0.94,	0.00,	0.42,	58.74
12	1.00,	1.04,	1.17,	0.93,	0.86,	0.00,	0.37,	56.47
16	0.97,	1.09,	1.16,	0.91,	0.87,	0.00,	0.37,	56.22
20	0.99,	1.09,	1.15,	0.89,	0.87,	0.00,	0.35,	54.62
21	0.99,	1.11,	1.14,	0.89,	0.87,	0.00,	0.34,	53.97
22	0.99,	1.14,	1.13,	0.87,	0.87,	0.00,	0.33,	53.28
26	1.00,	1.13,	1.12,	0.87,	0.88,	0.00,	0.33,	53.17
29	1.00,	1.13,	1.12,	0.88,	0.87,	0.00,	0.33,	53.04
31	0.99,	1.15,	1.11,	0.88,	0.87,	0.00,	0.33,	52.78
34	1.00,	1.14,	1.10,	0.88,	0.88,	0.00,	0.33,	52.70
41	1.00,	1.15,	1.11,	0.87,	0.87,	0.00,	0.32,	52.50
47	1.00,	1.16,	1.11,	0.87,	0.87,	0.00,	0.32,	52.24
51	1.00,	1.16,	1.10,	0.87,	0.87,	0.00,	0.32,	52.21
56	1.00,	1.17,	1.11,	0.86,	0.86,	0.00,	0.31,	52.12
61	1.00,	1.17,	1.12,	0.86,	0.86,	0.00,	0.30,	51.88
70	1.00,	1.17,	1.11,	0.86,	0.86,	0.00,	0.30,	51.86
75	1.00,	1.18,	1.11,	0.86,	0.85,	0.00,	0.30,	51.81
76	1.00,	1.17,	1.11,	0.87,	0.85,	0.00,	0.30,	51.74
80	1.00,	1.17,	1.10,	0.87,	0.86,	0.00,	0.30,	51.61
85	1.00,	1.18,	1.10,	0.87,	0.86,	0.00,	0.30,	51.54
92	1.00,	1.18,	1.10,	0.87,	0.85,	0.00,	0.30,	51.27
105	1.00,	1.19,	1.10,	0.86,	0.85,	0.00,	0.29,	51.17
108	1.00,	1.20,	1.10,	0.86,	0.84,	0.00,	0.29,	51.10
123	1.00,	1.19,	1.11,	0.86,	0.84,	0.00,	0.28,	51.02
140	1.00,	1.20,	1.10,	0.86,	0.84,	0.00,	0.28,	50.92
141	1.00,	1.20,	1.10,	0.86,	0.85,	0.00,	0.28,	50.89
267	1.00,	1.20,	1.10,	0.86,	0.84,	0.00,	0.28,	50.84
274	1.00,	1.20,	1.10,	0.86,	0.84,	0.00,	0.28,	50.84
303	1.00,	1.20,	1.10,	0.86,	0.84,	0.00,	0.28,	50.79
485	1.00,	1.20,	1.10,	0.87,	0.84,	0.00,	0.28,	50.77
558	1.00,	1.20,	1.09,	0.87,	0.84,	0.00,	0.28,	50.76
633	1.00,	1.20,	1.09,	0.87,	0.84,	0.00,	0.28,	50.73
766	1.00,	1.20,	1.09,	0.87,	0.84,	0.00,	0.29,	50.68

Fig. 6a: Optimization of a Fuel Shuffling Scheme by SHAKE

SHAKE Procedure for Fuel Sharing Optimization
SIEMENS KWU V231 (C) H. Moldaschl 07.91

JS - iteration number
Fxy - power peaking factor
SP - kind of shuffling [1 out-in, 0 in-out]
SS - corrosion layer thickness
Cycle Number = 5
Residence times TA - in, TE - out [fpd]

JS	Fxy						SP	SS[µm]
MAX	0.90,	1.20,	1.30,	0.90,	1.20,	0.00,		
TA	0	250	500	750	1,000	0		
TE	250	500	750	1,000	1,250	0		
2	0.88,	1.03,	1.01,	0.89,	1.19,	0.00,	0.66,	79.99
11	0.88,	1.03,	1.10,	0.85,	1.14,	0.00,	0.61,	74.86
21	0.88,	1.10,	1.05,	0.83,	1.13,	0.00,	0.58,	72.51
22	0.88,	1.19,	1.03,	0.76,	1.14,	0.00,	0.53,	72.04
23	0.86,	1.18,	1.04,	0.79,	1.12,	0.00,	0.54,	70.67
24	0.84,	1.18,	1.08,	0.81,	1.10,	0.00,	0.55,	69.84
29	0.84,	1.19,	1.09,	0.82,	1.06,	0.00,	0.53,	66.79
30	0.86,	1.17,	1.13,	0.82,	1.02,	0.00,	0.49,	63.80
32	0.86,	1.17,	1.14,	0.82,	1.00,	0.00,	0.48,	63.40
33	0.87,	1.15,	1.13,	0.85,	1.00,	0.00,	0.49,	62.93
37	0.85,	1.17,	1.14,	0.87,	0.97,	0.00,	0.48,	61.82
41	0.85,	1.20,	1.16,	0.83,	0.95,	0.00,	0.44,	60.80
49	0.89,	1.20,	1.17,	0.81,	0.93,	0.00,	0.40,	58.97
58	0.89,	1.19,	1.15,	0.83,	0.94,	0.00,	0.41,	58.89
61	0.89,	1.20,	1.16,	0.83,	0.93,	0.00,	0.40,	58.55
63	0.90,	1.19,	1.15,	0.83,	0.93,	0.00,	0.40,	58.24
70	0.89,	1.20,	1.15,	0.83,	0.93,	0.00,	0.40,	58.11
76	0.90,	1.20,	1.14,	0.84,	0.93,	0.00,	0.40,	58.05
80	0.90,	1.20,	1.13,	0.84,	0.93,	0.00,	0.40,	58.02
107	0.90,	1.19,	1.14,	0.84,	0.93,	0.00,	0.40,	57.99
116	0.90,	1.20,	1.14,	0.84,	0.93,	0.00,	0.40,	57.97
144	0.90,	1.20,	1.14,	0.84,	0.92,	0.00,	0.40,	57.80
154	0.90,	1.20,	1.14,	0.84,	0.92,	0.00,	0.40,	57.75
157	0.90,	1.20,	1.14,	0.84,	0.92,	0.00,	0.40,	57.71
174	0.90,	1.19,	1.14,	0.85,	0.92,	0.00,	0.40,	57.63
177	0.89,	1.20,	1.14,	0.85,	0.92,	0.00,	0.40,	57.59
179	0.90,	1.19,	1.13,	0.86,	0.92,	0.00,	0.40,	57.42
195	0.90,	1.20,	1.14,	0.85,	0.91,	0.00,	0.39,	57.27
237	0.90,	1.20,	1.14,	0.85,	0.91,	0.00,	0.39,	57.27
243	0.90,	1.20,	1.14,	0.86,	0.91,	0.00,	0.39,	57.27
249	0.90,	1.20,	1.14,	0.86,	0.91,	0.00,	0.39,	57.26
252	0.89,	1.20,	1.14,	0.86,	0.90,	0.00,	0.39,	57.24
264	0.90,	1.20,	1.14,	0.86,	0.90,	0.00,	0.39,	57.21
267	0.90,	1.20,	1.14,	0.87,	0.90,	0.00,	0.39,	57.13
269	0.90,	1.20,	1.14,	0.86,	0.90,	0.00,	0.39,	57.08
303	0.90,	1.20,	1.14,	0.86,	0.90,	0.00,	0.39,	56.97
418	0.90,	1.20,	1.14,	0.87,	0.90,	0.00,	0.39,	56.88
458	0.90,	1.20,	1.14,	0.87,	0.90,	0.00,	0.39,	56.87
461	0.90,	1.20,	1.14,	0.87,	0.89,	0.00,	0.39,	56.74
633	0.90,	1.20,	1.14,	0.87,	0.89,	0.00,	0.39,	56.74
657	0.90,	1.20,	1.14,	0.88,	0.89,	0.00,	0.39,	56.72
675	0.90,	1.20,	1.13,	0.88,	0.89,	0.00,	0.39,	56.71
690	0.90,	1.20,	1.13,	0.88,	0.89,	0.00,	0.39,	56.59
792	0.90,	1.20,	1.14,	0.88,	0.88,	0.00,	0.38,	56.58
801	0.90,	1.20,	1.14,	0.88,	0.88,	0.00,	0.38,	56.58
838	0.90,	1.20,	1.13,	0.88,	0.88,	0.00,	0.38,	56.55
1,022	0.90,	1.20,	1.13,	0.88,	0.88,	0.00,	0.38,	56.53

Fig. 6b: Optimization of a Fuel Shuffling Scheme by SHAKE

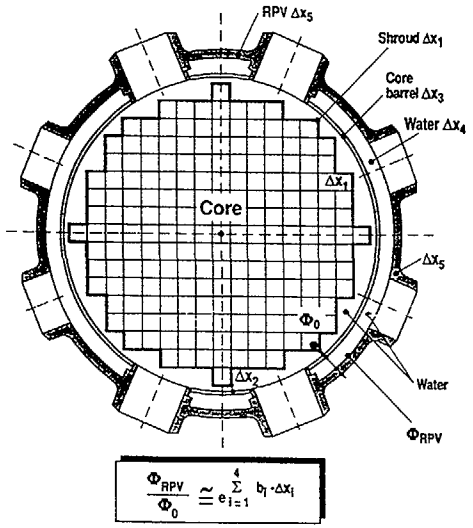

Fig.7: Calculation of the RPV Fluence

6 Conclusion

It can be recognized, that the claim for FCC optimization is comparatively large Therefore optimization efforts are worthwile to be performed One should notice here that for a 1300 MWe plant specific energy cost of 10^{-4} DM/kWh mean a sum of approx 10 Mio DM p a

Since there exist many interconnections between the relevant parameters of the plant, an optimization, using the common sophisticated and powerful design codes, may have no prospects This holds to a larger extent for the optimization of the whole plant

Case	Core Height [cm]	FA Number	FA Type	q' [W/cm]	q'' [W/cm²]	d_{corr} [µm]	1) ∫φdt norm	e_0 [%U235]	$\overline{BU}^{batch}_{EOL}$ [MWd/kg]	FC [DM/kg HM]	FCC [Dpf/ kWh]
Ref case	390	221	17x17-25	165 5	55 4	43	1 00	3 77	46 1	7875	1 90
Variant 1	360	221	17x17-25	179 3	60 1	50	1 08	4 05	50 0	8319	1 80
Variant 2	390	193	18x18-24	166 7	55 9	44	1 75	3 79	46 5	7916	1 89
Variant 3	390	193	17x17-25	189 5	63 5	57	0 36	4 26	52 8	8647	1 74
Variant 4	360	193	17x17-25	205 3	68 8	85	0 40	4 58	57 2	9155	1 66

q' - linear heat rate
q'' - heat flux
d_{corr} - waterside corrosion layer
∫φdt - RPV fluence (inner side of RPV)
e_0 - reload enrichment
$\overline{BU}^{batch}_{EOL}$ - reload burnup
FC - fuel cost
HM - heavy metal
FCC - fuel cycle cost
Dpf - 0,01 DM

1) shroud thickness, core barrel and RPV size for all cases identical

Fig. 8. Parameter Influence on the Fuel Cycle Cost

INFLUENCE OF PROLONGED NUCLEAR FUEL BURNUP ON SAFETY MARGINS OF ADVANCED PWRs

D. SPASOJEVIĆ, N MARINKOVIĆ, M V. MATAUSEK
Boris Kidrič Institute of Nuclear Sciences,
Belgrade, Yugoslavia

Abstract

Prolonged nuclear fuel burnup in advanced NPP with four or more instead of three one-year cycles, and/or 15- to 18-months instead of standard 12-month cycles, requires the fresh fuel with increased initial enrichment combined with burnable absorber. This causes changes in axial and radial power distribution during particular fuel cycles, so that detailed analysis of thermal reliability of reactor core becomes inevitable This paper presents the results of the analysis of the departure from nucleate boiling ratio (DNBR) for an equilibrium cycle of an advanced PWR core

INTRODUCTION

The basic goal of in-core nuclear fuel management is the minimum value of nuclear power production cost for the given system properties and safety margins. This goal is achieved if the total burnup of discharged fuel has the maximum possible value, while from both economic and safety reasons it is desirable that the radial and the axial burnup distribution in discharged fuel assemblies lie in the narrowest possible range. The direct approach in solving the so defined optimization problem is the power generation flattening, which for LWRs led to partitioning of reactor core into three radial zones containing fuel with different initial enrichment (first core) or different burnup histories (succeeding cores). In the course of its three years lifetime a fuel assembly occupies different positions during the three 12-month cycles Inserting the fresh fuel in the outer low neutron flux zone, and moving it gradually towards the center of reactor core (out-in reloading scheme), it is provided that the fuel containing higher percentage of fissionable material operates in the lower neutron flux, which results in better reactor core safety properties Since the burnup process itself leads towards power generation flattening, from the safety point view the beginning of each cycle is critical and thus it is used as the design basis

Recent developments in nuclear power production, however, dictate different criteria for in-core nuclear fuel management First, the tendency of nuclear power plant life extension, from present 30 years to possible 50 years, makes the preservation of reactor vessel integrity the goal of primary importance In order to minimize the radiation damage of reactor vessel, fresh fuel with high content of fissionable material is placed in the intermediate or the central core zone, while loading patterns are designed so to minimize the leakage of neutrons (particularly fast neutrons) from the core Second, increasing prices of back-end fuel cycle services, as well as the global delay of commercial use of fast reactors, result in a permanent requirement for increasing the total discharge burnup. Improvements in fuel production technology can already guarantee average discharge burnup of 50 instead of present 30-40 MWd/kgU This increased discharge burnup can be achieved either by increasing the power generation density, or by prolonging the fuel resident time in the reactor. In both cases, there appears the question of keeping up with safety margins.

Fuel designed to spend in a reactor four three-months or three 15- to 18-months cycles, instead of original three one-year cycles, must have increased initial enrichment in order to provide sufficient built-in reactivity for the prolonged operation. On the other hand, use of fuel with higher initial enrichment, which is no longer necessarily inserted in the lowest neutron flux zone, can seriously jeopardize safety characteristics of the system considered. Thus the expected peaks of power generation at the beginning of cycle are compensated by applying burnable absorbers, while control rods can be used for compensating high built-in reactivity. Obviously, this kind of in-core fuel management requires additional safety analysis

Having in mind that the future nuclear power plants will certainly be of the advanced type, with prolonged fuel cycles and extended lifetime, the nuclear characteristics of such systems were studied[1,7,8]. The following quantities were calculated:

- axial and radial distribution of neutron flux and power generation in a fuel rod for different burnup values;
- space (assemblywise) distribution of neutron flux and power generation in the reactor core having initial or equilibrium configuration and for different options of built-in reactivity compensation;
- isotopic fuel composition and fission product inventory for different burnup values The problem of worsened reactor core safety characteristics in the course of fuel burnup was noticed in the case when burnable absorbers were applied for power generation flattening, particularly towards the end of the cycle, when most of the burnable absorbers were already burnt The necessity of more detailed analysis of thermal reliability of the reactor core was pointed out

In the present paper the results of reactor core neutronic calculations presented in[1] are used as input data for calculating the temperature distribution in a fuel rod and a reactor core, as well as critical thermal flux ratio and the departure from nucleate boiling ratio (DNBR). The results of the thermal-hydraulic calculations are given for an equilibrium cycle of a typical 1000 MWe power plant[2], for the case of fresh fuel having standard initial enrichment, and for the case of fuel with increased initial enrichment and burnable absorbers An analysis of results obtained using different heat transfer correlations[3,4] suitable for this kind of reactor safety calculations has been performed

METHOD AND CORRELATION APPLIED FOR CALCULATION OF DNBR

Critical heat flux, q_{crit} is one of the main constraints for the power density generated in nuclear fuel, since the integrity of the first safety barriers, namely fuel element cladding, depends on its value[3,7]. Value of q_{crit} depends on the local conditions of the coolant and on the thermal conditions of the heating surface[3,5]. Value of the departure from nucleate boiling ratio (DNBR=q_{crit}/q_{clad}) is applied to validate the thermal reliability of the reactor core.

Having in mind the complexity of the procedure for determining heat flux distribution on the surface of the fuel cladding q_{clad}, on one hand and the correlation for calculating values of local heat flux q_{crit}, on the other hand, distribution of DNBR is represented in a very complex implicit form. That is why the direct determination of minimum DNBR value, which is the safety margin, is practically impossible.

Procedure for calculating the DNBR distribution performed in this analysis is the following:
Distribution of the heat flux on the surface of a fuel rod and its cladding $q_{clad}(z)$, is calculated by applying coupled code packages WIMSD-VAMPIR and HITOC-MOD3. For a chosen reactor core configuration, burnup Bu(r,z) and power P(r,z) distribution were computed by WIMSD-VAMPIR[1] code package. The so obtained heat distribution was used as input in the HITOC-MOD 3 code for calculating thermal and hydrodynamic parameters of the heating channel and the fuel rod. In this procedure choice and method of applying the correlation for calculating the critical heat flux q_{crit} has special significance. Among a number of available experimentally obtained correlations for q_{crit}[5,6], the following three correlations are applied for the analysis performed in this paper:

Correlation W-3:[5]

$$q_{crit}(z)=[2.002-0.0000624p+(0.1722-0.0000143p)e^{(18.177-0.000599p)x}]\,[0.00073474(0.1484-1.596x+0.1729x|x|)G+1.037]\,(1.157-0.869x)(0.2664+0.8357e^{124.1D_e})(0.8258+0.000341i_{inlet}) \quad (1)$$

which is valid for the following ranges of parameters:
p=6895 - 15860 kPa, x=-0.15- 0.15, G= 1356 - 6780 kg/m^{2}s, D_e=0.005 - 0.018 m.

Correlation RELAP 4 - MOD 5:[5]

$$q_{crit}(z)=\frac{25487\left(\frac{G}{1356}\right)^{0.1775\ln(x+1)}}{[(x+1)^{3.3906}\cdot 0.5356p^{0.3234}FFP^{1.053}]} \quad (2)$$

valid for the following ranges:
p=690 - 15200 kPq, x= -0.10 - 0.10 , G= 100 - 4100 kg/m^{2}s, FFP= maximum value of the fuel rod radial form factor.

Correlation GIDROPRESS:[4]

$$q_{crit}(z)=795000(1-x^{0.105p-0.5}\cdot G^{0.311(1-x)-0.127}\cdot(1-0.0185p) \quad (3)$$

valid for the following ranges:
p= 7450 - 16700 kPa, x=-0.7 - 0.4, G= 700 - 3800 kg/m^{2}s, D_e > 0.009 m

In the previously mentioned relations steam quality x is a function of axial coordinate z and it is calculated according to the following:

$$x(z)=-\frac{i_{inlet}}{r}+\frac{4}{D_e\cdot Gr}\int_0^z q(z)\,dz, \qquad D_e=4\frac{A}{O} \quad (4)$$

where i_{inlet} is the enthalpy of the coolant entering the core, A is the coolant cross section in the fuel element, and O is the wet perimeter of the fuel element.

RESULTS OF CALCULATION

Basic parameters of the system analyzed in this paper are shown in Table 1. Assemblywise radial distribution of form factor at the beginning of cycle (BOC) and at the end of cycle (EOC) for an equilibrium core is shown in Figure 1. This results from neutronic calculations of the core with burnable absorbers (IFBA).

Critical heat flux for chosen reactor types (PWR or VVER) is determined by applying the above correlations, but for a final comparison of DNBR at BOC and EOC with and without burnable absorbers, correlation W-3 was applied for PWR case while the correlation GIDROPRESS is applied for the VVER case. The results for VVER case are not cited here, because they are still in preliminary form.

Results of thermal-hydrodynamic calculations are shown in Table 2 and in Figures 2 - 4. Axial distributions of q_{clad}, q_{crit} and DNBR at the beginning and at the end of an equilibrium cycle are computed for the cases with and without burnable absorber by applying axial distribution at the fuel assembly maximum of generated heat fuel.

Effects of the reliability of applied experimental correlations for determining the critical heat flux and engineering uncertainty factors of reactor parameters are shown in Figure 5. It may be seen that in the case of extended fuel cycle analyzed here, the designed safety margin DNBR is jeopardized towards the end of cycle.

Table 1 Reactor core Thermal-hydraulic parameters

Parameter	PWR	VVER
Gross fission power output,Mw	2900	3000
Maximum transient overpower allowances,%	118	110
Specific power, kw/kgU	35 5	45 9
Power density, Mw/m³	88 8	108
Linear heat rating, kw/m		
Core average	15 16	16 6
Maximum steady state value	39 37	44 8
Maximum value in overpower transient	72 19	47 4
Heat transfer surface area, m²	5341 9	5176
Heat flux, kw/m²s		
Core average	529	580
Maximum at steady state	1375	1570
Maximum during overpower transient	2519	1660
Center fuel temperature, °C		
Core average	749	850
Maximum at steady state	1621	1660
Maximum at steady state transient	2593	1720
DNBR, dryout or critical heat flux ratio		
Maximum value at rated power	2 06/2 14	1 73
Minimum value at overpower	1 36/1 38	1 51
Confidence level	95	95
Corelation used to determine DNBR	WRB	GIDROPRESS
Cladding temperature, °C		
Core average, clean	333 3	340/320
Maximum value	350	400/345
Coolant flow, kg/s		
Total core	13990	82200
Effective flow for heat transfer	13000	82200
Bypass flow, %	8 5	3 1
Operating pressure, MPa	15 51	15 7
Core pressure drop, MPa	0 1127	0 142
Coolant temperature, °C		
Inlet	294 1	287
Average outlet	331 7	320
Outlet of hot channel	341.0	340
Fuel assembly parameters	square	hexagonal
lattice type	17x17	
No of fuel rods/assembly	264	317
Fuel rod pitch, mm	12 6	12 75
Active length	3657 6	3550
Fuel pellet diameter, mm	7 843	7 72
Fuel cladding inside diameter, mm	8 0	7 72
Fuel cladding thickness, mm	0 571	0 69

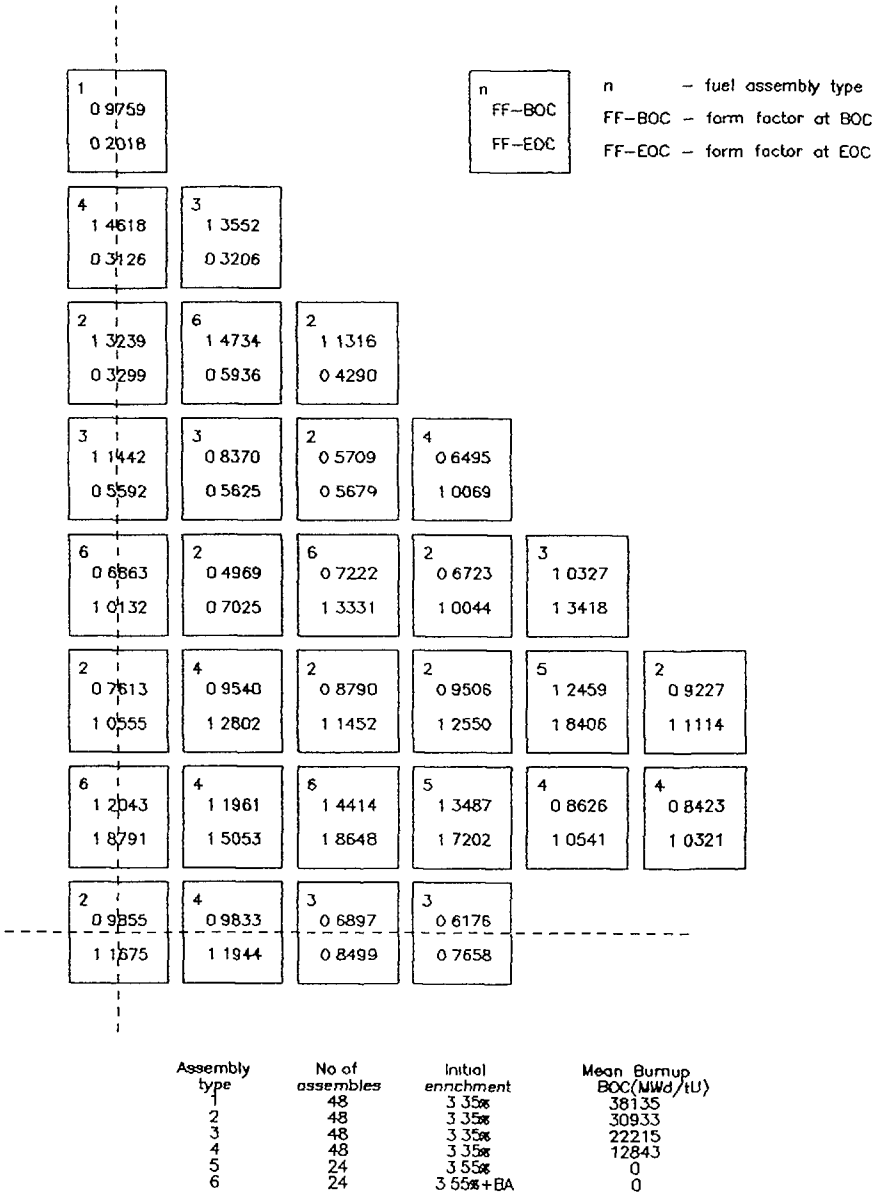

Assembly type	No of assembles	Initial enrichment	Mean Burnup BOC(MWd/tU)
1	48	3 35%	38135
2	48	3 35%	30933
3	48	3 35%	22215
4	48	3 35%	12843
5	24	3 55%	0
6	24	3 55%+BA	0

Fig 1 Assemblywise power distribution at BOC and at EOC for an equilibrium cycle Case with burnable absorber (BA)

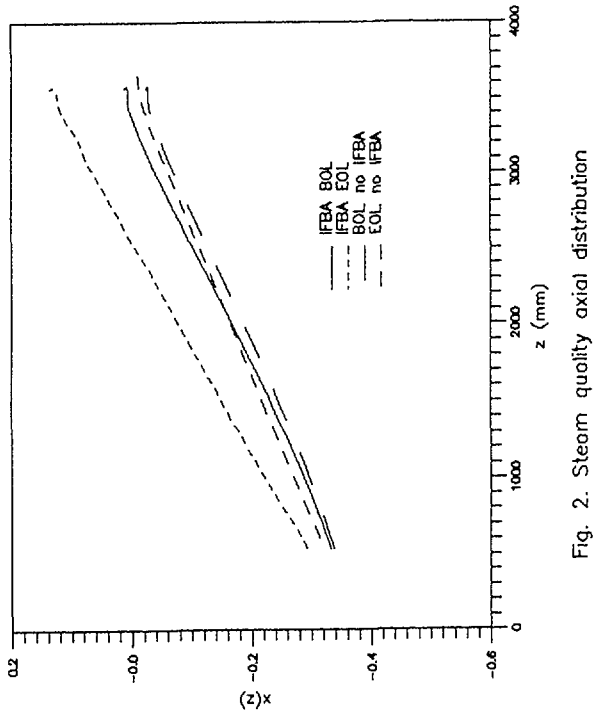

Fig. 2. Steam quality axial distribution

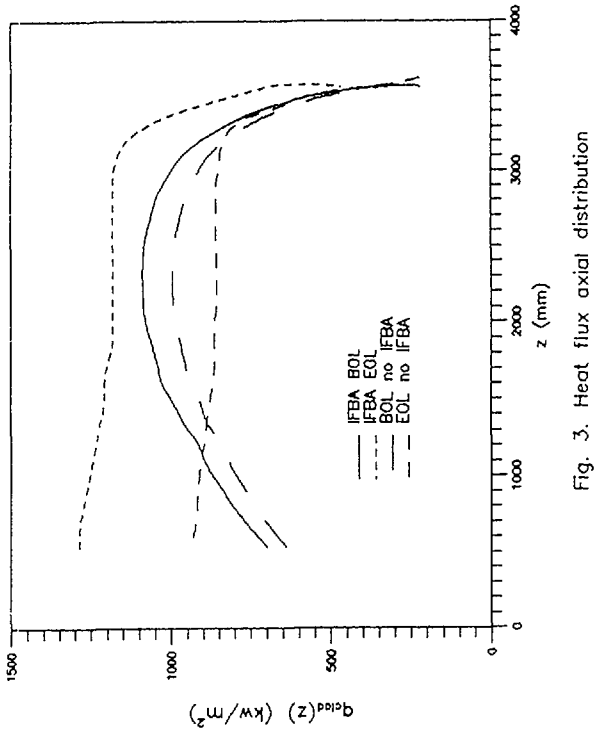

Fig. 3. Heat flux axial distribution

Table 2. Axial distribution of power and termohidraulic parameters for fuel assembly, equilibrium cycle without control rods and burnable absorbers

z (cm)	Maximum power peaking at BOC					Maximum power peaking at EOC				
	P	x(z)	$q_{clad}(z)$	$q_{crit}(z)$	DNBR	P	x(z)	$q_{clad}(z)$	$q_{crit}(z)$	DNBR
80.7	107.44	0.367	177.458	8160.3	45.98	101.63	-0.367	245.580	8147.6	33.18
134.5	245.57	0.365	342.240	8067.9	23.57	251.73	-0.365	362.703	8063.7	22.23
188.3	429.75	0.362	456.321	7949.1	17.42	505.80	-0.361	613.938	7899.3	12.87
268.9	736.72	0.357	507.023	7751.0	15.29	798.96	-0.356	708.395	7688.8	10.87
403.4	1289.25	0.348	547.585	7412.8	13.54	1122.58	-0.351	782.000	7506.9	9.60
537.9	1933.88	0.338	638.849	7040.9	11.02	1469.04	-0.346	837.190	7320.2	8.74
672.4	2632.23	0.327	692.086	6666.9	9.63	2403.05	-0.331	901.925	6795.3	7.53
806.8	3376.62	0.315	737.718	6297.2	8.54	3366.25	-0.315	930.995	6288.2	6.75
941.3	4159.38	0.303	775.745	5934.3	7.65	4319.72	-0.300	921.591	5856.7	6.36
1075.8	4980.51	0.290	813.772	5585.2	6.86	5269.30	-0.285	917.831	5463.1	5.95
1210.2	5825.43	0.276	837.348	5250.6	6.27	6213.04	-0.270	912.186	5103.3	5.59
1344.7	6719.47	0.262	886.023	4926.2	5.56	7147.05	-0.255	902.781	4773.8	5.29
1479.2	7637.30	0.247	909.599	4619.5	5.08	8072.33	-0.241	893.377	4490.9	5.03
1616.6	8588.89	0.232	943.063	4326.1	4.59	8986.88	-0.226	883.972	4211.6	4.76
1748.1	9555.83	0.217	958.273	4054.8	4.23	9891.70	-0.212	874.567	3971.0	4.54
1882.6	10538.12	0.201	973.484	3830.5	3.93	10786.79	-0.197	865.162	3732.8	4.31
2017.1	11535.75	0.185	988.695	3561.2	3.60	11681.88	-0.183	865.162	3526.9	4.08
2420.5	14567.04	0.137	996.300	2949.0	2.96	12576.97	-0.169	865.162	3335.7	3.86
2554.9	15564.67	0.121	988.695	2777.4	2.81	13466.23	-0.155	859.527	3157.7	3.67
2689.4	16546.96	0.106	973.484	2621.6	2.69	18801.79	-0.070	859.527	2305.6	2.68
2823.9	17513.90	0.090	958.273	2478.8	2.59	19681.27	-0.056	850.074	2195.3	2.58
2958.4	18450.15	0.075	927.852	2350.1	2.53	20550.98	-0.042	840.631	2091.8	2.49
3092.8	19348.15	0.061	889.825	2234.7	2.51	21371.83	-0.029	793.405	2001.3	2.52
3227.3	20176.83	0.048	821.377	2135.3	2.60	21931.50	-0.020	653.204	1941.6	2.97
3361.8	20898.19	0.036	714.902	2052.6	2.87	22175.17	-0.016	588.807	1915.8	3.25
3496.2	21435.38	0.028	532.374	1993.6	3.75	22357.92	-0.013	441.599	1896.8	4.30
3576.9	21604.21	0.025	278.863	1975.8	7.09	22486.33	-0.011	266.543	1884.2	7.07
3657.8	21727.00	0.023	202.809	1963.2	9.68	22554.00	-0.010	184.010	1889.9	10.27

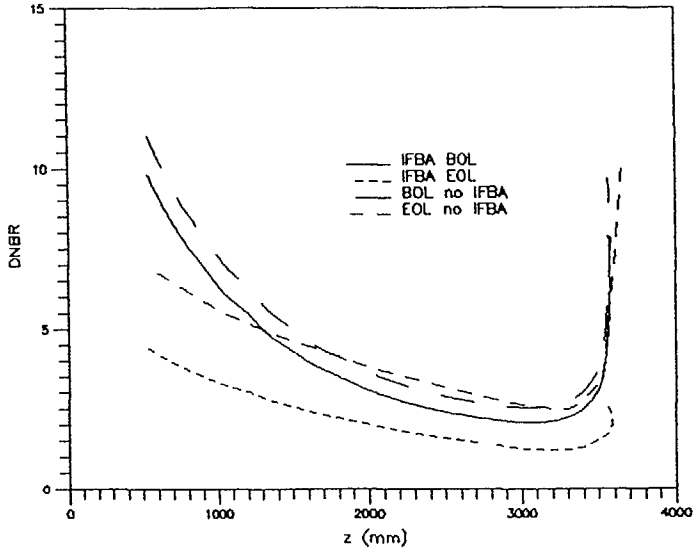

Fig 4 Axial DNBR distribution

CONCLUSION

Prolonged fuel cycles from original 12 months to 15 or more demand increase of fresh fuel enrichment and application of burnable absorbers. This causes variations of radial and axial power distribution during the cycle which impose the need for detailed analysis of the reactor core thermal reliability.
In this paper an analysis of the variation DNBR parameter is performed for a PWR fuel rod cladding. Results of the analysis show that reactor core having $(q_{crit}/q_{clad})_{min} \geq 2.5$ at the beginning of the cycle may change to $(q_{crit}/q_{clad})_{min} < 1.2$ at the end of cycle when the burnable absorber is applied. This is not acceptable from safety point of view since the accepted design value is $(q_{crit}/q_{clad})_{min}=1.36$

The analysis and the results given the present paper indicate that increasing the total discharge burnup and introducing advanced refuelling schemes require more sophisticated safety analysis, i e. more detailed both physical and thermal-hydraulic calculation models and methods

REFERENCES

/1/ M.V.Matausek, N Marinkovic, Prolonged Fuel Burnup in Advanced LWRs, IAEA Int. Topical Meeting on Burnup Determination of Water Reactor Fuel, Karlsruhe, 1988

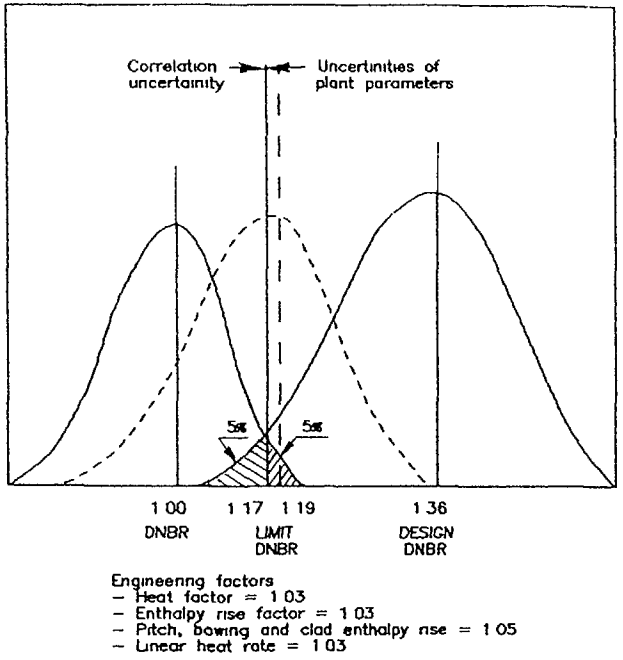

Fig 5 Uncertainity effects of the correlation for DNBR reactor parameters

/2/ US Government/Industry Seminar on Nuclear power technology, Bled, 1982.
/3/ Ginoux J.J , Two-Phase Flows and Heat Transfer with Application to Nuclear Reactor Design Problems, Hemisphere Publication Corporation, New York, 1978.
/4/ Z.Stosic, D Spasojevic, Modification Heat Influence to PWR Core Thermal Reliability Owing to Burnup, Proc. of the XXIV Yug. Conf of ETAN, Vol.IV, pp 105-110, 1980.
/5/ D.C. Groeneveld, C.W. Snoek, A Comprehensive Examination of Heat Transfer Correlations Suitable for Reactor Safety Analysis, Multiphase Science and Technology, Vol.2, 1984
/6/ L N. Polianin, M H. Ibragimov, G.I. Sabelev, Teploobmen v jadernih reaktorah, Energoizdat, Moscow, 1984.
/7/ D Spasojevic et al. Study of Nuclear Reactor Safety, pp 459, Beograd 1988, (in Serbian)
/8/ M V Matausek et al., Study Fuel Cycle Management, pp 148, Beograd 1989. (in Serbian)

CORE RELOAD PATTERN OPTIMIZATION ON DESKTOP COMPUTERS

A.Z. TANKER
Turkish Atomic Energy Authority,
Ankara, Turkey

Abstract

A method to find a low leakage core reload pattern that results in the highest possible burnup within the safety constraints is developed. The coupled burnable poison optimization problem is effectively separated by the use of Haling depletion. The method is based on a two-dimensional, effective-one-group nodal scheme for power distribution calculations in which assembly reactivities are related linearly to assembly burnup. Linear programming is used to select the the pattern with highest EOC k_{eff} under power peaking constraints.

Strong dependence on initial guess pattern was observed, and a set of distinctly different guess patterns is generated and evaluated in each case. Test applications indicate that the method converges to a few high k_{eff}, low leakage patterns having similar assembly distributions, which, are also similar to those found in reference studies. A 193-assembly core analysis, the reference of which takes 220 CPU seconds on a CYBER-205, took a total of 310 seconds on a 386-based personal computer. The method is found suitable for sifting through a large number of possible patterns, to select a few to be analyzed more accurately.

INTRODUCTION

Pressurized Water Reactor (PWR) core design is a complicated task which involves the evaluation of many physics and engineering parameters. Simultaneous solution of all the equations that govern such a complex system is far from reality, therefore, the problem is broken down into weakly-interrelated smaller problems. Core fuel management is one of these smaller problems and it is related to the rest of the variables of core design in terms of constraints such as:

- limit on fuel burnup - due to material considerations
- limit on peak-to-average power ratio - should not be larger than a predetermined value at any point in the core during the cycle
- enough excess reactivity in the core to overcome the xenon absorption
- ability to shut the reactor down at any time during the cycle.

When constraints such as these are considered, the fuel management problem is effectively separated from the structural, thermal-hydraulics, safety, etc. aspects of the core design.

In-core fuel management of a PWR core involves the following steps:

- the refueling cycle length is determined
- the batch size and enrichment are estimated
- the fuel reload pattern and absorber distribution are found to satisfy the safety requirements and constraints
- detailed calculations are performed to validate the proposed loading pattern.

The present work concentrates on the third step above, which includes:

- a criterion to select the best reload pattern
- power and depletion calculations on trial patterns to check the safety constraints
- an optimization method to determine the best pattern.

In the last decade low leakage fuel management became a popular trend because of the reduction of the leakage and the fluence on the pressure vessel. Burnable poisons are used extensively in low leakage cores to control power peaking and the placement of these rods constitutes a second optimization problem coupled to the fuel reload optimization. However, with the use of Haling depletion, the fuel assembly pattern problem and the burnable poison distribution problem can be separated. The latter problem will not be addressed in this work.

THEORY

In scoping studies, a two-dimensional, effective one-group (Ref. 1) nodal scheme with adjustable parameters is sufficiently accurate for the calculation of power distributions:

$$-\nabla^2\Phi_k = \left(\frac{1}{k_{eff}\,(1-\rho_k)} - 1 \right) \frac{1}{M^2}\,\Phi_k \qquad (1)$$

where

Φ_k = effective one-group neutron flux in the k-th node,
k_{eff} = criticality eigenvalue,
ρ_k = nodal reactivity, including a correction for thermal-group leakage (Ref. 1),
M = migration length.

This equation is solved at the end of cycle (EOC) assuming that all burnable poison in the core will be burned at the EOC.

By taking $\Phi_k \sim f_k(1 - \rho_k)$, Eq. 1 can be written as a function of f_k = the normalized nodal power, ρ_k = nodal reactivity, k_{eff} and M. The migration length is shown to be independent of burnup and assembly (Ref. 1). f_k is assumed to stay constant throughout the cycle (Haling depletion) whereas ρ_k and k_{eff} are EOC parameters. Since the available values are ρ_k^{BOC} - the initial reactivity distribution - and not ρ_k at the EOC, a way must be found to relate ρ_k and ρ_k^{BOC}. This is done by using the linear reactivity model (Ref. 2) in which the assembly reactivities are assumed to depend linearly on the assembly burnup:

$$\rho_k = \rho_k^{BOC} - A_k \, \Delta B_k \ .$$

The coefficients ρ_k^{BOC} and A_k in this relation are determined by curve fitting to detailed burnup calculations for the assemblies. This approximation greatly facilitates the determination of the state of the core at any time during the cycle. To relate the burnup ΔB_k of node k to the prechosen cycle burnup ΔB, a expression of the form $\Delta B_k = f_k \frac{m_{core}}{m_k} \Delta B$, where m denotes the heavy metal loading, is used. Now the EOC state is described by the reactivity distribution at BOC, M and f_k values which are taken to be independent of burnup, ΔB which is specified beforehand, and k_{eff} at the EOC. The problem is reduced to finding the highest EOC k_{eff} for different initial reactivity distribution patterns. The advantages of this method are the following:

- the resulting quadratic equation for f_k can be solved very fast,
- the memory requirements are extremely small, since all variables but ρ_k^{BOC} and A_k are lumped into assembly-independent M and h (node size),
- allows one step treatment of the depletion process,
- there is no need to further partition the one-eighth core into zones to keep the number of calculations at a reasonable level.

This calculational method reduces the time spent in power distribution calculations significantly and permits the reload assembly pattern analyses to be performed on desktop computers.

The optimization of initial reactivity distribution to maximize the EOC k_{eff} without having power peaking above the given limits has been done using a number of methods including dynamic programming, optimal control strategy, linear programming and direct search. The method used in this study is linear programming with the objective function :

$$\text{maximize} \quad J = k_{eff}(\rho_i) = k_{eff}^{p} + \sum_{i=1}^{N} \left(\frac{\partial k_{eff}}{\partial \rho_i} \right)^{p} (\rho_i - \rho_i^{p}) \ ,$$

where N is the total number of nodes in the core, and the BOC superscript of ρ_i is dropped. Three conditions are imposed on the reactivities:

$$\rho_{min} < \rho_i < \rho_{max} \ , \qquad i = 1,2, \ \ldots \ ,N \tag{2}$$

$$\sum_{i=1}^{N} w_i \rho_i = \text{const}, \tag{3}$$

where w_i is the total number of nodes in the full core that, because of symmetry, are identical to the i-th node in the one-eighth core,

$$f_{min} < f_i < f_{max} \ , \qquad i = 1,2, \ \ldots \ ,N \tag{4}$$

where f_i is the assembly power normalized to unity over the full core and is linearized with respect to the reactivities as (Ref. 3):

$$f_i = f_i^{p} + \sum_{m=1}^{N} \left(\frac{\partial f_i}{\partial \rho_m} \right)^{p} (\rho_m - \rho_m^{p}) \ , \tag{5}$$

(the superscript p indicates that the results of the previous iteration are to be used in the evaluation of the variable).

THE COMPUTER CODE

The theory described above is incorporated in a computer program consisting of power calculation, optimization, assembly matching and input-output modules. This modular structure allows improvement of a particular section such as the power calculation without changing other parts of the program. The flow diagram of the code is presented in Fig. 1.

The program starts by reading groups of assemblies and their enrichments. Throughout the work it was found that the convergence of the linear programming routine is strongly dependent on the initial guess pattern. Therefore, the code

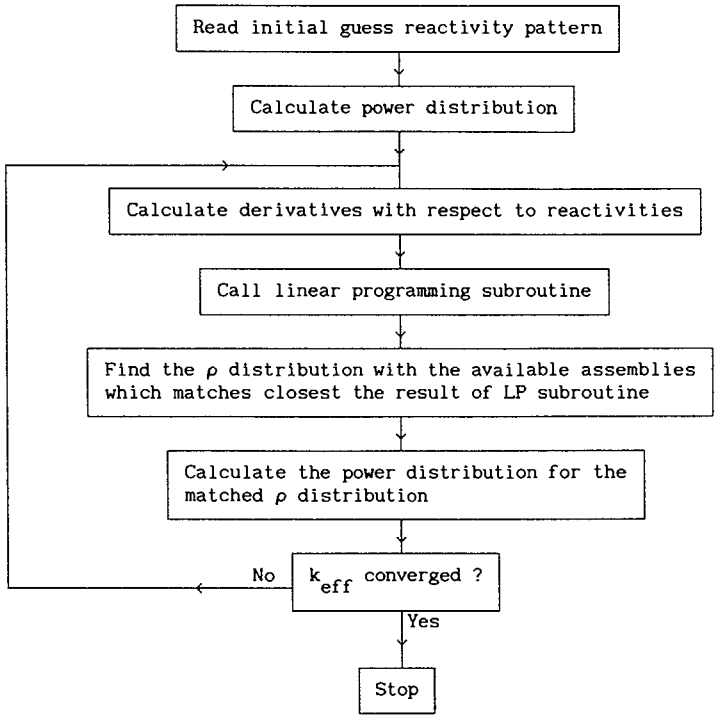

Fig.1 - Flow Diagram for Core Reload Pattern Optimization

is written such that it always creates 10 patterns which sample distinctly different distributions with the same assemblies, and calculates the results for each of them. The CPU times given in the next section include all 10 calculations.

In the second step the derivatives of k_{eff} with respect to increases in individual assembly reactivities are calculated to find the coefficients in the objective function. The procedure to do this is to assume a change $\Delta\rho_i$ in the reactivity of the i-th node, and, keeping all other reactivities constant, performing a power calculation, and finding the resulting change in k_{eff}. At the same time, the derivatives of the assembly powers with respect to changes in reactivities, $\partial f_i/\partial \rho_m$ in Eq. 5, are also calculated.

With these derivatives, the linear programming subroutine ZX3LP (Ref. 3) finds a distribution of reactivities, - which take values in the continuous range of Eq. 2, which respect the given power peaking limits of Eq. 4 and which maximizes the k_{eff} at the EOC. As observed in Ref. 4, power peaking limit permitting, the code converges to low leakage patterns.

The next task is to match the actually available assemblies with the optimized pattern of nodal reactivities. This is done by matching the assembly with the highest reactivity with the corresponding highest reactivity node. Note that, because of symmetry, nodes are repeated in the core 1, 4 or 8 times, which should be taken into account in matching the nodes with the assemblies.

Upon matching, a power calculation for the assembly pattern is done and the resulting k_{eff} is compared with the one for the previous pattern. The k_{eff} first increases, then starts decreasing at which point the iterations stop.

To test the validity of the suggested scheme two cases were used: The first one is a 44 node core with one-eighth core symmetry and 3 batches of assemblies. To serve as reference, all possible core patterns were separately created with a different code, and associated k_{eff}'s were calculated with the same power calculation module. The optimization code converged to the pattern with the highest EOC k_{eff} value among the 82 possible patterns of the reference study.

The second test case is taken from Ref. 5 and the assemblies used in that study are grouped into three reactivity intervals with average reactivities assigned to each group. In Ref. 5, the assemblies along the symmetry lines were shuffled only among themselves. Here, no such limitation is imposed. The optimization scheme converged to a pattern which, despite the simplicity of the model used, is remarkably close to the reference study.

These test cases are explained in more detail in the following paragraphs.

APPLICATION

1) 44-NODE CORE

The first test case consists of 12 assemblies with ρ = 0.2, 20 assemblies with ρ = 0.1 and 12 assemblies with ρ = 0.0 . The core layout is presented in Fig. 2. The migration area is taken as 4.0 cm^2. Although 1.30 is used as the power peaking factor in linear programming routine, when the resulting reactivity distribution is matched with the pattern of actually available assemblies, the

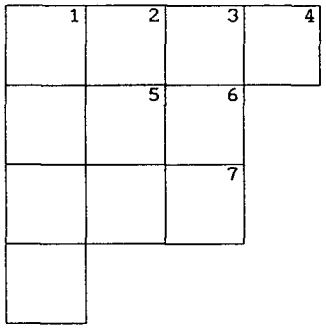

Fig. 2 - 1/8 Core Layout used in Test Case 1

power peaking becomes more pronounced. Therefore, not only the EOC k_{eff} but also the peaking is a factor to be considered when judging the patterns found by the code

Table 1 shows the results of a separate calculation to find the pattern with the highest k_{eff}. In the first column the values of the power peaking factor are divided into four groups All the possible patterns - for the given assemblies and the core structure - are evaluated. The neutronics model in this separate calculation is the same as the one used by the optimization code

11 reactivity distributions out of 82 has peaking lower than 1.40 Among these patterns the highest k_{eff} is 1 051 which belongs to pattern 1020121 (which should be interpreted as the BOC reactivity for node 1 is 0.1, for node 2 it is 0 0, for node 3 it is 0 2, and so on). 12 patterns result in power peaking in the range of 1.41 to 1 49, and among these the highest k_{eff} belongs to pattern 1120210. 7 patterns result in peaking between 1 50 and 1.59 among which pattern 1110220 has the highest k_{eff} value (1 069) This is also second to 1.074 in the combined peaking range of 1 41 to 1.59.

Table 1 - Number of cases and highest k_{eff} patterns in each peaking range

Power Peaking	# of cases	Max k_{eff}	Pattern
≤ 1 40	11	1 051	1020121
1 41 - 1.49	12	1 074	1120210
1 50 - 1.59	7	1 069	1110220
1 60 ≤	52	1 116	2210110

As explained earlier, the results are strongly dependent on the initial guess pattern, accordingly the optimization code generates 10 different starting patterns and performs the calculations for all of them Four out of these ten calculations converge to pattern 1120210 with k_{eff} = 1 074 Another four converge to pattern 1110220 with k_{eff} = 1.069. The remaining trials converge to 2110120 with peaking greater than 2.0, and to 1112200 with k_{eff} = 1.052 which is smaller than 1.069. Thus, the code predominantly finds the two patterns with the highest k_{eff} values.

2) 193-NODE CORE

The core of the second test case is shown in Fig 3. Power peaking factor is chosen as 1.30 in the linear programming subroutine, though, as explained in the first test case the resulting patterns with actually available ρ values may have peaking larger than this limit The full core contains 64 assemblies having ρ = 0.2, 64 assemblies having ρ = 0 1, and 65 assemblies having ρ = 0.0. The optimum pattern found by the code has k_{eff} = 1 1255 This pattern is going to be referred to in the following paragraphs as pattern 1 This pattern and its initial guess pattern are shown in Figs 4 and 5

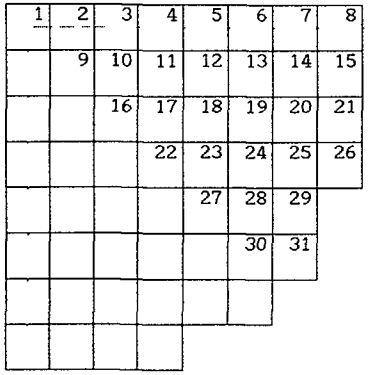

Fig. 3 - Core layout used in the second test case.

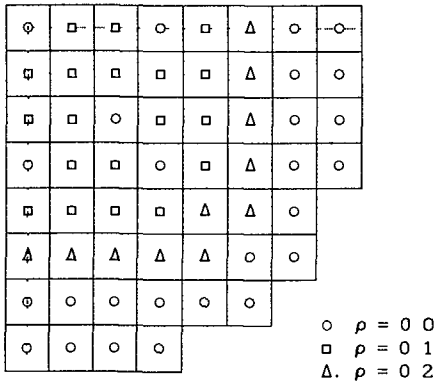

Fig 4 - Pattern 1 with the highest EOC k_{eff}

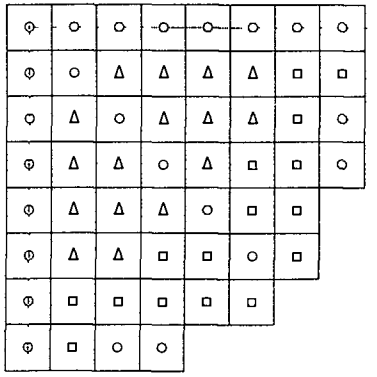

Fig 5 - Initial guess pattern used to generate Fig 4

The next-highest k_{eff} patterns have 1.1224, 1.1201, 1.1103 and 1.0886 as their k_{eff} values. For the remaining five guess patterns convergence cannot be achieved. Since 1.1224 and 1.1201 are quite close to the k_{eff} of pattern 1, nodes that are common among these three patterns are also of interest, to rule out the possibility that their similar k_{eff} values may be the result of similar initial patterns As can be seen from Fig 7 these three patterns have 10 out of

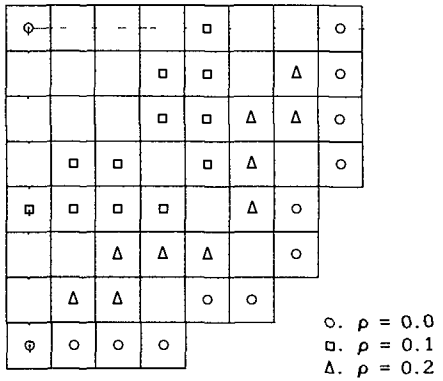

Fig. 6 - Common nodes of the 3 highest-k_{eff} patterns

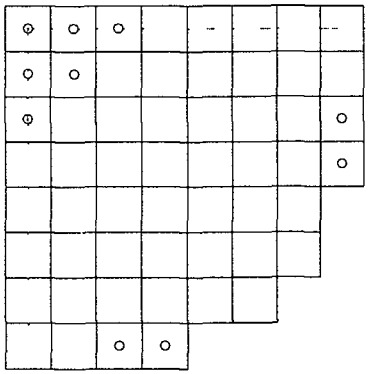

Fig. 7 - Common nodes of initial patterns that generate 3 highest-k_{eff} patterns

56 nodes in common in their initial quarter-core guess patterns. The converged optimized patterns, however, have 35 nodes out of 56 in common (Fig. 6). This result shows that the code has converged to similar final patterns starting from distinctly different guess patterns.

Figs. 8 and 9 show the results of Ref 5 which uses the same core Fig. 8 shows the initial pattern and Fig. 9 presents the resulting optimized, higher k_{eff} pattern which serves as reference in the present work. In that study the assemblies along the symmetry lines could be shuffled only among themselves. Fig. 9 was obtained under this restriction

Figs. 10 and 11 compare pattern 1 with the initial and final cases of the reference study, that is with Figs 8 and 9. This comparison shows that the optimization code used in this study starts from a pattern which has 25 nodes in common with the reference optimized pattern, it converges to a pattern having 35 nodes in common Considering the crudeness of the approximations used in this study the final pattern has a remarkable similarity to the reference pattern

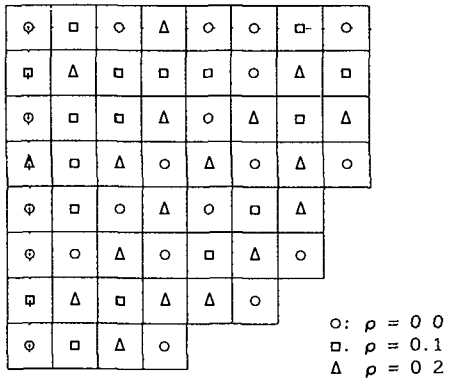

Fig. 8 - Initial core of Ref. 5

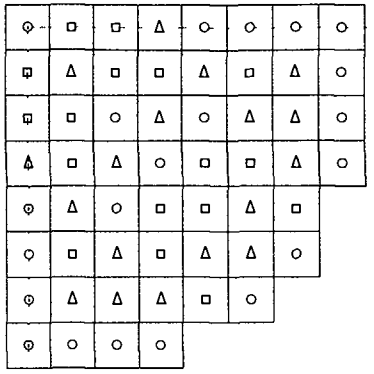

Fig 9 - Optimized, higher k_{eff} reference pattern

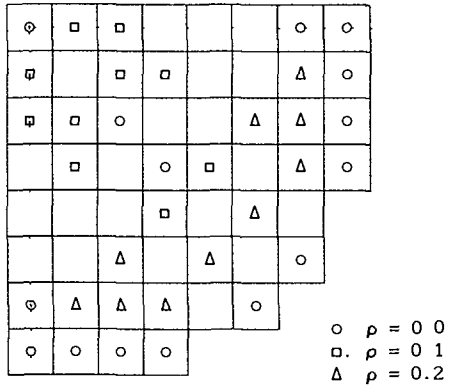

Fig. 10 - Nodes common between final cores of pattern 1 and the reference

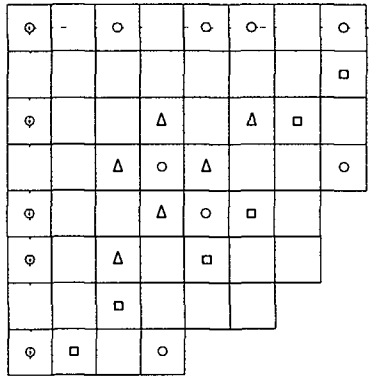

Fig 11 - Nodes common between initial core of pattern 1 and reference core

When the common nodes of the three highest k_{eff} patterns are compared with the reference initial and final patterns as shown in Figs. 12 and 13, the results are more pronounced

The number of nodes that are common in the initial cases of the three patterns and the reference initial pattern is only 5 By contrast, the final patterns have 23 common nodes with the reference final pattern In other words, starting patterns were distinctly different than the one used in the reference study, and

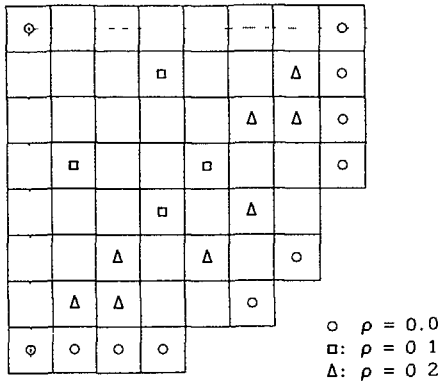

Fig. 12 - Nodes common between final cores of 3 highest k_{eff} patterns and the ref.

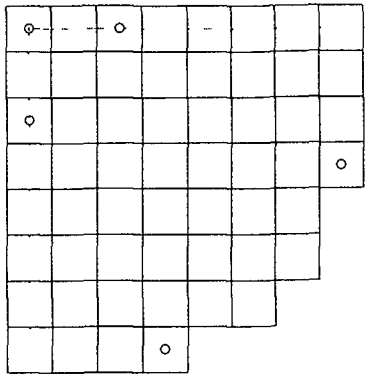

Fig 13 - Nodes common between init. cores of 3 highest patterns and initial reference core

so were from each other; but they all converged to final patterns that are similar to each other and to the reference one. The reference calculation took 220 CPU seconds on the CYBER-205 computer whereas all 10 initial patterns analyzed in this study with a 386-based Personal Computer took a total of 310 seconds.

CONCLUSIONS

In this study an optimization method for beginning-of-cycle fuel loading based on the linear reactivity model, effective one-group approximation to the diffusion equation, and linear programmming, is investigated. The method was found to converge to high EOC k_{eff} patterns, respecting power peaking limits. Strong dependence on initial guess pattern was observed, so that the method generates and calculates final patterns for each of the distincly different initial guesses These final patterns are to be analyzed by more accurate neutronics and depletion models to arrive at a single reload pattern.

The optimization method was found suitable for sifting through a large number of possible patterns, to select a few to be analyzed more accurately, on a desktop computer in an acceptably short time.

REFERENCES

1 Y.A. CHAO, C.W. HU, C.A. SUO, *Nucl. Sci. Eng.*, 93, 78 (1986).

2 M.J. DRISCOLL, T.J. DOWNAR, E.E. PILAT, *The Linear Reactivity Model for Nuclear Fuel Management*, Department of Nuclear Engineering, Massachusetts Institute of Technology, Cambridge, Massachusetts (1986).

3. "Problem-Solving Software System for Mathematical and Statistical FORTRAN Programming," International Mathematical and Statistical Libraries (1984).

4 J.S SUH, S H. LEVINE, *Nucl. Sci. Eng.*, 105, 371 (1990).

5 Y. KIM, T. DOWNAR, A. SESONSKE, *Nucl. Sci. Eng.*, 96, 85 (1987)

WORKSTATION COMPUTER SYSTEMS FOR IN-CORE FUEL MANAGEMENT

L. CICCONE, A.L. CASADEI
Westinghouse Commercial Nuclear Fuel Division,
Pittsburgh, Pennsylvania,
United States of America

Abstract

The advancement of powerful engineering workstations has made it possible to have thermal-hydraulics and accident analysis computer programs operating efficiently with a significant performance/cost ratio compared to large mainframe computer. Today, nuclear utilities are acquiring independent engineering analysis capability for fuel management and safety analyses. Computer systems currently available to utility organizations vary widely thus requiring that this software be operational on a number of computer platforms.

Recognizing these trends Westinghouse adopted a software development life cycle process for the software development activities which strictly controls the development, testing and qualification of design computer codes. In addition, software standards to ensure maximum portability were developed and implemented, including adherence to FORTRAN 77, and use of uniform system interface and auxiliary routines. A comprehensive test matrix was developed for each computer program to ensure the evolution of code versions preserves the licensing basis. In addition, the results of such test matrices establish the Quality Assurance basis and consistency for the same software operating on different computer platforms.

Introduction

The computer industry has changed rapidly over the past three decades. In previous years step changes in performance of computers were doubling every 3 to 5 years. Today, performance of computers are doubling every year and will probably move even faster to keep up with the rapidly changing software environment. The ability to move Fuel Management software to new platforms of hardware and software requires a strict development and migration process.

This paper will review the experience accumulated in migrating Fuel Management software to smaller computers and will discuss the experience to date of installation and operations of such systems in the US and abroad. In addition, the computer hardware evolution will be discussed with benchmark performance of the Westinghouse Advanced Nodal Code operating in several new workstation models recently released in the US market.

Evolution of Computing in the U. S.

The computing has changed significantly over time as illustrated in Figure 1. In the 1960's, the main thrust of the computer industry was central processing. Corporations installed these large processors and access was provided by punched card decks. This environment provided limited improvement in user productivity but began demonstrate computers could solve problems of minimal complexity.

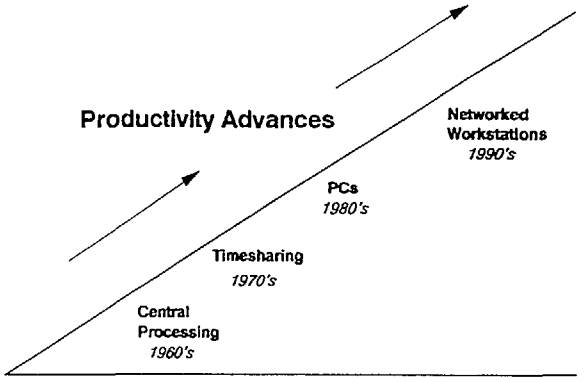

FIG. 1. Computing evolution.

Timesharing computing was the highlight of the 1970's. The large processors of the 60's were advanced by software developments that allowed users access via Cathode Ray Tubes (CRT). Users threw away their card decks and now could edit files interactively and submit application input data directly to the computer. This environment increased the productivity of users over central processing systems and began the era of sharing information via computers.

Probably the largest advance in computing was the introduction of the personal computer. This advance gave users dedicated power at their desk and provided an environment for the greatest advance in personal productivity software. Databases and graphical based software was being developed and users were incorporating these features into their daily job functions. Still, the sharing of data was limited at best in this structure.

Starting in the mid 1980's, the computing revolution moved to workstations. Initially, they appeared to be another version of the personal computer with more power but their development over the past 5 years has made them stand out. The first systems performed at around .5 million instructions per second (MIPS) and were used to perform simple calculations. Today, just 7 years later, machines are performing at 76 MIPS and cost about the same as the mid 1980s systems. This has placed desktop workstations in the same performance class as the large mainframes.

Software Migration Process

Westinghouse has experienced the computing evolution like many other corporations. Westinghouse has installed large central processors accessed via timesharing techniques, invested in personal computers and are now basing our development, testing and qualification of nuclear applications on workstations.

Migration from one platform to another is imperative to survive in the rapidly changing computing industry. Westinghouse has established a migration environment with several key elements that insure a Quality Assurance basis for its software. These elements include a software development life cycle process, development standards and a uniform systems interface.

The software development life cycle process provides an organized method for developing, testing and maintaining applications. The life cycle process is characterized by the following phases:

- o Preliminary Evaluation
- o Functional Specification
- o Software Design
- o Software Implementation
- o Software Verification
- o Release for Production/Acceptance Testing

The hallmark of this process is the rigorous application testing. Each application is validated for a specific range of calculations. This range is modelled in a series of applications tests called a "test matrix". Each time an application is modified or migrated to another platform, the test matrix is executed and checked against reference QA results. This process of testing each application and verifying against previously validated results maintains the Quality Assurance basis for our software.

The ability move between platforms to take advantage of computing technology advances has prompted Westinghouse to adopt software standards. These software standards insure maximum portability while

maintaining the software Quality Assurance basis. Standards have been developed for application software, utility packages and system dependent utilities. The application software standards include ANSI 1977 FORTRAN Full Language Standard, naming conventions, variable initialization, FORMAT statements, alphanumeric data handling, data packing, array subscript usage, file handling, data types, etc.

Software utility packages, adhering to the above standards, provide a repository for commonly used programs. This technique avoids duplication of software by each application. Finally, a uniform interface between the applications and the operating system centralizes all system dependencies.

The software development life cycle process, standards based software development and the uniform system interface technique are essential elements of a migration environment. These processes and standards greatly reduce the effort in migrating to other platforms.

Platform Implementations

The development of a computer infrastructure, standards and a software development life cycle enables Westinghouse to move efficiently between platforms. In the fuel design arena, Westinghouse supports four

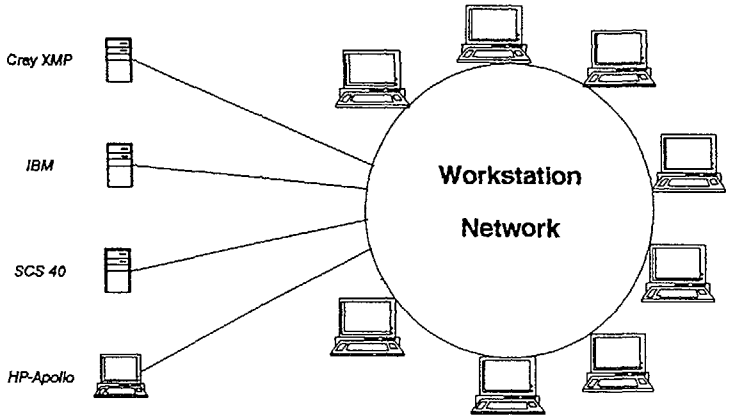

FIG. 2. Westinghouse CNFD software development network.

platforms (Figure 2) from their software development network. Platforms include specific operating systems for Cray, IBM, HP-Apollo and Scientific Computer Systems.

The software development and delivery process (Figure 3) was developed to ensure that all nuclear application software is developed and released consistently for all platforms. The software repository resides on the workstation where initial development is performed.

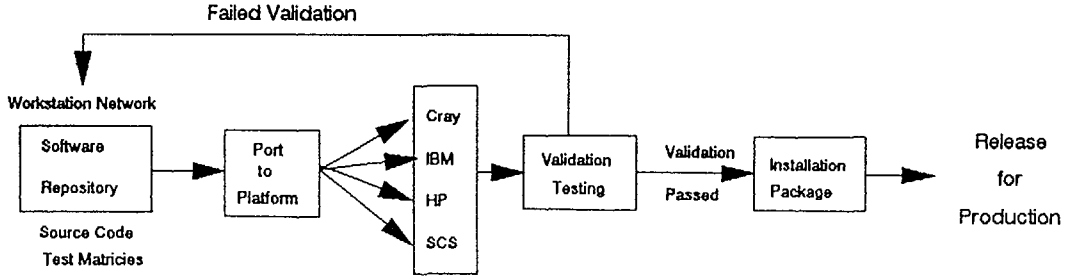

FIG. 3. Software development and delivery process.

After successful testing of modifications to an application, the source is generated for all supported platforms and tested in each environment. If any testing fails, changes are made to the applications in the software repository and retested on each platform. After all validation is successfully competed, software is then released for production.

The software delivery process uses the software life cycle, standards and uniform system interfaces as the basis for applications development and maintenance. This process insures that only one copy of the source is maintained for each application. This technique has improved our ability to maintain applications and has enhanced the portability of our nuclear software.

Workstation Hardware

The impact of workstations on the computing industry has been tremendous. Nuclear calculations that were only capable of being solved on mainframes can now be performed by smaller computers. Although these computers are physically smaller, their power is extremely impressive and their price/performance ratio is outstanding.

Westinghouse benchmarks many computers as a means of targeting platforms for development and to illustrate the performance of our applications in differing computer and operating system environments. Figure 4 shows benchmark results for the Westinghouse Advanced Nodal Code nuclear application. The benchmark is a representative analysis core consisting of 15 depletion steps for a Westinghouse four loop reactor. As can be seen, there is a wide spread on performance with a range of acceptable results for intermediate minicomputers to workstations. Until recently, this performance comparison chart only contained large mainframes and mini-computers. Last year, the Hewlett Packard (HP) 400 system made the chart and the recently announced HP 700 series computers' has broken into the elite group of computers rivaling Cray and IBM computers. Performance is only one component in selecting an implementation platform. Comparing costs in these differing environment provides the most dramatic improvement in computing. Mainframes and mini-computer

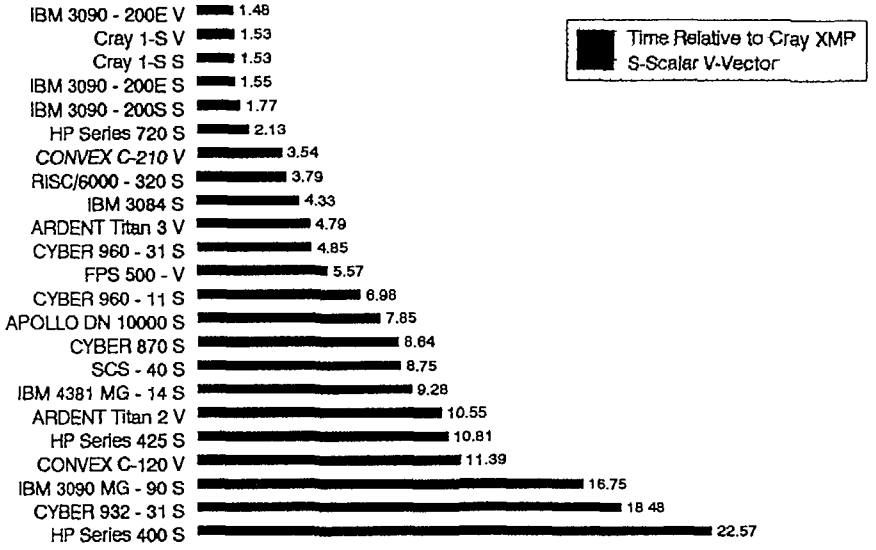

FIG. 4. 2D ANC benchmark results.

costs range from $100,000 to $1,000,000 and even higher. The typical workstation configuration, consisting of a 19" color graphics monitor, 16 megabytes of memory and 400 megabytes of disk, costs between $15,000 and $20,000. This price breakthrough has driven the cost/MIP to below $300.

Conclusion

Workstations are providing performance and price improvements that place significant power on the nuclear designers desk. There now exists a computer platform that will foster development of computer aided design applications for nuclear fuel management. Taking advantage of these improvements can only be possible with an infrastructure that provides a Quality Assurance basis for software applications. Software Development life cycle process and standards play a significant part in providing this Quality Assurance basis. Clearly the computing evolution has and will continue to impact the development of fuel management applications.

VERIFICATION OF KARATE: KALININ CYCLE-1

M. MAKAI, M. TELBISZ
Central Research Institute for Physics,
Budapest, Hungary

Abstract

The KARATE program system has been constituted to calculate WWER-1000 units. Test results obtained for the first fuel cycle of NPP Kalinin are given, including: the boron let down curve, k_q distributions at 17 and 235 full power days, outlet temperature distributions and a few axial power distributions. The calculated distributions suit well to the experimental results.

1.AVAILABLE MEASUREMENTS

Cycle 1 of Kalininskaya Power Plant's unit 1 has been proposed [1] for testing fuel cycle calculations of VVER-1000 type reactors. The available information concerning the operational history originates from the below given sources:

-a file [2] distributed in the TIC;
-a test problem specification [1] proposed on the XIX. Symposium of TIC;
-calculations [3,4] reported on TIC and IAEA meetings.

In Ref.[2] pointwise measured data have been given at 35 time points of the burnup cycle. The data include control rod positions, thermal powers, coolant flow values, boron concentrations and (core) inlet coolant temperatures. Comparing the powers of the time steps to the also available full power day values we have concluded that the available data refer rather to a given time point than to averages over time steps. The cycle history slightly differs in diverse sources that may indicate a posteriory introduced corrections on the measured data. In order to preserve the most important reactivity effects, a new history has been derived from the data. The power has been calculated from the given full power days (fpd) and from the given time. The values in Table 1 ,which show the history of the first burnup cycle, represent the values at the left of the given time interval.

In Ref.[2] not only the history but also outlet temperatures at T= 17 and 105 fpd are given, along with axial power profiles measured by self powered neutron detectors (SPND).

In Ref.[3] k_q distributions at T=17 and 235 fpd are given without specifying if the experimental values refer to SPND or thermocouple measurements.

Table 1.History of the Kalinin-1 first burnup cycle

No.	Power (MW)	Rod position (cm)	Burn-up (fpd)	Time (day)	T_{in} (C^o)
1	1450	195	0	0	280
2	1060	241	6.4	13.2	280
3	1500	224	11.5	27.6	282
4	1590	188	19.2	43.0	282
5	1560	259	27.5	58.7	282
6	2220	263	39.4	81.6	286
7	1380	266	47.3	92.3	286
8	2040	277	50.8	99.9	285
9	1650	245	58.1	110.6	284
10	2040	245	58.8	111.9	285
11	510	178	70.5	129.1	285
12	1710	266	72.0	137.9	285
13	1860	266	74.5	142.3	285
14	2370	266	84.6	158.6	286
15	2400	273	103.2	182.1	286
16	2370	256	123.5	207.5	286
17	1980	273	130.4	216.2	282
18	2310	252	132.7	219.7	287
19	2370	273	142.2	232.1	286
20	1740	234	154.8	248.0	285
21	2790	284	165.7	266.8	287
22	3090	316	180.2	282.4	287
23	1020	238	197.2	299.5	282
24	3090	291	200.0	340.3	287
25		284	235.3	340.3	287

In Ref.[4] k_q distributions at T=17 and 235 fpd are given both for SPND and thermocouple measurements. Axial distributions at different burnup values are also given but without specifying the assembly, in which the axial profile has been measured.

Neither T=17 fpd nor T=105 fpd occurs in our history as can be seen from Table 1. Hence the distributions to be compared to the experiments are taken at T= 27.5 fpd (instead of 17 fpd) and at T= 103.2 fpd (instead of 105 fpd). The error introduced this way must generally be negligible, although the error of the axial distributions is certainly larger than that of the outlet temperatures due to the difference in control rod positions.

2.CALCULATIONAL METHOD

The calculations were performed with the help of the KARATE system [6] developed at the Central Research Institute for Physics (KFKI). KARATE is able to model the neutron physical and thermal hydraulics processes taking place in the core of a VVER-1000 at normal and slow transient conditions.

KARATE involves three levels: cell, assembly and global levels. On the cell level the multigroup transport equation (TE) is solved in a cell, and the output cell averaged few group (i.e. 2 or 4 group) constants are placed in a suitable library. On the assembly level the few group diffusion eqation (DE) is solved for an assembly made up from homogeneous regions. Here a portion of the assembly's surroundings is also taken into account. The output of this level consists of assembly averaged cross-sections, organized in a suitable library. The power distribution and the burnup are calculated at the third, so called global level. The flux distribution is calculated by response matrix (RM) iteration. The RM's of a given assembly are calculated by means of analytical solutions to the DE in the given assembly.

The thermal hydraulic feed back is taken into account so that in the neutron physical calculations the thermal hydraulics variables (moderator density and temperature, steam fraction) are taken as parameters, and are calculeted by an adopted COBRA algorithm from the power distribution. The power distribution, moreover, is calculated in the neutron physical calculation with fixed thermal hydraulics parameters. Thermal hydraulics and neutron physical calculations are organized in a loop.

Reflector and structural materials around the core are described by albedo matrices. Also albedo matrices are utilized at the top and bottom of the core.

3.ADJUSTMENT OF PROGRAMS, ASSUMPTIONS

No adjustment has been made in the KARATE sytem although because of some lacking information we resorted to the assumptions as follows:

- -the structure of the space above and under the core is not known. In both cases α_g= 6 cm extrapolation distance has been taken.
- -the structure of the assembly at the end of the absorber rod is not known. After the end of the rod water is assumed.

The calculations were performed in a 60-deg sector (with 34 assemblies) and 14 axial mesh points were taken.

4.RESULTS

The boron let-down curve is shown in Fig.1. The measured values along with the BIPR-7 calculations originate from Ref.[4]. BIPR-7 apparently underestimates the boron concentration everywhere but at the fresh core. KARATE slightly overestimates the first two values but shows a fairly good agreement with the measured values. At 200 fpd KARATE seriously overestimates and

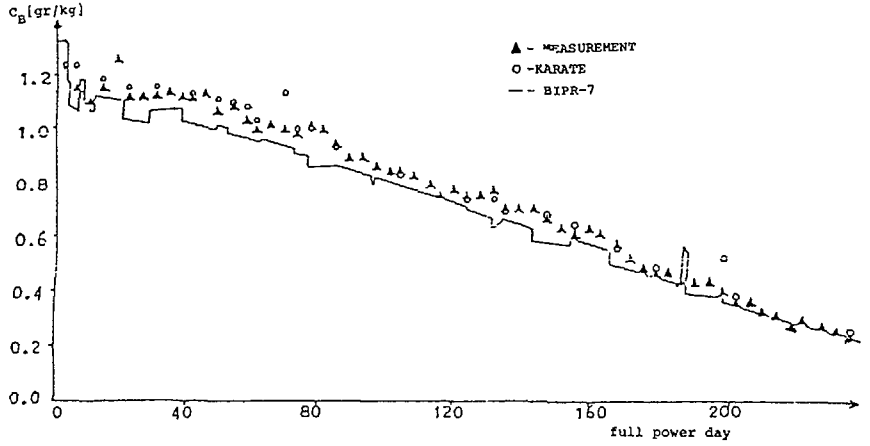

Fig.1. Comparison of boron concentrations
/Cycle 1 of Kalinin Unit 1/

the same effect can be observed with BIPR-7 though there the overestimation occurs 20 fpd earlier. The reason must be a reactivity effect having displayed in the models but not in the measurements. Such a reason may be a power change not represented in the given history.

Figure 2 compares the measured and calculated k_q distributions in a 30-deg sector at 27 fpd. The measured values are taken from Ref.[4]. Though neither the experimental methodology (the derivation of k_q from the measurements) nor the experimental error is known, the distribution calculated by KARATE seems to agree with the measurements within the presumable experimental error.

Figure 3 shows a similar comparison at 235 fpd, close to the end of the burnup cycle. Here considerable differences can be observed at positions 4, 8, 13, 18 and 19. Yet the measured values enclose the values calculated by KARATE at positions 2,3,5,6, and 19. The calculation seems to agree better with the SPND measurements than with the thermal measurements. There is a considerable difference between the SPND and thermal measurements as well.

Fig. 4 and 5 shows the measured and calculated energy release at 17 fpd and 105 fpd, respectively. The coordinate of the displayed assembly is 23-08. The good coincidence at the inner points of Fig.4 and the deviations at the first and last axial points may indicate the inadequacy of the extrapolation distances at the top and bottom of the core. It is very difficult

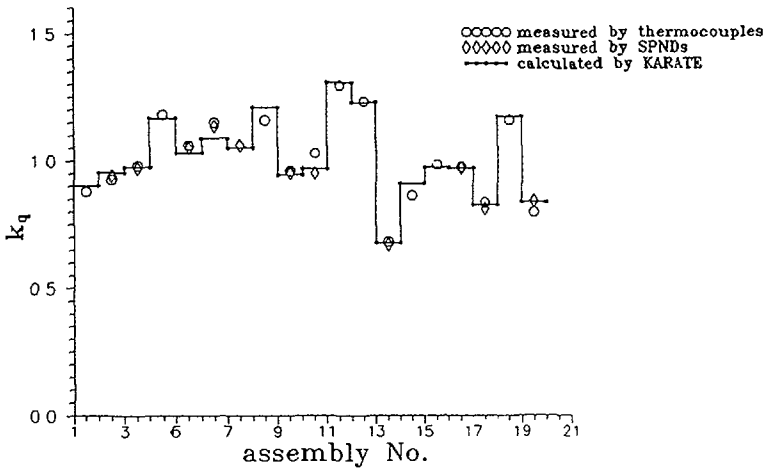

Fig. 2. k_q distribution comparison
T= 27 fpd W=1560 MW H_{10}= 259 cm

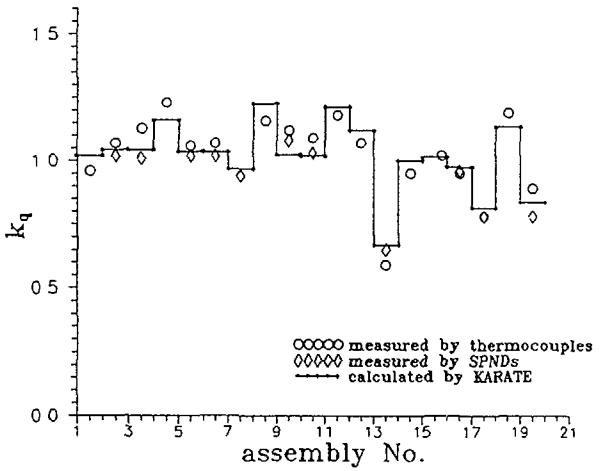

Fig.3. k_q distrubution comparison
T=235 fpd W=3040 MW H_{10}=284 cm

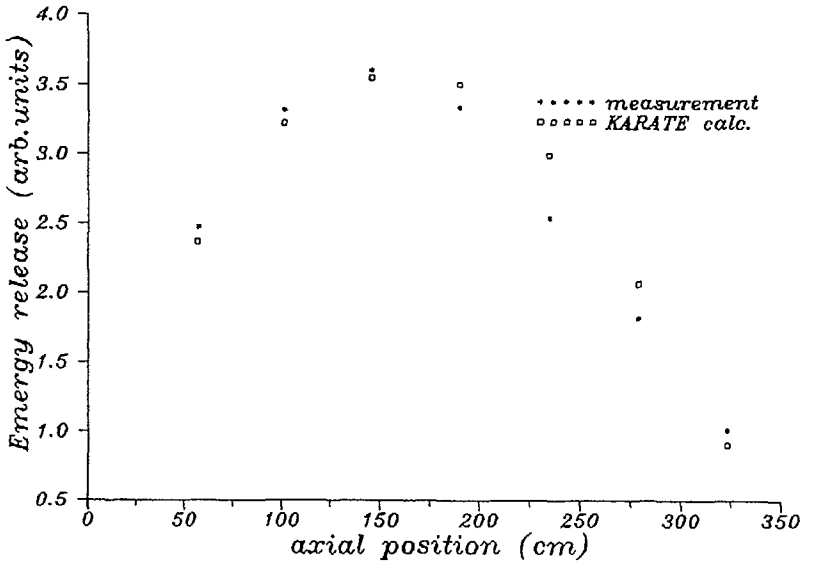

Fig. 4. KALININ 1/1 axial power 17 fpd
Assembly 23-08

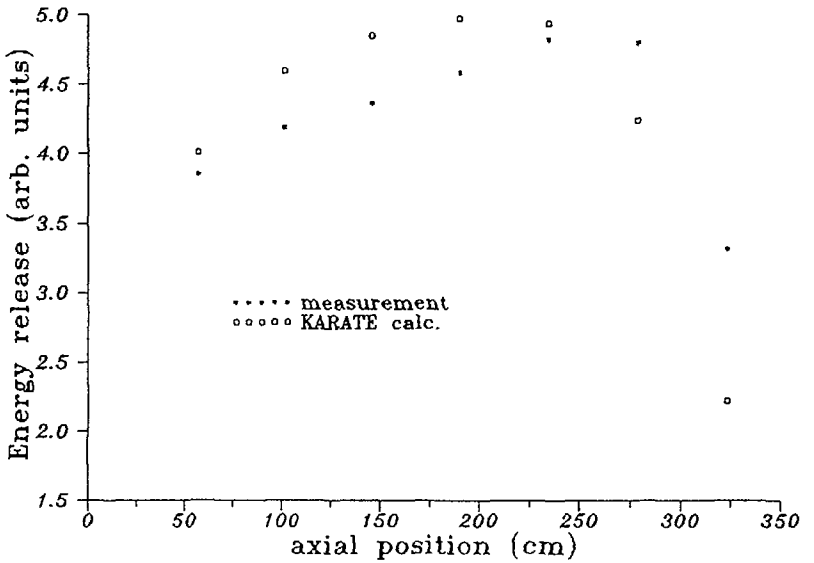

Fig 5 KALININ 1/1 axial power at 105 fpd
Assembly 23-08

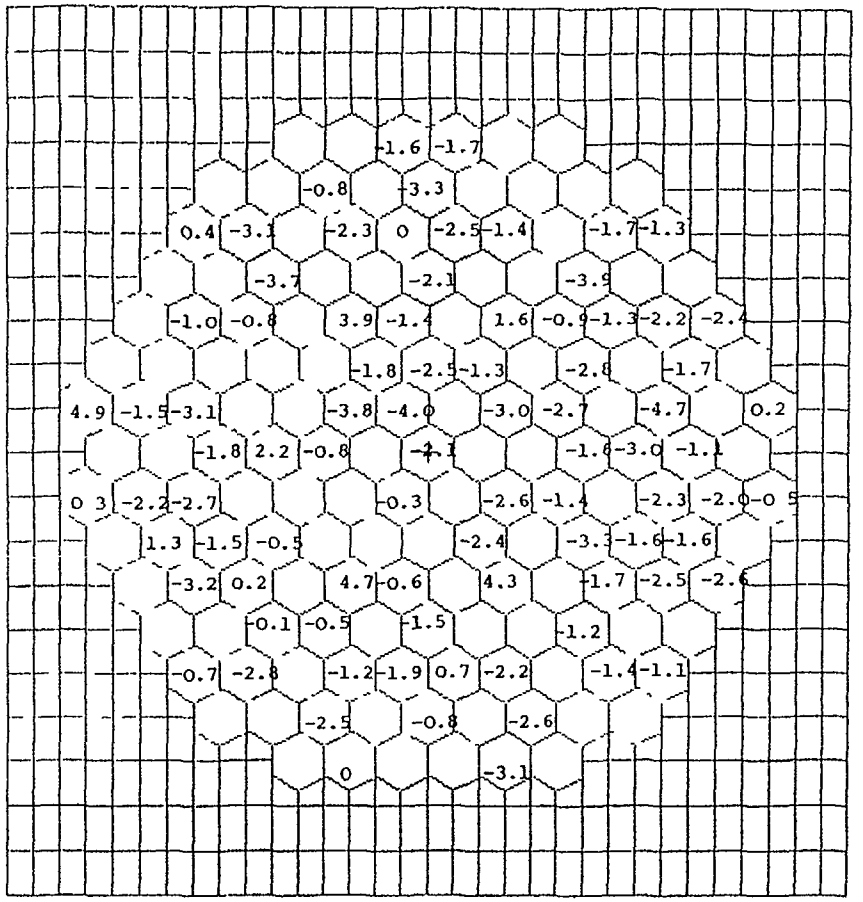

Fig. 6. Difference of Calculated and Measured Outlet Temperatures at 17 fpd

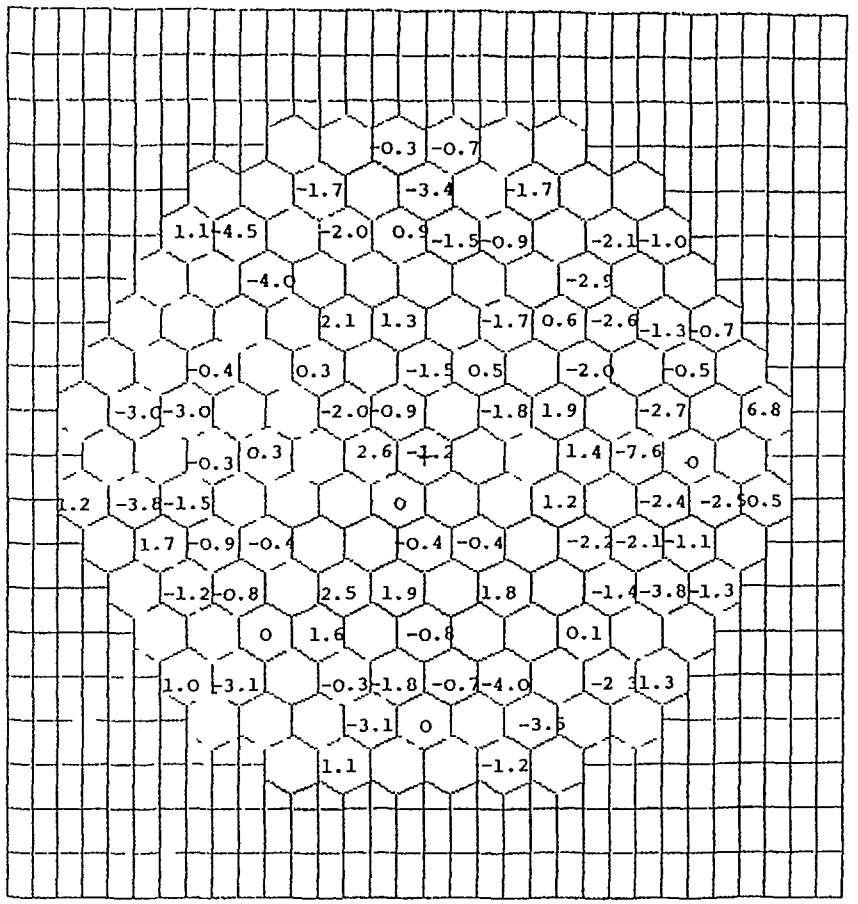

Fig. 7. Difference of Calculated and Measured Outlet Temperatures at 105 fpd

to say anything about Fig. 5. The axial shape suggested by the measurements is unrealistic and the calculated shape bears no resemblence to it. It should be pointed out that after comparing the measured and calculated distributions at every measured position the calculated and measured shapes are similar in general, the disagreement shown in Fig. 5 occurs only a couple of times out of the available 70 SPND measurements. In general the calculation agrees better with the measurements at 17 fpd than at 105 fpd. The reason, besides cumulating possible calculational errors, must be the cumulating uncertainty of the burnup cycle. It is known that rod position, local power and burnup all influence the local energy release and none of those quantities is known fully and certainly from the history.

Fig.6 and 7 shows the differences of calculated and measured outlet temperatures at 17 fpd and at 105 fpd, respectively. The maximal difference is 4.9 C° and 6.8 C°, respectively. Comparing measured values of symmetric positions we conclude the error of the temperature measurement must be somewhere about 2-3 C°. No significant deviation can be observed between the measured and calculated temperature distributions.

5. CONCLUSIONS

We have presented the first calculations by the KARATE system. The first burnup cycle of unit-1 of the Kalinin NPP has been calculated and the boron concentrations as well as the k_q values, axial shapes have been compared to measurements. The calculated boron concentrations agree fairly well with the measurements. The k_q distributions are also in accord with the measurements, though there the experimental values are sometimes contradicting. As to the axial shapes, the calculated shapes are not far from the measured ones in some cases and suggest corrections of the extrapolation distances at the top and bottom of the core.

REFERENCES

1. V. Saprykin et al. Benchmark Problems of Kalininskaya NPS, manuscript, 1990

2. The quoted file represents the conribution of USSR to the activity of the TIC working group called " тематическая группа по созданию информационного фаила эксплуатационных данных ВВЭР-440 и ВВЭР-1000" (group establishing information file on operational data of VVER-440 and VVER-1000). The file was distributed on the meeting of the group in Sofia.

3. A. A Suslov et al. Core Characteristics of Kalinin NPP Unit 1, p. 267-284, Proc. XIX. Symposium of Temporary International Collective (TIC), Siofok, Hungary, 1990

4. A. N. Novikov et al.: Problems of VVER In-Core Fuel Management, Proc. In-Core Fuel Management Practices Mtg., IAEA-TECDOC-567, p.325, Vienna, 1990

5. J. Gado. State of Calculational Complex KARATE, Proc. XVIII. Symposium of TIC. 1,175, Prahatice, CSSR, 1989

VALIDATION OF FUMACS CODE PACKAGE

B PETROVIĆ*, D. PEVEC**, T ŠMUC*, N URLI*

*Ruđer Bošković Institute
**Faculty of Electrical Engineering,
Zagreb University

Zagreb, Yugoslavia

Abstract

The FUMACS code package (an acronym for FUel MAnagement Code System) was developed at Ruđer Boškovic Institute with the aim to enable in core fuel management analysis of PWR core FUMACS encompasses computer codes PRELEO, PSU LEOPARD/RBI and MCRAC/RBI The computer code PRELEO is designed to fully automate preparation of input for the PSU LEOPARD/RBI code PSU LEOPARD/RBI is based on the PSU LEOPARD code with several options added, including the method to model integral fuel burnable absorbers The group constants generated by PSU LEOPARD/RBI are used to perform global reactor calculations using the MCRAC/RBI code MCRAC/RBI is improved version of the MCRAC code, including burnup modelling on quarter assembly level and local power peaking factor prediction The code package is completely written in FORTRAN 77 standard and it runs on a personal computer (IBM-PC or compatible) The validation of the FUMACS code package was performed by comparison of FUMACS results with design parameters for the first eight reload cycles of NPP Krško core The differences between critical boron concentrations calculated by FUMACS and design data are typically within 30 ppm The differences in assemblywise power and burnup distributions are typically within 6%, and the difference in power peaking factor is typically within 3% The comparison showed that the FUMACS code package is the fast and reliable code system suitable for repetitive and numerous in core fuel management calculations

INTRODUCTION

FUMACS code package has been developed at Ruđer Boškovic Institute (RBI) for in-core fuel management analysis of NPP Krško core[1] It is based on PSU LEOPARD and MCRAC codes which are obtained from Penn State University in the frame of IAEA expert service These codes were constantly improved and modified to enable modeling of innovations which were introduced in PWR technology in the last decade The experience accumulated in applying these codes to in core fuel management calculations of NPP Krsko

core has shown that these codes can be used with satisfactory confidence level for scoping calculations and for loading pattern development In order to transfer codes to NPP Krško it was necessary to modify codes to make them more user-friendly and to automate the application to NPP Krško core The result of efforts to achieve these goals is the FUMACS code package

This paper gives a short description of the FUMACS code package and results of validation process performed for eight reload cycles of NPP Krško

FUMACS CODE PACKAGE

FUMACS code package consists of the preprocessing code PRELEO, the cross section generating code, PSU-LEOPARD/RBI, and two-dimensional diffusion code, MCRAC/RBI The PRELEO code prepares ready-to-execute PSU-LEOPARD/RBI input data file PSU-LEOPARD/RBI generates a library of cross sections for various fuel types, represented by polynomial coefficients depending on burnup and boron concentration

The FUMACS code package is written in FORTRAN 77 and may be easily adapted for various computers The current version, V91 1, runs on personal computer(PC) The structure of the FUMACS code package is depicted in Figure 1

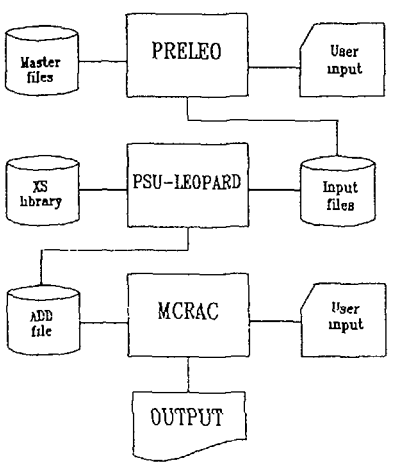

Figure 1 FUMACS code package organization

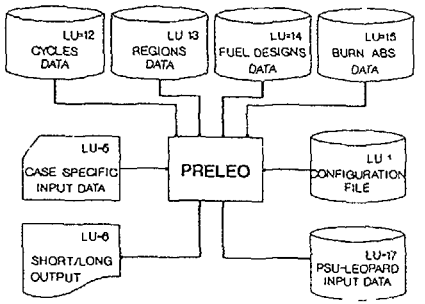

Figure 2 PRELEO input/output file organization

PRELEO

PRELEO[2] is a computer code for automated generation of PSU-LEOPARD/RBI input data files for NPP Krško fuel Attached to the code are four master files, containing all the relevant data about fuel design, fuel batches, cycles, burnable absorbers, etc , for the NPP Krško core The user specifies only the most basic data about the fuel depletion history, and PRELEO generates a complete, ready-to-execute, PSU-LEOPARD/RBI input data file The PRELEO code input/output organization is given in Figure 2

PSU-LEOPARD/RBI

PSU-LEOPARD/RBI[3] is improved version of PSU-LEOPARD code[4,5], which is developed at Penn State University PSU-LEOPARD code incorporates options to fit the group constants by polynomials in burnup and soluble boron concentration The polynomial coefficients are stored in a file called an ADD (Assembly Data Description), providing a complete set of group constants for automated fuel assembly depletion, in the format compatible with MCRAC code

The improvements and new features developed at RBI which are included in PSU-LEOPARD/RBI are.

- modeling of burnable poison rods and integral fuel burnable absorbers (IFBA)[6], numerically more stable polynomial fit,
- flexible output control, depletion restart option

MCRAC/RBI

MCRAC/RBI[7] is improved version of MCRAC code[8,9], which is developed at Penn State University MCRAC performs global analysis of PWR core using ADD file generated by PSU-LEOPARD

MCRAC/RBI Version 91 1 is specially developed to perform in-core fuel management calculations of NPP Krško core. The main characteristics of this version are

- core modeling by following separately quarter fuel
  assembly burnups,
- unfolding of core loading from quarter core level to
  full core level,
- pin-power reconstruction,
- simplified input structure,
  diversified output levels,
  fuel assembly interchange option including "rotations"

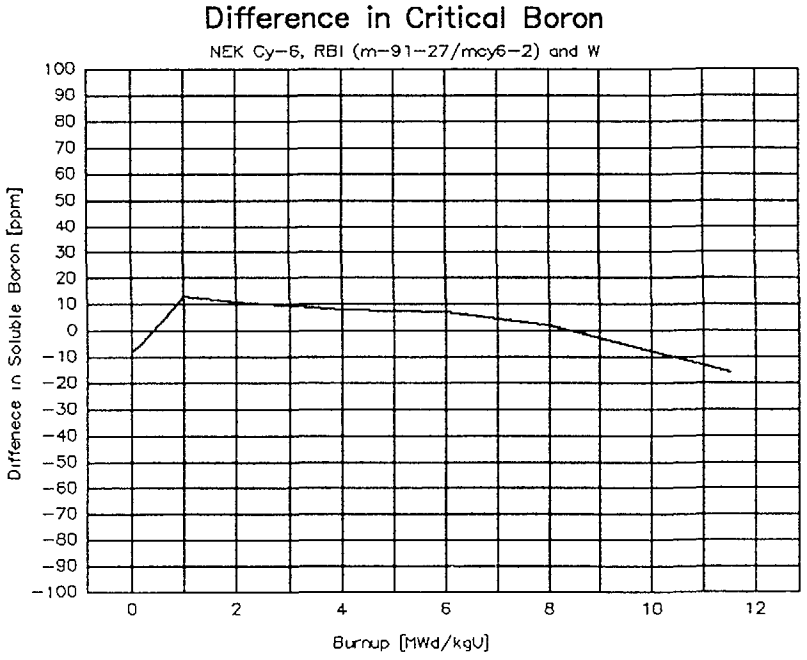

Figure 3 Difference in critical boron vs burnup for NPP Krško, cycle 6

FUMACS VALIDATION

The validation of the FUMACS code package has been made against operational data for cycle 2 to cycle 9 of NPP Krško The results for nominal conditions were compared with data from Westinghouse core design reports The parameters compared include critical soluble boron concentration, average and peak power and burnup per assembly during each cycle Differences in concentration of soluble boron, power peaking factor, and average fuel assembly power throughout cycle 6 of NPP Krško are depicted in Figures 3 to 5 EOC burnup difference distribution is given in Figure 6 A summary of the difference intervals for eight reload cycles of NPP Krško is given in the Table 1 and Table 2 The critical soluble boron differences are typically within 30 ppm The differences in assemblywise power and burnup distributions are typically within 6 %, and the difference in power peaking factor is typically within 3% The validation has shown that FUMACS code package can be used for performing in-core fuel management analysis of NPP Krško, even when complex loading patterns are considered

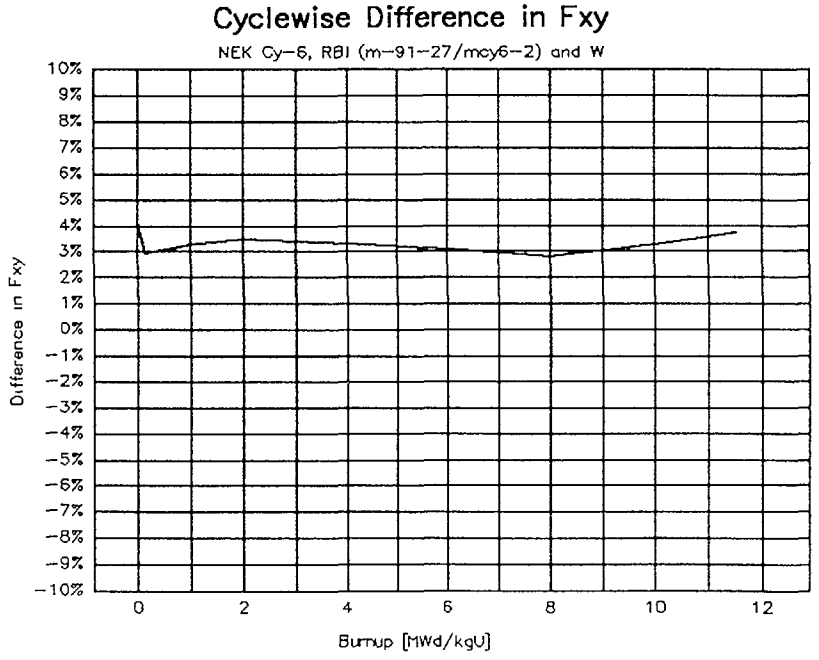

Figure 4 Difference in power peaking factor vs burnup for NPP Krško, cycle 6

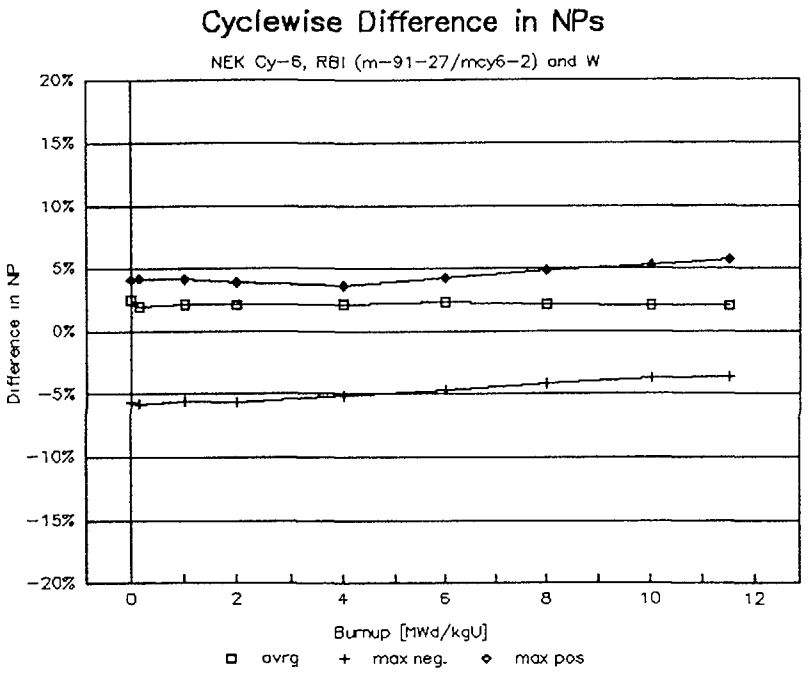

Figure 5. Difference in normalized power vs. burnup for NPP Krško, cycle 6

13476 13710 -1.7	12525 13048 -4.0	11792 12286 -4.0	15145 14612 3.6	12411 12712 -2.4	13742 13426 2.4	5732 6083 -5.8
12541 13061 -4.0	12389 12700 -2.4	12814 13108 -2.2	12462 12768 -2.4	13619 13481 1.0	13115 12969 1.1	6161 5987 2.9
11866 12355 -4.0	12860 13148 -2.2	11483 11824 -2.9	14664 14172 3.5	12800 12762 0.3	11287 10866 3.9	
15177 14636 3.7	12482 12787 -2.4	14674 14206 3.3	11904 12293 -3.2	12754 12693 0.5	5184 5223 -0.7	
12423 12732 -2.4	13632 13503 1.0	12810 12797 0.1	12757 12713 0.3	7533 7251 3.9		
13750 13460 2.2	13123 12993 1.0	11292 10887 3.7	5185 5229 -0.8			
5734 6090 -5.8	6165 5997 2.8					

Legend:

A B C

A FUMACS EOC burnup in MWd/tU
B Reference EOC burnup in MWd/tU
C Relative difference in %

Figure 6. Comparison of FUMACS and reference EOC burnup distribution for NPP Krško, cycle 6

Table 1

Cycle Number	Difference interval in boron concentr. (ppm)	Difference interval in power peaking factor (%)
2	(-15,+20)	(-1.5,+1.5)
3	(-10,+20)	(-0.0,+3.0)
4	(+30,+65)	(-1.0,+1.0)
5	(-25,+5)	(-1.0,+6.0)
6	(-15,+15)	(+3.0,+4.0)
7	(-10,+20)	(-1.0,+3.5)
8	(-50,+10)	(+2.5,+4.0)
9	(-10,+50)	(-1.5,+0.5)

Table 2

Cycle Number	Difference interval in normalized power (%)	Difference interval in EOC burnup (%)
2	(-6.0,+6.0)	(-5.8,+6.1)
3	(-6.0,+9.0)	(-4.7,+6.1)
4	(-9.0,+11.0)	(-7.1,+8.3)
5	(-5.0,+7.0)	(-4.6,+5.0)
6	(-6.0,+6.0)	(-5.8,+3.9)
7	(-5.0,+6.0)	(-8.7,+6.1)
8	(-9.0,+8.0)	(-4.0,+7.0)
9	(-6 0,+7.0)	(-3.7,+4.1)

CONCLUSION

FUMACS is simple, easy to use code package, developed for in-core fuel management calculations of NPP Krško core. It provides very simple preparation of input data, easy loading pattern search, and automatic generation of reports (extensive output information). The extensive validation has been performed by comparison of parameters with reference data for first eight reload cycles of NPP Krško. The differences between obtained results and reference data show that the FUMACS code package is the fast and reliable code system suitable for repetitive and numerous in-core fuel management calculations.

REFERENCES

(1) NPP Krško Final Safety Analysis Report, Westinghouse Electric Company (1978).

(2) B. G. Petrović and D. Pevec, "PRELEO - PC Preprocessor code for PSU-LEOPARD/RBI: User's Guide," Ruđer Bošković Institute (1991).

(3) B. G. Petrović, D. Pevec, and T. Šmuc, "PSU-LEOPARD/RBI, Version 91.1: User's Guide," Ruđer Bošković Institute (1991)

(4) S. H. Levine and S. S. Kim, "PSU-LEOPARD: User's Manual," The Pennsylvania State University, Breazale Nuclear Reactor (1984).

(5) D. Pevec, "IN-CORE FUEL MANAGEMENT: PWR Constants Generation Using PSU-LEOPARD Code", Workshop on Reactor Physics Calculations for Applications in Nuclear Technology, p. 328-359, World Scientific Publishing Company, Singapore (1991).

(6) D. Pevec and S. H. Levine, "Modification of LEOPARD to Calculate IFBA Depletion Cross Sections," Trans. Am. Nucl. Soc., Vol 56, 551 (1988)

(7) B. G. Petrović, D. Pevec, and T. Šmuc, "MCRAC/RBI, Version 91.1: User's Guide," Ruđer Bošković Institute (1991)

(8) H. Y. Huang, J. P. Colletti, Z. H. Kodah, and S. S. Kim, "User's Guide: MCRAC - Multiple Cycle Reactor Analysis Code," PSBR-315-497991, The Pennsylvania State University, Breazale Nuclear Reactor (1981).

(9) B. G. Petrović, "IN-CORE FUEL MANAGEMENT: PWR Core Calculations Using MCRAC Code" Workshop on Reactor Physics Calculations for Applications in Nuclear Technology, p. 360-398, World Scientific Publishing Company, Singapore (1991).

SAFETY ASPECTS OF VVER REACTOR CORE DESIGN AND ŠKODA COMPUTATIONAL SYSTEM

J. ŠVARNÝ, V. KRÝSL, P. MIKOLÁŠ, J. VACEK
Škoda Plzeň,
Plzeň, Czechoslovakia

Abstract

The paper presents the main principles and safety criteria stipulated in the Regulations of the Czechoslovak Atomic Energy Commission and methodology of the Final Safety Analysis Report with the emphasis to the normal operation and impairment of normal operation. The code system that is used in Skoda Plzen for reactor safety analysis for VVER - type reactor is described and brief description of VVER core and its mechanical design with basic project principles is given.

INTRODUCTION

In Czechoslovakia, there are now 8 VVER-440 reactors in operation and 4 VVER-440 and 2 VVER-1000 reactors under construction. Safety characteristics of VVER-440 reactor are more conservative than those of VVER-1000 and neutron-physical characteristics of VVER-1000 reactor with three-year fuel cycle meet the level corresponding to characteristics of modern large power reactors. Therefore, this paper deals only with the VVER-1000 reactor.

DESCRIPTION OF THE VVER-1000 REACTOR CORE

The VVER-1000 reactor core consists of 163 hexagonal fuel assemblies with fuel height equal to 355 cm and equivalent diameter of 316 cm.

The boron alloy burnable absorber rods are used to achieve the acceptable power peaking and to ensure the negative temperature coefficient of reactivity. 18 burnable absorber rods are inserted into the control absorber guide tubes of the most enriched (4.4%) fresh fuel assemblies. After the first year of operation they are removed from the assembly during refuelling.

To foster the power flattening, some of the fuel assemblies are profiled, i.e. 66 peripheral fuel rods are replaced by the rods with lower enrichment.

Reactivity is controled by 61 control absorber clusters. Each cluster consists of 18 absorber rods moving within thimble guide

tubes under control of the individual drive. Clusters are grouped into ten groups. The tenth group is the operating one, the fifth group consists of part length absorber rods and is used to control axial power distribution during Xenon transients.

SAFETY ANALYSIS REPORTS FOR THE VVER

The Rules [1] of the Czechoslovak Atomic Energy Commission (CAEC) require that each application for the construction permit of a nuclear reactor facility include a Preliminary Safety Analysis Report (PSAR) and each application for the operating license is accompanied by a Final Safety Analysis Report (FSAR).

In the 80's, the CAEC issued a series of the Safety Guides specifying in general terms the contents of the Safety Analysis Reports (SAR). The Guides are updated so that they reflect the current developments in the nuclear technology and reactor physics. Each edition is approved by the CAEC board.

The department of Physics of the Skoda Works Nuclear Engineering Plant is responsible for the Volume 3 of the SAR which deals with the reactor physics aspects of the reactor safety in normal, abnormal and emergency operating conditions. This volume contains the information relevant to the other SAR's volumes covering the thermohydraulic aspects and accident analyses.

Some of the safety considerations incorporated into the VVER-1000 core design are summarized in the this section.

An ultimate objective of nuclear fuel design is to produce nuclear fuel that will not release fission products to the primary coolant under any conditions of normal operation [1]. This is assured by the first general design fuel cladding integrity criteria [2,3]:

a) No more than 1 percent of the fuel elements can have defects of gas leakage type.
b) No more than 0.1 percent of the fuel elements disrupture with pellet - coolant contact.

These limits are defined only from the point of view of operation and repair. In reality, the probability of the occurence of such fuel element damages during VVER operation is lower than 0.007%.

For the accident with a rupture of the primary circuit (the maximum design breakdown), according to GRS the emergency cooling system must secure the following general design cladding integrity criteria:

a) The temperature of the cladding must be lower than 1200C.
b) The local depth of oxidation doesn't excceed 18 percent of the cladding thickness.
c) Chemical reaction Zr - H_2O doesn't exceed 1 percent of the total Zr mass.

The nuclear fuel design criteria require that the fuel is able to accomodate both normal operating transients as well as single component malfunections in the reactor control and protection system without loss of integrity. The malfunctions considered may be:

- failures in the reactor control and monitoring system,
- a loss of main circulating pumps feeding,
- an outage of the turbo-generator and heat removal systems,
- a complete loss of external power supplies,
- a leakage of the primary circuit which can be compensated by operational refilling systems.

Main fuel lattice parameters are fuel rod diameter, fuel rod pitch, geometry of the fuel rod lattice, and moderator/fuel ratio. Core design data for the VVER-1000 and a typical PWR of current generation are presented in Table 1.

Light water reactors of current generation are generally undermoderated at power operating conditions, because an under-moderated reactor has a negative temperature coefficient of reactivity and a higher conversion ratio, which improves the fuel economy. The moderator/fuel ratio of the $VVER_s$ and PWR_s is similar (or for $VVER_s$ little smaller then for many PWR_s).

Because diameter of the fuel rod in $VVER_s$ is smaller than in PWR_s, the fuel rod surface-to-mass ratio is higher. It causes an increase in the resonance absorption and a consequent decrease in k-inf of the $VVER_s$. Other consequence of the smaller rod diameter is the necessity of higher enrichment of the VVER fuel (4.4%). In the present VVER design the reload fuel enrichment is strictly determined and cannot be changed on the basis of the reqruirements of the cycle bein loaded like in the PWR projects.

As the fissile content of VVER fuel is higher than that of PWR fuel, the relative absorption in moderator decreases and the location of the k-inf maximum occurs at a higher moderator/fuel ratio, and also temperature coefficient of reactivity is more negative.

In VVER design, the fuel rod cladding (Zr + 1 % Nb) must accommodate thermal, pressure, and fatigue stress without failure in a high temperature and radiation environment for three years period. All these effects are both theoretically and experimntally explored.

In both normal and deviated from normal operating conditions the following criteria having a leading role in the core design must be fulfiled:

1. For operability of fuel elements, the criteria of strength are: the stability of cladding, the deformation criteria, and the acceptable crevice corrosion under stress in the presence of aggressive fission products. The last one is very important: A defect in the cladding /crevice/ accumulated during

Table 1. Comparison of the Main VVER and PWR Core Characteristics

		VVER	PWR
1.	Geometry of the fuel rod lattice	triangular	square
2.	Rod pitch, mm	12.75	>12.6
3.	Fuel rod outside diameter, mm	9.1	≥9.5
4.	Clad thickness, mm	0.69	0.57 (Fr.) 0.56-0.64 (West.) 0.64-0.72 (KWU)
5.	Pellet central hole, mm	2 4	-
6.	Composition of grids	steel	Zircaloy
7.	Core average active fuel height, cm	356	>356
8.	Height - to - diameter ratio	1.14	1.08... 1.14
9.	Number of guide thimbles per assembly	18	24
10.	Composition of guide thimbles	steel	Zircaloy
11.	Neutron absorber	B_4C	Ag-In-Cd
12.	Linear heat generation rate, KW/m	165.7	>170
13.	Power density, KW/ℓ	107	95--104
14.	Coolant pressure, MPa	15.9	~16

the cycle period must not exceed 60 μm in depth, with taking into consideration the permisible initial defect corresponding to 50 μm.

It is supposed that this criterium can be met during normal operation and predicted power transients only by minimizing deviations of the local power changes so that they should not exceed +13 percent of nominal values.

2. Temperature of the cladding should not exceed level about 400C.

   VVER cladding temperatures during normal operation are as follows:

cladding external surface	352C
oxide-metal layer	358C
cladding internal surface	416C

3. The diametral clearance between the fuel and cladding must be chosen so that during normal operation internal pressure doesn't exceed external pressure.

   After three years of operation the internal pressure reaches 16 MPa, which is equal to the pressure of the coolant. Maximum guaranteed permissible mean burnup value in most loaded element is 55.3 MWd/kgU. Design maximum burnup value after three years of operation is 54 MWd/KgU. Relatively high burnup limit is achieved by the presence of the central hole in the fuel pellet and small initial internal pressure (2MPa).

4. Fuel temperature must be more than 10 percent lower than the fuel melting point.

   The melting point of fresh fuel is ~3100C and for burnup 60 MWd/kgU it is ~2870C. During normal operation this criterium is fulfiled with 80 percent reserve.

5. The Departure from Nucleate Boiling Ratio (DNBR) must be greater then 1.15.

   In the actual VVER project under the most unfavourable combination of parameters deviations from nominal values the criterium for DNBR is fulfiled and reach value 1.19 (by both the Tong's and OKB Gidropress correlations). The 15 percent margin with confidence level of 95 percent is taken into account.

6. The power coefficient is a measure of the feedback that is associated with changes in power. In the VVER project, requirements of GRS[2] on negativity of the total power coefficient of reactivity are met in all critical states.

7. The last issue of GRS[4] requires the negativity of the temperature coefficient of reactivity ($\partial\rho/\partial T_M$) in all operating and start-up critical states. Negative value of $\partial\rho/\partial T_M$ in the VVER project is more suitable influenced than in the PWR project by the higher enrichment, leakage of neutrons from the core, and moderator/fuel ratio. Unfortunately, the prevailing effect of a soluble boron concentration causes that $\partial\rho/\partial T_M$ becomes positive in some critical states (e.g. during the reactor startup) This effect is closely connected with the chosen nonoptimal type of burnable absorbers made of boron alloy, high enrichment, and lifetime of the fuel cycle. The recommendation that each critical state must have temperature

higher than 260C enables to keep $\partial\rho/\partial T_M$ negative for the VVER core.

8 The shutdown margin is a design criterium requiring that the core should be subcritical at all times during the reactor operation with the most reactive control rod fully withdrawn This criterium is a weak point of the VVER project due to the relatively small worth of the control rods. At the end of the fuel cycle with zero boron concentration the VVER reaches secondary criticality after shutdown at temperature of 260C. During the accident with rupture of the main steam pipeline that causes quick decrease of the core temperature corresponding measures to avoid this secondary criticality are used.

One of the design values is the power peaking factor which is monitored by the in-core monitoring system.

In the fine-mesh calculations following nuclear factors are considered:

K_o - local heat flux nuclear power peaking factor (a ratio of the fuel rod maximum linear heat rate to the core average one);

K_r - fuel rod nuclear power peaking factor (a ratio of the fuel rod maximum specific power to the corresponding core average value).

Nuclear factors together with engineering safety factors establish restrictions for the core power peaking and are included into initial conditions for safety analysis

In the coarse-mesh calculations the analogues of K_o and K_r nuclear factors are

K_v - volumetric power peaking factor (a ratio of the discrete calculational element maximum power to the core average value),

K_q - radial power peaking factor (a ratio of the fuel assembly maximum power in the horizontal section of the core to the corresponding core average value)

Maximum design values of K_v and K_q factors are equal to 1.9 and 1 35 respectively.

The K_v or K_o limiting values depend on the core height and are established on the basis of the postulated LOCA accident.

The power limit equal to 44 8 KW/m is derived from the second general design fuel integrity criterium for cladding temperature to be less than 1200C. Then the maximum design value of K_o, and analogously also that of K_v , is determined by the relation

$$K_o^{max} = \frac{44.8}{\bar{q}_\ell \, K_N \, K_{eng}}$$ where $\bar{q}_\ell$, K_N , and K_{eng} are defined in Table 2.

The core power distribution control is based on neutron flux measurements using in-core instrumentation system and manual control of volumetric power peaking factor K_v , and axial offset value, AO, within the pre-set limits.

During load-follow operations and xenon oscillations the power-clad interaction (PCI) criterium is not explicitly checked. A strategy of power transient control aims to keep deviations in local power density in such way that should follow criterium number 1. An evaluation of the fuel design including possible combinations of chemical, thermal, irradiation, mechanical, and hydraulic interactions is not included into the Volume 3.

Table 2. Comparison of Design Safety Characteristics of VVER-1000 and South Texas PWR

	VVER-1000	South Texas NPS
1. Components of the fuel rod maximum linear heat rate		
1 1 Nuclear local heat flux power peaking factor, K_o	2.24	2.31
1.2. Engineering local heat flux safety factor including effect from power increase due to gaps between fuel pellets, K_{eng}	1.16	1.11
1.3. Uncertainty coefficient for determining and keeping reactor power, K_r	1 04	1.02
1 4. Maximum linear heat rate $\bar{q}_\ell$, KW/m	44 8	43 5
2. Components of the enthalpy rise factor in the subchannel		
2.1. Nuclear power peaking factor in the fuel rod, K_r	1.50	1.52
2.2. Engineering safety factor with account for non-uniformity of coolant flow distribution among the cells, K_{eng}	1.16	1.08
2.3 Maximum factor to calculate enthalpy rise in fuel rod cell	1 81	1 68

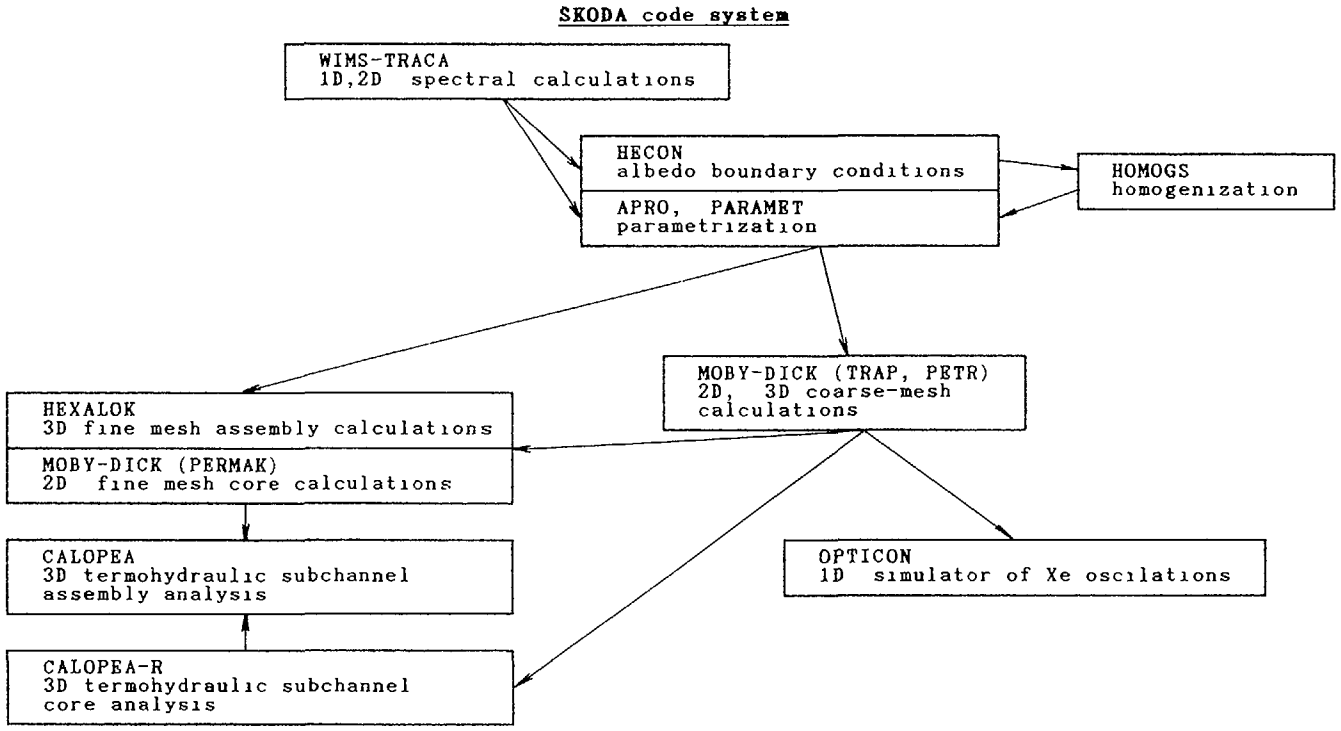

Fig.1. (physical and thermohydraulic codes for normal operation)

During coarse control (bank-bank), the value of axial offset is kept within its limits by part length rods. Control which assures suppression of power distribution xenon oscillations within the shortest period of time is realized. More refined power distribution control aimed at the minimization of the axial offset deviation (±5 %) from its stationary value is under development.

The main design safety characteristics of VVER-1000 and South Texas PWR, presented in Table 2, show that corresponding safety characteristics are comparable, the values of VVER safety factors being more conservative.

SKODA WORK'S CODE SYSTEM

The Skoda Work's system for physical and thermohydraulic calculation of VVER cores is presented in Fig.1. The backbone of this system, which is used for all SAR calculations, is a version of the WIMS code (WIMS-TRACA) used for the lattice calculations and original Skoda global core simular MOBY-DICK[7] based on the 3D coarse-mesh and 2D fine-mesh few-group difference diffusion approximation.

The code WIMS-TRACA[5] is used for the lattice calculations at a set of discrete lattice states that span the expected range of state variables. Both cell-averaged and assembly-averaged few-group diffusion constants can be produced for global reactor calculations. TRACA version was selected, as it allows region-wise homogenization and therefore several sets of data can be prepared simultaneously for different subregions of the modelled structure. For our calculational scheme it is also important, that we can model non-asymptotic cells by adding the extra region and average diffusion constants of the inner regions in the disturbed spectrum The applicability of WIMS to the preparation of few-group diffusion data for uniform and non-uniform lattices with control absorbers and water gaps was verified by the analysis of selected experiments[6].

The code HECON is a 1D code computing the heterogeneous constants by collision probability method. The calculations are performed in 10 groups with input data prepared by WIMS Resulting 2 or 4 group γ matrix coupling flux and current on the surface of the element, $J = \gamma \Phi$, is used to simulate boundary conditions in the coarse-mesh approximation of the MOBY-DICK code

HOMOGS is a few-group 2D finite difference diffusion code intended for the assembly homogenization. The fine-mesh diffussion constants obtained from WIMS and processed by the code PARAM or APRO are input to this code. The spectrum perturbations are modelled similarly as in WIMS by adding an extra region to the assembly and averaging the constants only over the volume of the assembly including the inter-assembly gap Advantage of this second stage homogenization is that code HOMOGS, in contrast to cylindrical model of WIMS, is able to treat the fuel assembly in the actual regular hexagonal representation

The correlation codes APRO and PARAM process the files prepared by WIMS in the form of few-group libraries based on the method of the least squares and perform search for the optimum regression polynomials While some parameters are separable, others are correlated and therefore mixed terms appear in resulting polynomials Up to now, the code has not been able to determine systematically the degree of the correlations and heuristic approach is used to select the appropriate combinations

MOBY-DICK[7] is a code system solving few-group diffusion equation It uses Borresen's modifications of the finite difference scheme by which averaged diffusion coefficient can be expressed like the geometric mean,

$$\bar{D}_{IJ} = \sqrt{D_I \, D_J}$$

Using the transformation

$$\Psi_I = \sqrt{D_I} \, \Phi_I \, ,$$

finite-difference equations can be written in a form allowing substantional reduction of computer memory and time The system allows to construct two computational paths

- triangular mesh with subdivision of the hexagonal mesh element to $6K^2$ triangles, used for 3D coarshe mesh core calculations,
- hexagonal mesh, used for 2D fine-mesh calculations of the layer of the core

Critical assemblies (i e the assemblies in which the safety margins could be violated) are usually determined on the basis of the three dimensional coarse-mesh calculation Pin-by-pin power distributions can then be determined by the code HEXALOK that performs a 3D fine-mesh diffusion calculations of the selected assemblies Non-homogenous boundary problem is solved, boundary conditions being determined on the basis of the preceding coarse-mesh core calculation

The code OPTICON is a 1D simulator of the Xenon oscillations during reactor operation The calculations are performed in 2 groups with input data prepared by MOBY-DICK. The code is intend ed for the quick analysis and preparation of recommendations for damping of axial xenon oscillations during start-up and normal operation of VVER-1000

Basic input data for coarse- and fine-mesh codes are parametrized in dependence on the burnup A, technological parameters V (fuel temperature, moderator temperature (or density), concentrations of soluble boron and Xe, Sm) and corrected by the instantaneous and the historical spectral corrections:

$$\Sigma = \Sigma^{AS} + K_v + K_{IN} + K_{IS} \qquad (1)$$

where Σ^{AS} = macroscopic cross section of the basic calculation (without spectral and V perturbations),
K_v = correction on perturbations of V,
K_{IN} = correction on instantaneous spectral perturbations,
K_{IS} = correction on historical spectral perturbations

Under spectral perturbation we understand the departure of the spectrum from the basic calculation and it is characterized by instantaneous spectral index (defined as the double ratio of epithermal to thermal flux) and historical spectral index (defined as the instantaneous spectral index averaged over the lifetime of the fuel element)

Shortly, preparation of the few-group library is realized in the folowing steps In the first step, one-dimensional spectral calculations (cell and supercell geometry) for nominal and perturbed spectra and technological parameters V are performed by the code WIMS Resulting equivalent cell constants are in next step processed by the codes PARAM (or APRO) into fine-mesh library of the form (1). With this library, the fuel assembly is homogenized by the code HOMOGS and homogenized data are then again processed by PARAM or APRO into coarse-mesh input libraries of global code MOBY-DICK in the form (1)

The program CALOPEA uses the subchannel analysis to predict thermohydraulic properties of the individual fuel assemblies and of the core in normal and transient operating modes. Program is based on methods employed in the code COBRA-III[9]. As inputs, coarse mesh (in case of CALOPEA-R) or fine-mesh (pinwise, in case of CALOPEA) power distributions created by MOBY-DICK, BIPR and HEXALOK, are used.

REFERENCES

1 Code of Regulations on the Nuclear Safety of Nuclear Facilities (in Czech), Prague, 1984

2 Общие положения обеспечения безопасности АЭС при проектировании, сооружении и эксплуатации (ОПБ-82), Энергоатомиздат, 1983

3 Правила ядернои безопасности атомных электростанции, (ОБЯ-04-74), Москва, Атомиздат, 1977

4 Общие положения обеспечения безопасности АЭС при проектировании, сооружении и эксплуатации (ОПБ-88), Энергоатомиздат, 1989

5 C Ahnert, J M. Aragones MARIA System A code Block for PWR Fuel Assembly Calculation, J E N 543, 1983

6 J. Vacek, P. Mikolas, J. Svarny, V. Krysl SKODA Computational System for WWER Reactors, Specialist Meeting on Advanced Calculational Methods for Power Reactors, Cadarache, France, September 1990

7 V. Krysl, M. Lehmann, J Machacek Theoretical foundations of a Modular Macrocode System "MOBY-DICK", Skoda Internal Report

8 А А Мараказов Методика расчета мощностеи кассет реакторов ВВЭР в двухгрупповом диффузионном приближении, Москва, 1977

9 D.S.Rowe· COBRA-III, A Digital Computer Program ... , BNWL-B-82 (1971)

PREWIMS-VVER: A WIMS-D/4 INPUT DATA PREPARATION CODE FOR VVERs

A. GONZALEZ-GARCIA, D. LOPEZ-ALDAMA,
D. MILIAN-LORENZO, C. ALVAREZ-CARDONA
Centro de Estudios Aplicados al Desarrollo Nuclear,
La Habana, Cuba

Abstract

The establishment of a fewgroup library requires the development of the different geometrical models to calculate the neutron and physical characteristics of the studied lattice In order to perform this work using the WIMS-D/4 code previous calculations and the preparation of the input data are needed. This is a tedious work liable to error

In this paper we describe the geometrical models developed to calculate a fewgroup constants library for VVERs lattices and also we show the relevant features of the PREWIMS-VVER code, which is able to prepare the WIMS-D/4 input data for different conditions

This work was under the International Atomic Energy Agency research contract 5701/RB.

1 INTRODUCTION

For the calculation of VVER lattices by means of WIMS-D/4 code, previous calculations and the preparation of input data for such code are needed This is a tedious work liable to errors. Therefore it is convenient to automatize this work in order to reduce the time for input data preparation as well the possibility of errors.

The PREWIMS-VVER module generates interface units containing input data for WIMS-D/4 code for different geometrical models considered for the calculation of neutron and physical characteristics of VVER reactors. For different conditions of temperature, boron concentration, fuel enrichment and lattice perturbations the module calculates.

- -Nuclear densities for basic materials and material mixtures
- -Water density as a function of temperature and pressure.
- -Dimensional expansions
- -Dancoff and Bell factors as a function of geometry, water density and resonance energies

This paper presents the PREWIMS-VVER general characteristics together with description of the geometrical and physical models considered Finally a sample problem is shown.

2. GEOMETRICAL MODELS.

For the definition of the geometrical models papers [1, 2] were taken as reference.

According to the VVER core structure five fundamental spectral cases were taken:

-Case K=1: Unperturbed fuel assembly.
-Case K=2: Perturbed with burnable absorbers fuel assembly.
-Case K=3: Perturbed with control absorbers fuel assembly.
-Case K=4: ARK assembly.
-Case K=5: Core + Reflector.

In all cases the cylindrization of hexagonal geometry is made assuring the volume equivalence.

These geometrical models are described below:

1) Unperturbed fuel assembly (K=1).

This model is used to describe unperturbed VVER-440 (VVER-1000) fuel assemblies for different typical UO2 fuel enrichment.

The model considers 10(14) annuli, 6(10) of them including fuel elements.The central annulus includes the homogeneized central tube and the last three annuli include the inner assembly water not considered into the elementary cells, as well as the assembly wall and water gap between assemblies. (fig.1)

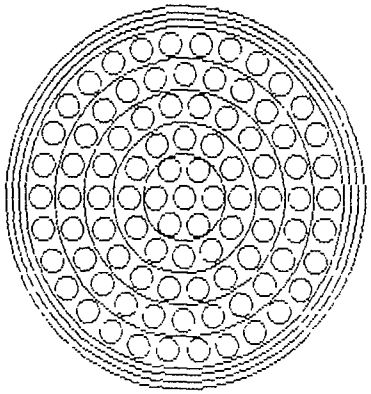

Fig.1. Case K=1. Unperturbed fuel assembly

2) Perturbed fuel assembly (K=2 and 3).

This type of fuel assembly is found in VVER-1000 reactors where control is made by means of clusters of absorber rods.

Fuel assemblies containing burnable absorber rods are also considered in spite of the actual assembly structure that does not includes such rods.

The main difference between this model and the former consists in that in this case rods with different material composition may be included in one annulus.

3) ARK type assembly (K=4).

The ARK supercell for calculations was set in correspondence with the VVER-440 core configuration . The ARK assembly was placed in the supercell center surrounded by its 6 complete nearest assemblies and the remaining of them was placed in the second neighborhood.

In this model 24 annuli are considered, the outermost annuli including fuel rods and the innermost ones 8 describe the ARK assembly containing its surrounding water.

4)Core + Reflector (K=5).

In this case a cylindrical model is also used and the core is divided into three regions. In principle these regions may have different enrichments (a mean value of 3.6 at% was taken). 11 annuli were used, the 3 first ones containing the fuel assemblies and the remaining ones describing the reflector up to the reactor vessel.

3. TRANSPORT SOLUTION.

In all cases the transport calculation is carried out using the multigroup Sn approximation. This option is available in WIMS-D/4 when the SEQUENCE 1 card is given in the prelude data. The number of transport groups and the order of the Sn approximation may be changed by the user in the PREWIMS-VVER input data.

4. PREWIMS-VVER MATERIAL LIBRARY.

The PREWIMS-VVER module has a basic material library. It includes values of material compositions for the different geometrical models. The geometrical models included represent the fuel assembly actual geometry, ARK assemblies, reflector as well as the density values (g/cm^3), the expansion coefficients and the number of isotopes for each material in VVER lattices. The expansion coefficient for UO2 in dependence of temperature is taken as described in [1].

A complete materials library for VVER is not available at present. For this reason some materials which should be taken from a VVER materials library were taken from a PWR materials library.

Standard values of material properties may be changed through input data giving NEWMAT (number of new materials in the library) a value different from zero.

Data for new materials introduced by NEWMAT are coded as followed:

J(L),L=1,NEWMAT Number of material L in the library.
N(L) Number of isotopes in material J(L).
RO(L) Density of material J(L) in cold condition.
AL(L) Linear expansion coefficient for material J(L).
AID(I,M) Identifier for isotope I in material M=J(L) in WIMS-D/4 code library.
FID(I,M) Nuclear density for isotope I in material M=J(L).

5. DIMENSIONAL EXPANSION.

The PREWIMS-VVER module calculates the changes in lattice dimensions arising from heating.

The algorithm of this module is based on methodology used in PREWIMS [1] code where it is assumed that :

-The lattice pitch increases according to the spacer grids material expansion for moderator temperature.
-The assembly pitch increases according to the expansion coefficient for shroud at moderator temperature.
-The fuel rod length does not change, assuming that gaps between fuel pellets are able to compensate for the linear expansion in axial dimension.

This algorithm consists in three steps:

1-Linear expansion (hot state dimensions calculations).
2-Volume expansion (volume fraction calculations).
3-Materials density change calculations.

The UO_2 density changes according to :

$$\Gamma_{UO2} = WUO2/\pi*RF^2*HF$$

The material density changes for remaining materials is calculated as:

Γ(hot state)=Γ(cold state)/linear expansion coefficient^3.

6. DANCOFF AND BELL FACTORS CALCULATION.

6.1. Dancoff and Bell factors calculations for fuel assemblies.

The PREWIMS-VVER module calculates the Dancoff factors considering the relative position of fuel elements inside the fuel assembly.

For the regular infinite lattice Dancoff factor calculation the module gives two possibilities:

-Dancoff factor calculation for infinite fuel regular lattice rod DANCR and for double step fuel lattice (central tube and control absorber rods) DANCV, using a similar methodology to the described in [3] and applied in [1].

- Dancoff factor calculation for regular infinite lattice as a function of moderator density and resonance energy as is given in [4]:

For VVER 440

-Resonance groups 15-17.

$$D(15\text{-}17)=0.147542 + 0.722204*\Gamma(H2O) - 0.231610*\Gamma^2(H2O)$$

-Resonance groups 18-27.

$$D(18\text{-}27)=0.152328 + 0.728344*\Gamma(H2O) - 0.23545*\Gamma^2(H2O)$$

For VVER 1000

-Resonance groups 15-17

$$D(15\text{-}17)=0.18869 + 0.75988*\Gamma(H2O) - 0.2571*\Gamma^2(H2O)$$

-Resonance groups 18-27

$$D(18\text{-}27)=0.19499 + 0.76325*\Gamma(H2O) - 0.25984*\Gamma^2(H2O)$$

For the N80 fuel elements in the periphery of the assembly the PREWIMS-VVER module considers the effect of the assembly wall and the water gap between assemblies on the Dancoff factor DANCB, as used in LWR-WIMS code [5] as well as in [1] and [6].

The module also calculates the mean Dancoff factor DANCM and the Dancoff factors for internal annulus DANCI following the principles used in [1].

The Bell factor is calculated by the expression given in [1] and also as a function of moderator density using the expressions taken from [4]:

VVER 440

Bell=1.12867+0.011463*Γ(H2O)

VVER 1000

Bell=1.13871

For Dancoff and Bell factors calculations in the case of core + reflector the methodology used is the same as for the fuel rods.

6.2. Dancoff and Bell factors for the ARK assembly.

Dancoff factors for the external rod annulus (including the assembly wall and a half of the gap between assemblies influence), average and for the internal annulus of ARK geometrical model are calculated in the PREWIMS-VVER module by the following expressions:

DBARK=(267.57*DANCB+36*DANARK)/303.57

DMARK=DANCR+δ and

δ=(135.43*(DANCV-DANCR)+267.57*(DANCB-DANCR)+
+36*(DANARK-DANCR))/1062

DIARK=(1062*DMARK-303.57*DBARK)/758.43

respectively, where:

DANARK: Dancoff factor for the external rod annulus corresponding to the 36 fuel rods allocated in the assembly periphery for fuel assemblies placed in the first ARK neighborhood, calculated with an optical thickness HARK.

DANCB: Dancoff factor for fuel elements in fuel assemblies not facing the ARK assembly; calculated taking into account the HGAP thickness.

DANCR : Regular infinite lattice Dancoff factor for the fuel elements.

DANCV: Double pitch Dancoff factor for fuel assemblies central tubes inside fuel assemblies and the central tube in ARK, and the 126 absorber rod cells in ARK assembly.

Bell factor for ARK assembly is calculated the same as for the fuel assemblies considering only geometrical dependence.For ARK assembly the average Dancoff factor is defined by DMARK in the expression for the Bell factor calculation.

7. INPUT-OUTPUT DATA FILES STRUCTURE DESCRIPTION.

A detailed input-output data description for the PREWIMS-VVER code is shown in reference [8]. Here only the table of files used during PREWIMS-VVER module execution and their function is shown below.

FILE	FUNCTION
1	File for input data.
2	File PREFLS (gives a resume of files created during a run).
3	File for previous results.
4	File to resume previous results.
5	Macroscopic cross sections file for HPS cards.
7	File for input data to WIMS-D/4 code.
10	Intermediate file for input to the module.

8. RESTRICTIONS FOR CALCULATIONAL TASKS SOLUTION.

The PREWIMS-VVER module fixes the dimensions for the arrays in order to describe enrichment values, geometry, groups structure, basic material library and burnup.

For work extending to dimensions outside the ranges of the array as fixed by the PREWIMS-VVER module, it becomes necessary to introduce the changes in the corresponding program units according to [8].

9. TECNICHAL REQUIREMENTS OF PREWIMS-VVER MODULE.

The PREWIMS-VVER module is written in FORTRAN-77 language, elaborated in a personal computer with an operative memory of 640 Kbytes, with processor 80286 (12MHz), with mathematical co-processor 80287(10 MHz) and a hard disk with 40 Mbytes. RMFORT compiler from Ryan Mcfarland corp. was used.

Typical running times for WIMS-D/4 input data preparation are:

-VVER-440 fuel assembly: 6.21 s
-VVER-440 fuel assembly including geometrical model changes: 12.96 s
-VVER-440 fuel assembly for three different enrichments in a single run: 8.02 s

Other tasks show similar typical run times.

10. PREWIMS-VVER input data sample case.

A sample problem corresponds to unperturbated VVER-440 assembly calculation (K=1) is shown in appendix 1.

Appendix 1. PREWIMS-VVER output sample case.

```
* conco440.016
CELL          7
SEQUENCE      1
NGROUP       25
NMESH        52
NREGION      10  6 22
NMATERIAL    12  6
NRODS       126  1  1  1  6  2  1
PREOUT
INITIATE
SUPPRESS      1  1  1  1  1  1  1  1  1  1  1  1  0  1  0  1  0
***   CALCULO DEL CONJUNTO COMBUSTIBLE 1.6%  BIBLIOTECA  DALE91
* CONJUNTO VVER  440   85.14 POT   TMOD= 280.00 C  1.60 A/D   2.86 g/Kg
ANNULUS       1    0.643494  1
ANNULUS       2    1.702524  2
ANNULUS       3    2.804924  2
ANNULUS       4    3.914218  2
ANNULUS       5    5.025845  2
ANNULUS       6    6.138537  2
ANNULUS       7    7.251804  2
ANNULUS       8    7.368681  3
ANNULUS       9    7.589742  4
ANNULUS      10    7.753570  5
ARRAY         1  ( 1     6.000000     1.173009     0.000000)
ARRAY         2  ( 1    12.000000     2.253724     0.000000)
ARRAY         3  ( 1    18.000000     3.359571     0.000000)
ARRAY         4  ( 1    24.000000     4.470032     0.000000)
ARRAY         5  ( 1    30.000000     5.582191     0.000000)
ARRAY         6  ( 1    36.000000     6.695171     0.000000)
RODSUB        1  1  0.381091  (  6    0.000000)
RODSUB        1  2  0.456306  ( 12    0.000000)
RODSUB        2  1  0.381091  (  7    0.000000)
RODSUB        2  2  0.456306  ( 12    0.000000)
RODSUB        3  1  0.381091  (  8    0.000000)
RODSUB        3  2  0.456306  ( 12    0.000000)
RODSUB        4  1  0.381091  (  9    0.000000)
RODSUB        4  2  0.456306  ( 12    0.000000)
RODSUB        5  1  0.381091  ( 10    0.000000)
RODSUB        5  2  0.456306  ( 12    0.000000)
RODSUB        6  1  0.381091  ( 11    0.000000)
RODSUB        6  2  0.456306  ( 12    0.000000)
MATERIAL      1 -1   553.15  4 $
    11.0  0.1743671E-04  2001.0  0.4190411E-01    16.0  0.2097821E-01 $
  1056.0  0.3924661E-04    56.0  0.9157541E-04    58.0  0.1939974E-04 $
    52.0  0.4228347E-04    91.0  0.7279027E-02  1000.0  0.7219108E-04
MATERIAL      2 -1   553.15  3 $
    11.0  0.2102977E-04  2001.0  0.5053900E-01    16.0  0.2530105E-01 $
  1056.0  0.1102366E-03    56.0  0.2572188E-03    58.0  0.5449037E-04 $
    52.0  0.1187666E-03
MATERIAL      3 -1   553.15  4 $
    11.0  0.2102977E-04  2001.0  0.5053900E-01    16.0  0.2530105E-01 $
  1056.0  0.1102366E-03    56.0  0.2572188E-03    58.0  0.5449037E-04 $
    52.0  0.1187666E-03
MATERIAL      4 -1   553.15  4 $
    91.0  0.4139711E-01  1000.0  0.1042199E-02
MATERIAL      5 -1   553.15  4 $
    11.0  0.2116634E-04  2001.0  0.5086721E-01    16.0  0.2546536E-01
MATERIAL      6 -1   859.99  1 $
   235.4  0.3452227E-03  2238.4  0.2123119E-01    16.0  0.4272131E-01 $
  3239.1  0.0000000E+00  1240.0  0.0000000E+00
MATERIAL      7 -1   859.99  1 $
   235.4  0.3452227E-03  2238.4  0.2123119E-01    16.0  0.4272131E-01 $
  3239.1  0.0000000E+00  1240.0  0.0000000E+00
MATERIAL      8 -1   859.99  1 $
   235.4  0.3452227E-03  2238.4  0.2123119E-01    16.0  0.4272131E-01 $
  3239.1  0.0000000E+00  1240.0  0.0000000E+00
MATERIAL      9 -1   859.99  1 $
   235.4  0.3452227E-03  2238.4  0.2123119E-01    16.0  0.4272131E-01 $
  3239.1  0.0000000E+00  1240.0  0.0000000E+00
MATERIAL     10 -1   859.99  1 $
   235.4  0.3452227E-03  2238.4  0.2123119E-01    16.0  0.4272131E-01 $
  3239.1  0.0000000E+00  1240.0  0.0000000E+00
MATERIAL     11 -1   859.99  1 $
   235.4  0.3452227E-03  2238.4  0.2123119E-01    16.0  0.4272131E-01 $
  3239.1  0.0000000E+00  1240.0  0.0000000E+00
MATERIAL     12 -1   569.15  2 $
    91.0  0.3876441E-01  1000.0  0.3844530E-03
BELL          1.13865578
DANCOFF       0.60028124  0.63341463
S             6
TOLERANCE  5.000000E-06
FEWGROUPS     2  3  4  5  6  8 11 14 15 21 25 26 27 32 35 38 41 45 48 $
             51 55 59 63 66 69
MESH          4  7  7  7  7  7  7  2  2  2
POWERC        1     33.0530    1.000000E-20     1
BUCKLINGS     0.00025363  0.00014713  0.00002536  0.00001471
BEGINC
PUNCH            0
ALPHA           16    16
SATURATE       135
THERMAL        7
BUCKLING      0.00025363  0.00014713
LEAKAGE       6
BEEONE        1
DNB           1  0.4190411E-01 0.0  0.2097821E-01 0.0
DNB           2  0.5053900E-01 0.0  0.2530105E-01 0.0
DNB           3  0.5053900E-01 0.0  0.2530105E-01 0.0
DNB           5  0.5086721E-01 0.0  0.2546536E-01 0.0
MATERIALS        0
BEGINC
* PASO  2          0.00 MWD/TU     2.86 g/Kg       1.0000 DEL XENON PREVIO
POWERC        1     33.0530    1.512722E+00     2
BEGINC
MATERIALS        0
BEGINC
* PASO  3         100.00 MWD/TU     2.86 g/Kg       1.0000 DEL XENON PREVIO
POWERC        1     33.0530    1.512722E+00     4
BEGINC
MATERIALS        0
BEGINC
* PASO  4         300.00 MWD/TU     2.86 g/Kg       1.0000 DEL XENON PREVIO
POWERC        1     33.0530    1.512722E+00     3
BEGINC
```

```
MATERIALS      -1
BEGINC
* PASO  5       450.00 MWD/TU    2.86 g/Kg      1.0000 DEL XENON PREVIO
POWERC       1      33.0530    1.512722E+00      3
BEGINC
MATERIALS       0
BEGINC
* PASO  6       600.00 MWD/TU    2.86 g/Kg      1.0000 DEL XENON PREVIO
POWERC       1      33.0530    1.512722E+00      3
BEGINC
MATERIALS      -1
BEGINC
* PASO  7       750.00 MWD/TU    2.86 g/Kg      1.0000 DEL XENON PREVIO
POWERC       1      33.0530    1.512722E+00      3
BEGINC
MATERIALS       0
BEGINC
* PASO  8       900.00 MWD/TU    2.86 g/Kg      1.0000 DEL XENON PREVIO
POWERC       1      33.0530    2.269083E+00      4
BEGINC
MATERIALS       0
BEGINC
* PASO  9      1200.00 MWD/TU    2.86 g/Kg      1.0000 DEL XENON PREVIO
POWERC       1      33.0530    2.269083E+00      8
BEGINC
MATERIALS       0
BEGINC
* PASO 10      1800.00 MWD/TU    2.86 g/Kg      1.0000 DEL XENON PREVIO
POWERC       1      33.0530    2.269083E+00      8
BEGINC
MATERIALS       0
BEGINC
* PASO 11      2400.00 MWD/TU    2.86 g/Kg      1.0000 DEL XENON PREVIO
POWERC       1      33.0530    2.269083E+00      8
BEGINC
MATERIALS       0
BEGINC
* PASO 12      3000.00 MWD/TU    2.86 g/Kg      1.0000 DEL XENON PREVIO
POWERC       1      33.0530    2.269083E+00      8
BEGINC
MATERIALS       0
BEGINC
* PASO 13      3600.00 MWD/TU    2.86 g/Kg      1.0000 DEL XENON PREVIO
POWERC       1      33.0530    2.269083E+00     12
BEGINC
MATERIALS       0
BEGINC
* PASO 14      4500.00 MWD/TU    2.86 g/Kg      1.0000 DEL XENON PREVIO
POWERC       1      33.0530    2.269083E+00     12
BEGINC
MATERIALS       0
BEGINC
* PASO 15      5400.00 MWD/TU    2.86 g/Kg      1.0000 DEL XENON PREVIO
POWERC       1      33.0530    2.269083E+00     12
BEGINC
MATERIALS       0
BEGINC
* PASO 16      6300.00 MWD/TU    2.86 g/Kg      1.0000 DEL XENON PREVIO
POWERC       1      33.0530    2.269083E+00     12
BEGINC
MATERIALS       0
BEGINC
* PASO 17      7200.00 MWD/TU    2.86 g/Kg      1.0000 DEL XENON PREVIO
POWERC       1      33.0530    2.593237E+00     14
BEGINC
MATERIALS       0
BEGINC
* PASO 18      8400.00 MWD/TU    2.86 g/Kg      1.0000 DEL XENON PREVIO
POWERC       1      33.0530    2.593237E+00     14
BEGINC
MATERIALS       0
BEGINC
* PASO 19      9600.00 MWD/TU    2.86 g/Kg      1.0000 DEL XENON PREVIO
POWERC       1      33.0530    2.593237E+00     14
BEGINC
MATERIALS       0
BEGINC
* PASO 20     10800.00 MWD/TU    2.86 g/Kg      1.0000 DEL XENON PREVIO
POWERC       1      33.0530    2.593237E+00     14
BEGINC
MATERIALS       0
BEGINC
* PASO 21     12000.00 MWD/TU    2.86 g/Kg      1.0000 DEL XENON PREVIO
POWERC       1      33.0530    2.593237E+00     14
BEGINC
MATERIALS       0
BEGINC
* PASO 22     13200.00 MWD/TU    2.86 g/Kg      1.0000 DEL XENON PREVIO
POWERC       1      33.0530    2.593237E+00     14
BEGINC
MATERIALS       0
BEGINC
* PASO 23     14400.00 MWD/TU    2.86 g/Kg      1.0000 DEL XENON PREVIO
POWERC       1      33.0530    2.593237E+00     14
BEGINC
MATERIALS       0
BEGINC
* PASO 24     15600.00 MWD/TU    2.86 g/Kg      1.0000 DEL XENON PREVIO
POWERC       1      33.0530    2.593237E+00     14
BEGINC
MATERIALS       0
BEGINC
* PASO 25     16800.00 MWD/TU    2.86 g/Kg      1.0000 DEL XENON PREVIO
POWERC       1      33.0530    2.593237E+00     14
BEGINC
MATERIALS       0
BEGINC
* PASO 26     18000.00 MWD/TU    2.86 g/Kg      1.0000 DEL XENON PREVIO
POWERC       1      33.0530    2.593237E+00     14
BEGINC
MATERIALS       0
BEGINC
* PASO 27     19200.00 MWD/TU    2.86 g/Kg      1.0000 DEL XENON PREVIO
POWERC       1      33.0530    2.593237E+00     14
BEGINC
```

```
MATERIALS       0
BEGINC
* PASO 28     20400.00 MWD/TU     2.86 g/Kg       1.0000 DEL XENON PREVIO
POWERC       1      33.0530     2.593237E+00     14
BEGINC
MATERIALS       0
BEGINC
* PASO 29     21600.00 MWD/TU     2.86 g/Kg       1.0000 DEL XENON PREVIO
POWERC       1      33.0530     2.593237E+00     14
BEGINC
MATERIALS       0
BEGINC
* PASO 30     22800.00 MWD/TU     2.86 g/Kg       1.0000 DEL XENON PREVIO
POWERC       1      33.0530     2.593237E+00     14
BEGINC
MATERIALS       0
BEGINC
* PASO 31     24000.00 MWD/TU     2.86 g/Kg       1.0000 DEL XENON PREVIO
POWERC       1      33.0530     2.593237E+00     14
BEGINC
MATERIALS       0
BEGINC
* PASO 32     25200.00 MWD/TU     2.86 g/Kg       1.0000 DEL XENON PREVIO
POWERC       1      33.0530     2.593237E+00     14
BEGINC
MATERIALS       0
BEGINC
* PASO 33     26400.00 MWD/TU     2.86 g/Kg       1.0000 DEL XENON PREVIO
POWERC       1      33.0530     2.593237E+00     14
BEGINC
MATERIALS       0
BEGINC
* PASO 34     27600.00 MWD/TU     2.86 g/Kg       1.0000 DEL XENON PREVIO
POWERC       1      33.0530     2.593237E+00     14
BEGINC
MATERIALS       0
BEGINC
* PASO 35     28800.00 MWD/TU     2.86 g/Kg       1.0000 DEL XENON PREVIO
POWERC       1      33.0530     2.593237E+00     14
BEGINC
MATERIALS       0
BEGINC
* PASO 36     30000.00 MWD/TU     2.86 g/Kg       1.0000 DEL XENON PREVIO
POWERC       1      33.0530     2.593237E+00     14
BEGINC
MATERIALS       0
BEGINC
* PASO 37     31200.00 MWD/TU     2.86 g/Kg       1.0000 DEL XENON PREVIO
POWERC       1      33.0530     0.000000E-01      1
BEGINC
MATERIALS      -1
BEGINC
```


REFERENCES

1. C. Anhert, J. M. Aragonés, MARIA SYSTEM: A code block for PWR fuel assembly calculations.

2. P. Mikolash, Spectral calculations of VVER lattices using WIMSD-4 code. TIC 16th Symposium. Moskow, 1987(in russian).

3. L.E. Strawbridge, R.F. Barry. Nucl. Sci. Eng. 3, 58 (1965).

4. P.Mikolash, I. Vacek, T. Kulikovska, Application of WIMS-D/4 code for few groups constants libraries calculations. TIC 15th Symposium. Rostock, 1986 (in russian).

5. F.J. Fayers, et al., LWR-WIMS, a modular computer code for the evaluation of light water reactors. Description of methods. AEEW-R-785. UKAEA, Winfrith (1972).

6. T.Kulikovska, B. Sadovska, Auxiliary programs for WIMS-D/4 in IBM/PC/AT. TIC 17th Symposium. Varna, 1988 (in russian).

7. P. T. Petkov, SPPS-1 version for XT and AT personal computers. TIC 17th Symposium. Varna, 1988 (in russian).

8. A. González, D. López, D. Milián, C. M. Alvarez, PREWIMS-VVER PC module for VVERs Input Data Preparation. IAEA Research Contract No. 5701/RB, Annual Final Report. Oct, 1990.

GADOLINIUM ABSORBERS IN WWER-1000 TYPE FUEL LATTICES

J. MIKUŠ, F. HUDEC, J. ROČEK, M. TRGIŇA,
L. VRBA, K. ZÁLESKÝ
Nuclear Research Institute,
Řež, Czechoslovakia

Abstract

A complex scheme based on the use of separate computer programmes to obtain the data needed for the WWER-type Gd-poisoned lattices has been built up and applied to a number of cores behaviour determination. The calculated values have been compared with the experimental ones from measurements carried out in the LR-0 reactor. Some preliminary results concerned with one of the cores considered are presented in this paper.

1. Introduction

A wide research programme has been prepared and carried out on the LR-0 reactor to obtain information needed for using fuel with burnable absorbers in the WWER-type reactors.

The previous activity was concerned with WWER-440 type lattices containing single fuel pins with homogeneous Gd_2O_3 admixture /1/. The present investigations are devoted to the cores consisting of WWER-1000 type assemblies with various number (up to 24) of fuel pins with gadolinium at them. A number of such cores was investigated and detailed analysis and comparison of the calculated and in the LR-0 measured values has been carried out.

In this paper a brief information only is given about some preliminary results concerned with one of the cores considered.

2. Experimental arrangement

The reactor core investigated consists of 7 WWER-1000 type fuel assemblies with 4.4 % enriched uranium, where in the central assembly 18 fuel pins were replaced by the fuel pins with 3.6 % enriched uranium containing 2.0 % (by weight) of Gd_2O_3 admixture (Fig. 1). Detailed description of the LR-0 reactor can be found in /2/, here a short information only is given concerning our experiment.

To compare the specific gadolinium-effects, series of measurements were performed both in the clean core (without gadolinium) and above mentioned one. The irradiations were made at room temperature with critical heights H_{cr} of the H_2O moderator levels being 226.64 mm (variant No 1 - clean core) and 266.10 mm (variant No 2 - core to be investigated with gadolinium).

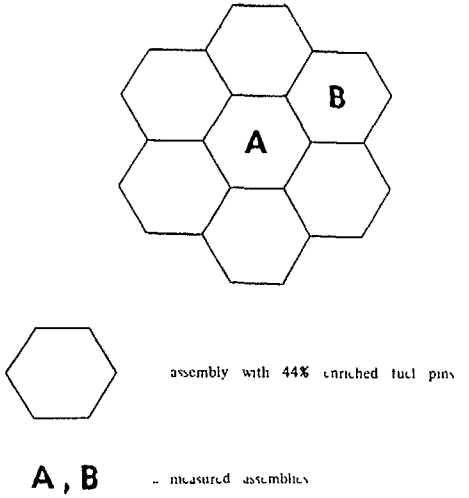

Fig. 1 - The scheme of the LR-0 core.

3. Method of calculation and codes used

A set of PC programmes has been developed and can be used to predict the behaviour of the WWER-type cores containing fuel pins with burnable absorbers.

The calculations for both cores considered were performed in two steps. In the first one the four - group constants of elementary cells and super-cells containing fuel pins with gadolinium (in the following text abbreviated as "Gd-pins") or water holes were calculated using the code MICROBE /3/. In the second step calculations in the 30° - sector of symmetry were performed by means of the code BŘETISLAV /4/. This code treats the two - dimensional four-group diffusion equations using the so called fine mesh method Results of this calculations are four-group flux densities and criticality factor for a given extrapolation height $H_{ex} = H_{cr} + d_{ex}$, where d_{ex} is the extrapolation distance, which value has been found to be 140 mm for cores of such a type

The calculated criticality factors are

$k_{eff} = 0.9861$ - variant No 1

$k_{eff} = 1.0015$ - variant No 2.

4. Results

In a plane perpendicular to the core axis, the fission rate distribution was determined for both variants of cores (clean and to be investigated) by means of irradiated fuel pins measuring of their gamma radiation in the energy range of 600 to 900 keV. The fuel pins to be measured were placed in 100 positions shown in Fig 2 The preliminary results of such measurements carried out both in the clean and investigated cores were published in the paper /5/, where the values of corresponding calculations were presented too

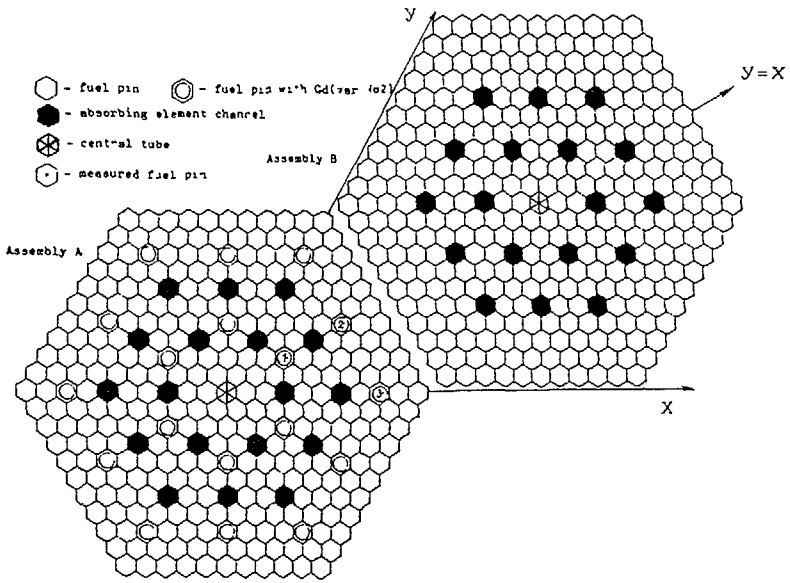

Fig. 2 - The positions of fuel pins to be measured.

To compare the experimental and calculated power distributions, a brief graphic information only is given in this work by means of Fig. 3 - 6, where the energy release per one fuel pin (abbreviated as "power") is plotted as a function of distance from the core axis. Following norm was used in this comparison mean energy release (in arbitrary units) per one measured fuel pin is equal to one.

All experimental and calculated data in the 30°-sector of symmetry are plotted in Fig 3 and 4 for both variants. Of course, this way of depicting causes a certain additional dispersion of points in both series Therefore, a comparison of "pure" data series along 30°-line (y = x) is shown in Fig. 5 and 6 for the clean core and the one with Gd-pins, respectively. Such a way of depicting is free of above mentioned additional dispersion

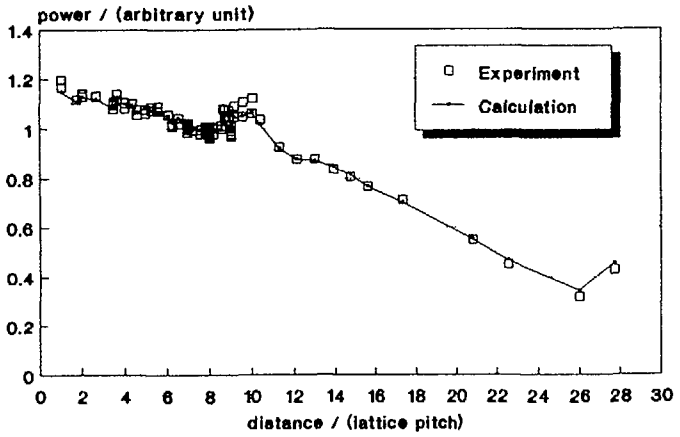

Fig.3: Variant No 1 - Clean core
All experimental and calculated
data in the 30 deg. sector.

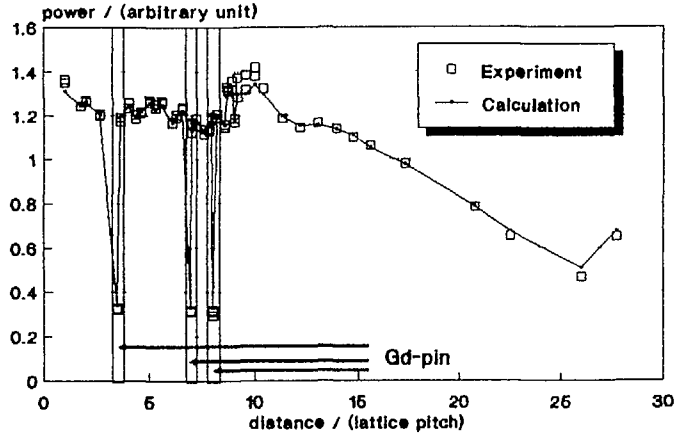

Fig.4: Variant No 2 - Core with Gd-pins
All experimental and calculated
data in the 30 deg. sector.

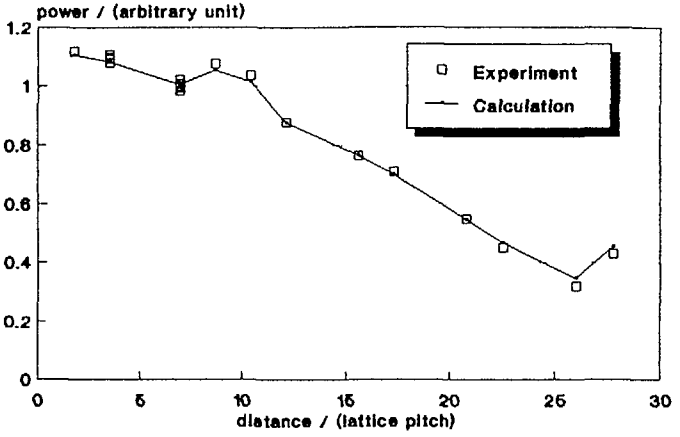

Fig.5: Variant No 1 - Clean core
Experimental and calculated data
along the 30 deg. line.

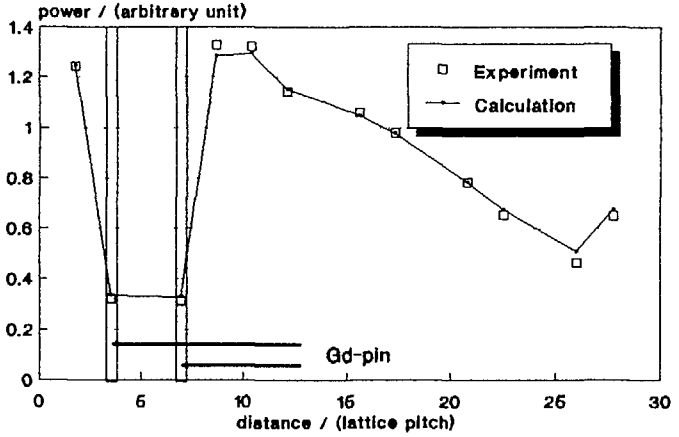

Fig.6: Variant No 2 - Core with Gd-pins
Experimental and calculated data
along the 30 deg. line.

Moreover, the depression of power distribution caused by the presence of Gd-pins in the central fuel assembly is illustrated in Fig. 7 and 8. In this case another norm of data is used: mean energy release on 12 fuel pins in peripheral assembly is equal to one.

Calculations and experiment are in fairly good agreement as it can be seen from Tab. 1 The mean value of the relative power distribution difference absolute values is 1.4 % for the clean core and 2.4 % for the core with Gd-pins.

The shape of the power distribution in the neighbourhood of a Gd-pin can be characterized by the following ratio:

Q = (average energy release at the ring of 6 fuel pins around a Gd-pin) / (energy release on that Gd-pin).

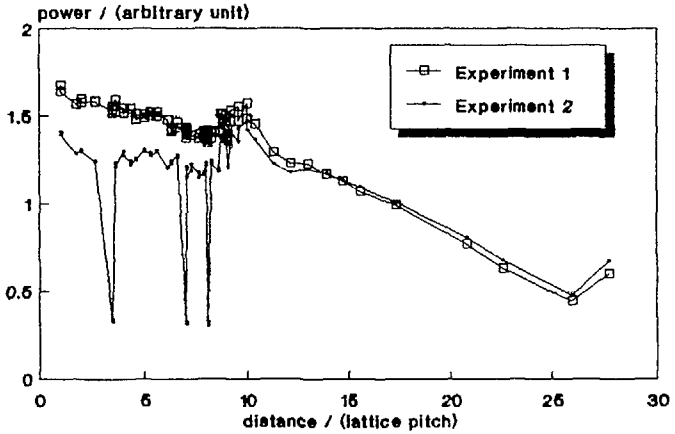

Fig.7: Variant 1 and 2 - Experiment
Comparison of experimental data for both variants in the 30 deg.sector

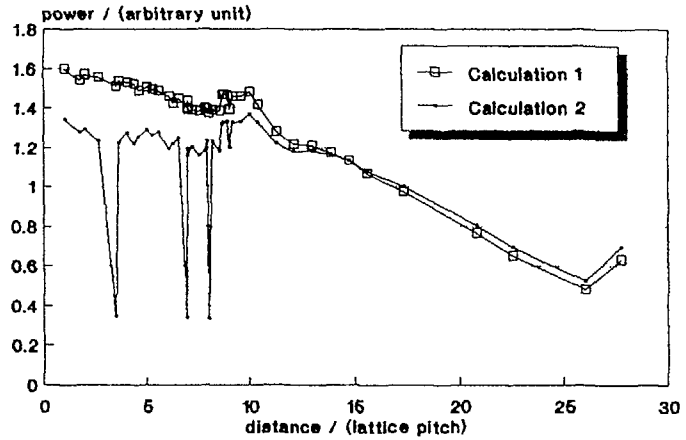

Fig.8: Variant 1 and 2 - Calculation
Comparison of calculated data for both variants in the 30 deg.sector

Tab.1 Comparison of experimental and calculated results

Value	Core	
	clean	with Gd-pins
Mean | difference |	0.013	0.017
Mean | relative difference |	1.4 %	2.4 %
Maximum positive rel. difference	5.3 %	6.2 %
Maximum negative rel. difference	-8.8 %	-12.7 %

difference = $P_t - P_c$

relative difference = $100 * (P_t - P_c) / P_t$

where P_t and P_c are the experimental and calculated values of energy release, respectively.

Tab.2 Core with Gd-pins. Comparison of experimental and calculated values of power ratio Q for three positions of Gd-pins.

No	Experimental ratio Q_E	Calculated ratio Q_C	Difference $d = Q_E - Q_C$	Relative differ. $100*d/Q_E$
1	3.718	3.553	0.165	4.4
2	3.669	3.501	0.168	4.6
3	3.694	3.523	0.171	4.6

Q = (average value of energy release on 6 fuel pins around a Gd-pin) / (energy release on Gd-pin)

Results for three different positions of Gd-pins are presented in Tab. 2, where a fairly good agreement between calculated and experimental power distributions can be seen too. The relative difference of quantity Q is about 4.6 % for all three positions of Gd-pins.

5. Conclusions

The results presented in this paper demonstrate a good agreement between calculated and experimental power distributions. It can be concluded that both the experimental and evaluating methods seem to be the hopeful tools for further investigations of reactor lattices with Gd-pins.

References

/1/ Bárdoš J., Hron M., Drexler J., Veselý P.: "Burnable Absorbers in WWER-Type Lattices", Meeting of participants in the Co-ordination Research Programme on "Safe Core Management with Burnable Absorbers in WWERs", IAEA, Viena, 11-14 December 1989.

/2/ Sochor Q., Starý R." "The Experimental Reactor LR-0 after Five Year's Operation". Nukleon, 1988, A special issue.

/3/ Záleský K.: "Manual of the Program MICROBE-02 for the Calculation of Local Burn-up" (in Czech). (Report ÚJV 6880-R,A). NRI Řež 1984.

/4/ Lelek V.:"BŘETISLAV - A Net Program for Calculation of a Reactor in Hexagonal Geometry" (in Russian). (Report ÚJV 7771-R,A). NRI Řež 1986.

/5/ Hudec F., Mikuš J., Roček J., Trgiňa M., Vrba L., Záleský K.: "Investigations with WWER-1000 Type Fuel Assemblies with Gd-Burnable Absorbers on the LR-0 Reactor", 1. Symposium AER, Řež, 23-28 September 1991

USE OF NEUTRONIC CODES FOR THE DESIGN OF MTR LEU CORES

M. MADARIAGA, M. HIGA
Comisión Nacional de Energía Atómica,
Buenos Aires, Argentina

Abstract

The Comisión Nacional de Energía Atómica from Argentina (CNEA) has been working in the last years in several LWR designs. Two lines could be destiguished:

a) experimental and/or radioisotope production reactors up to 22 MW, with LEU (20% U_{235} enrichment) or slightly enriched (about 5%) fuel.
b) power reactor about 15 MWe (or other applications) loaded with slightly enriched fuel with an intrinsically safe design (Carem reactor).

Many of the tools for neutronic calculations are the same in both lines. On the other hand it is in case a) that CNEA has made the complete process: basic and detail design, construction of the facility, fuel fabrication and start-up. This is the case of RA3 (Argentina), RP10 (Peru) and NUR (Argelia) reactors.

In case b) the design work is in progress, being now under construction a critical facility and a pressurize loop in order to check the main neutronic and thermohydraulic design parameters.

In this work it is at first presented a review of the LWR design that have been studied at CNEA in the last years. Next the neutronic calculation methods and codes are discussed related with the different stages of the core design. The particular case of HEU and LEU fuel conversion is considered.

The experimental results coming from the start up of RP10, NOR and RA3 are discussed with certain detail and compared with the design calculations. Finally, taking in account the radioisotope production requirements of RA3, the optimization of the fuel management and the equilibrium core is studied considering two levels: basic and detail with a realistic fuel management including the control fuel elements.

A good agreement of the calculated an experimental design parameters is concluded for the case of MTR, HEU and LEU cores. Thus the calculation methods are completely validate for case a) while they could be considered partially validate for case b).

1 Introductory Concepts

1.1 Introduction

The main purpose of this paper is to present a review of the neutronic design work done at the Atomic Energy Commission from Argentina (CNEA) in MTR cores during the last years, understanding by MTR cores those corresponding to open pool reactors with plate type fuel elements (FE).

CNEA, together with an associated company, INVAP, has been working during the last 10 years in several projects related to the design of LWR. Some of these projects (which are MTR type) have been completed including the reactor start-up. All of them but one are Low Enriched Uranium (LEU) cores (20 % enr.) corresponding to new reactors or conversions from Highly Enriched Uranium (HEU, 90 % enr.).

Although the calculation methods and neutronic codes used in the different projects are not the same they are quite similar and hence, general conclusions are obtained. The particular case of HEU to LEU conversion of the RA3 reactor is considered in some detail.

1.2 General ideas about MTR core design

The starting point for the design work is the conceptual definition of the reactor. In this connection, and speaking only about MTR reactors, we can distinguish 4 different (not excluding) items:

A) Critical facilities and reactors up to 0.5 Mw.

B) Radioisotopes production.

C) High flux performance.

D) HEU to LEU conversion.

Although many reactors can be classified in more than one of these types we can separate them according to the main differences in the design parameters to be optimized:

A) The core configuration is variable and the burnup of the fuel element (FE) is not significant so the design job is done mainly by considering one typical fresh core configuration.

B) The typical power range is between 1 Mw and 20 Mw. More than 20 or 30 Mw will probably require an ascending coolant flow while the lower powers use descending flows.
The utilization factor (UF)

$$UF = \% \text{ of full power operating days per year}$$

is about 60 % or more and thus, the economy of the fuel cycle has to be optimized. We can say that the boundary conditions for the design could be set as:

Discharge Burnup > Minimum (ie 40 % U_{235} consumed)

Neutronic flux in irradiation channels > Minimum (ie 10^{14} n/cm²sec / 5 Mw)

In this case the design optimization is performed on the equilibrium core and hence, a first fresh core is analyzed in connection only with the start up of the reactor

C) As it is known, the increase of neutronic flux in the irradiation channels, is normally obtained from a decrease of discharge burnup We can then say that the main difference between B and C is that the fuel cycle economy is no longer the first priority and hence, the increasing of the neutronic flux per Mw is the only main objective of the design This allows compact cores, highly sub-moderated, where the reflector (usually Be or D_2O) partially works as moderator obtaining large values of the thermal flu in the irradiation channels This design philosophy is used in medium flux reactors (more than 10^{14} and less than 10^{15}) with powers about 10 Mw or more, and high flux reactors (more than 10^{15}) with powers about 200 Mw

D) The HEU to LEU conversion has been widely analyzed in several meetings organized by the RERTR program and the IAEA We will here only recall that HEU to LEU conversion is a design task that could be done following two different criteria

D1) Obtain a LEU core with a similar performance than the existing HEU core and hence, the reference for the LEU design are the parameters of the existing HEU core In this case it is usual to set the following design condition

[Neutronic thermal flux in irradiation channels (LEU)] > [0 9 * HEU corresponding flux for the same operating power]

D2) Use the HEU to LEU conversion in order to define a different reactor by means of some other significant cnanges (for example a power increase) In this case the conceptual definition of the reactor is modified and the core design may be quite similar to the case of a new reactor

1 3 Calculation methods

Once the conceptual design is defined, different calculation levels are performed in agreement with the corresponding design steps We can briefly describe them as follows

Basic Design. Parametric studies are applied for the FE and core design optimization (geometry and composition) The models are simple for the sake of efficiency and smaller computer times The main output of this step is
- Geometry and composition of the FE
- Core geometry is defined but the detailed fuel management has *not been studied yet This means that the equilibrium burnup* distribution has been obtained with a simplified refuelling chain without considering for example control FE replacement
- The main parameters of the core are known, for example
  approximate flux distribution
  available flux for irradiation
  temperature and void coefficients
  excess reactivity
  shutdown margins
  cycle length (time and reactivity)
  xenon reactivity worth
  control rods worth
  total power peaking factor (most unfavourable case)
  Average discharge burnup

Detailed Design. Some details are studied at this step, for example
- The function of each control rod is defined At CNEA the control rod functions are usually split as follows

Control rod bank	5 rods	
Regulating rod	1	
		2 shim-safety rods
Safety rods	4	
		2 safety-rods only

The safety-rods-only are totally withdrawn during operation while the shim-safety rods could be in any desirable position in order to compensate reactivity or modify the flux distribution
- A detailed refuelling scheme is studied considering the refuelling of the control FE as well as dividing the whole core into several chains of 4 or 5 FE each The idea is to move only a fraction of the core in each refuelling
- The detailed equilibrium core calculation is performed and the (expected) flux distribution in the operating condition is obtained
- Oscillations of the discharge burnup due to a realistic FE *management are obtained*
- Definition and detailed study of the start-up core, including the calculation of several transients due to normal or accidental postulated conditions

The following calculation conditions are set depending on the design step

DIMENSION	ENERGY GROUPS	FE GEOMETRY DETAIL	CONTROL RODS
0 (B^2_{tot})	2 or more	Homogeneous	No
X-Y (B^2_z)	2 - 3	Homogeneous	No
X-Y (B^2_z)	2 - 3	Hom except CFE	Yes
X-Y (B^2_z)	2 - 3	Explicit Frames	Yes
X-Y-Z	2 - 3	Explicit Frames	Yes

The cross sections for the different materials, including control rods and reflectors are obtained from WIMS /1/ and in some special cases GGTC code /2/ HERMET /3/, a cell code (developed at CNEA) has also been used producing similar results as WIMS (it has the same nuclear data library)

The reactor and equilibrium core calculations were performed with PUMA /4/ (developed at CNEA) or with CITVAP /5/, a modified version of CITATION /6/ that performs burnup and equilibrium core calculations using a set of burnup dependent macroscopic cross sections

The reliability of each one of the calculation conditions together with the neutronic codes is estimated as compared to an experimental reference At CNEA, this reference was first provided by a set of measurements /7/ performed at the RA-2 critical facility (HEU) The knowledge of the discrepancy has been esential to extrapolate true results At present, LEU experimental data are also available

1 4 Review of LWR design at CNEA

In this section we briefly present those projects, related to LWR design, developed at CNEA and/or INVAP in the last years

Reactor-Project. RA-6, new reactor, 0 5 Mw (1978)
Type. (A) MTR, HEU 19 plates FE, 150 gr U_{235}/FE , general purpose and teaching
Comments. design process completed, reactor start-up on 1982 At present the reactor is in operation with its HEU core, basic studies are being performed in order to convert it from HEU to LEU together with a power increase from 0 5 Mw to 5 Mw in order to achieve a high flux performance (C)
Designer. CNEA-INVAP
Owner. CNEA
Location. Bariloche, Argentina

Reactor-Project. RP-10, new reactor, 10 Mw (1978)
Type. (B) MTR, LEU 16 plates FE, 280 gr U_{235}/FE, U_3O_8, Uranium density about 2 3 gr/cc Radioisotope production
Comments. design process completed, reactor start-up on 1988 At present the reactor is in operation
Designer. CNEA
Owner. Instituto Peruano de Energia Nuclear (IPEN)
Location. Huarangal (near Lima) Peru

Reactor-Project. RA-3 , HEU to LEU core conversion, 5 Mw (1980)
Type. (D) MTR, LEU 19 plates FE, 290 gr U_{235}/FE, U_3O_8, Uranium density about 3 0 gr/cc Radioisotope production (B)
Comments. design process completed, reactor start-up with the new LEU core in 1990 At present the reactor is in operation
Designer. CNEA
Owner. CNEA
Location. Buenos Aires, Argentina

Reactor-Project. CAREM, new reactor, 15 Mwe (1984)
Type. Power reactor for electricity production or (in a modified version) for heating Slighty enriched FE Intrinsically safe design
Comments. design work in progress At present a critical facility and a pressurized loop are under construction in order to check the main neutronic and thermohydraulic design parameters
Designer. INVAP
Owner. CNEA

Reactor-Project. NUR, new reactor, 1 Mw (1985)
Type. (A)-(B) MTR, LEU 19 plates FE, 290 gr U_{235}/FE, U_3O_8, Uranium density about 3 0 gr/cc General Purpose and teaching
Comments. design process completed, reactor start-up in 1989. At present the reactor is in operation
Designer. INVAP
Owner. Haut Commisariat a la Recherche
Location. Draria, Argelia

Reactor-Project. RPR, new reactor, 22 Mw (1986)
Type. (B)-(C) MTR, LEU 19 plates FE, 470-500 gr U_{235}/FE, U_3O_8 or U_3Si_2, Uranium density about 3 0 or 4 8 gr/cc Radioisotope production and FE irradiation
Comments. basic design completed Project cancelled because of budget problems
Designer. CNEA-INVAP
Owner. CNEA

Reactor-Project. TRR, HEU to LEU core conversion, 5 Mw (1987)
TYPE. (B) MTR, LEU 19 plates FE, 290 gr U_{235}/FE, U_3O_8, Uranium density about 3 0 gr/cc Radioisotope production
Comments. basic and detail design completed The reactor will be starting-up in the near term
Designer. INVAP
Owner. Atomic Energy Organization of Iran (AEOI)
Location. Tehran, Iran

2 RA-3 HEU to LEU conversion

2 1 First design step

During the first design step a considerable effort was done in order to define a calculation line with its error as well as the first approach to the new FE design parameters On the other hand the developing work done in the FE fabrication area produced (during this step) modifications in the maximum Uranium density available in the meat The existing 28 FE HEU core was taken as a reference in order to obtain the LEU FE by means of equilibrium core calculations in the same core

The output of this step was the basic LEU FE design The main changes introduced in the FE were

90 % enrich	20 % enrich
195 gr U_{235}/FE	290 gr U_{235}/FE
0 052 cm/meat	0 070 cm /meat
0 59 U gr/cc	3 0 U gr/cc

The number of plates (19) and the grid pitch remained constant

The main design result obtained with this FE was about 55-60% discharge burnup in a similar core as the HEU core (no central irradiation box) together with similar fluxes in the irradiation boxes, let us say more than 0 9 times the HEU case

2 2 Second design step

The second design step refers to the equilibrium core optimization The possibility of reducing the core size from 28 FE (HEU) to 25 FE was considered together with the possibility of introducing a high flux irradiation position at a central irradiation box (CIB) /8/ The feasibility of this CIB was related with the economical cost (due to the lack of discharge burnup) and safety requirements
In other words, the main questions to be answered with the design job were
-With 5 Mw, is it possible to achieve an irradiation thermal flux above 10^{14} n/cm^{2}sec using the designed LEU FE ?
-Which is the economical cost of the CIB ?
-Roughly speaking which kind of FE management is convenient IN-->OUT or OUT-->IN ?

The equilibrium core calculations were performed with the X-Y(B^2_z) 2 groups-Homogeneous scheme, with no Control FE Only one refuelling chain with 25 standard FE was considered Recent data coming from the NUR start up were used /12/ in order to improve the experimental reference for the calculated reactivity The results are presented in tables 1 and 2 Briefly the conclusions of this design step were
-It is possible to get the desired irradiation flux (10^{14}) in the CIB (5 Mw) in order to produce Ir_{192} and improve the Mo_{99} production

Table 1 Comparison between different FE managements

25 FE core configuration, 5 Mw
with Central Irrad Box (CIB)

FE Management	In - -> Out	Out ---> In
Cycle Length (T)	23 8 days	20 0 days
Discharged Burnup	49 8 % U_{235}	41 8 % U_{235}
Power Peaking Factor	4 0	3 0
Mean Neutronic Thermal Flux (CIB)	1 1 10^{14} n/cm^{2}sec	9 9 10^{13} n/cm^{2}sec

Table 2 Economic cost of the CIB

25 FE core configuration
(5 Mw)

C I B	with	without
Mean Neutronic Thermal Flux (best Irrad box)	10^{14} n/cm^{2}sec	6 7 10^{13} n/cm2sec
Discharged Burnup	45 % U_{235}	55 % U_{235}
FE per full power year	16 8	13 7

-The economical cost of the CIB, although significant (about 3 FE per full power operating year) is considered to be partially compensated with the reactor production increase The 25 FE core with CIB (fig 1) is adopted as final geometry for the equilibrium core
-An intermediate IN-->OUT, OUT-->IN refuelling scheme was selected in order to obtain a power peaking factor less than 3 5 and a discharge burnup about 45 % of U_{235} consumed

G	G	G	G	G	G	G	IB
G	IB					G	G
G	R5		R1				G
G		R4		CIB	R2		G
G			R3				G
G	IB					IB	G
G	G	G	IB	G	G	G	
			G				

Standard FE
R1 Control FE
IB Irradiation box
G Graphite reflector

Figure 1 25 FF configuration for the equilibrium core

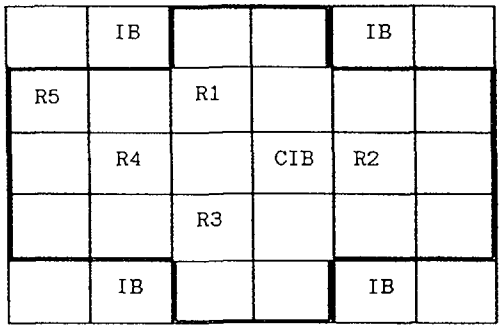

Figure 2 21 FE start-up core (water reflected)

2.3 Third design step

This step is related with the detailed analysis of the equilibrium and start-up cores. A smaller core is proposed /9/ as start-up core in fig. 2 . During a transition phase, 4 FE and 24 graphite reflector boxes will be added in order to get the final size of the equilibrium core.

2.3.1 Detailed fuel management

The detailed FE management /10/ is defined by a sequence of 7 refuelling chains indicated in fig.3. Refuelling chains 1 to 4 (C1 to C4) correspond to standard FE while C5 to C7 correspond to control FE. In the simulation with PUMA code the reactor was operated at a constant power of 5 Mw and no stop time step was taken in account. Each time step T, one refuelling chain Ci is executed, so one fresh FE is inserted each time T. The refuelling sequence is defined as follows:

C1 C2 C3 C5
C4 C1 C2 C6
C3 C4 C1 C7
C2 C3 C4 C5
C1 C2 C3 C6
C4 C1 C2 C7
C3 C4 C1 C5
C2 C3 C4 C6
C1 C2 C3 C7
C4 C1 C2 C5
C3 C4 C1 C6
C2 C3 C4 C7

From the analysis of the refuelling scheme it can be seen that each 48*T time steps the whole sequence will be repeated The

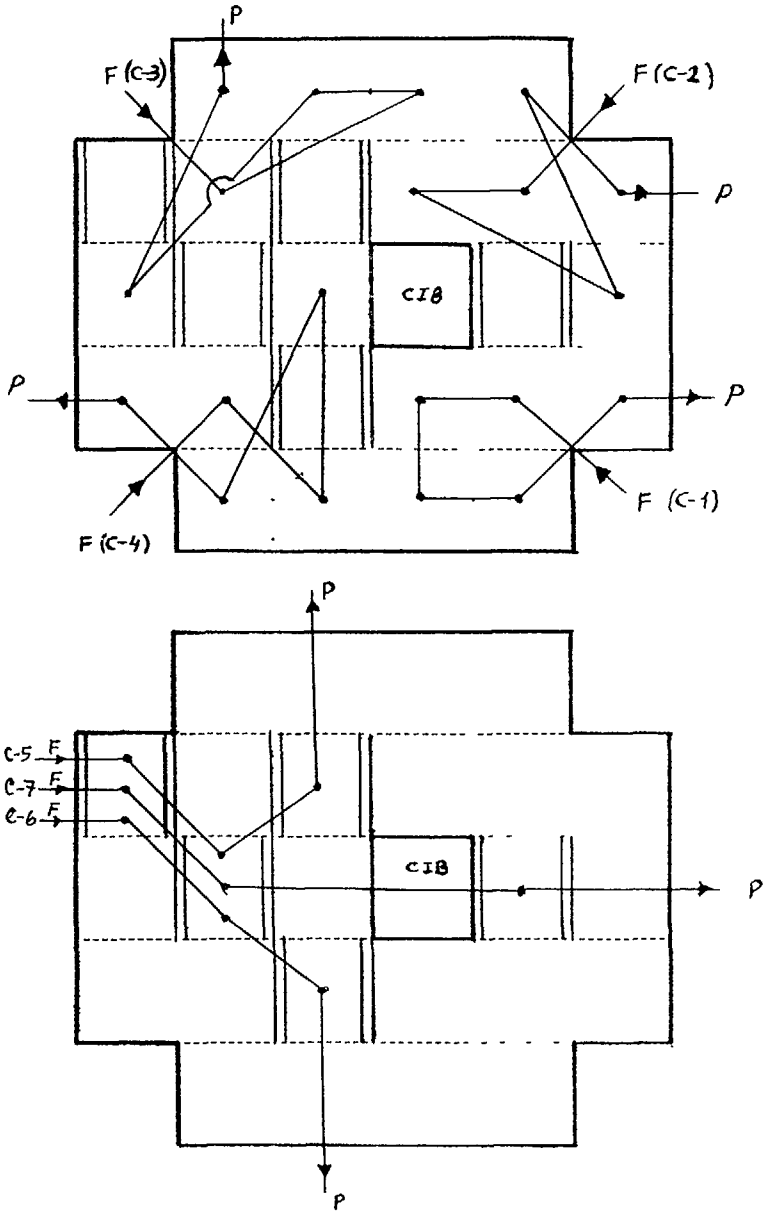

Figure 3 : refuelling chains (F= fresh, P=pool)

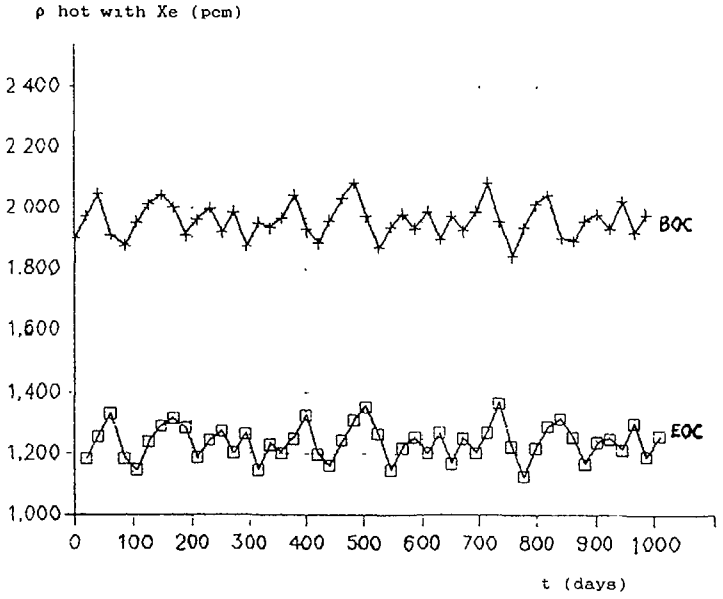

Figure 4 : BOC and EOC reactivity versus operation time

X-Y(B^2_z) 2gr homogeneous calculation scheme was applied, anyway, the control FE were included in the model in order to take the right volumes and U_{235} loadings into account. The insertion of control rod-4 during the operation was also considered.

Setting the condition:

EOC reactivity (hot with Xe) > 1000 pcm

a cycle length of T = 21 days was found in agreement with previous non detailed calculations. Once the equilibrium methods were applied and a BOC core state was obtained, a detailed simulation, starting from this BOC state was performed. During the 48*T = 1008 days the neutronic flux of the reactor was re-calculated after each refuelling (ie each 21 days). It was verified that the initial core was in equilibrium obtaining the oscillations of the different parameters during a macro-cycle (48*T). Fig. 4 shows the BOC and EOC reactivities versus the operation time, while table 3 gives the main parameters obtained with this detailed refuelling scheme.

Table 3: Detailed FE management results

	MINIMUM	MAXIMUM
BOC reactivity (hot,with Xe)	1869 pcm	2085 pcm
EOC reactivity (hot,with Xe)	1123 pcm	1365 pcm
U_{235} mass in the BOC core	5129.5 gr	5168.1 gr
U_{235} mass in the EOC core	5002.0 gr	5041.1 gr
$\Delta\rho$ BOC--->EOC	716 pcm	735 pcm
ΔM_{235} BOC--->EOC	126.85 gr	126.85 gr
$\Delta\rho$ / ΔM_{235}	5.64 pcm/gr	5.79 pcm/gr

ΔEnergy (BOC-->EOC) = 5 Mw * 21 days

DISCHARGED BURNUP :

Standard FE = (47.4 ± 2.1) % of U_{235} consumed
Control FE = (44.3 ± 1.0) % of U_{235} consumed

2.3.2 Operative core conditions

Usual design requirements have been put together in a set of conditions that shall be verified by the start-up core as well as the equilibrium core.

Let us consider:

ρ_{max} = core reactivity excess (ie calculated reactivity, cold, without Xe, all control rods withdrawn).

ρ_4 = calculated reactivity of the core (cold with no Xe) with the 4 safety-rods bank inserted

ρ_2 = calculated reactivity of the core (cold with no Xe) with any 2 safety rods inserted

Then we have the following static conditions to be verified in order to consider that a core is operable:

cond1 :

$$(\rho_{max} - \rho_4) / \rho_{max} > 1.5$$

cond2 :

$$-\rho_4 > 3000 \text{ pcm}$$

cond3 :

$-\rho_2 > 500$ pcm

cond4 :
The correct cooling of the core during operation must be verified Normally the thermohydraulic design has been performed assuming an upper value for the power peaking factor (PPF) with a minimum number of FE in the core In this case it was demonstrated that a 21 FE core with a PPF of 4 was correctly cooled by the existing cooling system, so it is enough to check that

$$PPF \leq 4\ 0$$

$$\text{Core FE Number} \geq 21$$

cond 5 :
This condition establishes a minimum value for the excess reactivity This value is in accordance with the reactivity requirements which approximately are.

Cold ---> Hot	400 pcm
Xenon	.3100 pcm
BOC ---> EOC	.1000 pcm
EOC minimum reactivity (Hot with Xenon)	.1000 pcm
ρ^{max}	> 5500 pcm

Conditions 1 to 5 defined above have been verified using the X-Y (B^2_z)-2gr-Explicit Frames model for the reactivity calculations and X-Y-Z-2gr-Explicit Frames model for the power peaking factor calculations The BOC with maximum reactivity was selected for calculating the detail reactivity balance together with the start-up core Fig 5 shows the burnup distribution of the BOC core and table 4 gives the reactivity balance for both cores

2.3.3 Detailed flux calculation

As it was mentioned the detailed flux calculation was performed on the BOC with maximum reactivity which was taken as a reference The calculated PPF for this core was 3.1 Figure 6 shows the mean fluxes in each box while fig 7 shows the thermal flux in a line perpendicular to the fuel plates crossing the center of the CIB

3 Design verifications

In the three cases, RP-10, NUR, and RA-3, during the start-up process several experimental verifications have been performed Different analysis of these results were done /11/, /12 /, /13/ The general conclusion is that the observed core parameters have been within the design values

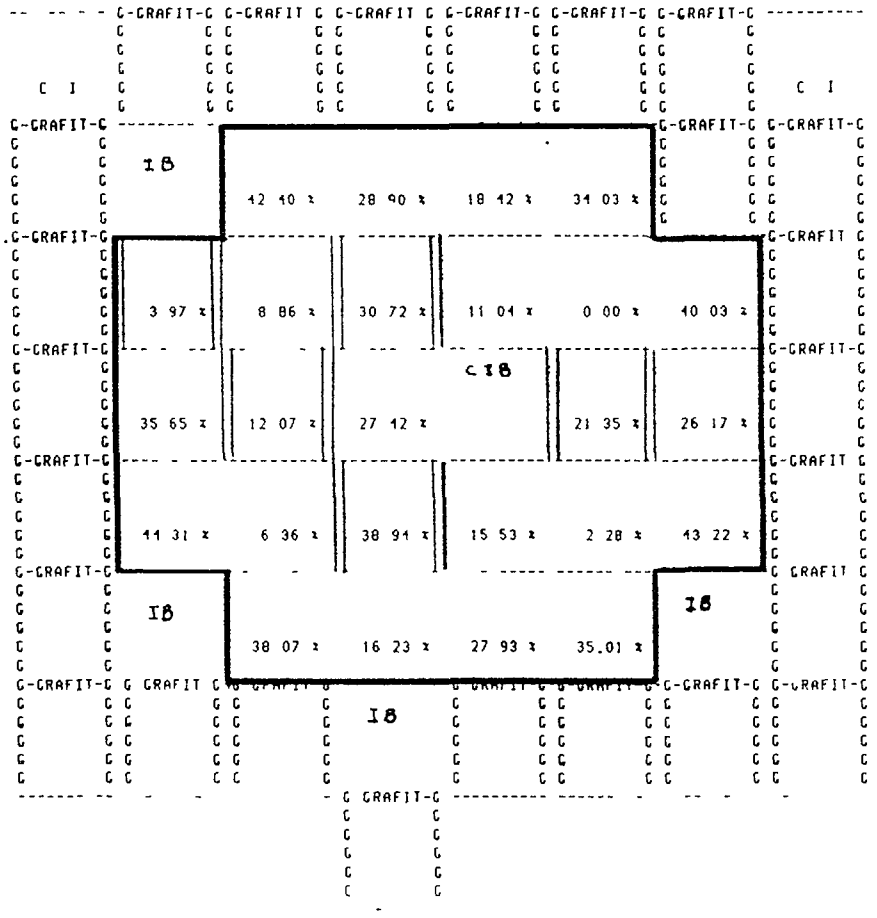

Figure 5 . BOC burnup distribution (in % of U_{235} consumed)

The X-Y(B^2_z) 2gr explicit frames model gives the reactivity results within a range of about 500 pcm. The experimental and calculated fluxes (X-Y-Z model) are also in good agreement within 10 %

The main differences between experimental and calculated reactivities are observed in large excess reactivity worth, let us say more than 3000 pcm We suppose that the main reason for this discrepancy is the strong interaction existing wher two or more

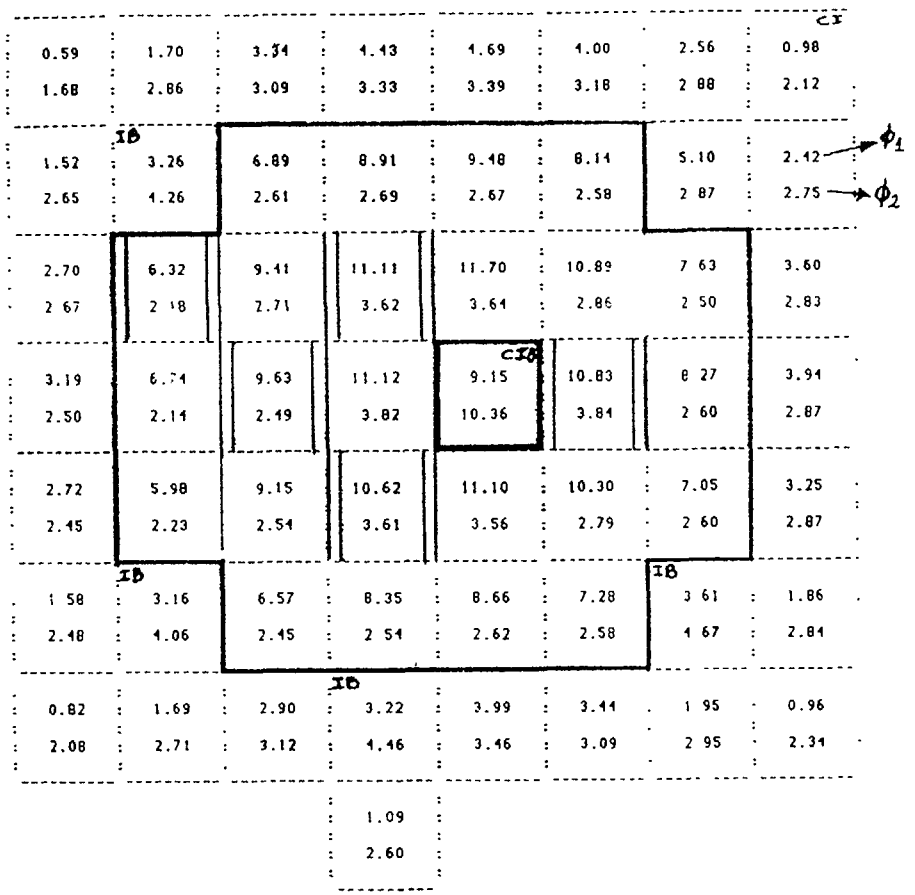

Figure 6 : BOC mean neutronic fluxes per region

control rods are inserted together. Normally the experimental core excess reactivity is obtained by adding linearly the control rods worth obtained from the control rod calibration which gives greater results than the calculated values. Figures 8 and 9 shows different cores that have been measured in the NUR and RA-3 reactor. The FE data are the same in both cases and can be obtained from table 5 (more details are given in /12/).

Table 4: Reactivity balance of the start-up and equilibrium cores

TEMP.	XENON	R1	R2	R3	R4	ρ (pcm) start-up	ρ (pcm) equilibrium
COLD 20 C	without					4981	5300
		1				897	1320
			1			2097	2280
				1		857	1330
					1	1202	1920
		1	1			-2621	-2020
		1		1		-3969	-2990
		1			1	-2413	-1630
			1	1		-2721	-2040
			1		1	-3100	-2400
				1	1	-2491	-1370
		1	1	1	1	-13775	-11800
HOT	without					4644	4950
HOT	with					1554	2120

R1 = 1 indicates control rod 1 100% inserted
R1 = blank indicates control rod 1 100% withdrawn

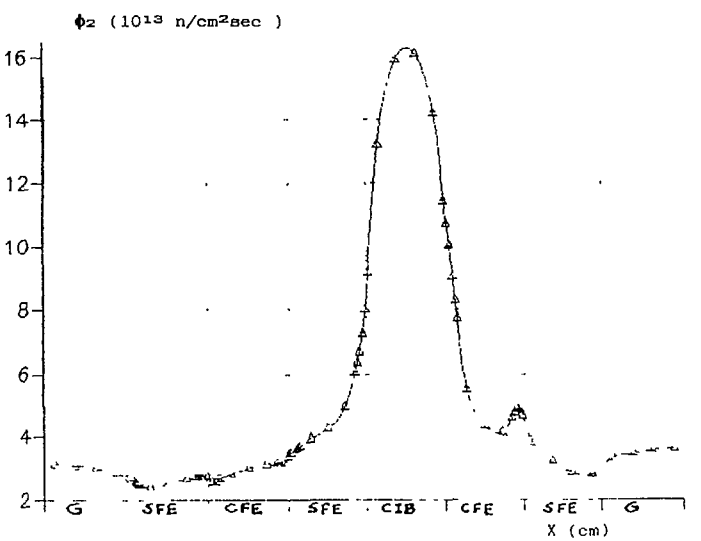

Figure 7: Neutronic thermal flux versus position in a central line perpendicular to the fuel plates

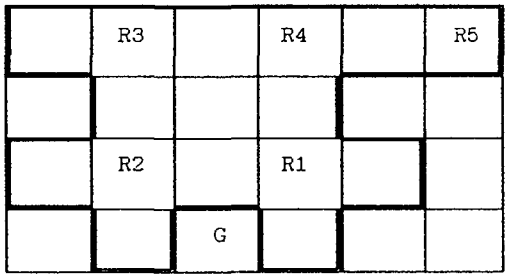

Experimental reactivity excess = 870 pcm

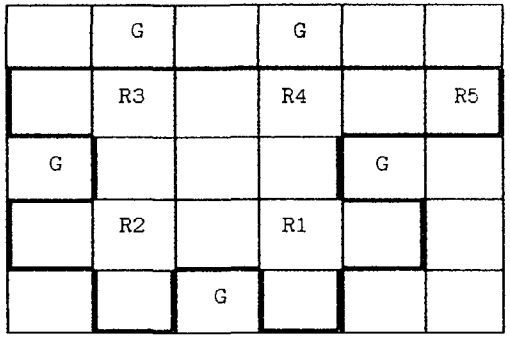

Experimental reactivity excess = 2300 pcm

Figure 8 : Measured LEU cores (x=8.1cm y=7 7cm)

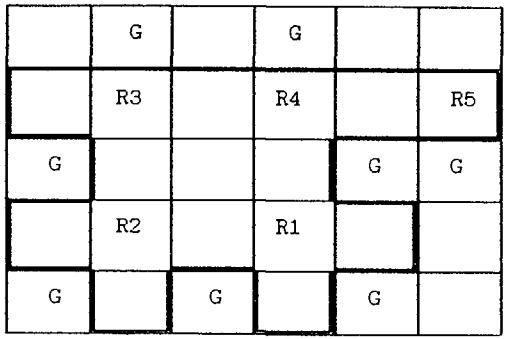

Experimental reactivity excess = 4020 pcm

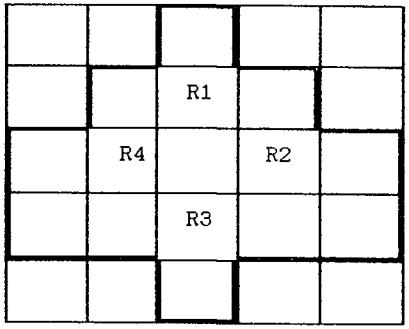

Experimental reactivity excess = 280 pcm

Start-up core (figure 2) Exper. react. excess = 5520 pcm

Figure 9 : Measured LEU cores (x=8.1cm y=7.7cm)

Table 5: Fuel Element data

Standard FE	
Fuel type	U_3O_8-Al
Enrichment	20 %
Uranium density in the meat	2.96 gr/cc
U_{235} mass per plate	76.5 gr
Void fraction in the meat	10 %
U_3O_8 density	8.1 gr/cc
U weight fraction in the U_3O_8	0.8477
Al density	2.7 gr/cc
Number of fuel plates	19
Plate thickness	0.150 cm
Meat thickness	0.070 cm
Clad thickness	0.040 cm
Water channel thickness	0.270 *cm*
Meat width	6.0 cm
Meat height (active height)	61.5 cm
Frame thickness	0.50 cm
Inner distance between frames	6.6 cm
Frame length	8.01 cm
Structural material (frames and clads)	Al 6061
Control FE	
Fuel plate	same as SFE
Number of fuel plates	14
water channel thickness	same as SFE
Frame thickness	0.45 cm
Inner distances between frames	6.7 cm
frame length	8.01 cm
Absorber material	Ag-In-Cd
(80%,15%,5%)	
Clad material for absorber	AISI 316
Material gap within the absorber	He
Guide plates material	Al 6061
Grid dimensions	7.7cm*8.1cm

In this report we wanted to describe how CNEA has developed its own calculation methods, successfully applied to the design of MTR cores. The complete design process has been followed beginning with the conceptual design and ending with the start-up of the facility (including the fuel fabrication) in most of the projects before mentioned.

References

/1/ Askew, Fayers and Kemshell; A general description of the lattice code WIMS, UKAEA, 1967 and 1981.

/2/ O.Chiovato, F.di Pasquantonio; GGTC-ENEL, CNA-CPL,1977.

/3/ Giust y Lecot; HERMET código de cálculo neutrónico de celda para combustibles MTR, Instituto Balseiro, 1987.

/4/ C.Grant; PUMA, sistema para la simulación del funcionamiento de reactores nucleares, CNEA-Re-163,1980.(Internal Report)

/5/ Villarino and Lecot; CITVAP an extended version of CITATION code, INVAP SE 1987.(Internal Report)

/6/ T.Fowler, D.Vondy, and G.Cunningam; CITATION a nuclear reactor core analysis code, ORNL-TM-2496,1972.

/7/ G.Ricabarra, M.B. de Ricabarra and M.Bang; MTR core experiments (part I and II), paper presented at the RERTR meeting 1987.

/8/ M.Higa, M.Madariaga y R.Waldman; Alternativas para definir el *núcleo de equilibrio del RA-3, CNEA-Re-CA-90-14.(Internal Report)*

/9/ M.Madariaga, D.Parkansky y R.Waldman; Propuesta y análisis de un núcleo con ECBE para el rearranque del RA-3, CNEA-Re-CA-90-16.(Internal Report)

/10/ M.Higa y M.Madariaga; Gestión de combustible y núcleo de equilibrio del reactor RA-3 con ECBE, CNEA-Re-CA-91-05.(Internal Report)

/11/ M.Higa y M.Madariaga; Análisis por cálculo de las experiencias físicas de la puesta en servicio del reactor Peruano RP-10, paper presented in the ARCAL V meeting, Chile 1991.

/12/ M.Madariaga E.Villarino, J.Relloso and R.Rubio; Calculation analysis of the neutronic experimental data coming from the NUR reactor start-up.

/13/ L.Cohen de Porto, M.T.Bang, G.Estryk y J.Quintana; Conversión del núcleo del RA-3 de elementos combustibles al 90% de enriquecimiento a elementos combustibles al 20% de enriquecimiento. Paper presented in the ARCAL V meeting, Colombia 1991.

CONTROL ROD WORTH, REACTIVITY AND POWER DISTRIBUTION IN A 1300 MWe PWR

M. NURDIN
National Atomic Energy Agency,
Jakarta, Indonesia

Abstract

The objectives of the presentation are to perform the amelioration of the precision in the burn-up calculation for the purpose of In-Core Fuel Management and implicitly the improvement of the reactor performance and the reactor safety. In generating the cross section set for the nuclear fuel assemblies having the absorber rods, a new procedure has been formulated to overcome the over-estimation of the worth of the control fuel assembly. The new procedure enables us to adjust the homogeneous nuclear constants by an adjustment factor taking into account the influence of the environment of control fuel assemblies in the core and the equivalence of the transport-diffusion calculation. The adjustment factor calculated at the beginning of life of the reactor has been proved rigorously to be sufficient for all core condition. Generation of the adjusted nuclear constants become a simple process. Hence this procedure enables us to improve three dimensional study of the core with reasonable computing cost and to anticipate the consequences of any movement of the absorber rods during operation of the reactor.

INTRODUCTION

The present study deal with the calculational scheme for pressurized water reactors aiming to improve the precision of core computation for the augmentation of safety and reactor performance. This is especially intended for the reactors operating as load follower, where the permanent movement of the control rods are needed. Hence it is really necessary to know correctly the worth of different group of rods insertion in the three dimensional calculation, where from computing cost point of view, they must be executed in homogeneous one.

In the calculational sequence known so far, the homogeneous or heterogeneous cross sections of fuel assembly are calculated in infinite medium.

Core calculations using one library per fuel assembly (homogeneous cross section) have good result compared to the reference if there is no control fuel element in the core, and if the rods are in the core they overestimate the control rod worth from 6 to 10% compared to the reference. On the other hand core calculation using cell by cell libraries give good result what ever the configuration of the core, but such computation is very expensive and need very high space of memory.

Concerning the calculational schema requiring new development, the study consist of two main subjects, first how to represent heterogeneously a certain fuel assemblies in the transport calculation and second how to improve the homogeneous nuclear constants of the control fuel assemblies. Hence the contribution of this study are :

1. On one hand, determination of the grouping procedure of the cell as a function of fuel enrichment, concentration of boron in the moderator, fuel burn-up etc. Using the transport code APOLLO1, based on the best discretisation of the fuel assembly, reactivity and power distribution per fuel assembly are calculated both at time zero and in burning-up (evolution) situation.

2. On the other hand, establishment of a method in calculating the homogeneous nuclear constants for the control fuel assemblies.

So the study covers the following analysis

- Pressurized Water Reactor 1300 MWe
- Calculational Method used for Cross Section Generation
- New Procedure for Generating Homogeneous Nuclear Constants of the Control Fuel Assemblies
- Generalisation of the Calculational Procedure
- Conclusion

I. PRESSURIZED WATER REACTOR 1300 MWe

I-1 Principal Characteristics of the Core

This system use light water reactor both as coolant and moderator Moderation ratio of a cell is 1.655 and for a standard fuel assembly the ratio is 1.982.
Active length of the core (H) is 426.7 cm and its equivalent diameter (D) is 337.03 cm. The core produce 3 800 MWth.
The first core of the reactor consist of 193 fuel assemblies having three different enrichments. There are 65 fuel assemblies with the enrichment of 1.50%, 64 fuel assemblies with enrichment of 2.40% and the rest is 2.95%
Loading pattern of the first core is shown in Fig. I-1.
There are 58 instrumented fuel assemblies in the core, equipped by mobile detector, intended for detail flux mapping.
For the first core, at beginning of life, with obligation to have negative temperature coefficient of the moderator, a certain fuel assemblies are equipped by burnable-poison (glass of borosilicate).
There are 80 burnable fuel assemblies in the core an after the first cycle all burnable rods will be removed from the fuel assemblies
For the purposes of reactor operation and safety, there are three control system available, i.e

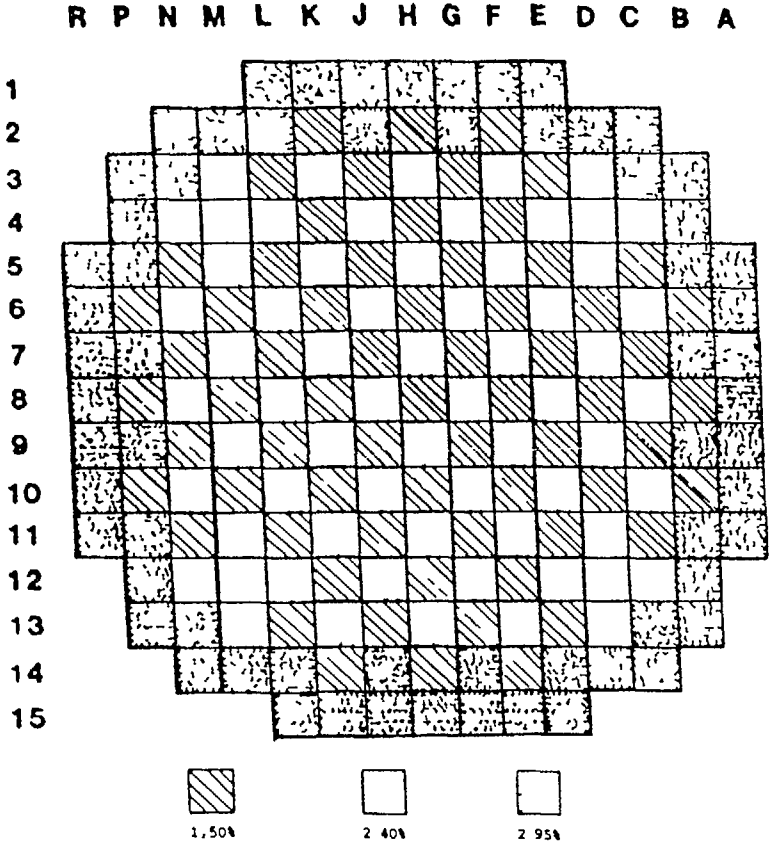

Fig. I-1 LOADING PATTERN OF THE FIRST CORE

1. Urgent shut-down of the reactor the system must be capable of stopping the reactor at any moment of operation.
2. Power regulation the objectives of the system are,
   - to regulate the variation of moderator average temperature during operation,
   - to regulate the power demand, regulation of reactor power level

3. Long term regulation, the system is intended to follow the reactivity during the evolution of the core, it means :
   - evolution of fuel assemblies, burn-up of fissile material,
   - evolution of xenon, the accumulation of fission product,
   - changement from shut-down and hot condition to shut-down and cold condition of the core.

The purpose of grouping the control rods as such are to minimize the maximum amplitude of power peaking due to the insertion of the rod to the core and to assure an optimum burn-up of the fuel.
The core configuration representing the position of standard fuel assemblies with three different enrichments, burnable fuel assemblies, groups of rods for regulation and for safety is shown in Fig. I-2.
The description of core reactor can be seen in Table I-1.

I-2 Description of Fuel Assembly

The fuel assembly is the type of 17 x 17, and the assembly is consisting of :
- 264 rods of Uranium dioxide (UO_2),
- 24 guide tubes, to accommodate the control rod, burnable rod and neutron source for start-up the reactor,
- 1 guide tube for instrumentation.

Salient feature of fuel assembly is shown in Table I-2.

II. CALCULATIONAL METHOD USED FOR CROSS SECTION GENERATION

II-1 General

The objectives of neutronic calculation is to determine evolution of reactivity, power distribution and the worth of control rod during the cycle of reactor operation.

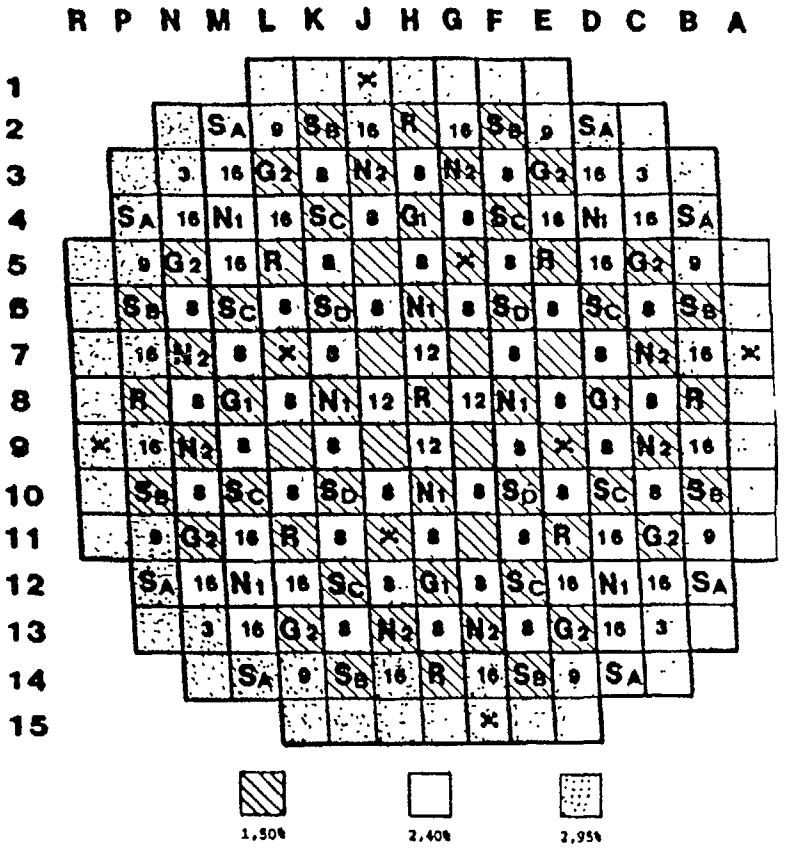

Fig. I-2 FIRST CORE CONFIGURATION OF PWR 1300

Neutronic calculational scheme of a nuclear reactor can be divided into two steps :
- cell or multi-cell (fuel assembly) calculation using the transport theory that enable us to obtain the nuclear parameters,
- space and energy calculation using the diffusion theory utilizing the nuclear parameters obtained at the preceding step.

TABLE I-1. DESCRIPTION OF REACTOR CORE

9	Thermal Power, MWth	3 800
	Percentage of Power produced in fuel (%)	97.4
	Disposition of Fuel Assembly	3 region
	Assembly with enrichment of 1.50% :	65
	Assembly with enrichment of 2.40% :	64
	Assembly with enrichment of 2.95% :	64
	Burnable fuel assembly (E=2.4% & E=2.95%)	80
	- Uranium, kg	103 909
	- UO_2, kg	117 880
	- Zircaloy, kg	24 700
	- Inconel, kg	1 110
	- Steel, kg	220
	- Water, kg	20 250
	Temperature of coolant, C :	
	- hot, zero power	297.20
	- inlet, hot, nominal power	293.10
	- average in core, hot, nominal power	311.80
	Nominal pressure in bars	155.10
	Average linear power, kw/m	17.02
	Power produced in core kw/kg uranium	36.60
	Power density, kw/l core	99.80

The cross section sets of each fuel assembly in 2 groups of energy used in the diffusion calculations are generated by the transport code "Apollo 1" using the approximation of multi-groups for energy spectrum (0 - 10 Mev) and collision probability method (best adaptation for heterogeneous thin mediums of the lattice).

The nuclear constants obtained from this calculation can be in two forms :

- heterogeneous nuclear constants, cell by cell library of an assembly,
- homogeneous nuclear constants, one library of an assembly.

Having two forms of library, we can have two calculational schemes :

- heterogeneous transport-diffusion,
- homogeneous transport-diffusion.

TABLE I-2. SALIENT FEATURE OF FUEL ASSEMBLY

Type of array	17 x 17
Side of the assembly, cm	21.504
Number of fuel rod per assembly	264
Number of guide tube per assembly	25
Number of grid along the active core	9
Number of grid along the fuel assembly	10
Material :	
- fuel	UO
- pressurization gas	Helium
- cladding	Zircaloy 4
- grid	Inconel 718
- cladding absorber rod	SS 304
Cold fuel cell dimension :	
- pitch, cm	1.260
- outer diameter of the cladding, cm	0.950
- inner diameter of the cladding, cm	0.836
- pellet diameter, cm	0.819
Cold guide tube dimension :	
- outer diameter, cm	1.224
- inner diameter, cm	1.143
Fuel enrichment	
- region 1, 65 assemblies (%)	1.50
- region 2, 64 assemblies (%)	2.40
- region 3, 64 assemblies (%)	2.95

At the first scheme, the calculation of core or a fraction of core (motif, assembly) is carried out for each cell in diffusion theory. This calculation is considered as the reference for the calculation of the second scheme.

II-2 Cross Section Generation

In this step, it is necessary to determine the representation of fuel assembly for the transport calculation, since most of the assemblies in the core are symmetric; after a certain verification basing on :

- correction factor of equivalence heterogeneous and homogeneous transport (factor SPH),
- level of integrated flux in 13 physical cells and in the fuel assembly,
- reactivity of each assembly,
- computing time,

it was refound that the symmetrical fuel assembly can be represented by 1/8 of the assembly, total cells of this presentation are 45, see Fig. II-1.
According to the core configuration, and taking into account the water layer between the assemblies, there are 8 generic cells in the core :

a. fuel cell at the corner of assembly
b. fuel cell at the periphery
c. inner fuel cell
d. water rod cell (TE)
e. water rod cell for instrumentation (TI)
f. grey rod cell (BG-ACIER)
g. black rod cell (BN-AIC)
h. black rod cell (BN-B_4C)
i. burnable rod cell (PC)

The distribution of these generic cell in the fuel assemblies are as follow :

REPARTITION OF GENERIC CELL PER FUEL TYPE

Genevic cell	Standard Fuel Assembly	Grey CFA	Black CFA		Burnable Fuel		
			AgInCd	B4C	8PC	12PC	16PC
a	1	1	1	1	1	1	1
b	8	8	8	8	8	8	8
c	30	30	30	30	30	30	30
d	5	-	-	-	4	3	2
e	1	1	1	1	1	1	1
f	-	3	-	-	-	-	-
g	-	2	5	-	-	-	-
h	-	-	-	5	-	-	-
i	-	-	-	-	1	2	3

Cold dimension of absorber rod used in our calculations is illustrated in Fig. II-2.

For each fuel assembly, it has 5 or 6 generic cells, each has different isotopic composition or different geometry, and due to the limit of code, we determine 13 physical cell. The complete schemes for the elaboration of nuclear constants at time zero and during evolution of core are illustrated in Fig. II-3a and Fig. II-3b.

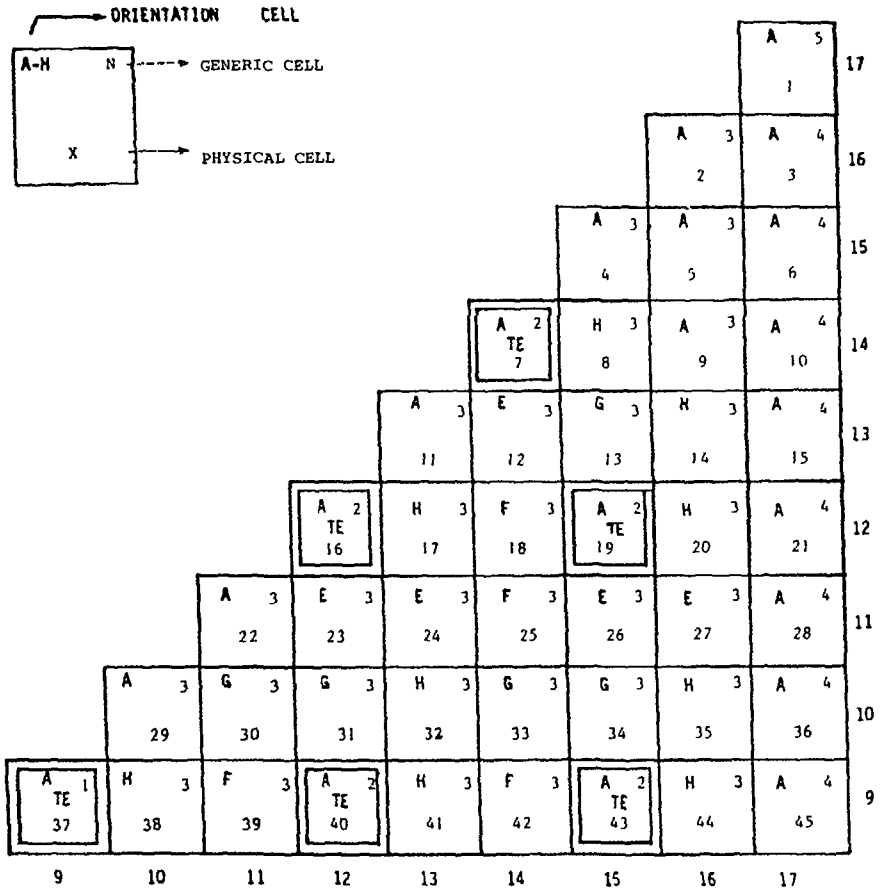

Fig. II-1 REPRESENTATION OF 1/8 FUEL ASSEMBLY

Using the two calculational schemes mentioned above, we have 9,24 and 22 groups of cells in the standard, grey and black control fuel assembly respectively.

For burnable fuel assemblies having 8,12 and 16 rods of pirex, we have respectively 20,27 and 24 groups of cells. Representation of 22 groups of cells for black control fuel assembly is shown in Fig. II-4.

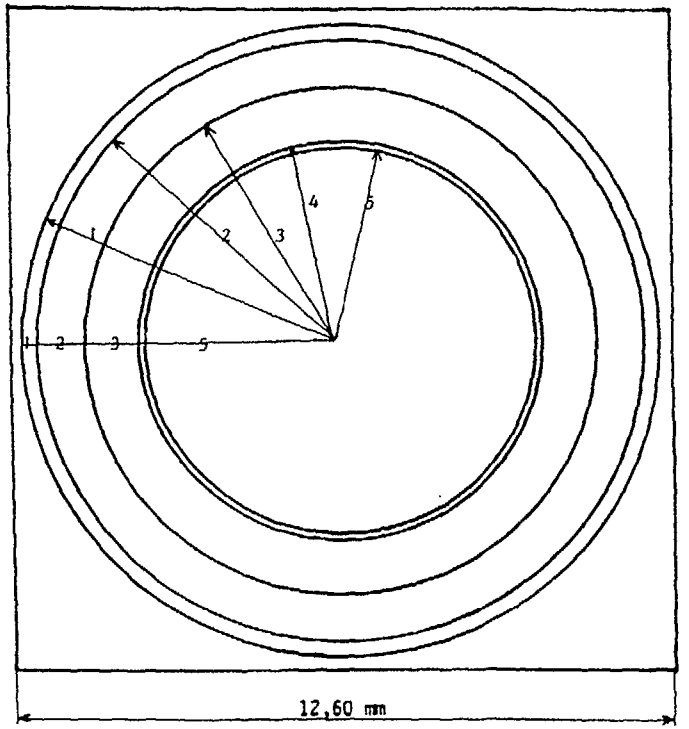

ZONE/RADIUS	MATERIAL	COLD RADIUS (cm)
1	Zircaloy (G.T.)	
2	Water	
3	SS 304	
4	Gap	
5	AIC or B_4C	

Fig. II-2 COLD DIMENSION OF ABSORBER CELL

The validity of cell grouping have been verified rigorously by taking into consideration, the following situations :

- level of discretisation,
- degree of enrichment,
- concentration of boron in moderator,

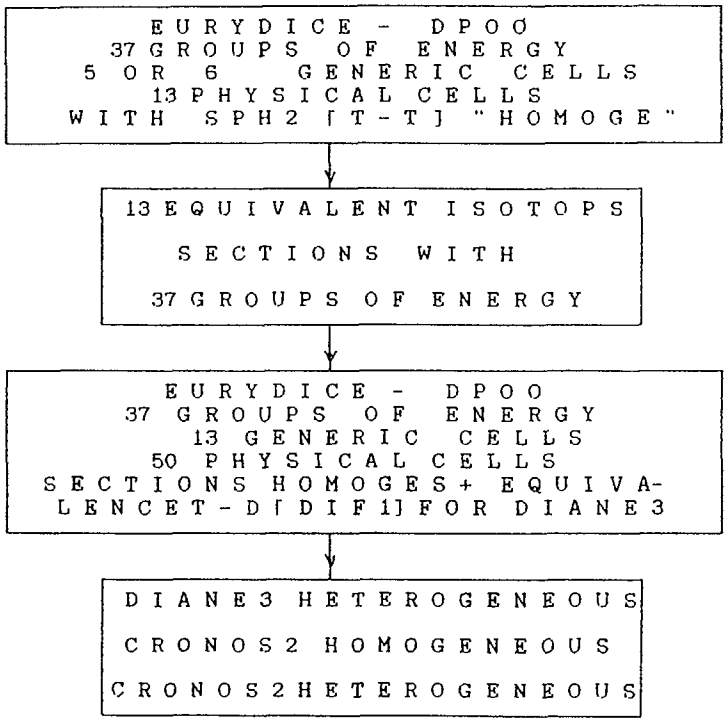

Fig. II-3a GENERATION OF CROSS SECTION AT STEP 0

- burn-up level,
- disparition of burnable poison in the fuel assembly.

The relative discrepancies of the power distribution compared to the reference are in the order of 1 or 2%. The cell at the corner present around 3 or 5%, fortunately the power in such kind of assembly is lower than the average one.

It is worth to mention that the grouping used for grey control fuel assembly can not be applicable for to the black control fuel assembly even the degree of discretisation of the former is better than the last one; the profile of physical interaction between the cells are not identic in those assemblies.

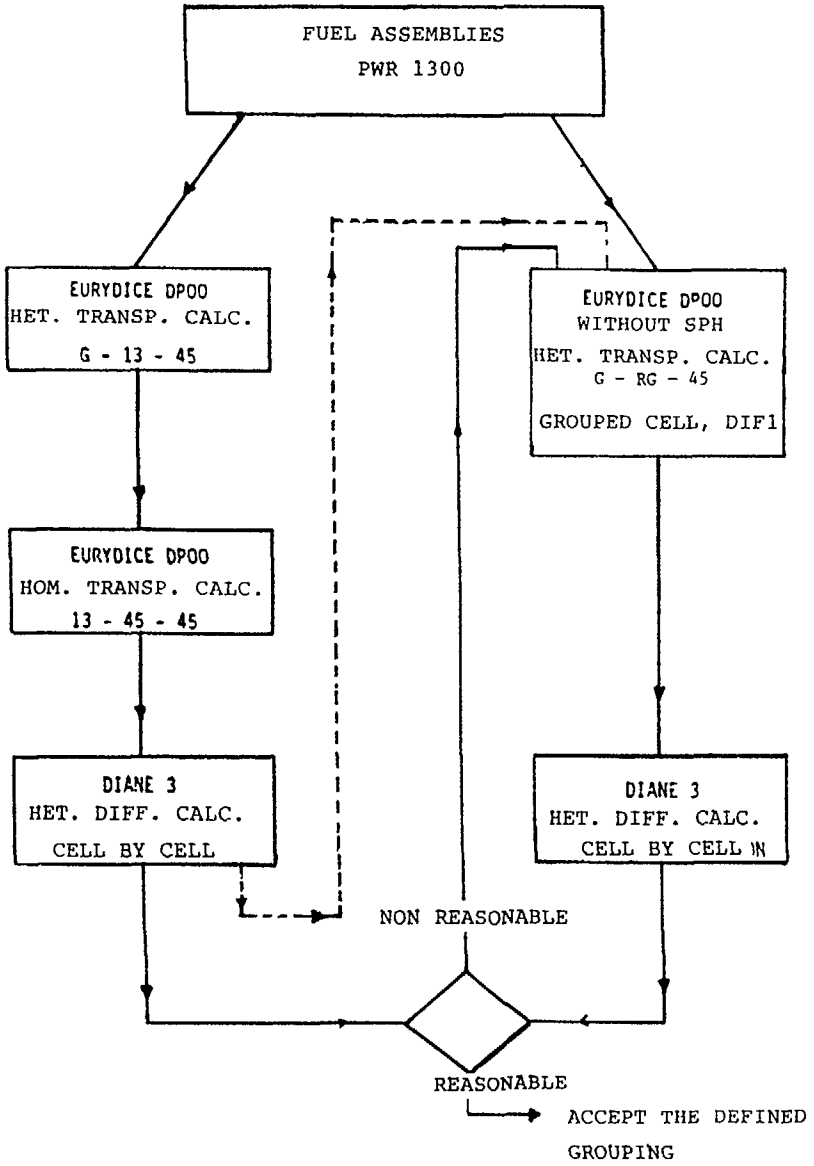

Fig. II-3b CALCULATIONAL SCHEME FOR GROUPING THE CELLS

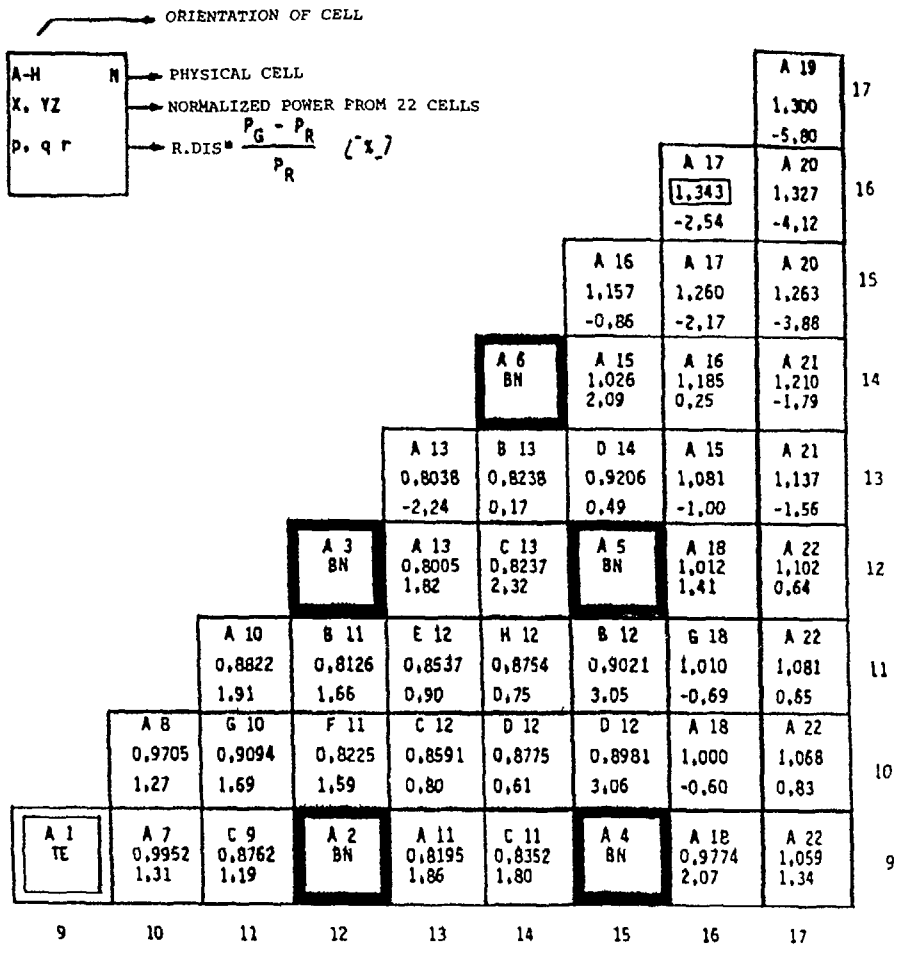

Fig. II-4 REPRESENTATION OF 22 PHYSICAL CELLS OF BLACK CONTROL FUEL ASSEMBLY /B_4C ABSORBER ROD/
ENRICHMENT = 1.5%
BORON CONCENTRATION = 1150 ppm
TE = WATER ROD
BN = CELL OF B_4C
WORTH = 48761 pcm

Cell grouping must of course be determined properly, otherwise we lose the precision. It is important to note here that cell grouping is relevant to minimize the computing cost, especially in generating the evolutive library where many steps of burn-up are required.

III. NEW PROCEDURE FOR GENERATING HOMOGENEOUS NUCLEAR CONSTANTS OF CONTROL FUEL ASSEMBLIES

III-1 General

In following the demand of the grid, PWR 1300 use the grey control assembly (G1, G2) and black control assembly (N1, N2 and R). For this purposes, it is really necessary to know precisely the worth of the rods and from safety point of view it is important to anticipate any consequences of the rods movement on reactivity, power distribution and peaking position.

III-2 Position of the Problem

Core calculations using one library per fuel assembly (homogeneous cross section) have good result compared to the referential ones if there is no control fuel element in the core, and if the rods are in the core they overestimate the control rod worth from 6 to 10% compared to the reference. On the other hand core calculation using cell by cell libraries give good result what ever the configuration of the core, but such computation is very expensive and need very high space of memory. To show this phenomena, it is necessary to have 6 motifs (each motif consists of 9 fuel assemblies) representing both the configuration of the core and the spectrum of neutron energy, they are as follow

1	2	1	3	5	3
2	c	2	1	c	5
1	2	1	3	4	1

Motif B Motif C

1	2	y	1	2	y	2	y	2	2	y	2
2	x	2	2	1	2	2	1	2	2	1	2
1	2	1	x	2	1	1	2	x	2	x	2

Motif D Motif E Motif F Motif G

Where : 1 = standard fuel assembly, E = 1.50%
2 = standard fuel assembly, E = 2.40% + 8 pyrex
3 = standard fuel assembly, E = 2.95%
4 = standard fuel assembly, E = 2.40% + 12 pyrex
5 = standard fuel assembly, E = 2.95% + 16 pyrex

C, X and Y = position for control fuel assembly.

Since we use the motifs to qualify our libraries, the references should be defined before.

Based on the work done on PWR 900 MWe (REP - CP1 (2)), operating in mode A, a series of measurement on the worth of their control rod were compared to the results of heterogeneous diffusion calculations as illustrated below

C o n t r o l r o d w o r t h

Group insertion	Measurement (pcm)	Heterogeneous diff. calculation (pcm)	Δ(%)
D	1310±26(±2.0%)	1318	+ 0 6
C	1120±33(±2.9%)	1132	+ 1 1
B	1857±57(±3.1%)	1906	+ 2.6

From the results in the above table, the heterogeneous calculation are slightly bigger than the measurement, but all of them are in the incertitude of the measurement. So we can take the heterogeneous diffusion calculation as the reference.
If the control fuel assembly are replaced by standard fuel assembly (6 motifs), the maximum difference in reactivity between heterogeneous and homogeneous calculation is only 83 pcm, it is negligible compared to the reactivity at the motif C. When absorber rods are inserted completely in those motifs (B, C, D, E. F and G), the relative discrepancies range from 6.6% to 7.95% in the motif B and motif C for the black control assembly and they range from 2% to 2.29% for the grey control assembly.
For the other motifs, the discrepancies are slightly decreased, but they are still untolerable.
From the above presentation, our conclusion is that the homogeneous nuclear constants of the control fuel assembly should be elaborated by certain amelioration.

III-3 Calculational Scheme for Control Fuel Assembly

Homogeneous nuclear constants generated in infinite medium do not take into account the following phenomena
- the environment of the control fuel assembly in the core,
- the equivalence of homogeneous transport-diffusion calculation.

According to the core configuration, the proper environment for the control fuel assembly is the burnable fuel assembly. The modul treating the equivalence of homogeneous transport-diffusion calculation is not available in the EURYDICE (direct homogenesation) Another constraint of Eurydice is in geometrical capacity

Taking into account those problems, modul MARSYAS is used to give the solution and the procedure for that are as follow :

1. Marsyas-motif, transport calculation done on a motif consisting of control fuel assembly and its environment. From this calculation we have homogeneous nuclear constants in two groups of energy. This homogeneous constants take already the equivalence transport--diffusion into consideration. The constants is named "JEU A".
2. Marsyas-assembly, transport calculation done on a control assembly in infinite medium. The constants in two groups of energy is named "JEU B".
3. Adjustment factor represents simultaneously the equivalence of homogeneous transport-diffusion calculation and the environment, in two groups of neutron energy, are defined as such :

$$\mathcal{L} = \frac{\text{JEU A [MOTIF]}}{\text{JEU B [MEDIUM } \mathcal{L}\text{]}}$$

4. By an assumption (hyphothese) that the factor is independent of the modul used in the calculation, so we have :

$$\mathcal{L} = \left[\frac{\text{JEU A}}{\text{JEU B}}\right]_{\text{MARSYAS}} = \left[\frac{\text{JEU A}}{\text{JEU B}'}\right]_{\text{EURYDICE}}$$

$$\Longrightarrow \underbrace{\text{JEU A}}_{\text{ADJUSTED (EURYDICE)}} = \mathcal{L} \times \underbrace{\text{JEU B}'}_{\text{EURYDICE MEDIUM } \mathcal{L}}$$

Calculational scheme for the elaboration of homogeneous nuclear constants of control fuel assembly is illustrated in Fig. III-1.

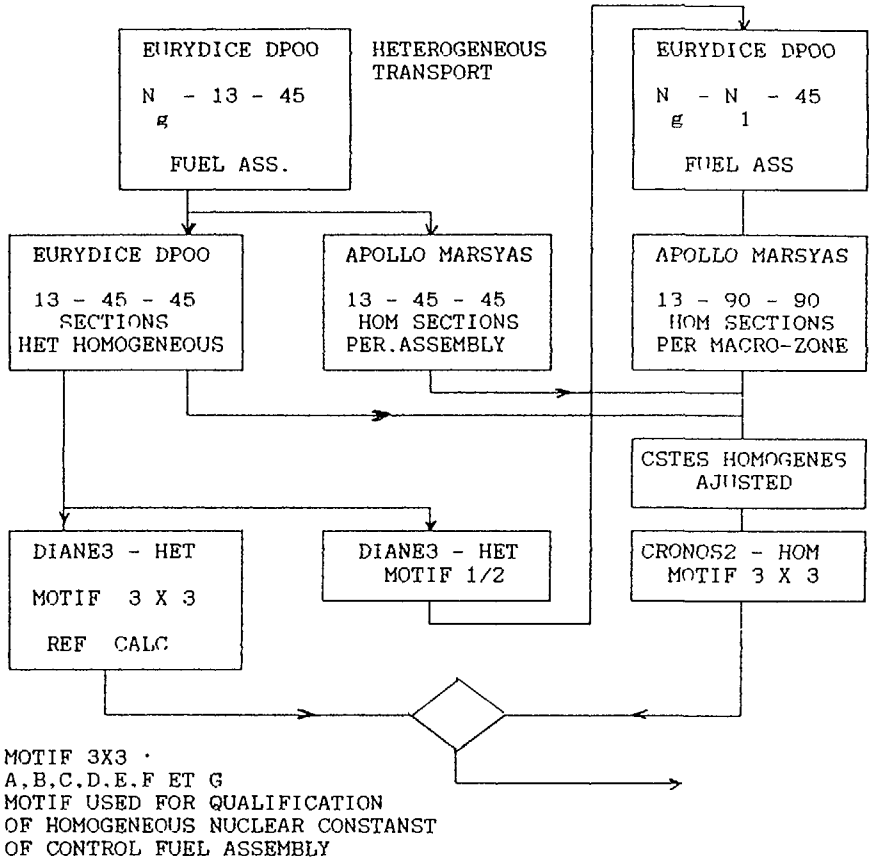

Fig. III-1

CALCULATIONAL SCHEMA USED

The homogeneous nuclear constants of the control fuel assembly produced by Eurydice through direct homogeneisation are corrected (adjusted) by the adjustment factors.
Utilization of adjusted nuclear constants in homogeneous diffusion calculation on the 6 motifs mentioned above give good results if we compare to the reference.The maximum relative discrepancy in the worth of rods is 1.43 % for the

black control assembly on the motif C, compared to the value of 8% using unadjusted homogeneous nuclear constants. From the power distribution point of view that the maximum relative discrepancy is 2.8% in the black control assembly, but for the peripheral assemblies only 1.4%, both in the fuel assembly having less power.

IV. GENERALIZATION OF THE CALCULATIONAL PROCEDURE

IV-1 General

After starting-up the reactor, all original characteristics begin to change, the evolution of the core are due to the following phenomenas and needs :

-. at beginning of life
1. depletion of fissile material,
2. dilution of boron or its depletion in the moderator,
3 accumulation of the fission product,
4. depletion of boron in the burnable rod,

-. beginning of the second core until equilibrium core :
5. depletion of fissile material and fission product accumulation in the control fuel element,
6. chargement of the environment due to fuel element shuffling

for the future cycle.

According to the various phenomenas mentioned above, does adjustment factor calculated at the beginning of life change? To answer this question, a series of sensitivity study is of course necessary; namely as a function of :

1. influence of the environment
2. influence of the boron concentration in the moderator
3. influence of burnable poison depletion
4. influence of the fuel evolution
5. influence of the changement of the environment due to fuel management path.

IV-2 Influence of the Environmental Modification

At the first cycle, the position of control fuel assembly are also side by side with the burnable fuel assembly having 9, 12 and 16 rods of pyrex and the enrichment of 2.40% and 2.95%. To know the concequences of this modification on the adjusted nuclear constants, we use the motif B and C as below :

1	2	1	3	5	3
2	c	2	1	c	5
1	2	1	3	4	1
Motif B			Motif C		

It is found that the maximum relative discrepancy on the control rod worth of B_4C is only 1.43%. So the adjustment factor is still applicable.

IV-3 Influence of Boron Concentration in Moderator

Due to the operational demand, boron is diluted and so the concentration decrease, for example until 25 ppm.
When the adjustment factor generated, the concentration of boron is 1150 ppm; there fore the simulation of boron concentration like 650 ppm, 250 ppm and 25 ppm are required to test the factor.

Using the same adjustment factor for each boron concentration, the adjusted homogeneous nuclear constants of the

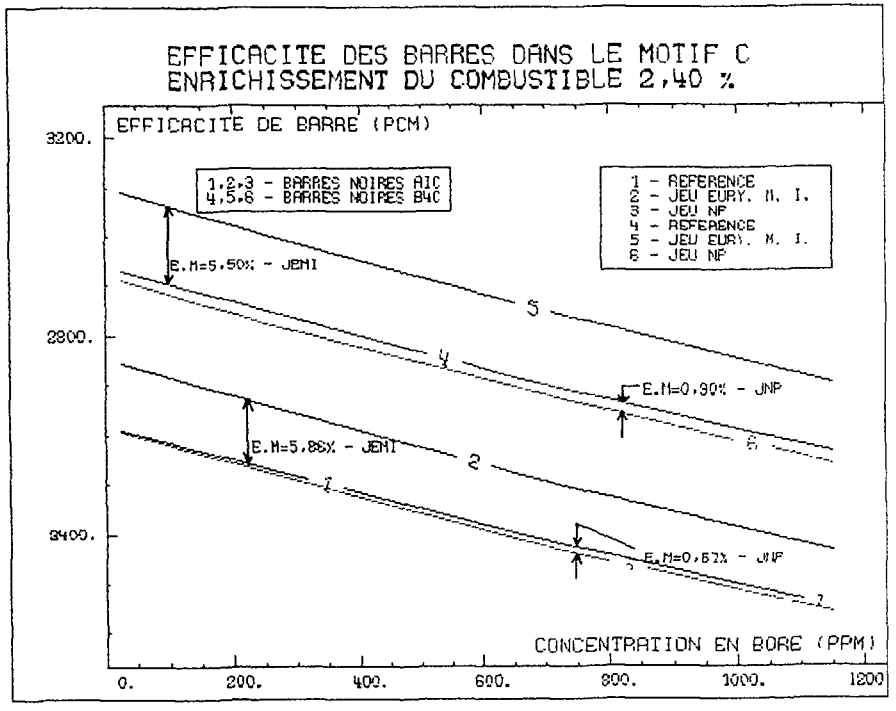

3	5	3
1	grappe	5
3	4	1

1 = assemblage sans poison (E=1,50%)

3 = assemblage sans poison (E=2,95%)

4 = assemblage empoisonné (E=2,40%, 12 pyrex)

5 = assemblage empoisonné (E=2,95%, 16 pyrex)

Fig. IV-1 CONTROL ROD WORTH AS A FONCTION OF BORON CONCENTRATION

control fuel assemblies having the fuel enrichment of 2.4% are calculated.

Utilization of these constants in the motif C give the maximum relative discrepancy of 0.8% for B_4C; as shown in Fig. IV-1.

IV-4 Influence of Boron Depletion in Burnable Fuel Assembly

To simulate this study, boron concentration of 75,50 and 25% from their natural concentration are taken as the basic of evaluation.

In this case, the environment itself change, but nothing to do with the control fuel. For control fuel with fuel enrichment of 2.40%, the maximum relative discrepancy in the motif C is 0.73% for B_4C at 75% concentration of boron in the burnable fuel assembly, it is shown in Fig. IV-2.

IV-5 Influence of Fuel Depletion

The conditions belong to this phenomena can be divided into 3 situations :

- evolution of core during the first cycle, there are still burnable rods in the core,
- evolution of core during the second and the third core, there is no anymore the burnable rod in the core, the original enrichment is still different,
- evolution of equilibrium core where the fuel assembly have the same initial enrichment.

The first case is much more complicated due to the heterogeneous medium in the core, so it will be shown here the result of verification both as a function of power distribution in the motif and reactivity/worth of the control fuel assembly.

It is worth to remind here again that the adjustment factor used is always the first one, it was elaborated at the beginning of life.

As shown in Fig IV-3 (A, A', B and B'), the maximum relative discrepancy are in the control fuel element for the power distribution, so it is well accepted, because this fuel ge-

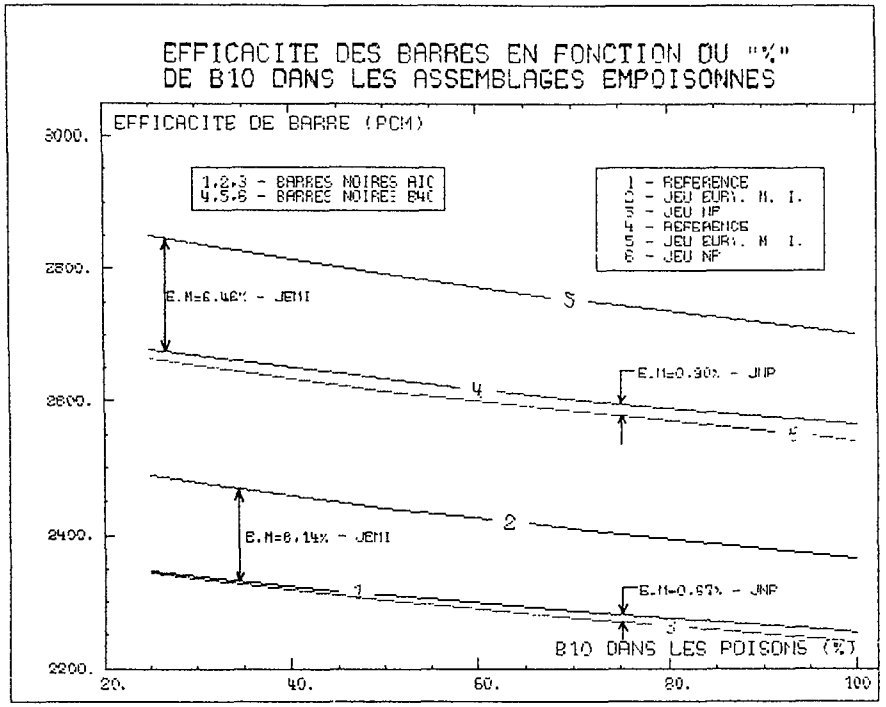

3	5	3
1	grappe	5
3	4	1

1 = assemblage sans poison (E=1,50%)

3 = assemblage sans poison (E=2,95%)

4 = assemblage empoisonné (E=2,40%, 12 pyrex)

5 = assemblage empoisonné (E=2,95%, 16 pyrex)

Fig. IV-2 CONTROL ROD WORTH AS A FONCTION OF BORON CONCENTRATION

nerate less power than the other fuel assemblies. From reactivity/worth of the rods point of view, the maximum relative discrepancy is negligible (very small).
From the power distribution point of view, the peripheral assembly are correctly calculated.

A

	ASP-0.0
	1,018 1,018 0,00
BNB-0,0	APC-0,0
0,4778 0,4667 -2,32 $\Delta\rho$ =0.21	1,113 1,115 +0,18

^{1}A

	ASP-5000
	1,026 1,028 +0,19
BNB-15000	APC-7000
0,4657 0,4515 -3,09 $\Delta\rho$ =0.22	1,107 1,109 +0,18

B.

	ASP-5000
	1,013 1,014 0,10
BNB-500	APC-7000
0,5059 0,4985 -1,46 $\Delta\rho$ =0.0	1,110 1,111 +0,09

^{1}B

ASP-11000	APC-13000	ASP-11000
0,9114 0,9114 +0,19	1,011 1,013 +0,20	0,9114 0,9131 +0,19
APC-13000	BNB-13000	APC-13000
1,094 1,094 +0,00	0,5131 0,5010 -2,36	1,094 1,094 +0,00
ASP-9000	BPC-9000	ASP-9000
1,099 1,100 +0,09	1,267 1,270 +0,24	1,099 1,100 +0,09

Fig. IV-3 REACTIVITY, CONTROL ROD WORTH AND POWER DISTRIBUTION

V. CONCLUSION

1. Cell grouping is a good tool to minimize the computing cost; especially for generating the evolutive libraries consisting of many burn-up steps.

2. Adjustment factor calculated at the beginning of life of the reactor, they can be used for any condition of the reactor; they are calculated 1 time and its utilization is justified for all condition of the reactor.

3. Application of this homogeneous cross section, enable us one day to modify all the constants for the purpose of three dimensional diffusion calculation by the new p.c.

4. Adjustment of the nuclear constants is then quite simple; but the result are well justified both by power distribution in the core on in the fraction of the core (motif) and by the reactivity & the worth of rods.

REFERENCES

1. M. NURDIN
   Reactor a eau sous pression de 1300 MWe:
   Amelioration de la representation des assemblages et du calcul des absorbants
   Ph.D Thesis. Universite de Paris XI. Centre d'Orsay
   June 1989

2. J. BERGERON
   Private communication

3. J. BILLECOCQUE
   Private communication

4. A. PUILL
   Private communication

5. M. NURDIN
   Calculational method for PWR burnable fuel assembly
   IAEA-TEC DOC-587
   VIENNA - December 1989

6. J. KREBS
   Utilisation dans Marsyas de Jeux de sections equivalentes transport. Comparaison EURYDICE - MARSYIAS
   Rapport DEMT/481

7. J. KREBS
   Private communication

8. APPOLO1 :
   - Note de principe. Report DEMT 85-450/SERMA 728/1
   - Note de informatique. Report DEMT 86-322/SERMA 728/2
   - Notice d'utilisation. Report DEMT 87-446/SERMA 954

9. J.L. FRANCOIS, R. LENAIN
   DIANE3 :
   Presentation de la procedure No:1.
   Report DEMT 85/457
   SERMA/LENR/85/733 "T"

10. CRONOS
    - Note de principe. Report DEMT 85-305/SERMA 704/1
    - Notice d'utilisation. Report DEMT/87-019/SERMA 704-3

11. M. DETOC
    Module TRISYNTHESE
    Report SERMA SPM 460 DR

12. R. LENAIN
    EUGENE :
    Un generateur externe de NEPLIB
    Note SERMA/LENR/85/1657
    February 1985

13. G. MATHONNIERE
    Bibliotheque neutronique a nombre restreint pour le calcul des reacteur a eau
    Ph.D Thesis. Universite de Paris XI. Centre d'Orsay
    October 1980

14. A. HEBER
    Private communication

CRITICALITY CALCULATIONS FOR A BWR SPENT FUEL POOL

M. BARCENAS-ROBLES, C. FILIO-LOPEZ
Comisión Nacional de Seguridad Nuclear y Salvaguardias
and
Escuela Superior de Física y Matemáticas,
Mexico City, Mexico

Abstract

In this paper we present the methodology used for calculating the effective multiplication constant (K_{eff}) for BWR spent fuel arrangements. The calculations were performed for the spent fuel pool specified in the Final Safety Analysis Report[1] for the BWR Nuclear Plant at Laguna Verde, Veracruz. The computer codes RECORD[2] and MIXQUIC[3] were used to perform these calculations. The macroscopic cross sections for two energy groups were obtained with the RECORD code assuming 3 w/o U-235 enrichment and no gadolinium for the fuel elements and stainless steel surrounding the fuel assembly. The spent fuel racks geometry and cross sections were used along with the MIXQUIC code to perform the two-dimensional criticality calculations with no neutron leakage along the axial axis. Additional calculations were performed changing the temperature, fuel assemblies pitch and tube wall thickness. The results show that the multiplication constant obtained is less than the value of 0.95 required as a limit for the design of a spent fuel pool.

GENERAL DESCRIPTION

The present mexican nuclear project comprises two Boiling Water Reactors (BWR/5) of 654 MWe, one is now in operation and the other is still under construction. Both reactors are located in Laguna Verde, Veracruz and were supplied by General Electric. In the first cycle of the operating plant the reactor was loaded with 444 fuel assemblies of the type GE5. There are three different types of fuel assemblies. The average enrichment are 2.19 w/o, 1.76 w/o and .711 w/o with several gadolinium contents.

Fuel Assemblies	U-235 Average Enrichment (w/o)
280	2.19
96	1.76
68	0.711

Each of the fuel assemblies consists of 62 fuel rods and 2 water rods surrounded by a square flow box (Figure 1.). The fuel rods have the following dimensions:

Parameter	Dim.
Pitch	16.256 mm
Pellet diameter	10.41 mm
Outer diameter of clad	12.268 mm
Inner diameter of clad	10.642 mm
Rod active length	3810 mm

SPENT FUEL RACKS

The spent fuel assemblies are stored in racks which are placed on the pool floor without any floor attachment, and laterally supported by the bracing system as illustrated in Figure 2.

The capacity of each of the spent fuel racks is 9 x 6 or 54 fuel assemblies. Each rack consists of tube cluster assemblies supported by a cross-braced framing system, a base plate, and four leg assemblies as shown in Figure 3.

One 36-space "special purpose rack" has been designed to store the control rods, the defective spent fuel bundles with

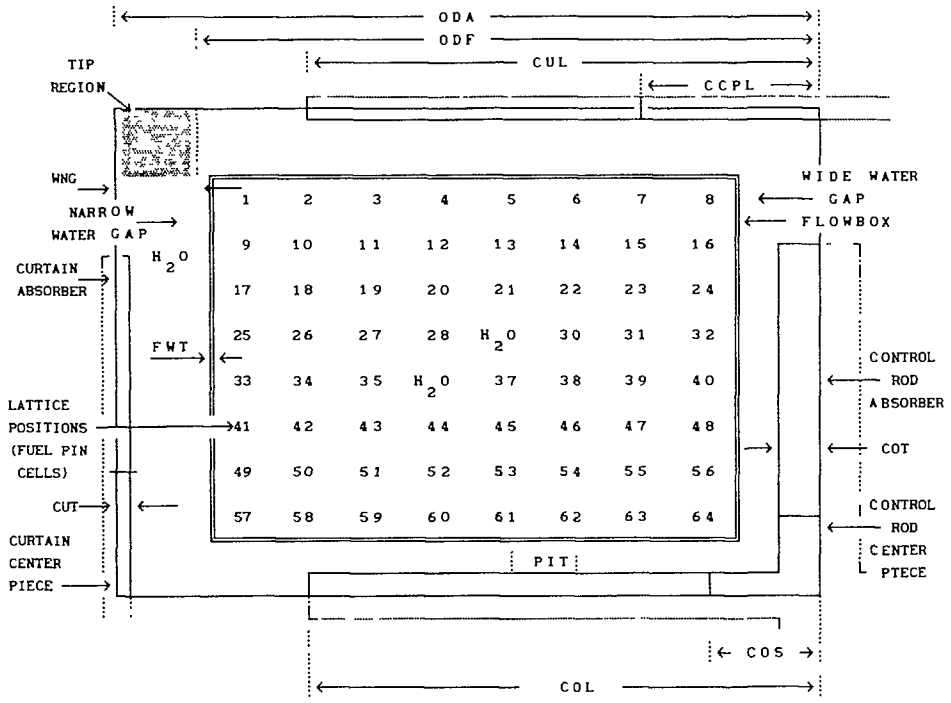

ODA	= Outer dimension of assembly cell	:16.57	cm
ODF	= Outer dimension of flowbox	:13.8125	cm
FWT	= Flowbox wall thickness	: 0.2032	cm
WNG	= Width of narrow water gap	: 0.8989	cm
PIT	= Lattice pitch	: 1.6256	cm
COL	= Effective control plate "half span"	:15.57	cm
COT	= Control plate "half thickness"	: 0.50	cm
COS	= Control plate centre-piece "half span"	: 0.00	cm
CUL	= Curtain "half span"	:15.17	cm
CUT	= Curtain "half thickness"	: 0.50	cm
CCPL	= Curtain centre piece "half span"	: 0.00	cm

FIG. 1. Geometrical representation of the BWR fuel assembly cell.

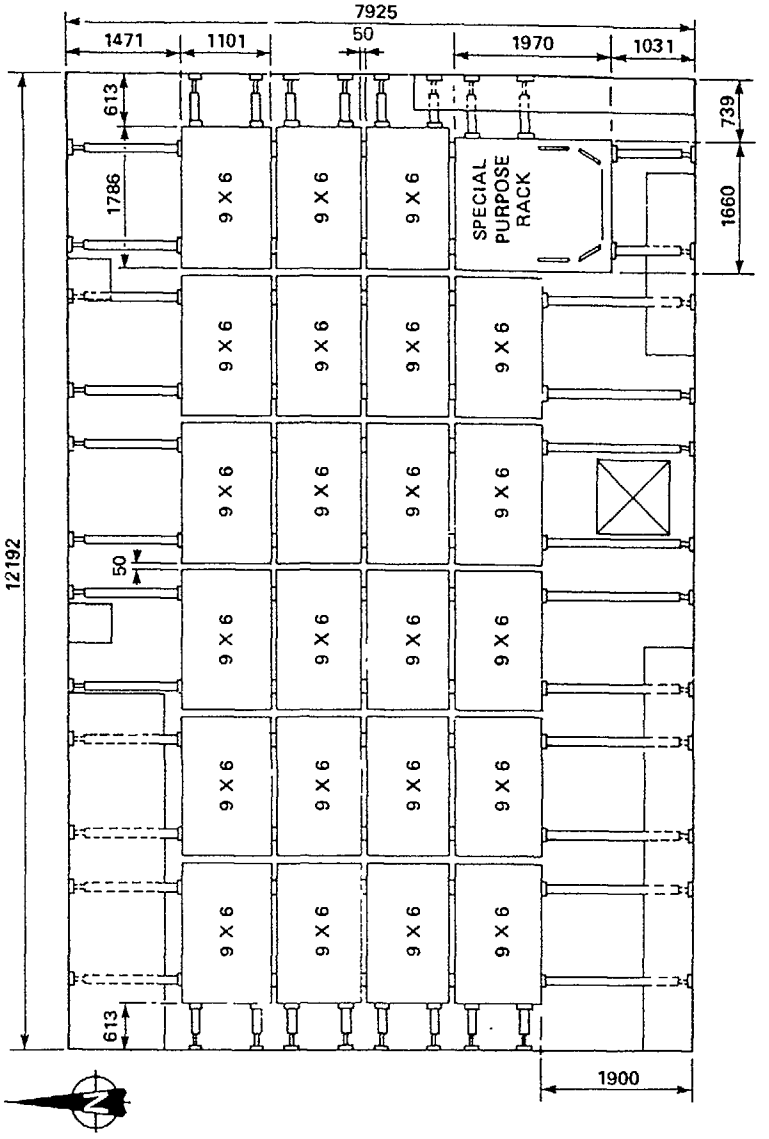

FIG. 2. Fuel pool arrangement (Laguna Verde nuclear power stations units 1 and 2 (Comisión Federal de Electricidad)).

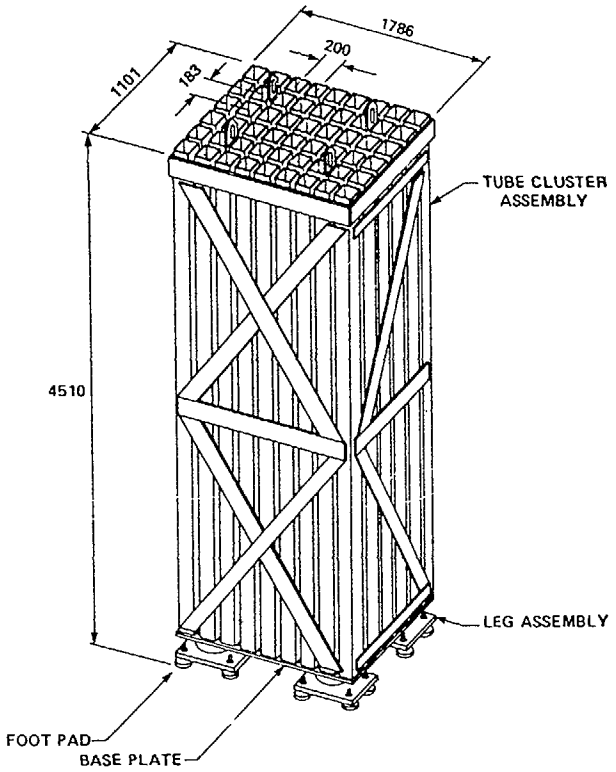

FIG. 3. Spent fuel rack (9 × 6) (Laguna Verde nuclear power stations units 1 and 2 (Comisión Federal de Electricidad)).

containers, and control rod guide tubes. This rack assembly is composed of twenty-seven 10-inch diameter and nine 12-inch diameter stainless steel pipes welded together in a array as shown in Figure 4.

The spent fuel racks as well as the special purpose rack are specified to be Type 304 stainless steel.

The spent fuel high density storage racks contain storage space sufficient for 280 percent of the core fuel assemblies.

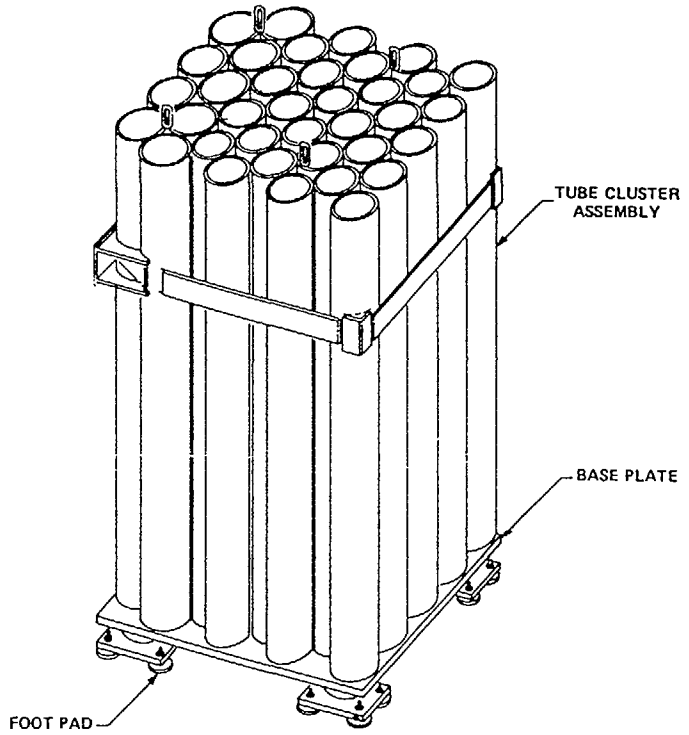

FIG. 4. Special purpose rack (Laguna Verde nuclear power stations units 1 and 2 (Comisión Federal de Electricidad)).

NUCLEAR SAFETY DESIGN BASES

The Final Safety Analysis Report for the BWR Nuclear Plant at Laguna Verde, Veracruz, specifies the following bases for the nuclear safety design.

a. Pool is filled with fuel with 3.3 w/o U-235 enrichment and no burnable poison. This fuel has a higher k_{∞} than any fuel which will be used in the core.
b. The water in the fuel storage pool is clean and unborated.

c. The pool temperature is 115°C. (No boiling)

d. No credit is taken for the fuel assembly support structure. However, the neutron absorption of the 5 mm thick stainless steel tubes in which the fuel assemblies are supported while in the storage racks is considered in the calculation.

e. Axial neutron leakage is not considered, that is, an infinite array is assumed in the axial direction.

The above assumptions are considered as a conservative base for the calculations.

For all spent fuel storage conditions:

Maximum $k_{eff} \leq 0.95$

NUCLEAR CALCULATIONS USING THE RECORD AND MIXQUIC CODES

In order to simulate a rack in the pool we considered a multiplicative and a non multiplicative region. For both regions, the RECORD code was used to calculate the two energy group macroscopic cross sections.

The calculations for the multiplicative region considered a cell to be formed by a fuel assembly, the surrounding water and a stainless steel tube of the rack. It was assumed that two stainless steel curtains and a stainless steel control rod with no boron, were the walls of a tube in the rack. For the non-multiplicative region, the water nuclear parameters were obtained from the water region surrounding the flow box in the RECORD cell (Figure 1.). The nuclear cell constants obtained are shown in Table I.

The MIXQUIC code solves the diffusion equation in X-Y geometry using numerical nodal finite element methods. This code was used to perform criticality calculations for the spent fuel pool using the rack's geometry (Figure 5.) and the nuclear constants obtained by the RECORD code. As stated in the FSAR, here we also assume no neutron leakage along the axial axis.

TABLE I

MULTIPLICATIVE REGION

Group	D	Σ_r	Σ_a	$\nu\Sigma_f$	χ
Fast	0.12319E+01	0.28650E-01	0.11050E-01	0.52714E-02	1.0
Thermal	0.33406E+00	0.0	0.10469E+00	0.12407E+00	0.0

(*) $\Sigma_r^M = \Sigma_r^R + \Sigma_a^R$ y $\Sigma_{1-2}^M = \Sigma_r^R$

Σ_r^M = 3.9700E-2 Σ_{1-2}^M = 2.8650E-2 Fast group

= 1.0469E-1 = 0.0 Thermal group

NON-MULTIPLICATIVE REGION

Group	D	Σ_r	Σ_a	$\nu\Sigma_f$	χ
Fast	1.4701	4.6000E-2	3.2098E-4	0.0	0.0
Thermal	1.9538E-1	0.0	1.7652E-2	0.0	0.0

Σ_r^M = 4.6318E-2 Σ_{1-2}^M = 4.6000E-2 Fast group

= 1.7652E-2 = 0.0 Thermal group

χ fision neutron fraction

(*) The removal cross section (Σ_r^M) for MIXQUIC code is given as the sum of removal (Σ_r^R) and absorbtion (Σ_a^R) cross sections of the RECORD code. The RECORD code removal cross section (Σ_r^R) is the scattering cross section (Σ_{1-2}^M) for the MIXQUIC code.

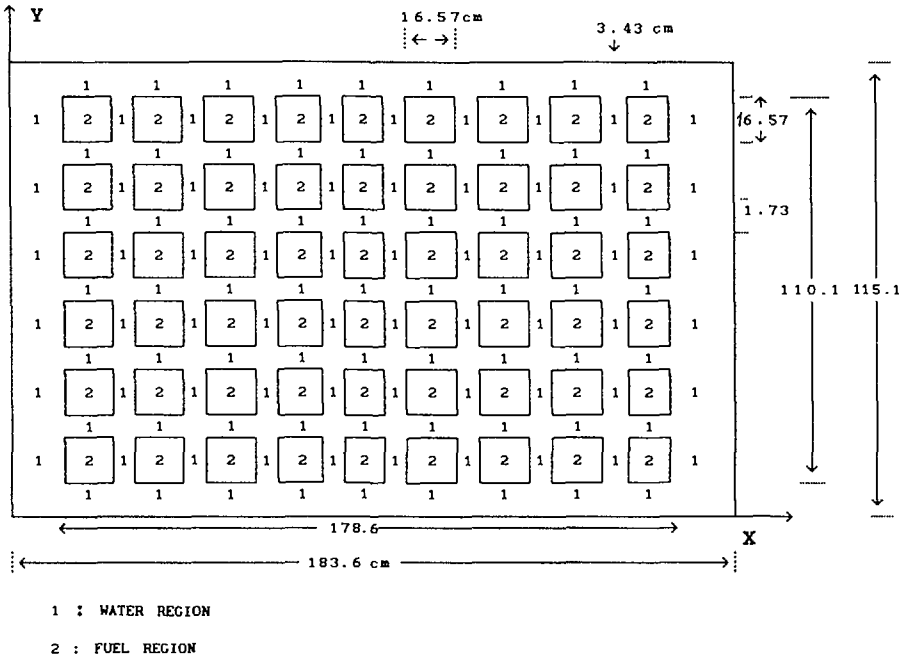

FIG. 5. MIXQUIC mesh for a rack.

Additional calculations were performed changing the temperature, lattice pitch and tube wall thickness, in order to take into account their tolerance effects.

For 1mm decrease in tube wall thickness we obtained a $\Delta K_w = 0.01589$, for a 2mm decrease in lattice pitch we obtained $\Delta K_p = 0.00856$ and for a 115°C temperature we obtained a $\Delta K_t = -0.0020$, therefore when these tolerances effects are included we have.

$$K_{eff} = 0.91746 + 0.01589 + 0.00856 - 0.002 = 0.9399$$

CONCLUSIONS

The results show that the multiplication constant obtained is less than the value of 0.95 required as a limit for the design of a spent fuel pool.

Since the macroscopic cross sections generated by the RECORD code can take into account fuel pins of different enrichment, gadolinium content as burnable poison and also their burnup, it is possible to perform less conservative calculations using these codes, although it should be noted that a homogeneous composition along the axial axis will be still considered since the MIXQUIC code is a two dimensional code.

There was a design change in the spent fuel pool which includes stainless steel mixed with boral for the racks's tube walls, this composition can be taken into account in the RECORD code since we can specify a boron fraction in the curtains and control rod materials.

REFERENCES

(1) Final Safety Analysis Report, Chap. 9.1.2 Vol. X, CFE 1974

(2) T. Skardhamar "User Manual For Record" FMS Vol. II Scandpower, 1983

(3) Del Valle, E., J.P. Hennart D. Meade, "Finite element formulations of nodal schemes for neutron diffusion and transport problems:. Advances in Nuclear Engineering Computational Methods, Vol.2,p.473, A.N.S, Knoxville, Tennessee, 1985 Nuc. Sci. Eng.,92,p.204,1986.

CRITICALITY CALCULATIONS FOR THE DESIGN ANALYSIS OF A 300 MWe PWR

Subhan GUL, Asif WASEEM, M. KAMRAM CHUGHTAI
Design and Engineering Department,
Pakistan Atomic Energy Commission,
Islamabad, Pakistan

Abstract

A 300 MWe PWR having nearly the same characteristics as the current PWR plants, analyzed for the criticality calculation. Lattice code WIMS-D4 and two dimensional diffusion code EXTERMINATOR-2 were employed for this purpose. Calculations were performed with three neutron energy groups, fast (10 MeV to 9118 eV) resonance (9118 eV to 4.00 eV) and thermal (4.00 eV to 0.00 eV). The reactivity for cold/clean, hot/clean zero power and hot/clean full power reactor states were found.

The Keff for the three states were 1.267, 1.222 and 1.200 respectively, which is quite in agreement with the available data. Further calculations are underway to calculate the same states of the reactor with burnable poison rods.

1. INTRODUCTION

Neutronic analysis techniques for PWR are well established. For detailed analysis and for licensing purpose the verifying analysis is based on finite difference solution of diffusion equation. For incore fuel management nodal and finite element methods have become standards because of their having short run time on computers.

The present paper describes the criticality calculations based on finite difference solution of diffusion equation for a 300 MWe PWR having nearly the same characteristics as the current PWR plants. The geometrical data and material specification are generally available from literature and IAEA directories. This is an initial exercise to be developed later through participation in IAEA coordinated research programs for incore fuel management and core design parameters.

2. REACTOR CORE

2.1 Description

For a 300 MWe PWR the number of fuel assemblies in the core is 121. All of the fuel assemblies have identical external dimensions and hydraulic characteristics. So they may be inserted in any position within the core array. The core height as reported in literature varies from 275 cm to 305 cm and the equivalent diameter varies from 248 cm to 255 cm. This is according to the development process in which the initial core design was cast, taking into account all other parameters.

The core is cooled/moderated by H_2O and surrounded by a stainless steel baffle. Each fuel assembly could consist of either a 14x14 or 15x15 rod array. The rod pitch within the fuel assembly could vary between 1.3 to 1.4 cm and the assembly pitch may be between 19.5 and 20.5 cm. The cladding material is Zircaloy 4. The fuel rods within each assembly are held by spacer grids and top & bottom fittings. The fuel assembly is also provided with guide thimbles for cluster of control rods. All other details and features are according to the standard PWR assembly.

2.2 Fuel Enrichment & Loading

Fuel assemblies of three different enrichments are used in the initial core, inorder to obtain the favourable radial power distribution.

Region I	2.28 to 2.45 $^{w}/_{o}$ U^{235}	41 fuel assemblies
Region II	2.50 to 2.80 $^{w}/_{o}$ U^{235}	40 fuel assemblies
Region III	2.90 to 3.50 $^{w}/_{o}$ U^{235}	40 fuel assemblies

The first two regions, which consist of the lower enrichments, are arranged in a modified checkerboard pattern towards the centre of the core. The third region of highest enrichment is arranged around the periphery of the core.

3. METHOD OF ANALYSIS

The methodology adopted in our analysis is based on the multigroup scheme to evaluate the neutron distribution in space and energy. This is achieved by solving transport equation in one dimension at the cell level.

Later flux weighted group constants for the few group model are produced. Finally finite difference method is applied to solve diffusion equation in two dimensions using few group model data, to determine the reactor criticality, flux distribution etc. The computational scheme is as follows:

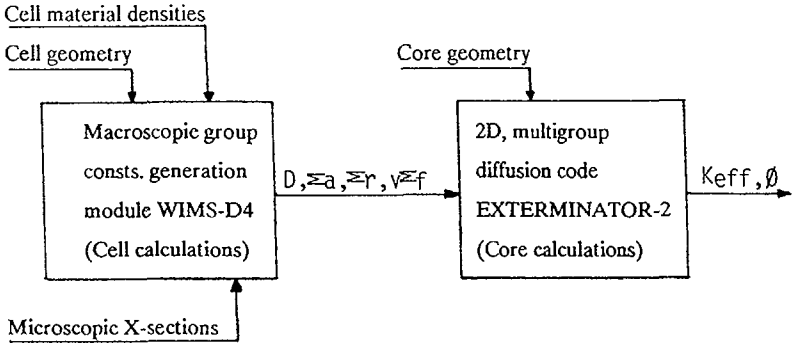

The cell calculations are performed using WIMS-D4 computer code. A variety of geometries can be treated in WIMS-D4, the basic ones are slab array including bundles of plates, regular rod array and rod clusters in cylindrical geometry. In our case we treated fuel lattice as a regular rod array form. Calculations were performed with three neutron energy groups, fast (10 Mev to 9118 ev) resonance (9118 ev to 4.00 ev) and thermal (4.00 ev to 0.00 ev). The scattering matrix included one upscattering and two down scatterings.

Lattice cells modeled for group constant generation are shown in figures 1 and 2. Cell parameters for each fuel enrichment are calculated. Similarly guide thimble and reflector cross-sections are generated. Parameters thus obtained for core are fed to EXTERMINATOR-2 code. Core calculations with EXTERMINATOR-2 can be performed

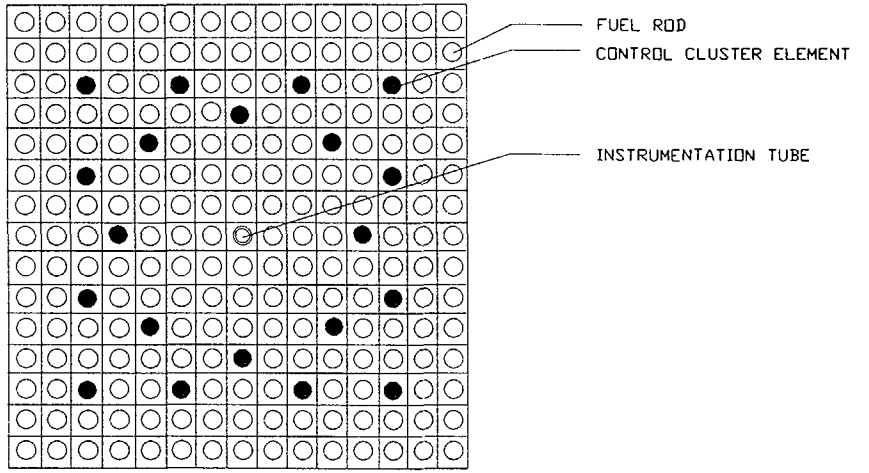

FIG. 1. 15 x 15 fuel assembly cross-section.

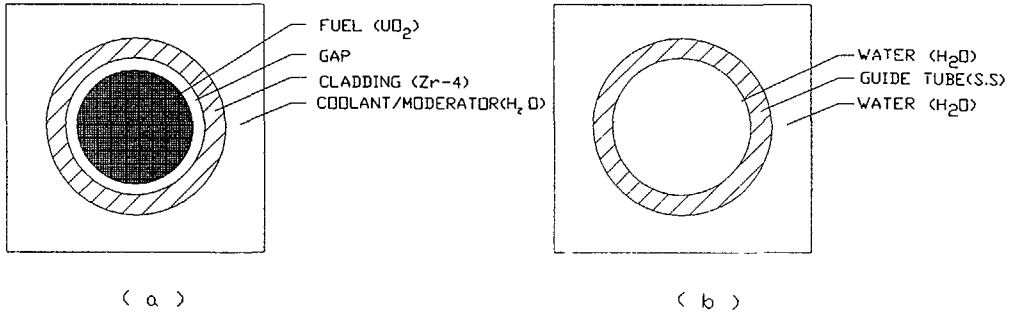

FIG. 2. (a) fuel lattice cell; (b) guide thimble cell.

by taking 1/4 core symmetry. Figure 3 shows 1/4 symmetry of the core with 91 rows and 91 columns in mesh specification. Three types of outer boundary conditions, zero flux, zero normal derivatives or periodic condition may be imposed according to problem requirement. Here we used X-Y geometry with zero flux and zero normal derivative boundary conditions.

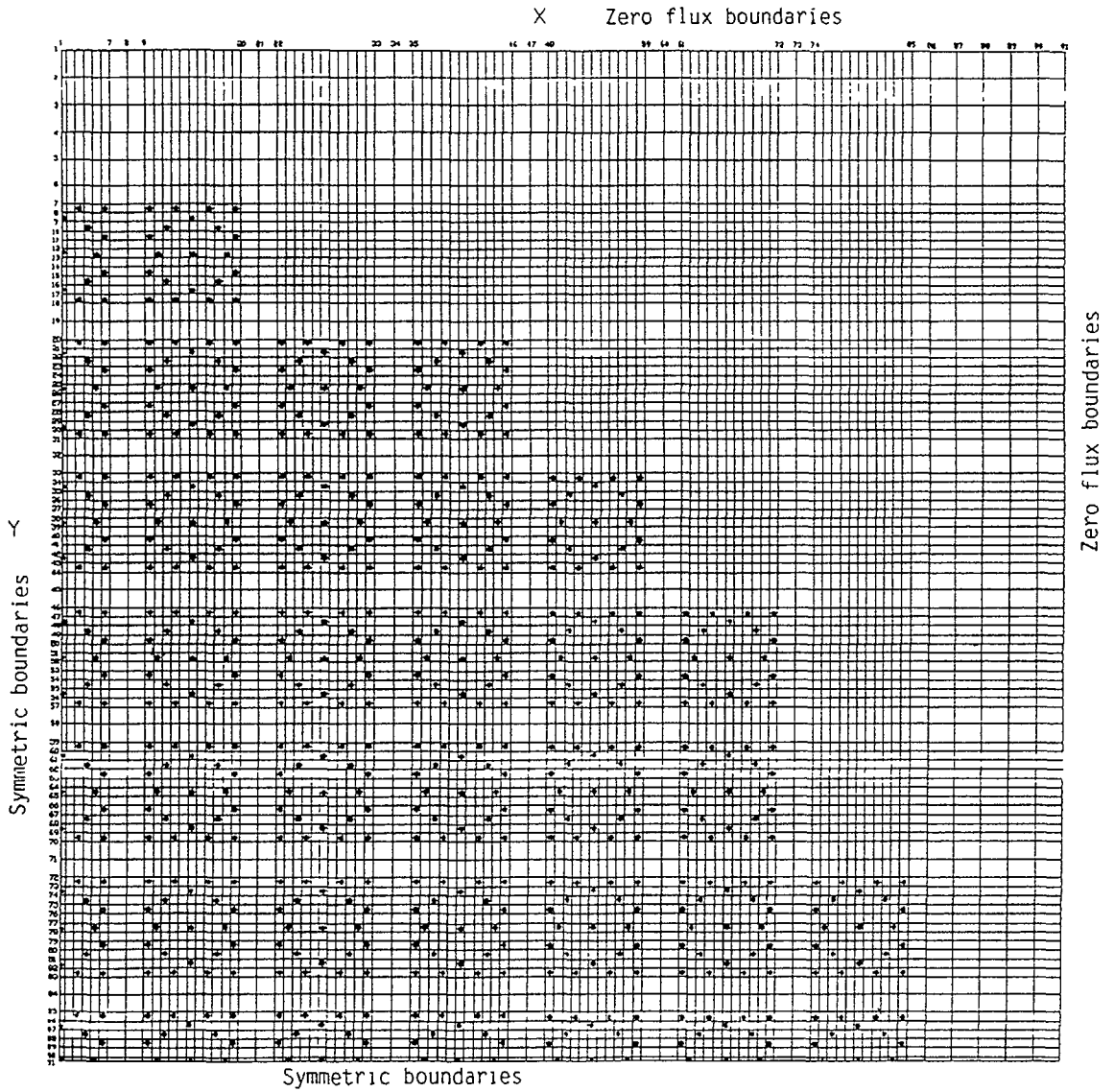

FIG 3. *Core mesh specification for ¼ core symmetry in* EXTERMINATOR-2

TABLE-1: GROUP CONSTANTS OF FUEL ASSEMBLIES CELL FOR COLD/CLEAN CORE CASE

ENRICHMENT REGION	ENERGY GROUP	DIFFUSION COEFF D(cm)	ABSORPTION X-SEC $\Sigma a(cm^{-1})$	REMOVAL X SEC $\Sigma r(cm^{-1})$	FISSION X-SEC $\nu\Sigma f(cm^{-1})$
Region I	1	1 43583	3 03948E 03	4 68054E-02	4 39476E-03
	2	0 60107	2 20367E 02	8 63089E 02	8 55206E-03
	3	0 42772	7 83527E 02	1 11833E-05	1 20821E-01
Region II	1	1 43600	3 07156E-03	4 67876E-02	4 47088E-03
	2	0 60071	2 26400E 02	8 60175E 02	9 55787E-03
	3	0 42519	8 28610E 02	1 18166E-05	1 31119E-01
Region III	1	1 43612	3 09295E-03	4 67756E-02	4 52166E 03
	2	0 60048	2 30328E-02	8 58284E-02	1 02154E-02
	3	0 42370	8 57255E-02	1 22338E 05	1 37642E-01

4 RESULTS AND DISCUSSION

Group constant generated for WIMS-D4 for cold/clean, Hot/clean zero power and Hot/clean full power cases are given in tables 1 to 6 The group constants are used in EXTERMINATOR-2 code for finding effective multiplication factor and power distribution in the core Keff calculated for each case are presented in table 7 Keff calculated for three reactor states compare fairly well with the values available in literature

The standard approach is to use LWR version of WIMS code, which is LWR-WIMS. Since it is proprietary code therefore we do not have any access to it Also an assembly code is not available with us which could be an intermediate step of calculations before going to global core calculations The basic aim in this work is to go through the available computer codes and to refine our calculations by minimizing assumptions made, which can effect the core criticality Later 3D calculations can be undertaken using CITATION It is also envisaged that participating in CRP will enable us to develop expertise in nodal and finite element based computer codes, which will have direct application for incore fuel management of PWR

TABLE-2: CELL AVERAGE SCATTERING CROSS SECTIONS FOR COLD/CLEAN CORE CASE

ENRICHMENT REGION	ENERGY GROUP	1	2	3
Region I	1	1 7681E 01	4 6786E-02	1 9086E 05
	2	0 0000E+00	4 6805E 01	8 6309E 02
	3	0 0000E+00	1 1180E-05	9 4739E-01
Region II	1	1 7676E-01	4 6768E-02	1 9079E 05
	2	0 0000E+00	4 6822E-01	8 6017E-02
	3	0 0000E+00	1 1810E-05	9 3419E 01
Region III	1	1 7674E 01	4 6757E-02	1 9074E-05
	2	0 0000E+00	4 6833E-01	8 5828E-02
	3	0 0000E+00	1 2209E 05	9 2621E-01

TABLE-3: GROUP CONSTANTS OF FUEL ASSEMBLIES CELL FOR HOT/CLEAN ZERO POWER CASE

ENRICHMENT REGION	ENERGY GROUP	DIFFUSION COEFF D(cm)	ABSORPTION X-SEC $\Sigma_a(cm^{-1})$	REMOVAL X SEC $\Sigma_r(cm^{-1})$	FISSION X-SEC $\nu\Sigma_f(cm^{-1})$
	1	1 67970	2 94810E-03	3 61095E-02	4 16662E 03
Region I	2	0 71314	2 17443E-02	6 14992E 02	8 37684E-03
	3	0 50788	6 02210E-02	2 18786E-05	9 41947E 02
	1	1 67998	2 98044E-03	3 60917E-02	4 24329E-03
Region II	2	0 71282	2 23167E-02	6 12220E-02	9 34577E-03
	3	0 50614	6 40812E-02	2 32607E-05	1 02739E-01
	1	1 68022	3 00739E-03	3 60767E-02	4 30716E-03
Region III	2	0 71257	2 27774E-02	6 10020E-02	1 01293E-02
	3	0 50489	6 71474E-02	2 43262E 05	1 09507E-01

TABLE-4: CELL AVERAGE SCATTERING CROSS SECTIONS FOR HOT/CLEAN ZERO POWER CASE

ENRICHMENT REGION	ENERGY GROUP	1	2	3
	1	1 5924E 01	3 6095E-02	1 4673E-05
Region I	2	0 0000E+00	4 0988E-01	6 1499E-02
	3	0 0000E+00	2 1863E-05	6 9192E 01
	1	1 5919E-01	3 6077E 02	1 4665E-05
Region II	2	0 0000E+00	4 1001E-01	6 1222E-02
	3	0 0000E+00	2 3222E-05	6 8383E-01
	1	1 5915E-01	3 6062E 02	1 4659E 05
Region III	2	0 0000E+00	4 1010E-01	6 1002E-02
	3	0 0000E+00	2 4296E-05	6 7771E-01

TABLE-5: GROUP CONSTANTS OF FUEL ASSEMBLIES CELL FOR HOT/CLEAN FULL POWER CASE

ENRICHMENT REGION	ENERGY GROUP	DIFFUSION COEFF D(cm)	ABSORPTION X SEC $\Sigma_a(cm^{-1})$	REMOVAL X-SEC $\Sigma_r(cm^{-1})$	FISSION X SEC $\nu\Sigma_f(cm^{-1})$
	1	1 72101	2 93595E 03	3 47861E-02	4 13288E-03
Region I	2	0 73176	2 25723E-02	5 81590E-02	8 31280E-03
	3	0 51939	5 87845E-02	3 19108E-05	9 21063E-02
	1	1 72130	2 96834E-03	3 47682E-02	4 20965E-03
Region II	2	0 73145	2 31363E-02	5 78867E-02	9 27169E-03
	3	0 51792	6 25679E-02	3 38703E-05	1 00467E-01
	1	1 72156	2 99533E 03	3 47533E 02	4 27360E-03
Region III	2	0 73121	2 35909E-02	5 76704E-02	1 00482E-02
	3	0 51688	6 55734E-02	3 53977E-05	1 07090E 01

TABLE-6: CELL AVERAGE SCATTERING CROSS SECTIONS FOR HOT/CLEAN FULL POWER CASE

ENRICHMENT REGION	ENERGY GROUP	1	2	3
	1	1 5713E 01	3 4772E 02	1 4126E 05
Region I	2	0 0000E+00	4 0291E 01	5 8159E 02
	3	0 0000L+00	3 1890E 05	6 6400E 01
	1	1 5709E 01	3 4754E 02	1 4119E 05
Region II	2	0 0000E+00	4 0303E 01	5 7887E 02
	3	0 0000E+00	3 3870E 05	6 5632E 01
	1	1 5705E 01	3 4739E 02	1 4113E 05
Region III	2	0 0000E+00	4 0311E 01	5 7670E 02
	3	0 0000E+00	3 5433E 05	6 5050E-01

TABLE-7: TYPICAL EFFECTIVE MULTIPLICATION CONSTANTS CALCULATED BY EXTERMINATOR-2 (BOL, NO BURNABLE POISON, SOLUBLE POISON AND CONTROL RODS)

STATE	K EFF (T R)
Cold/Clean Core	1 267
Hot/Clean Zero Power	1 222
Hot/Clean Full Power	1 200

REFERENCES

1 A general description of the Lattice Cell code WIMS D by J R Askew, F.J Fayers and P B Kemshell

2 WIMS D4 and cataloged procedure by C.J Taubman and J H Lawerence

3 EXTERMINATOR-2 A multigroup code for Solving Neutron Diffusion Equations in one and two dimensions, USAEC Report, ORNL TM 842, Oak Ridge National Laboratory, by T B Fowler, M L Tobies and D R Vondy

4 Nuclear Reactor Analysis by James J Duderstadt and Louis J Hamilton

5 Hand Book of Engineering Materials by MINER and SEASTONE

6 Directory of Nuclear Reactors IAEA

7 Directory of Nuclear Power Plants in world edited by Haruo Fujii of Japan Nuclear Energy Information Centre Co LTD, Tokyo Japan

8 World Nuclear Industry Hand Book special Nuclear Engineering International Publication 1988

A MODIFIED VERSION OF THE COBRA-IV-I SUBCHANNEL THERMOHYDRAULIC COMPUTER CODE

L.L. BIRO
National Commission for Nuclear Activities Control,
Bucharest, Romania

Abstract

This paper presents the study model used in COBRA-IV-I computer code for the analysis of the fuel rod temperatures distributions in non-uniform operating conditions induced by the heated generated rate and the heat transfer conditions.

An example of using the code is presented for LWR type fuel bundles with the 25 fuel rods model.

The subroutines which are added to COBRA-IV-I computer code perform the computations to determine the influences on the spatial heat flux and fuel rod temperatures distributions of the azimuthal and radial heat generation microdistributions, the azimuthal gap clading heat transfer coefficient distributions and the azimuthal coolant heat transfer coefficient distribution.

The models are based on using Fourier series for the heat generation rate and for the heat transfer coefficients in the fuel gap and on the outter fuel rod surface.

The numerical example presented in the paper provides some results obtained in assessing the degree of conservatism of the hot spot factors evaluation during the LWR core thermohydraulic design.

1. INTRODUCTION

The well known COBRA-IV-I [1],subchannel thermohydraulic computer code, it is designed to perform calculations for obtaining the spatial distribution of the thermohydraulic parameters in LWR fuel rods arrays type in steady-state and transients operation conditions. The main assumptions of this computer code do not include the azimuthal and radial micro-distributions of the heat generated rate in the fuel pellet and of the azimuthal distribution of the fuel gap thermal conductance. A more understanding of the fuel rods behaviour conditions can be obtained using an adequate post-proccesing techniques of the COBRA-IV-I computed results.

The influences of non-uniformities existing for the heat generated rate, for the fuel gap thermal conductance and for coolant heat transfer coefficient on the spatial temperature ditributions in the fuel pellet and cladding can be analysed with the Nijsing [2] analytical model.

Based on this analytical approch a number of subruotines were performed and coupled at the COBRA-IV-I computer code standard version.

2. COBRA-IV-I MODIFIED VERSION CHARACTERISTICS

The subroutines added to the COBRA-IV-I computer code deal with the effects of non-uniform heat generated rate and non-uniform heat transfer conditions on the temperature and heat flux distribution in thr fuel rods of a LWR fuel bundle type.

The mathematical model of this subroutines is based on the Nijsing's analytical approch and have the following assumptions:

- thermal conductivity is not dependent by the temperature;
- non-uniformities of the heat generated distribution, fuel-cladding contact resistance and coolant heat transfer coefficients can be simulated by the user by means of analytical expressions which are dependent by the local radial coordinate and azimuthal angle cosine;
- the temperature fields are obtained as general solutions of the heat conduction equation, founded by combining the solutions of the homogeneous and inhomogeneous parts of this equation;
- the coefficients of the Fourier series are obtained from the boundary conditions and from the continuity and symmetry requirements;
- the different types of non-uniformities are separatelly studied.

This subroutines provide a post-processing of the standard COBRA-IV-I computed results using the following procedures:

- based on COBRA-IV-I computed results the spatial position with the maximum heat flux and the maximum clad surface temperature are selected;
- the azimuthal variations of the coolant temperatures and heat transfer coefficients located in these specified positions are fitted to the subchannels local heat transfer conditions arround the selected fuel rod.
- according with the fuel temperature dependent thermal conductivity expression used in COBRA-IV-I and with computed temperature radial profile for uniform heat generated rate, the average value of the fuel thermal conductivity is computed;
- after these data preparation the absolute and relative values of the heat generated rate, temperatures and heat fluxes are computed for the fuel pellet and the cladding versus radial and azimuthal coordinates;
- finally, the isovalues curves for the heat generated rate and for temperature distribution are computed and plotted.

This COBRA-IV-I modified version is installed on CNCAN PC-386 type computer. The suplimentary memory reqiurements are 200 Kb more than standard version. For the complete non-uniformities calculations the computed run time increse with 60 seconds for each case.

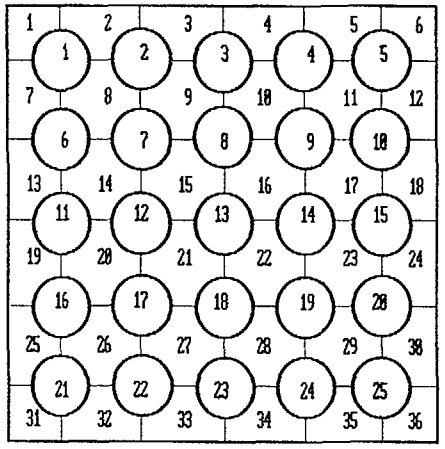

Fig. 1 Fuel rods and subchannel identification numbers.

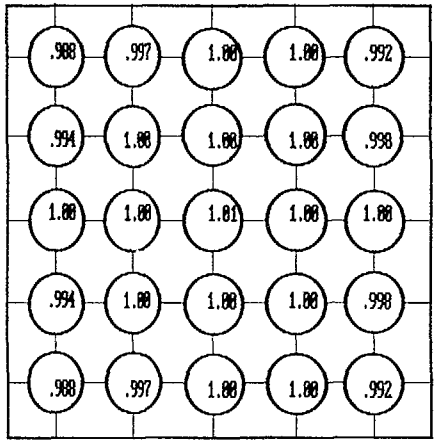

Fig. 2 Power fuel rod factors

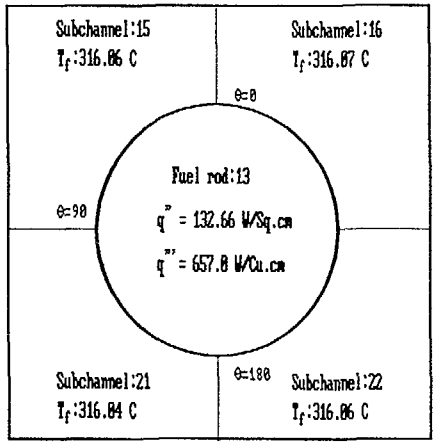

Fig. 3 Elementary cell for non-uniformities calculations.

Table No. 1
General input data

Rod diameter	: 10.7 mm
Pellet diameter	: 9.3 mm
Clad thickness	: 0.8 mm
Arrays pitch layout	: 14.3 mm
No. of fuel rods	: 25
No. of subchannels	: 36
Height of fuel bundles	: 3.9 m
Inlet mass velocity	: 3725 Kg/sq.m/s
Inlet pressure	: 158 Bar
Inlet temperature	: 291 C
Average heat flux	: 91 W/sq.cm
Axial step size	: 13 cm
Power rod factors	: see fig. 2

3. NUMERICAL EXAMPLE

A model with 25 fuel rods and 36 subchannels was selected to demonstrate the working procedure based on the coupling COBRA-IV-I standard version with the analytical post-processing techniques, above described. The used geometrical model shown in fig. 1, and represent a high fuel rod power factors part of the PWR-1300 [3] fuel assembly. The data presented in table I have been used to preparation of the COBRA-IV-I input data.

The UO2 temperature dependent thermal conductivity has been carried out using the derived [4] expression as following :

$$K(T)=10.41*\left(1.-1.316*10.E-3*T+7.255*10.E-7*T*T-1.284*10.E-10*T*T*T\right) \quad (1)$$

A constant clad thermal conductivity value of 14 W/m/C and a cosine axial profile heat flux are used too.

With default input data options, the COBRA-IV-I results indicate the centerline maximum fuel temperature about 1837.8 C for fuel rod no.13 at 208 cm axial position from coolant inlet.

This spatial location was selected by the post-processing subroutine added to the COBRA-IV-I computer code for the local non-uniformities analysis in elementary cell as shown in fig. 3.

The analysis was perform for the four cases :

a) fuel rod without non-uniformities (COBRA-IV-I results)

b) fuel rod with radial and azimuthal heat generated microdistribution given by the following equations :

$$Q'''=657.8*[0.9679+0.09679*(r/R)**2+0.09679*(r/R)*\cos(f)+0.009679*(r/R)**3*\cos(f)] \quad (2)$$

c) fuel rod with azimuthal distribution of the heat transfer coefficient in the pellet-clad gap given by the following equation :

$$G=10000./[1+0.3*\cos(f)] \quad (3)$$

d) fuel rod with azimuthal distribution of the coolant heat transfer coefficient given by the following equation:

$$A=40000.*[1-0.3*\cos(f)] \quad (4)$$

From the post-processing of the COBRA-IV-I computed values and taking into account the non-uniformties above described, the main results are presented in table 2 and in fig.4 to fig.14.

The effects of the non-uniformities types on the temperatures fields in the fuel pellet and cladding are in line with expections.

4. FINAL REMARKS

The COBRA-IV-I modified version could be used in the deterministic assessing of the thermohydraulic operational parameters of the LWR type reactor.

This allows to obtain a better values for the hot spot factors in fuel rod arrays without iterative procedure and based on the thermohydraulic subchannel mixing model results.

This version have been already used successfully by the author for the PHWR type reactor to evaluate the hot spot factors and to compute the spatial distribution of the thermohydraulic parameters in the framework of the CANDU-600 MWe nuclear safety analyses [5].

Table No. 2

Comparasion between COBRA-IV-I standard version computed results and non-uniformities operations conditions post-processing results.

Fuel rod No. 13
Axial position : 288 cm

No. crt.	PARAMETERS	COBRA-IV-I standard version results	Non-uniform heat generated case		Non-uniform fuel gap conductance case		Non-uniform coolant heat transfer coefficient	
			Absolute values	Relative values*)	Absolute values	Relative values*)	Absolute values	Relative values*)
1	Maximum fuel temperature (C)	1837.8	1838.4	0.033	1854.7	0.919	1848.9	0.683
2	Maximum fuel surface temperature (C)	576.8	585.1	1.439	623.2	8.044	585.6	1.525
3	Maximum fuel gap drop temperature (Grd. C)	152.64	159.08	4.690	284.51	33.98	153.08	0.288
4	Maximum inner clad surface temperature (C)	428.44	425.38	1.156	422.28	0.418	433.78	3.154
5	Maximum outer clad surface temperature (C)	349.25	358.98	0.472	349.98	0.186	363.18	3.965
6	Maximum clad drop temperature (Grd. C)	71.898	74.391	4.643	72.311	1.715	71.357	0.375
7	Maximum clad-coolant drop temperature (Grd. C)	33.258	34.781	4.684	33.816	1.782	47.827	41.43
8	Maximum pellet surface heat flux (W/Sq.CM)	152.64	159.66	4.688	155.22	1.698	153.33	0.452
9	Maximum inner clad heat flux (W/Sq.CM)	152.64	159.66	4.688	155.22	1.698	153.08	0.452
10	Maximum outer clad heat flux (W/Sq.CM)	132.66	138.77	4.682	134.92	1.708	133.27	0.456

*) (Absolute value - COBRA-IV-I value)/(COBRA-IV-I value) * 100 (%)

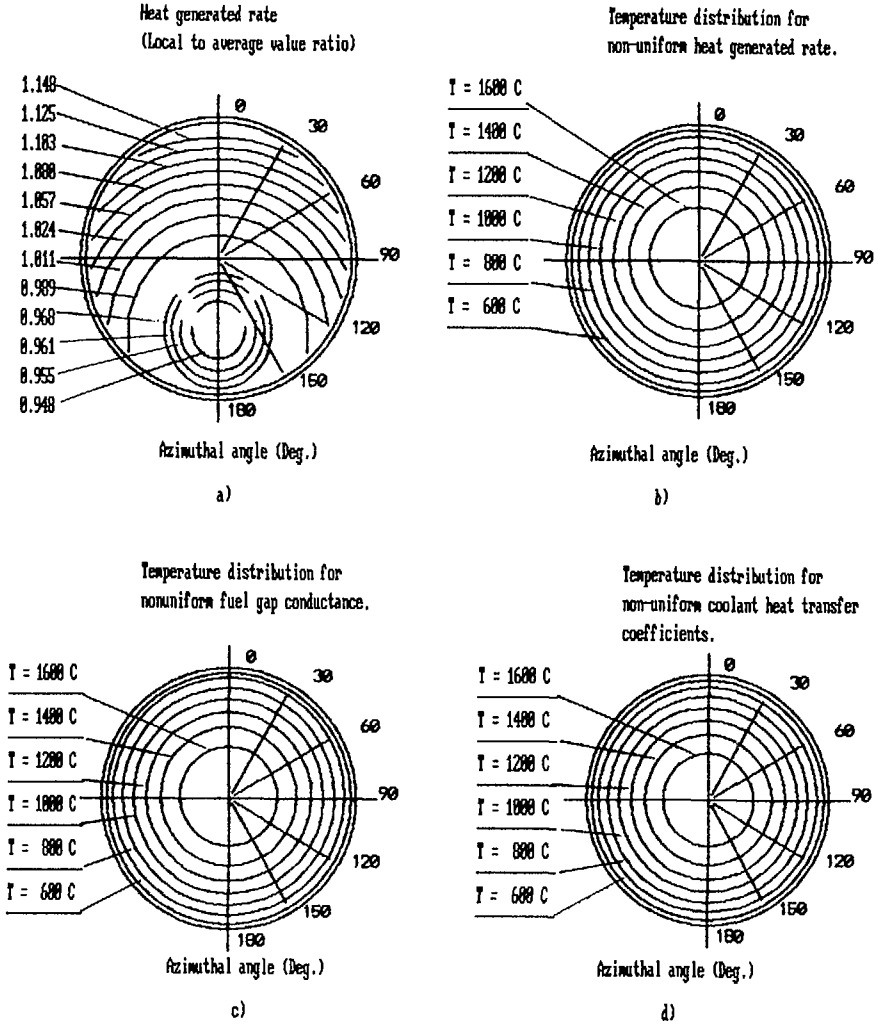

Fig. 4 ISOVALUES CURVES FOR FUEL PELET CROSS SECTION

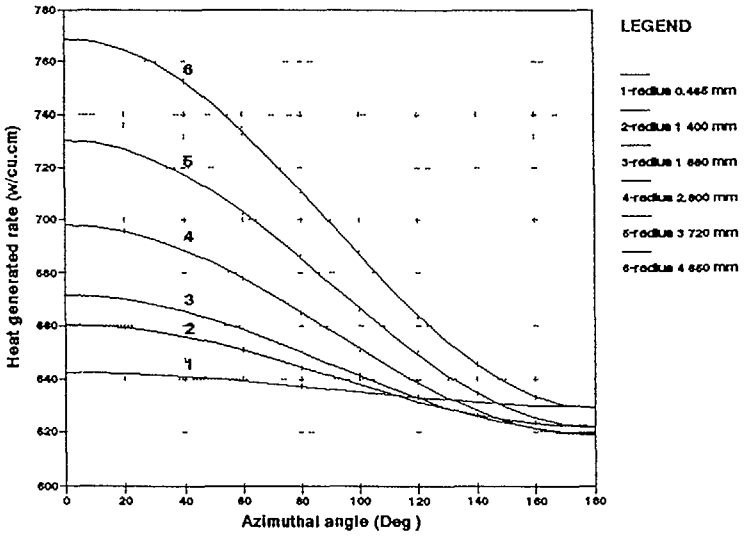

Fig. 5 Azimuthal distribution of heat generated rate.

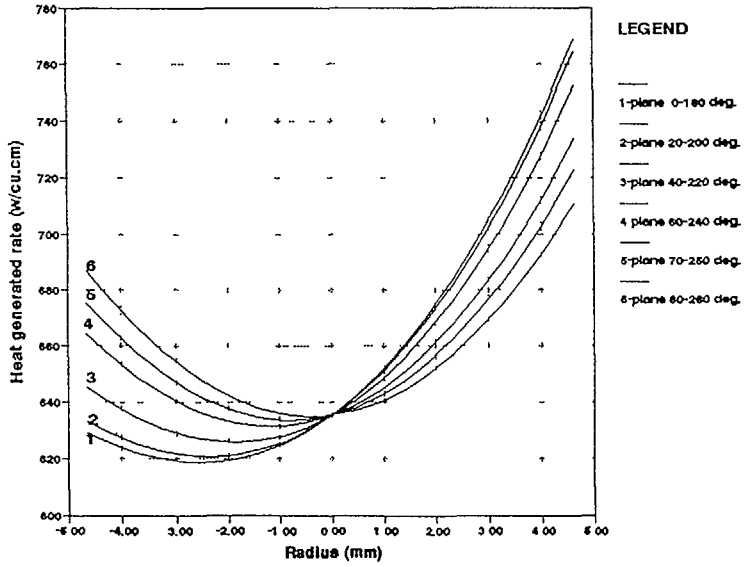

Fig. 6 Radial distribution of heat generated rate.

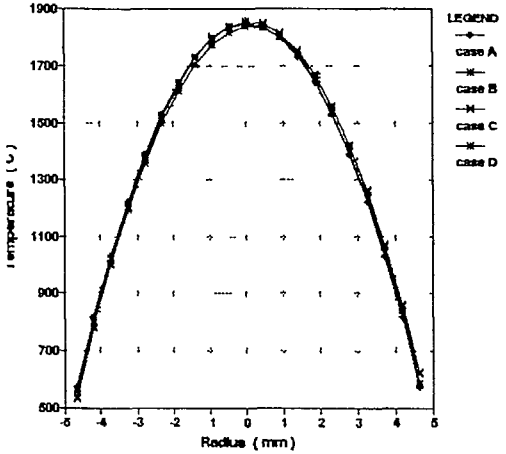

Fig 7 Fuel pelet radial temperature distribution

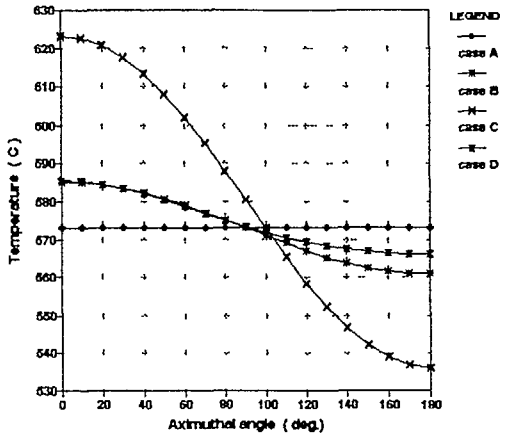

Fig 8 Fuel palet surface azimuthal temperature distribution

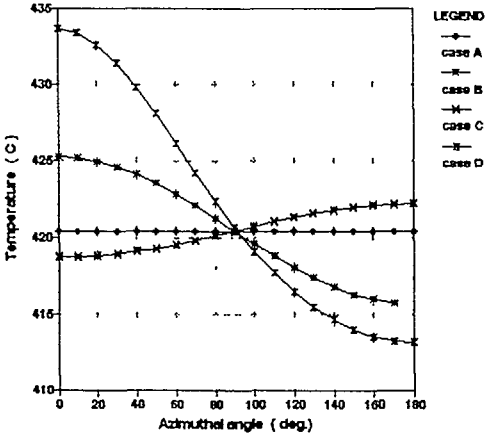

Fig 9 Inner clad surface azimuthal temperature distribution

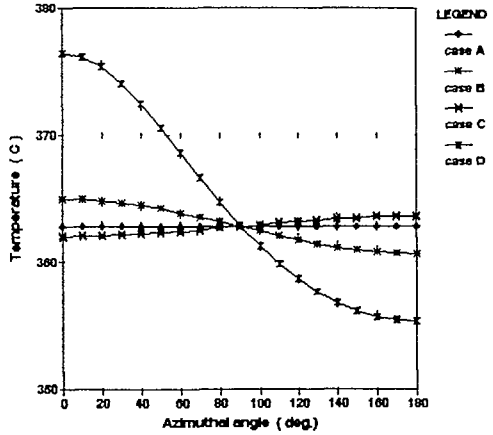

Fig 10 Outer clad surface azimuthal temperature distribution

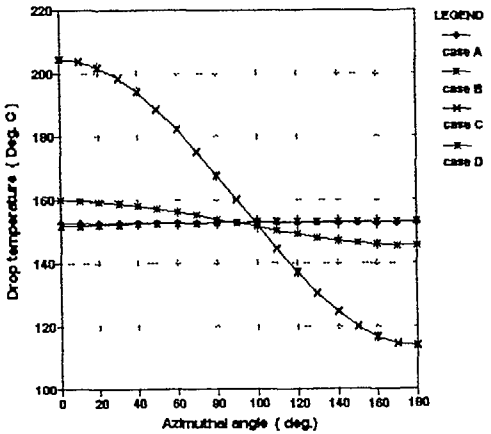

Fig 11 Fuel gap drop temperature azimuthal distribution

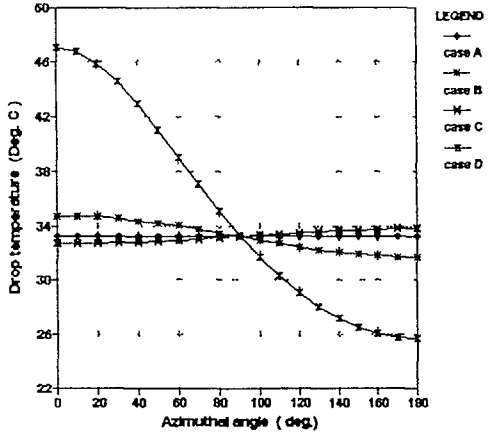

Fig 12 Clad-coolant temperature azimuthal distribution

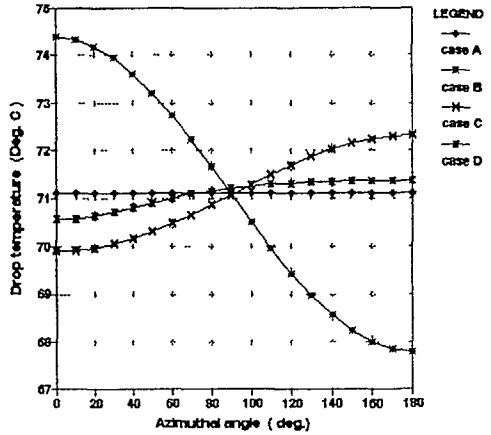

Fig 13 Clad drop temperaturev azimuthal distribution

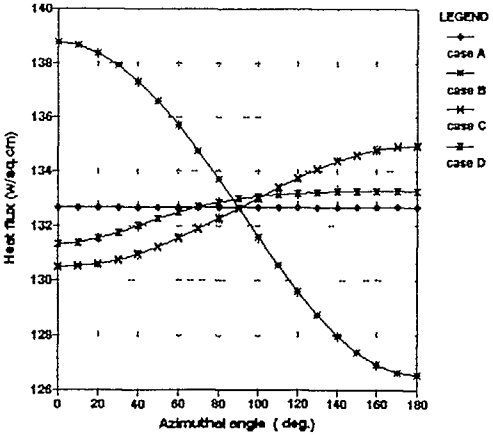

Fig 14 Fuel rod surface heat flux azimuthal distribution

NOTATION

A : coolant heat transfer coefficient (w/sq.m/grd.C)
G : fuel gap heat transfer coefficient (w/sq.m/grd.C)
f : azimuthal angle (deg.)
K : fuel thermal conductivity (w/m/grd.C)
r : current fuel radius (m)
R : pellet radius (m)
T : temperature (C)
Q''': heat generated rate (w/cu.cm)

REFERENCES

[1] C.L. Wheeler, et. al.,
"COBRA-IV-I: An Interim Version of COBRA for Thermal-Hydraulic Analysis of Rod Bundle Nuclear Fuel Elements and Cores", BNWL-1962/UC-32 ,March 1976, USA.

[2] R. Nijsing,
"Temperature and Heat Flux Distribution in Nuclear Fuel Element Rods",
Nuclear Engineering and Design 4(1966) 1-20, North-Holland Publishing Company, Amsterdam, Holland.

[3] A. Gruen,
"Physics of Pressurized Water Reactors",
Winter Courses on Nuclear Physics and Reactors, part. II, Trieste, February 1978, Italy.

[4] C.J. Hocevar, T. Wineiger,
"THETA-1B: A Computer Code for Nuclear Reactor Core Thermal Analysis",
USAEC, TID-4500, February 1971, USA.

[5] L.L. Biro,
"Arrays Effects in Thermo-Hydraulic Processes of Presurized Water Reactor Cores",
Bucharest, October, 1983, Romania.

CALCULATION OF TWO CYCLES OF KALININ UNIT-1

V. KRÝSL, P. MIKOLÁŠ, J. ŠVARNÝ
Škoda Plzeň,
Plzeň, Czechoslovakia

Abstract

This paper presents a overview of the new library for the ŠKODA multidimensional static computer program, MOBY-DICK, for core analysis. MOBY-DICK predictive capability was assessed by comparing its predictions of boron concentration and assembly power distributions against apropriate measured data. The first unit of the Kalinin Nuclear Power Plant (NPP) (so called serial version of WWER-1000) represents best documented test for WWER-1000. We have proposed for comparison of MOBY-DICK prediction versus core follow measurement two first cycles of that unit.

1. Overview of Preparation Library MILDA

The nuclear cross section library MILDA used by MOBY-DICK computer program contains macroscopic and microscopis (σ_{Xe},σ_{Sm}) cross section data based on 2/4 - energy-group structure which has been processed from WIMS [1,2] supercell one dimensional multigroup transport calculations and 2-group diffusion homogenization of fuel assembly by HOMOGS computer program [3]. The scheme of preparation of the library MILDA has been divided into two major steps.

In the first step, fine-mesh cross sections has been obtained by the one dimensional transport supercell calculations (incorporating fuel and non fuel regions) by code WIMS. Group collapse to 4 or 2 energy group has also been done.

The second step in the preparation process performs the homogenization by solving a standard diffussion equation of the whole subassembly and its vicinity. This step is based on the group-collapsed and homogenized fine mesh cross sections obtained from the first step ot solution.

Dependence of basic input data (cross sections, fission product yields, concentration of Xe and Sm and asymptotic spectral indices) on burnup A, technological parameters V (fuel temperature, moderator temperature (density), boron acid concentration, Xe and Sm poisoning) and instantaneous and long-term spectral perturbations has been accounted for according to the formula

$$\Sigma = \Sigma^{AS} K_V + K_{IS} + K_{DS} \qquad (1)$$

where Σ^{AS} is the cross section of the basic state (unperturbed technological parameters, assymptotic spectrum),

K_V is the factor accounting for the departure of technological parameters from their nominal values,

K_{IS} is the correction term describing the influence of long-term spectral perturbations,

K_{DS} is the correction term describing the influence of instantaneous spectral perturbations.

You see, that this cross section library has been developed in a manner consistent with existing AER methodologies (KAB Berlin).

Basic fine-mesh cross section tables has been prepared by one-dimensional calculations (by WIMS) of equivalent supercells for the selected range of perturbations in technological parameters and spectra. These tables has been then processed by computer program PARAMET [4] into coefficients of regression polynomials of the form (1).

Assembly homogenization has been then performed by program HOMOGS. Resulting coarse-mesh data has been again processed into polynomials of the form

$$\Sigma = \Sigma^{AS} K_{\gamma} \ . \qquad (2)$$

Boundary conditions, dependent on boron acid concentration has been choosen from previous library MAGRU and adjusted.

2. Core Follow Comparison

Presented core follow comparison between MOBY-DICK predicted and on Kalinin NPP measured values provide information about the accuracy of MOBY-DICK code and MILDA library.

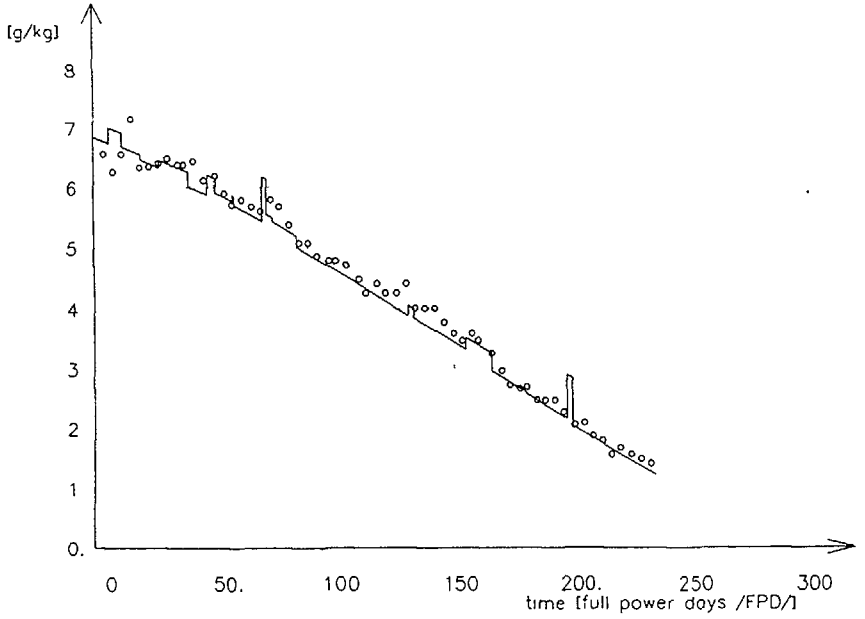

Fig 1a Comparison of critical boron concentration folow of cycle 1 of Kalinin NPP
[o — Measurement, ------ — Calculation by MOBY-DICK]

Analysis of the predicted soluble boron concentration versus time yields no significant deviations from experiments. A samples of the critical boron acid concentration versus time are shown in Figures {x}a ; the overall close-to-experimental boron concentration demonstrate the good stability of the MILDA library and methodology during burnup.

The comparison against directly measured assembly-wise relative power distribution from first two cycles of Kalininska NPS provides a good test of the WIMS-HOMOGS codes capability to provide cross sections to spatial design codes to calculate power and reactivity distribution. Figures {x}1b,c present the detailed analysis of the power distribution comparison using coarse-meshed diffusion theory code MOBY-DICK and WIMS-HOMOGS based few group cross sections. The overall agreement is good as demonstrated by a standard deviation.

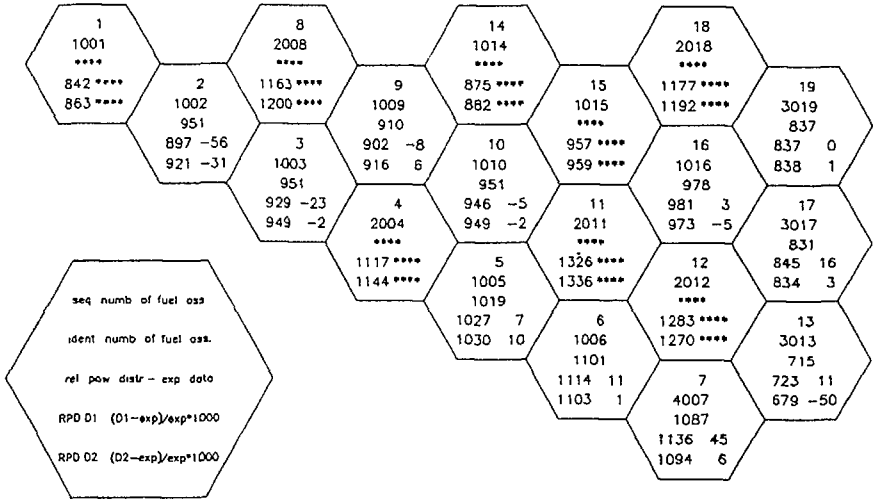

Fig 1b Relative power distributions of fuel assemblies at 17 FPD of cycle 1 of Kalinin NPP based on calculational and experimenal data and their comparison
data1,D1 —calculation by programme BIPR
data2,D2 —calculation by programme MOBY-DICK

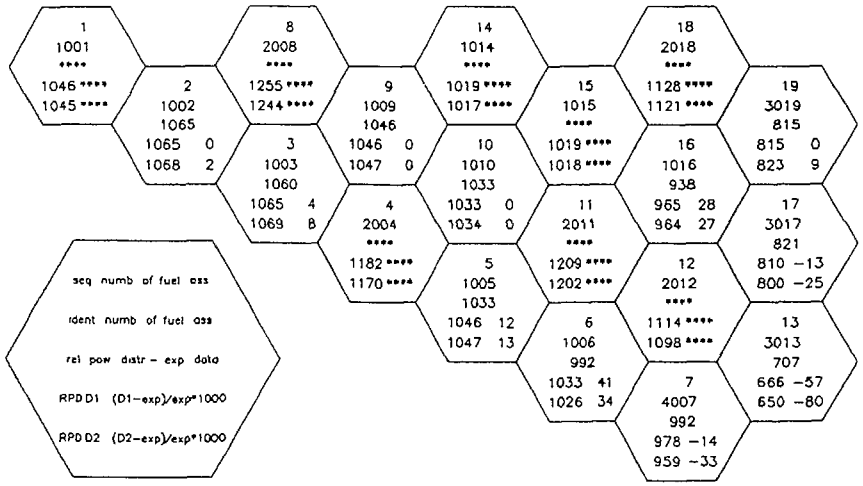

Fig 1c Relative power distributions of fuel assemblies at 235 FPD of cycle 1 of Kalinin NPP based on calculational and experimental data and their comparison
data1,D1 -calculation by programme BIPR
data2,D2 -calculation by programme MOBY-DICK

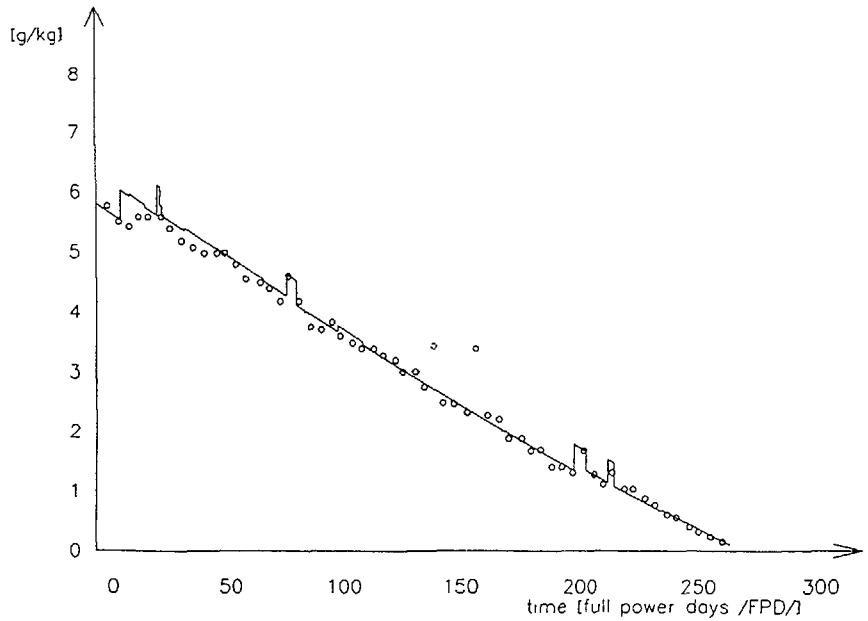

Fig 2a Comparison of critical boron concentration folow of cycle 2 of Kalinin NPP
[o - Measurement, ------ - Calculation by MOBY-DICK]

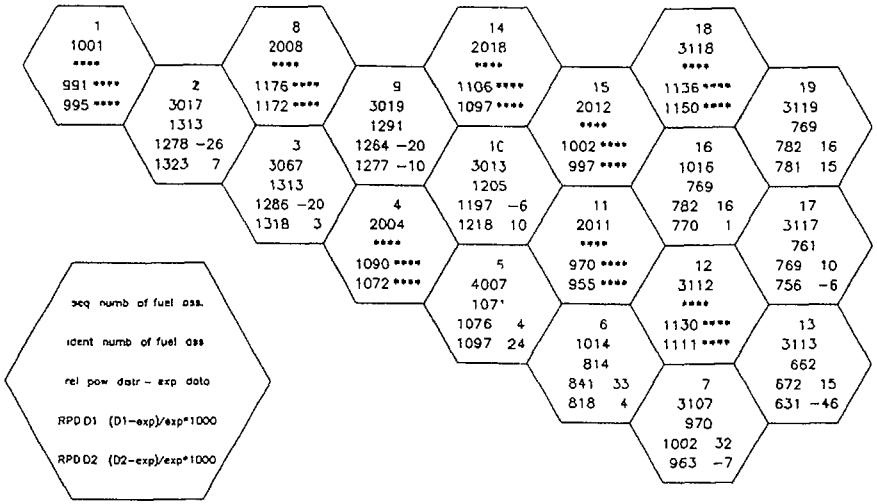

Fig 2b Relative power distributions of fuel assemblies at 92 FPD of cycle 2 of Kalinin NPP based on calculational and experimental data and their comparison
data1,D1 -calculation by programme BIPR
data2,D2 -calculation by programme MOBY-DICK

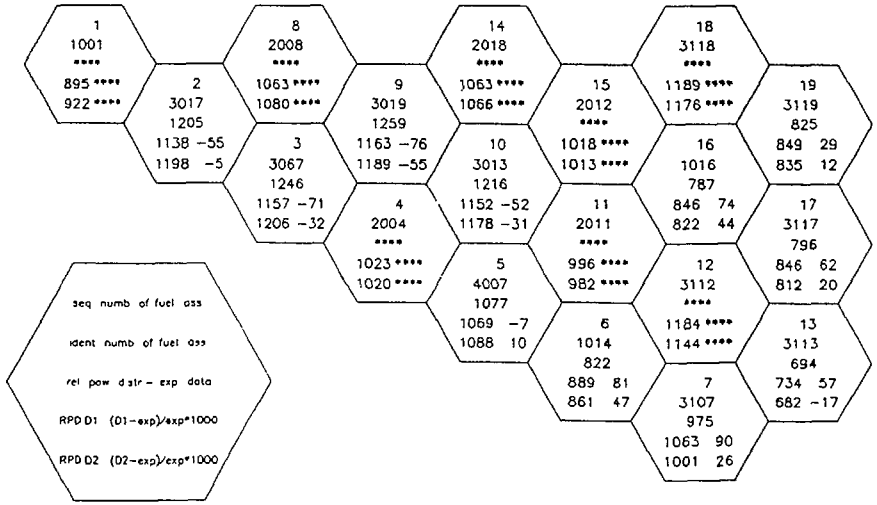

Fig 2c Relative power distributions of fuel assemblies at 208 FPD of cycle 2 of Kalinin NPP based on calculational and experimental data and their comparison
data1,D1 -calculation by programme BIPR
data2,D2 -calculation by programme MOBY-DICK

We must emphasise that for all comparisons presented, no adjustments nor biases were applied to library MILDA and any predicted quantities except for boundary conditions.

REFERENCES

[1] Roth, M.J., Taubmann, C.J., Lawrence, J.H.:
WIMS D4 - Version 101 and Cataloged Procedure,
AEEW-M 1925, Dorchester, 1982

[2] Ahnert, C., Aragones, J. M.:
MARIA System:
A Code Block for PWR Fuel Assembly Calculations,
J.E.N. 543, Madrid, 1983

[3] Svarný J.:
Short description of the HOMOGS program,
ZJS-5/91, Plzeň (CSFR), 1991

[4] Mach P., Mikoláš P., Svarný J.:
Description of the programme PARAMET,
ZJS-3/91, Plzeň (CSRF), 1991

LIST OF PARTICIPANTS

C. ALVAREZ-CARDONA
Higher Institute for Nuclear Science and Technology
Ave. Salvador Allende y Luacea
Quinta de los Molinos
Ciudad de la Habana
Cuba

T.G. APOSTOLOV
Institute for Nuclear Research and Nuclear Energy
Boul. Trakia 72
Sofia 1784
Bulgaria

J. BARDOS
Nuclear Research Institute
250 68 Rez
Czechoslovakia

L.L. BIRO
National Commission for Nuclear Activities Control
Bd. Libertatii nr. 12
Bucharest - 5
Romania

J. BROULIK
Nuclear Research Institute
250 68 Rez
Czechoslovakia

M.J. CRIJNS
International Atomic Energy Agency
Wagramerstr. 5
A-1400 Vienna
Austria

M.J. HALSALL
Winfrith Technology Centre
Dorchester, Dorset
United Kingdom

O. HRAZDIL
Nuclear Research Institute
250 68 Rez
Czechoslovakia

V. JAGANNATHAN
Bhabha Atomic Research Centre
Theoretical Physics Division
Bhabha Atomic Research Centre
Trombay, Bombay 400085
India

L. KORPAS
Paks Nuclear Power Station
P.O. Box 71
7031 Paks
Hungary

P.D. KRISHNANI
Bhabha Atomic Research Centre
Theoretical Physics Division
5th floor, Central Complex
B.A.R.C., Trombay, Bombay-85
India

CARLOS FILIO LOPEZ
SEMIP
Comision Nacional de Seguridad Nuclear y Salvaguardias
Mexico

J. KYNCL
Nuclear Research Institute
250 68 Rez
Czechoslovakia

V. LELEK
Nuclear Research Institute
250 68 Rez
Czechoslovakia

M.R. MADARIAGA
Comisión Nacional de Energía Atómica
Av. del Libertador 8250
1429 Buenos Aires
Argentina

M. MAKAI
Central Research Institute for Physics
KFKI/AEKI
Atomic Energy Research Institute
P.O. Box 49
H-1525 Budapest
Hungary

N. MARINKOVIC
Boris Kidric Institute of Nuclear Sciences
Nuclear Engineering Laboratory
P.O. Box 522
11001 Beograd
Yugoslavia

K.S. MERK
Siemens AG, UB KWU
Postfach 3220
W-8520 Erlangen
Germany

A. MIASNIKOV
Nuclear Research Institute
250 68 Rez
Czechoslovakia

P. MIKOLAS
SKODA Plzen
Nuclear Engineering Plant
316 00 Plzen
Czechoslovakia

J. MIKUS
Nuclear Research Institute
250 68 Rez
Czechoslovakia

H. MOLDASCHL
Siemens KWU
Power Generation Group
Hammerbacherstr. 12-14
P.O. Box 3220
D-8520 Erlangen
Germany

M. NASR
Atomic Energy Authority
101, Kasr El-Eini Street
Cairo
Egypt

T.Q. NGUYEN
Westinghouse Electric Corporation
P.O. Box 355
Pittsburgh
15230-0355 Pennsylvania
USA

M. NURDIN
National Atomic Energy Agency (BATAN)
Nuclear Technology Assessment Centre
P.O. Box 85 Kby
12710 Jakarta
Indonesia

B. OSMERA
Nuclear Research Institute
250 68 Rez
Czechoslovakia

M. PECKA
Nuclear Research Institute
250 68 Rez
Czechoslovakia

D. PEVEC
Faculty of Electrical Engineering
University of Zagreb
Unska 3
41000 Zagreb
Yugoslavia

J. ROCEK
Nuclear Research Institute
250 68 Rez
Czechoslovakia

V. RYPAR
Nuclear Research Institute
250 68 Rez
Czechoslovakia

L. SAUVAGE
Commissariat à l'Energie Atomique
C.E.N. Cadarache
13108 St. Paul lez Durance
France

HONG-GI SHIM
International Atomic Energy Agency
Wagramerstr. 5
A-1400 Vienna
Austria

A. SHUMSKY
Gidropress
Ue. Ordijonikidze 21
142103, Podolsk, Moscow region
Russia

G. SUBHAN
Chashma Nuclear Power Project
Chasnupp
P.O. Box 1133
PAEC, Islamabad
Pakistan

A. SUSLOV
I.V. Kurchatov Institute of Atomic Energy
I.V. Kurchatov Sg, 46
Moscow
Russia

J. SVARNY
SKODA Plzen
Nuclear Engineering Plant
316 00 Plzen
Czechoslovakia

C. SVOBODA
Nuclear Research Institute
250 68 Rez
Czechoslovakia

B. SZCZESNA
Institute of Atomic Energy
Nuclear Safety Analysis Dept.
Pl. 05-400 Otwock-Swierk
Poland

A.Z. TANKER
Energy Technologies Research Inst.
Saraykoy Research Center
Turkish Atomic Energy Authority
06105 Ankara
Turkey

S. THOMAS
Dep. NS4 (Core Design and Evaluation)
in Section 1 (Nuclear Power Plant)
Kraftwerks- und Anlagenbau AG
Allee der Kosmonauten 32
O-1140 Berlin-Marzahn
Germany

M.H. TUERGUT
CEKMECE
Nuclear Research and Training Center
P.O. Box 1 Havaalani
Istanbul
Turkey

T. TUERKER
CEKMECE
Nuclear Research and Training Center
P.O. Box 1 Havaalani
Istanbul
Turkey

J. VACEK
SKODA Plzen
Nuclear Engineering Plant
316 00 Plzen
Czechoslovakia

J. VANICEK
Nuclear Research Institute
250 68 Rez
Czechoslovakia

L. VRBA
Nuclear Research Institute
250 68 Rez
Czechoslovakia